TOWARDS THE UNDERSTANDING OF THE STEADY TILT PHENOMENON IN SEMI-SUBMERSIBLES

by

Mehmet Atlar, BSc, MSc

A thesis submitted for the Degree of Doctor of Philosophy in the Department of Naval Architecture and Ocean Engineering at the University of Glasgow

January, 1986

"To the Memory of my Mother and my Father"

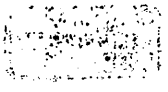

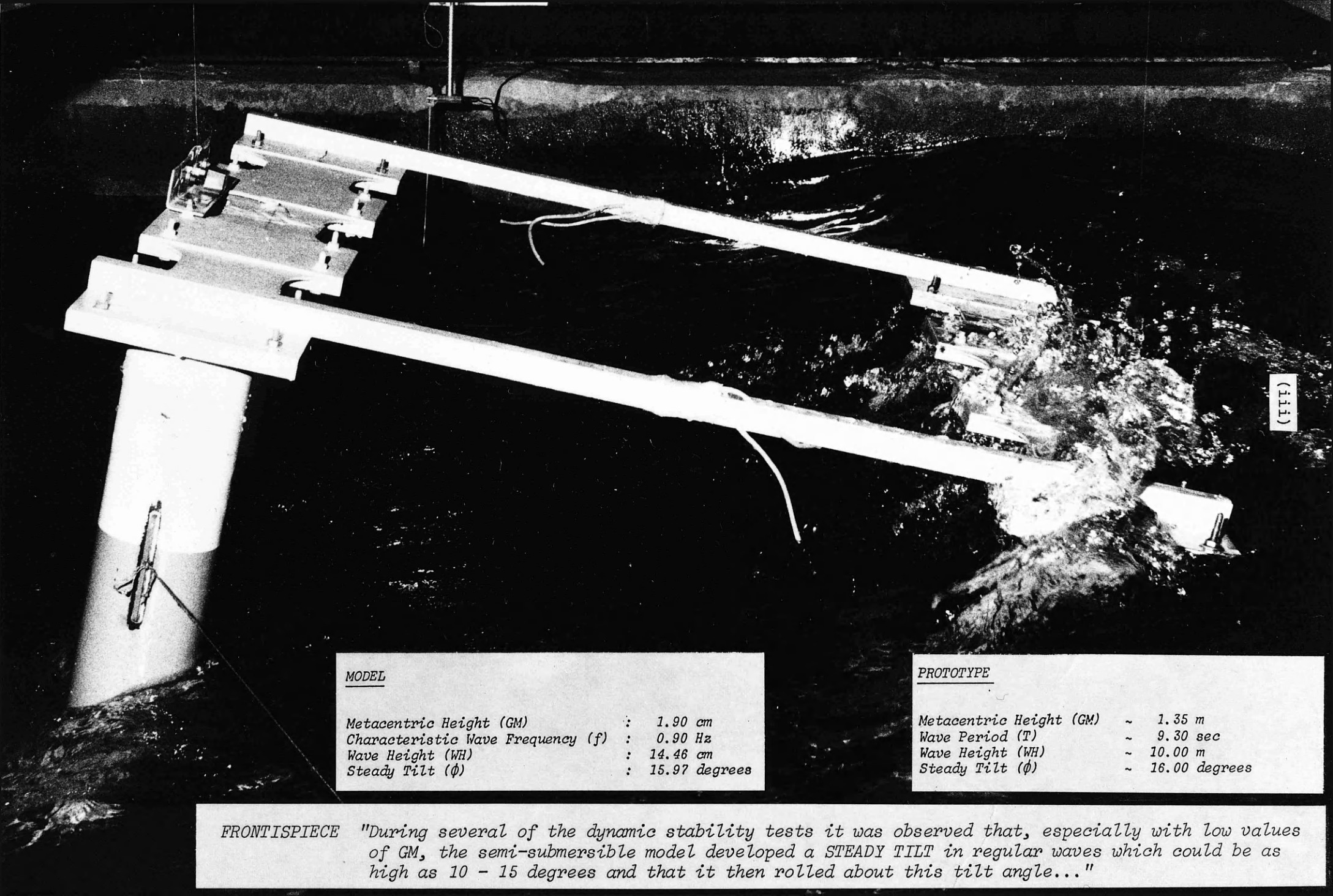

MODEL		
Metacentric Height (GM)	:	1.90 cm
Characteristic Wave Frequency (f)	:	0.90 Hz
Wave Height (WH)	:	14.46 cm
Steady Tilt (ϕ)	:	15.97 degrees

PROTOTYPE		
Metacentric Height (GM)	~	1.35 m
Wave Period (T)	~	9.30 sec
Wave Height (WH)	~	10.00 m
Steady Tilt (ϕ)	~	16.00 degrees

FRONTISPIECE "During several of the dynamic stability tests it was observed that, especially with low values of GM, the semi-submersible model developed a STEADY TILT in regular waves which could be as high as 10 - 15 degrees and that it then rolled about this tilt angle..."

SUMMARY

Dissatisfaction with the existing rules governing the intact stability of semi-submersibles has created one of the major research areas in recent years (post 1970). At that time several stability tests on models had shown that capsizing of a semi-submersible with minimum stability index in maximum environmental conditions had a very low probability due to its inherently good motion characteristics. This finding encouraged operators and designers to put pressure on the regulatory authorities and classification societies to relax the design rules by reducing the metacentric height ($\overline{GM}$). This would provide more deck load and possibly improved motion characteristics.

However, during several of these stability tests it was noted that, especially with low values of $\overline{GM}$, the models developed a "steady tilt" in regular waves which could be as high as 10° - 15° and that it then rolled about this tilt angle. This tilt was worst in short and steep regular waves but could be observed in a confused seaway, although it was then periodic in that it occurred most commonly at certain wave frequencies in the spectrum. This phenomena was called "slowly-varying tilt".

This behaviour was potentially dangerous since it could affect the motions non-linearly leading to large angles of inclinations and the deck edge becoming immersed; two conditions which could lead to dangerous stability problems, increased mooring tensions, structural damage due to slamming and operational difficulties with risers, helicopters, etc.

The majority of the research studies were originally designed to explore various aspects of the dynamic behaviour of semi-submersibles and the tilt effect was merely observed incidental to these tests. Thus the data recorded were of limited scope and in some cases of a conflicting nature. No documental cases of tilt on semi-submersibles in service had been recorded. As a result the various theoretical approaches to the problem lacked good experimental verification and no clear guidance regarding the reasons for tilt had been developed.

This thesis attempts to extend both the experimental and theoretical knowledge of this poorly understood and potentially dangerous phenomenon.

The first chapter of the thesis is of an introductory nature where the existing rules which govern the intact stability of semi-submersibles are reviewed and attention is drawn to the need to explore some dynamic aspects of the stability of the semi-submersibles with emphasis on the tilt behaviour.

The second chapter presents an historical review of past developments in the study of tilt behaviour. The results obtained from each tilt study are discussed with reference to the theory and experimental details which are provided in the appendix of this chapter. The conclusions drawn from this chapter determine that the primary requirement for the understanding of the phenomenon is some accurate experimental work devoted entirely to the tilt problem so that some of the conflicting reports in the early studies could be clarified and form a basis for a sound theoretical approach.

The third chapter of the thesis presents the experimental work carried out with a twin-circular 4-columns per hull semi-submersible model. In order to provide a reliable database for the present and future studies systematic tilt measurements were obtained over a wide range of regular beam seas and varying $\overline{GM}$s. Systematic force tests on the model hulls at various hull spacings and a number of other exploratory tests were carried out in order to clear up several hydrodynamic aspects some of which have been reported in previous studies.

In the fourth chapter, a theoretical analysis is presented with reference to the previous theoretical approaches and the test results carried out in this thesis. It is concentrated on the wave-induced loads in terms of the oscillatory (first-order) and the steady (second-order) components which are believed to be mainly responsible for the tilt behaviour. The main emphasis is placed on a proper determination of the wave-induced tilting mechanism which causes the steady tilt response and the determination of a minimum $\overline{GM}$ needed to limit tilt to some specified angle. The theoretical methods for the prediction of oscillatory forces and resulting motions and the main components of the steady tilting moments are presented. The experimental data produced in the thesis is utilised in order to validate the accuracy of the theoretical methods and several conclusions are drawn from the point of view of the hydrodynamic design and safety of semi-submersibles.

The final chapter reviews the whole study reported in the thesis with emphasis on the overall conclusions and some recommendations for design practice and future tilt studies.

It is concluded that tilt can occur in waves alone and can easily be confused with other steady effects on a moored vessel. For a twin-hull multi-column semi-submersible in regular beam seas it developed always in the leeward direction in a range of wave periods of approximately 12 sec to 7 sec on the full scale and wave height in excess of about 6 m. In the extreme case (about 9 sec of period, 10 m of wave height, 15° of tilt at 1.33 m of $\overline{GM}$) the leeward deck frequently became immersed but no tendency to capsize was observed.

The first impact of the waves, the location and style of the moorings and changes in viscous effects between the model and full scale affects the magnitude of the tilt but none of them was solely responsible for tilt. A possible non-linearity in the righting moment arm is not necessary to experience a steady tilt. The hydrodynamic interference between the hulls is not important for this particular design.

It is found that the prediction of tilt angle and the minimum $\overline{GM}$ needed to limit the steady tilt requires the precise determination of the wave-induced tilting moment. It is demonstrated that the two most important sets of wave forces contributing to this tilting moment are the steady vertical force on the lower hull due to potential effects and horizontal force on the columns due to drag effects.

The method presented in this study calculates this vertical force for any arbitrary cross-section of lower hull and demonstrates that the replacement of a rectangular hull with a circular one based on the same sectional area distribution underestimates this force and thus the tilting moment. The steady horizontal forces act as a starting tilt mechanism and induce steady tilt always in the wave travel direction, confirming the experimental observations.

The comparison of the predicted tilting moment on the basis of the above two force components with the body held in a fixed position gives consistently better agreement with the test data than when the body is allowed to oscillate freely. However, there is still an underestimation in tilting moment prediction indicating more theoretical work in three-dimensions is required, together with an improvement in our knowledge of the motion dynamics.

CONTENTS

DECLARATION

Except where reference is made to the work of others this thesis is believed to be original

* * *

LIST OF FIGURES

Appendix II.1

LIST OF TABLES

Chapter 1

INTRODUCTION

RULES FOR THE INTACT STABILITY OF SEMI-SUBMERSIBLES WITH REFERENCE TO TILT BEHAVIOUR

The chapter reviews the existing rules which govern the intact stability of semi-submersibles and draws attention to the need to explore several aspects of the dynamic stability including the problem of 'steady and slowly-varying tilt behaviour' in certain wave conditions.

There are various types of mobile units operating in offshore fields. Among these semi-submersibles are one of the most popular designs. They have good motion characteristics, a reasonable load-carrying capacity, wide diversity of performance for various types of tasks (e.g. operating as a drilling vessel or heavy-crane vessel or pipelaying vessel or support vessel, etc.). The operator usually wishes to have a high deck load because of the type of operation involving drilling derricks, cranes, accommodation blocks, helideck, etc. on the deck area. This leads to low metacentric heights ($\overline{GM}$). In addition to the gravitational deck loads, the non-aerodynamic forms of the columns above the water, the deck, deckhouses, helideck and lattice structures (e.g. drilling derricks, cranes, etc.) on the deck, lead to high-wind loading on this type of vessel compared to ships, etc. Moreover, semi-submersibles have large submerged underwater elements which are exposed to other dynamic effects such as current force, steady or slowly varying wave induced forces, mooring forces, etc.

All these effects can produce significant static heel and trim if the metacentric height is low.

In 1968, the American Bureau of Shipping (ABS) introduced the first regulations governing the intact and damaged stability of semi-submersibles[1]. They adopted for the intact stability of semi-submersibles the wind heeling moment criterion of the US Coast Guard's general ship stability which was itself taken from the US Naval Ship Criterion[2]. Other classification societies and regulatory authorities, for instance, the Det norske Veritas (DnV)[3], the Lloyd's Register of Shipping[4], tended to follow the same basic stability rules.

As shown in Fig. 1 the criterion for intact stability[1] is that a semi-submersible with an initial zero heel be able to withstand a beam wind of 70 knots for offshore service, 100 knots for the severe storm conditions and not less than 50 knots in normal operating conditions for sheltered locations. The resultant force of this wind on the projected surfaces is determined and is applied as a steady moment. The wind heeling moment with respect to the centre of lateral resistance of the underwater geometry is then compared to the righting moment available for the full range of representative conditions including transit conditions. The dynamic stability is considered sufficient when the area (A+B) under the righting moment is 1.3 times the area (B+C) under the wind heeling moment curve up to the downflooding or to the angle of second intercept of the curves, whichever occurs first.

An alternative stability criteria will be considered for approval for a particular semi-submersible if the wind heeling moment and dynamic properties for the representative model are derived from authoritative wind tunnel and motion tests in waves.

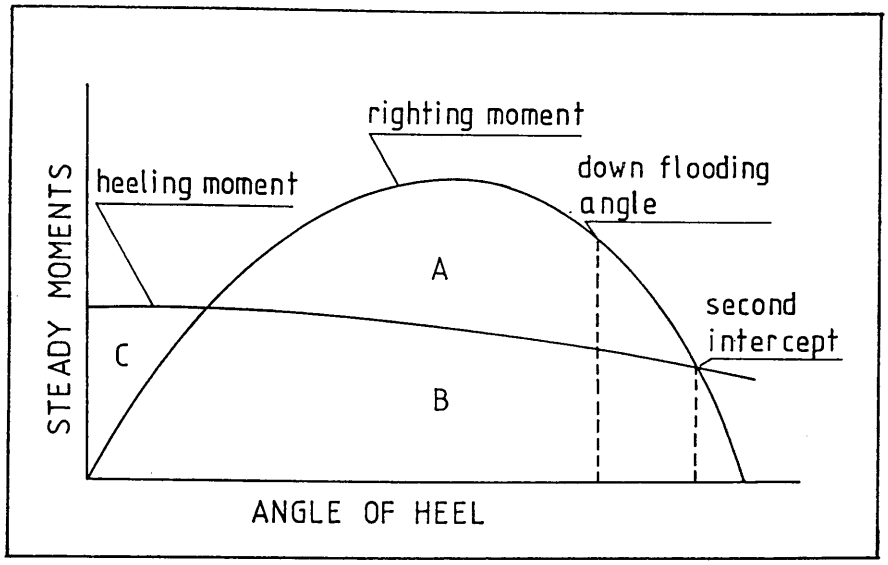

AREA (A+B) $\geq$ 1.3 AREA (B+C)

Fig. 1 - Intact stability criterion for semi-submersible units[1]

Before the introduction of the above rules, although there were many semi-submersible type vessels operating in the offshore fields, their historical background compared to conventional ships was very short. There was a lack of sufficient data on the full-scale exciting forces, moments and resulting responses of the actual semi-submersibles. The documented model tests and observations and rational analyses of the results to solve the stability problem and establish valid reliable relationships were lacking. Therefore, many problems related to semi-submersibles were treated as surface vessels with a lower motion response to the sea than ships and thus the stability criterion established was a modified version of a surface vessel criterion. This excludes the dynamic effects of realistic wind loadings, currents, wave induced forces, moorings and others. However, its static character has the advantage of being easy to be understood and applied in practice by naval architects.

The existing rules have been criticised on several occasions on the grounds of being too conservative especially with regard to this 1.3

figure and being inadequate because of the following reasons:

(i) It is obvious that the criterion based on the similar physical considerations for ships is not rational since there are differences in geometrical configurations and related differences in dynamic response. Therefore, one may expect that some of these differences, which are given in the following, may affect the intact stability of vessels[5].

For instance, the dimensions of the length, beam and depth of the semi-submersible are closely similar while the length of the ship is long compared to its beam and depth.

Semi-submersibles have higher righting arms ($\overline{GZ}$) over a relatively shorter range of stability (heel angles) compared to ships.

The natural frequency of roll of semi-submersibles is less than half the natural frequency of roll of ships. Therefore, in a realistic seastate the frequency of resonant roll behaviour of a semi-submersible is well below the frequency of peak energy in the wave spectrum, whereas the natural frequency of roll for a ship may fall within the range of encounter wave frequency. In ships this is highly affected by the speed and heading of the ship relative to the waves since the frequency of wave encounter depends on these factors. As semi-submersibles are usually stationary and have lower natural frequency of roll, the possibility of resonant roll behaviour is very low. On the other hand, the unsteadiness in the wind field may cover a range of frequencies which are very close to the natural frequency of roll of a semi-submersible. This may produce a resonant roll behaviour. However, this effect is very low for a ship since the natural frequency of roll is higher than this range of energy contained in the wind spectrum.

Semi-submersibles are usually vertical-sided vessels with small water plane areas. Therefore, the variation of $\overline{GZ}$ under certain combinations of waves relative to the position of the vessel (e.g. having a crest or trough of the wave at midships with various headings) is not important. However, for ships the variation of $\overline{GZ}$ due to waves is more dramatic because of its geometry. When this effect is combined with certain combinations of ship speed and heading (this is stated as the frequency of encounter being about twice the natural frequency of roll in following or quartering seas in ref. [6]), it may lead to unstable rolling and even capsizing.

(ii) The existing rules can be regarded as a 'static assessment' of the stability rather than its 'dynamic assessment'. This is because the dynamic effects of a semi-submersible and its environment are covered by the factor of 1.3 by which the static righting energy exceeds the steady wind energy in a static stability condition. In a way these effects which can contribute to the heeling energy are disregarded. Even the dynamic character of the wind energy is omitted by considering the wind force as a steady force. The dynamic effects can be listed as follows[7,8]:

- Wind Force (wind gusts, errors in accurate determination of wind heeling moment, etc.)
- Current Force
- Wave-induced Force (first-order force, second-order force, impact force)
- Mooring Force
- Others.

- In the present criterion, it is assumed that the magnitude of the wind force reaches its maximum value after an instantaneous increase

and remains constant with time although it may vary with heel or trim angle. The effect of gusts is not taken into account. This effect becomes very important on the lattice structures such as legs, cranes and drilling towers where the sensitivity to gusts increases. If average wind speeds are considered, it is suggested that the gust effect can be taken into account by means of a gust factor, which is the ratio of the average gust velocity to the average wind speed, determined from a dynamic force study or extrapolated data from land-based situations[9]. The random character of the gust effects can be considered in the time varying part of the wind velocity expressed as a special density function, for instance, the Davenport Spectrum[10]. As shown in ref. [5] for mean wind speeds of 50 and 100 knots, by using the Davenport Spectrum the maximum gusts occur at 30 and 60 secs which is the range of period covering the range of typical semi-submersible natural period of roll.

The accurate calculation or measurement of the wind heeling moment is one of the important factors in the determination of the intact stability and each authority has recommended procedures for its calculation. It is interesting that, although they all use the 1.3 factor criterion, they recommended different procedures for calculating the wind heeling moment. In ref. [11], it is shown that due to the differences in the assumed wind profile above the sea, differences in the design wind speed, differences in the recommended procedures for calculating the forces, differences in the drag coefficients to be used for different types of structures, the inclusion of lift effects in some cases and not in others, the wind heeling moments calculated according to different authorities could vary by 20 to 30%. None of these authorities give guidance on how to calculate the centre of lateral resistance of the underwater structure which is very dependent on the drag coefficients used, interference effects between adjacent circular

cylinders, etc. Different procedures here can give changes in height of the centre of resistance of the order of 1 m in a normal drilling semi-submersible and so the total uncertainty in a calculated wind heeling moment could be as high as 30%.

Many naval architects resorted to wind tunnel tests to give improved values of the wind heeling moment. Such models are necessarily on a relatively small scale, usually less than 1:50, in order to avoid blockage effects in the wind tunnel. This results in the Reynold's number (R_e) on the model being substantially lower than on the full scale, and on the cylindrical parts of the structure there will be substantial scale effects due to both changes in drag coefficients and changes in interference effects. Attempts are made to overcome this by using trip-wires or other turbulance stimulating devices, but their efficiency in simulating full scale flows will depend on the model R_e being close to 10^5 which, in the majority of cases, cannot be achieved. Most wind tunnels attempt to model the boundary layer above the sea but none can produce the wave conditions which must exist with high wind speed and thus the flow conditions in the air gap under the semi-submersible will not simulate the full scale conditions. The measured wind forces and moments have to be translated into full scale values and into a wind heeling moment which requires knowledge of the centre of lateral resistance. Tank tests on models cannot determine this since the scale effect problems are even greater than in the wind tunnels. Thus, although wind tunnel tests are to be preferred to calculation, they cannot give a precise answer and there can still be errors of the order of 15 - 20%.

- Another dynamic effect contributing to the overturning moment is the steady current force. Since semi-submersibles have large underwater elements the overturning moment due to current force on those

elements may have important effects on the stability and the mooring lines if they exist depending on the current velocity and fairlead position[8].

- The motion response of semi-submersibles due to the first- and second-order wave-induced forces combined with the other effects such as wind, moorings, currents, etc. could be another important mechanism for overturning. There is a very low possibility of the wave spectrum itself creating a large linear response due to the first-order forces unless another non-linear mechanism be involved such as non-linear restoring force or wind force. For instance, in the present criterion it is assumed that the initial value of roll is zero and the magnitude of the wind heeling moment increases instantaneously from zero to its final constant value and remains constant with time. In ref. [5] it is shown that if the effect of the dynamic roll induced by the wave is included, the roll response of semi-submersibles to the wind heeling moment may be increased.

The second-order wave-induced forces in the horizontal direction are generally considered to be small in magnitude in the excitation of semi-submersibles. But when the waves have large amplitudes and short periods, large steady drift forces are induced. For a semi-submersible moored in irregular waves, the slowly-varying wave drift forces cover the range of frequencies coinciding with the natural frequency of the horizontal motions of the vessel because of its low damping in the horizontal mode. This can lead to large amplitude resonant behaviour of the motions[12,13,14], extra tension forces in the mooring lines and an overturning moment depending on the mooring arrangements and fair-leads[8].

On the otherhand in some model tests of semi-submersibles, especially with low values of $\overline{GM}$, it was found that a 'steady tilt' developed in short and steep regular waves which could be as high as $10° - 15°$ and then the vessel rolled about this angle[15,16,17,18,8,19]. Although the steady tilt has not been reliably reported on the full scale, it seems to be a potentially dangerous mechanism to cause an overturning moment and needs to be considered in the stability assessment[15] and vessel design[18]. This phenomenon is related to the second-order wave forces in the vertical direction[15,20,21].

It is shown in refs [7,15,16] that if a semi-submersible with a minimum stability condition is exposed to maximum environmental conditions the motion response of the semi-submersible to the wave is still linear or near linear. However, the wave impact forces under the deck near to the leeward columns have important effects on the motion characteristics as well as providing severe slamming effects and the possibility of downflooding. This brings about an important parameter, the so-called 'underdeck clearance' which might be considered in the assessment of stability and design[18].

- One of the other possible effects to cause an overturning moment is the accumulation of green water on the deck from the water running through the openings at the lower deck (e.g. scuppers, exhaust, ventilators, rubbish shutes, etc.) in high and steep waves. This effect is vital for the damaged stability of the vessel[22]. Other possible effects for semi-submersibles operating in severe environmental conditions are: (1) in Arctic zones where heavy snow and ice accumulation cause a marked increase in the deck weight and in the exposed area which increases the wind force, and (2) storm surge caused by the wind shear and atmospheric pressure effects.

For a rational stability assessment, analytical methods based on ship characteristics are still lacking. There is a need for data collected from the full scale excitations and responses of actual semi-submersibles and documented tests and observations on models to support the analytical methods. Then the above mentioned dynamic effects can be analysed and valid and confident relationships can be established. However, data collection from the full scale seems difficult at this stage considering the limited number of semi-submersibles and their short historical background. It demands more effort and a long period of time. Therefore, initial efforts must be concentrated on the experimental studies backed up by theoretical analysis and supported by the documented tests and observations.

In the last decade in order to shed some light on the above matter the dynamics of different designs of semi-submersibles were studied experimentally in waves in a number of countries, e.g. refs [7, 15,16,17,18,8]. During these studies, attempts were made to find if the conditions leading to capsize conditions could be identified. These tests included wind and wave effects, the effects of moorings, including breaking of the seaward mooring and damage to one column to simulate a flooded condition. In all cases the vessels showed no tendency to capsize if the $\overline{GM}$s were those required to satisfy the regulations. Even if severely heeled by wind or damage effects, they tended to roll about the heeled angle, but due to their inherently low amplitude of motion this did not lead to a tendency to capsize. Obviously if such a vessel is heeled to a considerable angle its deck clearance becomes reduced and waves will slam against the structure which could lead to structural damage and potentially dangerous conditions, but as long as the deck structure remains intact capsize was an unlikely condition.

However, during several of these experiments it was noted, especially with low values of $\overline{GM}$, the models would develop a 'steady tilt' in regular waves which could be as high as 10° - 15° and that it then rolled about this tilt angle. The tilt was generally observed to occur in the direction of wave travel. This tilt was worst in short and steep regular waves but could be observed in a confused seaway, although it was then periodic in that it responded most to the presence of certain wave frequencies which was called 'slowly-varying tilt' or 'long period (low frequency) rolling'.

The remainder of this thesis is concerned with the experimental and analytical study of the tilt problem. In Chapter 2 a review of the existing state of knowledge at the beginning of this study is given. The experimental work carried out with a twin-circular hull semi-submersible model is presented in Chapter 3.

Chapter 4 contains a theoretical analysis of the tilt problem with reference to the results of the model tests in Chapter 3 and the previous theoretical approaches described in Chapter 2. The effect of a large number of factors which can effect the hydrodynamic behaviour is investigated in detail.

The final chapter (Chapter 5) reviews the whole study reported in the thesis with emphasis on the overall conclusions and some recommendations for design practice and future tilt studies.

Chapter 2

PAST DEVELOPMENTS IN THE STUDY OF TILT BEHAVIOUR OF SEMI-SUBMERSIBLES

2.1 INTRODUCTION

In this chapter a review is given of experimental and theoretical studies to explore the tilt behaviour of semi-submersibles which may be used to improve the existing methods for prediction of the steady tilt behaviour in regular waves.

In an endeavour to improve the present rules governing the intact stability of semi-submersibles several experimental and theoretical studies have been made since the late 1960's. During the experimental work the tilt behaviour was observed in some capsizing tests. After the existence of this behaviour was established there were a limited number of attempts to explore the phenomenon. Although the phenomenon seemed to be potentially very dangerous, there has been a little evidence from the full scale[23]. This might be due to the semi-submersibles in service having to satisfy the existing rules with higher $\overline{GM}$s than those which caused some problems in the model tests. Therefore there has not been much practical interest to the phenomenon. As will be discussed in the following, it is a complex problem which involves several other factors to be investigated by systematic tests and analysed by theoretical methods. However, the theoretical methods to be used are inexact and still under development since they are adopted from ship characteristics or provided from existing solutions with several assumptions and approximations. Many features of the tilt problem need systematic experimental effort in order to study

their individual contribution to the problem. However, as will be shown later in the thesis in discussing the tests carried out by the author, stability tests in waves, especially for small $\overline{GM}$ values are very difficult to perform experimentally and involved the possibility of experimental errors. Therefore, in the existing experimental studies a limited number of qualitative experimental results could be presented.

So far the studies in the past concerning the tilt behaviour can be listed as follows in the chronological order:

1. Numata and McClure[15] - Experimental
   Numata et al.[16] - Experimental and Theoretical
2. Miller[17] - Experimental
   De Souza[24] - Experimental and Theoretical
   De Souza et al[25,26,27] - Experimental and Theoretical
3. Kuo et al.[28] - Theoretical
   Martin and Kuo[20] - Mainly Theoretical
   Martin and Kuo[21] - Theoretical and Experimental
4. Morrall[29] - Experimental and Theoretical
5. Hineno et al.[18] - Experimental and Theoretical
6. Takarada et al.[8] - Experimental.

In the above studies the phenomenon was attributed to the 'second-order wave force in the vertical direction'[15,16] and an established simple method based on second-order wave theory demonstrated the correct order of magnitude with qualitative test results in regular waves[16]. Non-linear wave drag force itself produced a very small magnitude of steady tilt values[24]. However, the second-order theory alone could not explain several features of the tilt

phenomenon in particular the preferred direction of tilt[17,28]. Apart from second-order effects there were some additional physical factors which could cause a preferred direction of tilt[20]. Since the second-order wave theory would fail for high values and a shallow depth of submergence, tilt angles of large magnitude could not be predicted by this theory[20,21,28,29]. On the otherhand few attempts at the prediction of the slowly varying tilt behaviour in irregular waves indicated that the frequency domain solution, using the special low frequency tilt moment spectrum showed reasonable agreement with the tests[18]. However, there has been no complete solution of the slowly varying tilt behaviour in the time domain so far[8].

In the following these studies are reviewed in more detail and in particular experimental work which is very important to the understanding of this phenomenon. The results and discussions provided from these studies are presented in the text while the necessary formulations and the experimental data corresponding are provided in the appendix. One important point is that, in some of these studies, the range of the waves and the results from the tests are presented for the full scale. Although they are provided in the thesis as in their original presentation, the effect of scale on the results has to be borne in mind.

2.2 HISTORICAL REVIEW

2.2.1 In America in the early 1970's "the assessment of the intact stability of semi-submersibles" was identified as the most important and pressing problem to be explored by an authoritative research panel. This panel, called MS-3 of the Marine Systems Committee of the Society of Naval Architects and Marine Engineers, had representations from the

Offshore Petroleum Industry, the ABS, the US Coast Guard (USCG) and Navy[16]. In order to shed some light on this problem, during the years of 1973-74, research on the dynamics of different designs of semi-submersibles under various wind, wave loadings, stability conditions and mooring arrangements was carried out for this panel by Numata et al. at the Davidson Laboratory[7,15].

The main objective of this research was to test the adequacy of the present stability criterion and to determine more rational criteria with safe stability parameters by using model tests, state-of-the-art prediction methods for analysing the test results and the data collected on the full scale motion and environmental conditions to cross-check the findings. Finally, the criterion to be proposed should be acceptable by the ABS and USCG as valid for reassessing the present stability standards.

Two different types of designs were chosen to represent the majority of drilling semi-submersibles for the model tests in the research programme. They were a 4-column, footing type (vessel A) and a 6-column, twin rectangular pontoon type (vessel B) designs. The geometry and dimensions of these models, which were approximately to 1/96 scale are provided with the basic loading conditions in Figs I.1, I.2 and Tables I.1, I.2 in Appendix I.

The initial objective of these tests was to identify if there was any critical combinations of various dynamic effects (i.e. wind-induced heel, wave heading, deck loads, GM, mooring arrangements, etc.) which could cause capsizing of models. Therefore, both models with minimum stability index (max deck load, min GM) and maximum environmental conditions (max wind force, max wave height) required by the standard ABS Rules were tested in regular and irregular waves. Neither

model showed capsizing or near capsizing. Additional tests were run with a much lower stability index and a greater wind force than the standard ABS requirements including breaking of the seaward moorings. In all cases both models showed no tendency to capsize. If the $\overline{GM}$s were low, they heeled to leeward and the leeward deck was struck by the waves. A considerable amount of wave slamming (impact) against the leeward deck was observed.

From these tests it was concluded that the present criterion with its emphasis on overturning was inappropriate. Even in the extreme wind and sea conditions the possibility of capsizing was very low. The major need for adequate stability was to reduce the wave impact on the lower deck which could lead to structural damage and potentially serious conditions. Therefore, "the under-deck clearance" between the lower deck and the wave crest at the leeward column was considered as an essential parameter for stability and the second group of tests were concentrated on the relative motion of the model (i.e. the rise and fall of the water surface along the axis of the leeward column). In order to predict the statistics of responses in irregular waves, it was necessary to know the response operators (ratio of the motion amplitude to the wave amplitude) in regular waves. Then by assuming that the responses vary linearly with wave amplitude for a given frequency, the response spectrum in a required sea state could be obtained by combining the energy spectrum for that required sea with the response operators. Therefore, the relative motion values were measured in a wide range of wave periods varying from 6 to 24 secs and at a nominal wave height of 4.88 m corresponding to full scale values in regular waves for various wind heel angles. During these tests to check the linearity between the wave heights and the relative motions some runs were repeated at a period of 11 secs for 2.44, 4.88

and 6.70 m heights at 0°and 10.5° initial wind heel to leeward. The measured relative motion ratios (response operators) corresponding to those heights agreed to within 10% at zero wind heel. However, at 10.5° heel, the response ratios at 2.44 and 4.88 m agreed reasonably well but for 6.70 m height showed a 30% increase in the responses and also there was an increased "steady tilt" in the mean initial heel angle from 10.5° to 12° as shown in Fig. 2.

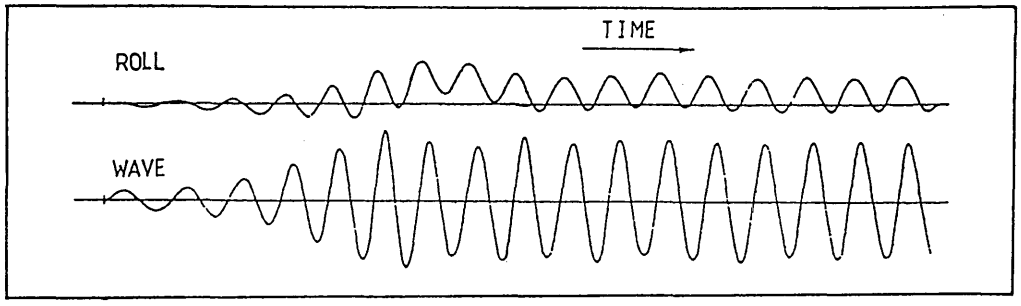

Fig. 2 - Chart record for roll response of vessel B in regular beam sea[16] (21.34 m of draught, 3.2 m of $\overline{GM}$, 10.5° of initial wind heel, 11 sec of period and 6.70 m of wave height)

The models were also tested in irregular waves having significant heights of 6.1 and 8.53 m at the same wind heel angles. As shown in Fig. 3 at 10.5° initial wind heel angle and a significant height of 6.1 m in beam sea, the model responded normally to a series of five short waves of moderate height. Then when a high and steep wave with a height of 7.92 m and apparent period of 11 secs (full scale) passed the model a "slowly-varying tilt" or "long-period rolling" behaviour was recorded to leeward at about the natural roll period (55 secs in full scale).

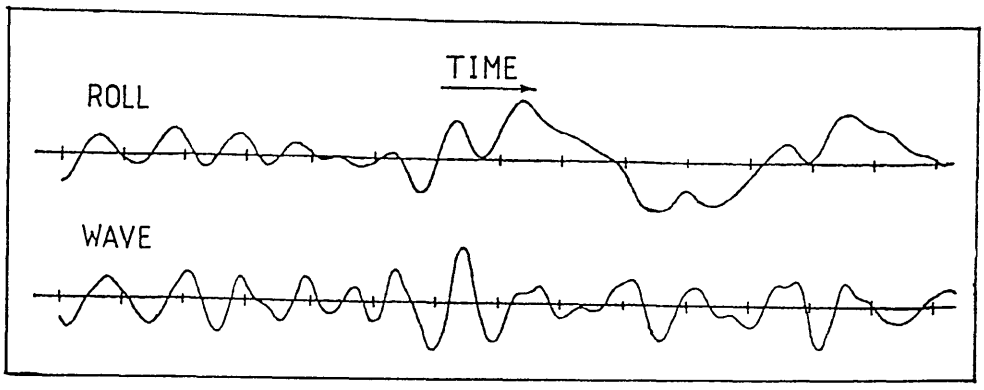

Fig. 3 - Chart record for roll response of vessel B in irregular beam sea[15] (10.5° of initial wind heel and 6.1 m of significant wave height)

It was obvious that such a long period (low frequency) response spectrum whose frequency was beyond the band of frequencies contained by the first-order wave energy spectrum could not be predicted by conventional spectral techniques. From this second group of tests it was concluded that a conventional response prediction method which uses response operators obtained by either model tests or analytical methods should be modified to include the effect of the "steady tilt".

The phenomenon in regular waves was attributed by Dalzell[16] to the second-order force in the vertical direction, the so-called "suction force" which had been investigated in the vertical motions of submarines[30]. This is due to the velocities of the water particles moving over the top of the hull being greater than those moving underneath due to the water surface proximity thereby producing a reduced pressure (set-down) on the top of the hull and thus a net steady lift force. The magnitude of this force was proportional to the square of the wave height for a given frequency and decreased exponentially as the depth of submergence increased.

In the case of a semi-submersible once an initial disturbance (e.g. initial heel due to wind) from the level condition took place, the pontoon or footing which was closer to the surface would experience a larger steady vertical force than the other pontoon or footings resulting in a "steady tilting moment". An equilibrium position could be established at a steady tilt angle when the tilting moment was balanced by the righting moment as shown in Fig. 4.

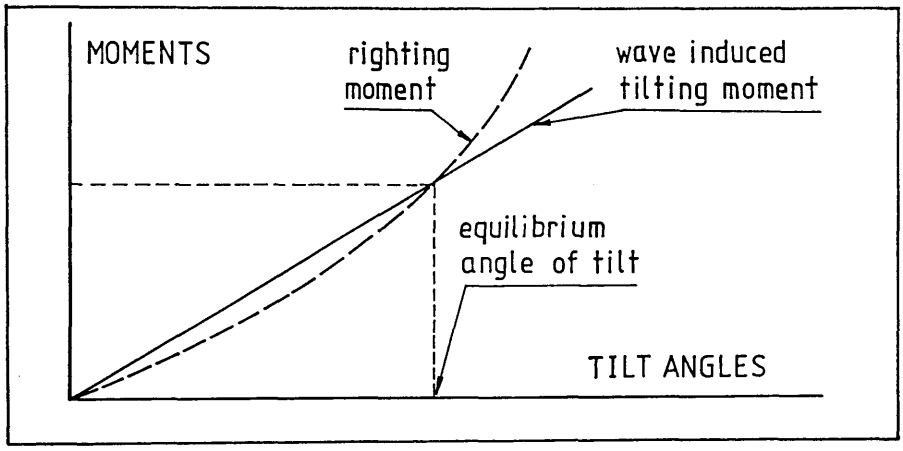

Fig. 4 - Simplified explanation of the wave-induced tilt[16]

The formulation of the above simple theory is provided in Appendix I from eq. I.1 through eq. I.7[16]. In the formulation Numata et al. used the 2-D approximate solution given by Ogilvie[31] for a horizontally submerged single circular cylinder under regular beam waves in order to calculate the second-order vertical force and moments acting on the pontoons or footings. This implied several assumptions and approximations as follows:

(i) The total steady vertical force on the semi-submersible was assumed to be dominated by the forces acting on the pontoons or footings. The forces on the vertical columns and bracings were ignored.

(ii) As shown in eq. I.1 of Appendix I, the steady force expression was a function of the modified Bessel Function of the first kind $I_1(2\gamma R)$ which was relatively insensitive to changes in the radius R. Therefore, the pontoons with non-circular cross-sections and footings could be replaced by a horizontal circular cylinder using equivalent areas and volumes as given in eq. I.2 through eq. I.4 of Appendix I, and so use the existing solution for circular cylinders.

(iii) Since the force solution was valid for a single submerged cylinder the steady force on each pontoon or footing was calculated as if they were isolated. The hydrodynamic interference between the pontoons was ignored.

(iv) Because of the approximate character of the solution it was assumed that the radius of the pontoon or footing was small compared to the wavelength (long-wave approximation) or depth of submergence was large (neglect of the free-surface effect).

(v) The existing solutions given by Ogilvie were either for restrained or freely floating cylinders. In the Numata study the restrained cylinder assumption was made. This was because the resultant vertical motions of the pontoon and footing, which were calculated by combining the measured heave and roll motion in short and steep waves, showed that they were approximately half of the orbital motion of the water particles measured at the same depths of submergence of pontoon or footing with phase angle of between 50° and 20°. If it was assumed that the models were freely floating the two motions would be equal with zero phase lag. This would produce a relatively small force compared to the restrained case and thus less conservative results.

In order to explore the phenomenon a third group of tests were prepared with both models in regular beam waves. From the previous tests it had been observed that the tilt behaviour occurred in short, steep waves having a period in the vicinity of 10 secs and a height in excess of 6.1 m full scale and its magnitude increased as either wave height increased or GM was decreased with a range of periods varying from 9 to 12 secs and heights from 6.1 to 12.2 m full scale. After the tests the calculated steady tilt moments at a range of tilt angles and the righting moments of the vessels corresponding to that range produced (see eqs I.5 and I.6 in Appendix I) the correct order of magnitude at the observed steady tilt angles for moderate waves (10 secs × 9.75 m) full scale as shown in Fig. 5. The prediction was not good for the limits of the range of period (i.e. 9 secs × 9.1 m and 12 secs × 12.2 m full scale) by about 40% difference in the predicted and measured values.

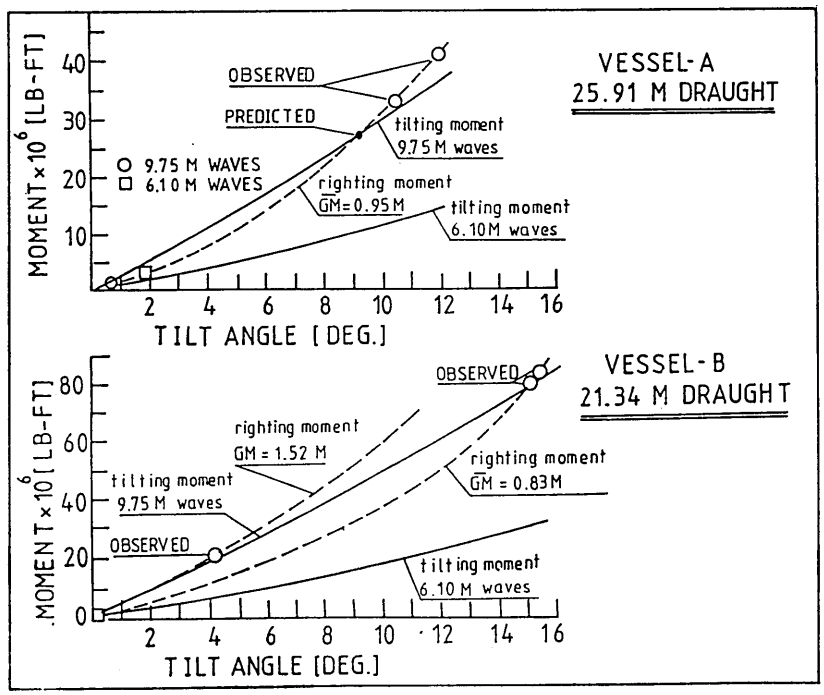

Fig. 5 - Predicted and observed steady tilt angles in 10 sec of period regular beam waves[16]

The tests performed under the wind and wave loading showed that the steady tilt angle under the combined condition was greater than the addition of the heel angle due to wind and wave acting alone as shown in Fig. 6.

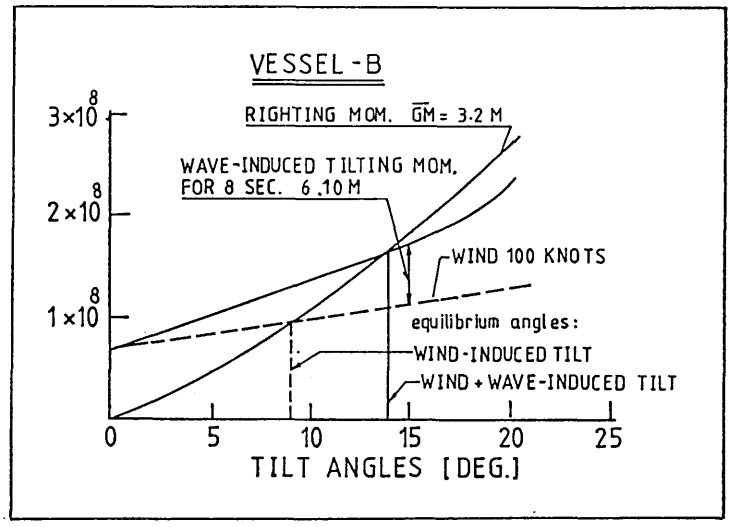

Fig. 6 - Wave plus wind heeling moment, Vessel B[16]

Since the prediction method worked reasonably well for the essential parameters such as frequency, wave height and $\overline{GM}$, a formula was established to give a "minimum $\overline{GM}$" value necessary to avoid a steady tilt in a given regular wave for a semi-submersible as given by eq. I.7 in Appendix I. Then the minimum $\overline{GM}$s for both vessels were calculated for a range of wave periods and heights where steady tilt occurred and shown in Fig. 7. This peak value of the $\overline{GM}$ was 1.52 m for vessel B and 1.16 m for vessel B full scale.

However, the final tests carried out with both models having their calculated minimum $\overline{GM}$ values (i.e. 1.52 and 1.16 m full scale) in irregular seas still produced a slowly-varying tilt for the particular range of periods where the "steady tilt" developed in regular waves. It was then concluded that for the better prediction of roll

responses in irregular seas with very low $\overline{GM}$s either the proposed procedure should be modified or a time-domain solution of roll response including slowly-varying tilt be presented.

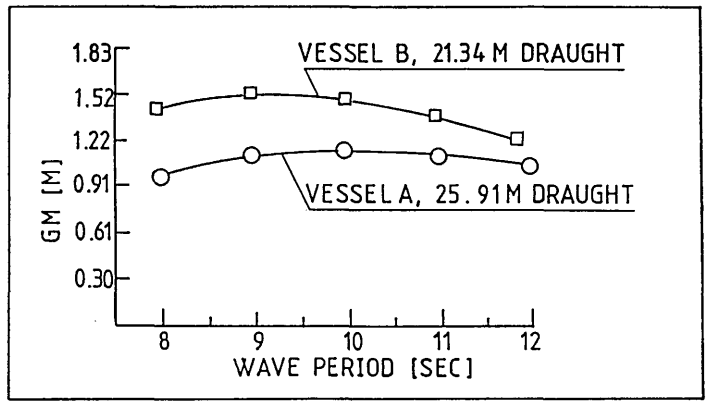

Fig. 7 - Calculated minimum $\overline{GM}$ to avoid wave-induced tilt[16]

A supplementary result to the above study[15,16] was given in ref. [32] on the "bi-stable" tilt behaviour which was the occurrence of tilt in either direction leeward or seaward. Although the simple theory produced bi-stable (or symmetric) tilt depending on the direction of the initial tilt, there was no result presented in refs [15,16] on the seaward tilt behaviour. However, in ref. [30] Numata indicated that in regular beam waves for a range of periods varying from 9 to 12 secs and heights in excess of 6.1 m full scale if the twin-pontoon model at $\overline{GM}$ values of 0.4 and 0.823 m full scale was inclined in a seaward direction by hand, a steady tilt to seaward could be sustained. However, when the GM increased to 1.524 m the tilt always developed in the leeward direction. The footing type model with similar $\overline{GM}$ conditions always had a steady tilt in the leeward direction even when a seaward tilt was imposed by hand.

2.2.2 In the UK a research programme similar to that carried out in the US, into the investigation of stability criterion of semi-submersibles was carried out for the Department of Energy by De Souza and Miller[17,11,25,26,27] at Glasgow University's Hydrodynamics Laboratory.

The main objective of the investigation was for a particular design of semi-submersible to determine whether there was any susceptibility to capsize or to conditions leading to capsize at any particular range of wave frequencies in regular waves and to provide experimental data which could be used to check theoretical calculations of the dynamic behaviour of this design type.

Tests were carried out with 3- and 4-column footing type designs. The reasons for choosing these two designs were the availability of the models at the beginning of the research period and the wish to compare the results for one of these models with those obtained for a similar design reported by Numata et al.[16]. In Appendix I, Figs I.4 and I.5 show the geometry and dimensions of the models tested with three different values of $\overline{GM}$s as given in Tables I.3 and I.4. They were approximately 1/100 scale.

During the tests with the lowest $\overline{GM}$ it was observed that the 3-column design at a period of 1 sec and 4-column design at 0.91 sec had a steady tilt of about 12° to leeward. This steady tilt only occurred over a narrow range of periods for any value of $\overline{GM}$s tested having peaks at those two frequencies. The angle of tilt increased when the $\overline{GM}$ reduced[17,27]. Some tests were performed with free models in order to eliminate the mooring effects which it has been suggested might have caused the tilt. The same behaviour was observed at about the same frequencies. The 4-column design with two higher $\overline{GM}$s were

tested with steady wind loading producing initial angles of heel of 4.3° for 7.5 cms $\overline{GM}$ and 7.2° for 4.7 cms $\overline{GM}$. At a period of about 0.9 sec, where the worst tilt was observed in the previous tests, the model with the lower initial heel had about 6° of steady tilt whereas with the higher initial heel the steady tilt measured was at about 10° as given in Table I.5 in Appendix I.

These tests demonstrated that the phenomenon appeared to be sharply tuned with respect to wave frequency. Since tilt occurred at a fixed frequency for a given model, it could be said to be a dynamic property of the model. A dangerous combination for capsizing could be created by a high wave flooding the deck or a strong wind load when the model was in this tilted position. For the possible explanations of the tilt attention was drawn to the following:

(i) The model scale effect due to, for example, the difference in the drag coefficients, added virtual mass coefficients, etc.

(ii) A possible combination of phase angles between the moments acting on the semi-submersible could produce a resulting moment which was always in one direction at a particular frequency.

(iii) Cross-coupling effects and the hydrodynamic interaction between the columns.

(iv) Errors in the restoring moment terms in linear theory and the neglect of dynamic pressure effects on $\overline{GM}$.

(v) Possible experimental errors such as in determining $\overline{GM}$, in wave height measurements, entrained water, etc.

The final tests indicated that an increase in the wind heeling angle from 4.3° to 7.2° did not yield great changes in the measured steady tilt angle. However, according to the Numata theory it was anticipated that higher initial heel would develop larger wave-induced tilt angles.

The theoretical approach taken by De Souza[24] for the calculation of the 'steady tilt' was different to that adopted by Numata et al. No potential second-order force was taken into account. It was hoped that the non-linearities in the wave drag force could explain the phenomenon. Therefore, the wave exciting forces were calculated by using Morrison's equation with constant coefficients. This implied the assumption of the diameters of footing and column being small compared to the wave length. The pressure, acceleration and velocity changes across these underwater members were ignored and interference effects between these elements were not taken into account. The calculations of the wave exciting forces demonstrated that due to the exponential term introduced by the integration of the pressure along the depth of submerged elements, the components of the force (see eqs I.8 through I.13 in Appendix I) particularly velocity components, which varied as the square of the wave amplitude, demonstrated a non-linear character. This non-linearity was very strong in the sway mode at a frequency about 7 rad/sec (or a period of 0.9 sec) as shown in Fig. 8. The breakdown of the roll exciting moment about the CG into its component is shown in Fig. 9. The contribution due to the heave exciting force was more linear and its value large compared to the non-linear contribution due to the sway exciting force which took its maximum at a frequency where the contribution due to the vertical force was nearly zero as the result of the model dimension and wave length. The integration of the resulting moment over a full cycle produced a non-zero average value in the leeward direction. However, the calculated steady tilt values by this method could produce only approximately 40% of values measured during the tests.

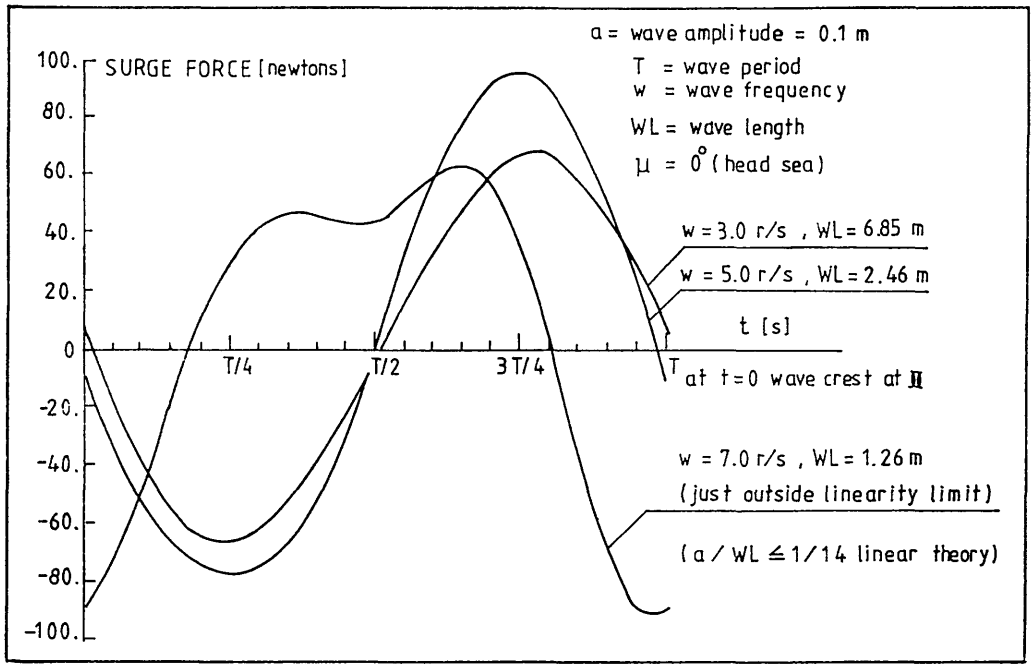

Fig. 8 - Surge exciting force calculated on 3-legged model [24]

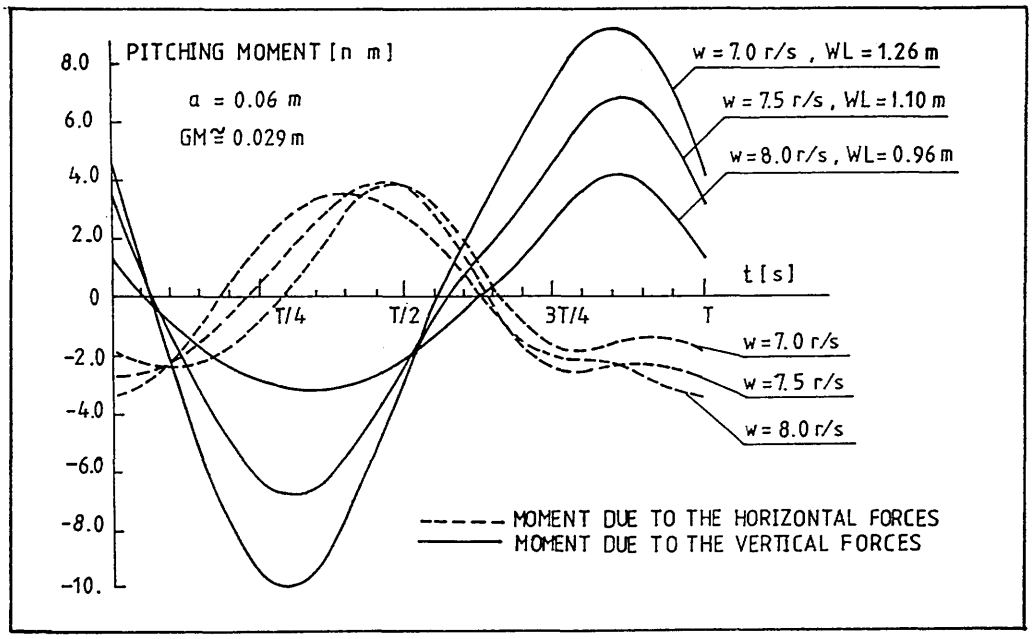

Fig. 9 - Breakdown of the roll exciting moment into its component about the COG for 3-legged model [24]

The first exploratory tests and the theory given by Numata et al. and the later tests and theoretical work by De Souza and Miller gave rise to the following problems:

(i) The tests performed by Numata et al. demonstrated that, in regular beam waves, exceeding a certain wave height (approx. 6.1 m in full scale) there was a range of period (varying from 8 secs to 12 secs in full scale) where steady tilt behaviour occurred. However, De Souza and Miller reported that beyond a certain wave height, which was higher than given by Numata, the steady tilt behaviour occurred at near one particular period for a given model.

(ii) Numata et al. reported that steady tilt had a 'bi-stable' character which could occur in either direction depending on the initial heel consistent with their theory. However, De Souza and Miller observed that steady tilt was always in the leeward direction confirming their theory.

(iii) The tests carried out by Miller with free and moored models in order to eliminate the mooring effects showed substantially the same behaviour at about the same period.

(iv) The tests performed under the wind and wave loading by Numata et al. showed that the tilt angle under the combined action was greater than the addition of the heel angle due to wind and waves alone as expected by the theory (i.e. the higher initial heel angle would develop a larger steady tilt angle induced by waves). However, the tests by De Souza and Miller showed that an increase in the wind heeling angle did not yield great changes in the measured steady tilt angles due to waves. However, this conclusion could be affected by the

different procedures in these tests. De Souza and Miller used an air jet blown onto a vane assembly on the deck of the model to simulate the wind loading whereas Numata et al. used a mechanism with hanging weights from pulleys which could create unrealistic inertia effects due to the weights.

(v) Numata et al. indicated that responsibility for the steady tilt was the potential second-order force in the vertical direction. In order to use the existing solution they made several assumptions and approximations which have been given earlier. The contribution of the viscous drag force to steady tilt was not taken into account. However, De Souza and Miller demonstrated the drag force in the sway mode itself could create steady tilt always in the leeward direction and its value could be 40% of the observed values.

2.2.3 Later in 1977 the above features of the steady tilt phenomenon were discussed by Martin and Kuo[20,21,28] in a mainly theoretical study supported by a few qualitative tests. A prediction method of the steady tilt for an idealised semi-submersible was given in regular beam waves by using the second-order wave theory with some additional factors explained in the following.

The main objective of this study was to improve Numata's method, which was lacking in several points although it produced the correct order of magnitude, by making less assumptions and simplifications.

In order to explore several factors experimentally, a set of tests were performed for simplified semi-submersible models with twin circular and rectangular pontoons in regular beam waves. The tests were qualitatively concerned with the observation of the steady tilt

behaviour rather than systematic measurements of tilt angles for various parameters. During the tests both models developed steady tilt when exceeding a certain value of wave steepness and this was observed over a wide range of wave periods and steepness. If the models were moored the magnitude of the tilt changed with the mooring arrangements. In the majority of runs the steady tilt was observed in the leeward direction except for the following cases where seaward tilt was observed:

- If the models were moored, sometimes depending on the mooring arrangement.
- The model with circular pontoon in the longest wave tested.

When the models were inclined in a seaward direction by hand after 2 to 5 passing waves a tilt to leeward was sustained. It was indicated that there were difficulties in the systematic tests to measure the small steady tilt values in the presence of the large oscillations due to the normal dynamic behaviour of the model.

The previous findings and the above observations indicated that the simple theory given by Numata et al., which produced correct order of magnitude of tilt, had to be improved in terms of the preferred direction of tilt and the neglect of several factors in order to use the existing solution. The inclusion of some of these factors neglected could provide a mechanism for a preferred direction of tilt as explained in the following:

(a) Effect of oscillations about the mean position,

(b) Effect of cross-section other than circles,

(c) The hydrodynamic interaction between the pontoons,

(d) Some other effects (non-linearities due to shallow depth of submergence, breaking waves, etc.).

In the simple Numata et al. theory the pontoons were assumed fixed and the steady tilting moment was calculated by neglecting the oscillation about the mean position. In an actual case the steady moment would be effected by the oscillatory first order forces and controlled by the moorings if they existed. The moments of the first-order forces at pontoon centres with respect to the centre of gravity would contribute to the steady tilting moment.

The assumption of a fixed circular cylinder under the regular beam waves yielded no steady horizontal drift force as shown by Ogilvie[31]. If the section was not circular or circular in general harmonic oscillation there would be a steady horizontal force which could contribute to the steady tilting moment and cause a preferred direction of tilt depending on the tilt angle and mooring arrangements. However, in the Numata theory the transformation of non-circular pontoon or footing to pontoon with circular cross-section would yield no steady horizontal force. This removed one possibility for a preferred direction of tilt.

The hydrodynamic interaction between the pontoons could be important if they were close together. At any separation distance the leeward pontoon always saw a wave diffracted by the seaward pontoon which in turn saw a wave reflected from the leeward pontoon and higher order 'mirror-effects' occurred. This effect was not significant for a fixed pontoon of circular cross-section since there would be no reflection according to the linear potential theory[33,34]. However, for moving pontoons of non-circular cross-section and any other fixed or moving pontoons the reflection would always exist and be different in the leeward and seaward tilt positions. This could cause another mechanism for a preferred direction of tilt.

During the model tests at higher waves and large tilt angles sometimes the top of the upper pontoon was very near to the surface and might even break the wave surface. For these extreme conditions one might expect second-order wave theory could fail. The experiments carried out by Salter et al.[35], with a shallow submerged fixed circular cylinder to investigate the behaviour of a 'nodding duck' power generator just below the waves, indicated that it was possible to have an average steady horizontal force opposite to the wave travel direction and an average steady vertical force downward in higher waves. The vertical component was often eight times larger than horizontal component. Later these results were verified by tests carried out by Longuet-Higgins[36] who discussed the possible explanations as follows:

(i) Higher harmonics, and

(ii) Breaking waves.

When the waves encountered the shallowly submerged cylinder without breaking the wave amplitude and horizontal particle velocities above the cylinder increased due to the local depth implying strong non-linearity and producing second harmonics. The frequency of the second harmonics was twice that of the first harmonics and their group velocity in deep water was half of the first harmonics. As derived in ref. [36] the steady horizontal force exerted on a shallowly submerged fixed circular cylinder (the reflection could be neglected) was given by:

$$\bar{F}_x^t = \frac{1}{4}\rho g\left(b - \frac{1}{2}a_{2T}^2\right)$$

where ρ = density, g = gravity, b = dissipation of energy,

a_{2T} = amplitude of the second harmonic transmitted wave.

As shown in the formula the sign of the force depended on a balance between the amplitude of the second harmonic transmitted wave and the dissipation of energy. When the second term (momentum flux in the second harmonic) was larger, the force would be in the opposite direction to the wave travel (seaward).

On the otherhand as the waves were passing over the cylinder there would be a mean pressure defect 'set down' due to the water surface proximity resulting in a mean upward force. If the waves had small amplitude, as demonstrated by Ogilvie[31] for a fixed or freely floating circular cylinder whose motion was identical to the water particles, there was no reflection of the waves due to the presence of the cylinder. Therefore, the 'set down' should be symmetric about the mid-point as shown in Fig. 10.

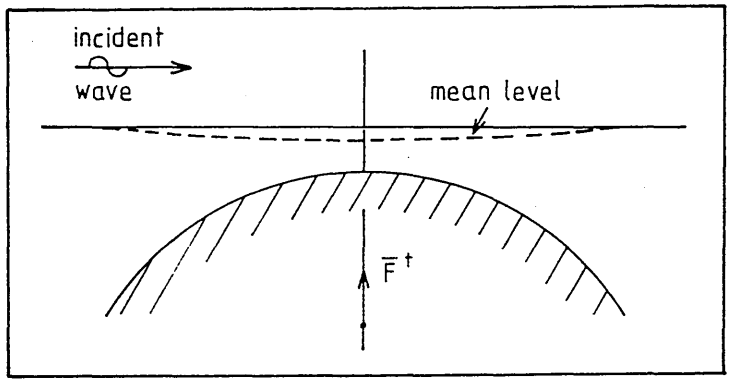

Fig. 10 - Schematic view of the symmetrical changes in mean sea level of waves in the presence of a submerged cylinder, if the waves are not breaking[36]

However, for the larger waves the set down could be unsymmetrical due to non-linearity and viscosity and this could produce a small mean horizontal force as well as a mean vertical force as shown in Fig. 11.

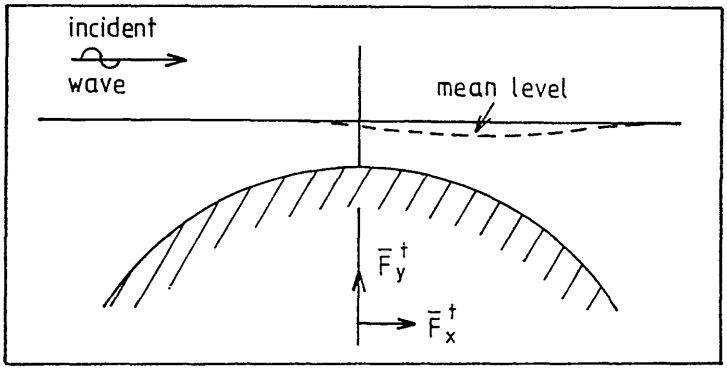

Fig. 11 - Schematic view of the unsymmetrical changes in mean sea level of waves in the presence of a submerged cylinder, if the waves are not breaking[36]

If the waves were breaking as shown in Fig. 12, the wave breaking began with a small set down until the breaking point B, when the wave height and momentum flux began to diminish. Then the static pressure increased producing a large rise ('set up') in mean level and downwards force (negative) on the cylinder in order to balance the loss of horizontal momentum flux. Now, if the set up was symmetrical there would be a large downwards force on the cylinder as shown in Fig. 12.

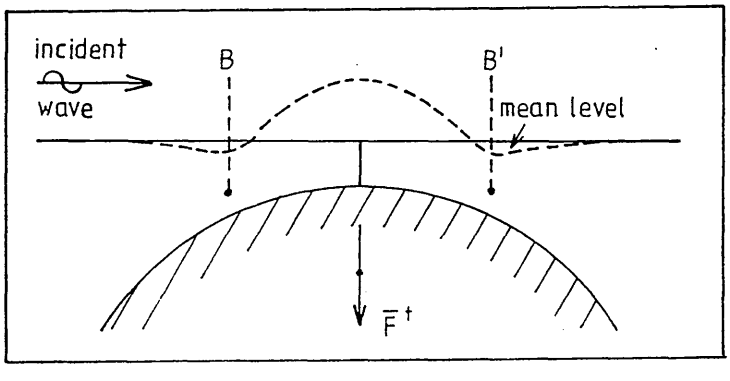

Fig. 12 - Schematic view of the symmetrical changes in mean level of waves in the presence of a submerged cylinder, if the waves are breaking[36]

If the set up was unsymmetrical there would be a mean horizontal force as well as the vertical force. The direction of the horizontal force depended on the wave length. If the wave length was short compared to the diameter of the cylinder, as shown in Fig. 13, the celerity of the wave and the change in the depth above the cylinder would be slow. In this case the breaker height, which was proportional to the local depth above the cylinder, would have time to adjust the local depth of water above the cylinder up to the mid-point. On the right of the mid-point when the depth began to increase, the breaking would suddenly cease since the waves would no longer be forced to try to become steeper. Therefore a net horizontal force would be exerted on the cylinder in the leeward direction.

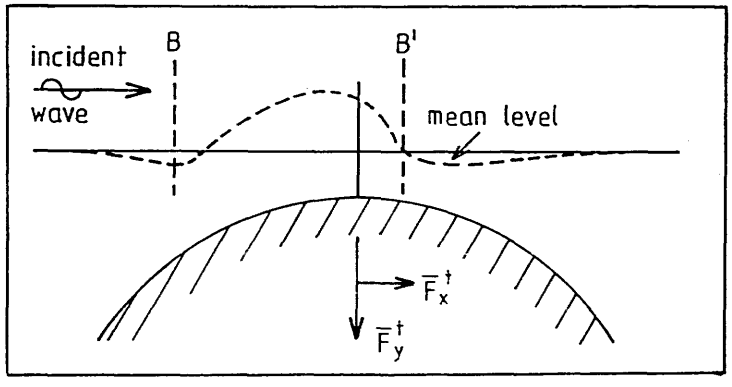

Fig. 13 - Schematic view of the unsymmetrical changes in mean level of waves in the presence of a submerged cylinder, if the waves are breaking (wave length not large compared to that of curvature)[36]

However, if the wave length was large compared to the diameter of the cylinder as shown in Fig. 14, because of the high celerity and short existence of the local depth, the wave could not find time to adjust the local depth, therefore breaking continued until some time after the depth began to increase again. This produced a set up on the leeward resulting in a net horizontal force in the seaward direction.

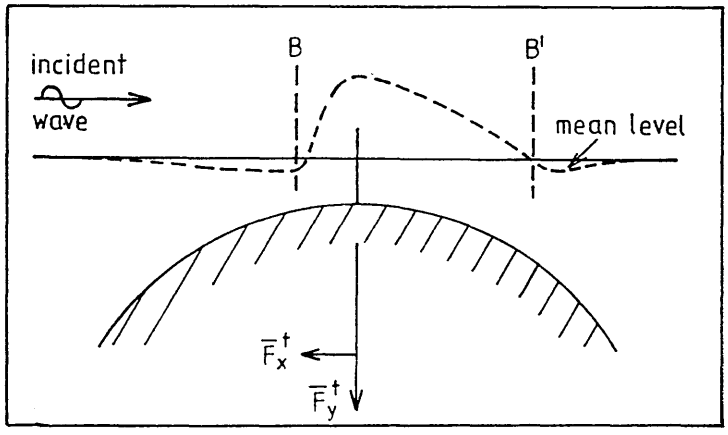

Fig. 14 - Schematic view of the unsymmetrical changes in mean level of waves in the presence of a submerged cylinder, if the waves are breaking (wave length large compared to that of curvature)[36]

The application of the above discussion to the pontoon of the semi-submersible implied that for shallow depth of submergence and higher waves, second-order wave theory could fail and in these cases there could be a strong mechanism for a preferred direction of tilt due to the steady horizontal forces.

In addition to the above factors in the simple Numata et al. theory the hydrodynamic effects of the vertical columns and bracings were ignored. This could remove one other possible mechanism for a preferred direction of tilt.

In the simple Numata et al. theory it was assumed that the semi-submersible was rotating about the fixed point CG where the steady tilting moment was calculated. In reality, in addition to the steady tilt motion the CG had translatory drift motion due to the horizontal and vertical forces respectively. This steady tilt and translatory motion values were coupled together. The steady horizontal force could be balanced by the mooring force or drag force. Whereas the steady vertical force should be balanced by the vertical restoring force.

Then the solution of the two coupled equations representing the balance of the steady tilting moment against righting moment and the balance of steady vertical force against vertical restoring force would yield the steady tilt angle and the mean elevation of the CG.

Martin and Kuo formulated and solved the steady tilt problem for an idealised semi-submersible in regular beam waves by using the second-order wave theory taking into account some of the above considerations. The semi-submersible consisted of twin circular pontoons which were long enough to apply two-dimensional theory. Thus the hydrodynamic effects of the columns and bracings were ignored while their hydrostatic effects were taken into account. The hydrodynamic forces on the pontoons were calculated by applying Ogilvie's study[31] to twin cylinders. The method was briefly as follows.

The initial equilibrium position of the semi-submersible in calm water was changed to a general position by applying an artificially suitable steady force and moment. Then the required forces, moments and motions which were of the same order as the wave steepness, were evaluated and the second-order forces and moments were calculated in the presence of the first-order oscillations. It was obvious that for each general position there would be a corresponding steady force and moment. When the steady vertical force and tilting moment about the CG were exactly balanced by the hydrostatic vertical force and righting moment there would be a possible mean position for a mean tilt and elevation of the CG. The sample computations were performed for a full scale idealised semi-submersible whose geometry and main dimensions are given in Fig. I.6 of Appendix I.

Figure 15 is given to show the effect of the assumptions as to which pontoons were assumed to be fixed or freely oscillating. It was

assumed that the semi-submersible with 5 m $\overline{GM}$ was artificially inclined in the leeward direction for 5° with no elevation. At this position the resulting steady wave-induced moment about the CG was calculated and plotted against the wave periods for the freely floating case by the solid line and for the fixed case by the dashed line. The tilting moment and period were expressed in terms of the following non-dimensional form:

$$C_G = \text{Steady Tilting Moment} / \rho g \ (\text{Incident Wave Amplitude})^2 \cdot (\text{Pontoon Separation})$$

$$2\ell/\lambda = \text{Pontoon Separation} / \text{Wave Length}$$

As shown in the figure the C_G for the fixed case was larger than that for the freely floating case by about 50% over most of the period. This indicated that the fixed pontoon assumption would yield an overestimated result. However, the free pontoon assumption could yield an underestimated result if there was any mooring and non-linear damping force. It was also indicated that there was no significant interference effect due to the twin hull configuration for this particular hull separation.

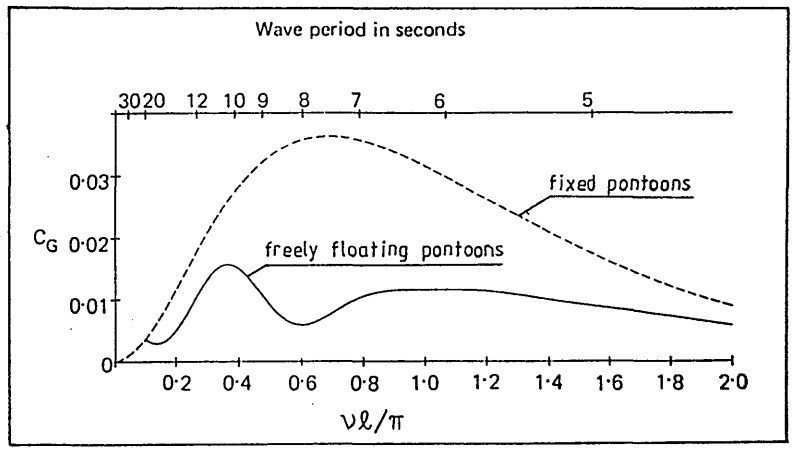

Fig. 15 - Comparison of steady moment coefficient C_G at 5° of tilt and zero elevation with 5.28 m of $\overline{GM}$ and 20 m of radius of gyration about the COG (where ν is wave number)[20]

The C_G curves were also used to study the tendency for a preferred direction of tilt. As shown in Fig. 16 the C_G values were obtained for the same configuration at artificially imposed tilt angles with no elevation from 10° in the leeward direction to 10° in the seaward direction (seaward direction represented by negative sign) including upright position (0° tilt). As could be seen there was a strong trend for a tilt in the leeward direction at about 10.5 secs for all positions. Even if the semi-submersible was artificially inclined in the seaward direction for 10° the steady moment curve was positive indicating a strong tendency for a leeward tilt. However, for the shorter waves the moment was always acting in the tilt direction indicating bi-stable behaviour.

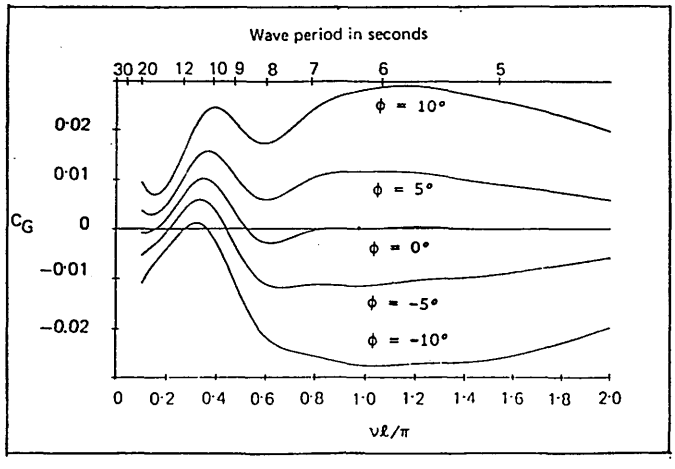

Fig. 16 - Steady moment coefficient C_G at zero elevation and various tilt angles ϕ, for 5.28 m of $\overline{GM}$[20]

The effect of $\overline{GM}$ on the tendency for a preferred direction of tilt is shown in Fig. 17 for various $\overline{GM}$s at zero tilt and zero elevation. As the $\overline{GM}$ was increased the tendency for a preferred direction of tilt was increased whereas the magnitude of tilt was reduced since the increase in the magnitudes of the righting moment were much greater than those in the steady tilting moment for the larger $\overline{GM}$s.

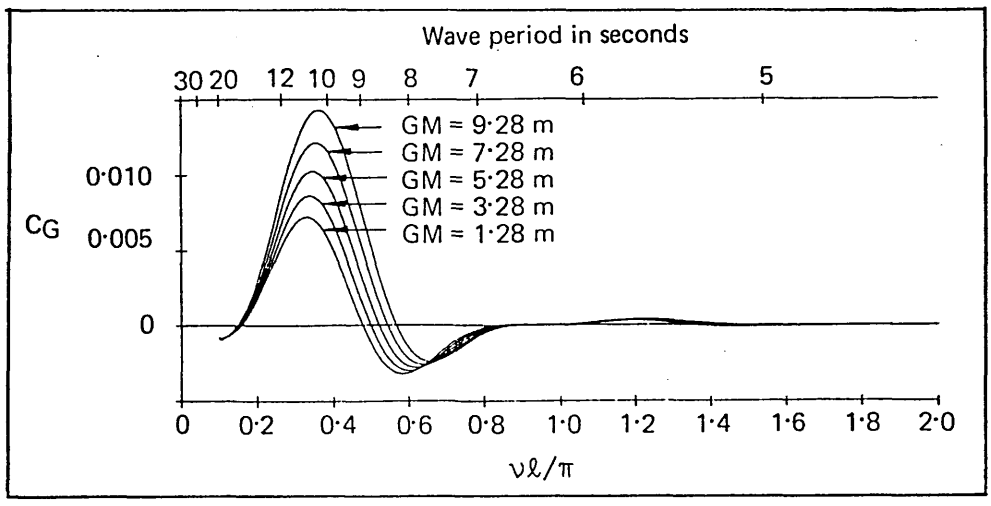

Fig. 17 - Steady moment coefficient C_G at zero tilt and zero elevation for 20 m radius of gyration about the COG and various $\overline{GM}$s [20]

From this study it was concluded that the more rational application of second-order wave theory with the inclusion of the additional factors could predict small stable tilt angles with a preferred direction. There was a limit to the application of the theory for predicting non-trivial tilt angles in terms of wave height (wave steepness) and depth of submergence. However, in order to give precise values for the limitation there was a need for reliable quantitative experiments.

These findings agreed with the tests of De Souza and Miller in terms of the preferred direction of tilt. Although no tilt in the seaward direction was observed in the tests of De Souza and Miller, Martin and Kuo observed the seaward tilt in the longest wave and some cases depending on the mooring geometry. However, Numata observed bi-stable tilt behaviour depending on the initial disturbance[32]. Even for larger tilt angles they demonstrated surprisingly good agreement for some cases between the measured and predicted values from the simple theory which was valid for large depth of submergence.

In order to compare the theoretical predictions with the observation made by Numata et al., a sample computation for the idealised semi-submersible with the lowest $\overline{GM}$ = 1.28 m was performed at a period of 10.5 secs where Numata observed large tilt angles at higher waves. The calculated tilt angles were plotted against the wave steepness. As shown in Fig. 18a the positions in the segment OM were stable and therefore the theory could predict the tilt angle $0 < \phi \leq 10°$. There was no stable mean position if the wave steepness $\varepsilon \geq 0.25$. This indicated that for large tilt angles and wave heights the steady tilt could not be predicted by second-order theory.

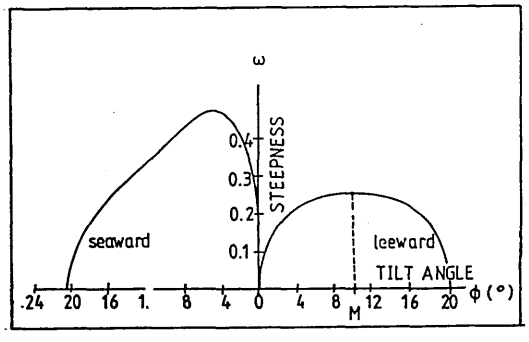

Fig. 18a - Wave steepness vs tilt angle for idealised semi-submersible configuration with GM = 1.28 m in waves with a period of 10.5 s. Only tilts in the range $\overline{OM}$ are stable[20]

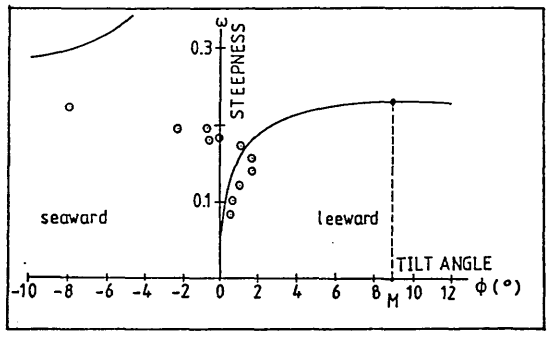

Fig. 18b - Wave steepness vs tilt angle for the simplified model at a frequency of 1.5 Hz. Comparison of theory and experiment. Only tilts in the range $\overline{OM}$ of the theoretical curve are predicted to be stable[20]

Martin and Kuo[20] also compared the theoretical predictions against experiments carried out with a simplified model which had a single degree of freedom (roll only) as shown in Fig. I.7 of Appendix I. As can be seen in Fig. 18b the comparison of the experiments and the present theory demonstrated a fair agreement for the magnitudes of tilt angle for small wave steepness ($\varepsilon \leq 0.15$). For the larger waves ($\varepsilon > 0.15$), as expected from the theory, there was no agreement at all, even the direction of tilt was wrong due to the non-linear effects.

In order to identify whether second-order theory could explain the tilt phenomenon by itself or not, the most realistic way was to investigate experimentally the behaviour of the steady vertical force which was thought to be mainly responsible for the steady tilt. It was known from theory that the second-order steady forces were very small in magnitude compared to the first-order oscillatory forces. Therefore, it demanded more sophisticated measuring techniques and careful analysis of small steady outputs from the large oscillatory outputs.

2.2.4 In 1978 Morrall[29] from the National Maritime Institute investigated the effect of the second-order steady vertical force, which was experimentally measured, on the stability of semi-submersibles.

The main objective of this study was to cross-check the simple Numata et al. theory by experimentally measured force values and to identify the limit of the wave height and depth of submergence at which second-order wave theory remained valid.

The tests were carried out on two models: one with a single footing, and another a single pontoon representing the main underwater elements of two different types of designs which were a 3-column, footing type and a 4-column twin-pontoon type semi-submersibles. The geometry and dimensions of the two models which were approximated to a scale of 1/30 are given in Figs I.8 and I.9 of Appendix I. Measurements were taken only on the footing and pontoon of the models which were held in fixed positions. The steady vertical force on the vertical column was not measured as it was neglected in the Numata et al. theory. The models were tested in regular beam waves. The wave heights and steepnesses used in the tests were the same as those used by Numata et al. in which the wave period and wave height, corresponding to full

scale values, varied from 8 to 12 secs and 7.38 to 12.01 m with wave steepness ratio from 0.0735 to 0.0535 respectively. In order to study the depth effect the measurements were taken at four different draughts as shown in Figs I.8 and I.9 of Appendix I.

From these tests it was found that the steady second-order vertical force was heavily overlaid by the large first-order oscillatory forces. The ratios of those forces were found to be 1/7 for the pontoon type model and 1/10 for the footing type model. As shown in Figs 19a and 19b the magnitude of the steady vertical force decreased with increasing draught about 15 m draught. For the draughts smaller than 15 m and for the higher waves the force rapidly decreased and in some cases changed its direction from upwards to downwards verifying the possibility for non-linearity discussed by Longuet-Higgins in the previous study. The observation of the flow at the smaller depths indicated it was highly disturbed by the vertical columns for both models. For the pontoon type model at smaller depths and higher waves a periodic reversal in flow direction was observed.

In this study the measured steady vertical force values were compared with:

(a) A simple method developed by using linear wave theory in which the steady vertical force on the simplified submerged parts of the semi-submersibles were expressed with the equations given in eqs I.14 and I.15 of Appendix I.

(b) The simple Numata et al. method.

(c) The three-dimensional source-sink method.

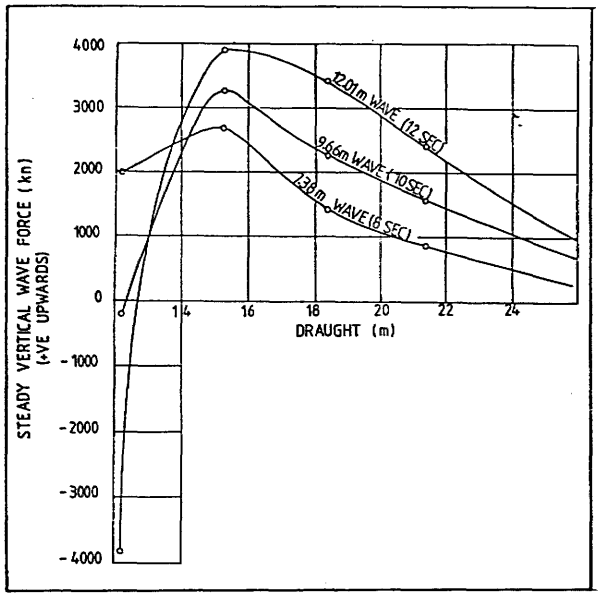

Fig. 19a - Measured steady vertical force vs draught for pontoon type semi-submersible[29]

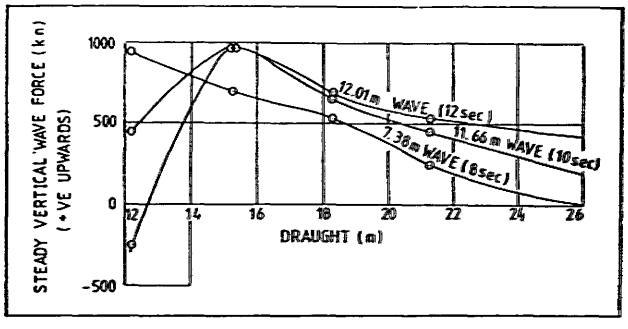

Fig. 19b - Measured steady vertical force vs draught for footing type semi-submersible[29]

As shown in Figs 20 and 21 there was a reasonable agreement between the measured and calculated force values at the larger draughts, but less satisfactory agreement for shallower draughts indicating that the existing methods based on the linear wave theory could fail at shallower depths as expected.

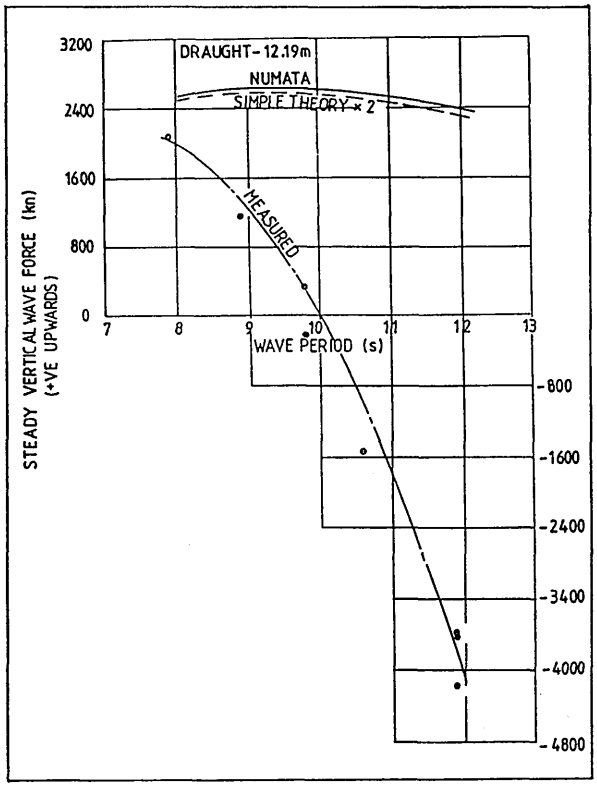

Fig. 20a - Steady vertical force vs wave period for pontoon type semi-submersible at the shallowest draught[29]

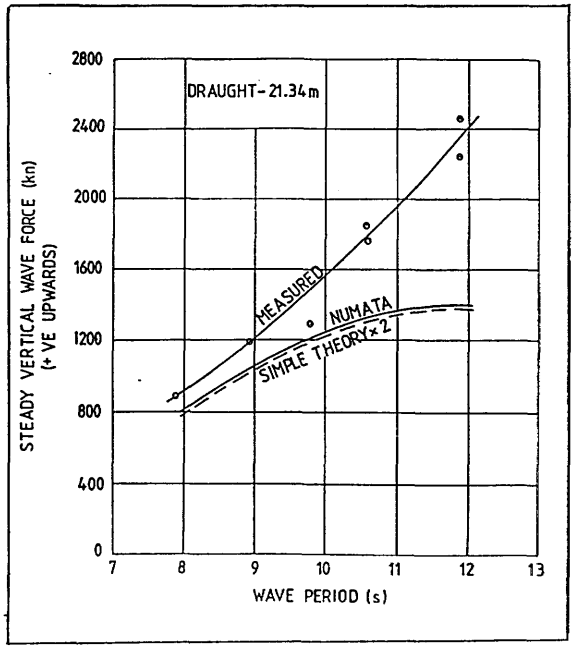

Fig. 20b - Steady vertical force vs wave period for pontoon type semi-submersible at the largest draught[29]

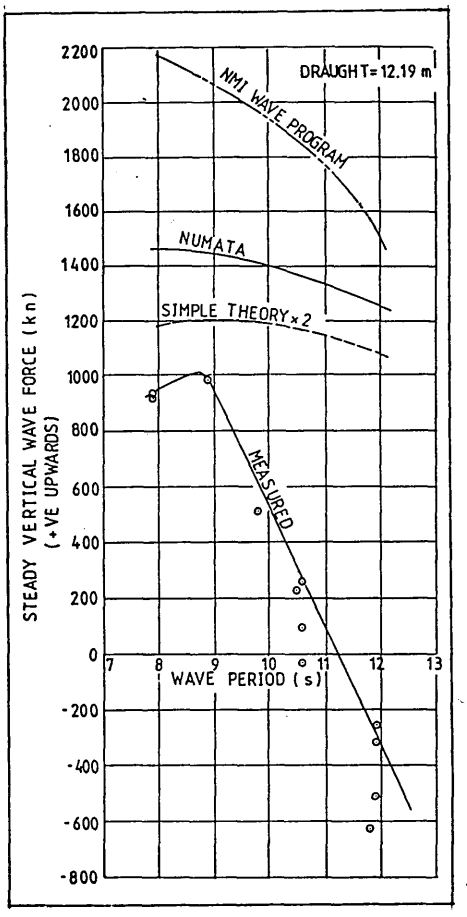

Fig. 21a - Steady vertical force vs wave period for footing type semi-submersible at the shallowest draught[29]

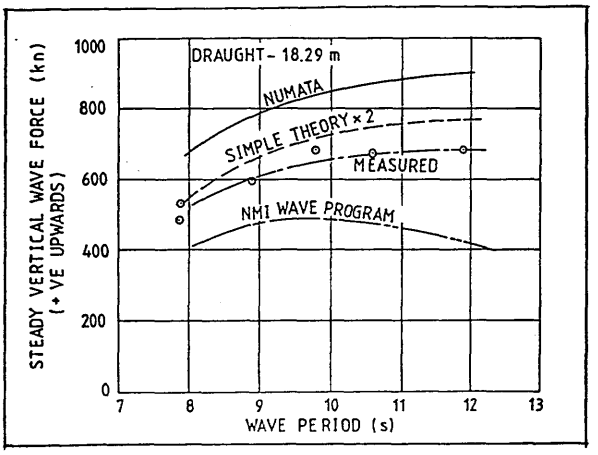

Fig. 21b - Steady vertical force vs wave period for footing semi-submersible at the largest draught[29]

Since the agreement at the largest draught (21.34 m) was best, by using the measured force value at this draught the wave-induced tilting moment and righting moment were plotted on the same charts for both models. The $\overline{GM}$s used to calculate the righting moments were the min $\overline{GM}$ values just satisfying the present wind heeling criterion up to 10° heel angle. It was 6.77 m at 70 knots wind speed for the footing type and 4.64 m at 100 knots for the pontoon type semi-submersible. As shown in Figs 22a and b the wave-induced tilting moments for the higher and longer waves diminished when the heel angles were greater than 5 degrees for both vessels. However, the minimum righting moment was found to be much greater than the steady wave-induced tilting moment for all cases. Therefore, it was concluded that the possibility of the occurrence of the steady tilt in the full scale was very low if the semi-submersibles complied with the current stability regulations.

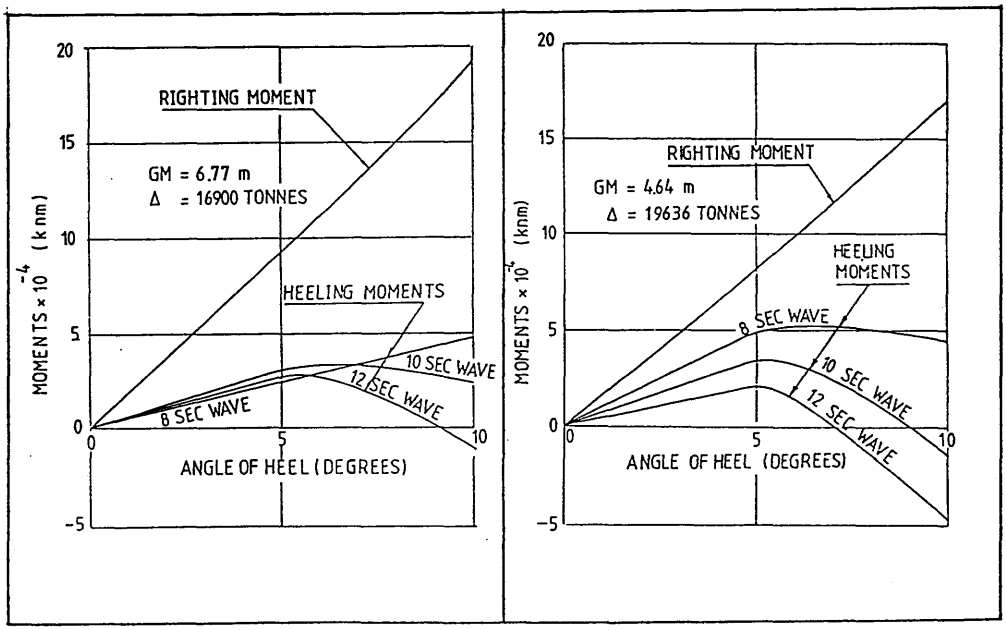

Fig. 22a - Footing type semi-submersible 21.34 m draught

Fig. 22b - Pontoon type semi-submersible 21.34 m draught

Fig. 22 - Righting and wave induced heeling moments vs heel angles (heeling moments based on measurements in regular beam waves[29]

As mentioned earlier during the capsizing tests of semi-submersibles attention was drawn to "the under-deck clearance" since capsizing had a very low probability. It was indicated that this could be an essential parameter for stability as well as for design to perform good motion characteristics and maintain safe and consistent operations with low stability index in extreme environmental conditions.

The under-deck clearance depended on the relative motion which was calculated from the heave, roll and wave elevation by taking into account the phase difference among these components. When a semi-submersible had low $\overline{GM}$ values a large steady tilt or slowly-varying tilt could affect the relative motion causing a decrease of under-deck clearance and extra forces and moments on the mooring lines. As indicated by Numata et al., in an irregular sea state the comparisons of experimental relative motion values with the predicted values derived from the motion responses in regular waves demonstrated under-estimated values because of the slowly varying tilt behaviour. Therefore it was concluded that the conventional response prediction technique, using motion amplitude operators obtained either from model tests or by calculation, should be modified in order to take into account this phenomenon.

2.2.5 In Japan, Hineno et al.[18] investigated the effect of slowly-varying tilt behaviour on the under-deck clearance of a semi-submersible. The main objective of this research was to provide a method to predict the required under-deck clearance of a semi-submersible when exposed to the effect of slowly-varying tilt in irregular waves.

The method presented started with motion tests in regular beam waves with a model approximately to a scale of 1/90 of an 8-column twin rectangular pontoon type semi-submersible. The geometry and main dimensions are given in Fig. I.10 and Table I.6 of Appendix I. Two

different $\overline{GM}$ values, corresponding to full scale values, were of 0.4 and 2.1 m. During this group of tests in beam seas, regular waves were generated in a range of period, corresponding to full scale, varying from 6 to 27 secs with wave steepnesses of 1/15 to 1/50. The main objective of these tests was to identify the existence of the steady tilt in regular waves and to calculate the steady tilting moment at observed steady tilt angles. In Figs 23 and 24 the measured tilt angles and corresponding experimental tilt moments C_G represented by:

$$C_G = \text{Steady Tilting Moment} / \rho g \text{ Beam Pontoon Length} \times [\text{Incident w. Amplitude}]^2$$

are given for two different $\overline{GM}$s and various wave heights. No seaward tilt or bi-stable tilt observation was reported in the study. In Fig. 24 by using the simple Numata method the steady tilting moments were calculated at the observed steady tilt angles and plotted on the same figure. As seen, although the measured and calculated values had a peak about 8 secs they did not agree over the range of period tested.

The measured steady tilt moment coefficient was used with the Pierson-Moskowitz type seaway spectrum to calculate the low frequency tilt moment spectrum in irregular waves by the method developed by Pinkster[14]. Since the first-order wave spectrum could not contain a frequency band to induce such a low frequency moment, an equivalent wave spectrum was defined corresponding to this moment by using the transfer function of roll moment per unit regular wave[37]. Then by using this equivalent wave spectrum and the transfer function of roll amplitude per unit regular wave the required low frequency roll motion spectrum was obtained. The transfer function of roll amplitude was calculated excluding the effects of the sway exciting force. On the

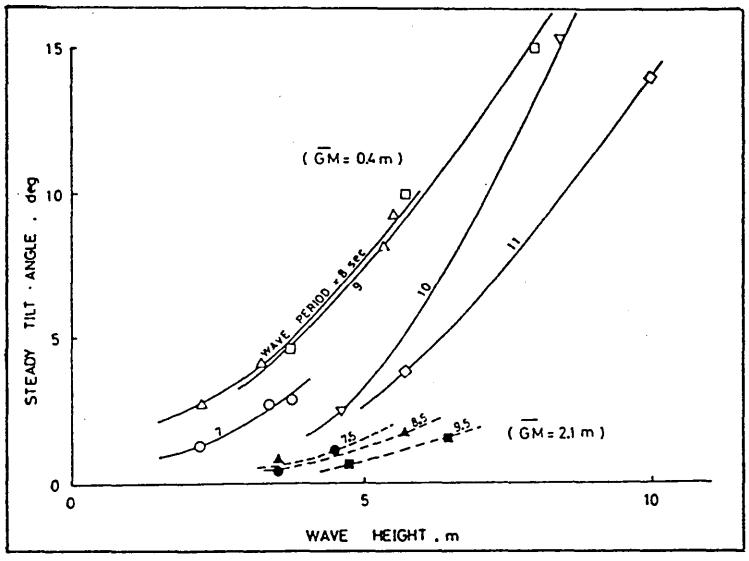

Fig. 23 - Measured steady tilt angles vs wave height[8]

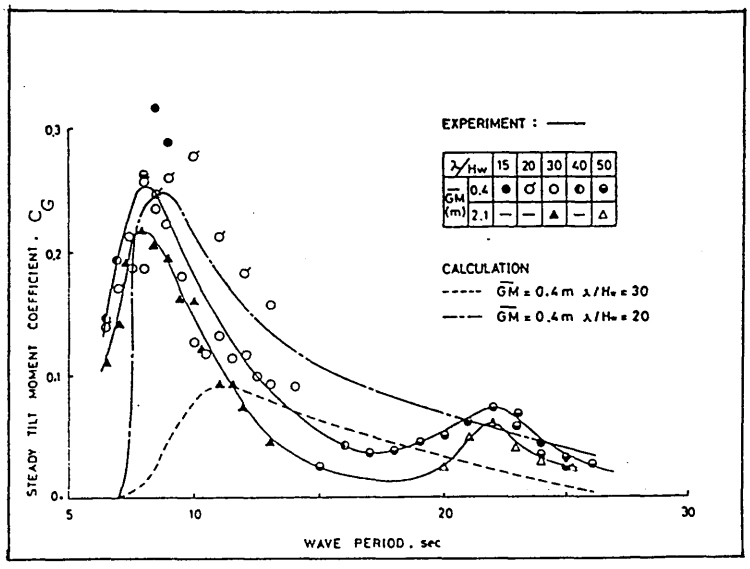

Fig. 24 - Steady tilting moment coefficient vs wave period[8]

(λ/H_w is wave length / wave height)

otherhand the roll motion spectrum for the higher frequencies was obtained by applying the transfer function of the roll motion amplitude per unit regular wave to the first-order wave spectrum, the transfer function only taking account of the first-order wave exciting roll moment. The overall spectrum of roll motion was obtained by summing the low and high frequency roll motion spectrums. The roll motion spectrum calculated in this way was found in good agreement with the test results as shown in Fig. 25.

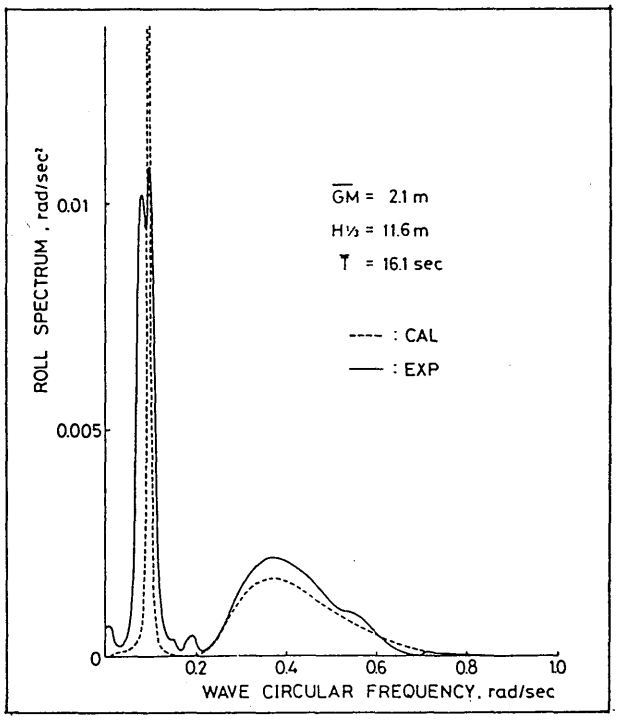

Fig. 25 - Roll motion spectrum vs wave frequency. Comparison of theory and experiment[8]

Following the above procedure the relative motion spectrum was processed in the low and high frequency ranges. In the range of low frequency the contribution to the relative motion due to heave mode was almost zero and the other contribution due to the wave elevation was non-existent. Therefore, the low frequency relative motion could

be calculated from the low frequency roll motion spectrum only. In the higher frequency ranges the relative motion spectrum was expressed by the first-order wave spectrum and transfer function of relative motion by the unit regular wave. The overall spectrum of the relative motion was obtained by summing the low and high frequency spectrums. The final spectrum had two peaks at low and high frequencies. It was assumed that the low frequency roll motion was independent of the high frequency one without the relative interference in phase and the spectrum at the roll resonant frequency predominant in the region of low frequencies. Then the calculated maximum roll motion amplitudes by the above method were in good agreement with the measured values from the tests. However, the calculated relative motions demonstrated a discrepancy with the measured values. The discrepancy was attributed to the non-linear behaviour of the wave elevation.

The above study demonstrated that, although the relative motion displacement could not be predicted accurately, the predicted non-linear effect of roll motion (slowly-varying tilt) was in good agreement with the test results as compared with the conventional techniques using the linear response assumption. The relative motion prediction could be improved if the non-linear effect of the irregular waves could be taken into account.

In the previous chapter it was indicated that the 1.3 figure could not satisfactorily represent the dynamic effects of a semi-submersible and its environment. More realistic presentation of those effects would provide a more rational stability criterion.

2.2.6 In Japan another experimental research on a moored semi-submersible has been carried out by Takarada et al.[8] in 1982. The research was still continuing when the first results were presented. Therefore the following assesses only a part of this work.

The main objective of this research was to explore the dynamic effects of current and wave-induced second-order forces on the stability of semi-submersibles in the presence of other dynamic effects due to moorings. It was concentrated on the steady and slowly-varying tilt combined with the effects of moorings. This study was interesting since:

(i) It demonstrated the importance of the effect of the mooring lines on the steady and slowly-varying tilt behaviour.

(ii) The first attempt was made for simulation of the slowly-varying tilt in a regular wave group.

(iii) It showed the importance of the horizontal drift force on the slowly-varying tilt behaviour.

The series of model tests with the 1/60th scale model of an 8-column twin rectangular pontoon type semi-submersible were carried out in regular, regular wave group and irregular waves. The main geometry and dimensions of the model and testing conditions are given in Fig. I.11 and Table I.7 of Appendix I. It was believed that the tilt would be influenced by the location of the fairleads as well as the $\overline{GM}$. Therefore, the tests were performed with the model moored by eight spread moorings at four different fairlead heights and three $\overline{GM}$s as shown in Figs I.12 and I.13 of Appendix I. The tests in regular beam seas were carried out in a range of wave periods varying from 1.12 to 1.73 secs and wave heights 10 to 25 cms. The results

demonstrate the effect of the fairlead position on the steady tilt angle as shown in Fig. 26.

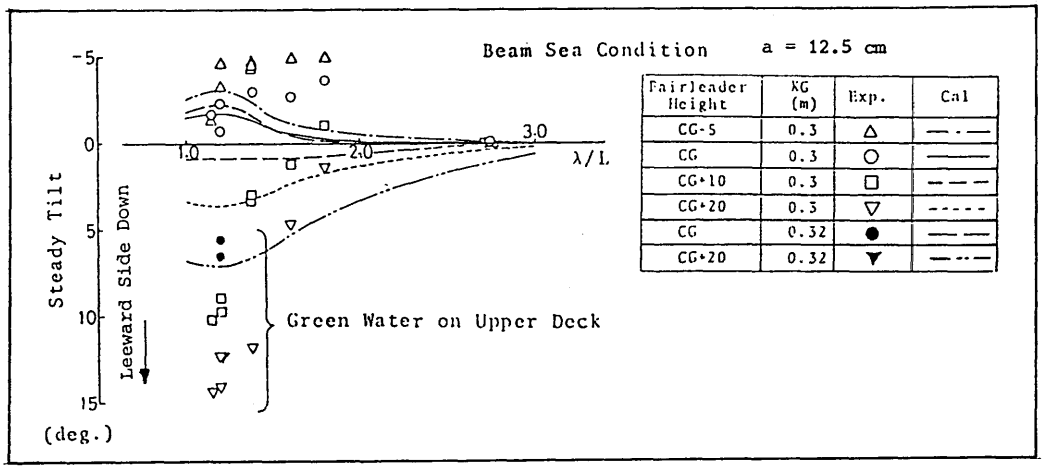

Fig. 26 - Comparison of the measured and calculated steady tilt for varying fairleader heights (λ is wave length, L is pontoon length and a is wave amplitude)[18]

As seen in Fig. 26 the magnitude of the steady tilt angle increased with the increasing distance of the location of the fairlead from the CG. When the fairlead was higher than that of the CG the model had a tendency to tilt in the seaward direction. It was observed that at the larger tilt angles sometimes the waves caused green water on deck which led to larger inclinations of model. In such positions the effect of the fairlead height was very important for the vessel's stability. The results obtained from the regular sea tests for various $\overline{GM}$s demonstrated similar trends to the results in the previous studies in which the magnitude of the steady tilt increased with decreasing $\overline{GM}$.

According to the method formulated in eqs I.16 through I.18 of Appendix I, the steady tilt angles were calculated from a quasi-static analysis of the steady and horizontal drift in the presence of the mooring forces. In the formulation it was assumed that the main

responsible for the steady tilt was the steady drift force in the horizontal direction. This steady force and its moment with respect to the CG were balanced by the restoring force and tension force in the mooring line and their moments at the steady tilt angles. However, as seen in Fig. 26 the predicted steady tilt angles by this method were underestimated.

It was indicated that the prediction of the slowly-varying tilt behaviour of a moored semi-submersible in irregular seas by using the quasi-static solution was very difficult. As shown in Fig. 27 a typical roll motion records showed unsteady non-linear behaviour which could be predicted in the time domain.

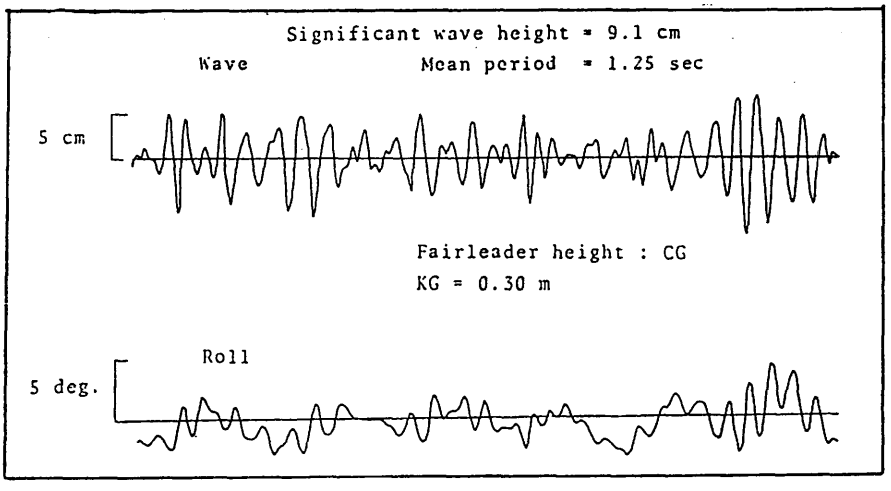

Fig. 27 - Experimental chart records of moored model roll motion response in irregular seas[18]

In order to start with the simplest case of the irregular sea state which was the regular wave group, some tests were carried out with the unmoored model in regular wave groups with a wave period varying from 1.1 to 1.4 secs. In Fig. 28 a typical motion record was shown. The magnitude of the slowly-varying tilt increased rapidly as the wave period became smaller where the drift force had large values.

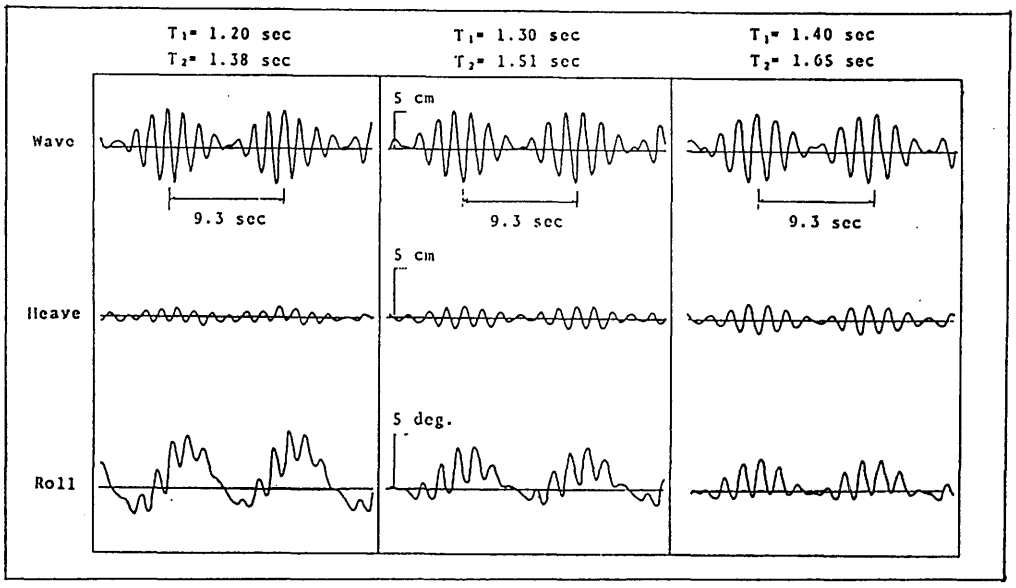

Fig. 28 - Experimental chart records of unmoored model roll motion response in regular wave groups[18]

Although no information was given for the calculation procedure, a computer simulation of the roll motion was given in this study as shown in Fig. 29. The breakdown of the slowly-varying tilt into its components due to the second-order vertical and horizontal force demonstrated that the contribution due to the vertical component was small compared to the horizontal component.

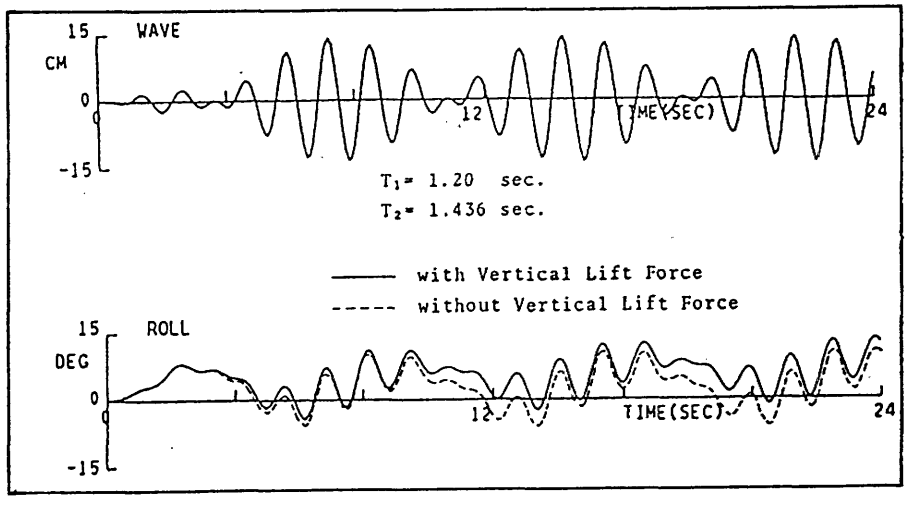

Fig. 29 - Computer simulation of unmoored model roll motion response in regular wave groups[18]

Some model test results with and without moorings in irregular seas obtained using the ISSC spectrum were given. Since the research had not been completed no complete results and theoretical calculations were given. However, the available results obtained from the irregular sea tests demonstrated the similar roll motion spectrum to that found by Hineno et al.[18] in which two peak values for low and high frequency ranges were obtained. As shown in Fig. 30 at the low frequency region the model with moorings had a larger tilt than the model in the unmoored situation. At the higher frequency region the unmoored model had a larger tilt.

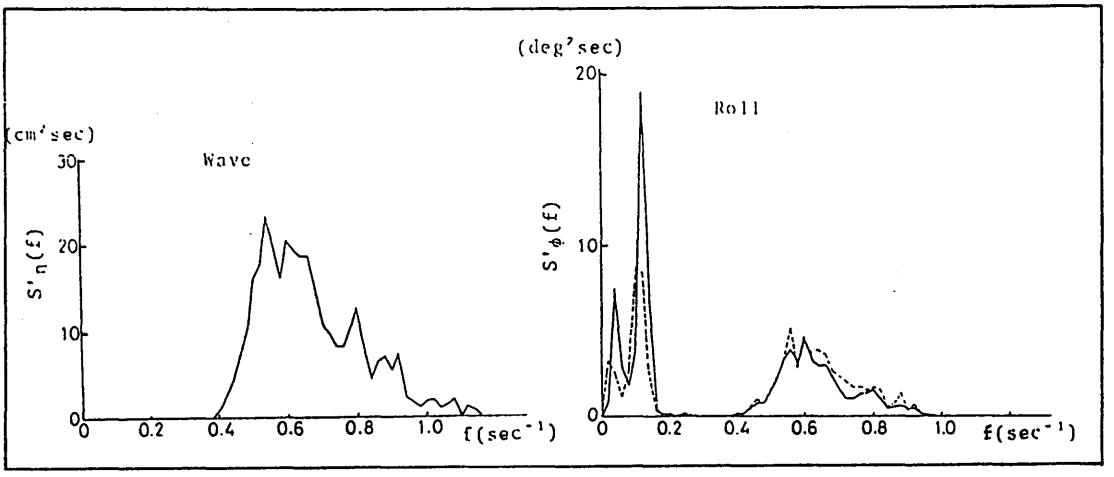

Fig. 30 - Experimental wave and the roll motion response spectrum[18]

From the available results of this study it was concluded that, the effects of the moorings on the magnitude and the direction of the tilt were significant. In regular waves the magnitude of the steady tilt was increased with increasing distance of the fairlead from the CG. If the fairlead height was higher than that of the CG a steady tilt in the seaward direction could develop. In irregular waves the slowly-varying tilt in the low frequency region was more significant

than in the high frequency range. The presence of moorings increased the magnitude of slowly-varying tilt in the low frequency region while it decreased it in the high frequency region. The first simulation study indicated that in irregular waves the contribution of the second-order horizontal force to the slowly-varying tilt was greater than that of the second-order vertical force.

2.3 CONCLUSIONS

The following were obtained from the study of previous theoretical and experimental work on tilt behaviour and these determined the objectives of the thesis.

Importance of the Phenomena

It has been revealed in several stability tests that capsizing of a semi-submersible with minimum stability index in maximum environmental conditions has a very low probability because of its inherently good motion characteristics. This finding encourages operators and designers to put pressure on the regulatory authorities and classification societies to relax the present rules by reducing $\overline{GM}$. This will provide more deck load and relatively good motion characteristics. In such a case, tilt behaviour is a very serious problem, which has to be considered in terms of the safety and design of the vessel. It could affect the motions non-linearly causing considerable stability losses due to large tilts, structural damage due to slamming and mooring problems due to extra mooring tensions.

The above statement implies that there could be an optimum between the conservative stability rules and the demands of the operators and designers encouraged by the model tests and very low

probability of the occurrence of the semi-submersible capsizing in practice.

This could be achieved by providing a complete explanation of the phenomena, but it would be dangerous to modify the rules in the absence of a complete understanding.

Factors Causing a Delay in Obtaining a Complete Explanation of the Phenomena

(i) Tilt behaviour has been observed during the model tests of semi-submersibles. So far, there has been no well documented reports of tilt being observed on full scale semi-submersibles, except some verbal statements suggesting it has occurred in one or two instances and it was attributed to wind, current and mooring effects. Therefore, this experimental behaviour has not been a serious problem on the full scale and not enough research studies have been carried out to explore the phenomena.

(ii) In addition, due to the shortage of the required research work, in the majority of existing studies tilt was investigated along with other dynamic aspects of semi-submersibles [e.g. motion response predictions, intact and damage stability assessment, determination of underdeck clearance, etc.]. Therefore the phenomena itself was not explored rigorously. The experimental studies have produced conflicting reports on several characteristics of this behaviour and these have not been cleared up by later work.

(iii) The complicated nature of the problem is a major cause of delay The existing studies show that it is composed of many factors [e.g. the effect of first and second-order wave forces, hydrodynamic interaction, moorings, viscosity, scale, non-linearity,

etc.] which depend on various parameters [e.g. wave frequency, wave height, $\overline{GM}$, draught, underwater geometry, etc.]. In order to identify the phenomena these effects should be explored by systematic research studies which require much effort and time.

Contributions from the Studies in the Past to the Development of the Phenomena

By reviewing the six research studies explained in the foregoing the following can be concluded.

(i) The research work performed by Numata et al. has been the most important one for the exploration of the phenomena. It was the first time tilt behaviour was noticed and its basic explanation based on second-order wave theory was presented. Several approximations and simplifications were made to use the existing second-order solutions which demonstrated a qualitatively correct order of magnitude with experimental results. The approximate character of the study produced 'bi-stable' tilt behaviour depending on the initial disturbance. In order to avoid the steady tilt in regular beam waves a calculation procedure for the minimum $\overline{GM}$ needed was provided. However, the model tests with this calculated $\overline{GM}$ still produced low-frequency roll motions in irregular waves. Thus, it was concluded that this procedure should be modified for irregular waves. This could be achieved ideally by predicting the low-frequency roll motion either in the frequency domain or time domain by a new technique to be developed.

(ii) The work carried out by De Souza and Miller was the interesting study compared to the others because of the different experimental findings and theoretical approach to the problem. They

reported that the steady tilt was sharply tuned with respect to the wave frequency for a particular model and it always developed in the leeward direction. By considering this finding the phenomena was attributed to the non-linear variations in the sway exciting force due to the drag component. This demonstrated preferred tilt in the leeward direction depending on the footing separation at one particular frequency where the steady tilt was observed in the tests. Although the predicted tilt angles were only approximately 40% of the measured angles, this study drew attention to the steady effects of the viscous drag forces.

(iii) The most comprehensive theoretical explanation of the phenomena was given by Martin and Kuo for the mathematical model semi-submersible. It was shown that second-order theory could not explain several features of the phenomena. Beside the second-order effects there were some additional factors [e.g. effects of first-order motions, hydrodynamic interaction, cross-section, moorings, non-linearity, etc.] which caused the preferred direction of tilt. Second-order theory could only predict small stable tilt angles since it would fail for high waves and shallow draughts. The theoretical solution of the behaviour based on second-order wave theory for the idealised model with circular pontoons demonstrated a small stable preferred direction of tilt. This study needed to be backed up by systematic motion tests for small stable tilt angles.

(iv) The only work, investigating experimentally the effect of steady vertical force on the phenomena, was performed by Morral. This force component was measured on the simple underwater elements of the semi-submersible models. The limits of the

validity of the second-order solution for this force component was confirmed by these tests. It was demonstrated that there was a scatter between the theoretically calculated force by the linear theories and the measured force increasing with increasing wave heights and reducing draughts. Consistent with the non-linear theory a downward (negative) force was recorded for very shallow draughts and high waves. However, it was difficult to appreciate the contribution of this force component to the actual tilt behaviour by the force measurements only without motion tests.

(v) Hineno et al. demonstrated that the low-frequency roll motion in irregular waves could be predicted satisfactorily by using the equivalent low-frequency wave spectrum corresponding to the wave-induced steady tilting moment at experimentally observed tilt angles and roll response in regular waves. However, the tilting moment which was calculated from the Numata theory and tests were not in agreement despite the similar trends. This study demonstrated that if the theoretical methods for calculating the tilting moment in regular waves were improved, the low-frequency roll motion could be predicted satisfactorily by the method suggested in the frequency domain. Otherwise there was a need for regular sea tests to establish the wave-induced steady tilting moment.

(vi) The work carried out by Takarada et al. investigating the effects of the moorings on the tilt behaviour indicated that the moorings played an important role in the magnitude and direction of the tilt depending on the fairlead position. The quasi-static formulation of the steady tilt problem taking into account only horizontal drift force and mooring tensions

demonstrated underestimated tilt values compared to the test results in regular beam seas. The time simulation of the tilt in regular wave groups showed that the contribution of the second-order horizontal drift force was considerably larger than that of the vertical second-order force.

Requirements for the Understanding of the Phenomena

The primary requirements were some accurate experimental work devoted entirely to the tilt problem so that some of the conflicting results reported earlier could be clarified and form a basis for theoretical developments.

Therefore in the following a list of experimental requirements which are considered in the thesis are given:

(i) The steady and slowly-varying character of the tilt behaviour requires that the motion tests be performed in regular and irregular seas. However, in the thesis, work is concentrated on systematic motion tests in regular beam seas because:

(a) As indicated by the experimental studies, the persistence of the regular sea makes the tilt worst and several characteristics of the behaviour are more accentuated compared to those in irregular seas. This is desirable for the systematic investigations and safety point of view.

(b) The majority of the existing theoretical studies are based on regular beam sea calculations but not enough quantitative experimental data are available to validate these studies.

(c) As demonstrated in ref. [18], the steady tilt values measured in regular seas can be used for predicting the slowly-varying tilt behaviour in irregular seas.

Hence at this stage it may be desirable to concentrate on the regular sea tests, but the investigation must be extended to irregular seas in future studies.

(ii) The wave-induced forces and the low $\overline{GM}$ are mainly responsible for the tilt behaviour with some other secondary effects. As stated earlier there are different theoretical approaches for the mechanism causing the tilt in terms of the wave-induced forces.

Although it was not verified by the motion tests, there has been at least one experimental study[29] investigating the influence of the vertical second-order force on the tilt phenomenon. However, no experimental study has been carried out investigating the effects of the oscillatory forces on the phenomena, but an unequal distribution of the maximum forces on each hull could be a mechanism for tilt.

In order to explore this matter, in the thesis, the first-order oscillatory force measurements are taken on the main hulls of the model at various hull separations with emphasis on the effect of hydrodynamic interference.

(iii) The effect of viscosity could be a possible major effect causing or contributing to the tilting. In order to gain an idea of this effect, experimentally, the flow conditions around the submerged part of the model can be changed by using stimulators. This is investigated in the thesis by motion tests with the model coated with a roughened paper.

(iv) One factor causing the tilt behaviour could be a non-linear variation of the roll restoring moment due to changes in vessels position and the wave form. This is investigated during inclining tests in the still water. One cannot expect that the changes in the wave form will affect very much the roll restoring moment of a semi-submersible because of the small volumes of the columns.

(v) The effect of wave frequency on the tilt behaviour was reported differently in the previous studies. Although it occurs in short waves there are conflicting reports whether it occurs at a range of short waves or at a particular short wave for a particular model. This is cleared up in the thesis by the model tests over a wide range of frequencies.

(vi) The tilt behaviour is also highly dependent on the wave heights. There are different reports about the lower and upper limits where tilt behaviour occurs and breaks down and becomes worse. The build-up of tilt with wave heights has not been investigated by enough numbers of test runs.

Therefore the model tests are carried out over a wide range of wave heights at each frequency. This would provide the build-up of tilt-height curve which could characterise the nature of the behaviour.

(vii) One of the common conclusions of the previous studies is the effect of $\overline{GM}$ on the tilt. This effect was investigated in these studies by one or two low $\overline{GM}$ values experimentally. However, the character of the build-up of tilt at different $\overline{GM}$s could be

different since it will be dominated by the wave-induced tilting moment at small $\overline{GM}$s and by the restoring moments at higher $\overline{GM}$s.

This effect is investigated in the thesis, by testing the model over the wide range of $\overline{GM}$ values compared to the previous studies.

(viii) As known from the theory, depending on the underwater geometry, the viscous effects could be very important about the resonant frequencies where large motion amplitudes are observed and these forces increase with the increasing motion amplitudes. This is considered in the thesis by testing the model at resonant frequencies.

(ix) The experimental findings on the effect of moorings from the previous studies demonstrate conflicting results. This is considered in the thesis by testing the model with and without the moorings at particular frequencies in order to clear up the previous findings.

(x) There are also conflicting statements about the direction of the tilt observed in the previous studies. This is investigated by the exploratory motion tests in the thesis.

The above stated considerations are investigated in the thesis by the two main groups of experiments supported by the same exploratory tests. However, there may be a need for further investigations which cannot be studied experimentally because of the limits of the thesis and/or existing facilities in the laboratory. These will be stated later in the main conclusions.

The Main Objectives of the Present Study

In the scope of the above considerations this thesis attempts to extend both the experimental and theoretical knowledge of this poorly understood and potentially dangerous phenomenon.

The main objective of the experimental work is to provide reliable quantitative tilt measurements for a wide range of waves and $\overline{GM}$s in order to use for the comparison of the existing and future theoretical studies. Several factors some of which have been reported in the previous studies are investigated and cleared up by a number of other exploratory tests.

The primary objective of the theoretical work is to improve the theoretical understanding of the tilt behaviour in regular waves based on the systematic model test data provided by the experimental work. The main emphasis is to be placed on a proper determination of the wave-induced steady tilting moment mechanism from which a minimum $\overline{GM}$ to limit an undesirable amount of tilt could be obtained as proposed by Numata et al. Several hydrodynamic aspects which are related to the phenomenon are investigated in terms of wave loading and motion response of the twin hull model considered.

Chapter 3

EXPERIMENTAL WORK

3.1 INTRODUCTION

In the previous chapter, the experimental requirements to provide a more precise explanation of the phenomena were considered. In this chapter a description is given and the results presented for a major series of tests in Glasgow University's 76m × 4.6m × 2.4m model test tank. It has a plunger type wave maker at one end, a wave absorbing beach at the other. The tests were:

(i) Motion tests on a twin-circular pontoon four columns per hull semi-submersible (see Fig. 31) in regular beam seas over a range of wave frequencies and heights for five different $\overline{GM}$ values. About 300 individual runs were carried out. The wave data and the heave and roll motion response were collected as precisely as possible in all cases.

(ii) Force tests on two circular pontoons of the same diameter as the semi-submersible model but without the columns being present (see Fig. 31) in regular beam seas over the same range of wave frequencies and heights. Over 150 individual runs were carried out. The heave and sway exciting force on the single isolated pontoon and the twin pontoons were measured in captive condition at four different hull separations.

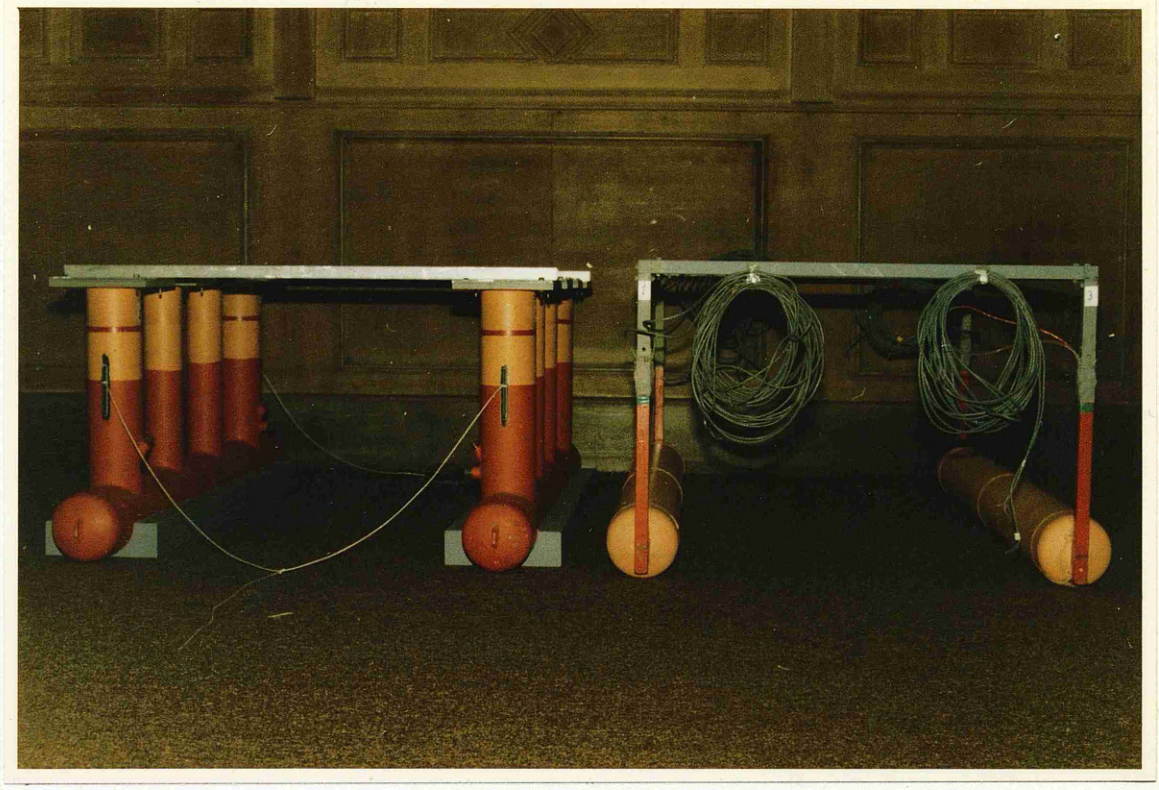

Fig. 31 - View of the models used for the motion test (on the left) and for the force test (on the right)

Beside these tests a number of other tests were carried out. These were the inclining tests, the natural frequency tests, motion tests with the coated model, motion tests with unmoored model, motion tests for the investigation of preferred direction of tilt and the effect of fairleads.

3.2 MOTION TESTS

The model used during the motion tests was a twin circular pontoon with four circular columns per hull. The intermediate columns have a smaller diameter than the end columns (see Figs 32 and 33).

The primary reason for choosing this particular design was the availability of the model at the beginning of the research. It was also thought sensible to compare the results with the existing studies which were mainly based on circular cross-section pontoons.

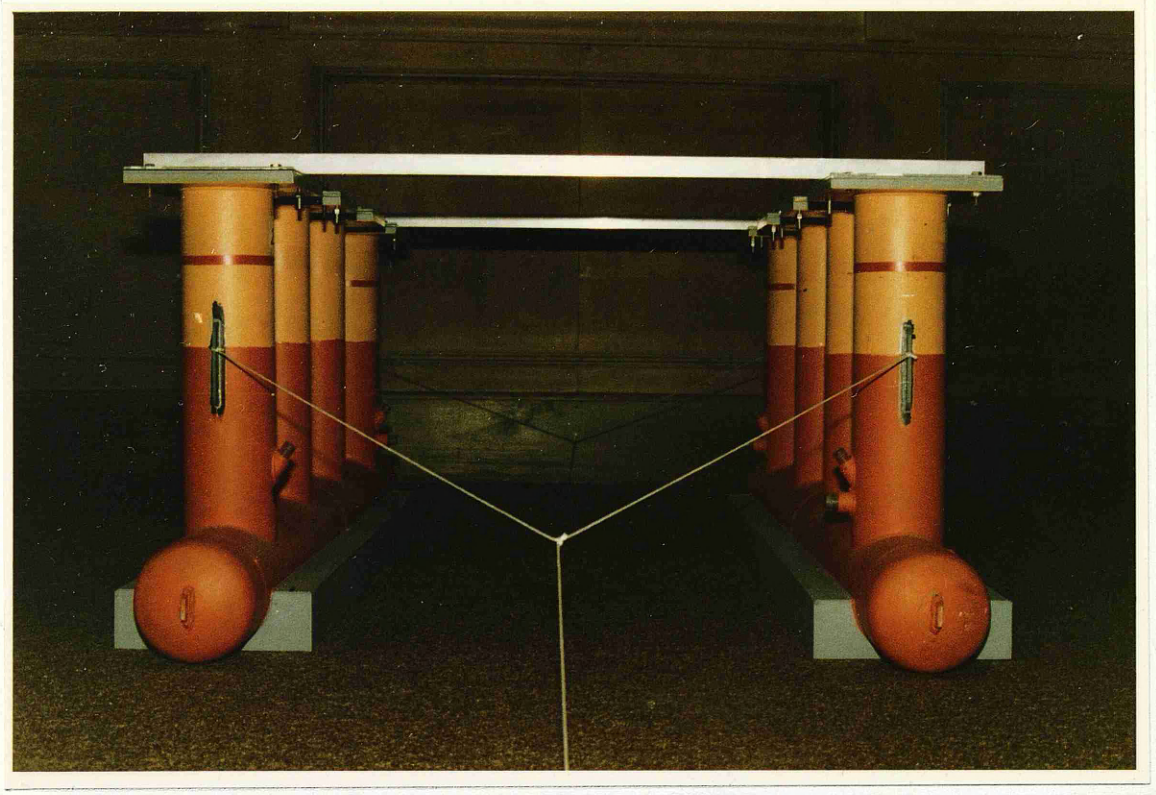

Fig. 32 - Front view of the 8-columns per hull twin-circular semi-submersible model used for the motion tests

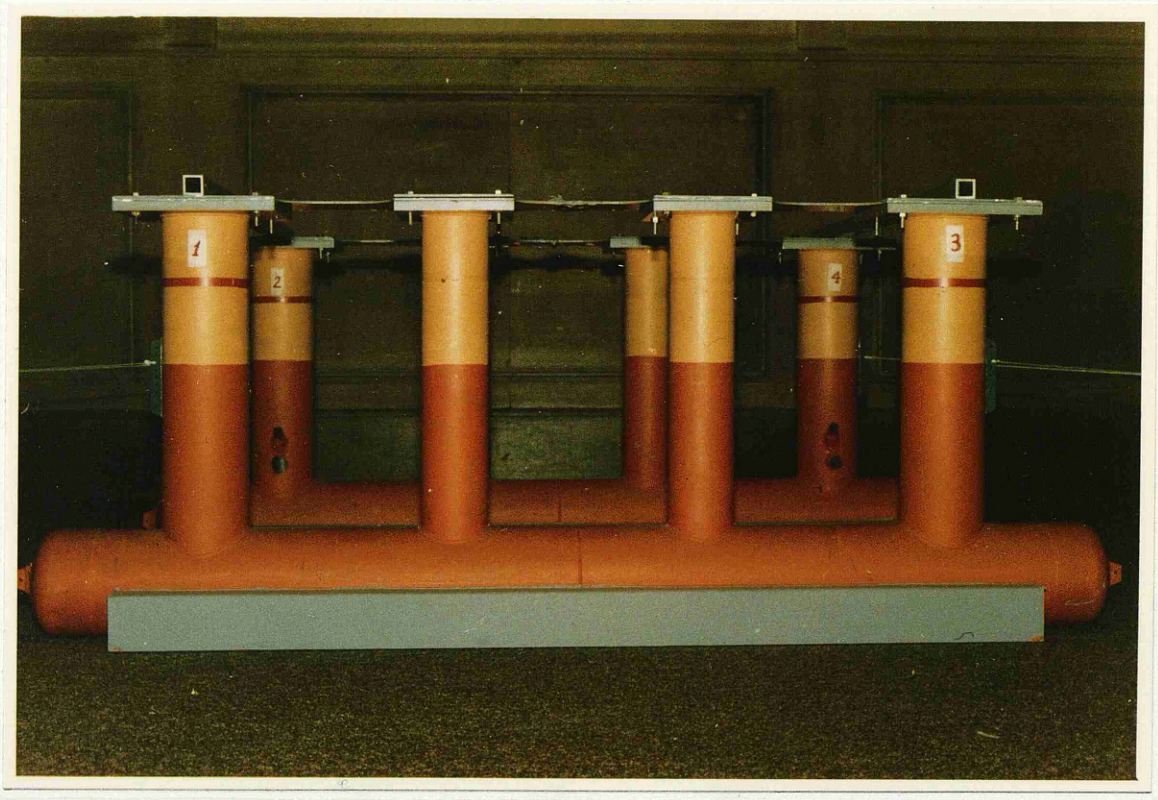

Fig. 33 - Side view of the semi-submersible model

Description of Model

The model was made to a scale of 1/70 of a prototype semi-submersible. It was constructed in two halves and connected with two transverse beams. Figure 34 shows the disassembled picture of the model.

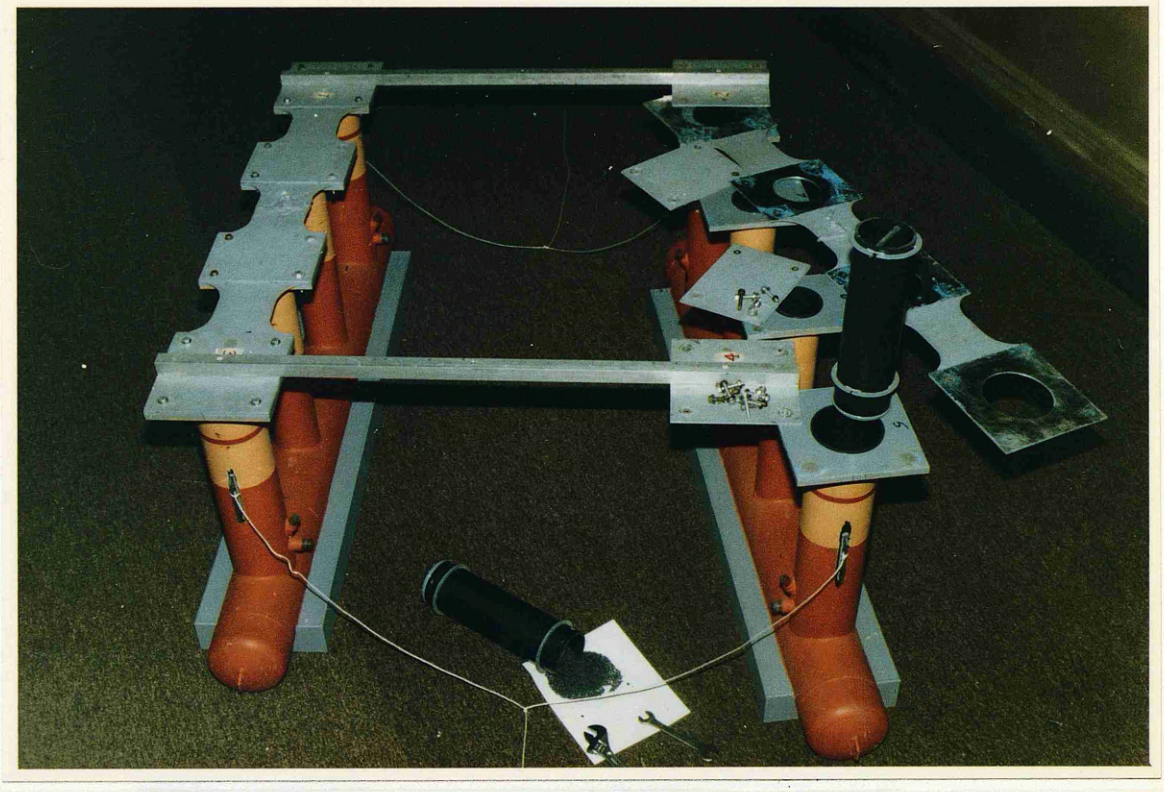

Fig. 34 - Disassembled view of the model

Although the original design had horizontal and vertical bracings, these were removed as it was believed that this complicated the analysis and introduced non-linear effects. The columns and pontoons were constructed in PVC piping and connected to each other with PVC welding. The deck was an aluminium plate running longitudinally along the model supported by PVC square plates on the columns. Transverse beams were made from aluminium tubes with square cross-sections bolted to the deck at the four corners.

The model was ballasted to 36 cms draught by using special ballast containers (see Fig. 34) which were made in PVC piping and could be moved vertically so as to adjust the CG of the model to the

$\overline{GM}$s desired. These containers were filled by leadshot and arrangements made to prevent any movement of the ballast due to model motion.

At each corner column a mooring was attached to the fairlead at a height corresponding to the CG desired as shown in Fig. 35. As shown in Figs 32 and 33 clearly, other fairleads were located at the centre of each pontoon end. The mooring arrangement for the tests are shown in Fig. 36.

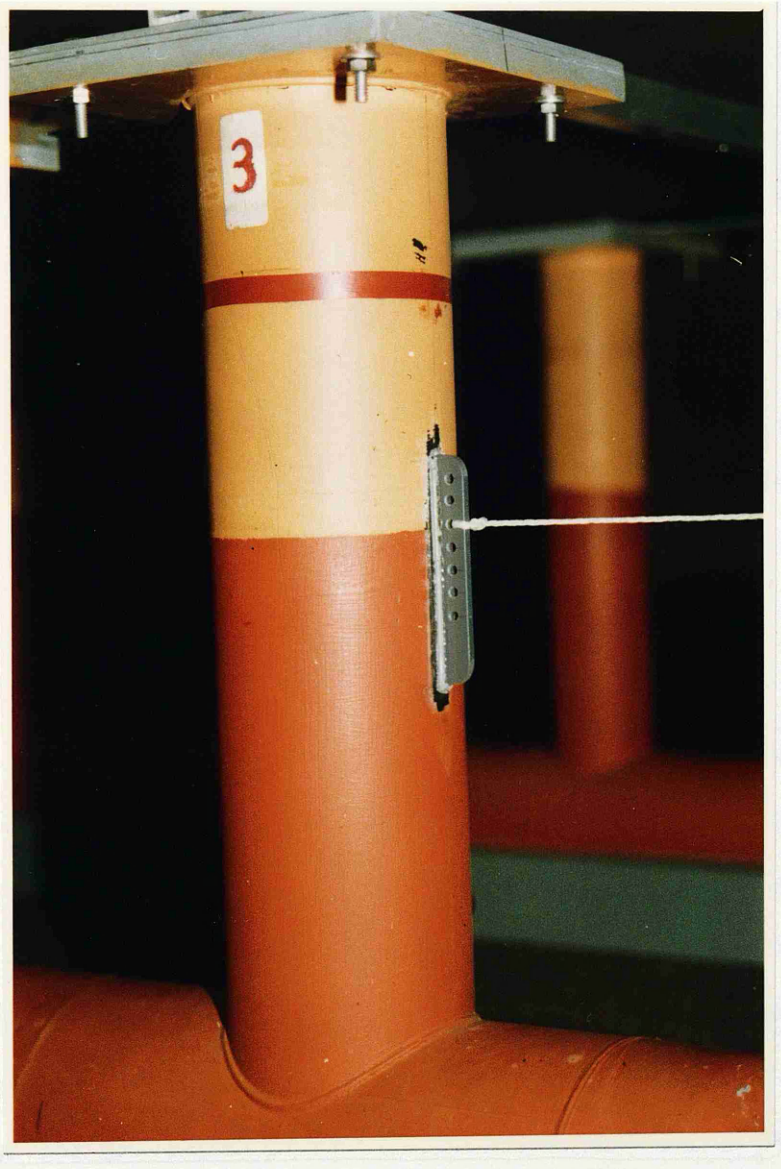

Fig. 35 - View of a fairlead attached to the corner (outer) column of the model

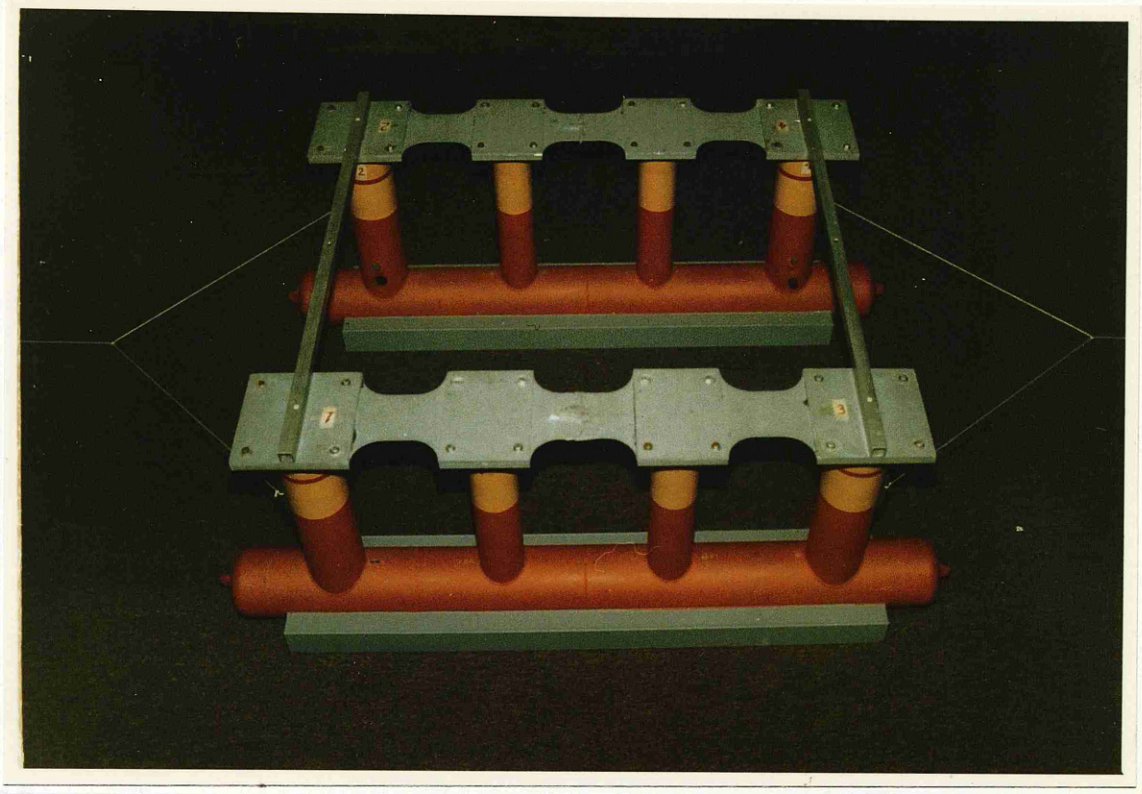

Fig. 36 - Arrangement of the moorings used for the motion tests

The main dimensions and particulars of the model are given in Fig. 37 and Table 1. In Table 1 the $\overline{GM}_T$, $\overline{KG}$, $\overline{k}_{xx}$ values and natural periods of the model as deduced from the inclining and natural period tests are given. See Appendix II.1 for the calculation of the mass moment of inertia and the radius of gyration $\overline{k}_{xx}$ for rolling.

The model hydrostatic characteristics are given in Table 2 [38] and Fig. 38. A detailed description of the mass distribution in the model for use in checking on the $\overline{GM}$ values to be tested is given in Table 3. In this table each item was weighed and its mass (w_i) and the centre of the gravity ($\overline{KG}_i$) was identified before assembly into the model. By using this data, the total displacement weight (Δ), the centre of the gravity from the baseline ($\overline{KG}$) and the metacentric height ($\overline{GM}$) of the model was calculated.

However, the actual $\overline{GM}$ and $\overline{KG}$ of the model was found from the inclining tests as follows.

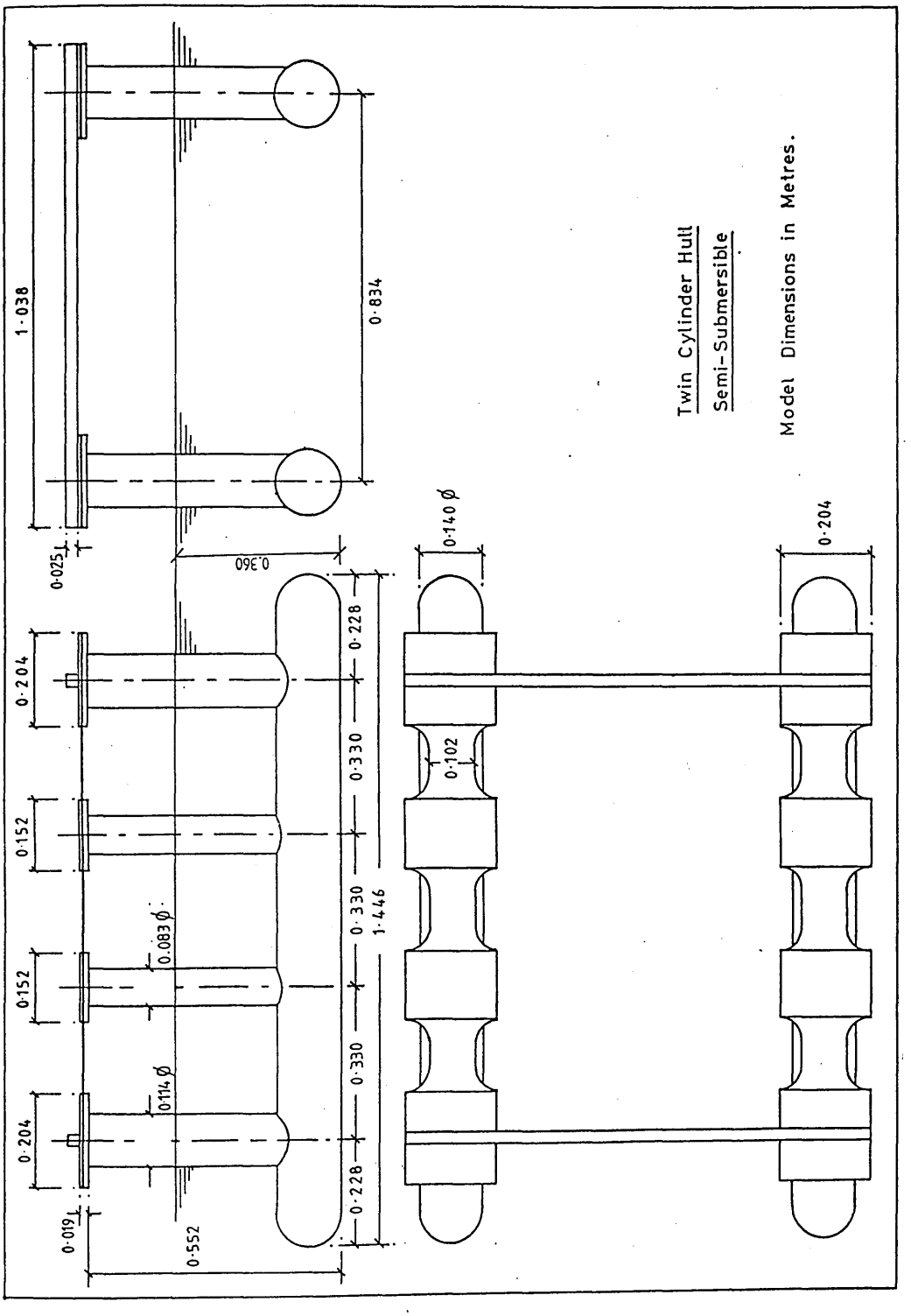

Fig. 37 - General arrangement of the semi-submersible model tested

Particulars of the Model		1/70 Model	Prototype
Length of pontoon		1.45 m	101.50 m
Radius of pontoon		0.07 m	4.90 m
Pontoon separation		0.834 m	58.38 m
Radius of small column		0.0415 m	2.905 m
Radius of large column		0.057 m	3.99 m
Draught		0.36 m	25.20 m
Displacement		58.30 kg	1996.90 ton
$\overline{KB}$		0.1125 m	7.875 m
$^{*}\overline{BM}_T$		0.188 m	13.16 m
$^{*}\overline{GM}_T$	Test series 1	0.019 m	1.33 m
	2	0.029 m	2.03 m
	3	0.038 m	2.66 m
	4	0.056 m	3.92 m
	5	0.079 m	5.53 m
$\overline{KG}$	Test series 1	0.280 m	19.60 m
	2	0.270 m	18.90 m
	3	0.261 m	18.27 m
	4	0.243 m	17.01 m
	5	0.220 m	15.40 m
$\overline{k}_{xx}$ (roll radius of gyration)	Test series 1	0.447 m	31.30 m
	2	0.448 m	31.36 m
	3	0.449 m	31.43 m
	4	0.450 m	31.50 m
	5	0.455 m	31.85 m

Natural (Period - Charac. Frequency - Radian Frequency)		S	Hz	rad.s^{-1}	S	Hz	rad.s^{-1}
Heave		2.44	0.41	2.60	20.4	0.050	0.31
Roll	Test series 1	9.00	0.11	0.69	75.3	0.013	0.08
	2	7.00	0.14	0.88	58.6	0.017	0.11
	3	6.25	0.16	1.00	52.3	0.019	0.12
	4	5.00	0.20	1.26	41.8	0.024	0.15
	5	4.00	0.25	1.57	33.5	0.030	0.19

*Subscript T indicates 'transverse'

Table 1 - Main particulars of the semi-submersible model

Draft (cm)	Displacement (cm^3)	Displacement (grms)	KB (cm)	LCB (cm)
2.25	4612.95	4728.27	1.33	72.25
4.50	12337.11	12645.54	2.64	72.25
6.75	21221.49	21752.02	3.89	72.25
9.00	26335.95	26994.34	4.56	72.25
11.25	31472.25	32259.06	4.62	72.25
13.50	39092.08	40069.38	5.48	72.25
15.75	45558.22	46697.17	7.19	72.25
18.00	46963.09	48137.17	7.48	72.25
20.25	48367.97	49577.17	7.82	72.25
22.50	49772.84	51017.16	8.20	72.25
24.75	51177.72	52457.16	8.62	72.25
27.00	52582.60	53897.16	9.08	72.25
29.25	53987.47	55337.16	9.58	72.25
31.50	55392.35	56777.16	10.11	72.25
33.75	56797.22	58217.15	10.66	72.25
36.00	58202.10	59657.15	11.25	72.25
38.25	59606.97	61097.14	11.86	72.25
40.50	61011.85	62537.14	12.49	72.25
42.75	62416.72	63977.14	13.15	72.25
45.00	63821.60	65417.14	13.82	72.25

Draft (cm)	BM (cm)	BML (cm)	Water Plane Area (cm^2)	Total Surface Area (cm^2)
2.25	2689.01	4484.09	2971.93	3334.65
4.50	544.72	533.01	3779.17	4874.59
6.75	339.21	331.53	4043.42	6207.69
9.00	261.92	256.18	3877.34	7524.56
11.25	181.25	177.74	3214.92	8992.07
13.50	67.85	66.84	1501.69	11169.17
15.75	23.97	23.34	624.39	13137.45
18.00	23.26	22.64	624.39	13694.17
20.25	22.58	21.98	624.39	14250.89
22.50	21.94	21.36	624.39	14007.61
24.75	21.34	20.78	624.39	15364.33
27.00	20.77	20.22	624.39	15921.06
29.25	20.23	19.70	624.39	16477.78
31.50	19.72	19.20	624.39	17034.50
33.75	19.23	18.72	624.39	17591.22
36.00	18.77	18.27	624.39	18147.95
38.25	18.32	17.84	624.39	18704.67
40.50	17.90	17.43	624.39	19261.39
42.75	17.50	17.04	624.39	19818.11
45.00	17.11	16.66	624.39	20374.83

Table 2 - Hydrostatic data of the semi-submersible model

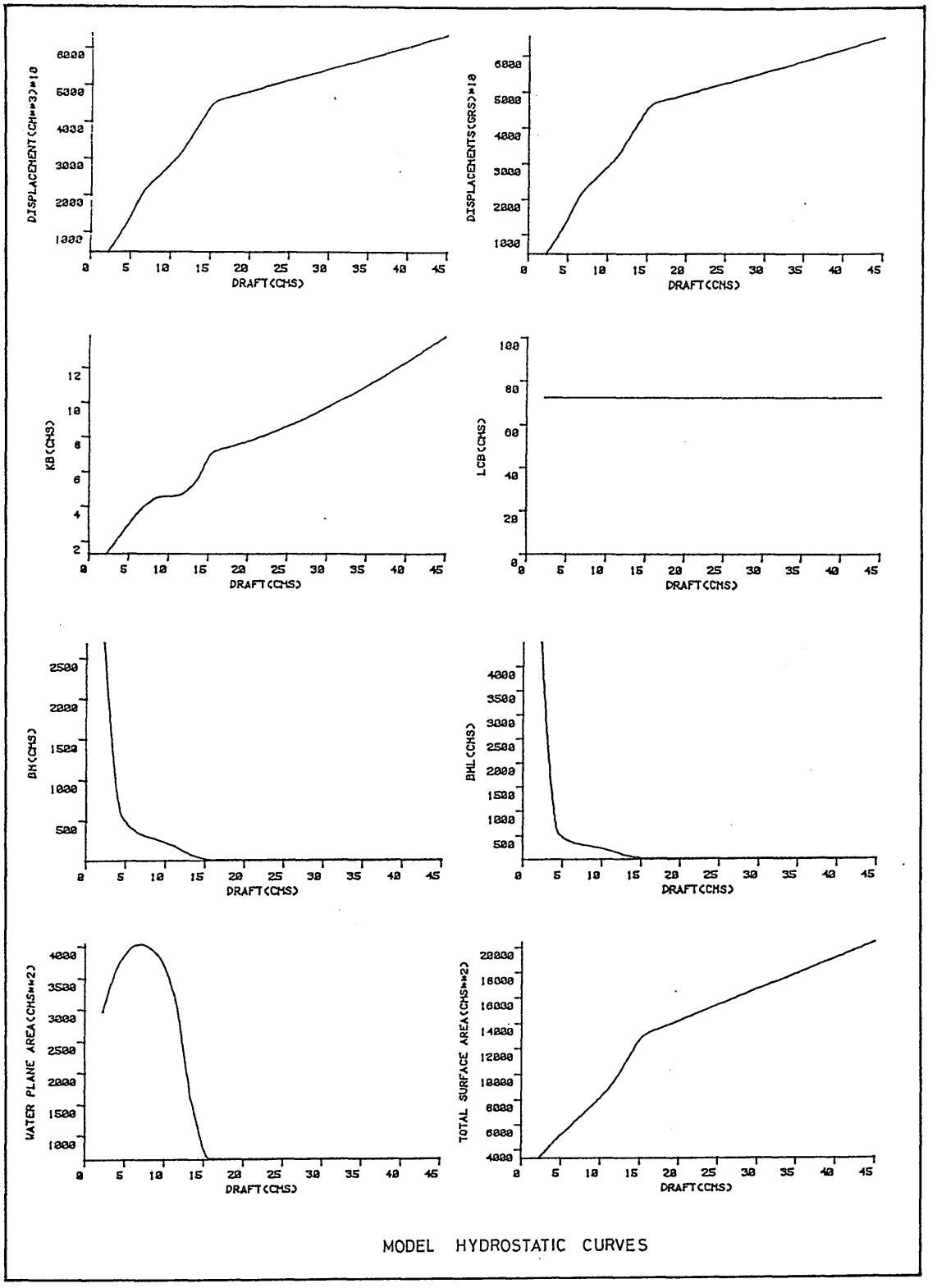

Fig. 38 - Hydrostatic curves of the semi-submersible model

Item	Number of Item i	Mass w_i (kgs)	CG from the Base Line $\overline{KG}_i$ (cms)
Hull	2	6.55	7.00
Vertical Column	8	1.00	35.35
Deck	2	4.70	57.00
Transverse Beam	2	0.825	58.25
Ballast Containers	4	0.632	17.70
Ballast	4	5.712	10.70
Bolts	32	0.015	57.00
Aluminium Brackets	2	0.100	58.00

Table 3 - Weight distribution of the semi-submersible model

Determination of $\overline{GM}$ for Each Loading Condition

$\overline{GM}$ is the essential parameter governing the tilt behaviour. Lower $\overline{GM}$'s will produce higher tilt magnitudes, so it is desirable to get a low $\overline{GM}$ in order to study the build-up of tilt with various parameters.

Therefore, in the beginning, the model's $\overline{GM}$ was set to a value close to zero by adjusting the ballast position. In this condition, it was found that, even with small wave excitations, the deck edge tended to enter the water rapidly and caused extra forces and moments due to the negligible righting moment. The model performed asymmetric motion responses (yawing, pitching) even when it was tested beam onto waves. After several trials the lower limit for the $\overline{GM}$s to be tested was identified at about 2 cms (1.4 m on full scale) for this particular vessel.

It was then decided to test this model at five different values of $\overline{GM}$ over a range varying from 2 cms to 8 cms, which was the design $\overline{GM}$[38].

By using the weight distribution data in Table 3, the model was set to approximately 2 cms $\overline{GM}$ (the ballast containers were raised from their original positions with various thicknesses of polystyrene supports inserted underneath them) for the first test series. Before the model was put into water, it was weighed and its displacement (Δ) was found as 58.300 kgs. As one loading condition was considered only, this displacement was not changed throughout all the tests and calculations. After this preparation the model was ready for the inclining test for the first test series of $\overline{GM}$ required.

3.3 INCLINING TESTS

The main objective of the inclining tests was to identify the actual $\overline{GM}$ of the model before each set of test series.

Instrumentation

The instrumentation for the inclining tests was the same as for the motion tests. The heave and roll motion response of the model was measured by a pair of gravity type LVDT (Linear Variable Differential Transformer) vertical displacement transducers with a ± 202 mm range. As shown in Fig. 39, they were attached to the subcarriage and connected with piano wires to the leeward and seaward side of the deck of the model, which was situated beam onto waves. The wires were suspended over a pulley to measure the vertical displacement at both sides. The weights of the transducers were balanced out by counter weights to avoid any inertia effects on the transducers due to motion of the model. The parameter signals, induced as a result of the motion of the model from the transducers, were digitised by the analog to digital converter (operating range bi-polar - 2.5^{V} to 2.5^{V}) and stored in files on the PDP 11/40 computer. They were also simultaneously recorded on charts by the multi-channel pen recorder.

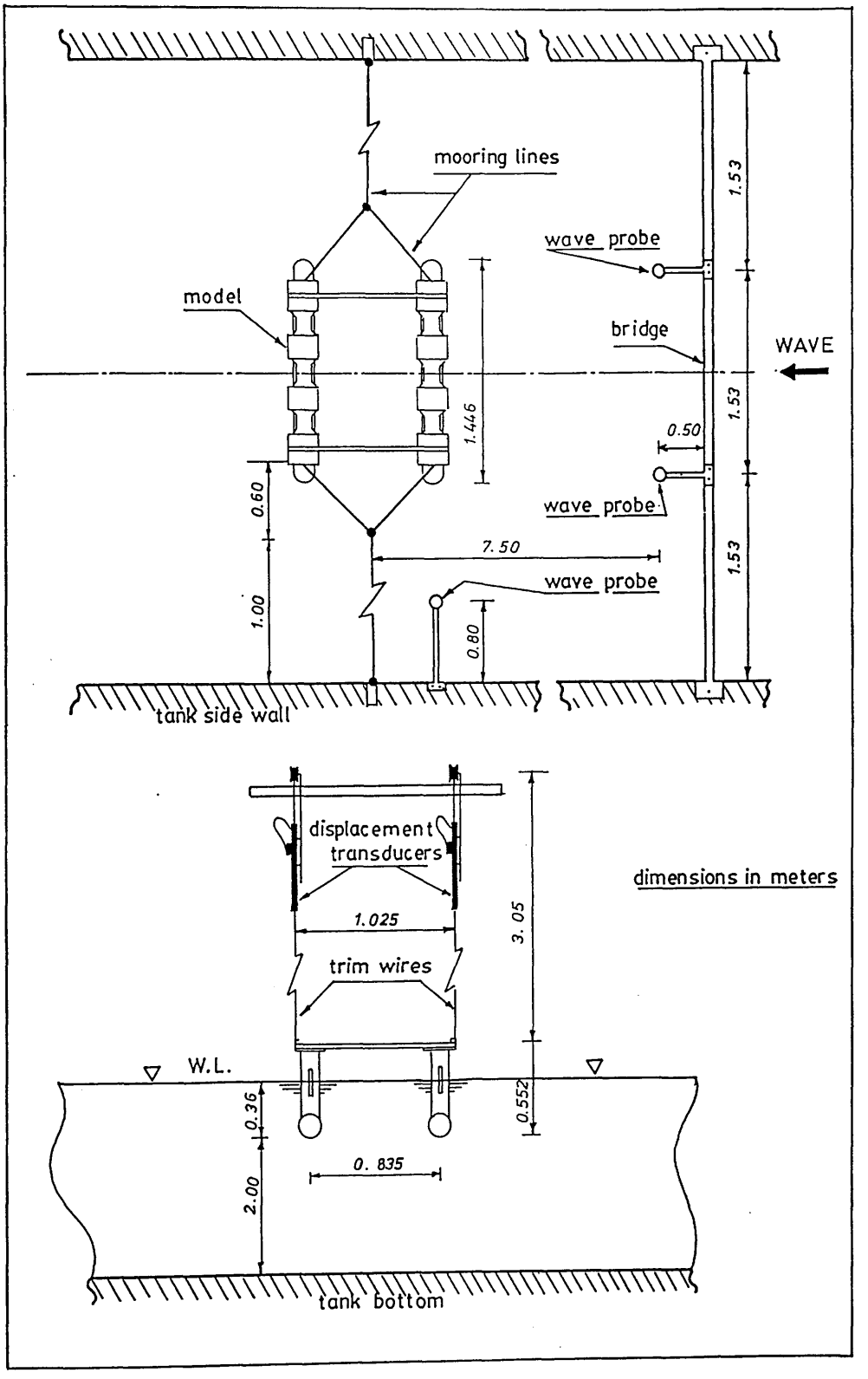

Fig. 39 - Experimental setup for the inclining test and the motion test

In order to record the model's motion responses four channels were used: two channels for the signals received from the transducers measuring the vertical motions of the leeward and seaward hulls and the other two for the signals due to the heave and roll motion responses received from a special amplifier which sums and differences the signals from the transducers to produce an output proportional to heave and roll motion response.

Calibration of Vertical Displacement Transducers (LVDT)

The model was floated in calm water at its set loading condition. Zero deflections were recorded by the pen recorder from both transducers attached to the model. Then the transducers were displaced ± 100 mm using a vertical vernier attached to the piano wire which connects the model to the transducers. At the same time, the pen deflection corresponding to the transducer was marked. The same procedure was carried out with the other transducer.

From the calibration records it was found that the responses of both transducers were identical and linear within the range of calibration. The calibration factor [K] was found by:

$$K = \frac{\textit{Vertical Displacement of Model / Corresponding Voltage}}{\textit{Deflection of Pen / Corresponding Voltage}}$$

The calibration factor K was obtained from the existing calibration program CALIBR [39] within the computer also.

Inclining Test Procedure

After the calibration, a known group of test weights were placed at the longitudinal symmetry of the deck in a row and symmetric with respect to both the longitudinal and transverse axis of the model. This provided no trim and heel on the model. The deflection corresponding to

zero level due to the addition of the test weights was marked on the chart. Progressively the centre line weights were transferred through an equal distance from the centre line of the model to the leeward direction (the weights were always kept in the same horizontal plane) and resultant heel was recorded. This was carried on up to 8° or 10° static heel was achieved. Then the weights were returned to their original position at the centre line. The same procedure was repeated by transferring the weights to the seaward side.

In Tables 4,5,6,7,8 the data belonging to the inclining tests are tabulated.

where i = number of shifts carried out

w_i = the sum of test weights transferred each time. A plus sign (+) indicates a shift from the centre line to leeward, a negative sign (-) indicates from the centre line to seaward

d_i = horizontal shift of the weights (d_i = 41.75 cms for weight transfers)

y_i = total deflection of the pen on the chart (due to sum of vertical displacement of the leeward and seaward transducers)

Y_i = total heel on the model calculated by:

$$Y_i = K \times y_i \qquad \ldots \quad (1)$$

where calibration factor K=2 found from the calibration test

ϕ_i = total heel angle calculated by:

$$\phi_i = \text{atan}[Y_i/\ell] \qquad \ldots \quad (2)$$

where ℓ is the distance between the vertical axes of the transducers, and its value ℓ=102 cms for these tests

m_i = static moments of the test weights calculated by:

$$m_i = w_i \times d_i \quad \ldots \quad (3)$$

$\overline{GM}_i$ = metacentric height, which includes the effect of test weights, after each shift calculated by:

$$\overline{GM}_i = m_i/(\Delta+w_i)\tan\phi_i \quad \ldots \quad (4)$$

$\overline{GM}$ = mean metacentric height calculated by:

$$\overline{GM} = \sum_{i=1}^{N} \overline{GM}_i/N \quad \ldots \quad (5)$$

where $\overline{GM}$ includes the effect of test weights which should be corrected to have the model's actual GM.

In the following the procedure for this correction is given only for the first test series (smallest $\overline{GM}$) by using Table 4. The remaining $\overline{GM}$s were corrected as shown in Tables 5 through 8 by the same procedure.

From Table 4 and eq.(5), $\overline{GM}$ value to be corrected is found:

$\overline{GM}$ = 1.695 cms

The model displacement Δ_c = 58.300 kgs

The sum of test weights Σw_i = 0.400 kgs

Number of shifts i = 1 to 8

Total displacement $\Delta = \Delta_c + \Sigma w_i$ = 58.700 kgs

In order to find $\overline{KG}$ value corresponding to the total displacement (Δ), the following relationship is used:

$$\overline{KG} = \overline{KB} + \overline{BM} - \overline{GM} \quad \ldots \quad (6)$$

by substituting:

$\overline{KB}$ (vertical buoyancy centre) = 10.86 cms for Δ = 58.700 kgs from Fig. 38 or Table 2

$\overline{BM}$ (transverse metacentre) = 19.07 cms for Δ = 58.700 kgs from Fig. 38 or Table 2

into eq.(6) it follows that KG = 28.23 cms.

The static moments of the model and weights together about the base line are equal to the sum of the moment due to the model itself and weights, i.e.

$$\overline{KG}\ \Delta = \overline{KG}_c\ \Delta_c + \overline{Kg}_i\ \Sigma w_i \qquad \ldots \quad (7)$$

where $\overline{KG}_c$ = corrected $\overline{KG}$ value of the model which excludes the effect of test weights

$\overline{Kg}_i$ = $\overline{KG}$ values of the test weights ($\overline{Kg}_i$ = 60 cms since the weights were kept in the same horizontal plane).

By substituting the values of KG, Δ, Δ_c and $\overline{Kg}_i$ into eq.(7) the corrected $\overline{KG}_c$ is found as:

$\overline{KG}_c$ = 28.02 cms

On the other hand $\overline{KB}_c$ and $\overline{BM}_c$ values corresponding to the displacement Δ_c = 58.300 kgs from Fig. 38 or Table 2 are:

$\overline{KB}_c$ = 10.70 cms and $\overline{BM}_c$ = 19.20 cms

The substitution of $\overline{KG}_c$, $\overline{KB}_c$, $\overline{BM}_c$ into eq.(6) yields the corrected $\overline{GM}_c$ as follows:

$\overline{GM}_c$ = 1.88 cms

i	w_i (grs)	d_i (cms)	y_i (cms)	Y_i (cms)	ϕ_i (Degrees)	m_i (gr × cm)	$\overline{GM}_i$ (cms)	Δ_c = 58300 grs Σw_i = 400 grs Δ = 58700 grs
1	+ 100	41.75	2.00	4.00	2.24	4175	1.81	$\overline{GM}$ = 1.695 cms
2	+ 200	"	4.20	8.40	4.71	8350	1.74	$\overline{KB}$ = 10.86 cms
3	+ 300	"	6.35	12.70	7.10	12525	1.72	$\overline{BM}$ = 19.07 cms
4	+ 400	"	8.10	16.20	9.02	16700	1.80	$\overline{KG}$ = 28.23 cms
5	- 100	"	2.35	4.70	2.64	4175	1.55	$\overline{KG}_c$ = 28.02 cms
6	- 200	"	4.60	9.20	5.15	8350	1.59	$\overline{KB}_c$ = 10.70 cms
7	- 300	"	6.65	13.30	7.43	12525	1.65	$\overline{BM}_c$ = 19.20 cms
8	- 400	"	8.62	17.20	9.57	16700	1.70	$\overline{GM}_c$ = 1.88 cms

Table 4

i	w_i (grs)	d_i (cms)	y_i (cms)	Y_i (cms)	ϕ_i (Degrees)	m_i (gr × cm)	$\overline{GM}_i$ (cms)	Δ_c = 58300 grs Σw_i = 600 grs Δ = 58900 grs
1	+ 200	41.75	2.775	5.55	3.11	8350	2.61	$\overline{GM}$ = 2.63 cms
2	+ 300	"	4.125	8.25	4.62	12525	2.63	$\overline{KB}$ = 10.94 cms
3	+ 500	"	6.90	13.80	7.70	20875	2.62	$\overline{BM}$ = 19.01 cms
4	+ 600	"	8.15	16.30	9.10	25050	2.66	$\overline{KG}$ = 27.32 cms
5	- 200	"	2.675	5.35	3.00	8350	2.70	$\overline{KG}_c$ = 26.98 cms
6	- 200	"	4.20	8.40	4.71	12525	2.58	$\overline{KB}_c$ = 10.70 cms
7	- 500	"	6.95	13.90	7.76	20875	2.60	$\overline{BM}_c$ = 19.20 cms
8	- 600	"	8.15	16.30	9.10	25050	2.66	$\overline{GM}_c$ = 2.92 cms

Table 5

i	w_i (grs)	d_i (cms)	y_i (cms)	Y_i (cms)	ϕ_i (Degrees)	m_i (gr × cm)	$\overline{GM}_i$ (cms)	Δ_c = 58300 grs Σw_i = 800 grs Δ = 59100 grs
1	+ 200	41.75	2.175	4.35	2.44	8350	3.31	$\overline{GM}$ = 3.37 cms
2	+ 400	"	4.325	8.65	4.85	16700	3.33	$\overline{KB}$ = 11.02 cms
3	+ 700	"	7.475	14.95	8.34	29225	3.37	$\overline{BM}$ = 18.95 cms
4	+ 800	"	8.725	17.45	9.71	33400	3.30	$\overline{KG}$ = 26.60 cms
5	- 200	"	2.10	4.20	2.36	8350	3.43	$\overline{KG}_c$ = 26.14 cms
6	- 400	"	4.25	8.50	4.76	16700	3.39	$\overline{KB}_c$ = 10.70 cms
7	- 600	"	6.375	12.75	7.12	25050	3.39	$\overline{BM}_c$ = 19.20 cms
8	- 800	"	8.33	16.66	9.24	33400	3.46	$\overline{GM}_c$ = 3.76 cms

Table 6

Tables 4,5 & 6 - Inclining test data for varying $\overline{GM}$'s

i	w_i (grs)	d_i (cms)	y_i (cms)	Y_i (cms)	ϕ_i (Degrees)	m_i (gr × cm)	$\overline{GM}_i$ (cms)	Δ_c = 58300 grs Σw_i = 1000 grs Δ = 59300 grs
1	+ 200	41.75	1.35	2.70	1.51	8350	5.32	$\overline{GM}$ = 5.04 cms
2	+ 400	"	2.75	5.50	3.10	16700	5.22	$\overline{KB}$ = 11.10 cms
3	+ 800	"	5.75	11.50	6.43	33400	5.00	$\overline{BM}$ = 18.88 cms
4	+1000	"	7.10	14.20	7.92	41750	5.05	$\overline{KG}$ = 24.94 cms
5	- 200	"	1.50	3.00	1.68	8350	4.79	$\overline{KG}_c$ = 24.34 cms
6	- 400	"	2.85	5.70	3.20	16700	5.04	$\overline{KB}_c$ = 10.70 cms
7	- 800	"	5.80	11.60	6.50	33400	4.95	$\overline{BM}_c$ = 19.20 cms
8	-1000	"	7.25	14.50	8.1	41750	4.95	$\overline{GM}_c$ = 5.56 cms

Table 7

i	w_i (grs)	d_i (cms)	y_i (cms)	Y_i (cms)	ϕ_i (Degrees)	m_i (gr × cm)	$\overline{GM}_i$ (cms)	Δ_c = 58300 grs Σw_i = 1600 grs Δ = 59900 grs
1	+ 400	41.75	2.05	4.1	2.30	16700	6.93	$\overline{GM}$ = 7.08 cms
2	+ 800	"	4.00	8.00	4.48	33400	7.11	$\overline{KB}$ = 11.35 cms
3	+1200	"	6.10	12.2	6.82	50100	6.99	$\overline{BM}$ = 18.70 cms
4	+1600	"	7.80	15.8	8.8	66800	7.19	$\overline{KG}$ = 22.97 cms
5	- 400	"	2.02	4.04	2.27	16700	7.03	$\overline{KG}_c$ = 21.95 cms
6	- 800	"	3.9	7.8	4.37	33400	7.29	$\overline{KB}_c$ = 10.70 cms
7	-1200	"	6.0	12.0	6.70	50100	7.12	$\overline{BM}_c$ = 19.20 cms
8	-1600	"	8.10	16.20	9.02	66800	7.02	$\overline{GM}_c$ = 7.95 cms

Table 8

Table 7 & 8 - Inclining test data for varying $\overline{GM}$'s

As shown in Tables 4 through 8 $\overline{GM}_c$ values, which were calculated at the positions after each transfer of weights differ from each other by 14% in the first test series, and average 5% in the other test series. This experimental error was the worst in the first test series since the model was very sensitive to small asymmetric shifts of the weights which produced relatively large asymmetric heel angles and thus magnified the errors in $\overline{GM}$.

Therefore this error was borne in mind and the above calculated $\overline{GM}_c$ and $\overline{KG}_c$ value was approximated to the values presented in Table 1. (Note that there is no subscript (c) in the notations of this value in Table 1. From now on wherever $\overline{KG}$ and $\overline{GM}$ are mentioned, it will be understood that they are the actual corrected values.)

3.4 NATURAL PERIOD TESTS

Before commencing each series of motion tests, the natural heave and roll periods were found from the free motion tests.

For the natural period in heave mode, the model was pushed down symmetrically at a certain draught and released to perform a free oscillation. Its motion response was recorded on the pen recorder chart as shown in Fig. 40. The heave period was determined by taking average cycle time over a number of cycles. The same procedure was repeated at least three times for each series of tests and mean values taken.

For the roll mode the model was heeled to one side symmetrically by applying a downward force and released to perform free roll oscillations. The roll response was recorded as shown in Fig. 40. This procedure was repeated by applying the downward force to the opposite side. The roll periods were measured as in the heave mode and average values taken.

By making use of the natural period test measurements, the added mass and the non-dimensional damping factor were evaluated as explained in Appendix II.2.

The measured natural periods and frequency values for each test series are presented in Table 1.

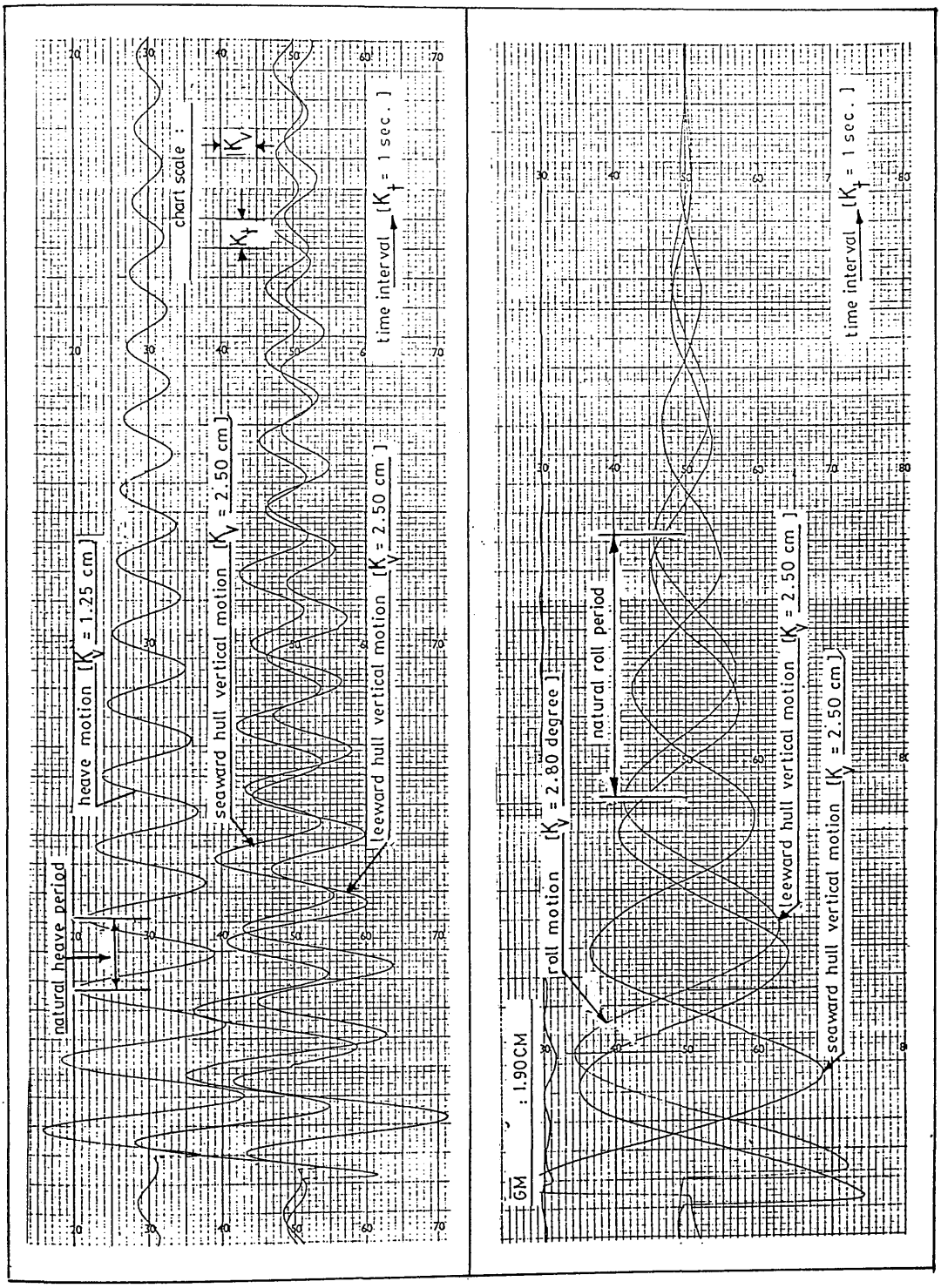

Fig. 40 - Chart records for the natural heave and roll period test

Instrumentation for the Motion Tests

During the majority of the tests the model was moored beam onto the waves on the centre line of the tank. The mooring was light nylon lines attached at the level of the CG of the model and to the tank sides to give a soft spring effect (see Fig. 39). The instrumentation was set to record the amplitudes of the regular wave trains as well as the amplitudes of the heave and roll motions of the model.

As mentioned earlier in the inclining tests instrumentation, the heave and roll motion response was measured by two linear displacement transducers.

The regular waves were created by a plunger type wavemaker driven by an electronically controlled hydraulic pump. The wave heights were measured by three resistance type wave probes. Two probes were placed between the wavemaker on the bridge and the model and one alongside the model as shown in Fig. 39. The distance between two probes on the bridge and the one alongside the model was about 7.0 m. These probes induced an electrical signal whose strength changes as the waves pass the probes. The signals were amplified, digitised and stored in a file in the computer during the tests. They were also simultaneously recorded on the pen recorder charts. The wave height measurements can be made to an accuracy of the order of ±2 mm but due to the presence of small transverse waves at some frequencies, the height measurement of the wave travelling along the length of the tank may be in error by ± 3 mm.

As the model surges, its position relative to the wave probe will vary and thus the phase angle between the wave and model motion as recorded are open to some error due to this effect.

Calibration of Wave Probes

All wave probes were submerged up to 3/4 of their lengths into the tank when the water was calm and zero readings on the wave probe amplifiers were taken. At the same time the positions of the pens corresponding to the zero deflections were marked on the charts. Progressively the calibration process was continued by lifting the wave probes gradually at about 5 cms intervals up to 15 cms and at each step the new deflections were recorded. From the calibration records linear relationships were found between the displacement of the wave probes and deflections of the pens on the charts.

Then the calibration factor (slope of the calibration curve) K_w was calculated by:

$$K_w = \frac{\textit{Displacement of Probe / Corresponding Voltage}}{\textit{Deflection of Pen / Corresponding Voltage}}$$

K_w was obtained from the calibration program CALIBR as well.

Description of Wave Range

The producible range of waves by the wavemaker in the model tank is shown in Fig. 41[40]. The limits for the characteristic frequency range were 0.3 Hz to 1.4 Hz and for wave heights, 2 cms to 20 cms. In full scale these limits correspond to a radian frequency of 0.23 to 1.05 rs^{-1} (a period of 6 to 28 sec) and a height of 1.4 to 14 m.

Prior to commencing systematic measurements, the model with the smallest $\overline{GM}$ condition was tested through the above range of wave frequencies with an increment of 0.1 Hz. The test demonstrated steady tilt at a range of frequencies as shown in the first row of Table 9.

After the frequency range was determined, the wave heights imposed were varied in a wide range as shown in Table 9. In order to study the effect of wave height on the tilt, there was a need for test

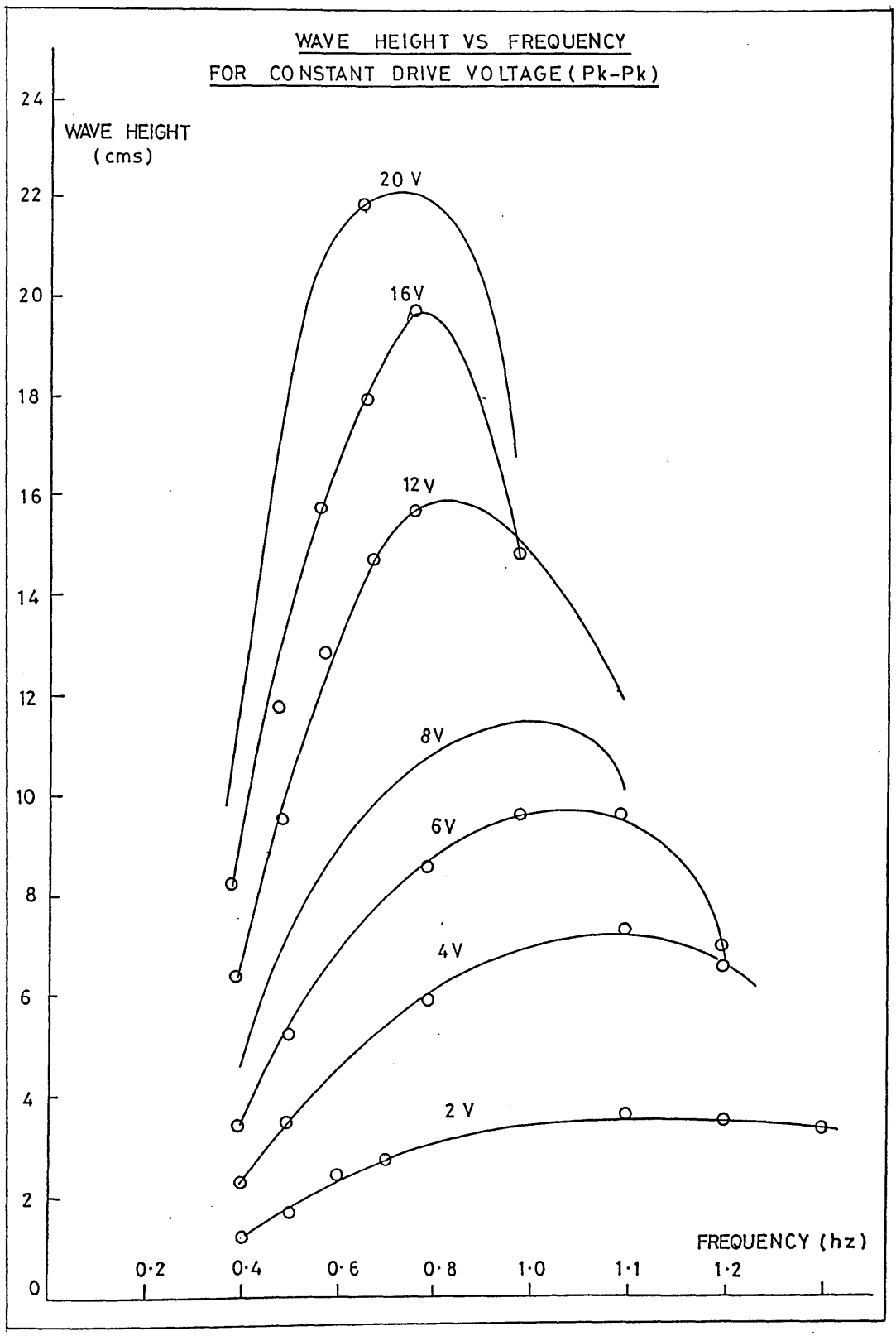

Fig. 41 - The producible range of waves by the wavemaker in the model tank[40]

runs at this wide range of wave heights with fine increments which could cause large changes in tilt magnitude for small $\overline{GM}$s.

Obviously the range of the wave to induce a noticeable tilt was dependent on the $\overline{GM}$ tested as presented in Table 9.

$\overline{GM}$ (cms)	Characteristic Frequency (Hz)	W. Amplitude (cms)
1.9	from 0.4 to 1.2 by 0.1 increment	from 8.0 to 19.0
2.9	" " " " " " "	" 8.6 to 19.0
3.8	" " " " " " "	" 9.0 to 19.0
5.6	" " " " " " "	" 10.6 to 19.0
7.9	" 0.3 " " " " "	" 10.8 to 20.0

Table 9 - The range of waves tested for the motion tests

Motion Test Procedure

As defined earlier the signals from a total of 7 channels (2 for the vertical motion of the leeward and seaward pontoon, 1 for the heave motion, 1 for the roll motion, 3 for the wave elevations) were recorded and stored by the multichannel pen recorder and computer simultaneously.

Each test run was preceeded and followed by a 'zero' measurement in calm water. Before a test run was recorded, the wavemaker was started and a period of time allowed for the waves to arrive at the model and wave height to stabilise at the correct value. The duration of a test run was 1.2 minutes and 64 secs (512 sample intervals) of this period were stored by the data collecting program RUNDAT[39]. A generous time was allowed for the tank to calm between test runs.

Description of Motion Records

Typical time history records of the motions are shown in Fig. 42 obtained from the multi-channel pen recorder and Fig. 43 from the stored data by the computer for the same test run.

As shown in Fig. 42, the records are the deflections versus real time scaled by a chart speed factor. As denoted on the chart, two records present the deflections received from both transducers due to the vertical motion of the leeward and seaward pontoons. The other two records are the deflections due to the heave and roll motions of the model received from the sum and difference amplifier. The last record on this chart is the deflection for the wave elevation received from the wave probe alongside the model.

The scale factors for the deflections and time are denoted by $[K_v]$ and $[K_t]$ and given for each record separately as shown in Fig. 42.

Figure 43 was produced from the stored data by the computer file for the same sample run. Figure 43a shows the vertical motion of the leeward and seaward hull, while Fig. 43b shows the corresponding heave motion. The roll motion is shown in Fig. 43c, while Fig. 43d is the wave elevation record.

As shown in Fig. 43c, at the beginning of the test a large tilt developed following the first impact of the wave and it then settled down to a lower value about which it oscillates. In order to investigate the variation of this behaviour, the back-bone curve was plotted in Fig. 44 by calculating the mean value of each peak point.

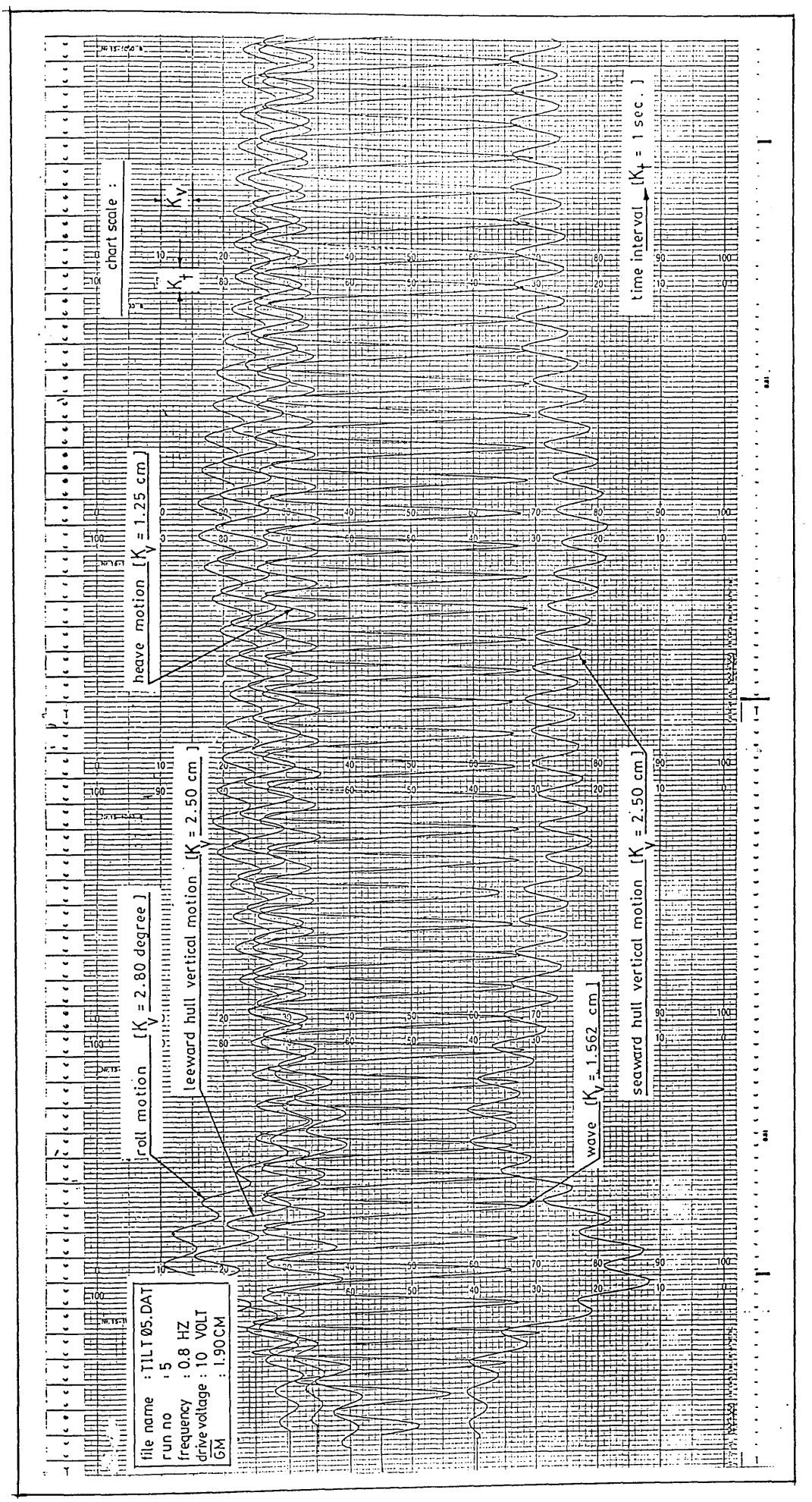

Fig. 42 - Chart record for the motions of the model from the multi-channel pen recorder

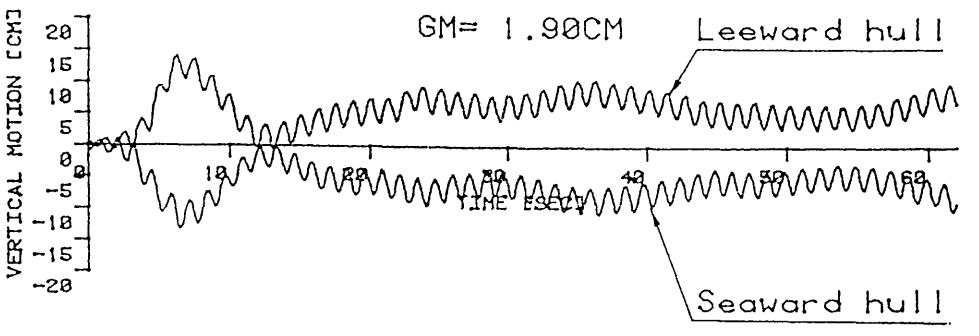

Fig. 43a

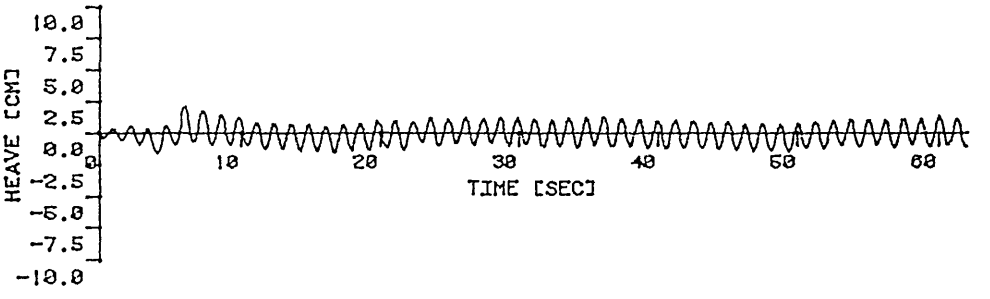

Fig. 43b

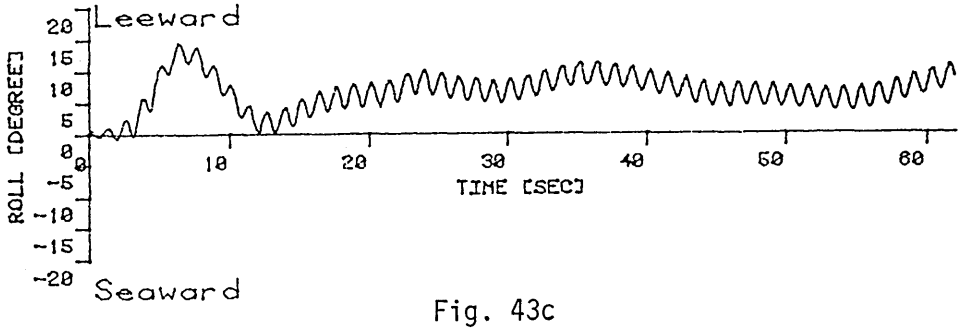

Fig. 43c

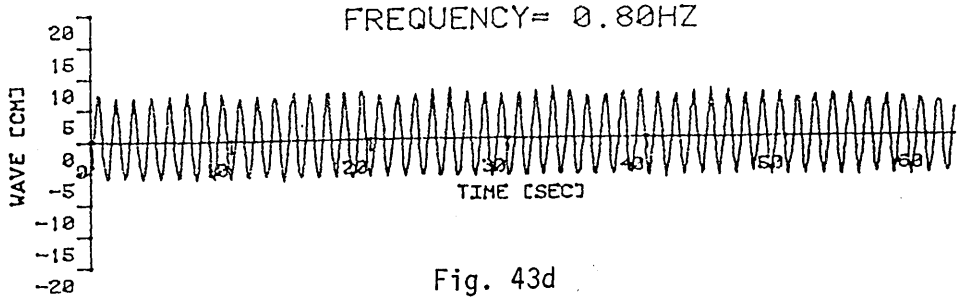

Fig. 43d

Fig. 43 - Chart record for the motions of the model from computer file [TILTØ5.DAT]

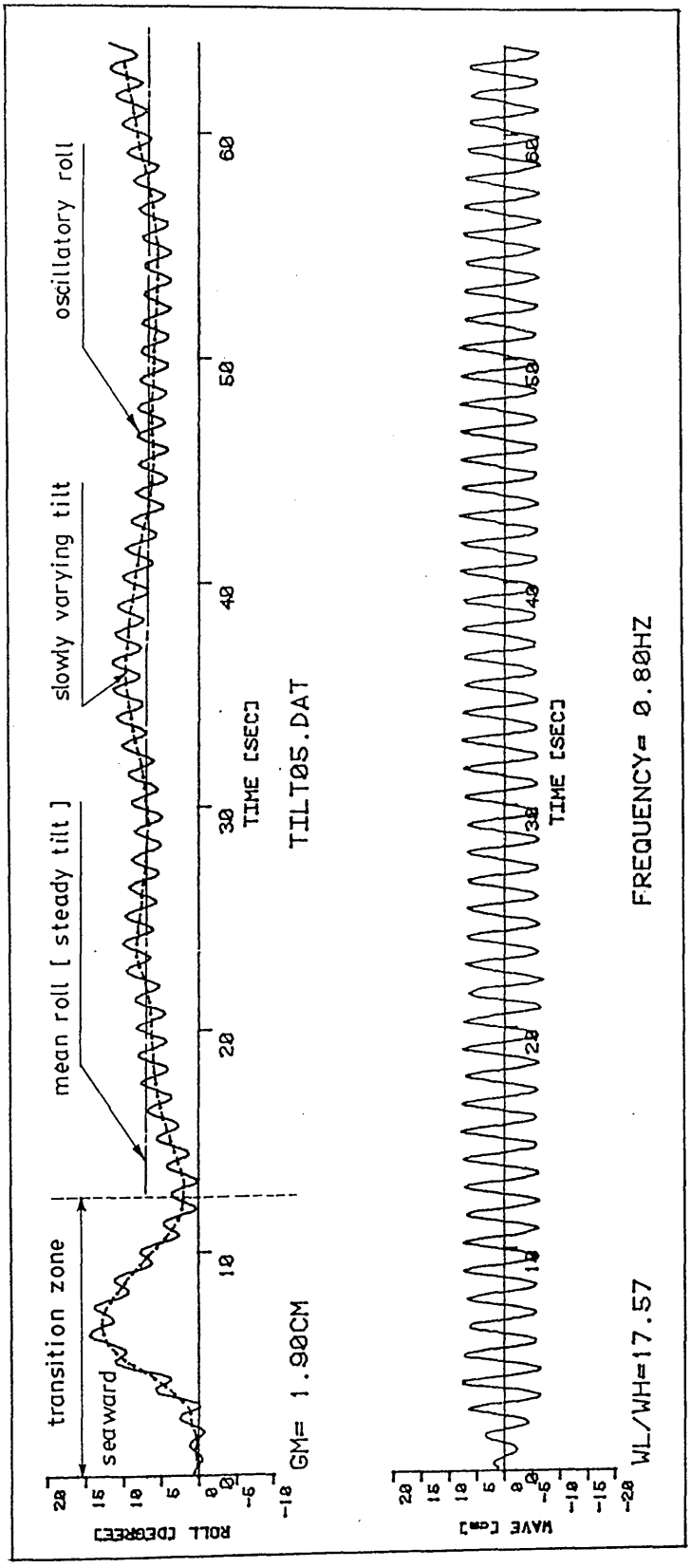

Fig. 44 - Illustration of the oscillatory roll, steady tilt and slowly varying tilt motion on a sample chart record. (Where WL and WH indicate the wave length and wave height respectively.)

Analysis of Measurements

In the typical time history records given in Figs 42, 43 and 44, the vertical motion, heave and roll motion response was observed in two different characters:

(i) A steady translation (usually slowly-varying as a result of the changes in wave height) about the initial position, and

(ii) Oscillatory motion about this steady position.

In Tables 10 through 14 the wave characteristics and the resulting two different characters of the motion responses are presented for each test series. The columns in these tables are explained as follows:

Column 1: Test run files, where the motion data stored by the computer presented as in the form of -TILT [run number].DAT - (e.g. TILTØ5.DAT). Each test run has an individual file which is identified with run number and each file has 5 different records collected over 512 sample intervals [1 sample = 0.125 sec].

Column 2: The characteristic wave frequencies used during the tests are presented in (Hz).

Column 3: The wave amplitudes calculated at each peak excluding the duration corresponding to the transient wave impact zone (see Fig. 44) and average taken over the peaks considered for each test run. The values presented are in (cms).

Although the wave elevation was measured at three different places to see the effects of reflections due to the tank walls, the wave beach, the model, etc., in this column the wave elevation, which is measured by the wave probe next to the model, is considered. The difference between the other probes measurements are discussed later in the thesis.

Column 4: The ratio of wave length to wave height (WL/WH)

Column 5: The magnitudes of the steady tilt in (degrees). As shown in Fig. 44, following the transient behaviour due to the first impact of the wave, the rolling oscillation takes place about a steady tilt position. Although this tilt is fairly steady once it settles down, there is some fluctuation (slow variation) which is believed to be due to slight changes in the wave conditions. The magnitude of the steady tilt was calculated by taking the mean value of the motion curve over the recording time by excluding the transient zone.

A minus sign indicates the tilt developed in the seaward direction.

Column 6: The steady heave motion response in (cms) calculated by the same procedure explained in Column 5. A minus sign represents the steady heave in the downward direction.

Column 7: The oscillatory roll motion response presented as Response Amplitude Operator (RAO) in (Degrees/cms) defined by:

RAO = Motion Amplitude / Wave Amplitude

where the motion amplitudes were calculated in the same manner in Column 3 at each peak and average taken over the peaks considered.

Column 8: The oscillatory heave motion response presented by the RAO for heave similar to Column 7.

Each table shows the measurements of each test series with different $\overline{GM}$.

$\bar{GM}$ = 1.90 cm

1	2	3	4	5	6	7	8
Run Data File No:	Characteristic W.Frequency (Hz)	W.Amplitude (cm)	W.Length / W.Height	Steady Tilt (Degree)	Steady Heave (cm)	Oscillatory Roll RAO (Degree/cm)	Oscillatory Heave RAO
TILT46.DAT	0.4	5.09	95.86	0.97	-0.11	0.220	2.275
TILT47.DAT		5.39	90.52	0.87	0.05	0.186	2.309
TILT44.DAT	0.5	6.40	48.79	0.16	0.10	0.263	0.265
TILT41.DAT	0.6	6.60	33.00	1.06	0.18	0.314	0.391
TILT42.DAT		8.47	25.60	2.02	0.13	0.279	0.346
TILT43.DAT		9.48	22.87	1.52	0.26	0.271	0.334
TILT35.DAT	0.7	6.04	26.38	1.90	0.23	0.307	0.297
TILT40.DAT		6.74	23.64	2.97	-0.02	0.284	0.278
TILT36.DAT		7.27	21.91	5.92	0.15	0.292	0.277
TILT39.DAT		7.77	20.50	3.32	0.24	0.286	0.282
TILT37.DAT		8.49	18.75	8.51	0.08	0.281	0.293
TILT38.DAT		9.47	16.83	12.15	0.05	0.296	0.291
TILTØ7.DAT	0.8	5.90	20.67	2.89	0.23	0.276	0.151
TILTØ9.DAT		6.42	19.00	5.58	-0.11	0.269	0.163
TILTØ5.DAT		6.94	17.57	6.92	0.10	0.271	0.162
TILT1Ø.DAT		7.85	15.53	15.71	0.05	0.292	0.193
TILT11.DAT	0.9	5.18	18.61	3.25	0.46	0.287	0.054
TILT12.DAT		5.64	17.09	7.81	0.57	0.303	0.074
TILT13.DAT		6.36	15.16	11.78	0.40	0.302	0.099
TILT14.DAT		7.23	13.33	15.97	0.09	0.297	0.119
TILT17.DAT	1.0	4.86	16.06	1.88	0.21	0.241	0.049
TILT18.DAT		5.25	14.87	2.33	0.33	0.242	0.045
TILT19.DAT		5.30	14.71	3.37	0.51	0.270	0.048
TILT2Ø.DAT		5.91	13.21	10.70	0.24	0.300	0.071
TILT21.DAT		6.27	12.45	15.23	0.03	0.315	0.095
TILT23.DAT	1.1	4.30	15.00	1.13	0.29	0.187	0.083
TILT24.DAT		4.94	13.06	1.81	0.27	0.181	0.076
TILT25.DAT		5.49	11.76	1.53	0.30	0.184	0.067
TILT26.DAT		6.16	10.46	2.16	0.49	0.170	0.061
TILT27.DAT		6.44	10.01	7.33	0.18	0.180	0.046
TILT28.DAT		6.71	9.61	12.16	0.15	0.171	0.041
TILT29.DAT	1.2	4.51	12.02	0.98	0.11	0.083	0.090
TILT30.DAT		4.94	10.97	1.23	0.18	0.083	0.090
TILT32.DAT		5.13	10.57	1.53	0.26	0.101	0.108
TILT31.DAT		5.17	10.48	1.32	0.21	0.083	0.085
TILT33.DAT		5.28	10.27	2.35	0.14	0.093	0.083
TILT34.DAT		5.32	10.19	4.11	0.00	0.099	0.082

Table 10 - Experimental wave and motion data analysed for $\bar{GM}$ = 1.90 cms

$\overline{GM}$ = 2.90 cm

1	2	3	4	5	6	7	8
Run Data File No:	Characteristic W.Frequency (Hz)	W.Amplitude (cm)	W.Length / W.Height	Steady Tilt (Degree)	Steady Heave (cm)	Oscillatory Roll RAO (Degree/cm)	Oscillatory Heave RAO
TILT144.DAT	0.4	4.75	102.71	2.83	1.90	0.368	2.749
TILT143.DAT		5.76	84.71	2.02	1.64	0.280	2.073
TILT141.DAT	0.5	6.78	46.06	0.08	0.16	0.206	0.231
TILT142.DAT		8.08	38.65	0.121	-0.40	0.250	0.301
TILT138.DAT	0.6	6.27	34.58	0.38	0.00	0.333	0.420
TILT139.DAT		8.78	24.64	-0.40	-0.25	0.265	0.333
TILT140.DAT		9.54	22.73	0.04	0.21	0.245	0.322
TILT130.DAT	0.7	5.51	28.91	0.35	0.06	0.299	0.279
TILT131.DAT		6.52	24.41	1.30	0.21	0.280	0.267
TILT132.DAT		7.29	21.86	1.70	0.22	0.294	0.262
TILT133.DAT		7.59	20.98	1.34	0.45	0.284	0.263
TILT134.DAT		7.75	20.54	1.61	0.43	0.272	0.295
TILT135.DAT		8.69	18.33	6.91	0.38	0.288	0.283
TILT136.DAT		9.43	16.88	4.77	0.63	0.278	0.269
TILT103.DAT	0.8	6.26	19.49	0.94	0.29	0.243	0.140
TILT104.DAT		6.48	18.81	2.07	0.42	0.261	0.160
TILT105.DAT		6.74	18.08	1.47	0.35	0.271	0.163
TILT110.DAT		7.36	16.56	1.82	0.49	0.247	0.139
TILT107.DAT		7.76	15.71	6.26	0.67	0.274	0.153
TILT109.DAT		8.48	14.39	9.94	0.34	0.261	0.174
TILT111.DAT		8.68	14.05	8.68	0.49	0.281	0.171
TILT112.DAT		9.33	13.07	9.33	0.07	0.287	0.180
TILT95.DAT	0.9	4.79	20.13	0.87	0.38	0.256	0.042
TILT96.DAT		5.87	16.41	2.55	0.29	0.279	0.055
TILT97.DAT		6.28	15.33	3.91	0.52	0.281	0.067
TILT99.DAT		6.42	15.00	7.21	0.09	0.301	0.077
TILT100.DAT		7.26	13.27	12.35	-0.22	0.313	0.099
TILT102.DAT		7.86	12.26	11.86	-0.14	0.280	0.095
TILT101.DAT		8.34	11.56	14.91	-0.22	0.295	0.126
TILT113.DAT	1.0	4.28	18.25	0.17	-0.26	0.261	0.04
TILT114.DAT		4.79	16.28	1.15	0.36	0.264	0.031
TILT115.DAT		5.29	14.74	1.45	0.40	0.270	0.027
TILT116.DAT		5.73	13.63	2.05	0.51	0.264	0.028
TILT117.DAT		6.51	11.98	4.27	0.64	0.267	0.035
TILT118.DAT		6.72	11.61	4.85	0.90	0.270	0.032
TILT119.DAT		7.75	10.07	10.54	0.29	0.242	0.038
TILT121.DAT	1.1	4.14	15.58	0.20	0.55	0.210	0.070
TILT120.DAT		4.75	13.58	0.05	0.26	0.164	0.071
TILT122.DAT		5.95	10.84	0.08	0.49	0.135	0.063
TILT123.DAT		6.39	10.10	0.17	0.66	0.145	0.057
TILT125.DAT		6.90	9.35	0.51	1.11	0.155	0.052
TILT126.DAT		7.06	9.14	1.11	1.37	0.150	0.044
TILT127.DAT	1.2	4.83	11.22	0.71	0.84	0.088	0.083
TILT129.DAT		4.94	10.97	0.66	0.77	0.081	0.082
TILT128.DAT		5.44	9.96	0.61	0.53	0.074	0.070

Table 11 - Experimental wave and motion data analysed for $\overline{GM}$ = 2.90 cms

$\bar{GM}$ = 3.80 cm

1	2	3	4	5	6	7	8
Run Data File No:	Characteristic W.Frequency (Hz)	W.Amplitude (cm)	W.Length / W.Height	Steady Tilt (Degree)	Steady Heave (cm)	Oscillatory Roll RAO (Degree/cm)	Oscillatory Heave RAO
TILT94.DAT	0.4	5.12	95.29	0.72	-0.05	0.097	2.202
TILT91.DAT	0.6	7.07	30.67	0.10	-0.02	0.291	0.358
TILT92.DAT		8.42	25.75	-0.06	0.00	0.271	0.345
TILT93.DAT		9.59	22.61	0.34	-0.07	0.235	0.324
TILT88.DAT	0.7	6.40	24.89	1.09	-0.01	0.258	0.270
TILT89.DAT		8.00	19.91	0.92	0.36	0.289	0.277
TILT90.DAT		9.20	17.32	2.31	0.61	0.291	0.262
TILT72.DAT	0.8	5.57	21.89	0.63	0.02	0.262	0.143
TILT73.DAT		6.89	17.70	0.81	0.05	0.257	0.150
TILT79.DAT		6.96	17.52	1.16	0.09	0.261	0.143
TILT74.DAT		8.26	14.77	2.75	0.37	0.239	0.165
TILT77.DAT		8.44	14.46	6.65	0.77	0.285	0.165
TILT78.DAT		8.66	14.08	6.00	0.82	0.266	0.157
TILT75.DAT		8.92	13.66	8.73	0.49	0.277	0.184
TILT76.DAT		9.26	13.18	10.95	0.19	0.279	0.178
TILT65.DAT	0.9	5.40	17.85	1.08	0.49	0.263	0.049
TILT66.DAT		5.73	16.81	1.65	0.53	0.281	0.063
TILT67.DAT		6.86	14.04	3.32	0.75	0.273	0.060
TILT69.DAT		7.26	13.28	5.33	0.87	0.292	0.073
TILT71.DAT		7.44	12.95	6.32	0.51	0.273	0.041
TILT70.DAT		7.82	12.32	8.51	0.86	0.306	0.084
TILT68.DAT		8.16	11.81	10.97	0.85	0.320	0.173
TILT80.DAT	1.0	4.35	17.93	0.21	0.30	0.259	0.039
TILT81.DAT		5.40	14.44	0.40	0.41	0.234	0.035
TILT82.DAT		6.40	12.20	0.94	0.52	0.241	0.024
TILT83.DAT		6.98	11.18	1.83	0.74	0.243	0.020
TILT85.DAT	1.1	5.07	12.72	0.05	0.30	0.169	0.069
TILT86.DAT		6.07	10.63	0.20	0.46	0.168	0.060
TILT87.DAT		6.80	9.49	0.68	0.48	0.154	0.051

Table 12 - Experimental wave and motion data analysed for $\bar{GM}$ = 3.80 cms

$\overline{GM}$ = 5.60 cm

1	2	3	4	5	6	7	8
Run Data File No:	Characteristic W.Frequency (Hz)	W.Amplitude (cm)	W.Length / W.Height	Steady Tilt (Degree)	Steady Heave (cm)	Oscillatory Roll RAO (Degree/cm)	Oscillatory Heave RAO
TILT2Ø4.DAT	0.4	4.62	105.61	0.39	-0.01	0.266	2.622
TILT2Ø3.DAT		4.69	104.03	0.30	0.05	0.213	2.243
TILT2Ø1.DAT	0.6	6.75	46.26	-Q.01	0.21	0.236	0.341
TILT2Ø2.DAT		8.09	35.60	0.13	0.08	0.211	0.243
TILT198.DAT	0.6	6.46	33.57	0.1	0.75	0.249	0.368
TILT199.DAT		7.15	30.33	0.25	-0.21	0.276	0.408
TILT2ØØ.DAT		9.31	23.29	0.23	0.32	0.236	0.341
TILT191.DAT	0.7	6.35	25.07	0.52	0.14	0.276	0.283
TILT192.DAT		6.83	23.32	0.80	0.20	0.271	0.273
TILT193.DAT		7.56	21.06	0.83	0.33	0.269	0.259
TILT195.DAT		8.34	19.10	1.51	0.61	0.257	0.289
TILT196.DAT		9.16	17.39	2.80	0.49	0.257	0.276
TILT197.DAT		9.85	16.17	2.33	0.97	0.259	0.265
TILT164.DAT	0.8	5.54	22.02	0.32	0.18	0.268	0.153
TILT165.DAT		6.36	19.18	0.56	0.34	0.260	0.150
TILT166.DAT		7.10	17.18	1.07	0.48	0.256	0.153
TILT167.DAT		7.94	15.36	1.53	0.72	0.245	0.160
TILT168.DAT		8.33	14.65	2.30	0.75	0.247	0.145
TILT169.DAT		9.13	13.36	3.52	0.98	0.271	0.148
TILT170.DAT		9.30	13.11	4.12	0.77	0.256	0.165
TILT178.DAT	0.9	5.26	18.33	0.58	0.43	0.264	0.050
TILT171.DAT		5.30	18.18	0.55	0.34	0.267	0.058
TILT172.DAT		5.54	17.40	0.66	0.43	0.275	0.059
TILT173.DAT		6.45	14.94	0.93	0.52	0.261	0.059
TILT174.DAT		6.64	14.52	1.22	0.63	0.264	0.054
TILT175.DAT		7.15	13.47	1.67	0.72	0.278	0.072
TILT176.DAT		7.41	13.01	1.93	0.92	0.278	0.064
TILT177.DAT		7.96	12.10	4.32	0.93	0.284	0.071
TILT180.DAT	1.0	5.46	14.30	0.54	0.53	0.244	0.029
TILT181.DAT		5.60	13.93	0.67	0.60	0.258	0.032
TILT182.DAT		6.12	12.76	1.04	0.72	0.262	0.019
TILT183.DAT		6.21	12.57	1.27	0.86	0.276	0.024
TILT184.DAT		6.91	11.30	1.27	0.98	0.264	0.014
TILT185.DAT		7.08	11.03	1.06	1.03	0.253	0.019
TILT190.DAT	1.1	5.24	12.31	0.60	0.24	0.107	0.081
TILT189.DAT		5.49	11.75	0.34	0.18	0.087	0.069
TILT186.DAT		5.61	11.50	0.11	0.39	0.158	0.065
TILT187.DAT		6.95	9.28	0.28	0.53	0.153	0.052
TILT188.DAT		7.21	8.95	0.48	0.54	0.152	0.049

Table 13 - Experimental wave and motion data analysed for $\overline{GM}$ = 5.60 cms

$\overline{GM}$ 7.90 cm

1	2	3	4	5	6	7	8
Run Data File No:	Characteristic W.Frequency (Hz)	W.Amplitude (cm)	W.Length / W.Height	Steady Tilt (Degree)	Steady Heave (cm)	Oscillatory Roll RAO (Degree/cm)	Oscillatory Heave RAO
TILT243.DAT	0.3	2.72	318.90	-0.01	-0.10	0.193	1.572
TILT244.DAT		3.33	260.50	0.20	0.24	0.254	1.407
TILT241.DAT	0.4	5.49	88.87	0.08	-0.14	0.064	2.04
TILT242.DAT		7.11	68.62	0.44	-0.24	0.079	1.75
TILT2Ø6.DAT	0.5	7.20	43.37	0.14	-0.13	0.193	0.233
TILT2Ø7.DAT		8.49	36.78	0.12	0.02	0.178	0.227
TILT2Ø8.DAT	0.6	7.35	29.50	0.20	0.09	0.233	0.336
TILT2Ø9.DAT		8.00	27.11	0.16	0.28	0.236	0.354
TILT21Ø.DAT		9.04	23.99	0.17	0.18	0.220	0.344
TILT211.DAT	0.7	7.55	21.10	0.56	0.37	0.249	0.267
TILT212.DAT		8.50	18.73	0.80	0.50	0.243	0.278
TILT213.DAT		9.90	16.08	1.23	0.90	0.232	0.259
TILT214.DAT	0.8	5.46	22.32	0.26	0.24	0.262	0.154
TILT215.DAT		6.18	19.74	0.30	0.37	0.247	0.149
TILT216.DAT		6.70	18.20	0.44	0.69	0.247	0.159
TILT217.DAT		7.48	16.29	0.57	0.58	0.237	0.149
TILT218.DAT		8.00	15.24	1.05	0.68	0.241	0.154
TILT219.DAT		8.76	13.92	1.07	0.88	0.238	0.166
TILT221.DAT		9.20	13.25	1.44	1.03	0.246	0.173
TILT222.DAT	0.9	5.38	17.91	0.35	0.42	0.261	0.057
TILT223.DAT		5.84	16.50	0.53	0.50	0.261	0.057
TILT224.DAT		6.35	15.17	0.75	0.59	0.260	0.062
TILT225.DAT		6.64	14.52	0.97	0.70	0.277	0.069
TILT226.DAT		7.17	13.44	1.28	0.77	0.266	0.069
TILT227.DAT		7.63	12.63	1.36	0.86	0.259	0.069
TILT228.DAT		7.94	12.14	2.21	0.97	0.273	0.067
TILT229.DAT	1.0	4.78	16.31	0.16	0.38	0.241	0.031
TILT230.DAT		4.95	15.78	0.28	0.44	0.253	0.030
TILT231.DAT		5.33	14.64	0.32	0.57	0.272	0.022
TILT232.DAT		5.54	14.08	0.43	0.69	0.277	0.022
TILT233.DAT		6.06	12.87	0.46	0.78	0.276	0.023
TILT234.DAT		6.48	12.04	0.50	0.90	0.274	0.015
TILT235.DAT		7.38	10.57	0.66	0.97	0.248	0.016
TILT236.DAT	1.1	6.13	10.52	0.13	0.37	0.161	0.060
TILT238.DAT		6.93	9.31	0.26	0.47	0.167	0.053
TILT237.DAT		7.12	9.06	0.19	0.51	0.161	0.046
TILT239.DAT	1.2	5.42	10.00	0.23	0.11	0.102	0.068
TILT240.DAT		5.54	9.78	0.21	-0.20	0.109	0.069

Table 14 - Experimental wave and motion data analysed for $\overline{GM}$ = 7.90 cms

Presentation and Discussion of Results

Oscillatory motion response:

In Figs 45, 46, 47, 48 and 49 the heave motion response, and in Figs 51, 52, 53, 54 and 55 the roll motion response are presented for each test series as Characteristic Wave Frequency versus Response Amplitude Operators (RAO).

In order to investigate the effect of wave height more than one wave height was tested for each frequency, therefore in the figures each spot corresponds to a test run with a different wave height. The solid lines pass through the mean value of these spots.

An interesting finding noticed in these typical motion response curves is the scatter in the RAO's corresponding to different wave heights. At a first glance this can be attributed to higher waves, because if the small amplitude wave theory assumption is violated one can not expect the motion response to be linearly proportional to the wave amplitude. However, if the figures are carefully examined the magnitude of the scatter depends on the $\overline{GM}$ tested. As the $\overline{GM}$ increases, the scatter vanishes (compare Fig. 45 with Fig. 49 for heave, and Fig. 51 with Fig. 55 for roll mode). This scatter was worst in the first test series with the smallest $\overline{GM}$ and a frequency region between 0.8 and 1.0 Hz where the tilt was at its worst.

This finding suggests that besides non-linear effects of the higher waves, there were also non-linear effects on the oscillatory heave and roll RAO due to the steady tilt behaviour.

The other possibility for the scatter in the measured motion values (or defined RAO's) could be the difference in the wave amplitudes which were measured at three different places of the tank. As stated earlier, the steady motions and oscillatory RAO's were defined with

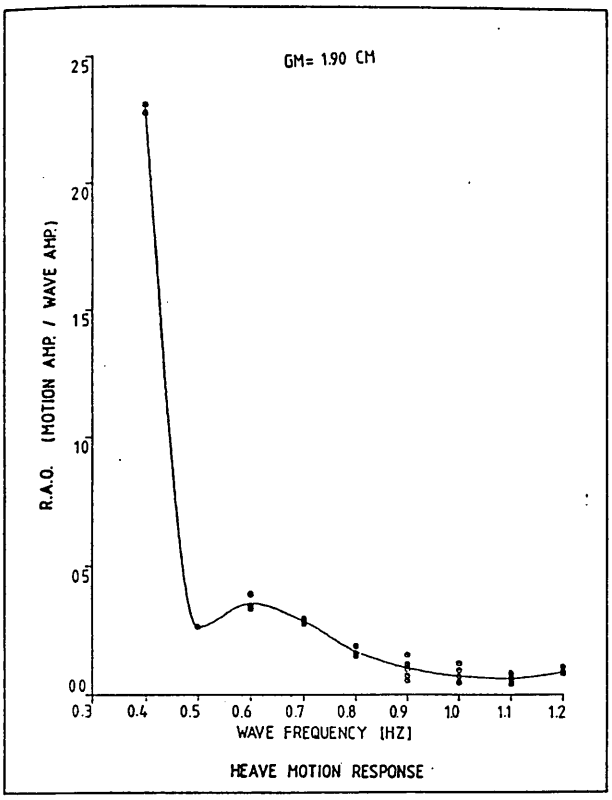

Fig. 45 - Experimental oscillatory heave motion response for $\overline{GM}$ = 1.90 cms

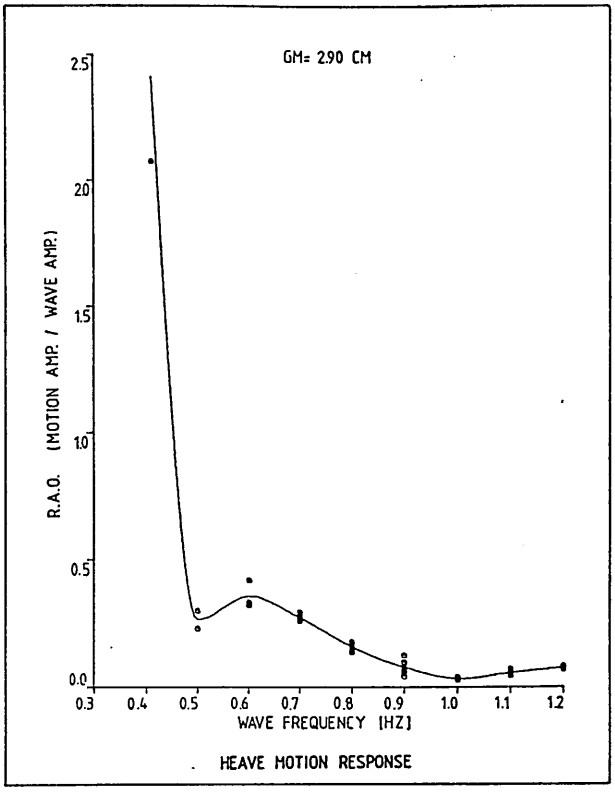

Fig. 46 - Experimental oscillatory heave motion response for $\overline{GM}$ = 2.90 cms

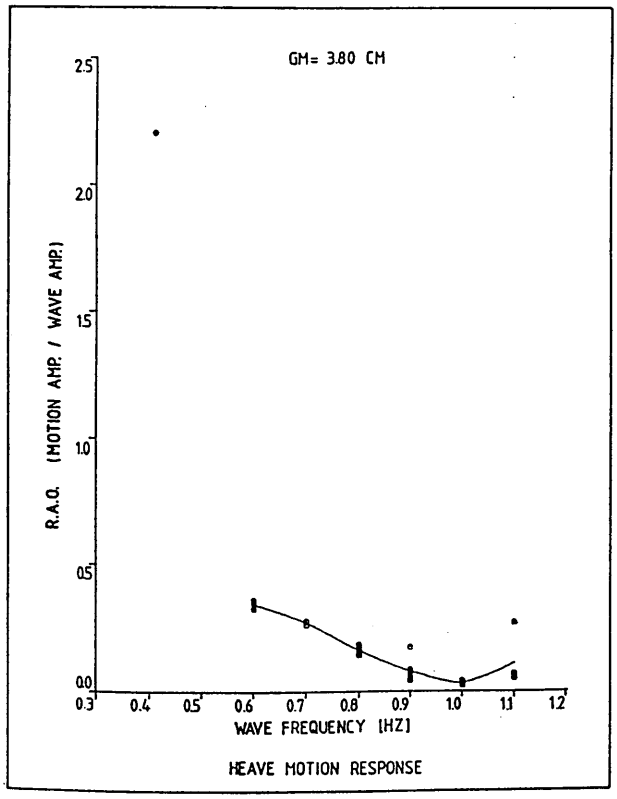

Fig. 47 - Experimental oscillatory heave motion response for $\overline{GM}$ = 3.80 cms

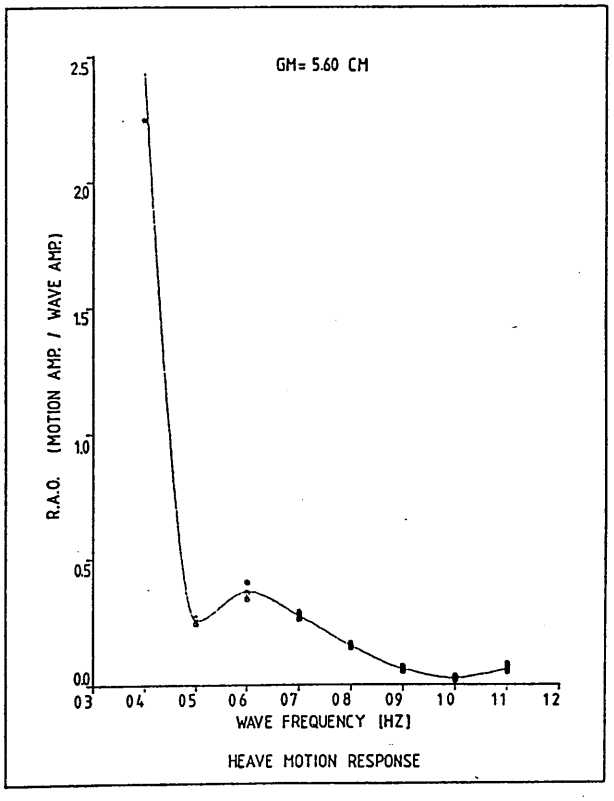

Fig. 48 - Experimental oscillatory heave motion response for $\overline{GM}$ = 5.60 cms

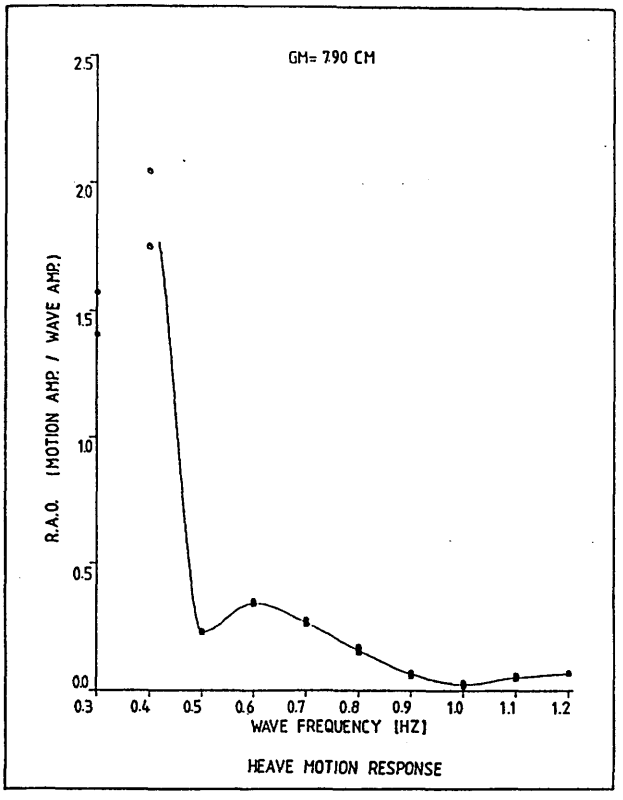

Fig. 49 - Experimental oscillatory heave motion response for $\overline{GM}$ = 7.90 cms

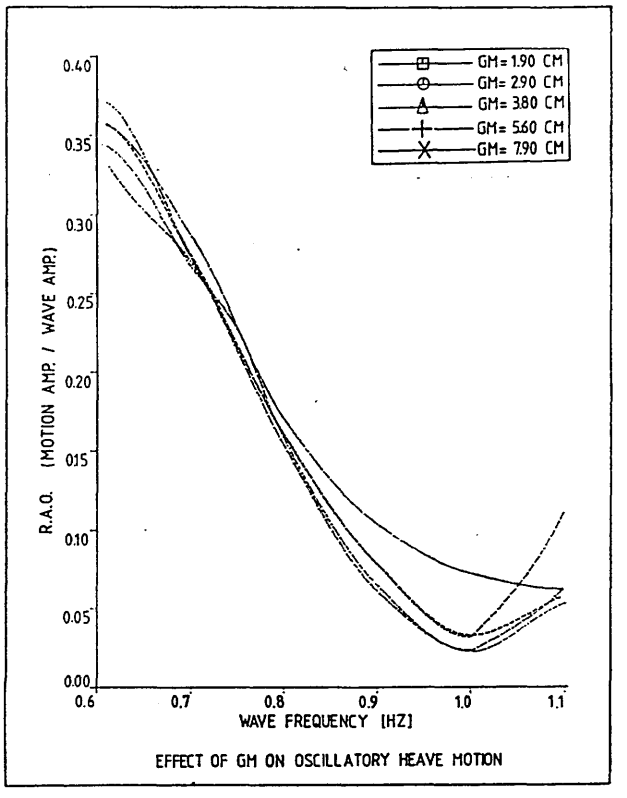

Fig. 50 - Effect of $\overline{GM}$ on the experimental oscillatory heave motion

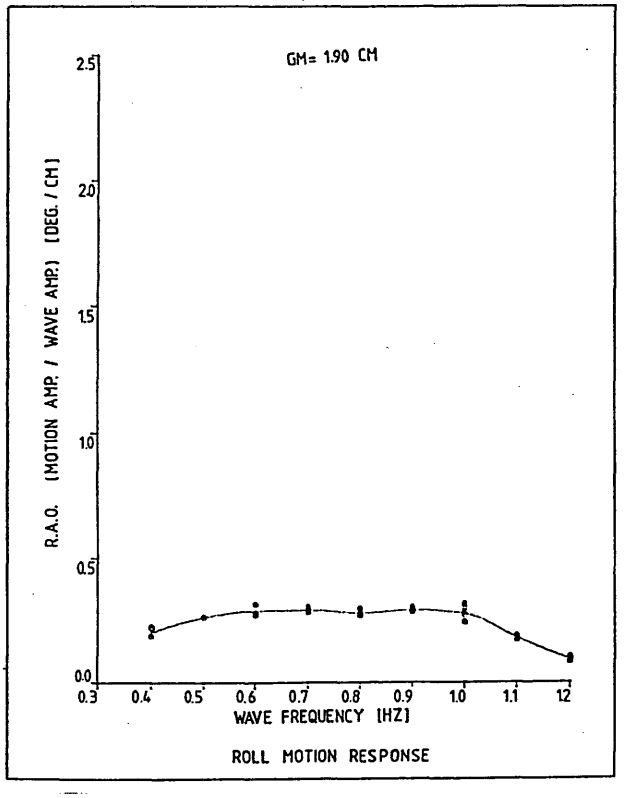

Fig. 51 - Experimental oscillatory roll motion response for $\overline{GM}$ = 1.90 cms

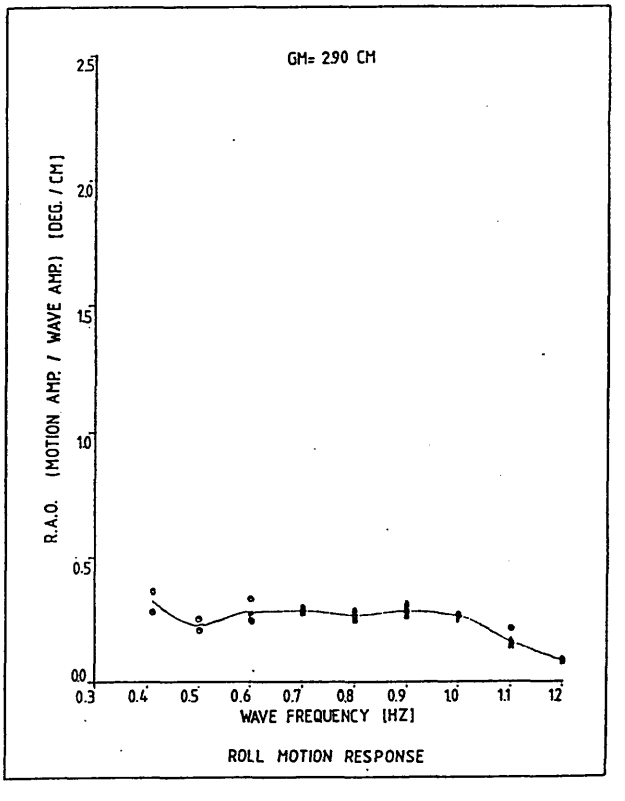

Fig. 52 - Experimental oscillatory roll motion response for $\overline{GM}$ = 2.90 cms

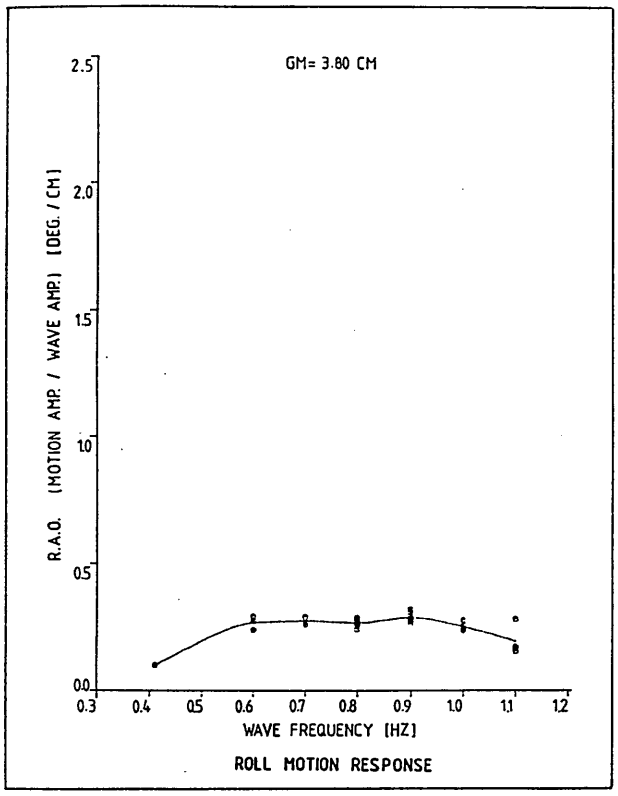

Fig. 53 - Experimental oscillatory roll motion response for $\overline{GM}$ = 3.80 cms

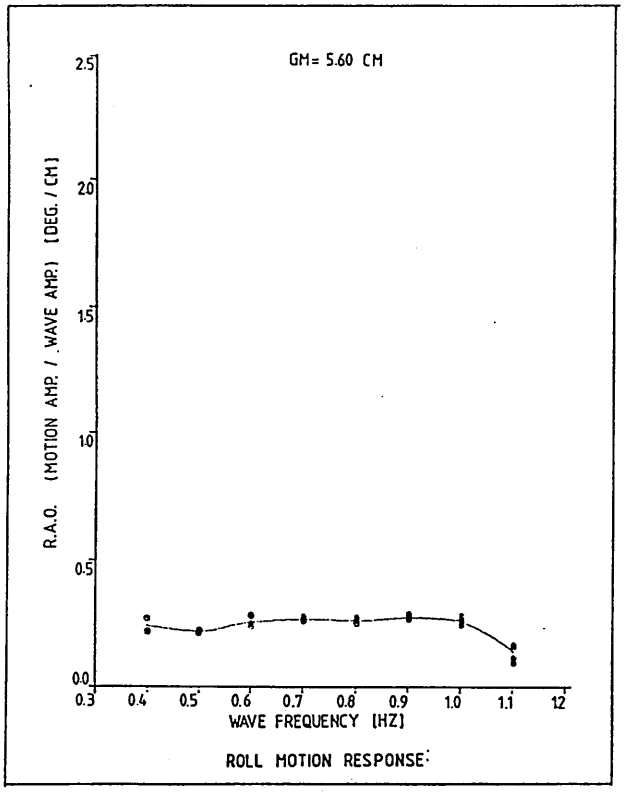

Fig. 54 - Experimental oscillatory roll motion response for $\overline{GM}$ = 5.60 cms

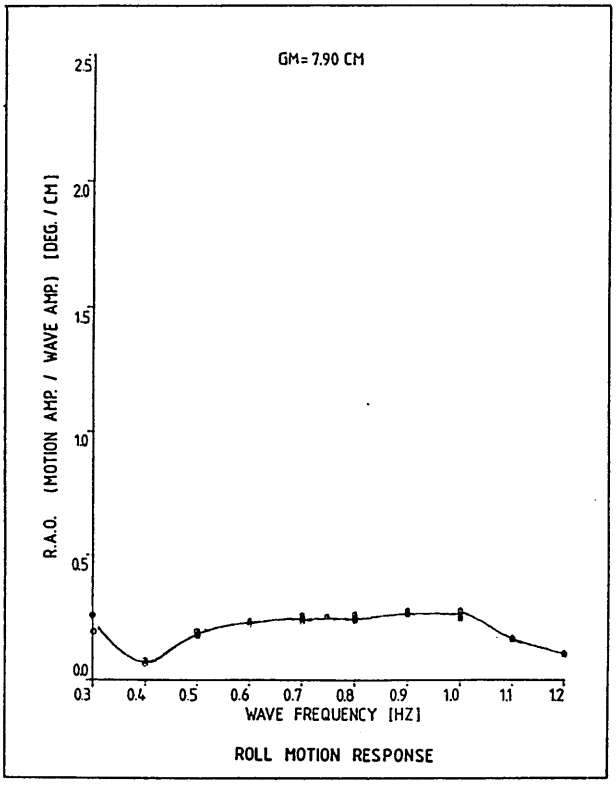

Fig. 55 - Experimental oscillatory roll motion response for $\overline{GM}$ = 7.90 cms

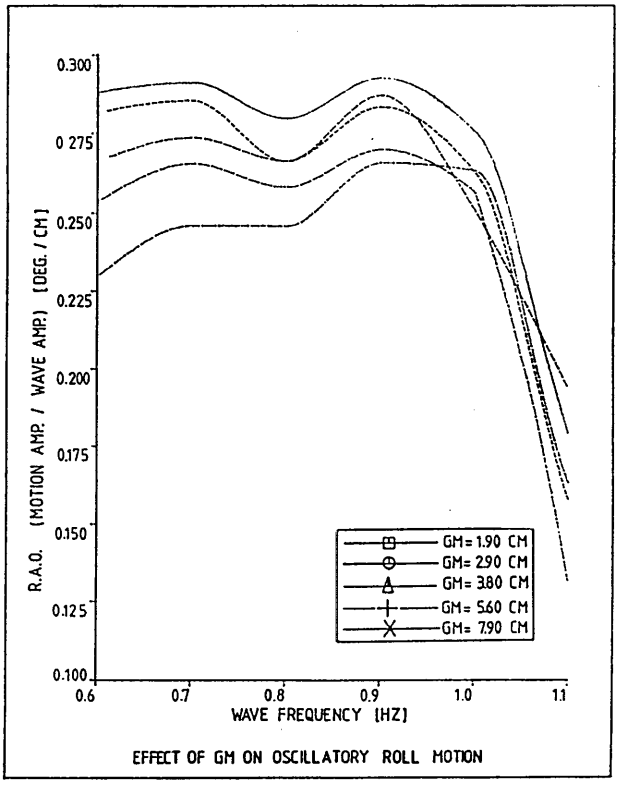

Fig. 56 - Effect of $\overline{GM}$ on the experimental oscillatory roll motion response

respect to the wave amplitude (ζ_M) obtained from the wave probe by the model. As shown in Fig. 39 this probe was 0.8 m clear from the model and the right side wall of the tank. In Table 15 as an example for a particular frequency of 0.7 Hz five different wave amplitudes ζ_M, ζ_R (obtained from the wave probe on the right side of the bridge), ζ_L (on the left side of the bridge) and corresponding first-order motion values are given.

Col.No: 1	2	3	4	5	6	7	8	9	10	11
Run Data File No:	ζ_M (cms)	ζ_R (cms)	ζ_L (cms)	$\zeta_B = \frac{\zeta_R+\zeta_L}{2}$ (cms)	Roll Amp. (degrees)	Heave Amp. (cms)	$\frac{\text{Roll}}{\zeta_M}$ (deg/cms)	$\frac{\text{Roll}}{\zeta_B}$ (deg/cms)	$\frac{\text{Heave}}{\zeta_M}$	$\frac{\text{Heave}}{\zeta_B}$
TILT191.DAT	6.35	6.30	6.12	6.21	1.75	1.79	0.276	0.282	0.283	0.288
TILT192.DAT	6.83	6.70	6.66	6.68	1.85	1.86	0.271	0.277	0.273	0.278
TILT193.DAT	7.56	7.50	7.30	7.40	2.03	1.96	0.269	0.275	0.259	0.265
TILT195.DAT	8.34	8.29	8.32	8.31	2.14	2.41	0.257	0.258	0.289	0.290
TILT196.DAT	9.16	9.10	8.86	8.98	2.35	2.53	0.257	0.261	0.276	0.282
TILT197.DAT	9.85	9.70	9.81	9.75	2.61	2.61	0.259	0.261	0.265	0.267

Table 15 – Wave amplitudes measured at three different places at the model tank and corresponding motion RAO's for a wave frequency of 0.7 Hz

As shown in Colums 2, 3 and 4 ζ_M was always greater than ζ_R and ζ_L. This was observed in the majority of test runs. The wave probes on the bridge were located side by side with a clearance of 1.53 m from each other and the side walls. Therefore one can expect that ζ_R and ζ_L would be the same in magnitude. But as shown in Columns 3 and 4 there is a difference in some cases with a maximum of 2.4 mm indicating that

the waves generated could be asymmetric along the tank breadth. Therefore in Column 5 the average values ζ_B taken. The difference between ζ_B and ζ_M has a maximum of 1.8 mm (the distance between two probes was about 7 m).

By considering these effects the RAO's defined with respect to the ζ_M and ζ_B for roll and heave were given in Column 8 through 11. If one compares Columns 8 and 9, the use of the wave ζ_B obtained from the bridge probes did not remove the scatter in the RAO's of roll but slightly increased the magnitudes. The same finding was valid for the RAO's of heave as given in Columns 10 and 11.

As demonstrated in this example check, the measured wave heights at the different places along the tank could differ by a maximum of 2.5 mm. This difference could change the magnitude of the motion values but it cannot remove the scatter in the motion values.

In Fig. 50 the effect of $\overline{GM}$ on the oscillatory heave motion is presented. In theory the changes in $\overline{GM}$ should not affect the oscillatory heave motion if there was no effect due to the steady tilt. However as shown in Fig. 50 there was a difference between each test series, the worst heave (maximum 60% increase on the heave with the smallest $\overline{GM}$ compared to the test with the highest $\overline{GM}$) occurring at the frequency region where the tilt was worst.

The effect of $\overline{GM}$ on the oscillatory roll motion is shown in Fig. 56. It is obvious that $\overline{GM}$ will affect the oscillatory roll motion response since it governs the roll restoring moment. This effect was reflected in the curves in that as the $\overline{GM}$ increased the roll response decreased. At a frequency of 0.7 Hz and 0.9 Hz this effect takes its peak values. It is interesting that at these frequencies the steady tilt takes peak values too as will be shown in the following. This trend suggests that there could also be an effect of steady tilt behaviour on the oscillatory roll motion response.

Steady motion response

In Column 6 of the Tables 10 through 14 the steady heave motion response of the model was given as a reference. Although this steady motion will not be studied in the thesis it was considered interesting that it could be greater than the maximum amplitude of the oscillatory heave motion at the higher frequencies. As shown in the tables, the magnitude of this steady motion increased non-linearly with increasing wave height. The ratio of the steady heave to the maximum amplitude of the oscillatory heave was not very significant at lower frequencies up to 0.7 Hz (not more than 20%). Between 0.7 Hz and 1.1 Hz as the amplitude of the oscillatory heave decreased, this ratio increased and at frequencies of 0.9, 1.0 and 1.1 Hz the steady heave became greater than the maximum amplitude of the oscillatory heave. However, at this frequency range since the magnitude of the heave motion was practically negligible this large ratio was not very important. At the majority of frequencies the steady heave motion was in the upward direction but sometimes was in the downward direction in particular at lower frequencies. This non-linear behaviour is another particular problem of semi-submersible type vessels which needs to be explored.

As stated earlier, a semi-submersible model can take on a steady tilt if the three main factors which are namely wave frequency, wave height and $\overline{GM}$, are in a certain range of values. When the steady tilt takes place these parameters govern the behaviour simultaneously with the other factors.

In order to identify this range or value, the variations of the measured steady tilt angles with varying wave frequency, wave height and $\overline{GM}$ are presented in Figs 57 and 58. In the figures the solid lines are the best-fit curves through the experimental data. It can be seen that

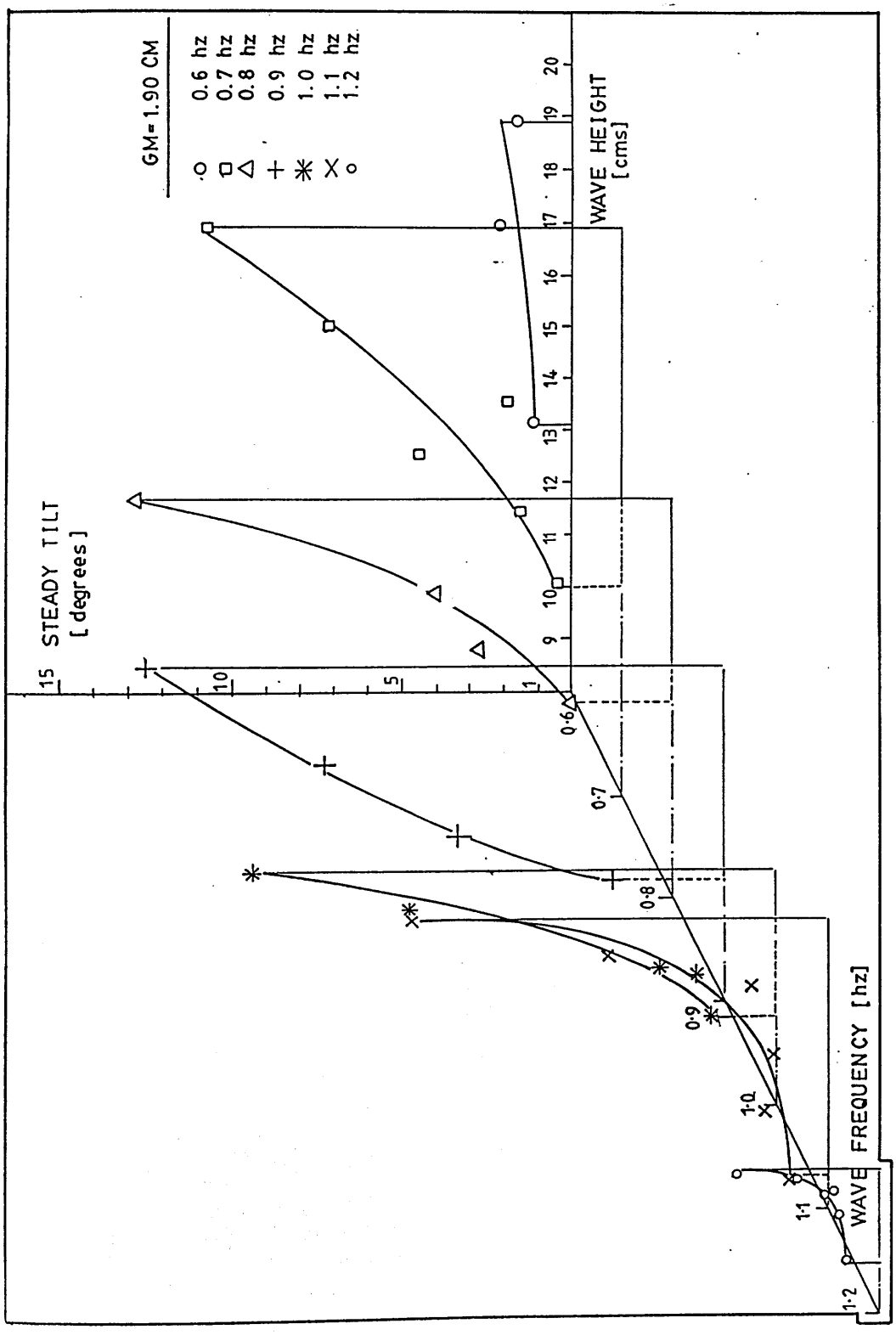

Fig. 57 - Three dimensional representation of the experimental steady tilt varying with wave frequency and wave height for the smallest GM tested (GM = 1.90 cms)

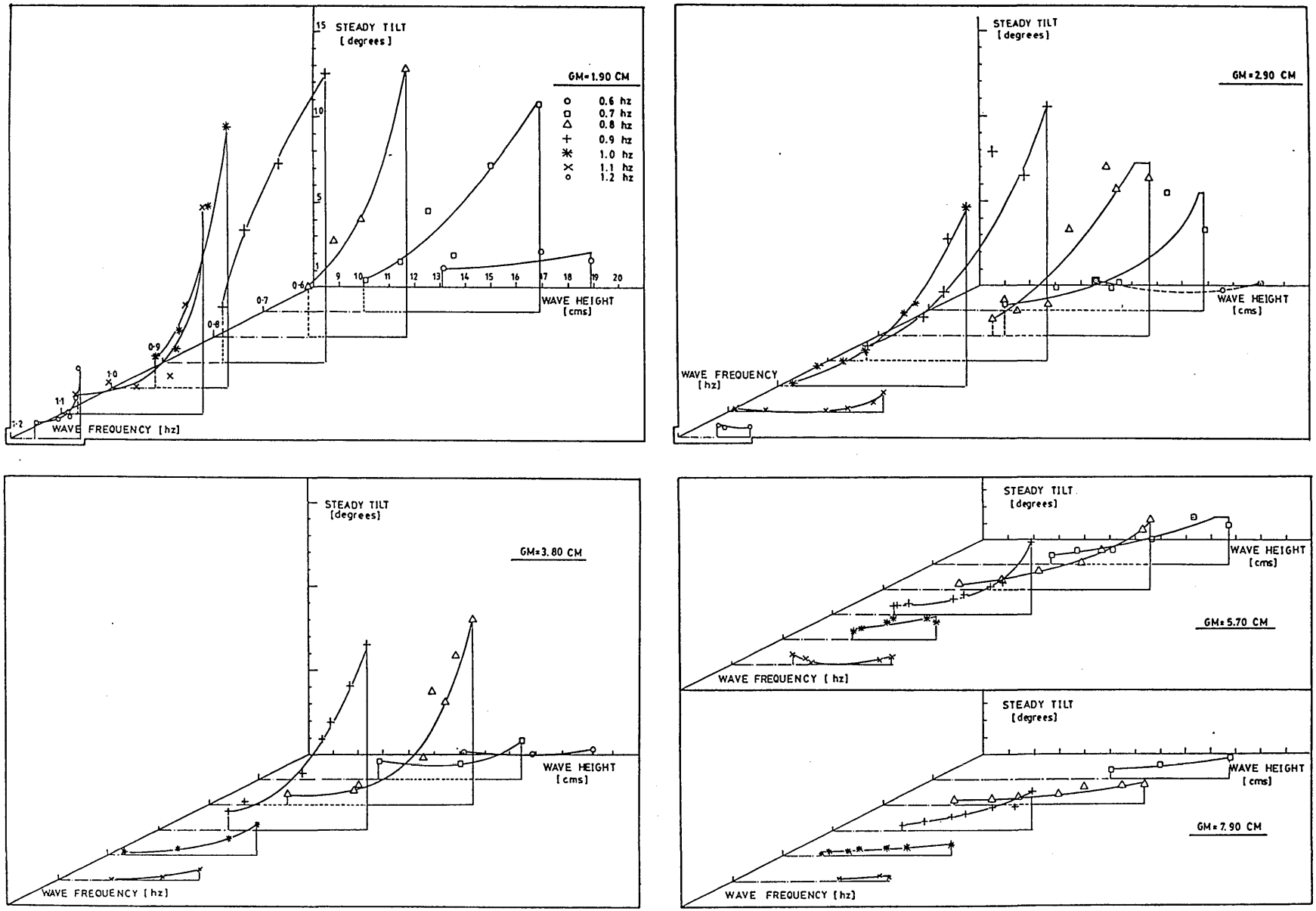

Fig. 58 - Three dimensional representation of the experimental steady tilt varying with wave frequency and wave height for differing $\overline{GM}$'s (the scale of the axes are the same for all the figures)

there is some scatter which reflects the sensitivity to wave heights. However, the trend is quite clear and once tilt has begun an increase in wave height causes a very sharp rise in tilt angle. This occurs over quite a wide frequency range and reflects the dependency on the non-linear variation of wave height.

The range of the wave frequencies and wave heights where tilt occurred, is demonstrated in Fig. 57 which presents the values measured with the smallest $\overline{GM}$. This is because at small $\overline{GM}$s tilt will be dominated mainly by the wave-induced tilting moment and thus the wave-induced effects will be strongly emphasised; where as at high $\overline{GM}$s the behaviour will be dominated by the vessel's restoring moment and no tilt or slight tilt would be observed in the range of waves which has the potential to cause tilt.

As seen in Fig. 57, the steady tilt occurred clearly (larger than 2°) over the range of characteristic wave frequencies varying between 0.7 Hz and 1.2 Hz (a range of wave period 12 sec to 7 sec on full scale) having a peak at about 0.9 Hz (a period of 9 sec on F.S.). Outside this range no major tilt was recorded except a slight tilt of 2-3° around the natural heave frequency of 0.4 Hz (a period of 21 sec on F.S.).

Because of its relevance to the limits of the frequency range it is worthwhile considering the performance of the wavemaker; below the lower frequency limit (frequency < 0.7 Hz) as shown in Fig. 40 the wavemaker could produce reasonably high waves (maximum 20 cms, i.e. 17 m on F.S.) down to 0.4 Hz when the form of the waves became non-sinusoidal. The tests between 0.7 Hz and the frequency, where the waves became non-sinusoidal, did not produce tilt in spite of the high waves. However, at the heave resonance frequency a slight tilt was observed even with moderate wave heights (10 cms). On the other hand, above the upper frequency limit (frequency > 1.2 Hz) the wavemaker

could produce a maximum wave height of 10 cms. The tests in this high frequency region with the extreme wave heights did not demonstrate tilt at all and waves became 'breaking waves'.

As shown in Fig. 58, $\overline{GM}$ affects the limits of this frequency range. As the $\overline{GM}$ increased, the tendency to tilt disappeared at the higher frequencies but remained around the 0.7 Hz frequency; i.e. the range of tilt frequencies decreased with the lower end of the range remaining fixed. (For example, $\overline{GM} \geq 2.90$ cms no tilt was observed at 1.2 Hz and gradually 1.1 Hz whereas small magnitude of tilts were still observed at 0.7 Hz.)

Referring to Fig. 57, to have a tilt over 2° the lower limit for wave heights should be at least over 10 cms (about 7 m on F.S.), and for wave heights above 15 cms (about 10 m on F.S.) the leeward deck was flooded. These limits were also dependent on the frequency and $\overline{GM}$.

Figure 59 presents the variations of the steady tilt angles with varying wave frequency and WL/WH - the ratio of the wave length to wave height for the smallest $\overline{GM}$. In Fig. 60 the same presentation is given for all the $\overline{GM}$s tested. As shown in Fig. 59 the range of WL/WH, where the tilt was observed, varies between about 10 and 20 and depends on the frequency and GM as seen in Fig. 60.

Since the tilt values were measured at more than one wave height for each frequency the presentations in Fig. 57 through 60 appear to be complicated but this was necessary to see if there was any trend in these curves. In order to demonstrate a simple presentation it is thought to be advisable to have a constant wave slope at each wave frequency and varying frequency. Physically this reflects that at sea, as the waves get longer, the maximum slope decreases

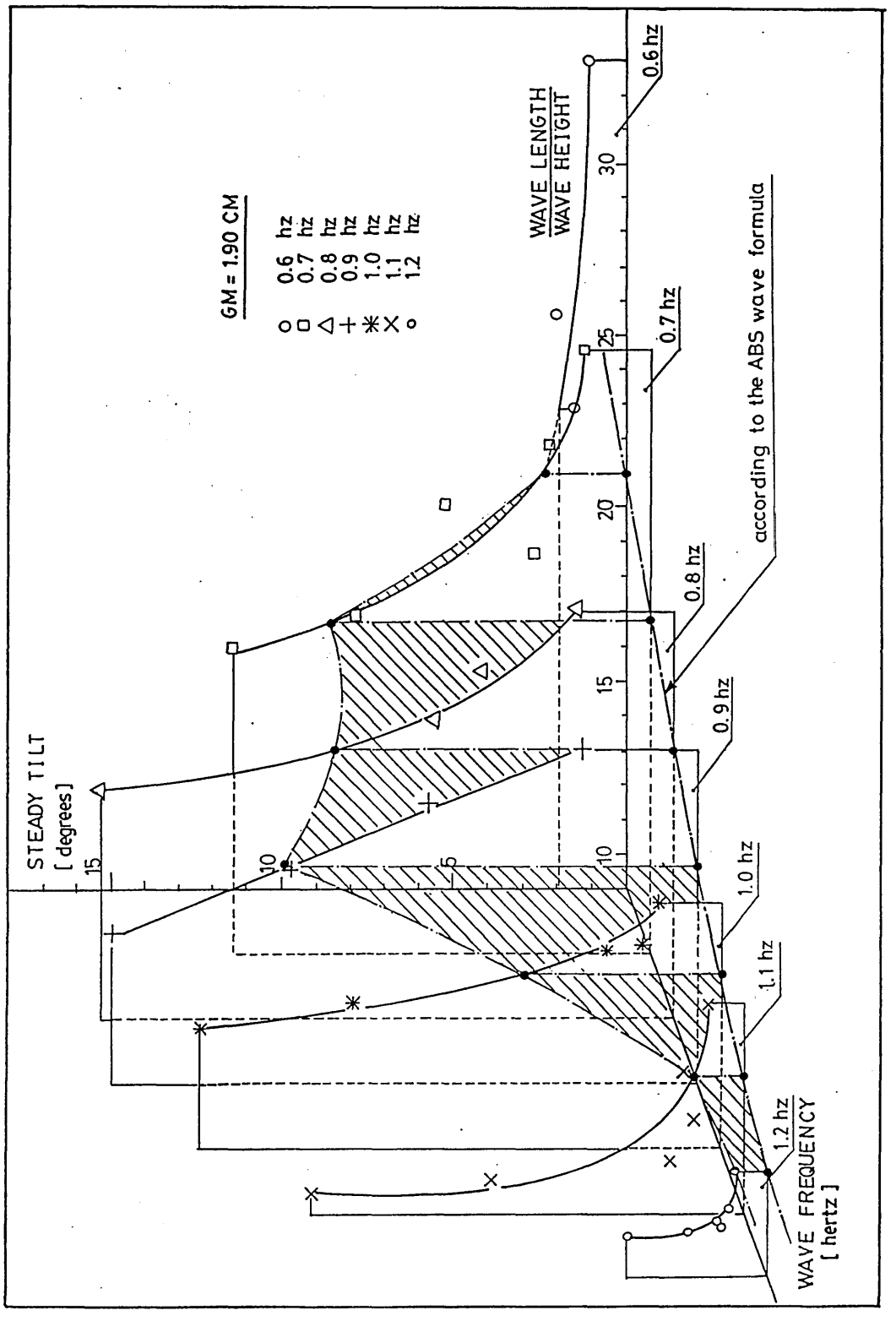

Fig. 59 - Three dimensional representation of the experimental steady tilt varying with wave frequency and WL/WH ratio for the smallest GM tested (GM = 1.90 cms)

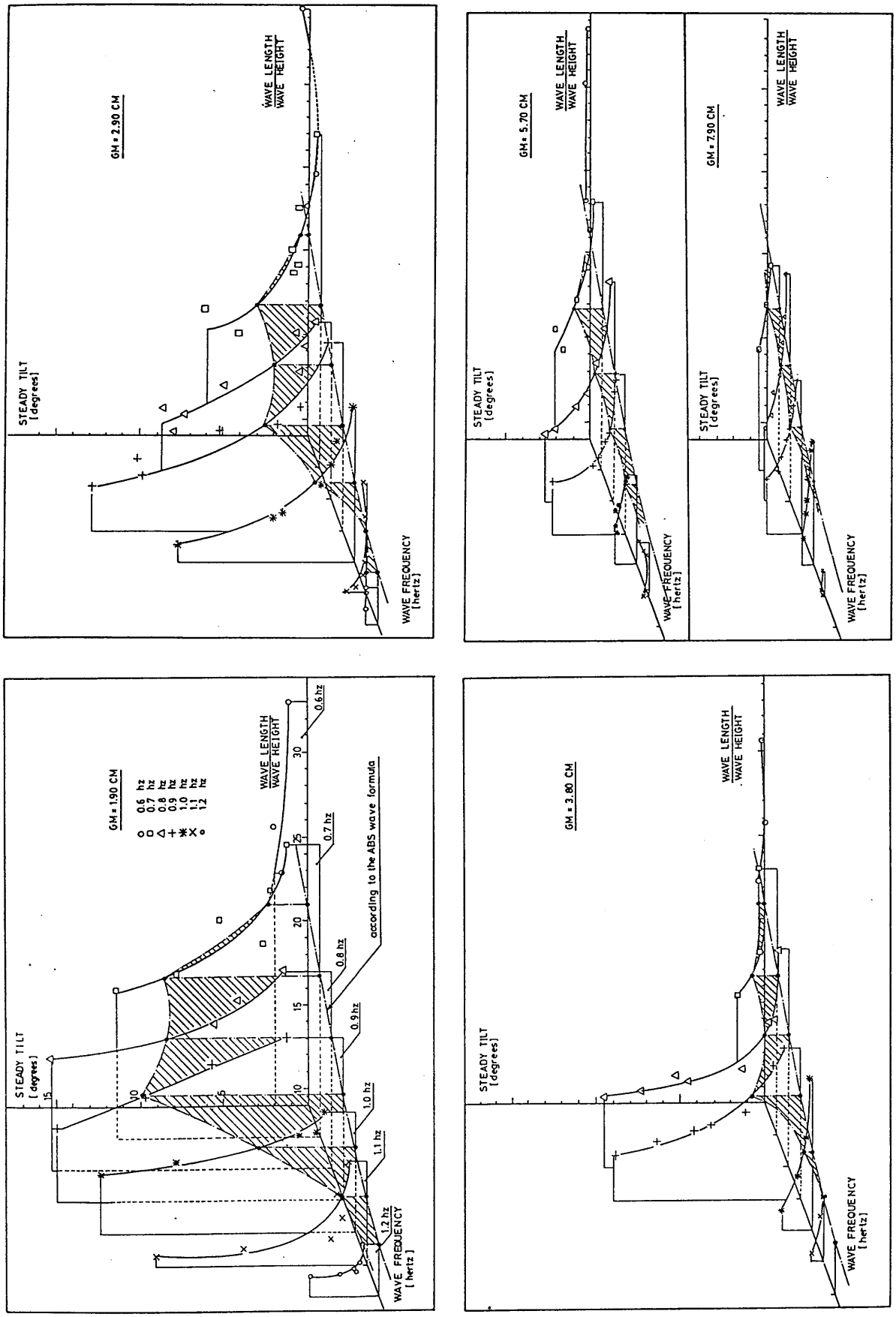

Fig. 60 - Three dimensional representation of the experimental steady tilt varying with wave frequency and WL/WH ratio for differing GM's (the scales of the axes are the same for all the figures)

This characteristic of waves is presented by the classification societies with various figures or empirical formulae, which relate the wave length to wave height obtained from statistical measurements at sea.

Among these DnV [41] presents the following formula for the maximum wave height of regular waves for design purposes:

$$WH = T^2/[4.5 + 0.02\ (T^2 - 36)] \quad \text{for } T > 6 \text{ sec} \qquad \ldots \quad (8)$$

where WH = wave height, T = wave period.

Numata et al. [16] consider the modified ABS wave height formula given as:

$$WH = 0.75\ (WL)^{0.6} \quad \text{[in feet]} \qquad \ldots \quad (9)$$

where WL = wave length.

The values calculated from these 2 formulae were tabulated in Table 16 over a range of wave frequency for full and model scales.

FULL SCALE					MODEL SCALE		
Charac.Freq. (Hz)	Period (sec)	Radian Freq. (rs^{-1})	Wave Length/Wave Height ABS	Wave Length/Wave Height DNV	Char.Freq. (Hz)	Wave Height (cms) ABS	Wave Height (cms) DNV
0.08	12.5	0.502	19.33	10.78	0.67	18.03	32.33
0.09	11.11	0.505	17.59	9.76	0.75	15.65	28.21
0.10	10.00	0.628	16.17	9.02	0.84	13.79	24.72
0.11	9.09	0.691	14.98	8.48	0.92	12.30	21.73
0.12	8.33	0.754	13.98	8.07	1.01	11.08	19.19
0.13	7.69	0.817	13.11	7.75	1.09	10.06	17.01
0.14	7.14	0.879	12.36	7.50	1.18	9.21	15.17
0.15	6.67	0.942	11.69	7.28	1.25	8.48	13.61

Table 16 – Comparison of the regular design wave formulae suggested by the ABS[16] *and the DnV*[41]

As shown in this table the difference in the wave slopes calculated from the two society formulae was about 40%. The DnV formula gives very steep waves compared to the ABS one. In order to produce waves with the same slopes in the model tank, the required wave heights according to these formulae are given in Table 15 as well. When these wave heights were compared with the waves which were producible by the wavemaker, it was found impossible to generate the wave heights required by the DnV formula in the model tank since they were too high. However, the ABS formula presented a range of wave heights which was producible by the wavemaker at the frequencies required. Therefore the ABS wave height formula had to be used for the further analysis of the results.

The other reason for using the ABS formula was that it gives a smaller wave slope than DnV or indeed the maximum slopes possible at sea; if the model or theory indicates tilt at this slope, the tilt is likely to be much more severe in the steeper wave conditions. Therefore from the design point of view it is desirable to check the behaviour in these less severe conditions.

In order to use this relationship in the experimental analysis, the curve given in Fig. 61 in the model scale was plotted three dimensionally in Figs 59 and 60 where the horizontal plane gives the axis of the characteristic wave frequency and WL/WH ratio. Now if one considers the shaded vertical planes which are normal to the horizontal planes and pass through the ABS curve, the heights of the intersection lines of the shaded planes and the other vertical planes at each frequency would give the steady tilt values for this particular wave height suggested by the ABS formula.

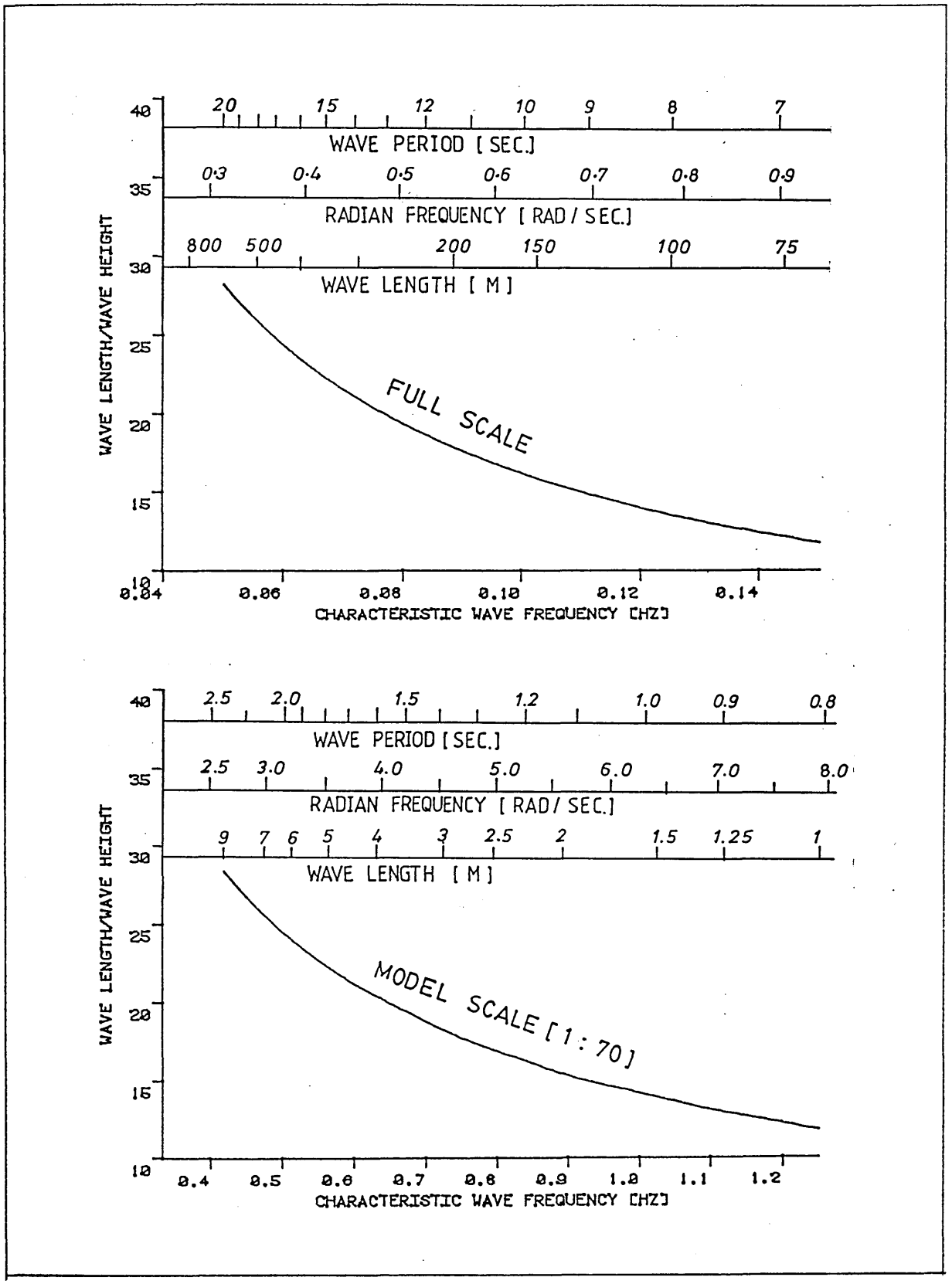

Fig. 61 - WL/WH ratio vs wave frequency obtained from the modified ABS design wave formula[16]

In Fig. 62 these steady tilt values were plotted against wave frequency, wave length/hull separation and WL/WH ratio for each $\overline{GM}$ at this particular wave. In this figure, the curves have a general trend in which the steady tilt has a local peak at a frequency of 0.7 Hz (a period of 12 sec on F.S.) apart from the main peak at a frequency of 0.9 Hz (a period of 9.3 sec on F.S.). These peaks occurred when the wave length equals to 3.8 and 2.3 times the hull separation and WL/WH ratio was about 18.7 and 15.3.

This trend is the same for all the small $\overline{GM}$s but as $\overline{GM}$ increases the main peak (worst tilt) seems to be replaced with the local peak.

The effect of $\overline{GM}$ on the magnitude of tilt is quite clear; as $\overline{GM}$ increases the magnitude of the tilt decreases non-linearly at all frequencies considered.

So far the effects of these three parameters have been presented in the frequency domain. However, it will be interesting to see if the same effects exist in the time history records as well.

In Fig. 63 the effect of frequency on steady tilt is shown for the smallest $\overline{GM}$. In these records the waves selected have the closest WL/WH ratios to that suggested by the ABS. It was difficult to have the exact WL/WH required by the formula. As shown in these records, the steady tilt clearly develops at 0.7 Hz and it takes the worst value at 0.9 Hz. While there was no tilt observed at 0.5 Hz there is a slight tilt at 0.4 Hz (natural heave frequency) despite the smaller wave steepness. The tilt at lower frequencies is fairly stable but as the frequency increases it becomes slowly varying. This is an important point to be borne in mind, because during the analysis this slow variation of tilt was ignored. However, looking at these curves suggests that the frequency domain analysis of the behaviour may not be correct.

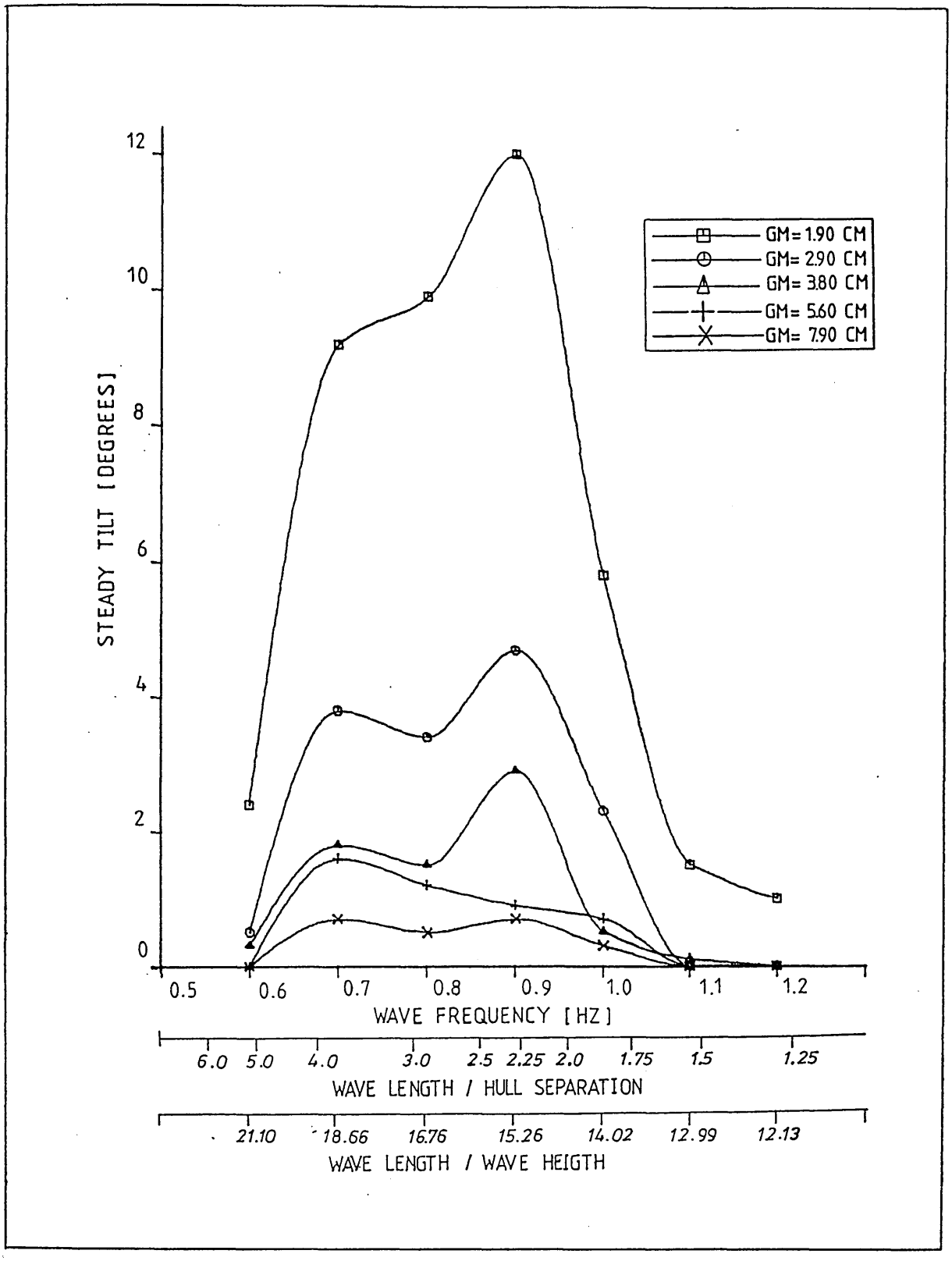

Fig. 62 - Experimental steady tilt vs wave frequency, wave length/hull separation and WL/WH ratio for varying $\overline{GM}$'s.
(The analysis is based on the modified ABS design wave formula[16].)

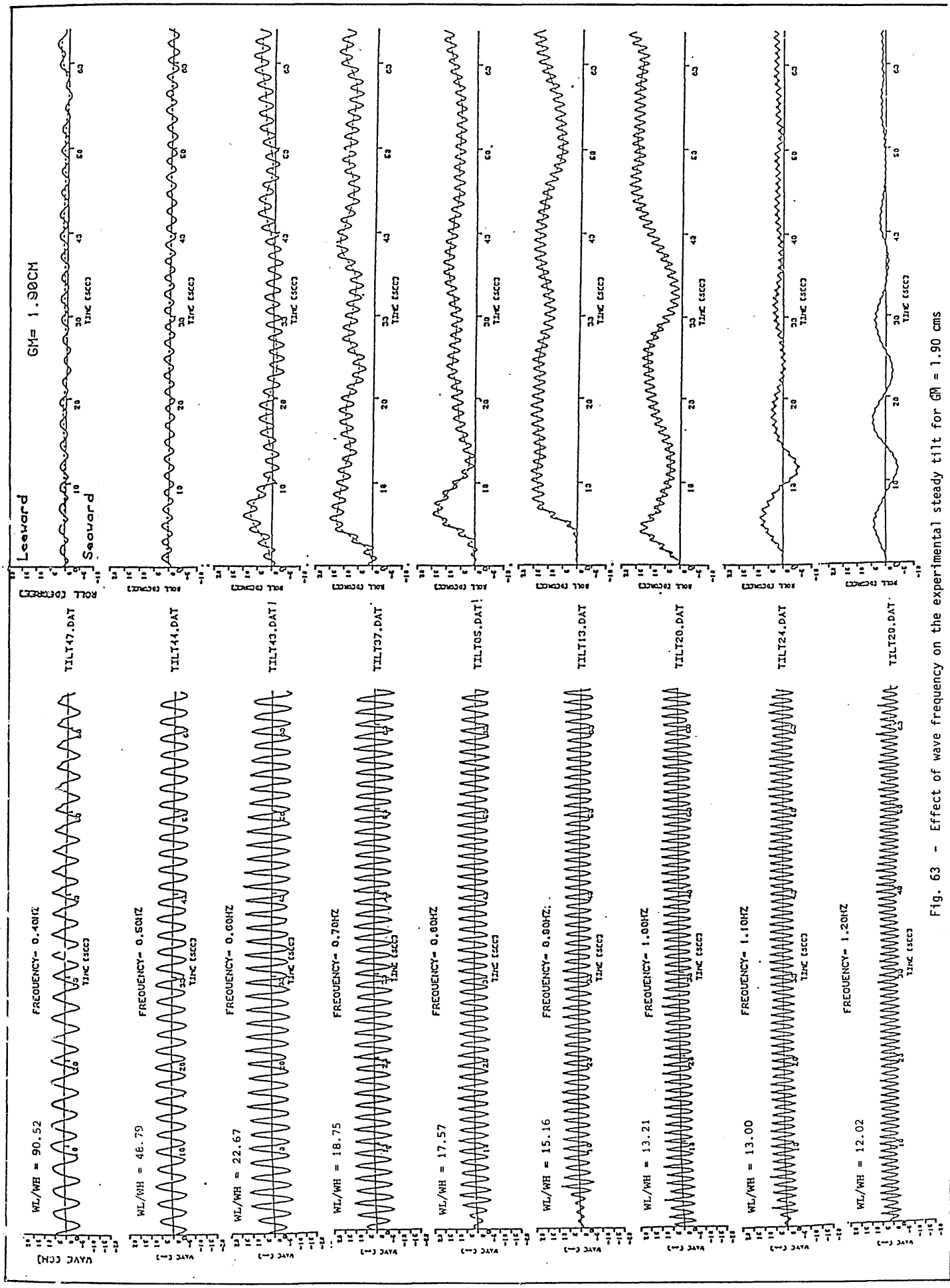

Fig. 63 - Effect of wave frequency on the experimental steady tilt for GM = 1.90 cms

However the investigation of about 300 test runs demonstrated that there was no general pattern followed by these curves at each particular frequency over the run duration. Figure 64 shows the pictures taken during the test runs at three different frequencies (TILT44, TILTØ5 and TILT29.DAT) in order to demonstrate the effect of frequency.

In Fig. 65, the effect of wave height on the steady tilt is demonstrated at the main peak (0.9 Hz) for the smallest $\overline{GM}$. As shown in these records once one had reached a height sufficient to induce tilt, it rapidly grew very large with slight height increments. Figure 66 demonstrates how tilt increased non-linearly with increasing wave heights at this particular frequency and $\overline{GM}$. In this figure ϕ_o and WH_o are the reference tilt and wave height values which are given in the figure.

Figure 68 shows the pictures taken during the tests relevant to the test runs considered (TILT11, 12, 13, 14) to demonstrate the effect of wave height.

Figure 69 shows the effect of $\overline{GM}$ on the steady tilt at the frequency of 0.9 Hz. To be able to make a comparison of the records the wave conditions should be the same. However this is practically impossible. Therefore as shown in the wave records of Fig. 69, the waves with the heights which are very close to each other (~ 14.5 cms) are considered. As shown in these records as the $\overline{GM}$ increased the steady tilt decreased non-linearly. The variation of the steady tilt with varying $\overline{GM}$ is shown in Fig. 67 for this particular wave frequency and height. In this figure ϕ_o and $\overline{GM}_o$ are the reference tilt angle and the smallest $\overline{GM}$.

In Fig. 70 the pictures taken during the tests relevant to the test runs considered (TILT14, 100, 69 and 226) to demonstrate the effect of $\overline{GM}$ on the tilt behaviour are given.

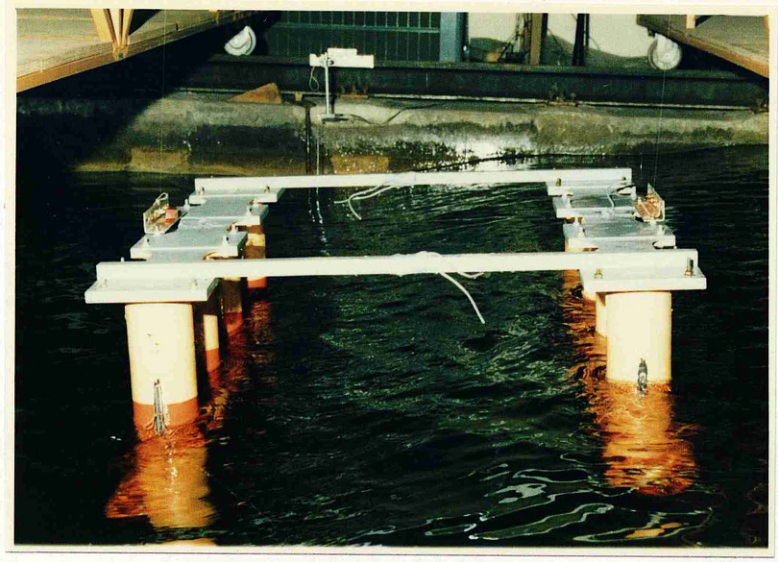

Test run file = TILT44.DAT
GM = 1.90 cms
W. Frequency = 0.5 Hz
W. Height = 12.80 cms
Steady tilt = 0.16°

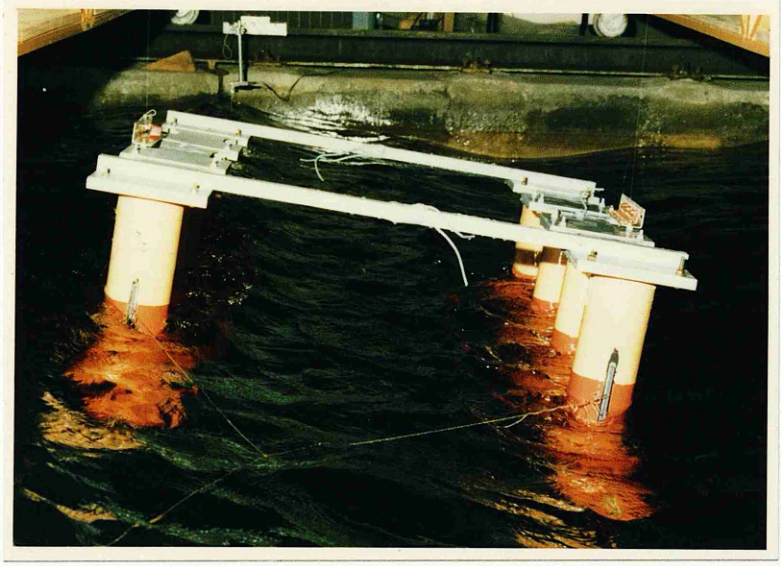

Test run file = TILTØ5.DAT
GM = 1.90 cms
W. Frequency = 0.8 Hz
W. Height = 13.88 cms
Steady tilt = 6.92°

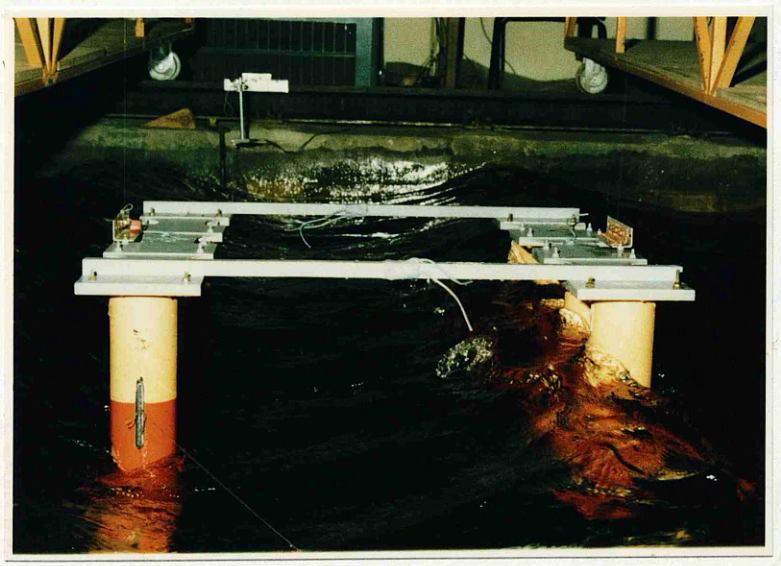

Test run file = TILT29.DAT
GM = 1.90 cms
W. Frequency = 1.2 Hz
W. Height = 9.02 cms
Steady tilt = 0.98°

Fig. 64 - Motion views illustrating the effect of wave frequency for $\overline{GM}$ = 1.90 cms

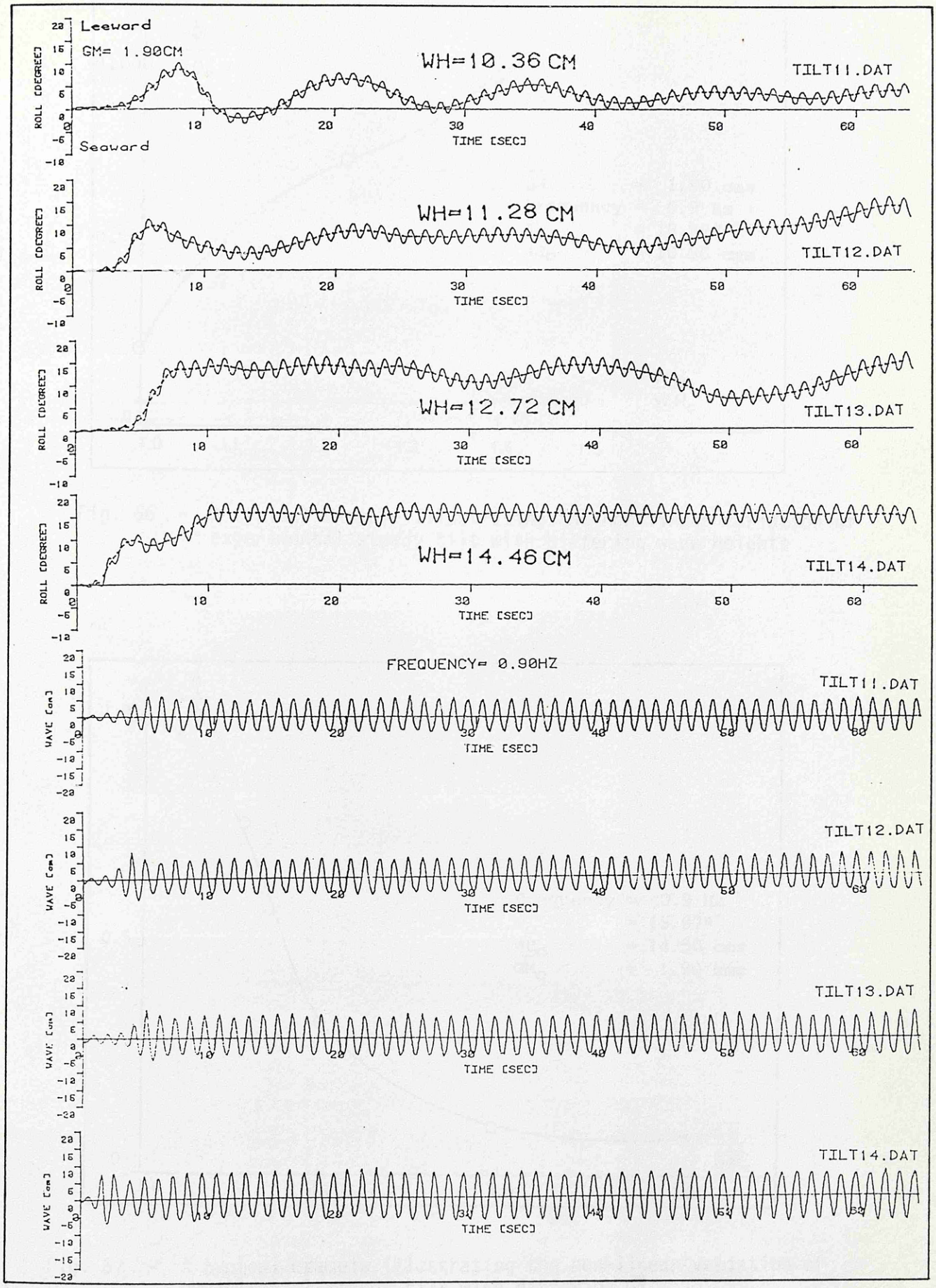

Fig. 65 - Effect of wave height on the experimental steady tilt for GM = 1.90 cms and frequency = 0.9 Hz

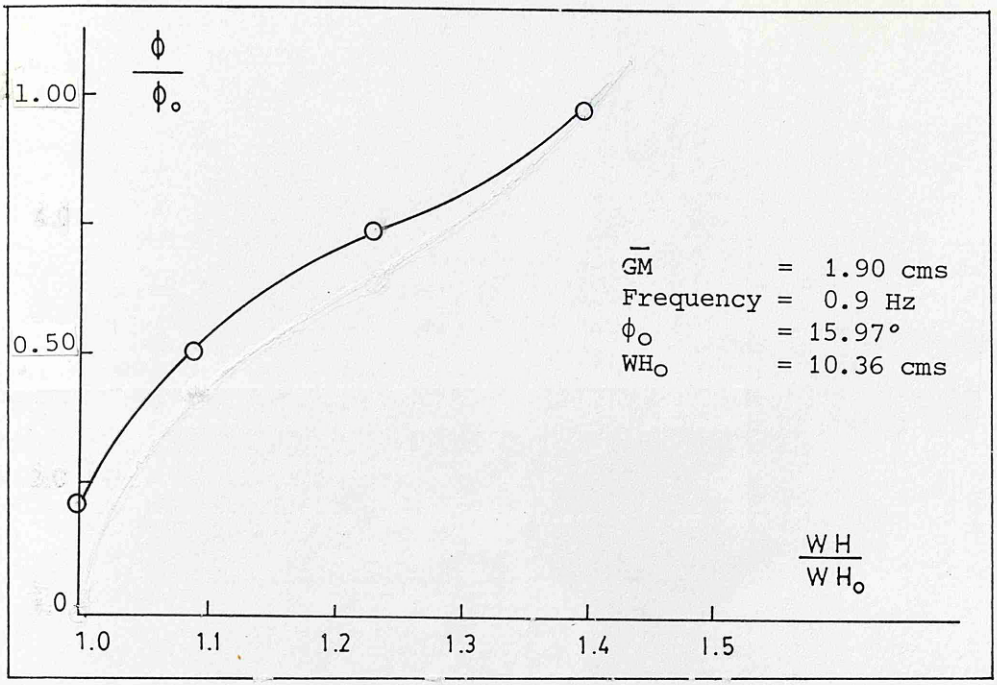

Fig. 66 - A typical example illustrating the non-linear variation of experimental steady tilt with differing wave heights

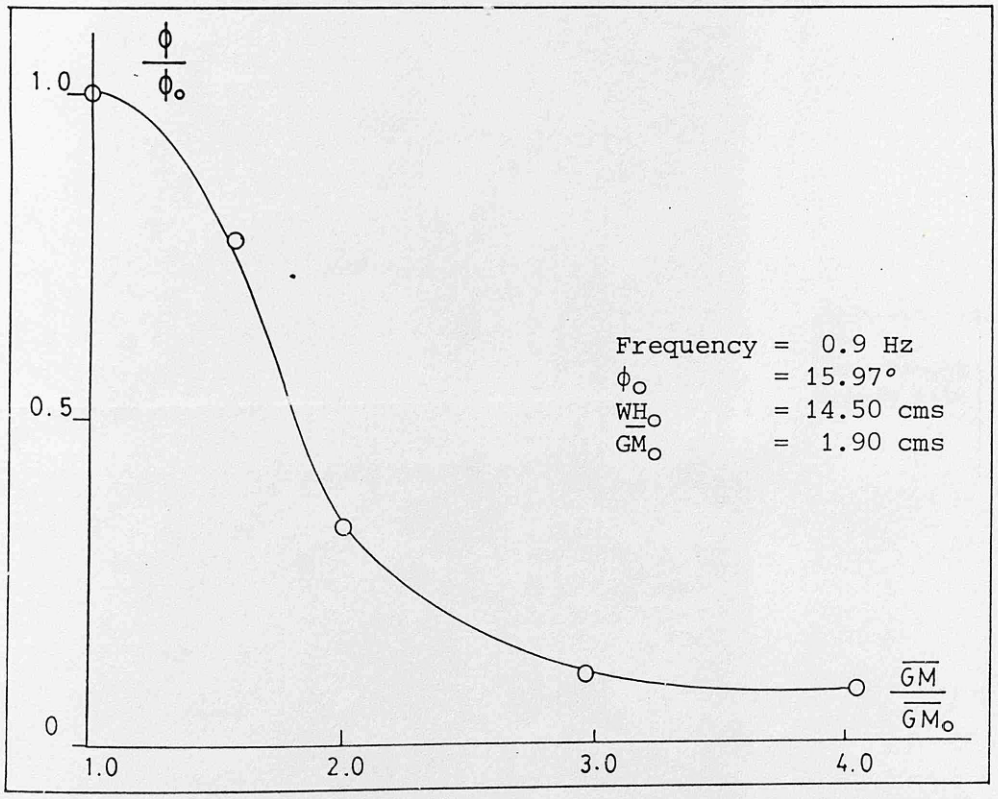

Fig. 67 - A typical example illustrating the non-linear variation of experimental steady tilt with differing $\overline{GM}$'s

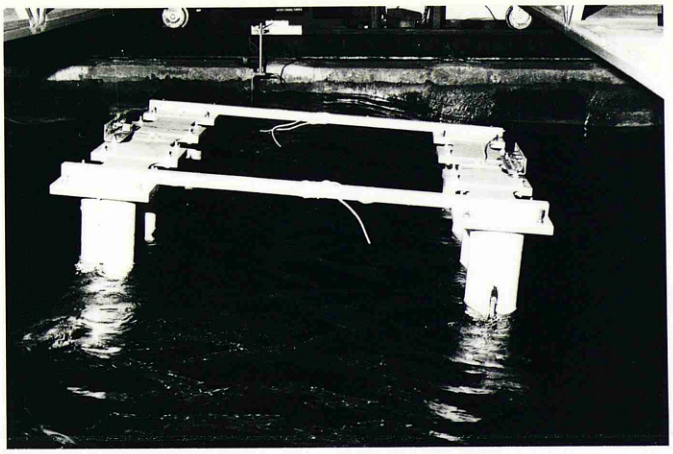

Test run file = TILT11.DAT
GM = 1.90 cms
Wave height = 10.36 cms
Steady tilt = 3.25°

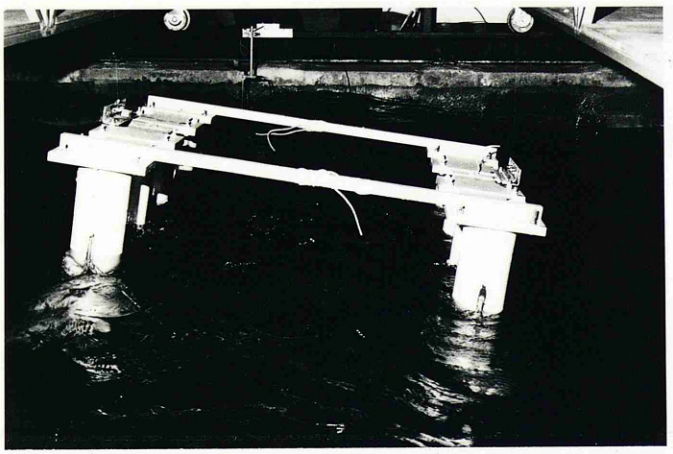

Test run file = TILT12.DAT
GM = 1.90 cms
Wave height = 11.28 cms
Steady tilt = 7.81°

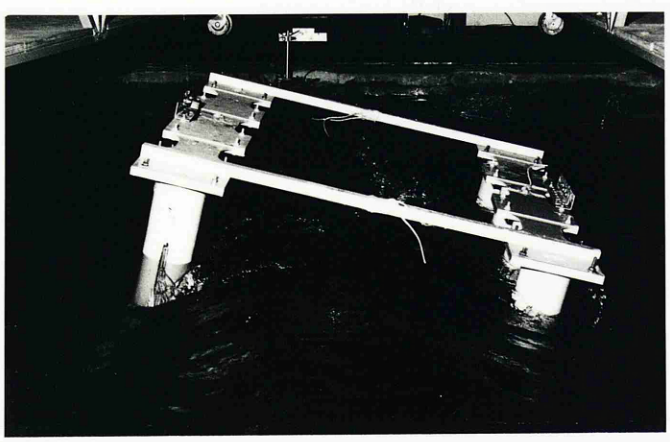

Test run file = TILT13.DAT
GM = 1.90 cms
Wave height = 12.72 cms
Steady tilt = 11.78°

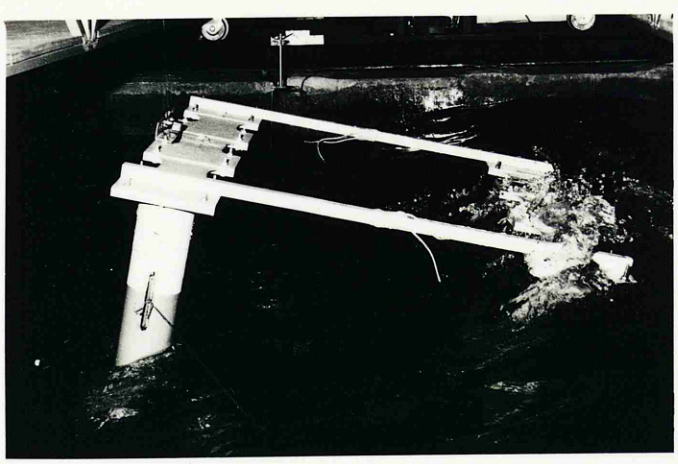

Test run file = TILT14.DAT
GM = 1.90 cms
Wave height = 14.46 cms
Steady tilt = 15.97°

Fig. 68 - Motion views illustrating the effect of wave height for $\bar{GM}$ = 1.90 cms

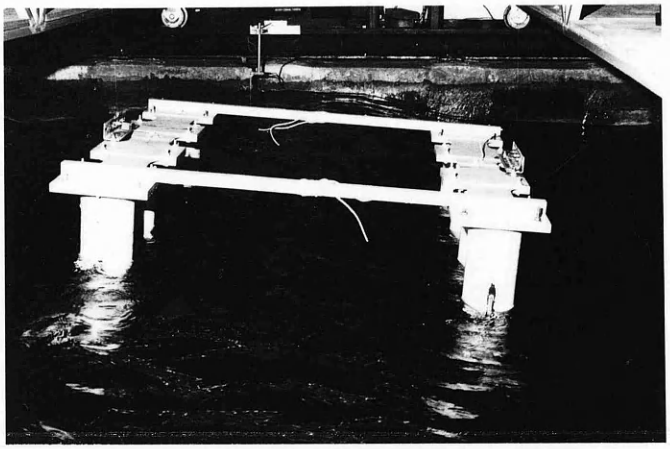

Test run file = TILT11.DAT
GM = 1.90 cms
Wave height = 10.36 cms
Steady tilt = 3.25°

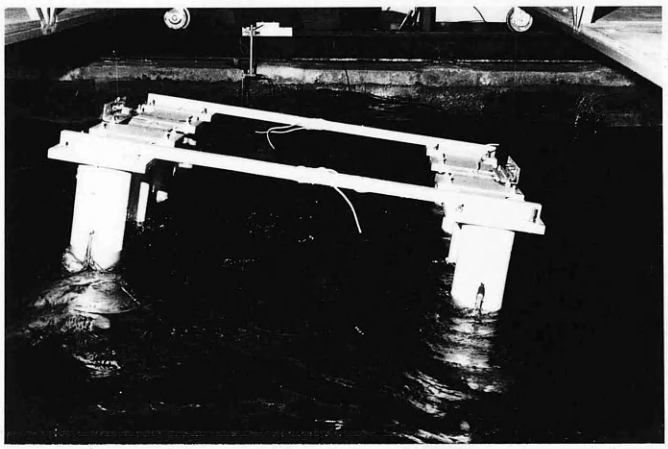

Test run file = TILT12.DAT
GM = 1.90 cms
Wave height = 11.28 cms
Steady tilt = 7.81°

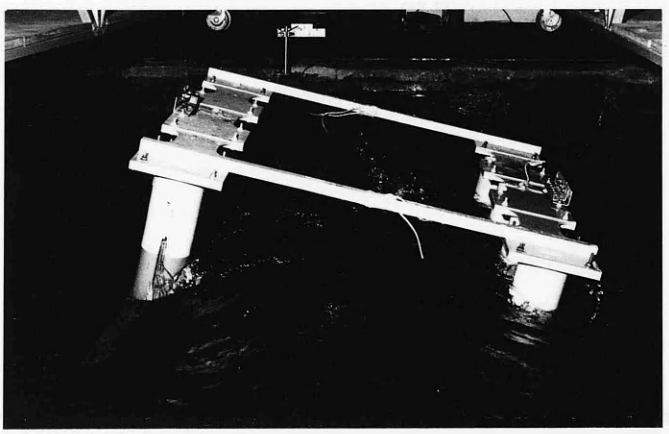

Test run file = TILT13.DAT
GM = 1.90 cms
Wave height = 12.72 cms
Steady tilt = 11.78°

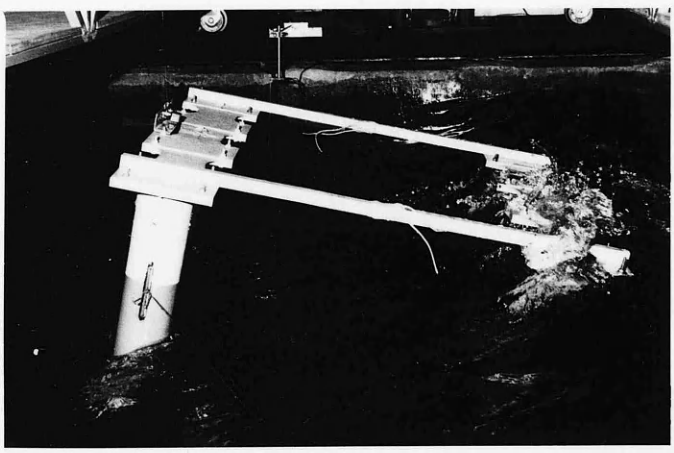

Test run file = TILT14.DAT
GM = 1.90 cms
Wave height = 14.46 cms
Steady tilt = 15.97°

Fig. 68 - Motion views illustrating the effect of wave height for $\overline{GM}$ = 1.90 cms

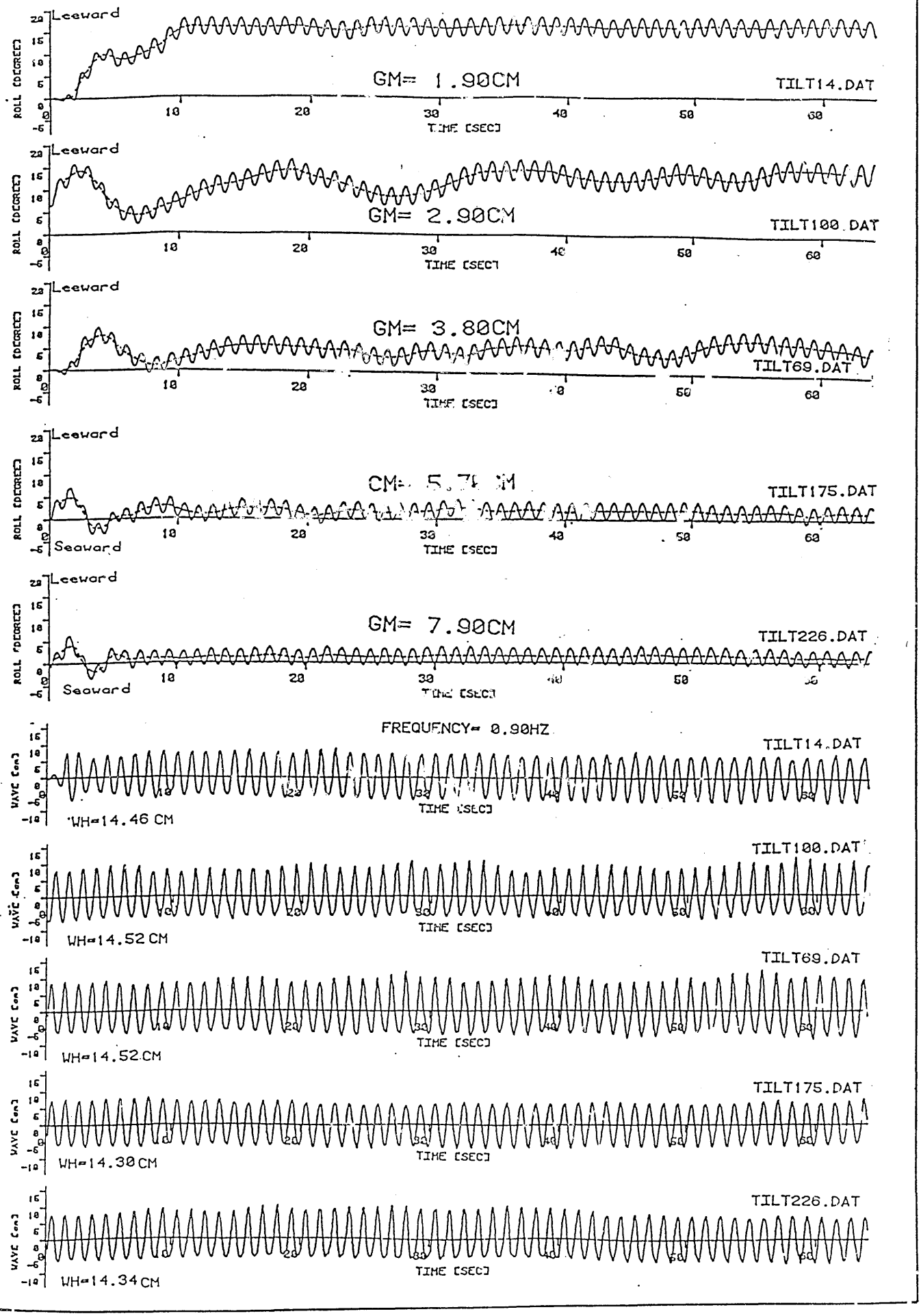

Fig. 69 - Effect of GM on experimental steady tilt for wave heights about 14.5 cms and frequency of 0.9 Hz

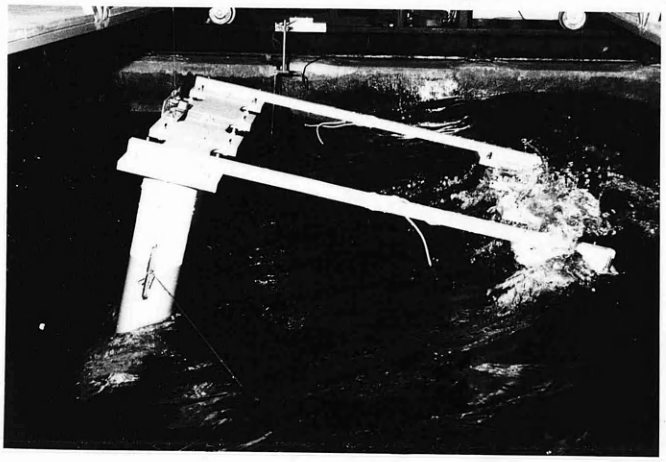

Test run file = TILT14.DAT
GM = 1.90 cms
W. Frequency = 0.90 Hz
W. Height = 14.46 cms
Steady tilt = 15.97°

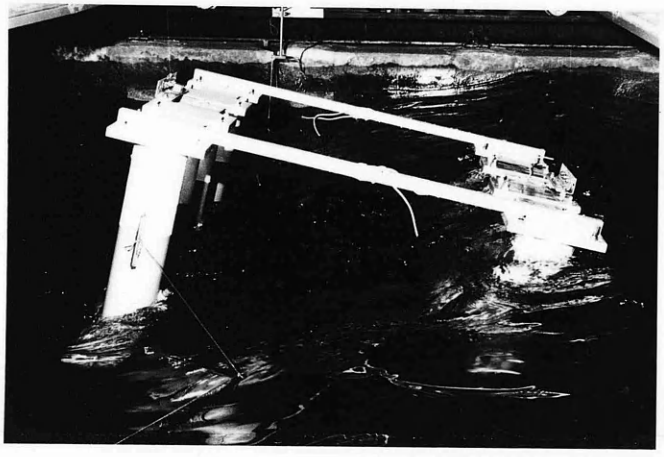

Test run file = TILT100.DAT
GM = 2.90 cms
W. Frequency = 0.90 Hz
W. Height = 14.52 cms
Steady tilt = 12.35°

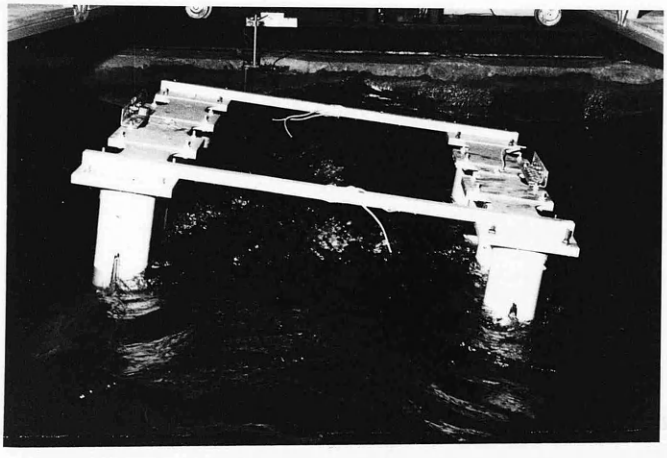

Test run file = TILT69.DAT
GM = 3.80 cms
W. Frequency = 0.90 Hz
W. Height = 14.52 cms
Steady tilt = 5.33°

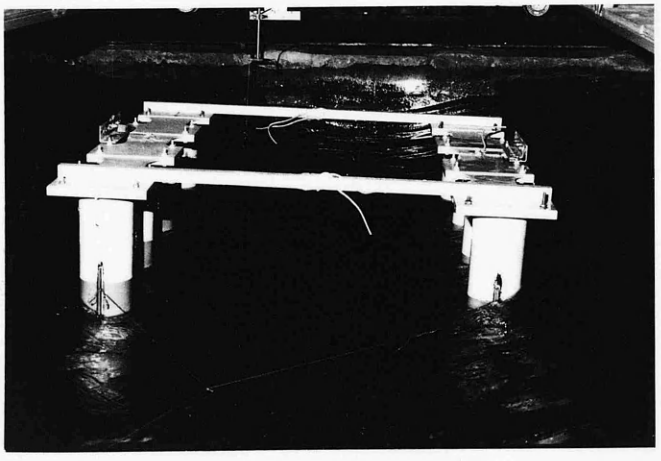

Test run file = TILT226.DAT
GM = 7.90 cms
W. Frequency = 0.9 Hz
W. Height = 14.34 cms
Steady tilt = 1.28°

Fig. 70 - Motion views illustrating the effect of $\overline{GM}$ for a frequency of 0.9 Hz

During the observations of the tests it was noticed that the first impact of the waves induced very large tilt angles and if the model was forced to drift, it was restrained by the mooring lines.

At one stage it was thought that this impact effect could be the starting mechanism for tilt and combined with the moorings could be responsible for the tilting. In order to investigate this effect, in the frequency region where the tilt was observed, the model was held in captive condition at the level position until the first group of waves passed the model and then released. In Fig. 71 two sample records among these exploratory tests are shown. As shown in these typical results, this did not affect the development of the tilt. But the duration of the development (transition time) was reduced considerably. As soon as the model was released tilt developed very quickly.

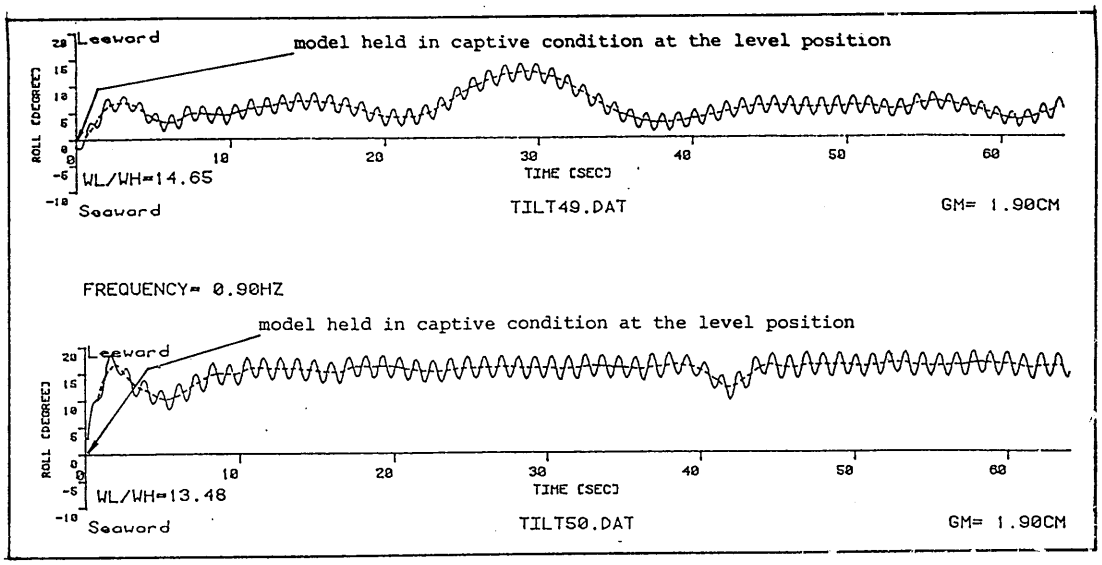

Fig. 71 - Effect of the initial impact of the waves on the steady tilt

In the majority of the tests the model was moored beam onto the waves with the mooring arrangement as shown in Figs 36 and 39. One of the possible mechanisms to cause the tilt could be the mooring lines. Therefore some tests were repeated without mooring lines at the frequencies where the tilts were observed. In Fig. 72 samples are shown of the response of the model when moored and freely floating at two different frequencies with very nearly the same wave height. Steady tilt developed in both cases although there are some differences in the magnitudes. It is difficult to say if the difference is due to effect of moorings only, because the wave heights are not the same for the same frequency and therefore there should be an effect due to wave height difference. As a matter of fact the main purpose of these exploratory tests was to see whether the moorings themselves were the mechanism to cause the tilting moment rather than to see the mooring effects on the magnitude of tilts. This requires precise measurements with and without the moorings under the same wave conditions.

During the tests it was observed that the model always developed its tilt in the leeward direction if it developed any tilt at all. In the foregoing Tables 11 through 15, the magnitudes of the tilt were tabulated at Column 5 in which the minus sign demonstrated the tilt developed in the seaward direction. In over 250 test runs only on 3 or 4 occasions tilts developed in the seaward direction with a negligible magnitude at lower frequencies. Even with these cases it is hard to define them as 'seaward tilts' because it was varying about the zero level and the area under the backbone curve on the seaward side was slightly greater than the leeward side.

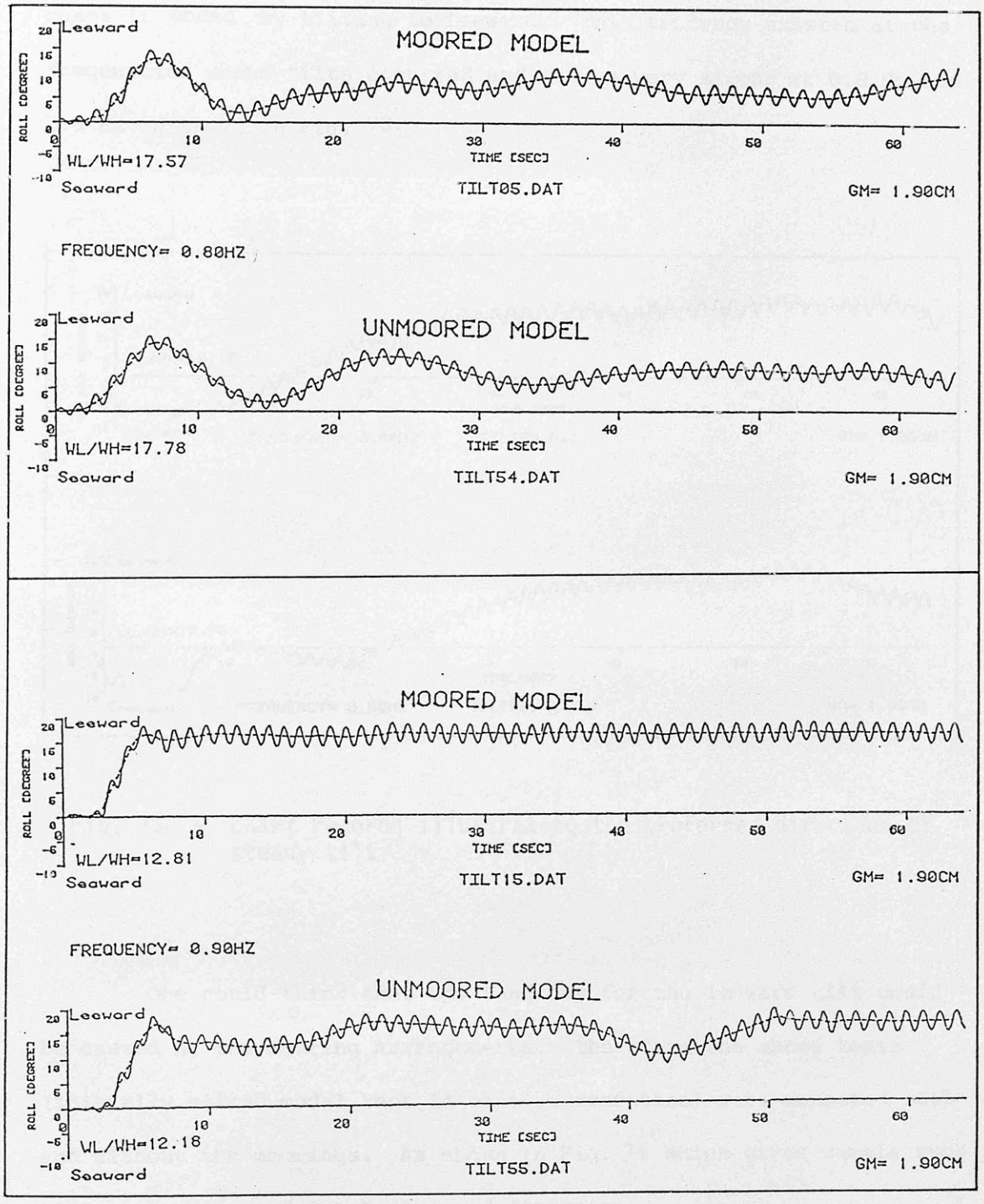

Fig. 72 - Effect of moorings on the steady tilt

In order to investigate if there was any tendency for a steady tilt in the seaward direction, at certain frequencies, the model was deliberately tilted to seaward at the beginning of the tests but in all cases it ended by tilting to leeward. This tendency existed at the frequencies where tilts occurred and it was very strong at 0.8 Hz and 0.9 Hz as shown in Fig. 73.

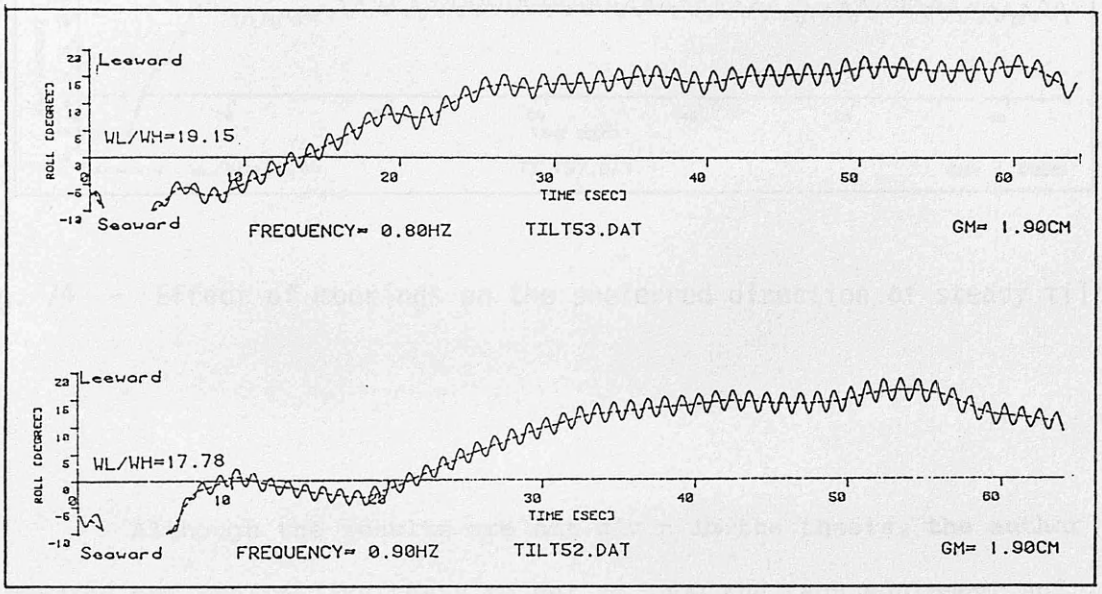

Fig. 73 - Chart records illustrating the preferred direction of steady tilt

One could think that the tendency for the leeward tilt could be caused by the mooring arrangements. Therefore the above tests (initially tilted model kept in captive condition) were repeated with and without the moorings. As shown in Fig. 74 which gives sample runs tilt again occurred in the leeward direction.

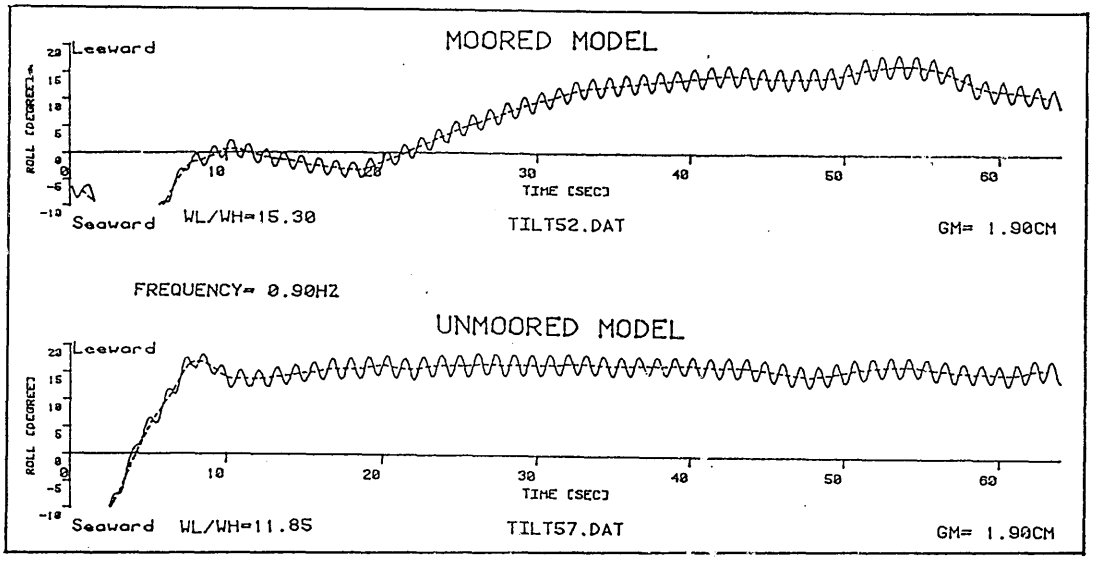

Fig. 74 - Effect of moorings on the preferred direction of steady tilt

Although the results are not given in the thesis, the author carried out preliminary tests to get to know the tank equipment and to observe the phenomena. In these tests the model did not have fairleads at the columns. Its original fairleads were located at the mid-end of the pontoons as shown in Fig. 32. Therefore the model was moored from these fairleads with the same type of arrangement under the water. However, the findings were very similar to those obtained from the tests in the thesis. No seaward tilt was observed and the frequency region where tilt occurred was the same as in the present tests.

In the foregoing it was stated that at about the natural heave resonance frequency there was an increase in the measured tilt values compared to the adjacent frequencies. This is shown by the time history records in Fig. 75. The closest frequencies to the natural heave frequency (0.4 Hz) were 0.3 Hz and 0.5 Hz. It was practically impossible

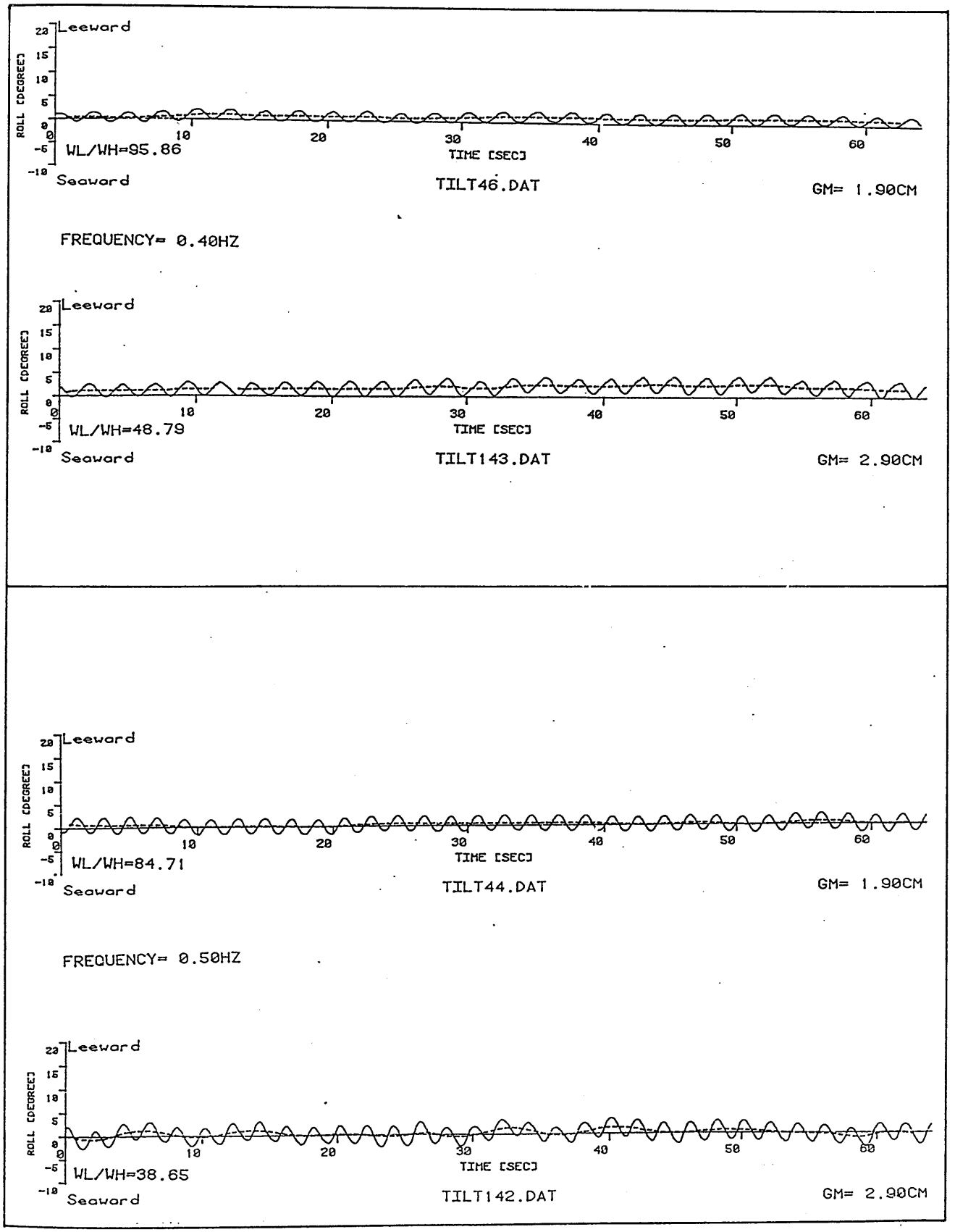

Fig. 75 - Chart records about the natural heave frequency

to carry out a test run at 0.3 Hz since the waves became non-sinusoidal. However the test runs at 0.5 Hz with steeper waves demonstrated virtually no tilt compared to the tests at natural heave frequency whereas slight tilt of about 2°-3° was observed with moderate waves.

3.5 ROUGHENED MODEL TESTS

In order to investigate if the viscous effect played any significant role for tilting, the model's underwater geometry was coated by a roughened paper which provided a roughness of about 0.75% of the pontoon diameter (see Figs 76 and 77).

It was decided to test the coated model at a frequency of 0.8 Hz and 0.9 Hz where the worst tilt was observed with the smooth model. If there was any mechanism creating or contributing to the tilt behaviour, this would be reflected in the measurements.

The addition of the roughened paper changed the model's $\overline{GM}$. From the inclining tests the new $\overline{GM}$ was found to be 3.50 cms. The measurements with this $\overline{GM}$ at these particular frequencies are given in Table 17.

In order to compare the tilts measured with the roughened and smooth model, in Fig. 78, the above measured tilt values and the previous measured tilt angles with 3.80 cm $\overline{GM}$ (the closest to 3.50 cms) were plotted at these two particular frequencies. The solid and dashed lines are the best-fit curves passing through the experimental data. As indicated in this figure the roughened model experienced larger magnitudes of tilt but followed the same trend as the smooth model. It was believed that this constant increment was due to the slight difference in the $\overline{GM}$s.

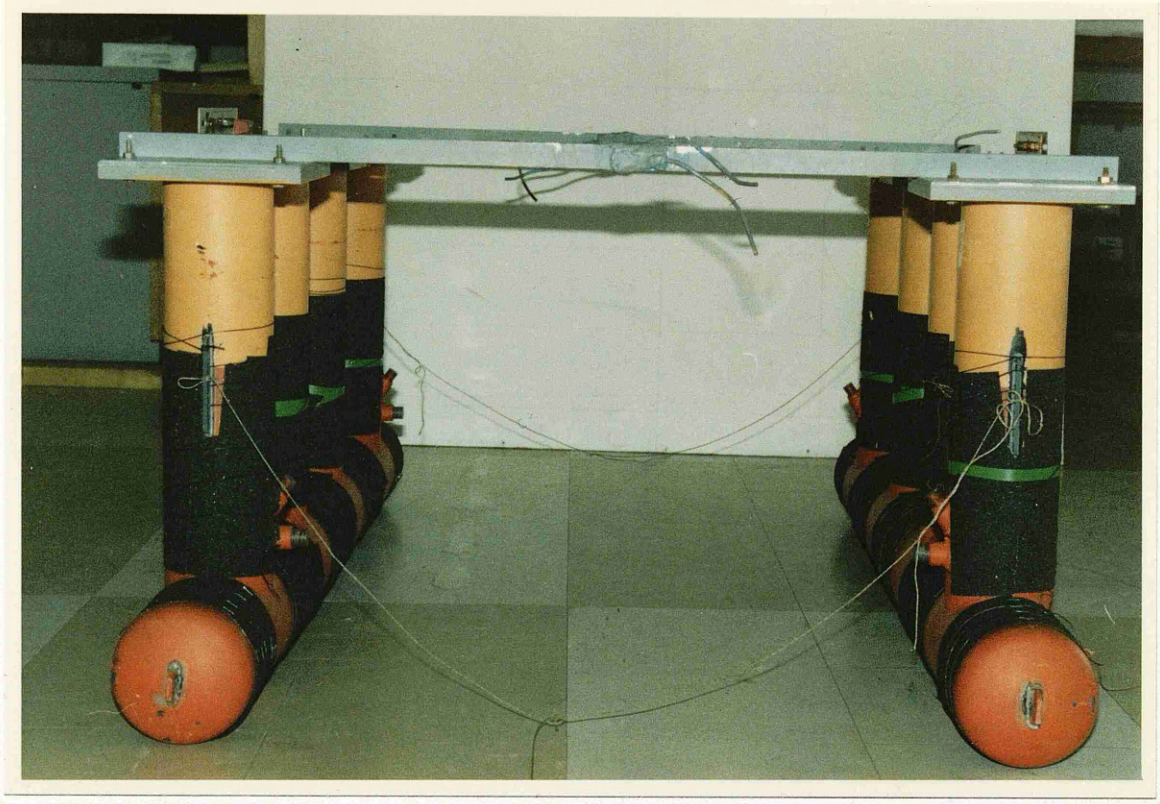

Fig. 76 - Front view of the coated model by abbrasive paper

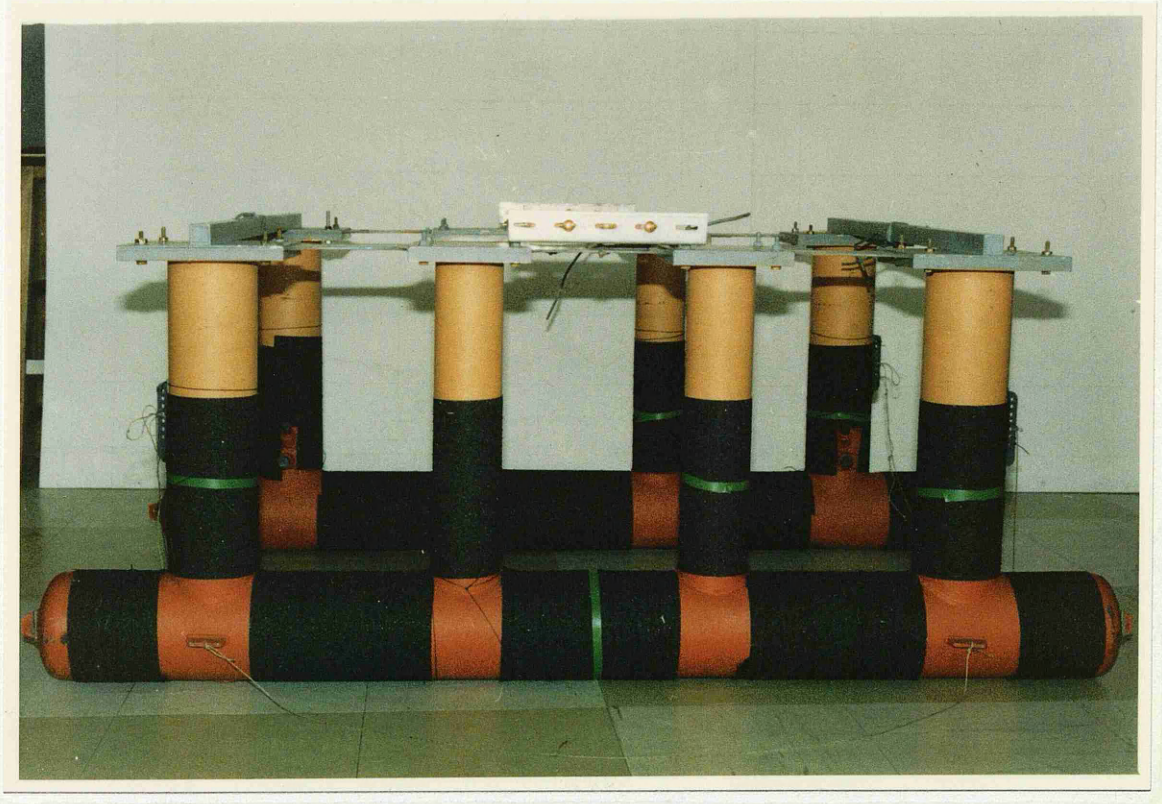

Fig. 77 - Side view of the coated model by abbrasive paper

Run Data File Number	Characteristic W. Frequency (Hz)	W.Amplitude (cm)	W.Length / W.Height	Steady Tilt (degree)	Steady Heave (cm)	Oscillatory Roll RAO (degree/cm)	Oscillatory Heave RAO
TILT147.DAT		5.16	23.64	1.03	0.32	0.298	0.166
TILT148.DAT		5.50	22.16	1.06	0.37	0.292	0.171
TILT150.DAT		5.78	21.10	1.43	0.55	0.298	0.183
TILT149.DAT	0.8	6.76	18.04	2.21	0.61	0.271	0.173
TILT151.DAT		7.29	16.73	4.34	1.06	0.305	0.178
TILT152.DAT		8.42	14.49	8.77	1.03	0.313	0.190
TILT153.DAT		8.46	14.41	11.97	0.60	0.347	0.227
TILT154.DAT		5.16	18.67	1.16	0.68	0.298	0.058
TILT155.DAT		5.27	18.27	1.58	0.69	0.305	0.057
TILT156.DAT		6.16	15.64	2.36	0.89	0.301	0.065
TILT157.DAT	0.9	6.52	14.78	5.90	0.94	0.319	0.084
TILT158.DAT		6.65	14.48	7.91	0.95	0.337	0.093
TILT159.DAT		7.31	13.18	9.37	0.70	0.317	0.107
TILT160.DAT		7.70	12.52	12.93	0.70	0.356	0.137

Table 17 - Experimental wave and motion data of the roughened model for $\overline{GM}$ = 3.50 cms

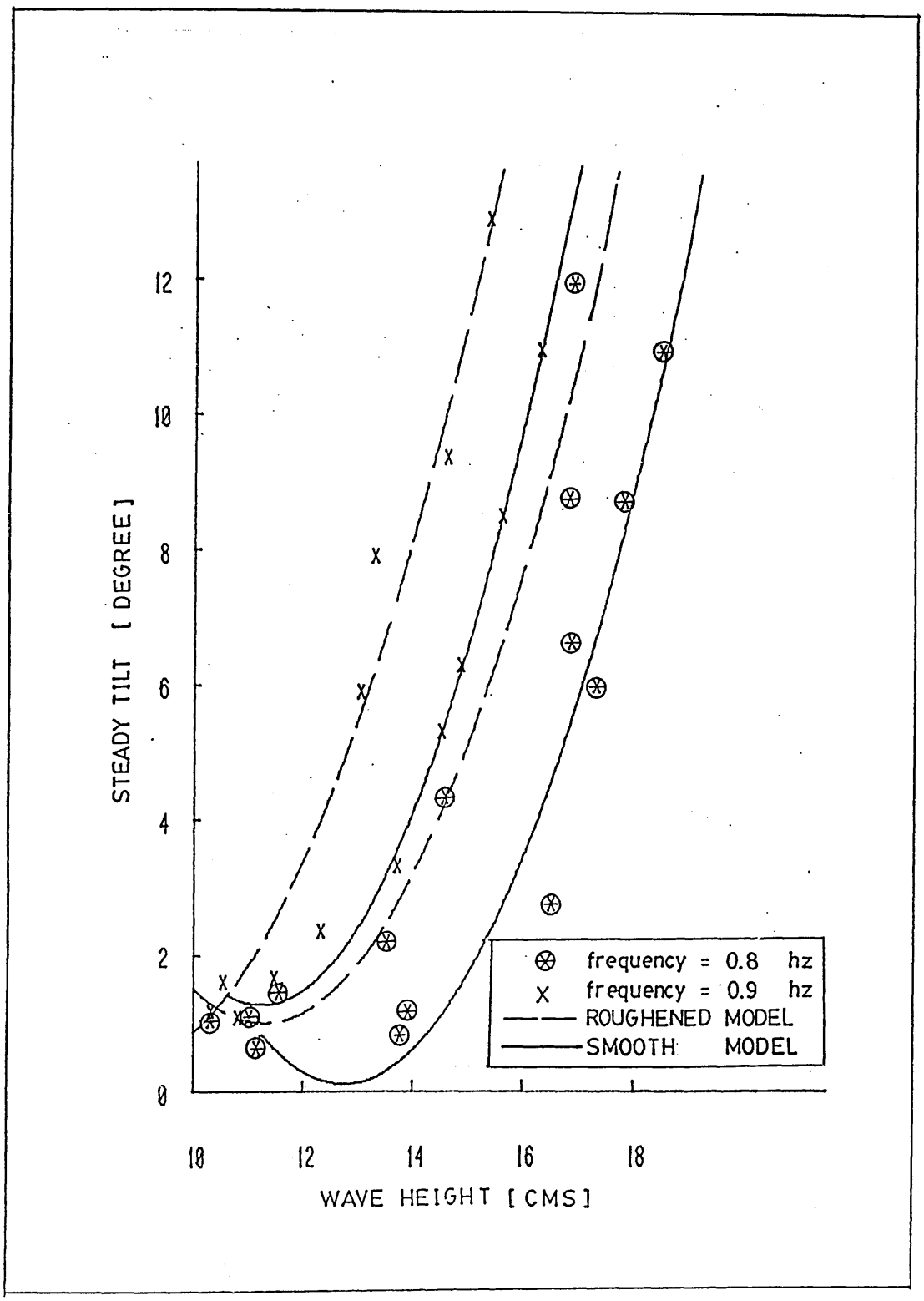

Fig. 78 - Comparison of the steady tilt measured with the roughened model ($\overline{GM}$ = 3.50 cms) and smooth model ($\overline{GM}$ = 3.80 cms)

In Fig. 79, this effect is shown with the time history records at about the same conditions. As shown in the figure it is difficult to find any major difference in the trend of the curves except the difference in the magnitudes which was due to the difference in the $\overline{GM}$s.

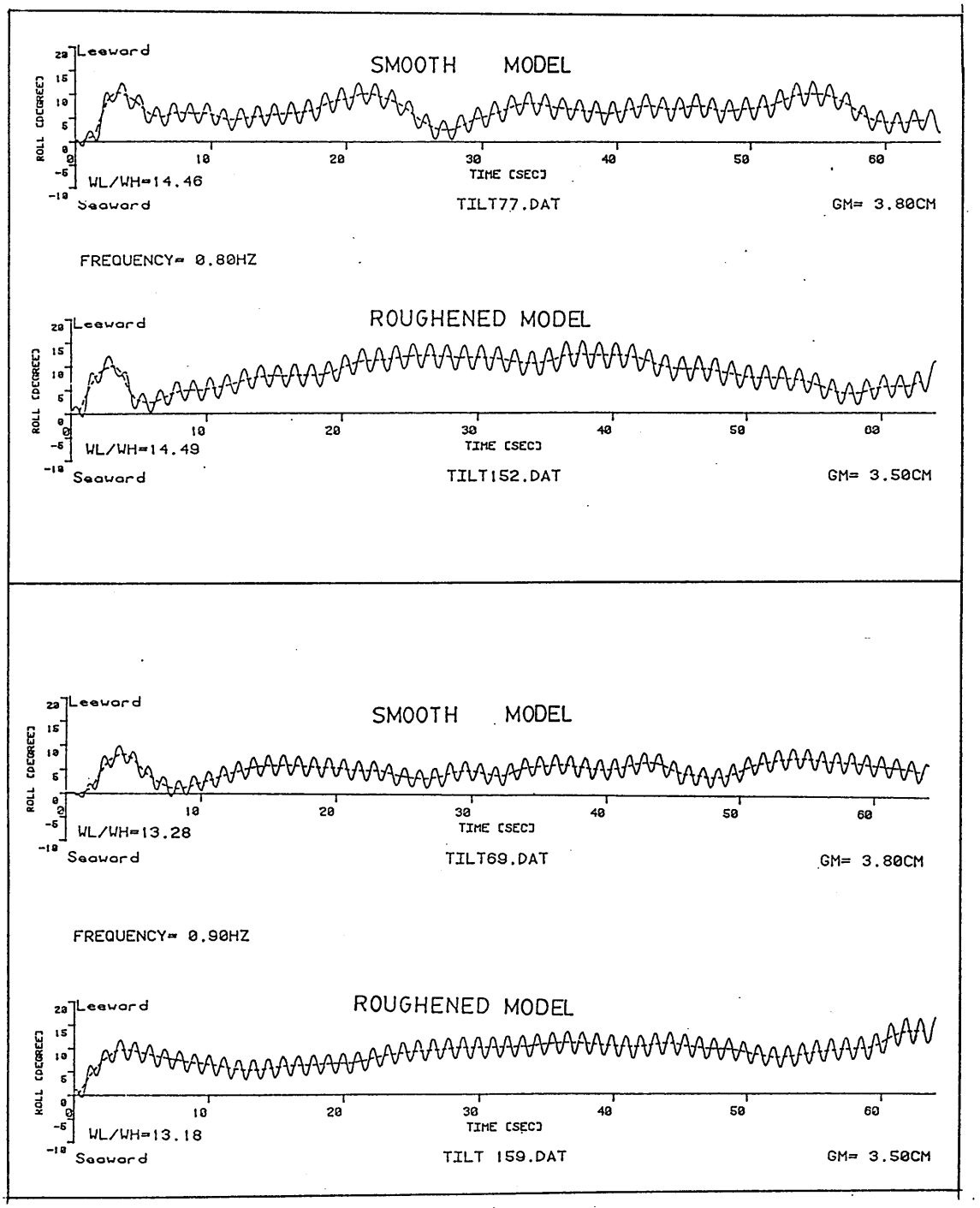

Fig. 79 - Chart records illustrating the effect of roughness on the the steady tilt motion

Finally, as stated earlier, abrupt changes of the underwater geometry at different positions and wave conditions could cause a tilting. However, as can be seen in Tables 4 through 8, the inclining tests in calm water demonstrated that there was no non-linearity in roll restoring moment ($\Delta \overline{GM} \sin\phi_i$) up to 10°. By using additional test weights this angle was extended up to 17° at which the deck became immersed and the roll restoring moment was still linear.

3.6 FORCE TESTS

The main objectives of the force tests were to determine the wave exciting force distribution on the pontoons of the semi-submersible since an unequal distribution of the oscillatory wave exciting force on each hull could be a mechanism to cause the tilting problem. It was also hoped to obtain the effect of hull separation on the wave load distribution.

It was assumed that the total wave-exciting force on the model was dominated by the forces on the pontoons. Therefore a simplified model, which consisted of two circular hulls only, was used as shown in Figs 80 and 81. It was originally intended to complete these tests by measuring the wave loads on the original model (columns and pontoons together) to determine the effect of columns on the phenomena. However, experimental difficulties, which arose during the tests with the simplified model showed that the set up for the original model could be difficult and inconclusive. Therefore it was not carried out.

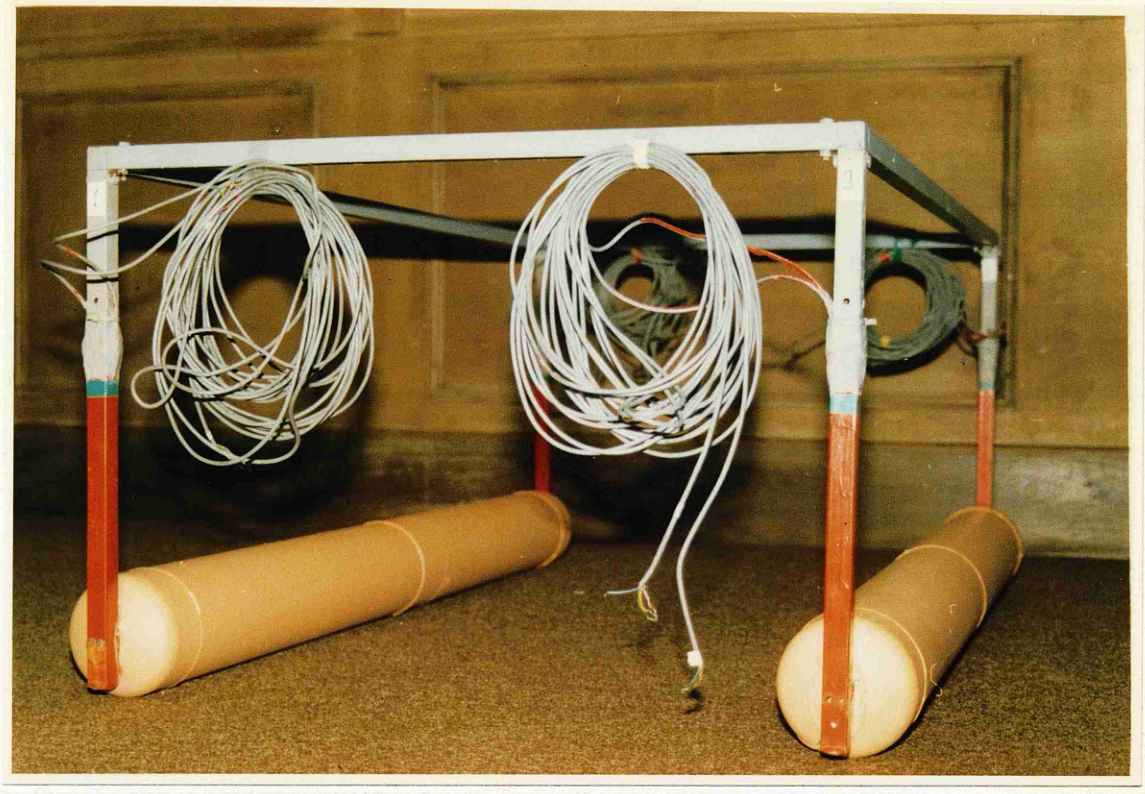

Fig. 80 - Front view of the twin circular pontoons used for the force tests

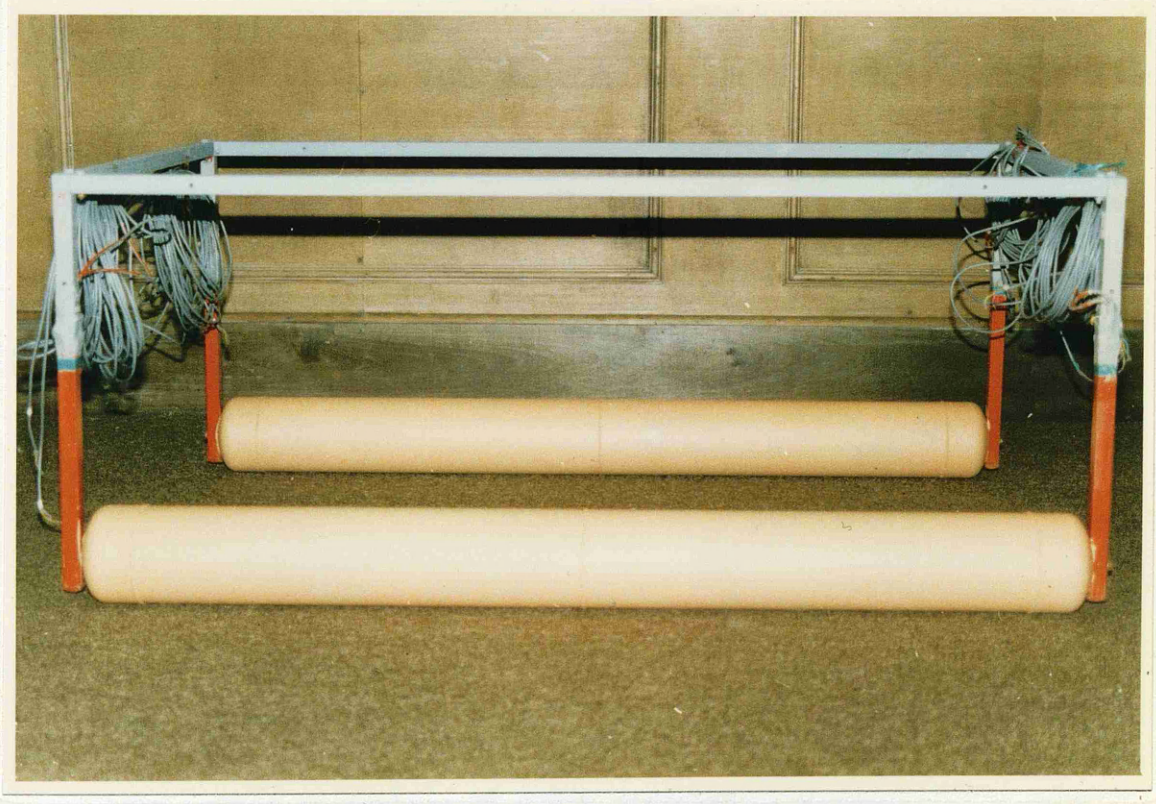

Fig. 81 - Side view of the twin circular pontoons used for the force tests

Description of Model

As shown in Figs 80 and 81 the simplified model consisted of two circular hulls, which were made of PVC piping and a frame work to carry the hulls. The main dimensions are shown in Fig. 82. The frame work had four legs supporting the hulls at their ends and two transverse and two diagonal beams connecting these legs together at their tops. The two transverse beams were adjustable in length in order to study the effect of hull separation. The whole frame work was constructed of rectangular cross-section steel tubes (25.4 × 25.4). This type of material was required to obtain rigidity for the system.

Instrumentation

The wave exciting forces in the heave and sway modes were measured on each hull in two steps by using 'load cell transducers'. Two legs (legs 1 and 4), which hold one hull, were converted into load cells by using strain-gauges (S/G). The model was oriented beam onto the waves and clamped onto a stout platform which was situated halfway along the tank length. Figure 83 shows the general arrangement of the set up. The draught was set at 36 cms as for the original model. Four wave probes were used to measure the wave heights at three different places as shown in Fig. 83.

As a matter of interest and to measure the interference effect, the first group of tests were carried out on the single isolated hull only. Therefore the other half of the model was removed. For the remaining tests, the model was assembled and the heave and sway exciting forces exerted on one hull measured in the presence of the other. The measurements were taken in a range of S/R = 2.0, 3.0, 4.0, 5.96 (2S = hull separation centre to centre; 2R = D = diameter of a hull).

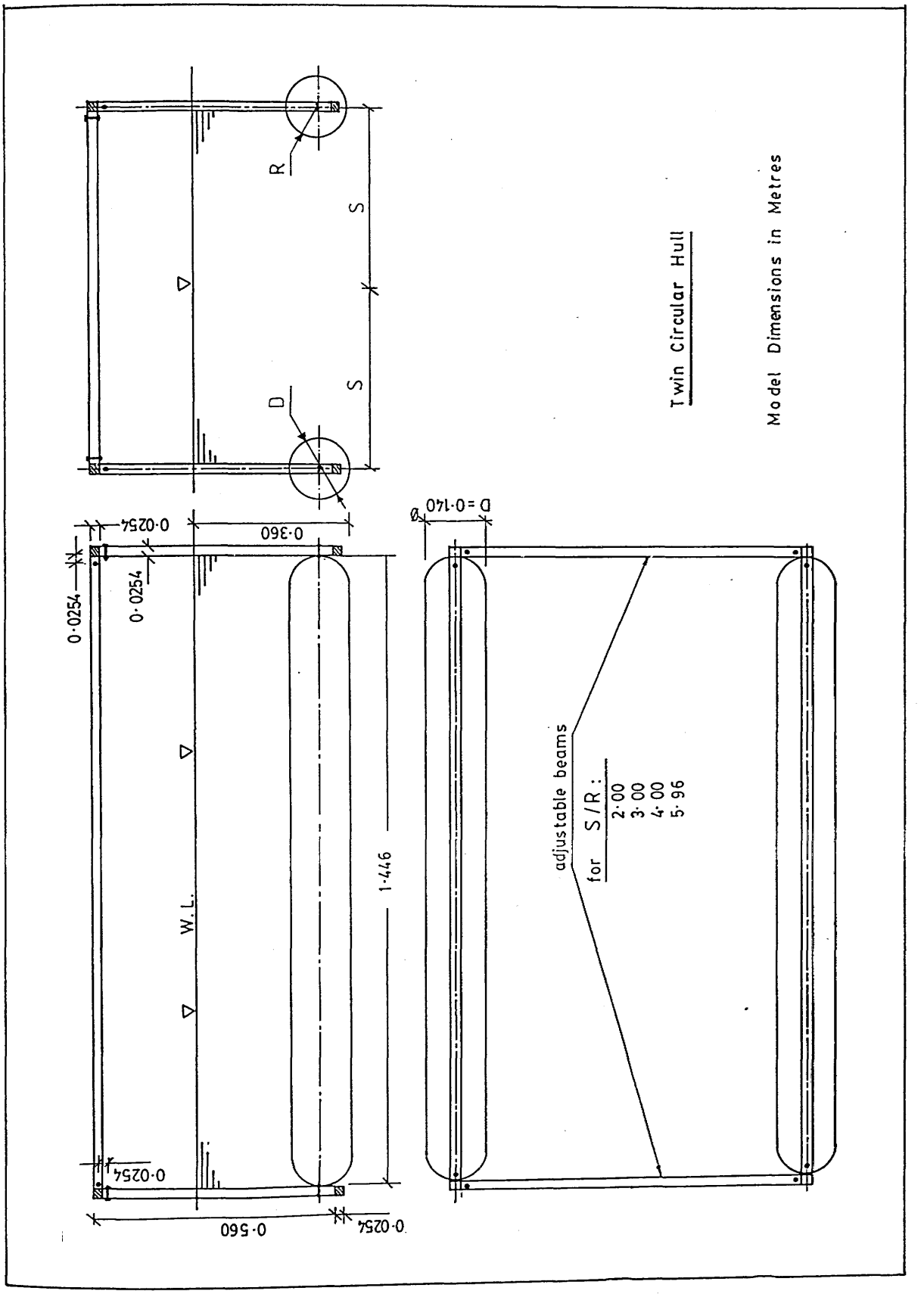

Fig. 82 - General arrangement of the twin circular pontoon model tested

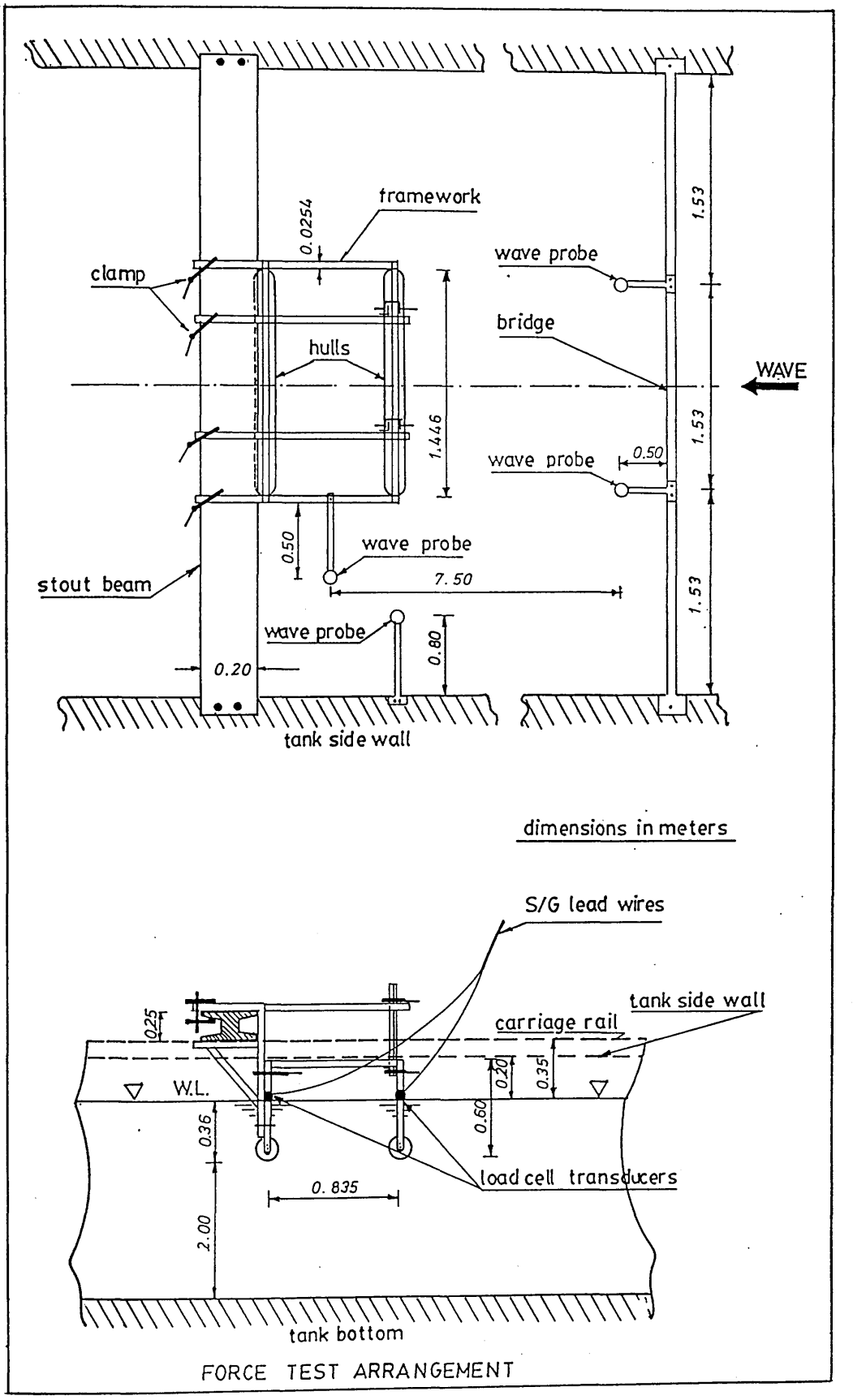

Fig. 83 - Experimental setup for the force tests

Since the S/G's were installed on two legs which held one hull, the total force acting on the hull was the sum of the corresponding force value on each leg. In this way, if there was any change in the wave height along the hull length, this would be taken into account. Otherwise the measurements on one leg would give half the total force on the hull. In fact the tests demonstrated that the force was substantially equally distributed on each leg.

In order to measure the forces on each hull separately, the tests were carried out in two steps at each spacing. Firstly the measurements were taken on the seaward hull and secondly, the model was turned through 180° and the measurements were repeated on the leeward hull. This was done to reduce the amount of measuring and recording equipment. It might be argued that if the forces were measured on both the hulls simultaneously the results could be different since in the above procedure it would be impossible to simulate the same wave conditions in both tests. This could introduce an error depending on wave height and changes in the model position, because as will be shown later, the forces were not exactly linearly proportional to wave height.

In order to clear up this uncertainty the tests at the largest hull separation were repeated with a new set of load cells which were fitted to one leg of each hull (the previous tests demonstrated the forces on each leg of one hull were very much equally distributed, therefore one transducer on one leg of each hull was satisfactory). The total force on each hull was calculated by doubling the measured force value on the leg. Fortunately this did not bring about any major difference compared to the previous measurements.

Load Cell Transducers

The wave exciting forces in heave and sway mode on the hulls were measured by 'load cell transducers' [42,43]. They were made up with the existing facilities in the laboratory by converting the legs into the load cells with the aid of the foil-type electrical resistance S/G's [42,44]. By calibrating the load cell to read in load units other than strain, the wave loads on each leg could be measured directly.

In order to measure the wave exciting force in heave mode four S/G's were mounted at the central region of the leg above the water level as shown in Fig. 84. According to the procedure given in refs [42,45] two opposite S/G's were in the vertical direction on face-1 and face-3 and the other two were in the transverse direction on face-2 and face-4.

To measure the sway forces another four S/G's were fitted, just above the previous S/G. They were vertically oriented with a pair on two opposite faces - face-4 and face-2 in the wave travel direction (see Fig. 84).

For the strain gauge installation the procedures given in refs [45,46] were followed and they were protected and waterproofed by special protective coatings and aluminium foil to avoid gauge instability, mechanical damage and chemical attack as shown in Fig. 85.

As described above the load cell was composed of the S/G's which were passive resistors. Therefore there was a need for a power source in order to interpret the changes in the resistance caused by mechanical strain (or loads) measured. This could be achieved by a bridge circuit which produced an out of balance voltage. Furthermore, this voltage had to be amplified and displayed so as to represent the required force units. At this stage 'the Wheatstone Bridge', which is the most common bridge circuit, was used as a direct readout device where the output voltage was

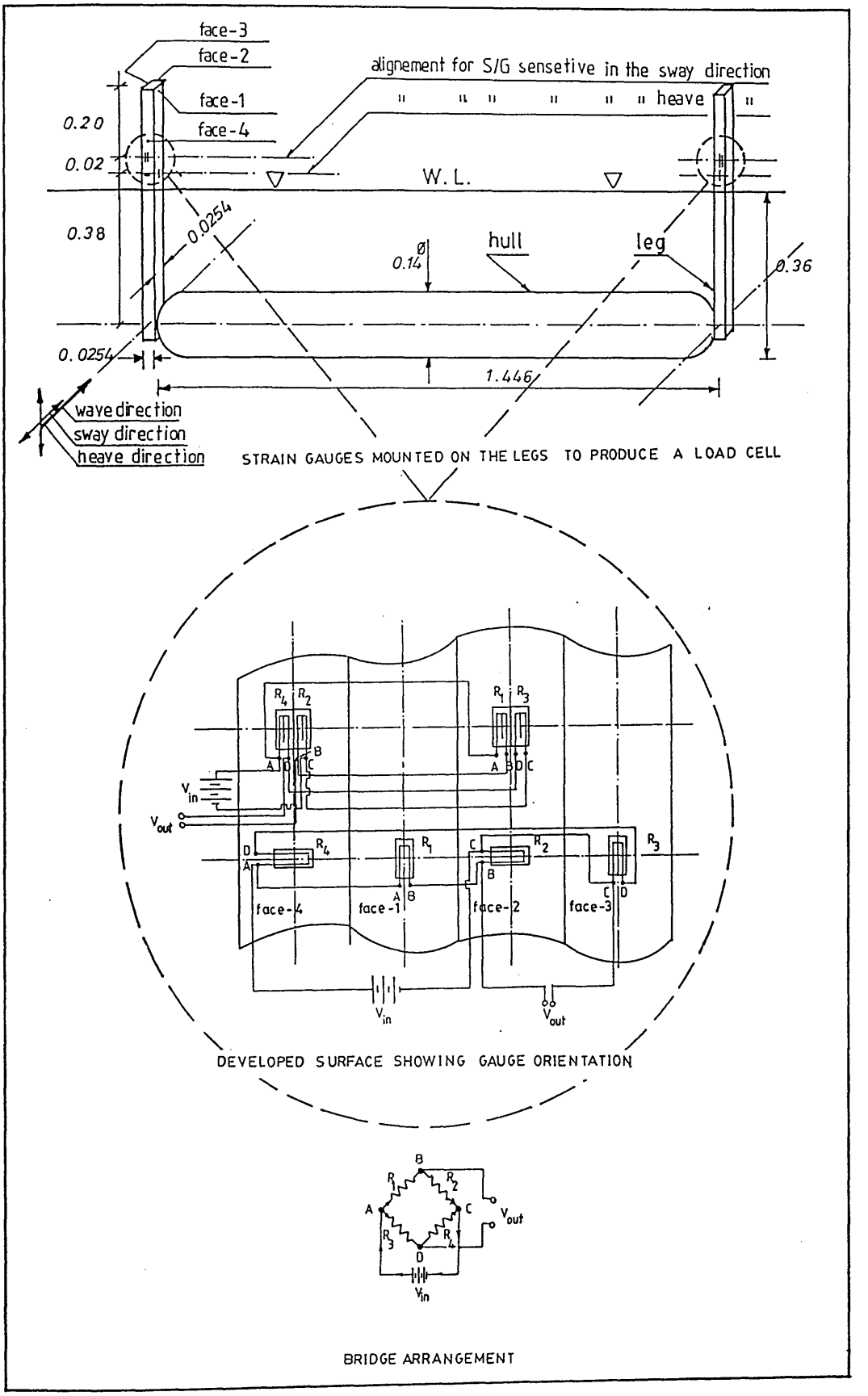

Fig. 84 - General arrangement for the load cell transducers

measured or related to strain (or load). The four active S/G's were placed in the bridge with one S/G in each of four arms - the full bridge arrangement - as shown in Fig. 84[42]. This type of arrangement further increases the sensitivity of the measuring system, gives improved temperature compensation and minimal errors due to connection of the system since the leadwires from the measuring point to the instrumentation were outside the measuring circuit. Before the system was loaded to the Wheatstone Bridge, it was balanced (i.e. by satisfying $R_1/R_4 = R_2/R_3$) as the output voltage $V_{out} = 0$. When the system was loaded a change in the resistance would unbalance the bridge and produce an output voltage ΔV_{out} across the output terminal. By measuring this voltage and using the calibration curve, the voltage readout was converted into the required load values.

However, during the tests the measurements in the axial direction were troublesome. Although the load cell arrangement in heave mode, as shown in Fig. 84, was essentially sensitive only to changes in the axial direction (i.e. independent of either bending or torsional loads) when the legs were subjected to the bending due to sway force only, while there was no load in the axial direction a slight readout in the axial direction was recorded. The contribution was a maximum of about 7 to 8% for a 4 kg force sway force in the wave travel direction. It was impossible to do any correction by using calibration curves for this error since its magnitude and direction was changing randomly as the sway force changed. Theoretically this type of installation of S/G's should not produce any error as far as the design principal of the load cells is concerned, as explained in ref. [42].

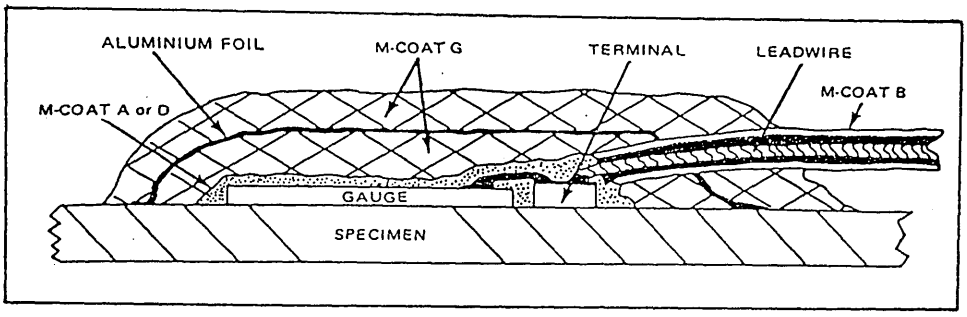

Fig. 85 - Cross-sectional view of long term gauge installation

The other possible reasons for this error could be the low strains obtained from the steel tube legs with 1.3 mm thicknesses, the lack of symmetry in the tube, the surface preparation, bonding, alignment, soldering of read-wires, coating, etc. Despite repeating the installations several times, unfortunately this error could not be removed.

Another reason could be electrical noise. Since the output voltage for the axial load was very small (maximum of 10 mv), in order to scale up this value on the pen recorder very high scale factors were used. Obviously this increased the magnitude of the electrical noise and drift on the records which could produce errors in the readouts.

Before the tests, it was intended to store the measurements in the data files and carry out the analysis by computer. However, the output voltage obtained from the load cells was too small in the axial direction (e.g. 4 mv readout for 4 kg-force heave force) while it was reasonable in the transverse direction (e.g. 700 mv readout for 4 kg-force sway force). Since the operating range of the analog to digital converter was bi-polar -2.5 v to +2.5 v, the signals in the axial direction could not be collected by the existing facilities at that time and the results were recorded on the charts by the multi-channel pen recorder.

Calibration of Load Cell Transducers

The calibration of wave-probes were the same as defined in the motion tests. The load cells were calibrated after the model was clamped onto the platform. The set up for the calibration in calm water is shown in Fig. 86.

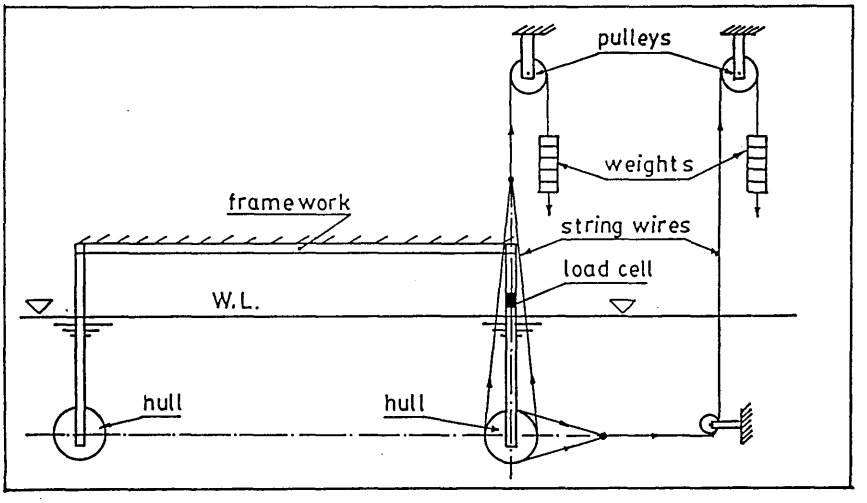

Fig. 86 - Experimental setup for the calibration of the load cell transducer

After taking the zero readings from the load cells, the test weights simulating the wave loads were step-by-step increased from 1 kg-f to 8 or 10 kg-f. During this procedure the change in the output voltage of the bridge was recorded by the pen recorder for each increment of the test weight. This process was carried out for axial and transverse loads separately. From the tests it was found that, the responses of the load cells were linearly proportional with increasing test weights in the range of weights applied. There was a difference in the slopes of the calibration curves belonging to the transducers on different legs related to the differences in the installation conditions and S/G characteristics. The slope of the calibration curves before and after the tests were found to be slightly different in some cases. Therefore the average value of the readings was taken. Another undesirable finding was the slight

difference in the calibration curves when the direction of the applied force was changed. However, this effect was not taken into account during the analysis.

From the above process the calibration factor K_L was calculated as:

$$K_L = \frac{\sum_{i=1}^{N} \{Applied\ Force\ [kg\text{-}f]\ /\ N \times Corresponding\ Voltage\ [mv]\}}{Deflection\ of\ Pen\ [mm]\ /\ Corresponding\ Voltage\ [mv]}$$

where N = number of test weights used.

The natural frequency of the vibration of the leg in sway mode was measured and found to be about 4 Hz which was well above the wave frequency range tested so that resonance effects could have little influence on the readings.

Test Procedure

A total of 8 channels, 4 channels for the load cells and 4 channels for the wave probe readings were recorded by the pen recorder. Each test run was preceded and followed by 'zero' measurement in calm water. Before a test run was recorded the wavemaker was started and a period of time allowed for the waves to arrive at the model and the wave height to stabilise at the correct value. The duration of a test run was approximately 50 sec. A generous time was allowed for the tank to calm between runs.

The wave frequency was varied from 0.5 Hz to 1.25 Hz and the wave heights from 8 cms to 20 cms as given in Table 18.

Characteristic Wave Frequency (Hz)	Wave Height (cms)
From 0.5 to 1.2 by 0.1 increment	From 8 to 15
From 0.55 to 1.25 by 0.1 increment	From 8 to 20

Table 18 - The range of waves tested in the force tests

Description of Records

Typical time history records of the forces on the single isolated hull are shown in Fig. 87. They are output voltage versus real time scaled by the chart voltage factor (K_v) and speed factor (K_t) as given for each record on the chart. The top two records are the deflections received from each leg in heave mode while the two bottom records are the deflections due to the sway force. The record in the middle of the chart is the deflection received from the wave probe aligned in the longitudinal symmetry line of the hull.

Analysis of Measurements

As stated earlier the analysis was carried out manually since the response signals in the axial direction were too small for the analog to digital converter. In order to find the motion and wave amplitudes at each test frequency at least three to five amplitude readings were averaged and these values were normalised by the corresponding averaged wave amplitudes. For this analysis the wave amplitudes, which were obtained from the wave probe alongside the front hull, were considered.

In Tables 19 through 23 the measured maximum wave and force values were tabulated for the single hull and twin hull configurations.

Single Isolated Hull

Character Wave Frequency (Hz)	Wave Height (cm)	Force Max. for Sway (kg-f)	Force Max. for heave (kg-f)
0.6	11.07	4.56	3.80
0.7	13.19	6.14	4.70
0.8	12.88	6.82	5.45
0.9	11.87	7.42	5.40
1.0	11.07	7.25	5.20
1.1	10.82	6.95	4.80
1.2	9.11	5.54	4.15
0.55	15.82	4.95	4.32
0.65	17.67	6.88	5.30
0.75	15.98	7.24	5.82
0.85	15.19	8.12	6.20
0.95	14.87	8.19	6.45
1.05	12.40	7.80	5.80
1.15	11.64	6.23	4.50
1.25	9.30	5.23	3.95

Table 19 - Experimental wave and force data for single circular hull in isolation

Twin Circular Hull (S/R = 2.00)

Characteristic Wave Frequency (Hz)	Seaward Hull			Leeward Hull		
	Wave Height (cm)	Force Max. for Sway (kg-f)	Force Max. for Heave (kg-f)	Wave Height (cm)	Force Max. for Sway (kg-f)	Force Max. for Heave (kg-f)
0.6	10.32	4.44	4.07	12.69	5.85	4.85
0.7	12.97	6.03	4.60	14.49	7.39	5.70
0.8	13.64	7.48	5.80	13.61	7.89	6.88
0.9	11.45	7.62	5.40	12.31	8.57	6.35
1.0	9.43	7.03	5.00	11.30	8.05	6.35
1.1	10.92	7.80	4.80	10.89	7.62	5.93
1.2	8.61	5.94	4.05	7.44	5.47	4.03
0.55	15.76	4.26	4.70	14.14	5.85	4.83
0.65	18.10	6.70	6.20	16.69	9.02	6.20
0.75	16.36	6.62	6.35	15.47	8.79	6.45
0.85	14.68	7.38	6.20	15.16	9.88	6.55
0.95	13.83	7.50	6.25	13.89	9.47	6.60
1.05	12.47	7.16	5.60	12.12	8.66	6.25
1.15	10.41	5.86	4.55	11.93	6.71	4.97
1.25	8.67	4.95	3.70	7.72	6.06	4.22

Table 20

Twin Circular Hull (S/R = 3.00)

Characteristic Wave Frequency (Hz)	Seaward Hull			Leeward Hull		
	Wave Height (cm)	Force Max. for Sway (kg-f)	Force Max. for Heave (kg-f)	Wave Height (cm)	Force Max. for Sway (kg-f)	Force Max. for Heave (kg-f)
0.6	15.79	4.44	4.40	12.82	4.84	4.35
0.7	15.09	5.40	5.05	14.62	6.45	5.32
0.8	12.91	5.96	5.10	13.91	6.86	6.09
0.9	11.93	6.52	5.47	13.89	7.72	6.10
1.0	11.71	6.60	5.10	12.28	7.72	6.07
1.1	10.41	5.92	4.60	11.58	6.82	5.50
1.2	8.54	5.10	3.70	8.97	5.12	4.45
0.6	17.79	5.31	5.17	13.58	5.88	4.25
0.7	18.29	6.41	6.05	13.92	7.58	5.35
0.8	16.87	6.77	5.90	13.42	8.83	6.75
0.9	15.25	7.50	6.40	12.34	9.07	6.25
1.0	14.08	7.50	6.3	9.64	7.80	5.55
1.1	12.88	7.20	5.70	9.53	7.63	5.47
1.2	10.92	4.84	3.70	8.96	6.86	4.35

Table 21

Twin Circular Hull (S/R = 4.00)

Characteristic Wave Frequency (Hz)	Seaward Hull			Leeward Hull		
	Wave Height (cm)	Force Max. for Sway (kg-f)	Force Max. for Heave (kg-f)	Wave Height (cm)	Force Max. for Sway (kg-f)	Force Max. for Heave (kg-f)
0.6	13.04	5.01	3.68	11.49	5.15	3.82
0.7	14.65	6.30	5.47	13.97	6.98	5.42
0.8	13.51	7.07	5.31	13.25	7.91	6.08
0.9	12.18	7.37	5.06	11.70	8.37	6.03
1.0	11.87	7.50	4.91	10.54	8.11	6.23
1.1	11.17	7.07	4.91	9.87	7.15	5.57
1.2	9.99	6.09	3.99	9.05	5.91	4.60
0.55	16.01	4.80	4.24	15.63	5.64	4.47
0.65	18.61	6.62	5.06	17.12	7.50	5.47
0.75	16.55	7.24	5.47	15.69	7.86	5.47
0.85	13.86	8.02	5.52	14.52	9.05	6.26
0.95	14.27	8.57	6.18	14.11	9.40	6.75
1.05	12.66	8.23	5.52	12.34	8.80	6.21
1.15	12.21	6.30	4.55	10.95	6.97	4.73
1.25	9.84	6.09	4.39	8.48	5.27	3.73

Table 22

Twin Circular Hull (S/R = 5.964)

Characteristic Wave Frequency (Hz)	Seaward Hull			Leeward Hull		
	Wave Height (cm)	Force Max. for Sway (kg-f)	Force Max. for Heave (kg-f)	Wave Height (cm)	Force Max. for Sway (kg-f)	Force Max. for Heave (kg-f)
0.6	13.45	5.13	4.16	13.70	5.83	4.43
0.7	13.75	6.12	4.70	13.04	6.77	5.28
0.8	14.27	7.22	5.19	12.82	8.07	6.39
0.9	13.35	7.86	5.74	9.52	7.7	5.28
1.0	12.18	7.95	5.87	8.73	7.33	5.44
1.1	11.94	7.29	5.84	9.65	7.84	5.97
1.2	8.13	5.79	4.65	8.73	6.49	4.96
0.55	13.13	4.21	3.79	15.06	5.60	4.54
0.65	13.68	5.61	4.47	16.23	7.05	5.39
0.75	12.21	6.45	5.27	14.94	8.07	5.76
0.85	12.37	7.33	5.22	13.99	9.24	6.71
0.95	11.23	7.29	5.50	13.26	9.71	6.55
1.05	10.35	6.45	5.06	11.80	9.10	6.40
1.15	8.92	5.62	4.47	11.52	7.00	5.17
1.25	8.76	5.20	3.77	8.48	6.25	4.59

Table 23

Table 20 to 23 - Experimental wave and force data for twin circular hulls for varying hull separations

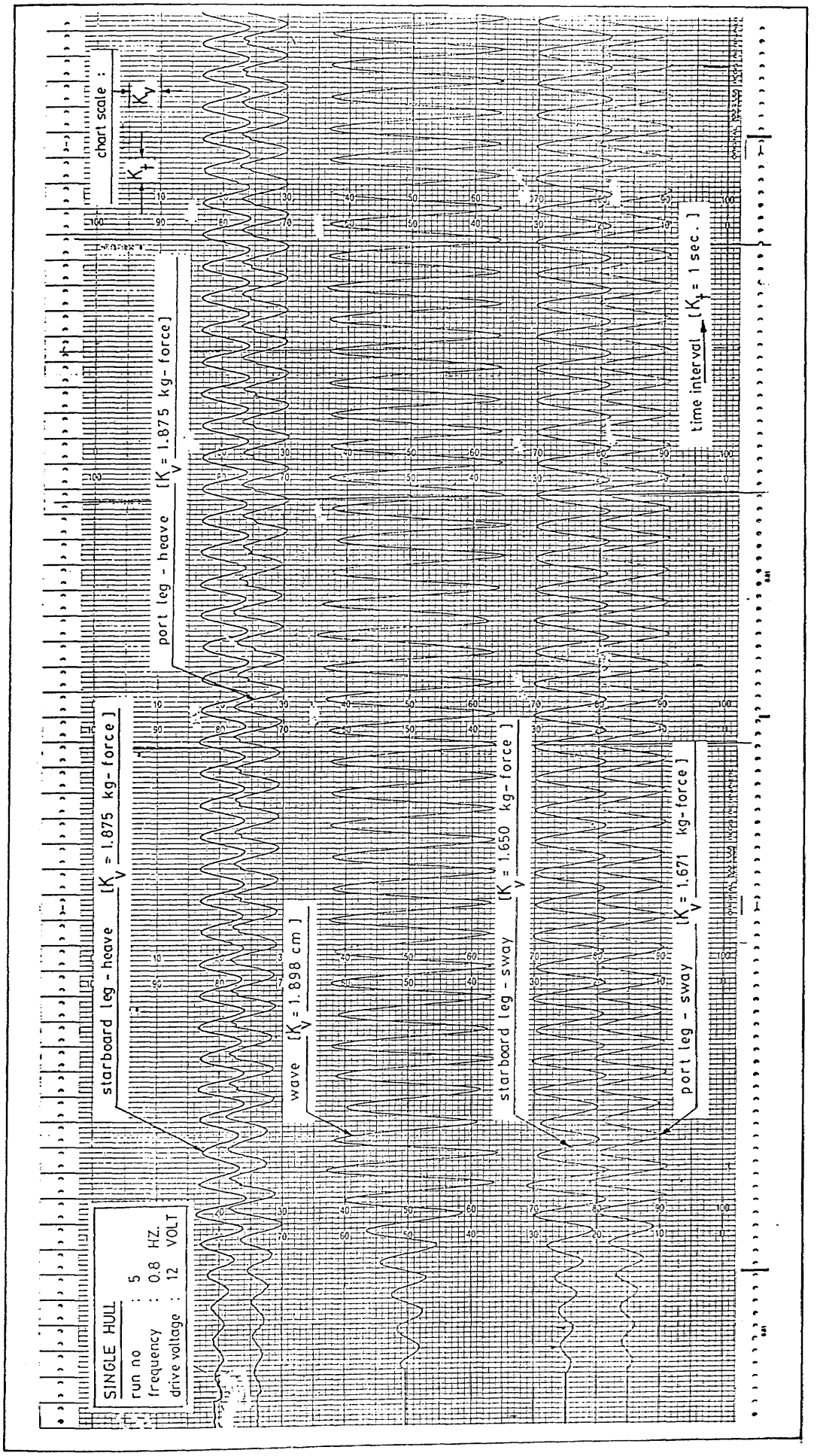

Fig. 87 - Chart record of the forces on the single circular hull in isolation from the multi-channel pen recorder

Presentation and Discussion of Results

In Fig. 88 the measured force values on the isolated single hull are presented as maximum force per unit wave height versus characteristic wave frequency. The dashed and solid lines are the best fit curves through the experimental data in heave and sway mode respectively.

As shown in the figure both forces increase as the frequency increases and reach their maximum smoothly at about 0.9 and 1.0 Hz and then decrease gradually by following the same pattern. There is a scatter in the experimental data reflected from the different wave heights used at the adjacent frequencies. This indicates that the wave force is not exactly linearly proportional to the wave heights tested. Despite the same trends of the curves there is a difference in the magnitude of sway and heave force at about a maximum of 25% of the maximum sway force at the peak point.

In Figs 89 and 90a,b,c,d the load distribution for heave and sway mode on the leeward and seaward hulls are given at each hull separation. The dashed and solid lines are the best fit curves passing through the experimental data corresponding to the seaward and leeward hull measurements.

At a first glance, both figures suggest that the experimental data on each hull are scattered into each other's and it is difficult to distinguish a trend indicating an unequal load distribution. However, when the data is curve-fitted it can be seen that there is a constant load increment on the leeward hull relative to the seaward hull (a maximum of 15% of the maximum value of the heave force on the leeward hull at S/R = 4.00 and maximum of 20% of the maximum value of the sway force on the leeward hull at S/R = 3.00).

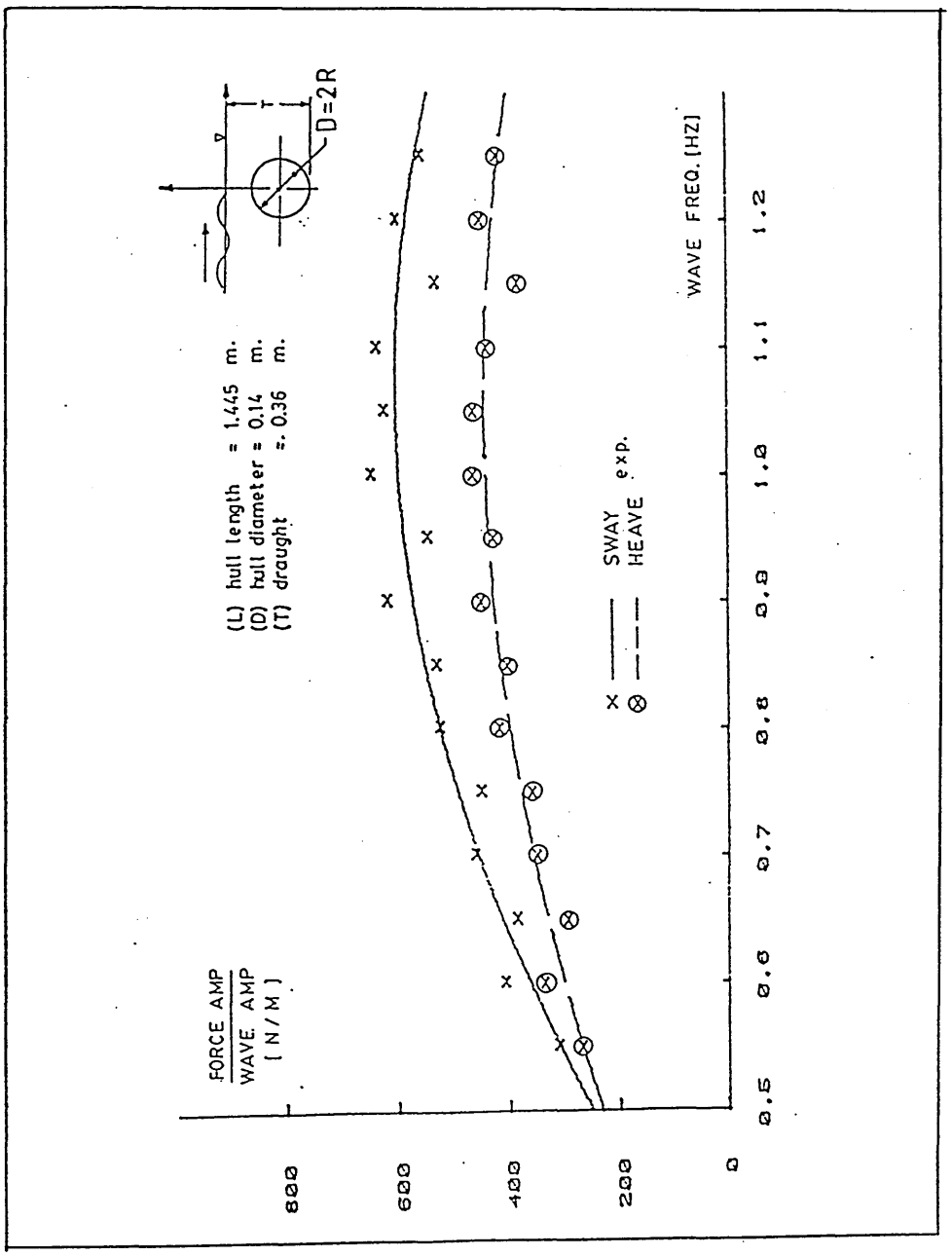

Fig. 88 - Experimental wave exciting force on the submerged single circular hull

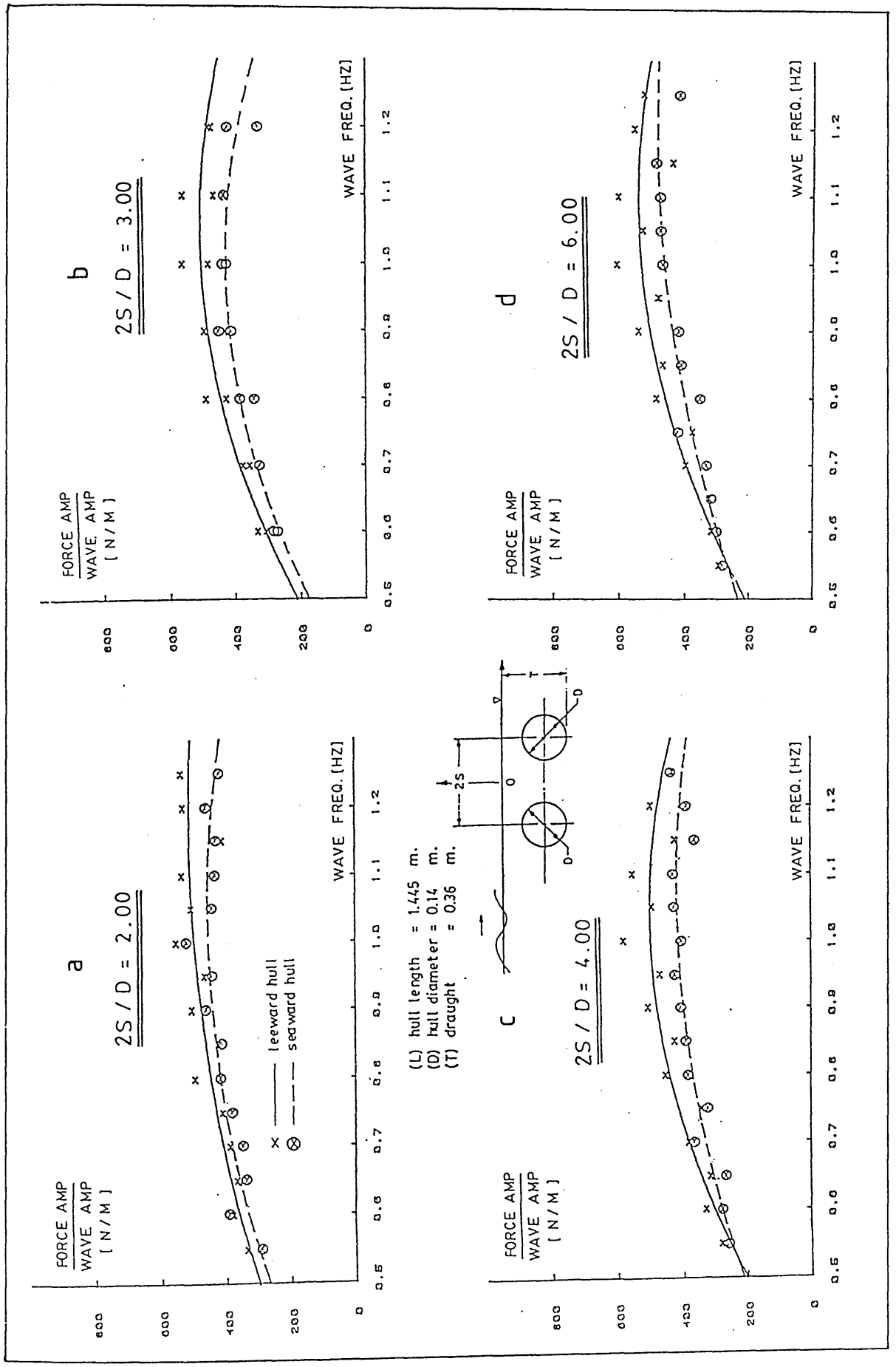

Fig. 89 - Experimental heave exciting forces on the submerged twin circular hull

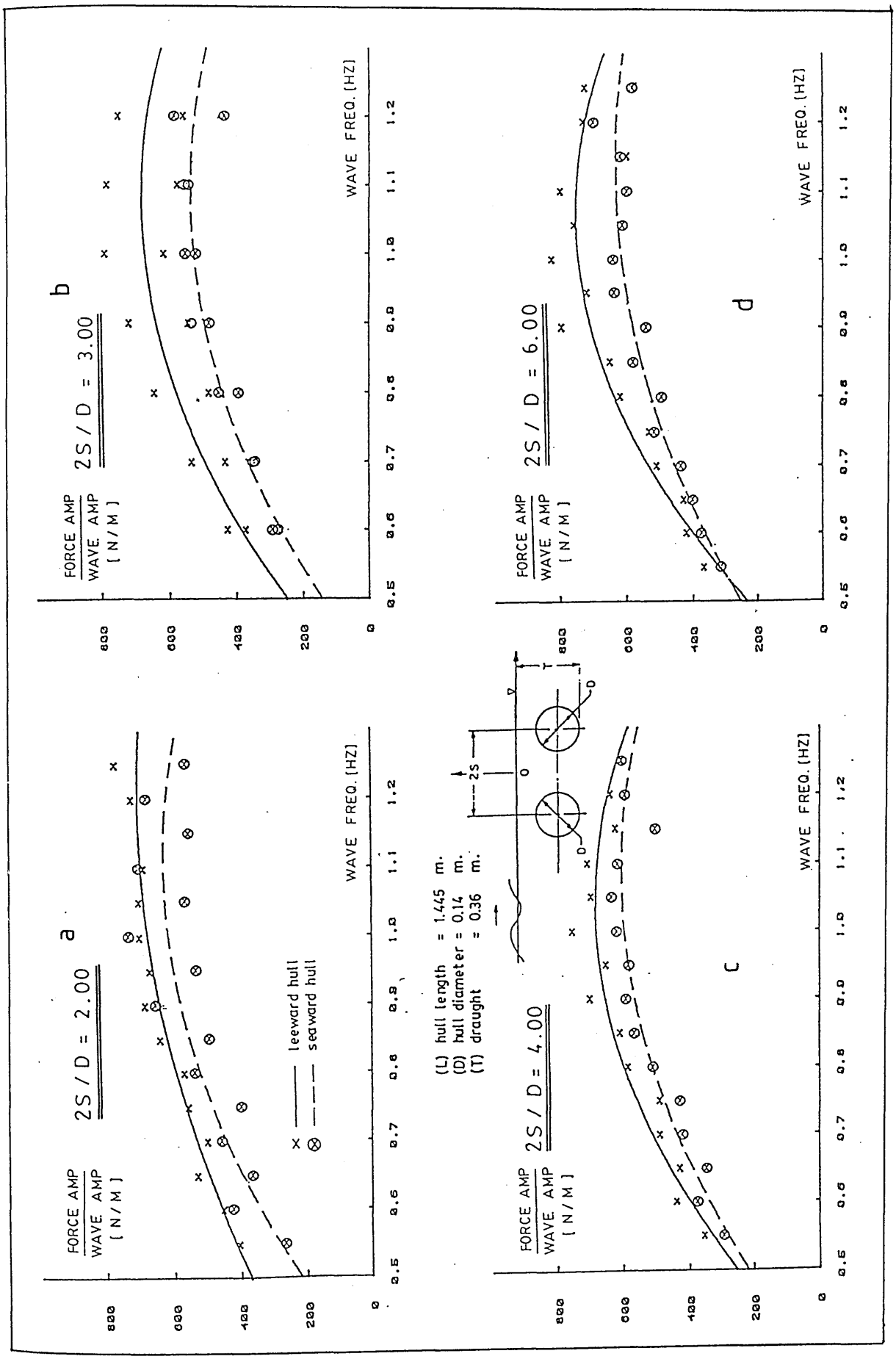

Fig. 90 - Experimental sway exciting forces on the submerged twin circular hull

The load difference between the hulls in heave mode is relatively small compared to that in the sway mode in proportion to the magnitudes of the forces. As shown in Fig. 89a at the closest hull separation the forces on each hull are very close. Whereas in Fig. 89b, c and d the same difference occurs at each spacing.

In the sway mode as shown in Fig. 90, the force difference at the hull separation of S/R = 2.0 and S/R = 4.0 are relatively small compared to those at S/R = 3.0 and 6.0 where the big differences in the wave heights causes a non-linear force increase.

Although it is not valid for each hull separation, the force differences in the hulls occurs mainly between 0.5 Hz and 1.3 Hz.

Figure 91a,b,c,d show the effect of hull separation on the measured load values at each hull separation relative to the isolated single isolated hull values.

As shown in Fig. 91a and c as the frequency increases the forces in heave and sway mode on the leeward hull take increasingly larger values compared to those on the isolated single cylinder (about a maximum of 15% of the maximum single cylinder force value). From the theory it is expected that as the hull separation increases the force acting on each hull approaches the single isolated hull value. However, the tests demonstrate, contrary to the theory, the forces at the largest hull separation (S/R = 6.00) are larger than on the single isolated hull and the smaller hull separations. The changes in the hull separation do not bring great changes in the measured force values at S/R = 2.0, 3.0 and 4.0.

On the otherhand Fig. 91b and d demonstrate that the sway and heave force on the seaward hull have nearly the same magnitude as the single isolated hull has, except for S/R = 3.00 for sway mode (about 15%

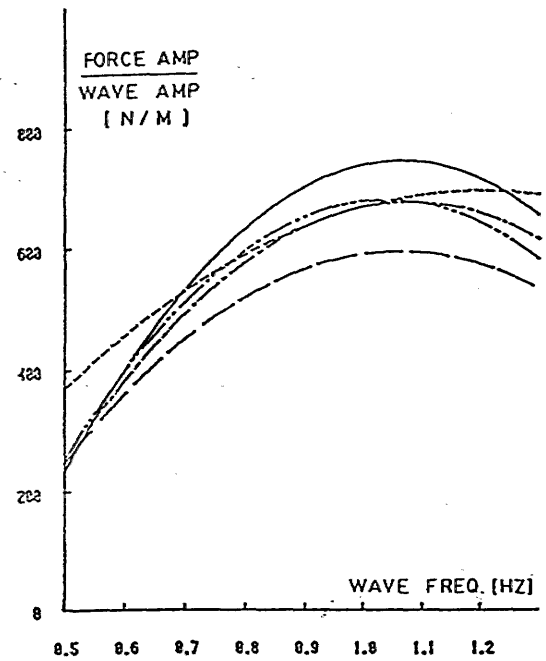

Fig. 91a - Experimental sway exciting force on the leeward hull

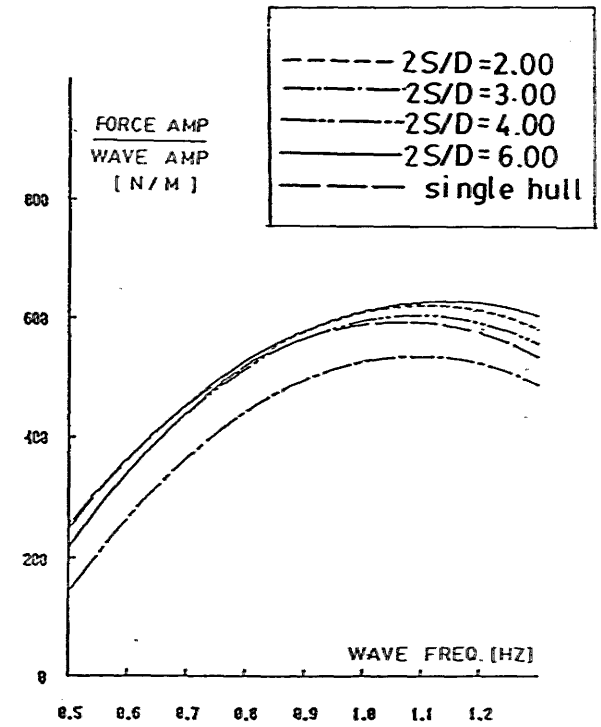

Fig. 91b - Experimental sway exciting force on the seaward hull

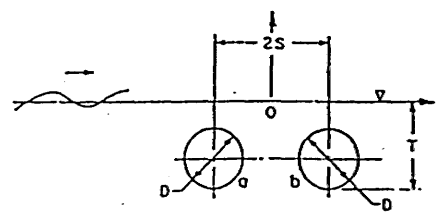

(L) hull length = 1.445 m.
(D) hull diameter = 0.14 m.
(T) draught = 0.36 m.

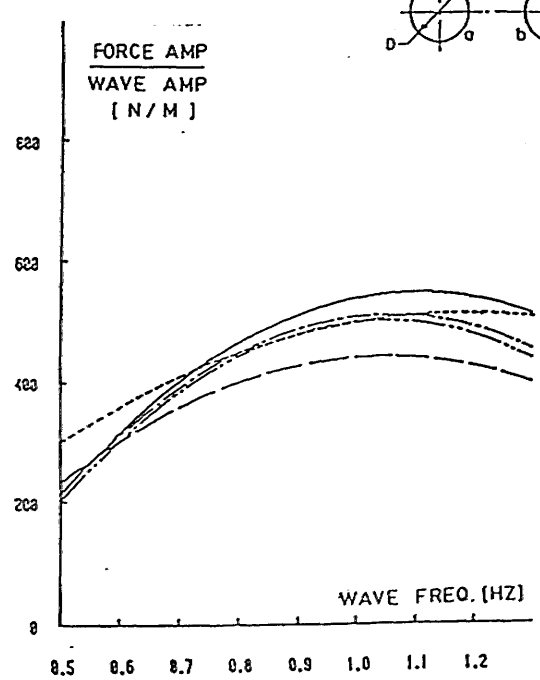

Fig. 91c - Experimental heave exciting force on the leeward hull

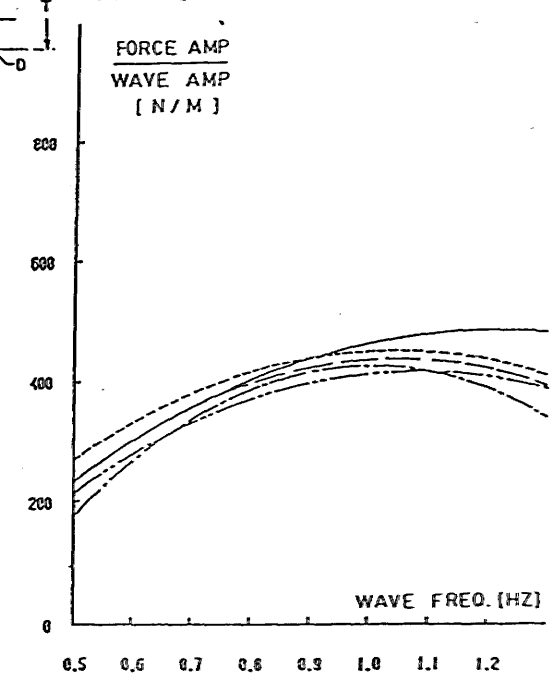

Fig. 91d - Experimental heave exciting force on the seaward hull

Fig. 91 - Effect of hull separation on the heave and sway exciting force

smaller than the force measured at other spacings). This could be related to the higher waves used. The changes in the hull separation do not demonstrate a major difference in the measured force values. These findings imply that the seaward hull could be treated as a single isolated hull.

Figure 92a and b shows the pictures taken during the tests at S/R = 3.0 and 6.0 at three different frequencies.

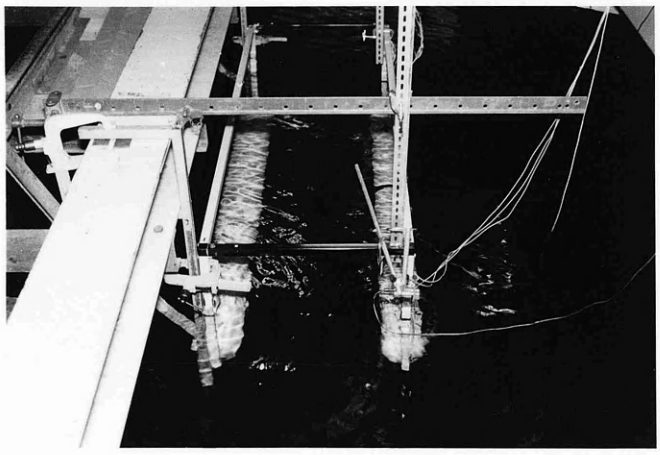

2S/D = 3.00
W. Frequency = 0.7 Hz
W. Height = 15.09 cms

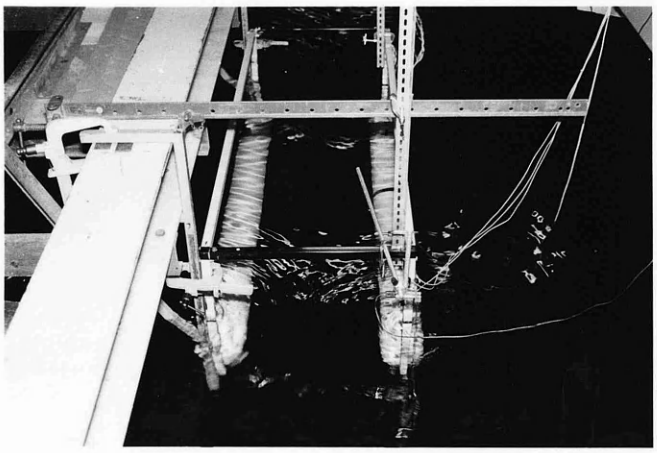

2S/D = 3.00
W. Frequency = 0.9 Hz
W. Height = 11.93 cms

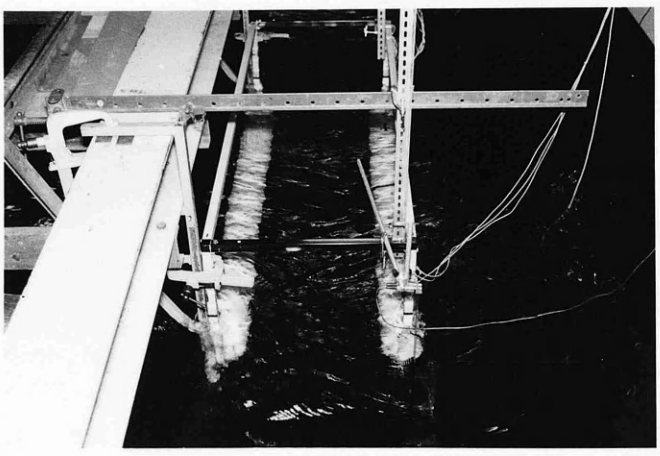

2S/D = 3.00
W. Frequency = 1.2 Hz
W. Height = 8.54 cms

Fig. 92a - Views of the force tests at varying frequencies for hull separation (2S) to hull diameter (D) ratio of 3

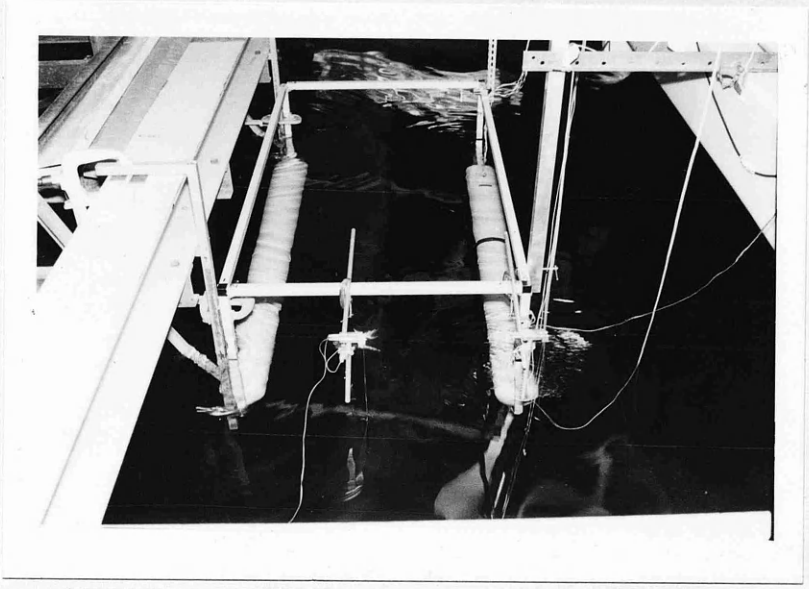

2S/D ≃ 6.00
W. Frequency = 0.7 Hz
W. Height = 13.75 cms

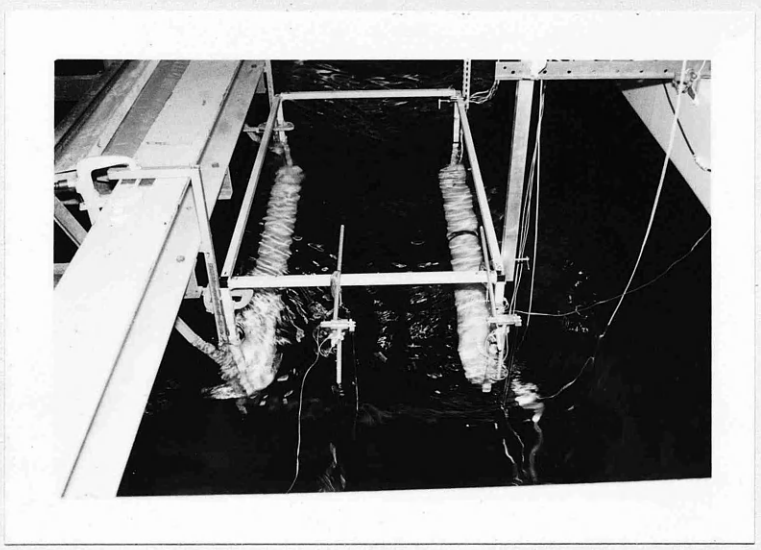

2S/D ≃ 6.00
W. Frequency = 0.9 Hz
W. Height = 13.35 cms

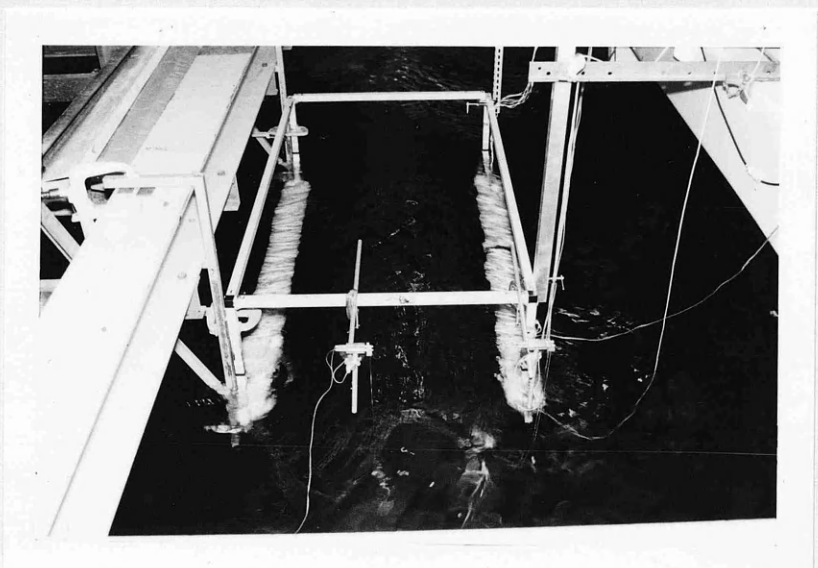

2S/D ≃ 6.00
W. Frequency = 1.2 Hz
W. Height = 8.13 cms

Fig. 92b - Views of the force tests at varying frequencies for hull separation (2S) to hull diameter (D) ratio of 6

3.7 CONCLUSIONS

1. For this particular model the steady tilt developed in regular beam seas with a range of frequency varying between 0.7 Hz and 1.2 Hz (a range of period 12 sec to 7 sec on full scale) and wave height in excess of 8 cms (about 6 m on F.S.). The worst tilt observed was 16° for the smallest $\overline{GM}$, for the largest $\overline{GM}$ it was 2.5°, both of these occurring at a frequency of 0.9 Hz (a period of 9 sec on F.S.). It had a further local maximum at a frequency of 0.7 Hz.

2. As the $\overline{GM}$ increased, the tendency to tilt disappeared at the higher frequencies but remained around the 0.7 Hz frequency, i.e. the range of tilt frequencies decreased with the lower end of the above defined range remaining fixed.

3. Although 2 to 2.5° of steady tilt occurred at the natural heave frequency of 0.4 Hz (a period of 21 sec on F.S.), it was found that there was no tilt at adjacent higher and lower frequencies. In the cases where the roll frequency fell with the experimental range a similar result occurred.

4. The magnitude of the tilt increased rapidly and non-linearly for very small increments of the wave height once a sufficient wave height to create tilt was reached.

5. The tilt also increased non-linearly with decreasing $\overline{GM}$. The trend of the $\overline{GM}$ curves with varying frequencies was the same for the three smaller $\overline{GM}$s, whereas it demonstrated a different trend for the two higher $\overline{GM}$s.

6. The steady tilt occurred always in the leeward direction if it occurred at all. The exploratory tests demonstrated that there was a mechanism for the leeward tilt which was very strong at the region where the tilt was worst.

7. The steady tilt behaviour was caused by the exciting mechanism in regular beam waves and controlled by the restoring moments and the moorings if they existed. The effects of the wave parameters on the tilt were accentuated when the model's $\overline{GM}$ was very close to zero. However, in this case it was impossible to perform the model tests for systematic measurements because of unstable behaviour of the model with poor restoring moment. The limiting $\overline{GM}$ for this model was determined as 1.90 cm (1.33 m on F.S.).

8. Several factors, which are listed below, were investigated and it was found that although each individual factor was not the sole mechanism to create the tilt each could affect the magnitude of the tilt. These are:

(i) the first impact of the waves

(ii) the moorings which were arranged as defined in the diagrams and text,

(iii) the different locations of the fairleads at the centre of gravity and the centre of gravity of the pontoons, and

(iv) the different type of flow condition created by the stimulators around the underwater geometry.

9. Inclining tests in calm water indicated that there was no non-linearity in the roll restoring moments with varying tilt angles until the deck became immersed in the water about 17°.

10. In addition to the investigation for the tilt mechanism given in 8 above, the measurements of the wave exciting force on the fixed pontoons of the model demonstrated that:

(i) the interference effects between the pontoons did not show any noticeable load difference between the hulls to cause a steady tilt, but there was a slight force increase on the leeward hull relative to the seaward hull when the wave height increased,

(ii) the force measured on the seaward hull for each hull spacing was more or less the same as on the single isolated hull measured,

(iii) the motion tests demonstrated that the worst tilt occurred at a ratio of the wave length to hull separation of 2.3 and a second peak occurred at a ratio of 3.8. However, the force measurements at various hull spacings did not show noticeable force difference at the corresponding ratios, and

(iv) the measured force in the sway mode was always greater than that in the heave mode for both twin and single hull;

11. In both the motion and the force tests it was observed that, in the range of wave height tested, the variation of the first-order motion and force values with wave height was not quite linear as expected from the linear theory. It was interesting that increase in wave height caused a load difference on the measured force values on the twin hulls and scatter in the motion response amplitude operators.

12. Since tests were carried out for more than one wave height at each frequency, it is desirable to have a wave height formula, which gives a constant slope for each frequency, to analyse the results. In the thesis the ABS wave height formula was chosen because:

(i) for this scale of model the ABS formula gave a wave height which could be produced by the existing wavemaker in the model tank, and

(ii) the ABS formula produced a smaller wave slope than the DnV or indeed the maximum slope found at sea; if the model or theory indicated tilt at the ABS slope, the tilt is likely to be much more severe in steeper wave conditions. Therefore from the design point of view it was desirable to check this behaviour in these less severe conditions.

13. The measurements of the wave elevations at different places in the tank demonstrated differences in readings of 2 or 3 mm due to the effect of tank wall, wave beach reflections, etc. However, this difference was not the cause for the scatter in the measured motion response values.

14. The steady tilt affected the first-order roll and heave response amplitude operators non-linearly. As the $\overline{GM}$ decreased higher roll and heave motion RAO's were obtained in the frequency region where tilt was recorded.

15. The duration of a test run was 1.2 minutes. This length of time was required to observe the several characteristics of the tilt behaviour. One could argue that in this long duration, the sine form of the waves generated could be destroyed by the reflection and interference. This was sometimes observed at the high frequencies.

16. The determination of the small $\overline{GM}$s required very accurate inclining tests. A small asymmetric distribution of the mass of the model or test weights could cause magnified errors due to small $\overline{GM}$.

17. The free motion tests for the determination of the natural period demonstrated very consistent time intervals between each cycle for each set of $\overline{GM}$ values. However, the ratio of the amplitude of the motion for the cycles did not vary exponentially in particular for small $\overline{GM}$ values. This would affect the experimentally calculated added moment of inertia and damping moment for small $\overline{GM}$s.

Chapter 4

THEORETICAL WORK

4.1 INTRODUCTION

As stated in Chapter 1, a semi-submersible is exposed to dynamic external loads due to waves, wind, current and other agencies. Under steady conditions, the loads due to wind, current and others are the constant quantities which can cause steady tilt behaviour when the appropriate environmental conditions are present.

However, during the simulation of the steady tilt behaviour by model tests, in the absence of these steady loads, it was observed that the wave-induced loads often had the potential to cause and sustain this steady behaviour in spite of their unsteady character. It was also found that a mooring system was not necessary to develop the steady tilt though it affected its magnitude.

Therefore, keeping in mind the importance of the other steady external loads, this chapter concentrates on the theoretical analysis of the wave-induced loads which is believed to be mainly responsible for the steady tilt behaviour.

The methods and results analysed in this chapter have been presented by the author in refs [48,49,50,51,52,53] in more detail. Therefore, frequent reference to these studies is made where appropriate in the text.

Wave-Induced Loads

When a semi-submersible is subjected to surface waves, hydrodynamic forces and moments are exerted on its body. These forces and moments will not only have large, first-order, unsteady oscillatory components but also small, second-order, steady (mean) or low frequency components due to various non-linear effects[14].

The first-order forces (or moments) are linearly proportional to wave height and cause the oscillatory motions of the semi-submersible with frequencies equal to the frequencies in the wave spectrum. They are induced by the particle motions in waves.

The second-order forces (or moments) are linearly proportional to the square of the wave height and can cause large amplitude resonant behaviour of motions with very low damping. The frequencies of the second-order low frequency component are associated with the frequencies of wave groups occurring in irregular waves.

The second-order forces are induced essentially by two main properties of the surface waves which are:

(i) Momentum transportation,

(ii) Particle motions close to the surface.

When the incident wave encounters the semi-submersible,part of the surface waves will be diffracted and the rest will be transmitted. If the semi-submersible is floating freely, its motions will generate waves radiating outwards. According to the conservation of wave momentum principle there will be a resulting net force on the body for each passing wave[54]. This force is usually known as the "wave drift force" since it acts on the semi-submersible in the direction of wave travel[12].

Since the semi-submersible has deeply submerged lower hulls and other submerged elements, it is possible to avoid breaking of the waves. For these members, the velocity of the water particles moving over the top of the hull or submerged element will be greater than those moving underneath caused by the surface proximity. This creates a reduced pressure on top of the body contour with respect to the bottom (a mean depression of the free surface from the level) resulting in a net force in the upward direction. This force is sometimes termed "wave suction force" since it causes the body to rise relative to the free surface[30].

A regular wave train induces "mean or steady" second-order forces resulting in a static shift of the position of the semi-submersible. Whereas in irregular waves or regular wave groups, varying sequences of the wave height in time with a certain period result in an average force varying with the same period. Since the variations of the average force amplitude and zero-crossing points are slowly-varying with the time, the resulting second-order force is in "slowly-varying" form (or termed as "low-frequency" second-order force)[13,55].

Both components of the wave-induced loads, the first- and second-order, act on the semi-submersible and cause the oscillatory and steady motions. As reviewed in Chapter 2 the tilt behaviour is induced by both components in combination. Therefore in the following these components are analysed separately with their several hydrodynamic aspects.

4.2 FIRST-ORDER WAVE-INDUCED LOADS

As shown in Table 24, the first-order hydrodynamic loads on the semi-submersible can be divided into two major components which are:

(i) wave-exciting forces, F_W, induced by the wave motion,

(ii) Radiation forces, F_R, induced by the response motion of the semi-submersible.

These forces are subdivided into two components as follows:

The wave-exciting force, F_W, consists of

(i.1) The Froude-Krylov force, F_I, caused by the undisturbed incident wave pressure when the wave passes across the semi-submersible.

(i.2) The diffraction force, F_D, resulting from the hydrodynamic disturbance introduced by the presence of the semi-submersible into the waves.

The diffraction force component, F_D, can be further decomposed into two components as follows:

(i.2.1) The inertial force, F_{AD}, in phase with the acceleration of the wave motion.

(i.2.2) The velocity force, F_{BD}, in phase with the velocity of the wave motion.

Similarly, the radiation force, F_R, consists of

(ii.1) The inertial force, F_A, caused by the added virtual mass of the water surrounding the semi-submersible and it is linearly proportional to the acceleration of the motion.

(ii.2) The velocity force, F_B, caused by the dissipation of energy (damping) in radiating surface waves from the response motion of the semi-submersible which is also linearly proportion to the velocity of the motion.

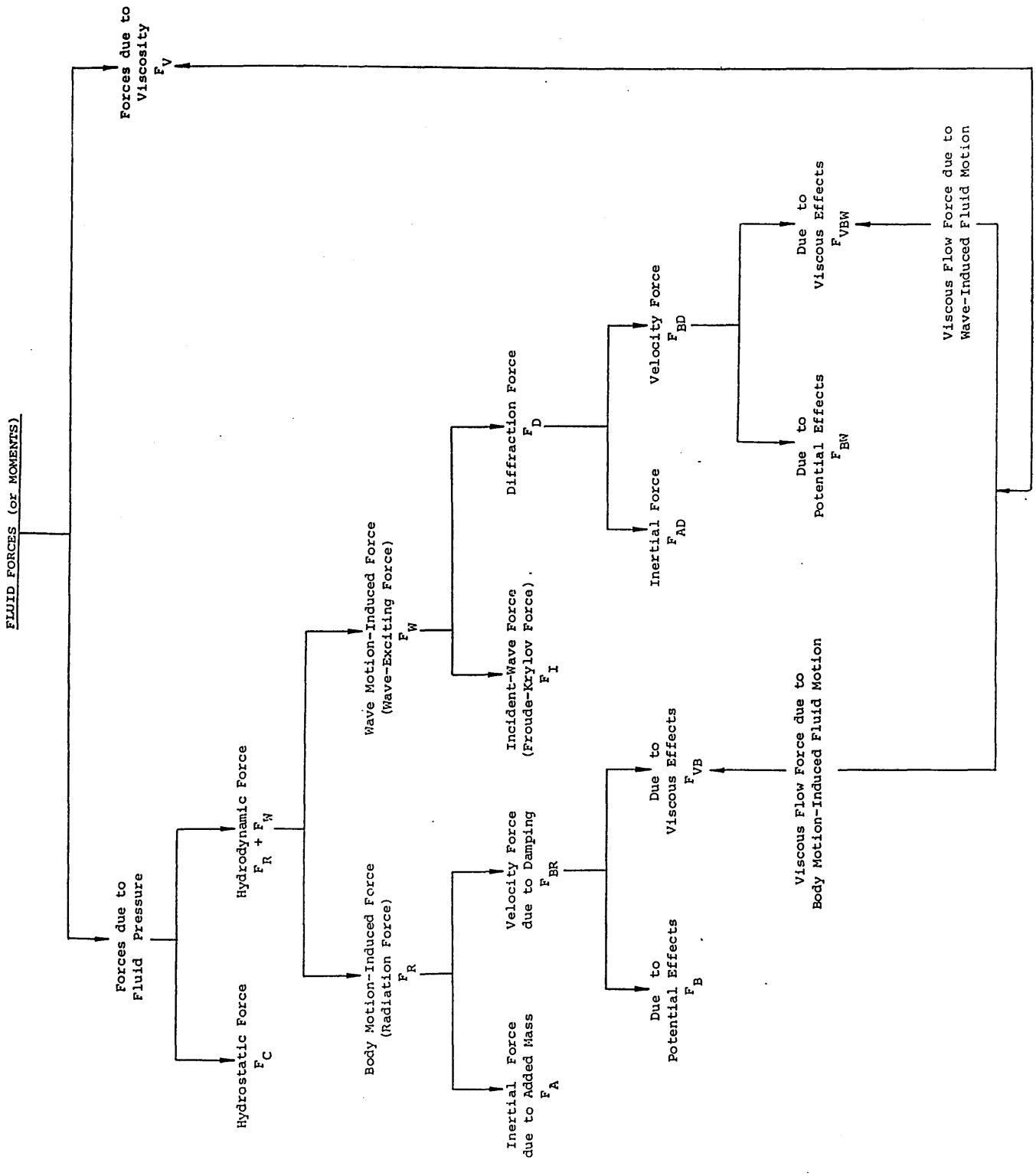

Table 24 - Breakdown of the oscillatory fluid forces (or moments)

Both forces, F_W and F_R, have also viscous components associated with the flow velocities about the underwater geometry of the semi-submersible. These are

(i.2.2.1) The viscous wave force, F_{VBW}, caused by the wave-induced viscous fluid motion.

(ii.2.1) The viscous damping force, F_{VB}, caused by the semi-submersible motion-induced viscous fluid motion.

Strictly F_{VBW} and F_{VB} should be combined into a single viscous force, F_V, resulting from the relative velocity due to both the motion of the semi-submersible and the wave particles in combination.

There are two fundamentally different approaches to the calculation of first-order wave-induced loads: one mathematical, the other empirical.

The mathematical method is used in the design of ships and wide body structures. It involves the mathematical solution of equations describing wave diffraction and radiation by the body and ideal fluid assumption (e.g. methods based on two- and three-dimensional source distribution techniques[56,57,14,58]. By using this method, the most important parameters from the point of view of tilt effect can be taken into account for the computation of hydrodynamic loads. These parameters are as follows:

- Frequency Dependence
- Free Surface Proximity
- Hydrodynamic Modelling of Underwater Geometry
- Hydrodynamic Interference between the Underwater Elements

However, in some cases, there are other non-linear parameters such as the effect of viscosity, large amplitude wave and response motion, wave breaking, etc., which may play an important part in the tilt behaviour.

The viscous effect is generally considered to be significant only for structural members with section dimensions which are small in comparison with the wave particle orbit width which is equal to the wave height in deep water. They are important if the body shape is such that the forces due to fluid pressure are small and it has low damping characteristics. For instance, heaving vertical cylinders with very large draughts compared to the diameter, rolling cylinders with nearly circular cross-sections, moored small cylinders with long cables, small cylinders in long waves, etc.[59].

Although the earlier mentioned parameters can be represented by the mathematical methods in potential theory, the viscous effect is represented by the drag term in the empirical Morison equation[60]. This term is a non-linear term which varies with the square of the relative velocity induced by the fluid motion and response motion in combination. Thus the viscous wave and motion induced forces are accentuated for finite long period waves and in resonant motions with large amplitudes[61].

Depending on the flow regime the drag component of the wave forces on semi-submersible members is taken into account. According to linear theory, for a typical member with diameter D in regular deep waves of height H, a rough criterion for neglect of drag force is $D/H > 0.2$[58,62]. In the case of horizontal drag forces, since the horizontal velocity is maximum at the wave crest, the additional force contributed by the crest needs to be considered and this is discussed in greater detail later.

In Chapter 3, both the force and motion tests indicated that the measured values were strongly frequency dependent. Thus, this effect is the most important parameter to be taken into account.

The free surface effect may not be important at the relatively deeply submerged lower hull of the models tested. However, it is important on the surface-piercing columns at any draught and the lower hulls at a shallow depth of submergence (e.g. in a tilted position). As shown in Fig. 93, this effect is reflected in the motions of the model at large tilt angles so that the vertical motion of the seaward hull, which is closer to the free surface, is larger in magnitude than that of the leeward hull.

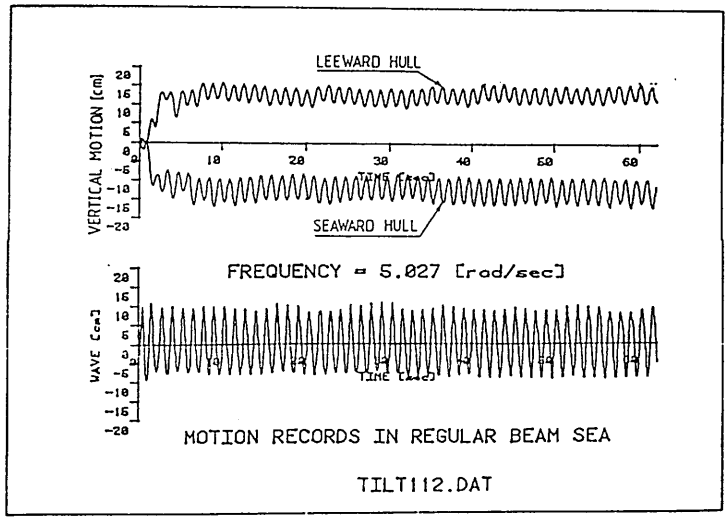

Fig. 93 - Typical chart records of motions displaying the effect of free surface on the vertical motions of the leeward and seaward hull of the model

In extreme cases, in which very large tilt develops, the upper hull comes very close to the surface or even causes wave breaking. This type of non-linearity can be covered up to a certain point (e.g. shallow depth of submergence) by the linearised free surface effect, but the physical interpretation of the theoretical findings still need to be explored (e.g. occurrence of a negative added mass for a rectangular pontoon just below the free surface[63]).

Semi-submersibles consist of a number of underwater elements of different types in various orientations (e.g. horizontally submerged lower hulls, surface-piercing vertical columns, horizontal and

diagonal bracings, etc.). The hydrodynamic modelling of this complex geometry requires three-dimensional techniques and thus usually considerable computational effort[14,58].

However, for a twin-hull semi-submersible having two long slender lower hulls which experience most of the total hydrodynamic load on the entire body of the vessel, the use of a two-dimensional technique combined with the strip method can be justified[64,65,66,67,51]. During the hydrodynamic modelling of the lower hulls the effect of cross-section should be taken into account. This effect combined with the free surface effect will be accentuated in a tilted position for a lower hull with non-circular cross-section[68].

Having represented the lower hulls by two-dimensional techniques, it is anticipated that the use of a similar technique in the column sections, which are relatively short and whose cross-sectional dimensions are similar in magnitude to the hull separation and the draught, may induce considerable errors due to three-dimensional effects. In such cases, the loads on the legs may be computed independently from the loads on the lower hulls by using three-dimensional techniques[67].

In the two-dimensional strip method, procedures for the hydrodynamic representation of the columns are either treated independently from the lower hulls as vertical cylinders in isolation[65] or as surface-piercing extensions of the lower hulls (i.e. column and hull combination) to include into the strip computation. These procedures can be applied to many SWATH ships and semi-submersibles whose vertical columns are a significant proportion of the length of the hulls[64,66,67,51,69,70,71]. The hydrodynamic representation of an inclined column in a tilted position is also possible by these procedures[68].

The spatial distribution of the underwater elements creates various types of hydrodynamic interference problems. Amongst them, the

following are the most important:

(i) the interference between the hull sections,

(ii) the interference between the columns and the lower hull of each hull and column combination.

The theoretical and experimental investigations on the first type of interference phenomenon indicate that the hydrodynamic forces of twin-hulled configurations differ significantly from those equivalent single hull throughout the frequency range[72,73,74,75,76,64,66,52]. This type of interference is more serious for surface-piercing sections compared to a submerged section since the waves at the surface generated by radiation or diffraction can be trapped between the inner walls of the sections. The two-dimensional theory on which the strip approximation is based requires that according to the reflection principle at certain frequencies, which are called "resonant frequencies" these waves interact and take a form of standing waves[73,74]. Depending on the mode of oscillation these standing waves can be of symmetric or asymmetric form[52,77]. As the oscillation frequency varies, changes in the energy of the standing waves and others travelling outwards result in sharp discontinuities in the motion-induced coefficients (e.g. negative added mass, zero damping) and the wave-induced coefficients, e.g. refs [74,76].

Depending on the oscillation frequency and the phase relation between this frequency and that of the generated waves, the ensuing variations occupy a significant portion of the low frequency range and induces sharp discontinuities within a narrow band of the intermediate or high frequency range.

If the hulls are very close to each other the force values will differ from those of a single hull. Even if they are separated many wave

lengths apart, at a certain number of frequencies, which correspond to the resonant frequencies, standing waves will occur inducing sudden changes in force magnitudes on the surface-piercing sections.

For completely submerged elements, there will be no equivalent resonant behaviour since there is no physical boundary at the surface to trap the waves. Some effects of hydrodynamic interference still exist at small hull separation but these effects are much less compared to those on the surface-piercing sections.

The above mentioned features of this hydrodynamic interference effect is a real physical phenomenon in two-dimensions corresponding to the resonant behaviour of waves confirmed by the tests, e.g. refs [74, 75]. However, the occurrence of this behaviour on a semi-submersible is open to question. This is mainly because of the three-dimensional effects expected as well as the leakage of the energy of the trapped waves in the longitudinal direction and the irregular motion of the sea-way. In addition to this physical uncertainty, the hydrodynamic representation of the interference effect at a tilted position which gives rise to asymmetric underwater geometry and its physical interpretation will be controversial.

In spite of the three-dimensional effects or random excitations, for semi-submersibles whose vertical columns are a significant proportion of the length of the lower hulls (such as pipelaying and derrick barges, SWATH ships, etc.) these peaks and deviations cannot be removed completely as a hydrodynamic property of the twin-hull geometry. From the hydrodynamic design point of view it is advisable to avoid these types of column with elongated water plane areas which increase the physical boundary length at the water surface and thus the possibility for the resonant behaviour.

This may not be possible for seagoing semi-submersibles like SWATH but for stationary semi-submersibles it is better to have circular columns. Another disadvantage of having columns with elongated water plane area is that in beam seas or near beam seas they cause large horizontal drift forces since the reflection of the incident waves at the columns is considerable.

The contribution of the lower hulls to the resonant phenomenon may not be important at relatively deep depths of submergence. However, in the transit condition the potential damping increases with shallow depth of submergence. Therefore the deviations in the damping from a maximum to zero value results in large deviations in the motion and wave-induced forces. If the shallowly submerged lower hulls have wall sided shapes this may work as a physical boundary to build up a resonant condition. In such a case having circular or elliptical cross-section of lower hulls may have advantages compared to rectangular or rectangular with rounded corners shapes of hull from the hydrodynamic design point of view.

Moreover as indicated in ref. [63], shallowly submerged rectangular hulls with large width can have negative added mass and sharp peaks in the damping and added mass coefficients in the heave mode. This is induced by resonant standing waves occurring in the shallow region on top of the large rectangle and it is undesirable as it causes discontinuities in the hydrodynamic loading.

The second type of interference phenomenon occurs during the hydrodynamic representation of the columns and lower hulls in combination. This results in a "wave-excitationless" frequency at relatively low frequencies in the heave mode induced by the cancellation of the Froude-Krylov force, F_I, on the column section and the inertial diffraction force, F_{AD}, of opposite sign on the submerged lower hull

section[51,90]. This interference effect can be taken into account automatically by representing the columns as the surface-piercing extensions of the hulls[67]. Moreover, as demonstrated by the author et al.[68], this type of representation indicates a third interference effect between the above stated two so that as the hull separation decreases the wave-excitationless frequency shifts towards a higher frequency.

Finally, some tests done with twin surface-piercing cylinders with different cross-sections showed that if the cylinders have vertical sides at the free surface such as semi-circular or rectangular, linearity exists between the body oscillations and the hydrodynamic radiation force, but if the cylinder had sloped sides such as triangular, the relationship is non-linear at the lower frequencies[75]. This finding implies that elongated waterplane area of columns with fairing (or sloped sides) is undesirable from the hydrodynamic design point of view.

4.2.1 *Outline of Theoretical Approach for the First-Order Wave-Induced Loads*

As will be presented in section 4.4.1, there are several effects inducing steady second-order loads. Amongst others the oscillatory motion response induced by the first-order wave forces is one of them[14,58].

From the point of view of steady tilt behaviour, this effect will be important as it influences the magnitude of steady wave-induced tilting moment in roll mode as well as in other modes as indicated in ref. [21].

The fundamentals of vector analysis indicate that a change in a vector quantity can occur only by a change in length and/or a change in direction[78]. Regarding the steady tilt behaviour of semi-submersibles, the distance vectors from the centre of the rotation to the application point of the oscillatory first-order wave forces on each hull are fixed

in its body. (There have been arguments about the precise centre of roll for semi-submersibles and the application point of the forces on each hull for moment considerations, but in practice they are usually assumed at the centre of gravity and centre of lower hulls as chosen in ref. [21].) Although the lengths of the distance vectors are fixed in the moving semi-submersible, their direction changes as the vessel moves in space. The change in these vectors is a change in direction brought about by the rotation of the semi-submersible and does not depend on the translation of the vessel. Considering the beam sea case this change will be induced by the first-order roll motion only in oscillatory form and small in magnitude justifying linear theory assumptions.

During the derivation of the steady wave-induced tilting moment about the centre of rotation, the product of first-order forces on each hull and the distance vectors, which both oscillate sinusoidally, produces a steady moment and a second harmonic moment component. This effect reduces the steady wave-induced tilting moment on the semi-submersible which is assumed restrained[21].

In the foregoing section although this effect is omitted by the assumption of complete restraint, the author realises its importance and presents a method for the computation of the first-order forces as follows.

The method formulated here is the most rigorous application of the strip theory. It assumes that the semi-submersible is split into many beamwise strips along its length and the hydrodynamic interaction between adjacent cross-sections in the longitudinal direction is neglected. This assumption produces a two-dimensional hydrodynamic force problem in surface-piercing column sections, which are assumed as the extensions of the lower hulls, and in submerged lower hull sections.

It is assumed that the amplitudes of the incident wave and the resulting motions of the semi-submersible are moderate compared to the diameters of the main underwater elements. Thus the fluid forces will be dominated by the component due to pressure and viscous effects can be neglected. This assumption implies that even at large tilt angles, the hydrodynamic forces should be linear resulting in moderate amplitudes of harmonic motions about this tilted position.

Under these linear theory assumptions the sectional hydrodynamic loads on the semi-submersible cross-sections are computed by using the Frank Close-fit technique[79] which is based on the Green's Function Integral Equation Method. This method is applicable to any two-dimensional simply connected shape. It has a great advantage in that it represents the fluid potential directly due to any shape of disturbance. This facility allows the computation of hydrodynamic forces on the asymmetric hull section at tilted positions.

In spite of the three-dimensional effects anticipated, the use of the beamwise strip method will also facilitate the investigation of both the interference problems. Since the columns are assumed as the extensions of the hulls, the second type of hydrodynamic interference stated earlier is automatically taken into account. However, in the course of formulation of the first type of hydrodynamic interference problem the reflection principle is used[75,48,49]. Therefore the hull sections must be symmetric longitudinally with respect to the vertical mid-plane of the twin geometry. This restriction implies that the interference between the hull sections can be investigated only in the upright position of the twin geometry.

Moreover, since in the Frank Close-fit technique the required velocity potential is represented directly by a distribution of pulsating point sources around the wetted strip contour, the pressure distribution

around the contour can be obtained automatically. Such a facility will give information to obtain the hydrodynamic pressure centre where the hydrodynamic forces act on the section[50].

The Frank Close-fit technique was developed by Frank[79] and has been used extensively in several ship motion programmes developed in the David Taylor Model Basin (DTNSDC)[80,81,82]. By making use of the technique developed in these programmes, the author applied this method for the asymmetric single sections, symmetric twin-sections and computed the coupled motion-induced coefficients in plane modes[48,49]. He used the same technique to represent the two-dimensional diffraction potential [84,65,66] and computed the wave-exciting forces for single and twin sections in oblique seas[49]. He also studied the distribution of the hydrodynamic radiation pressures around semi-submersible types of cross-sections[50].

In the following a brief outline of the above hydrodynamic force problem is presented for regular beam seas based on the Frank Close-fit method. The effect of the earlier stated parameters, i.e. the frequency, the free surface, the section geometry, the interference and the tilt, are presented for the semi-submersible model tested.

4.2.2 *Formulation of the Theoretical Method*

It is assumed that the fluid is ideal, of infinite depth and that its motion is irrotational. Since the incident wave and resulting motion response is assumed sufficiently small in amplitude to justify a linear description, this general motion problem can be assumed to be a linear superposition of the following boundary value problems:

(i) The incident wave encountered by the semi-submersible section will be diffracted from it assuming the strip section is rigidly held in its fixed position. This is called the "Diffraction Problem".

(ii) As soon as the incident waves are diffracted due to the presence of the section, it is assumed that the motion can be represented by the oscillation of this section in initially calm water with the same frequency as the waves. This is known as the "Radiation Problem".

Thus, the total velocity potential of the fluid motion generated by sinusoidal beam waves with the stationary strip section undergoing small amplitude oscillation can be described by a time-dependent potential,

$$\Phi = \Phi_I + \Phi_D + \Phi_R \qquad \ldots \quad (10)$$

where Φ_I = the incident wave potential (Froude-Krylov potential) representing the incoming beam waves

Φ_D = the diffraction potential representing the disturbance of the incoming wave diffracted by the section

Φ_R = the radiation potential representing the motion-induced disturbance of the initially calm water.

The nature of the linear boundary value problems imposes the following conditions which should be satisfied by the sectional velocity potential:

(i) The Laplace equation in the fluid domain.

(ii) The linearised free surface condition on the free surface.

(iii) The bottom condition at the sea floor.

(iv) The radiation condition at a large distance from the strip section.

(v) The kinematic boundary condition on the section contour given by

$$\frac{\partial \Phi}{\partial n} = \frac{\partial}{\partial n}\left(\Phi_I + \Phi_D + \Phi_R\right) = V_n \qquad \ldots \quad (11)$$

where V_n = normal velocity component of a point on the section contour.

Within the linear analysis further decomposition of the kinematic boundary conditions yields the following for the radiation problem:

$$\frac{\partial \Phi_R}{\partial n} = V_n \qquad \ldots \quad (12)$$

and for the diffraction problem it is assumed that the body is rigidly held, thus:

$$\frac{\partial \Phi_I}{\partial n} + \frac{\partial \Phi_D}{\partial n} = 0 \qquad \ldots \quad (13)$$

In the strip domain, taken vertically in a beamwise direction, the incident wave profile, Froude-Krylov, radiation and diffraction potentials are expressed in the strip section as follows, Fig. 94[49]:

The incident wave (h) progressing across the x-axis given by:

$$h = a\, e^{i(\gamma x - \omega t)} \qquad \ldots \quad (14)$$

where a = maximum of the incident wave

ω = radian wave frequency

$\gamma = \frac{\omega^2}{g}$ = wave number

g = acceleration due to gravity

The Froude-Krylov velocity potential Φ_I which generates this wave in the beamwise direction at the strip contour is given by:

$$\Phi_I(x,y;t) = -\frac{i g a}{\omega} a^{\gamma y}\, e^{i(\gamma x - \omega t)} \qquad \ldots \quad (15)$$

The radiation potential Φ_R is represented by a distribution of wave source potentials along the strip section wetted perimeter with the aid of Green's formula, given by[79,49]:

$$\Phi_R^{(m)}(x,y;t) = \int_S Q_R^{(m)}(\xi,\eta)\, G(x,y;\xi,\eta)\, e^{-i\omega t}\, ds \qquad \ldots \quad (16)$$

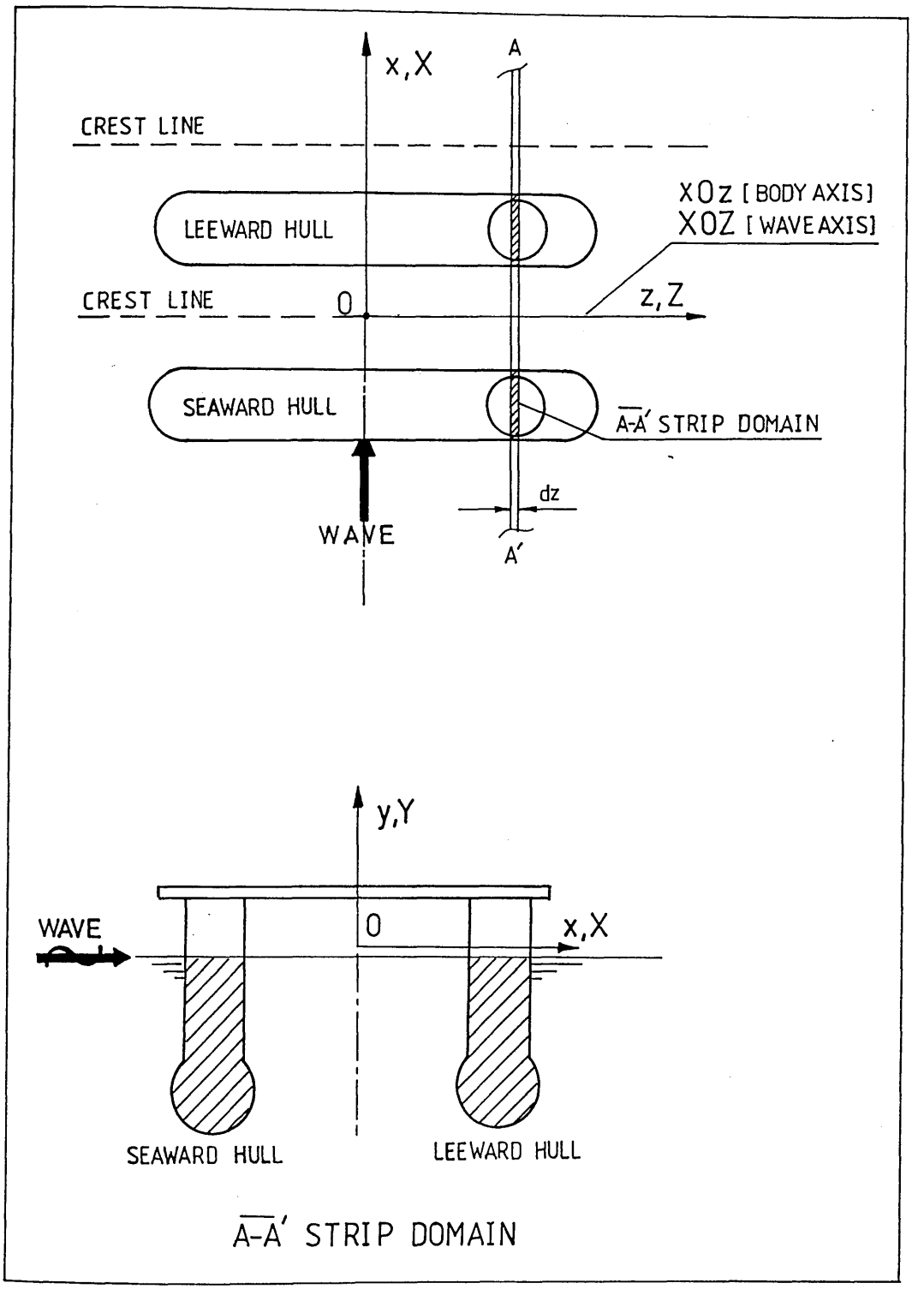

Fig. 94 - Definition of the coordinate systems and strip section

where Q_R = unknown source strength

G = pulsating source potential of unit strength at a point (ξ,η) on the strip contour. See refs [84,85,49].

$\underline{s}$ = wetted contour of the strip section

m = mode of oscillation takes 2, 3 and 4 for sway, heave and roll respectively.

Since the diffraction is also a disturbance, the diffraction potential Φ_D, is expressed in the same manner[83,49]:

$$\Phi_D^{(m)}(x,y;t) = \int_{\underline{s}} Q_D^{(m)}(\xi,\eta)\ G(x,y;\xi,\eta)\ e^{-i\omega t}\ ds \qquad \ldots \quad (17)$$

The radiation potential is employed to solve for the sectional motion-induced force coefficients (added mass/inertia and damping). The diffraction potential and the Froude-Krylov potentials are combined and utilised to obtain the sectional wave-induced forces (exciting force/moment) with accompanying phase angles as follows.

The Radiation Problem

The unknown source strengths $Q_R^{(m)}$ of eq. (16) are found by the application of the kinematic boundary condition eq. (12) on the strip contour as follows:

$$\begin{aligned} RE\left\{(n.\nabla) \int_{\underline{s}} Q_R^{(m)}(\xi,\eta)\ G(x,y\ \xi,\eta)\ ds\right\} &= 0 \\ IM\left\{(n.\nabla) \int_{\underline{s}} Q_R^{(m)}(\xi,\eta)\ G(x,y\ \xi,\eta)\ ds\right\} &= \omega\ A^{(m)} \cos(n,m) \end{aligned} \qquad \ldots \quad (18)$$

where $A^{(m)}$ = maximum of the motion of the strip in the mode of motion (m)

$\cos(n,m)$ = direction cosine depending on the mode of motion (m)

n = outward unit normal vector.

According to the Frank Close-fit procedure, the strip contour is approximated by a series of straight line segments with a single pulsating

source located at the mid-point of each segment. For the symmetric single and twin-section configurations by using the reflection principle the problem can be reduced to half of a symmetric section or one part of a twin section. In Fig. 95, typical section segmentations are shown for a column section in twin, single symmetric and single asymmetric cases. The strengths of the sources are assumed constant along the segment length but vary from segment to segment. Consequently, the above two sets of coupled integral equations, eq. 18, become a set of 2N linear algebraic equations, i.e. i=1,2, ... N.

$$\sum_{j=1}^{N} Q_j^{(m)} I_{ij}^{(m)} + \sum_{j=1}^{N} Q_{N+j}^{(m)} J_{ij}^{(m)} = 0$$

$$- \sum_{j=1}^{N} Q_j^{(m)} J_{ij}^{(m)} + \sum_{j=1}^{N} Q_{N+j}^{(m)} I_{ij}^{(m)} = \omega A^{(m)} \cos(n,m) \qquad \ldots \quad (19)$$

where

$$RE\left\{Q_R^{(m)}(\xi,\eta)\right\} = Q_j^{(m)} \quad \text{and} \quad IM\left\{Q_R^{(m)}(\xi,\eta)\right\} = Q_{N+j}^{(m)} \qquad \ldots (20)$$

and $I_{ij}^{(m)}$ and $J_{ij}^{(m)}$ are the "influence coefficients" given by Frank[79] and studied by the author in more detail in ref. [48].

By solving the above algebraic equation system, the unknown source strengths and, thus, the radiation potential is evaluated. The resulting potential consists of components in phase with acceleration and velocity. The hydrodynamic pressure along the strip contour is obtained from this potential using the linearised Bernouilli equation. Integration of the component pressures along the body contour yields the corresponding sectional added mass/inertia in phase with the acceleration and the potential damping in phase with the velocity[49].

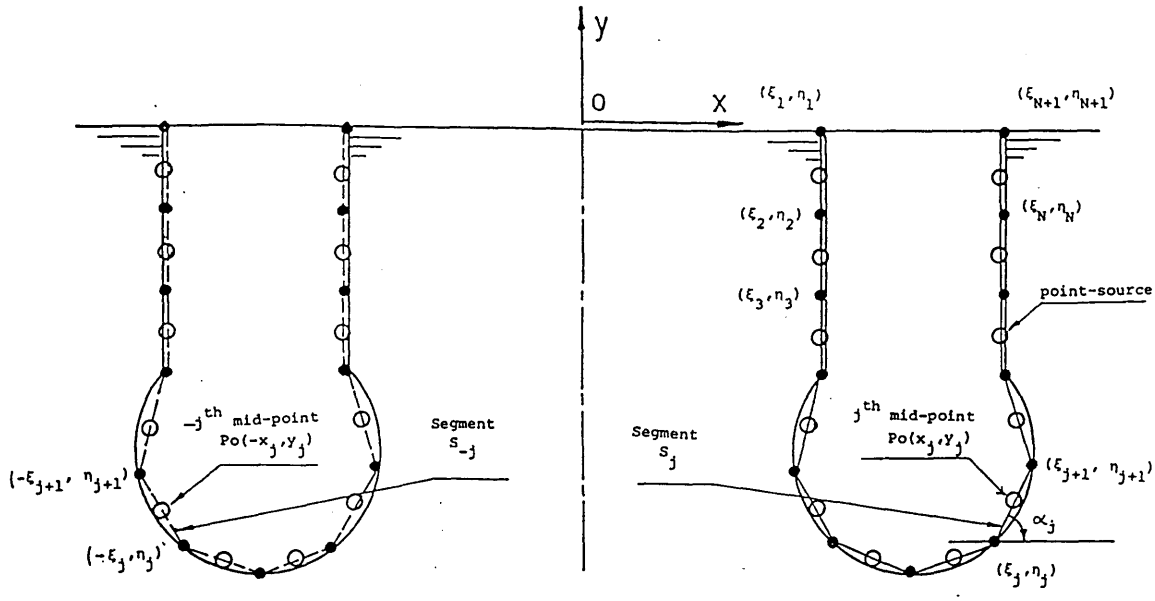

Fig. 95a - Twin-section segmentation

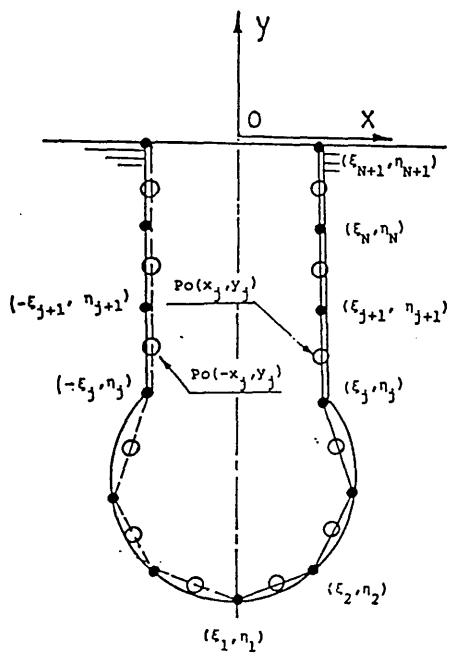

Fig. 95b - Symmetric single section segmentation

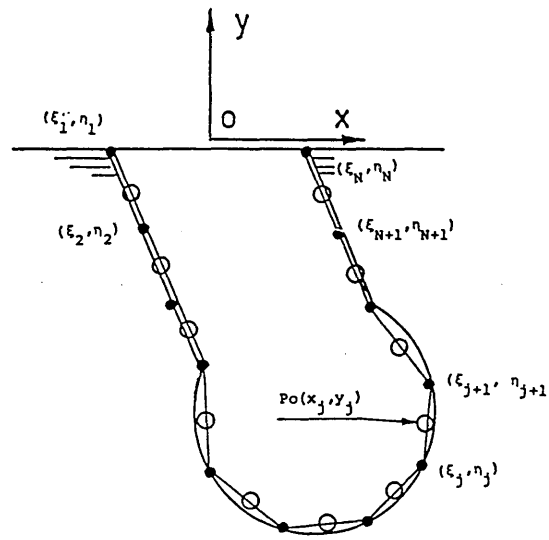

Fig. 95c - Asymmetric single section segmentation

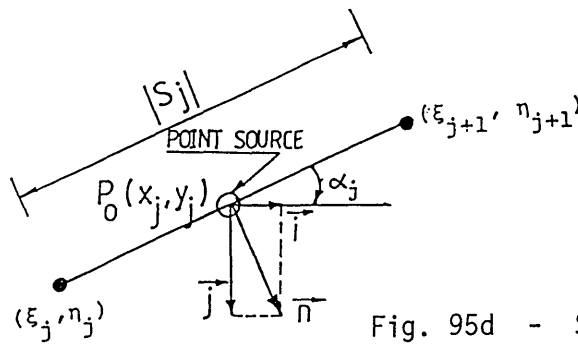

Fig. 95d - Segment geometry

Fig. 95 - Typical section segmentations according to the Frank Close-Fit Method

The Diffraction Problem

The Froude-Krylov force given in eq. (15) is broken into its real and imaginary parts per unit amplitude of the incident wave corresponding to its odd (o) and even (e) components in the form:

$$\frac{1}{a}\Phi_I^{(o)} = \text{RE}\left\{\Phi_I\ (x,y\ t)\right\} = \frac{g}{\omega}e^{\gamma y}\sin(\gamma x)\cos\omega t$$

$$\frac{1}{a}\Phi_I^{(e)} = \text{IM}\left\{\Phi_I\ (x,y\ t)\right\} = -\frac{g}{\omega}e^{\gamma y}\cos(\gamma x)\sin\omega t \qquad \ldots \quad (21)$$

which generates the appropriate modes of fluid motion. The even potential is applied to represent the symmetric flow about the y-axis whereas the odd potential function is applied to generate the asymmetric flow field about the same axis. The required potential per unit wave amplitude, which represents the flow due to the incident wave and the diffracted wave in the presence of a fixed strip section Φ_W, is written according to the mode of excitation[83,49]:

$$\begin{bmatrix}\Phi_W^{(2)}\\ \Phi_W^{(3)}\\ \Phi_W^{(4)}\end{bmatrix} = \frac{1}{a}\begin{bmatrix}\Phi_I^{(o)}\\ \Phi_I^{(e)}\\ \Phi_I^{(o)}\end{bmatrix} + \begin{bmatrix}\Phi_D^{(2)}\\ \Phi_D^{(3)}\\ \Phi_D^{(4)}\end{bmatrix} \qquad \ldots \quad (22)$$

The kinematic boundary condition given in eq. (13) will be different for the symmetric (heave) and asymmetric (sway and roll) modes thus:

$$\frac{\partial\Phi_D^{(3)}}{\partial n} = -\frac{\partial\Phi_I^{(e)}}{\partial n}$$

$$\frac{\partial\Phi_D^{(2,4)}}{\partial n} = -\frac{\partial\Phi_I^{(o)}}{\partial n} \qquad \ldots \quad (23)$$

Substituting the potential expression of eq. (17) and eq. (21) into eq. (23) by using the relation given by eq. (22) and utilising the Close-fit technique, the following algebraic equation systems are obtained:

(i) for heave

$$\sum_{j=1}^{N} Q_j^{(3)} I_{ij}^{(3)} + \sum_{j=1}^{N} Q_{N+j}^{(3)} J_{ij}^{(3)} = 0$$

$$\sum_{j=1}^{N} Q_j^{(3)} J_{ij}^{(3)} - \sum_{j=1}^{N} Q_{N+j}^{(3)} I_{ij}^{(3)} = \omega e^{\gamma y_i} \{\sin(\gamma x_i) \sin \alpha_i + \cos(\gamma x_i) \cos\alpha_i\} \quad \ldots \quad (24)$$

(ii) for sway (and, similarly roll)

$$\sum_{j=1}^{N} Q_j^{(2)} I_{ij}^{(2)} + \sum_{j=1}^{N} Q_{N+j}^{(2)} J_{ij}^{(2)} = - \omega e^{\gamma y_i} \{\cos(\gamma x_i) \sin\alpha_i + \sin(\gamma x_i) \cos\alpha_i\}$$

$$\sum_{j=1}^{N} Q_j^{(2)} J_{ij}^{(2)} - \sum_{j=1}^{N} Q_{N+j}^{(2)} I_{ij}^{(2)} = 0 \quad \ldots \quad (25)$$

where α_i is the segment slope of the i^{th} segment mid-point on the section contour, Fig. 95.

By solving each of the above equation systems as appropriate, the unknown source strength $Q_j^{(m)}$ and $Q_{N+j}^{(m)}$ and consequently the required diffraction potential is obtained. Both the diffraction potential and the Froude-Krylov potential comprise terms in phase with the acceleration and terms in phase with the velocity. The integration of the pressure around the wetted contour produces the sectional wave exciting force/moments in phase with the acceleration and velocity[49]. Thus:

$$f^{(m)} = |f^{(m)}| \cos(\varepsilon^{(m)} - \omega t) \quad \ldots \quad (26)$$

where

$$|f^{(m)}| = \left(f_R^{(m)2} + f_I^{(m)2} \right)^{\frac{1}{2}} \quad \ldots \quad (27)$$

is the force maximum and

$$\varepsilon^{(m)} = \tan^{-1} \left(f_I^{(m)} / f_R^{(m)} \right) \quad \ldots \quad (28)$$

is the phase shift of the force maximum from the incident wave maximum at the origin.

4.2.3 *Computations for the First-Order Wave-Induced Loads*

In this section based on the theoretical method used, the wave-induced loads on the semi-submersible model tested in Chapter 3 are computed. In spite of the appreciably large three-dimensional effects expected, a rigorous application of the strip method for this particular model illustrates several hydrodynamic aspects. Among these the effect of frequency, section geometry, hydrodynamic interference, surface-piercing columns and steady tilt are accounted for. Taking advantage of the two-dimensional procedure used, a major part of the investigation of these effects is carried out on the sectional loads as well as on the total (integrated) loads on the model in the upright position. The measured wave-exciting forces on the single hull and twin lower hull of the model given in Chapter 3 are compared with forces computed by the present method.

Presentation of Results

In order to facilitate the presentations, the results are presented in three groups as follows:

(i) Presentation of the sectional and total hydrodynamic loads on the particular model tested with emphasis on the effects stated above except for the tilt.

(ii) Presentation of the effect of hydrodynamic interference between the hulls, steady tilt and hull section shape on the sectional loads with various parameters.

(iii) Presentation of the comparison of the experimental and theoretical wave-exciting forces on the single and twin lower hull of the model in heave and sway mode.

It is appropriate that the hydrodynamic loads are usually represented by two distinct groups of force coefficients which are used in

the motion equation:

- Motion-induced coefficients (i.e. added mass/inertia and damping)
- Exciting wave-induced coefficients with accompanying phase angles.

Since a semi-submersible has two different types of cross-sections along the hull, it is also appropriate to represent these coefficients for:

- completely submerged (hull) section
- surface-piercing (column + hull combination) section.

(i) The hydrodynamic coefficients for the semi-submersible model are computed over the frequency range chosen according to the waves generated during the model tests, i.e. $1.885 \leq \omega \leq 7.54$ rs^{-1}. The coefficients are generated for all in-plane modes (heave, sway and roll) including the coupled sway-roll motion induced coefficients in the upright position of the model.

As shown in Fig. 96, three equally spaced vertical strips in the beamwise direction are taken for each column and one strip is taken for the hulls neglecting appendages. Thus, there is one completely submerged circular hull (section A-A) and four surface-piercing column (and hull combination) sections with differing widths at the waterline (section B-B and C-C at the outer columns; section D-D and E-E at the intermediate columns).

As outlined in the theoretical part, the Frank Close-fit technique requires the segmentation of the immersed section contour. Increasing the number of segments along the contour increases the accuracy of the results but simultaneously increases the computer time requirements. Consequently a compromise is normally made to limit costs.

If the demi-hull section is symmetric about its vertical mid-plane and hydrodynamic interference between the demi-hull sections is disregarded, a considerable saving in computing time is attained by utilising the symmetry and considering only one half of a demi-hull section. This facility is employed to determine the hydrodynamic coefficients of a single symmetric section in the upright position. The same facility is also used to determine the hydrodynamic coefficients of twin-hulled sections including the effect of hydrodynamic interference, in which case one complete demi-hull section is considered in the calculation.

However, when the section is forced into a tilted position, the resulting underwater geometry becomes asymmetric and requires the segmentation of each one of the complete demi-hull sections for the purposes of computation.

Figure 97 shows the segment distributions of the five typical cross-sections considered by using 24 straight line segments for one demi-hull.

In all figures the abscissa is a non-dimensional frequencey γR (R is hull radius). The sectional added mass and damping have been non-dimensionalised as in Table 25.

Mode of Motion	Added Mass Coefficients	Damping Coefficients
Heave	Added Mass/ρ S_A	Damping Force/ω ρS_A
Sway	Added Mass/ρ S_A	Damping Force/ω ρS_A
Roll	Added Inertia/ρ S_A S^2	Damping Inertia/ω ρS_A S^2
Sway-Roll	Added Moment/ρ S_A S	Damping Moment/ω ρS_A S

where S_A is instantaneous cross-sectional area, S is half of the hull separation.

Table 25 - Presentation of the hydrodynamic motion-induced coefficients

The sectional exciting forces and moments are presented in the form of amplitudes $|f^{(m)}|$ and phase angles $\varepsilon^{(m)}$ in the m^{th} in-plane mode of motion. These can be written in a time dependent form as:

$$|f^{(m)}| \cos(\varepsilon^{(m)} - \omega t)$$

where $\varepsilon^{(m)}$ is the phase shift of $|f^{(m)}|$ from the crest of the incident wave at the origin of the wave axis system (0-XY). This is taken at the intersection point of the water level and the vertical symmetry axis of the twin sections, Fig. 97. It should be noted that $|f^{(m)}|$ is the amplitude of the sum of the sinusoidal forces acting on the individual hull section and presented by the coefficients given in Table 26.

Mode of Excitation	Wave-exciting Force/Moment Coefficients
Heave	Exciting Force/$a\rho gR$
Sway	Exciting Force/$a\rho gR$
Roll	Exciting Moment/$a\rho g\ S^2$

Table 26 - Presentation of the hydrodynamic wave-induced coefficients

For the presentation, the rolling centre is located at the centre of the wave axis system (0-XY).

The computed sectional hydrodynamic coefficients of the five typical cross-sections shown in Fig. 97, are presented in Figs 98a,b to 104a,b. The figures termed by (a) show the coefficients of the twin sections where the hydrodynamic interaction between the hull sections are not accounted for (i.e. each hull in isolation). However, the physical interference (phase relation) between the hull sections owing to the orientation of each hull relative to the wave is accounted for in the wave-induced coefficients.

Whereas, the figures termed (b) present the same coefficients in the corresponding modes when account is taken of the hydrodynamic interference for the motion-induced coefficients and both the hydrodynamic and physical interference for the wave-induced coefficients.

The total hydrodynamic loads on the model, which are found by integrating these sectional loads along the length of the model, are presented in Figs 106 to 112 and compare the values in isolation with those for hydrodynamic interference. The results are presented in dimensional form against non-dimensional frequency values.

In order to investigate the hydrodynamic effects of the surface-piercing columns, the total hydrodynamic loads are presented by separating the loads on the two lower hulls of the model and those on the whole model (Figs 113 to 119). In this presentation the hydrodynamic interference between the hulls is not accounted for.

(ii) In the first group of investigations, the effect of hydrodynamic interference is presented for the model with a ratio of hull separation-to-hull diameter of 6.0 which is relatively large. In fact, this investigation must be carried out systematically over a range of hull separations rather than for a single value. Similarly, the effect of tilt on these force coefficients also demands a systematic study over a range of tilt angles.

Hence, both the effects of hydrodynamic interference and tilt on the force coefficients of two different cross-sections were investigated over a range of these parameters including cross-section shape effects.

The range of demi-hull sections comprises circular and rectangular geometries, the latter with an aspect ratio of 2.0. The circular submerged hull and surface-piercing column sections are two typical cross-sections, which are similar in size, to the model tested. The

column thickness to hull diameter (breadth) ratio of the geometrically related hull-column combination is 0.5, Fig. 120a. The beam of the rectangular section is similar to the hull diameter of the circular hull. It is to be noted that although the draught of the circular and rectangular hull and column section is different, the depth of submergence of each hull (upright) top surface below the free surface is kept the same, Fig. 120a.

The numerical results presented herein are based on a total of 24 segments distributed along the contour of each single completely submerged lower hull section and a total of 32 segments in the case of a surface-piercing column section. Figure 120b shows a typical segment distribution for the circular section generated by the computer in a tilted position.

The hydrodynamic coefficients are generated at 40 frequencies within a wide range, $0 < \omega \leq 12$, and for the so-called 'infinite-frequency' for added mass at the tilt investigated. These infinite frequency coefficients, termed 'I', appropriate to each submergence are shown in the key box of each added mass figure.

In order to ascertain the importance and nature of hydrodynamic interference effects between the hulls of the cross-sections, the coefficients are generated for single submerged hull and surface-piercing sections in isolation and compared to the coefficients obtained when accounting for hydrodynamic interference. Hull separation- to-beam ratios, S/B, of 1.5, 3.0, 6.0 are used during this investigation for both cross-sections.

In Figs 121 to 130 the effect of hydrodynamic interference on the hydrodynamic coefficients of both the circular and rectangular cross-sections are presented by typical examples in heave and sway mode. The full range of presentation is given in ref. [52].

The investigation of the effect of tilt on the hydrodynamic coefficients is based on the assumption that the immersed demi-hull sections do not interact with each other hydrodynamically. The hull separation-to-hull beam ratio chosen for this phase of the work is 6.0 as for the model's hull separation. Using specially prepared computer routines, each of the four types of stripwise twin-hulled section are rotated about the point of intersection between the centreline of lateral symmetry and the waterline as shown in Fig. 131. Numerical data is generated for the asymmetrical sections tilted in the leeward direction at tilt angles of 3°, 6°, 9°, 12° and 15°. Corresponding upright, single section data is generated at the equivalent depth of submergence, here measured below the free surface to the centre of area of each hull as shown in Fig. 132. This equivalent depth of submergence is different for the seaward, H_s, and leeward, H_ℓ, demi-hull sections. It is so defined to filter out the effect of the depth of submergence between the asymmetric tilted section and the equivalent upright section thus retaining solely the effect of the tilt angle. An examination of the effect of tilt is carried out by comparing the results computed for the leeward and seaward sections and the corresponding upright sections which are presented separately on the same figures.

The results are presented in Figs 133 to 151 by typical examples chosen in the heave and sway modes for both the circular and rectangular cross-sections. The full range of this investigation is also given in ref. [52]. In these figures the abscissa is a non-dimensional frequency γB. The sectional added mass, damping and wave-exciting force coefficients are presented as defined in group (i). It should be noted that, while for the purposes of the hydrodynamic interference study, $|f^{(m)}|$ is the amplitude of the sum of the sinusoidal

forces acting on the individual (leeward and seaward) hull, in the case of the tilt investigation $|f^{(m)}|$ is the amplitude of the force acting on each hull separately.

(iii) In the force tests, the wave-exciting force on the lower hulls of the model was measured at the hull separation-to-hull diameter ratios for 2.0, 3.0, 4.0 and 6.0 as well as on that of the single hull in isolation.

In the following this experimental force data is compared with theoretical results.

As stated in Chapter 3, during the model tests the wave-exciting forces were measured on each hull separately in the presence of the other hull. Therefore the measured force on each hull includes the hydrodynamic effect of the other hull. In order to present the sum of the forces acting on the twin hull the physical interference between the hulls is taken into account by using the theoretical phase angle, $\varepsilon^{(m)}$ of the single hull in isolation.

The comparison of the experimental and theoretical data with accompanying phase angles are presented in Figs 152 to 157 for the single hull in isolation and twin hull at four hull separations. In these figures the abscissa is non-dimensional frequency (γB) while the sectional force has been non-dimensionalised as for the previous presentations, i.e. by $a\rho gB$.

Discussion of Results

The discussion of the results is given in the same groups as described above.

(i) i.1 Sectional Hydrodynamic Coefficients: As illustrated in Figs 98 to 104 the sectional hydrodynamic coefficients are presented for two typical cross-sections of the model. These are:

Completely submerged twin hull-section (section A-A)

Surface-piercing twin column (and hull combination) section with differing ratios of column width at WL to hull diameter (column thickness ratio) of 0.51 (section D-D), 0.59 (section E-E), 0.71 (section B-B) and 0.81 (section C-C).

In these figures it is noted that having surface-piercing extensions with differing column thickness ratios changesthe hydrodynamic coefficients of the completely submerged hull section dramatically. This effect is different for each mode and depends on the column thickness ratio.

If one disregards the effect of the hydrodynamic interference, Figs 98a to 101a, while the inclusion of this extension decreases the added mass in the heave mode throughout the frequency range, its effect varies in the asymmetric modes (sway, roll, coupled sway-roll) with varying frequency particularly in the low frequency range.

The trend of the damping curves of the asymmetric modes is different from those in the symmetric heave mode. The inclusion of the column extension increases the damping of the submerged hull section enormously in the asymmetric modes throughout the frequency range while in the heave mode it increases it in the low frequency region and diminishes towards the higher frequency region.

The effect of the surface-piercing extension on the wave-exciting force coefficients follows the same trend as the damping coefficients reflecting the Haskind-Newman relationship[86] in the heave and sway mode as shown in Figs 98a, 99a and 102a,b. However, the force coefficients indicate a "critical-frequency" at about 0.26 where the forces on each hull section cancel each other out due to the physical interference.

As illustrated in Fig. 102a, the "wave-excitationless" frequency caused by the hydrodynamic interference between the surface-piercing extension and the submerged lower hull section occurs at relatively higher frequencies, where the damping also becomes zero, for section E-E and D-D. As the column thickness ratio increases the wave-excitationless frequency shifts towards the higher frequency region.

In order to ascertain the hydrodynamic interference between the hull sections if Figs 98a to 104a are compared with Figs 98b to 104b respectively, it is noted that this effect brings about two distinct discontinuities for the surface-piercing sections. These are in the vicinity of a non-dimensional frequency of 0.10 in the symmetric mode and that of 0.3 in the asymmetric modes.

The discontinuity about the non-dimensional frequency of 0.3 is caused by the two-dimensional interference phenomenon as stated earlier. At this resonant frequency the half length of the corresponding surface wave is equal to the distance between the inner walls of the column sections. This wave is a half antisymmetric standing wave trapped between the inner walls. It has a symmetry about the vertical symmetry axis of the twin sections, where its maximum or minimum occurs. Its zero-crossing points are at the intersection points of the column inner walls and the waterline.

By using the relation between the wave frequency and length, these non-dimensional resonant frequencies, K_r, can be located by the following formula as suggested in refs [73,74]:

$$K_r = n \frac{\pi}{S-x} R \qquad \begin{matrix} (n=1,2,3, \ldots \text{ for symmetric modes}) \\ (n=0.5,1.5,2.5, \ldots \text{ for asymmetric modes}) \end{matrix} \quad \ldots \quad (26)$$

where x is half column width at WL.

Equation 26 yields the first possible non-dimensional resonant frequencies in the asymmetric mode (i.e. n=0.5) for each surface-piercing section as follows:

K_r = 0.288, 0.292, 0.299 and 0.305 for section D-D, E-E, B-B and C-C respectively.

This indicates that the discontinuity at about 0.3 in the asymmetric modes is induced by the resonant behaviour.

However, the discontinuity in the heave mode cannot be explained by the resonant behaviour which does not occur for the sections and frequency range tested here (e.g. $K_r \simeq 0.5$ for n=1).

This discontinuity is attributed to the "irregular frequency" phenomenon induced by the singular behaviour of the Green's Function Integral Equation method for certain types of surface-piercing sections[79]. This is a mathematical failure and thus the computed values at this frequency do not represent any physical condition and should be disregarded or filtered out by using smoothing techniques[87,71]. As suggested in ref. [87] the irregular frequencies can be located by scanning the value of the determinant of the matrix coefficients used in determining the source strengths on the section contour. As shown in Fig. 105a in the vicinity of a non-dimensional frequency 0.10 the value of the determinant becomes very small relative to its neighbouring values in the symmetric mode. However, it is interesting that as illustrated in Fig. 105b, the value of the determinant also presents a sudden drop about the non-dimensional resonant frequency of 0.3 in the asymmetric modes. Thus, although no irregular frequency is observed in the case where the demi-hull section is in isolation, the irregular frequencies can occur in a complicated form when the hydrodynamic interference between the hull sections is accounted for. There may be a case where the irregular frequency may be nearly coincident with the

resonant frequency or close to each other affecting the width of the deviation band around these frequencies. In such a case it is impossible to distinguish between the two phenomena [68,77].

The comparison of Figs 98a to 104a with 98b to 104b indicates that at this hull separation ($S/R \simeq 6.0$) the effect of the hydrodynamic interference on the submerged hull section is negligible whereas it is considerable on the magnitude of the surface-piercing section coefficients in addition to the complicating resonant and irregular frequency phenomenon.

i.2 Total Hydrodynamic Loads: As illustrated in Figs 106 to 109, if the above explained discontinuities are disregarded, the effect of the hydrodynamic interference (between the demi-hulls) on the added mass of the model is small. However, the damping of the model is reduced considerably when this effect is accounted for in all the modes. This interference effect on the heave-exciting force on the model is less sensitive and practically unimportant, Fig. 110, while it is relatively less in the roll mode, Fig. 112. It is large on the sway exciting force resulting in considerable differences in magnitude with a different trend in which the critical-frequency, where the zero force occurs due to the physical interference, disappears, Fig. 111, as also reported in ref. [76].

The complicating occurrence of two discontinuities are observed at the same frequencies in the wave exciting force curves since the disturbance caused by the diffraction of the incident wave is represented by the same technique for the radiation case.

The effect of the existence of the columns is analysed when the hull sections are in isolation. This is preferred to eliminate the discontinuities encountered when accounting for the hydrodynamic inter-

ference between the hulls. As shown in Fig. 113, the inclusion of the columns brings about a constant reduction of 10% in the total added mass of the model through the frequencies tested. In the asymmetric modes this inclusion increases the added mass of the submerged hull considerably in the low frequency range while it does not affect it at the higher frequencies as shown in Figs 114 to 116.

The total damping of the lower hull increases considerably in the asymmetric modes throughout the frequencies when the columns are included. However, this effect is not very strong in the heave mode and varies as the frequency varies.

The inclusion of the columns presents a wave-excitationless frequency at a non-dimensional frequency of 0.05 caused by the hydrodynamic interaction between the submerged lower hull and submerged columns in the heave mode, Fig. 117. The inclusion of the column greatly increases the magnitude of the sway-exciting force on the lower hulls while its effect is relatively small on the roll-exciting moment of the lower hulls, Figs 118 and 119.

(ii) ii.1 The Effect of Hydrodynamic Interference on the Sectional Hydrodynamic Coefficients:

Motion-induced Coefficients

Submerged sections: Although the deeply submerged single, circular section coefficients in the heave and sway mode are the same, their values differ when hydrodynamic interference is taken into account, Figs 121 and 122. Whereas the heave values generally increase with decreasing hull separation, the corresponding added mass and damping values decrease in the sway mode. Notably the added mass values for S/B ratios greater than 3 are approximately of the same magnitude as those of the single hull. Apart from the effect of geometry and aspect ratio on the coefficients the differences in the trends of the rectangular section

results from those of corresponding circular section results are negligible, Figs 121a,b and 122a,b.

Surface-piercing sections: A decrease in the hull separation induces an increase in the added mass and damping values in the heave mode, Fig. 123. Hydrodynamic interference induces slight variations in the heave added mass coefficients in comparison with those of the single hull in isolation. The corresponding variations in damping with hull separation and the magnitude of the damping throughout the frequency range are negligible.

Although all curves have the same trend, the inclusion of the hydrodynamic interference brings about sharp discontinuities related to the resonant and irregular frequency phenomenon as stated earlier.

Table 27 represents the possible resonant frequencies derived from eq. 26 for the symmetric and asymmetric modes in the first 3 modes of the oscillations (i.e. n=1,2,3 for symmetric mode, 0.5,1.5,2.5 for asymmetric mode. The resonant frequencies in the shaded part are outwith the range tested here.

Asymmetric Modes (sway, roll)

S/B	n = 0.5	n = 1.0	n = 1.5	n = 2.0	n = 2.5	n = 3.0
1.5	1.57	3.14	4.71	6.28	7.85	9.42
3.0	0.63	1.26	1.8	2.51	3.14	3.77
6.0	0.28	0.57	0.86	1.14	1.43	1.71

Symmetric Modes (heave)

Table 27 - Location of resonant frequencies

Referring to Table 27 the discontinuity at a non-dimensional frequency of about 0.57 in the heave mode for the largest hull separation is because of a symmetric standing wave taking place between the inner walls of the columns of wave length equal to hull separation and maximum wave elevation at the centreline (i.e. n=1 in eq. 26). For narrower hull separations the resonant frequencies occur at higher frequencies outwith the range tested in the thesis.

However, in the low frequency region (a non-dimensional frequency range between 0.1 and 0.2), except for the single section case, the remaining curves have sharp discontinuities at frequencies which do not coincide with a resonant frequency. These are attributed to the irregular frequency phenomenon stated earlier and should be disregarded or filtered out.

The twin-hull asymmetric modes are dominated by the resonant frequency (or perhaps combined with the irregular frequency) behaviour at larger hull separations as shown in Figs 124a and b. Referring to Table 27 no resonant frequency occurs at the smallest hull separation. The discontinuity at a non-dimensional frequency of 0.63 for $S/B = 3.0$ and the discontinuities at 0.28 and 0.86 for $S/B = 6.0$ are caused by the asymmetric standing waves between the inner walls of the column section for $n = 0.5$ and 1.5.

Hydrodynamic interference reduces the twin-hull damping and added mass coefficients in this mode in comparison with those of the single hull although variations in the hull separation do not affect the results for all practical purposes (except for the resonant behaviour). As shown in Figs 123a,b and 124a,b the trend in the curves in the heave and sway mode for both circular and rectangular sections is similar in terms of the peaks and troughs. The magnitude of the heave added mass of the rectangular section is greater than that of the circular while for the damping the opposite is the case.

Wave-induced Coefficients

Submerged sections: For submerged sections in heave and sway changes due to hydrodynamic interference are negligible except for the smallest hull spacing (S/B = 3.0) and the moderate frequency range, Figs 125 to 128. Whether hydrodynamic interference is accounted for or not the largest force is observed at the smallest hull separation in the relatively low frequency range. As the hull separation increases local peaks occur because of the physical interference and result in a smaller force magnitude (which takes zero value at certain frequencies). For a given hull separation the occurrence of zero total force at certain frequencies is purely owing to the phase relation between the demi-hulls, Figs 127 and 128. This behaviour does not appear to be affected by hydrodynamic interaction in the case of a fully submerged section.

Surface-piercing sections: Typical force results for surface-piercing sections are given in Figs 129 and 130. For rectangular sections in the sway mode, the single section force values which do not include hydrodynamic interference follow the same trend exhibited by the submerged sections. However, this pattern of behaviour is altered and the magnitude of the force reduces dramatically when hydrodynamic interference is taken into account.

The wave-excitationless frequency in the heave mode, Fig. 129, shifts towards a higher frequency as the hull spacing decreases. As stated in the foregoing, since the diffraction potential is represented using the same technique employed to represent the radiation potential, the complicating occurrence of resonant and irregular frequencies are to be expected.

As for the submerged section case, zero forces are induced at certain frequencies. However, in the case of surface-piercing sections,

accounting for hydrodynamic interference leads to cancellation of zero-force frequencies, except for the wave-excitationless frequency referred to.

The trends observed for the rectangular hull interference and those of the circular are similar in nature.

ii.2 The Effect of Tilt on the Sectional Hydrodynamic Coefficients: The influence of a tilt angle on the hydrodynamic coefficients manifests itself through the change in the section area projected normal to the direction of motion, the depth of submergence (or draught) and in the case of roll and coupled sway-roll, through the change imposed on the moment arm to the centre of rotation of the section. Its effects on a submerged hull section differs from that experienced by a surface-piercing column. Furthermore, significant differences are induced in the hydrodynamic coefficients of the leeward and seaward demi-hulls.

Motion-induced Coefficients

Submerged sections: The influence of tilt on circular sections is non-existent in all the in-plane modes of motion throughout the frequency range and tilt angle range examined except for those changes due to the altered depth of submergence, Figs 133 and 134. Its effect on the rectangular sections depends on the mode of motion considered. As shown in Figs 135 and 136 if one compares figs a with c and b with d, the effect of pure tilt (i.e. effect of depth of submergence is filtered out) due to rotation on the heave and sway coefficients is negligible for all practical purposes except for tilt angles exceeding 10° for which slight variations are found. Significant variations exist between the leeward and seaward demi-hull. It may be observed that the greatest variations occur in the seaward hull values due to its greater

proximity to the free surface. Since the leeward hull increases its depth of submergence with increasing tilt angle, the variations in its coefficients with frequency are much smaller than those of the seaward hull. The magnitude of the coefficients of the seaward hull is always greater than that of the leeward hull in $0 < K \simeq 0.5$ for the range of tilt angles and sections examined. This trend may vary beyond this frequency.

Surface-piercing sections: Even if the effect of the draught is filtered out, a tilt angle induces significant changes in the non-dimensional frequency range < 0.4 in the heave mode at angles greater than 5° (compare fig. a with c and b with d in Figs 137 and 138). The modifications imposed on the sway coefficients are limited to the same frequency range and tilt angles greater than 10° where slight changes can be induced (see by comparison of fig. a with c and b with d in Figs 139 and 140).

Figure 138 indicates that whereas the damping assumes a zero value in the upright condition, it does not in a tilted position. This phenomenon is explained when discussing the wave-induced coefficients of surface-piercing sections.

If the motion coefficients of the seaward and leeward hulls at the equivalent upright positions are compared, the seaward hull experiences a larger force than the leeward hull in the heave mode, figs c and d in Figs 137 and 138. The same coefficients at the actual tilted position indicate the opposite trend so that the leeward hull experiences a larger force than the seaward hull, figs a and b in Figs 137 and 138. However, sway hydrodynamic coefficients of the leeward hull are always greater than those of the seaward hull whether it is in the upright or tilted position.

Wave-Induced Coefficients

Submerged sections: The effect of tilt on the force amplitude and phase of the circular section can be explained by the change due to depth of submergence. The seaward hull always experiences a larger force than the leeward hull throughout the frequency range, Figs 141 to 146. If the effect of the submergence is filtered out the pure effect of tilt on the force and phase angle of the rectangular section is small and limited to angles exceeding 10° for which minor changes occur, reflecting the slight changes induced in the wave damping.

Surface-piercing sections: The changes imposed by a tilt angle on the force amplitude and phase of surface-piercing sections are significant and particularly noteworthy. As has been illustrated when discussing the motion-induced coefficients, Fig. 138, there exists a 'critical frequency' at which the wave damping and, therefore, the wave-exciting forces, will vanish for single column sections having a small waterplane area and a large submerged volume. This wave-excitationless frequency appears to no longer exist once a tilt angle is imposed on the section, Figs 147 and 148.

The modifications due to the tilt angle are most significant in the non-dimensional frequency range $K < 0.4$ and manifest themselves through changes in both the amplitude and phase of the force. In the tilted positions, Figs 147a and b, as the tilt angle reaches very large values ($\phi > 10°$) the heave-exciting force on the leeward hull becomes larger than that on the seaward hull. Whereas in the equivalent upright position, Figs 147c and d, the seaward hull always experiences a larger heave exciting force than the leeward one particularly in the high frequency region.

Changes imposed on the wave-induced coefficient in the sway mode due to pure tilt effect (the effect of draught is filtered out) are limited to

tilt angles greater than 10° and are relatively minor, Fig. 150.

In the actual tilted position and equivalent tilted position, the sway-exciting force of the leeward hull is always greater than that of the seaward hull (compare fig. a with b and fig. c with d in Fig. 150).

These conclusions apply to both circular and rectangular hull sections.

(iii) Comparison of the Experimental and Theoretical Wave-exciting Force on the Lower-hulls of the Model

iii.1 Single Hull in Isolation: As illustrated in Figs 152 and 153, the theoretical method, which is based on the two-dimensional potential theory, indicates a similar magnitude of wave-exciting force for the single hull in the heave and sway mode. However, the experiments indicate a greater sway-exciting force compared to the heave force particularly in the high frequency range. The correlation between the theory and experiments is good in the heave and fair in the sway mode.

iii.2 Twin-hull at Various Hull Separations: As shown in Fig. 154 in the heave mode, the agreement between theory and experiment is very good at relatively low frequencies and good in the high frequencies at the four hull separations tested.

However, similar to the single hull case, the theory underestimates the experimental sway-exciting force. The agreement is worst at the smallest hull separation and improves as the hull separation increases, Fig. 156.

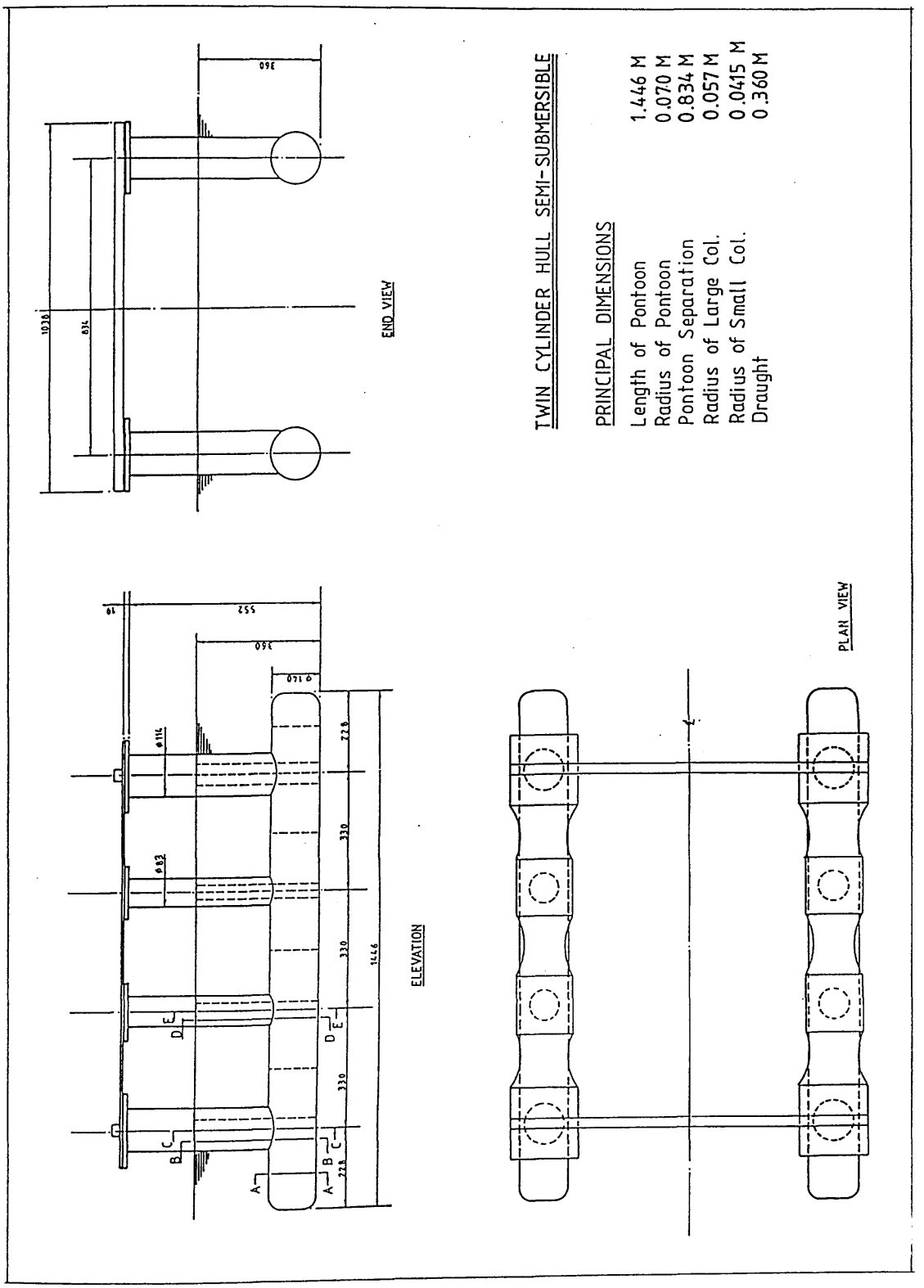

Fig. 96 - Illustration of the strip section A-A, B-B, C-C, D-D and E-E on the semi-submersible model

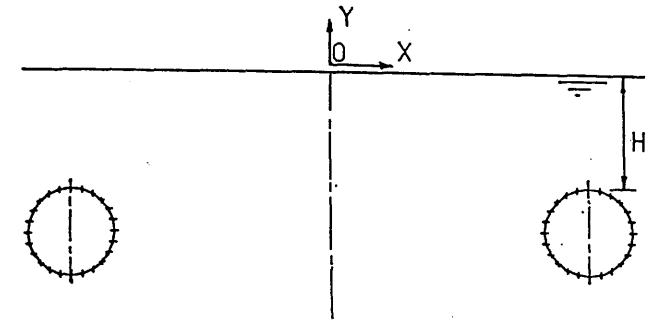

SECTION A-A

SECTION GEOMETRY	:	CIRCULAR
NO. OF SEGMENTS	:	24
RADIUS	:	0.07 H
HALF HULL SEPARATION	:	0.42 H
DEPTH OF SUBMERGENCE TO UPPER FACE(D		

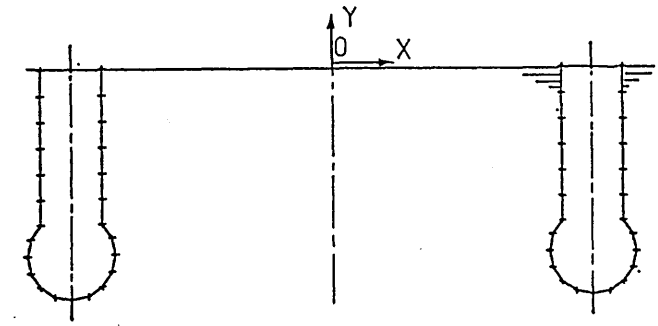

SECTION B-B

HULL GEOMETRY	:	CIRCULAR
NO. OF SEGMENTS	:	24
HULL RADIUS	:	0.07 H
SHR	:	0.71
DRAFT	:	0.38 H
HALF HULL SEPARATION	:	0.42 H

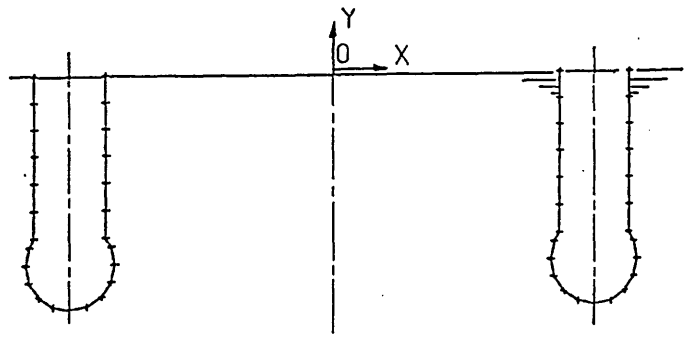

SECTION C-C

HULL GEOMETRY	:	CIRCULAR
NO. OF SEGMENTS	:	24
HULL RADIUS	:	0.07 H
SHR	:	0.81
DRAFT	:	0.36 H
HALF HULL SEPARATION	:	0.42 H

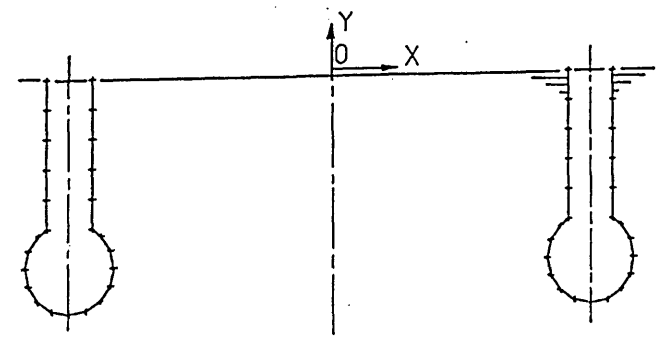

SECTION D-D

HULL GEOMETRY	:	CIRCULAR
NO. OF SEGMENTS	:	24
HULL RADIUS	:	0.07 H
SHR	:	0.51
DRAFT	:	0.30 H
HALF HULL SEPARATION	:	0.42 H

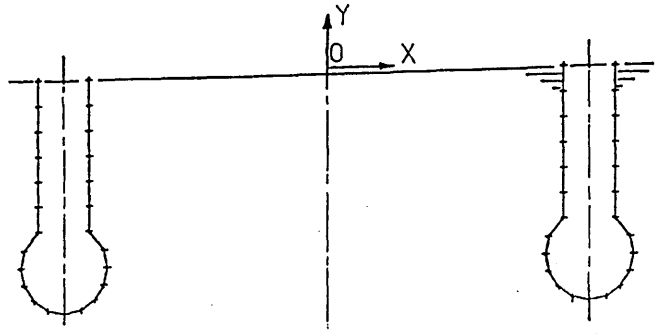

SECTION E-E

HULL GEOMETRY	:	CIRCULAR
NO. OF SEGMENTS	:	24
HULL RADIUS	:	0.07 H
SHR	:	0.59
DRAFT	:	0.30 H
HALF HULL SEPARATION	:	0.42 H

Fig. 97 - Segment distributions of the typical cross-sections considered

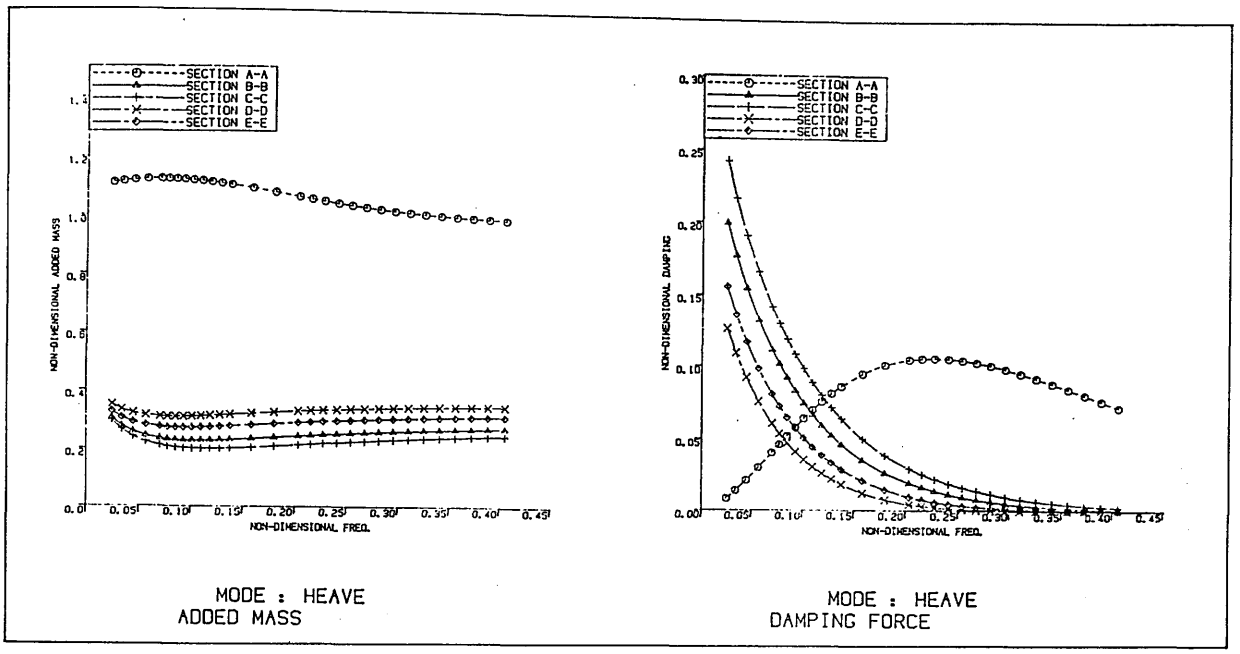

Fig. 98a - Sectional motion-induced coefficients for the heave mode in the absence of the hydrodynamic interaction between the twin sections

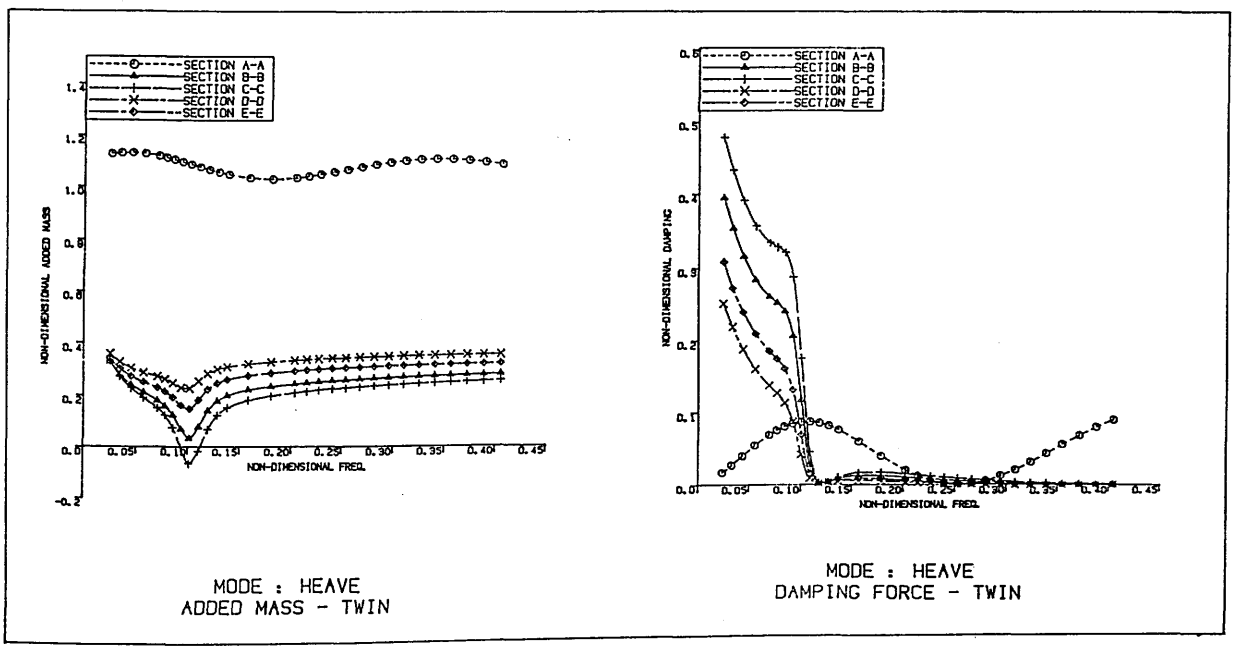

Fig. 98b - Sectional motion-induced coefficients for the heave mode in the presence of the hydrodynamic interaction between the twin sections

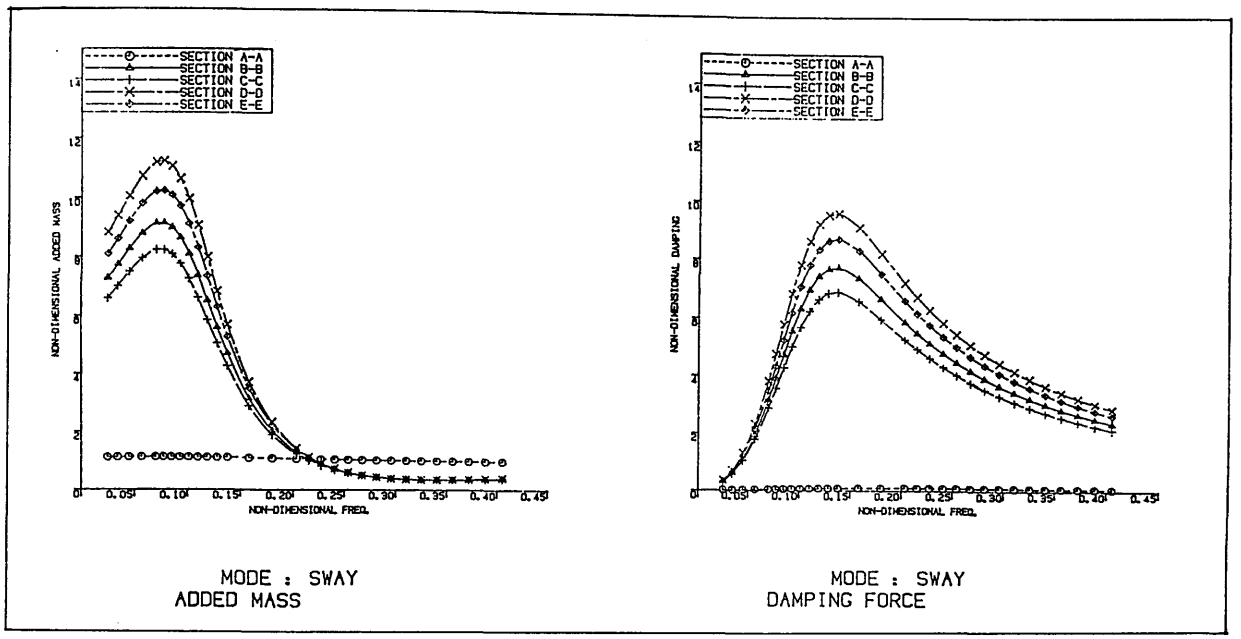

Fig. 99a - Sectional motion-induced coefficients for the sway mode in the absence of the hydrodynamic interaction between the twin sections

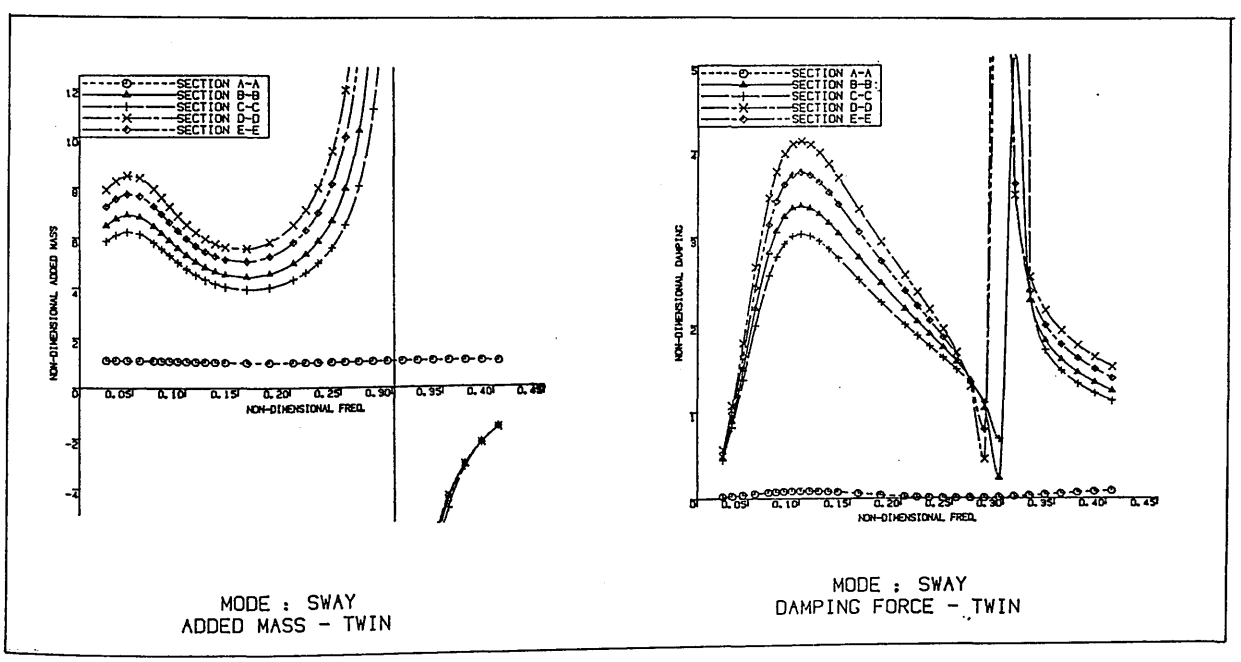

Fig. 99b - Sectional motion-induced coefficients for the sway mode in the presence of the hydrodynamic interaction between the twin sections

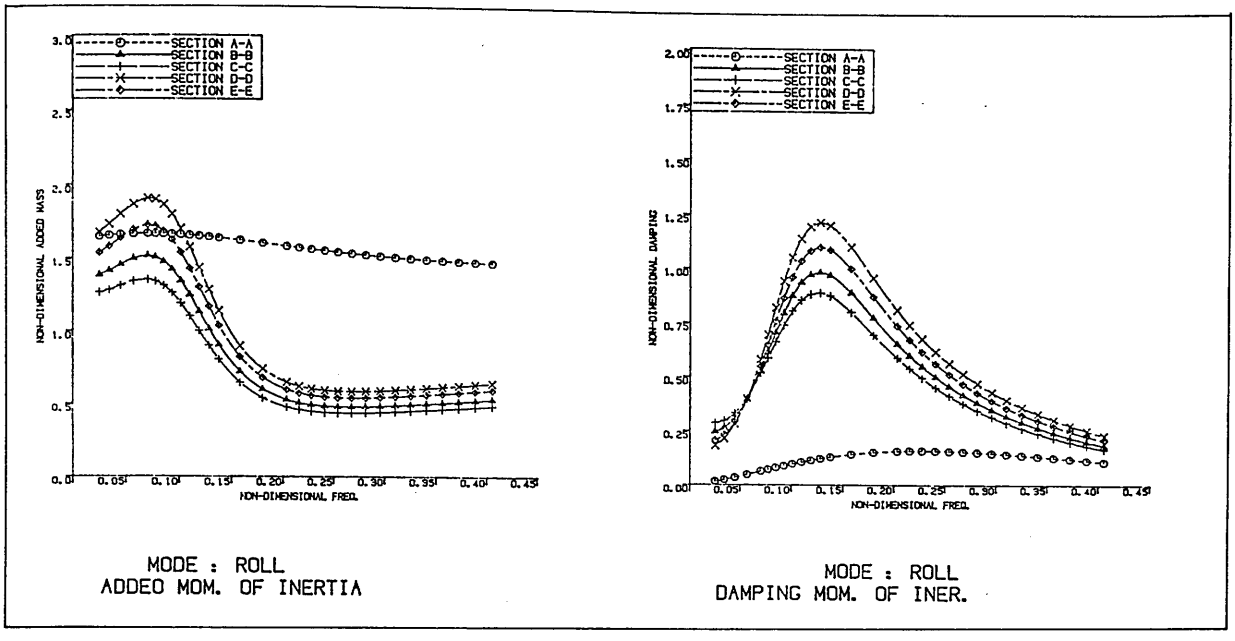

Fig. 100a - Sectional motion-induced coefficients for the roll mode in the absence of the hydrodynamic interference between the twin sections

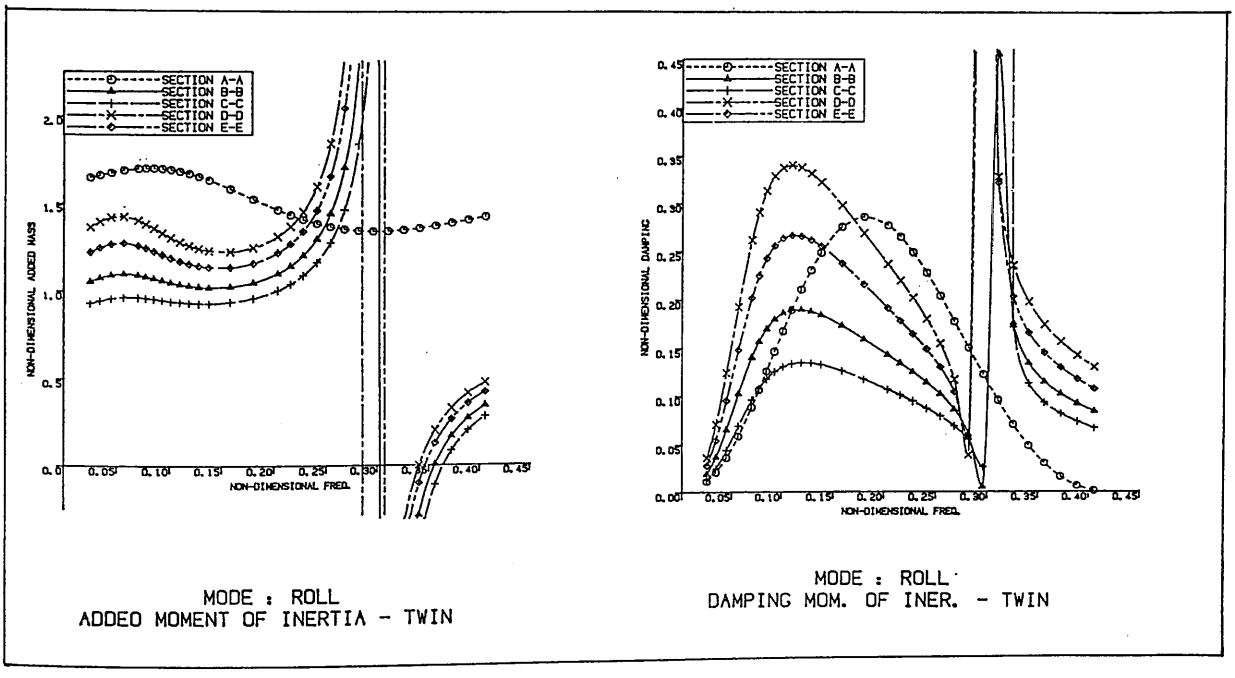

Fig. 100b - Sectional motion-induced coefficients for the roll mode in the presence of the hydrodynamic interference between the twin sections

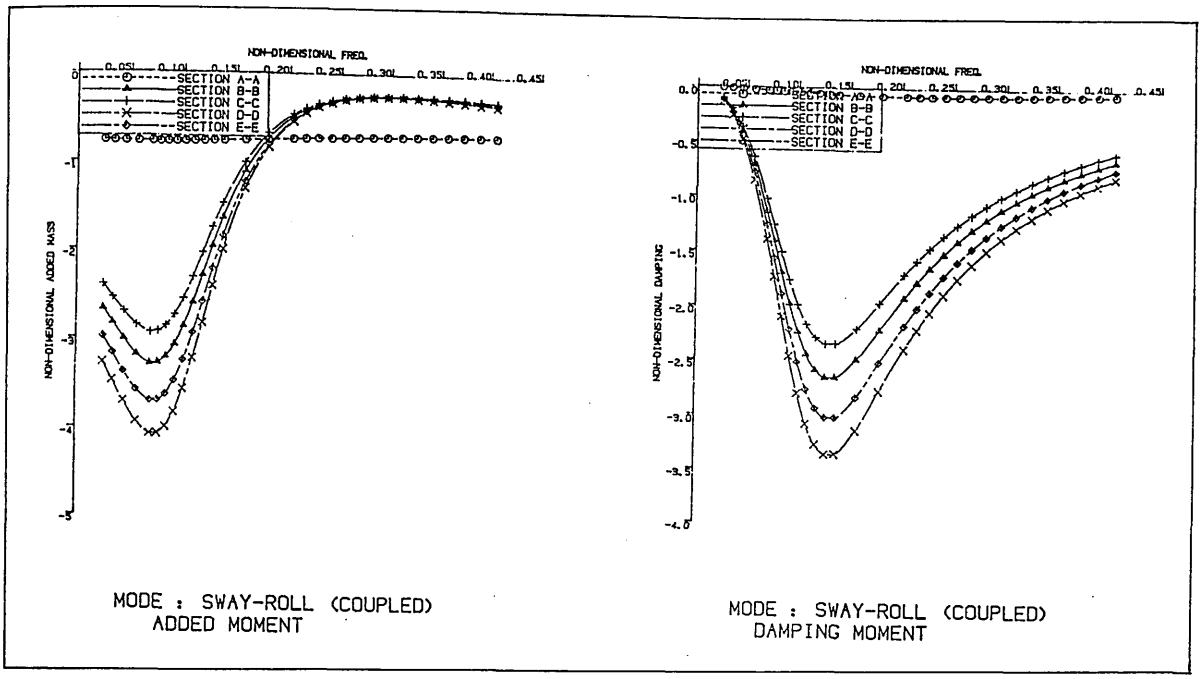

Fig. 101a - Sectional motion-induced coefficients for the coupled sway-roll mode in the absence of the hydrodynamic interference between the twin sections

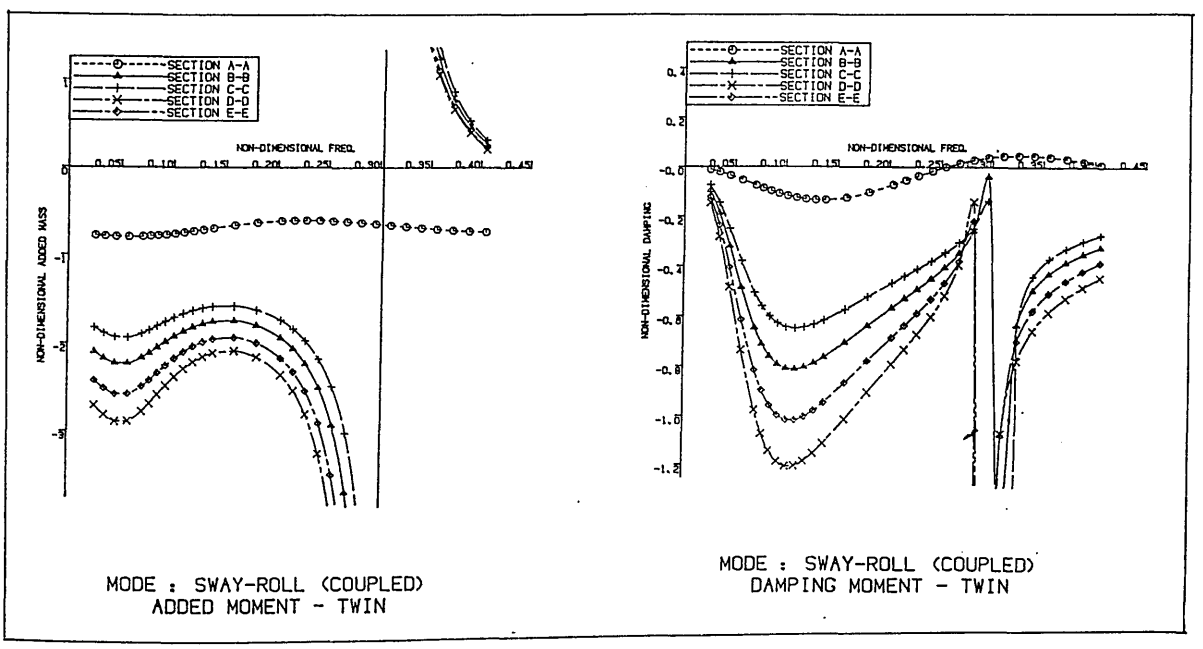

Fig. 101b - Sectional motion-induced coefficients for the coupled sway-roll mode in the presence of the hydrodynamic interference between the twin sections

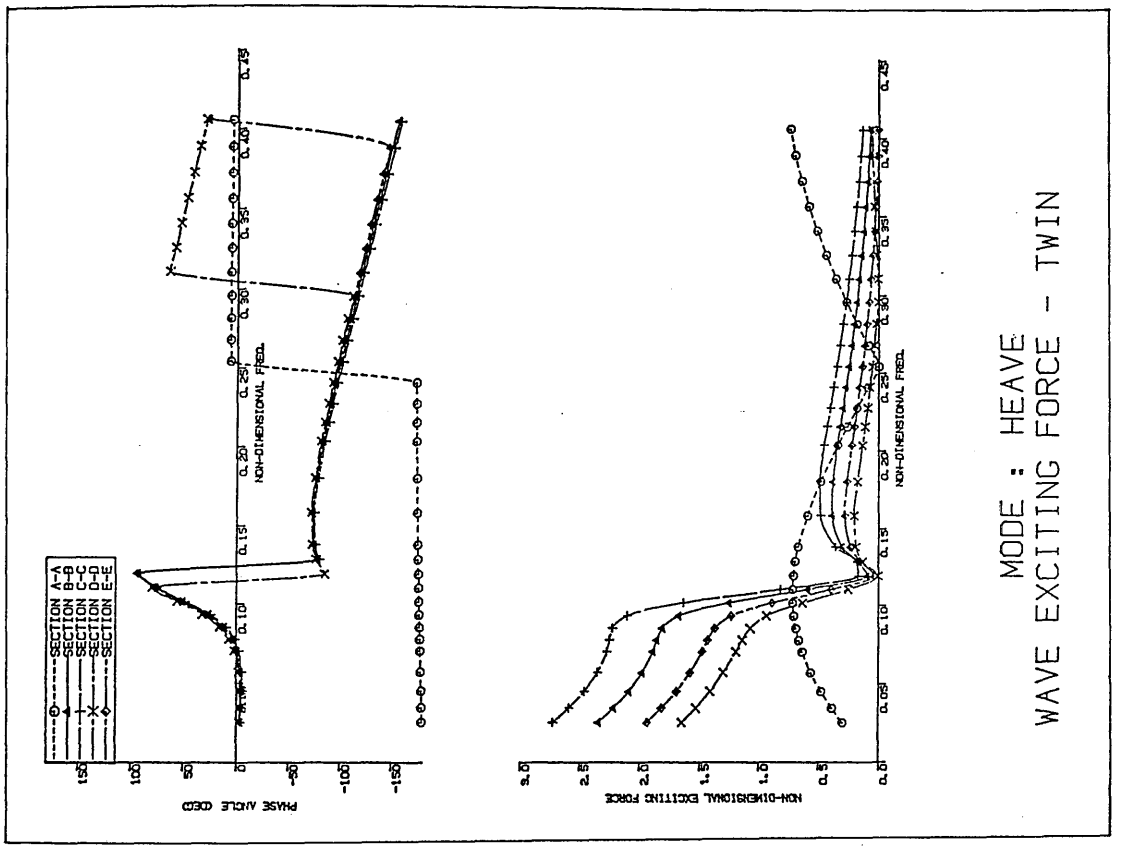

Fig. 102b - Sectional wave-induced coefficients for the heave mode in the presence of the hydrodynamic interaction between the twin sections

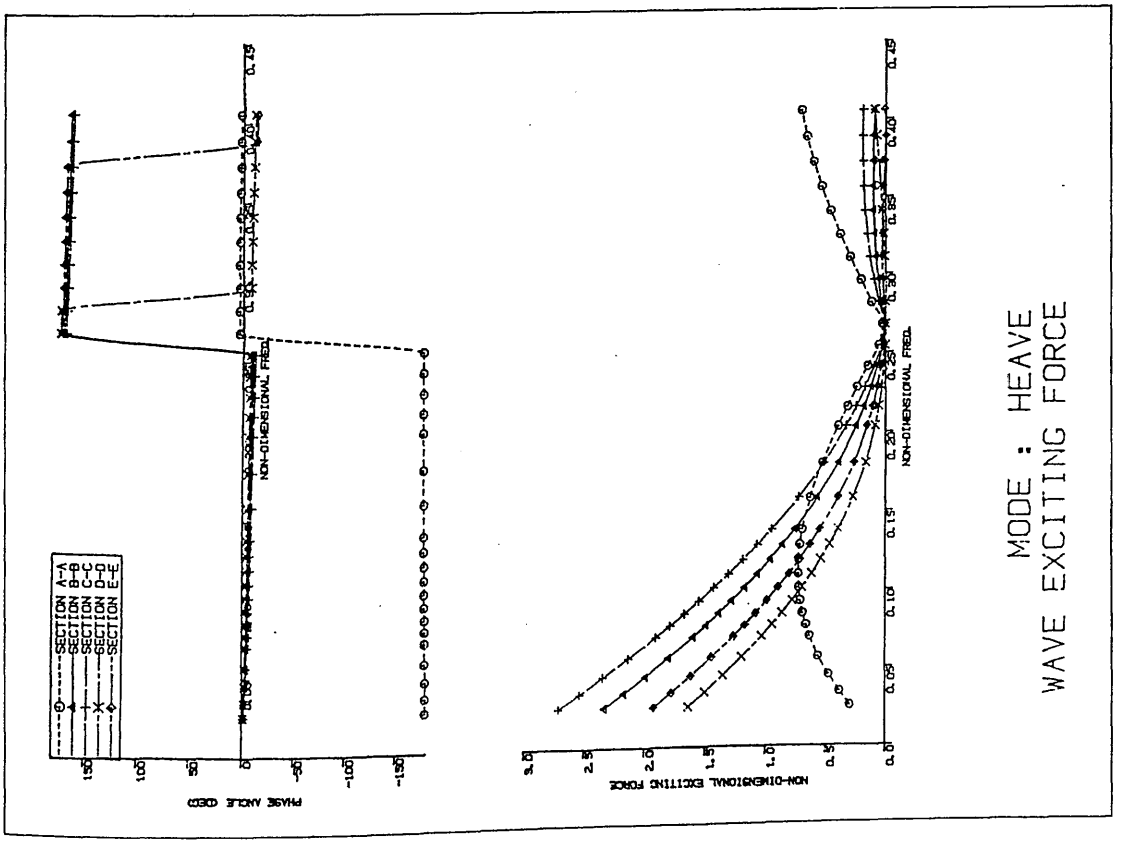

Fig. 102a - Sectional wave-induced coefficients for the heave mode in the absence of the hydrodynamic interaction between the twin sections

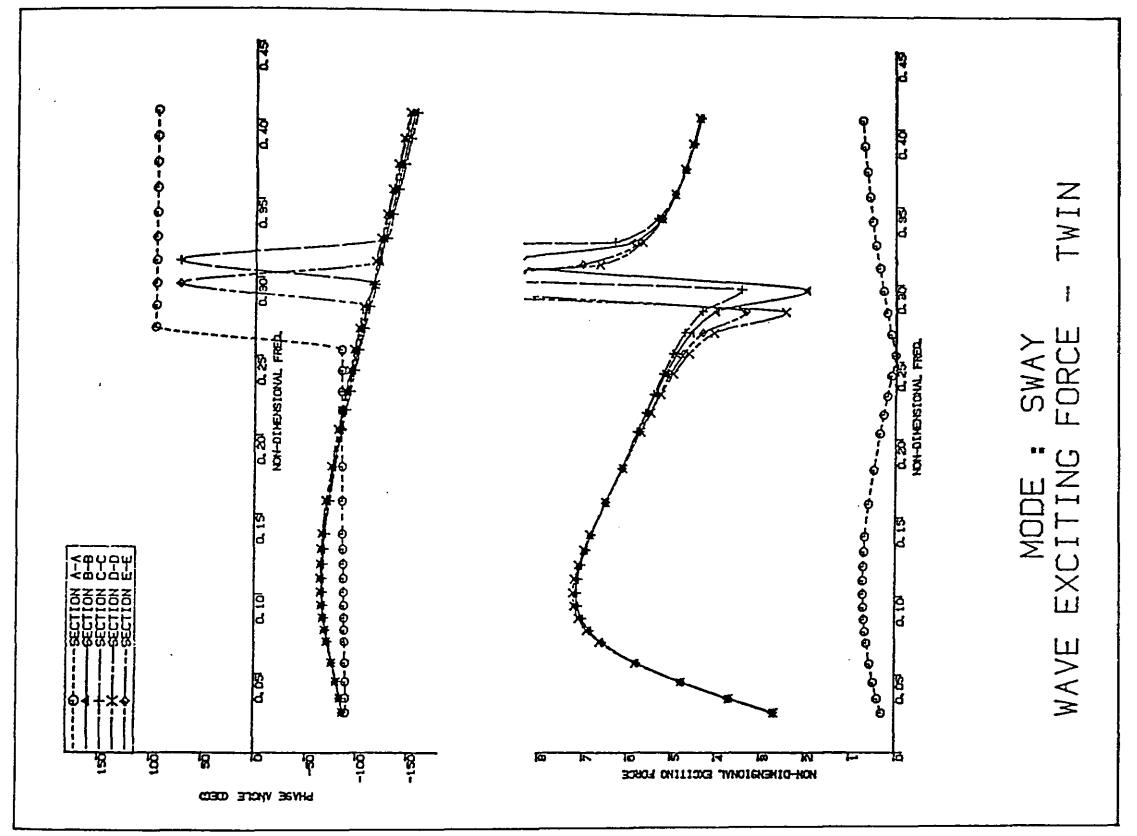

Fig. 103b - Sectional wave-induced coefficients for the sway mode in the presence of the hydrodynamic interaction between the twin sections

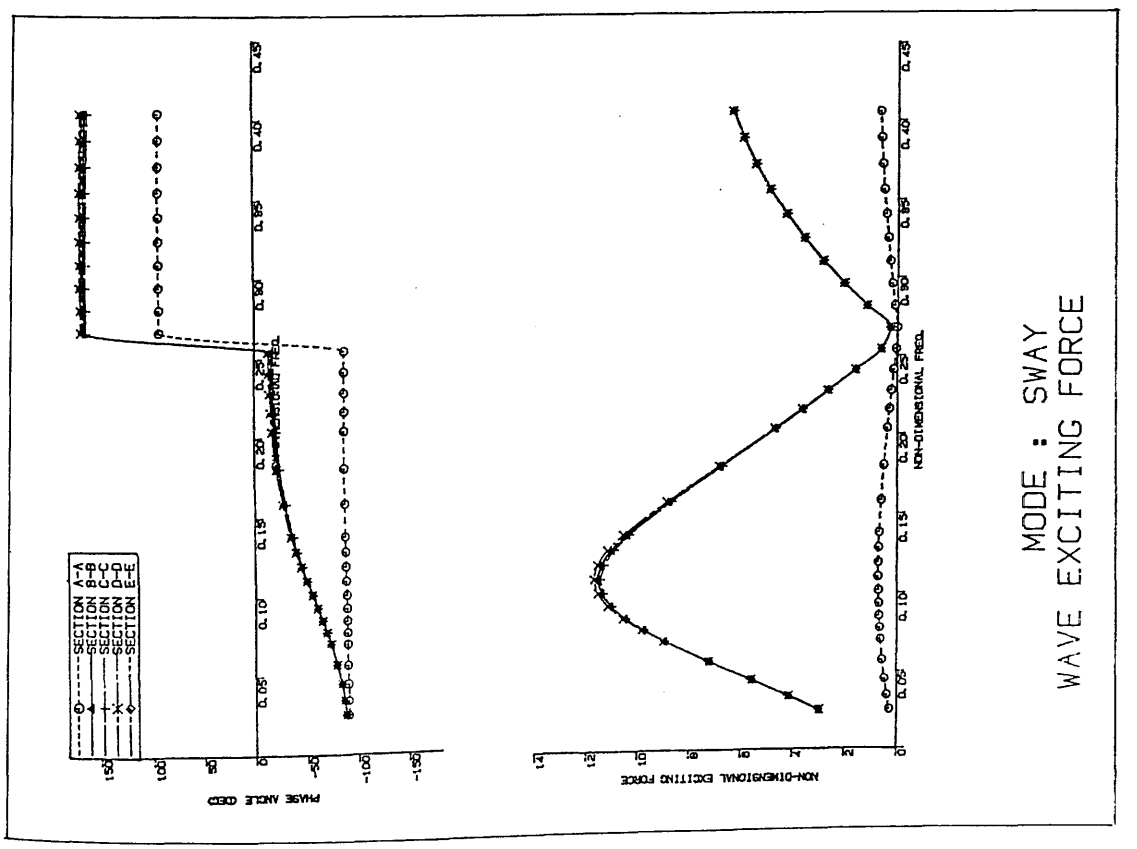

Fig. 103a - Sectional wave-induced coefficients for the sway mode in the absence of the hydrodynamic interaction between the twin sections

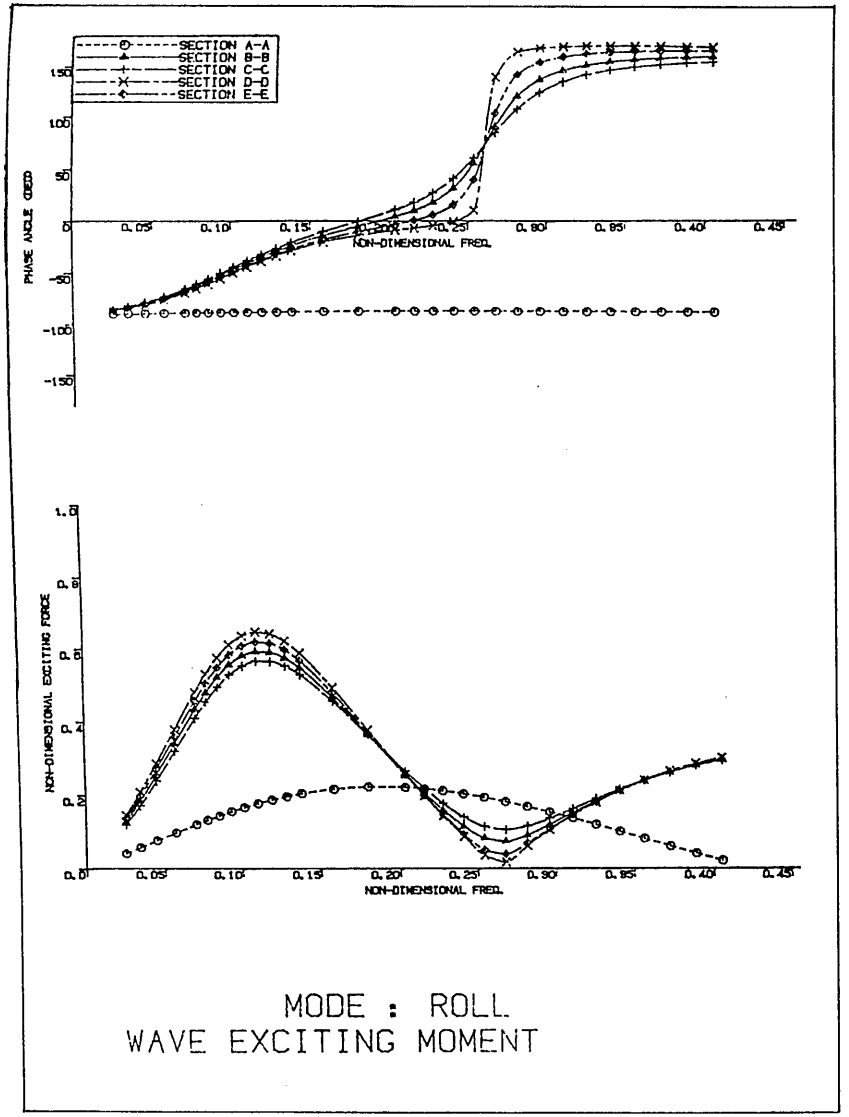

Fig. 104a - Sectional wave-induced coefficient for the roll mode in the absence of the hydrodynamic interaction between the twin sections

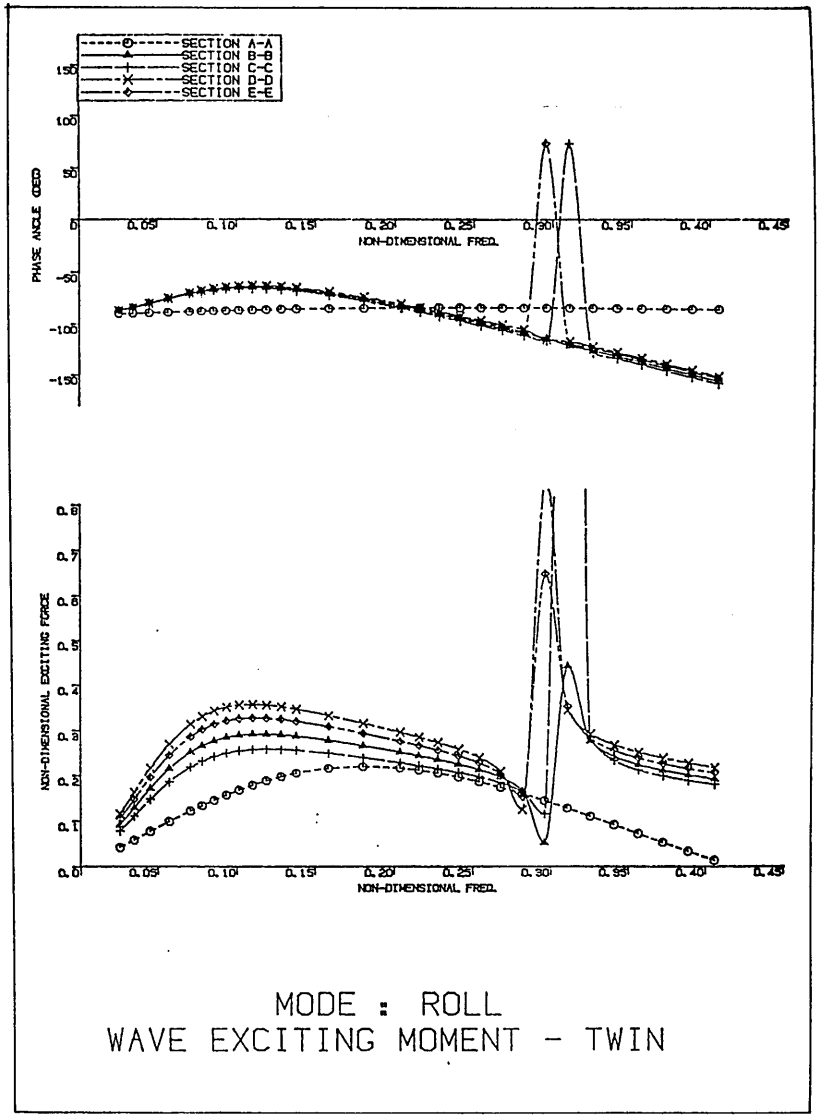

Fig. 104b - Sectional wave-induced coefficient for the roll mode in the presence of the hydrodynamic interaction between the twin sections

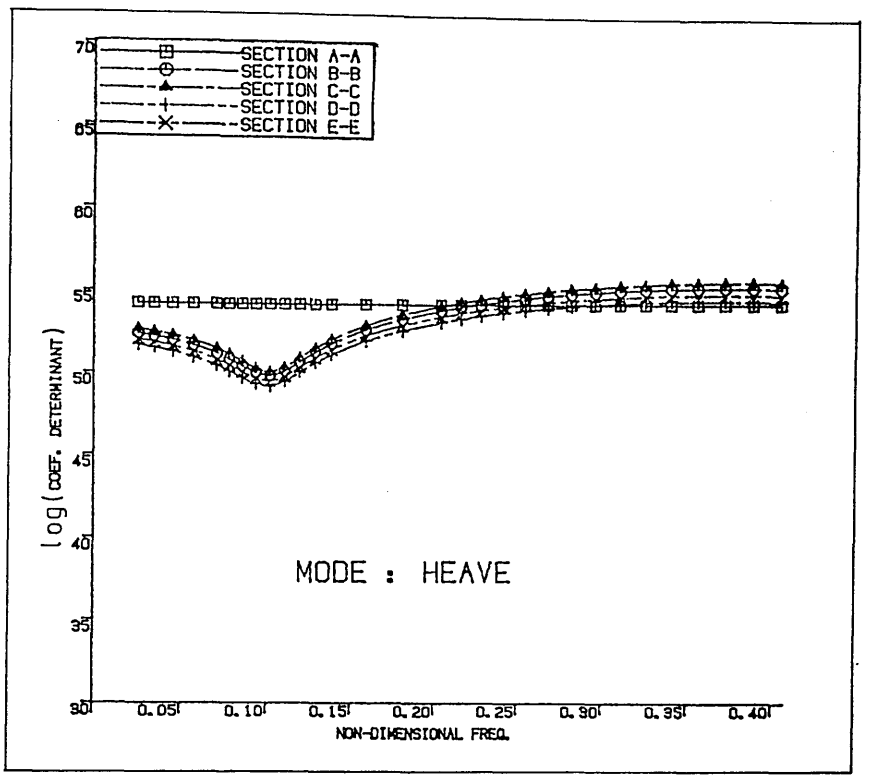

Fig. 105a - Determinant of the influence coefficient matrix for the heave mode

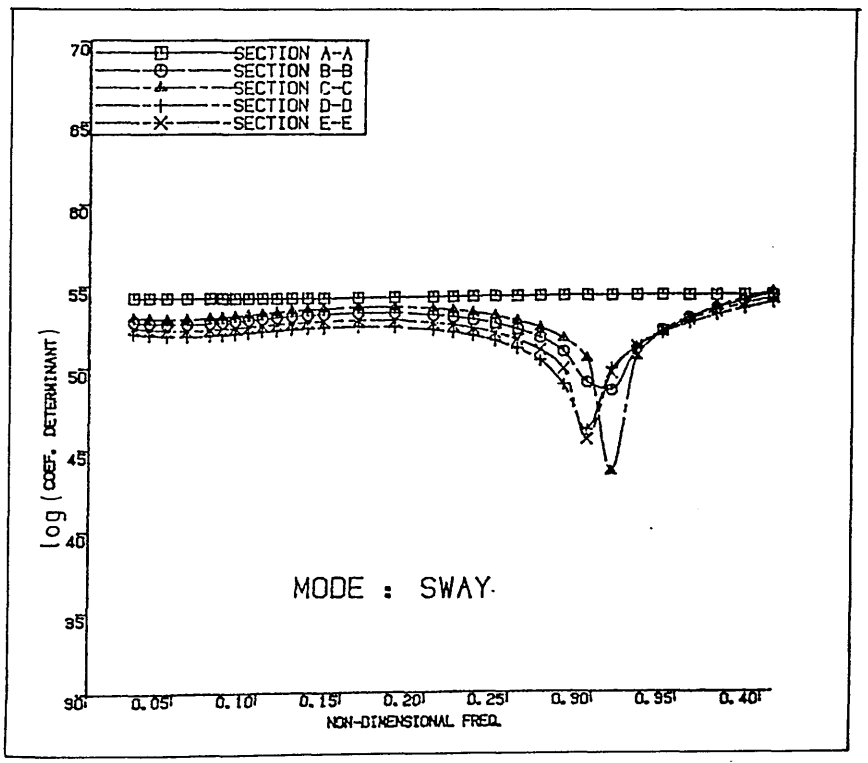

Fig. 105b - Determinant of the influence coefficient matrix for the sway mode

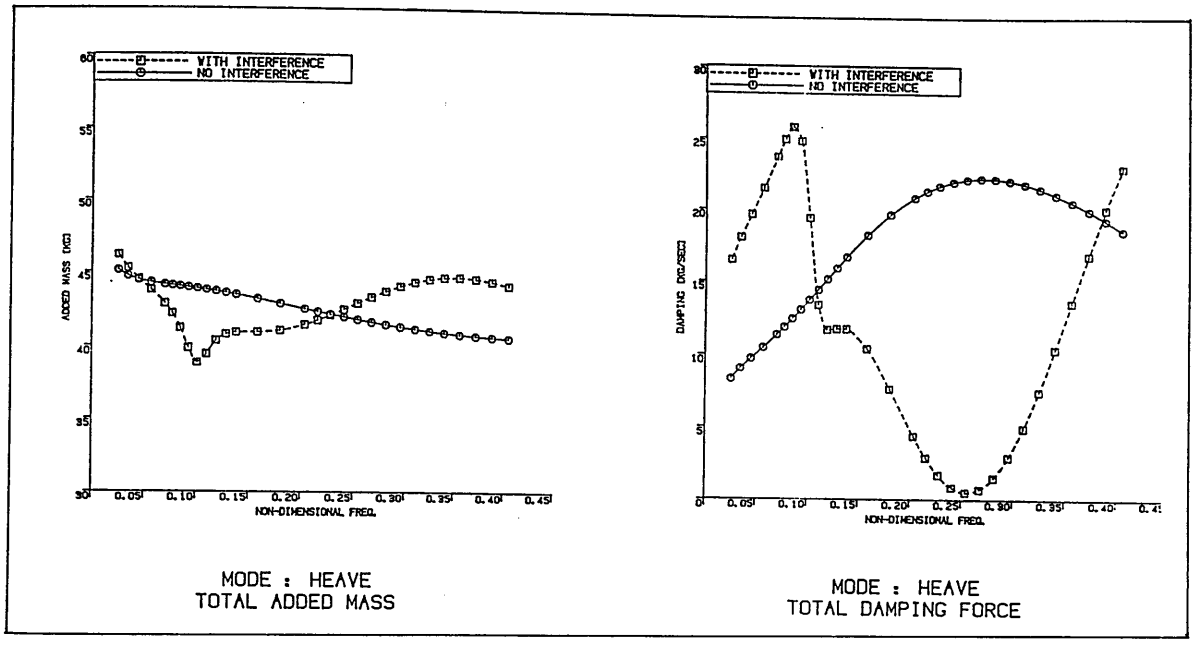

Fig. 106 - Comparison of the motion-induced coefficients of the model in the heave mode illustrating the hydrodynamic interaction effect between the hulls

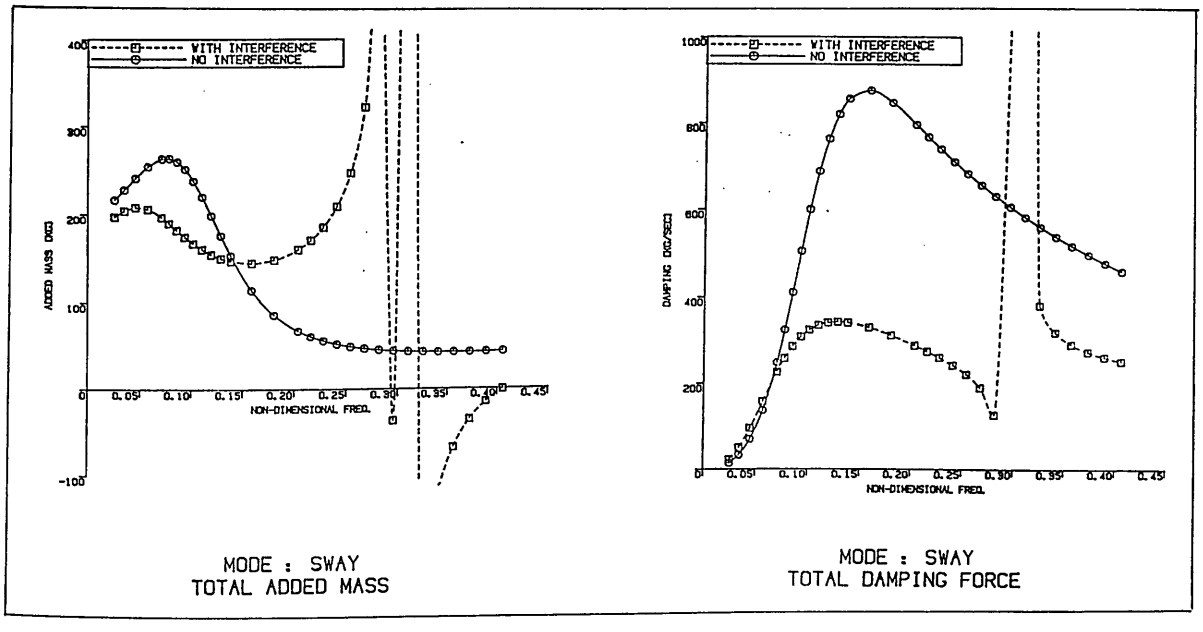

Fig. 107 - Comparison of the motion-induced coefficients of the model in the sway mode illustrating the hydrodynamic interaction effect between the hulls

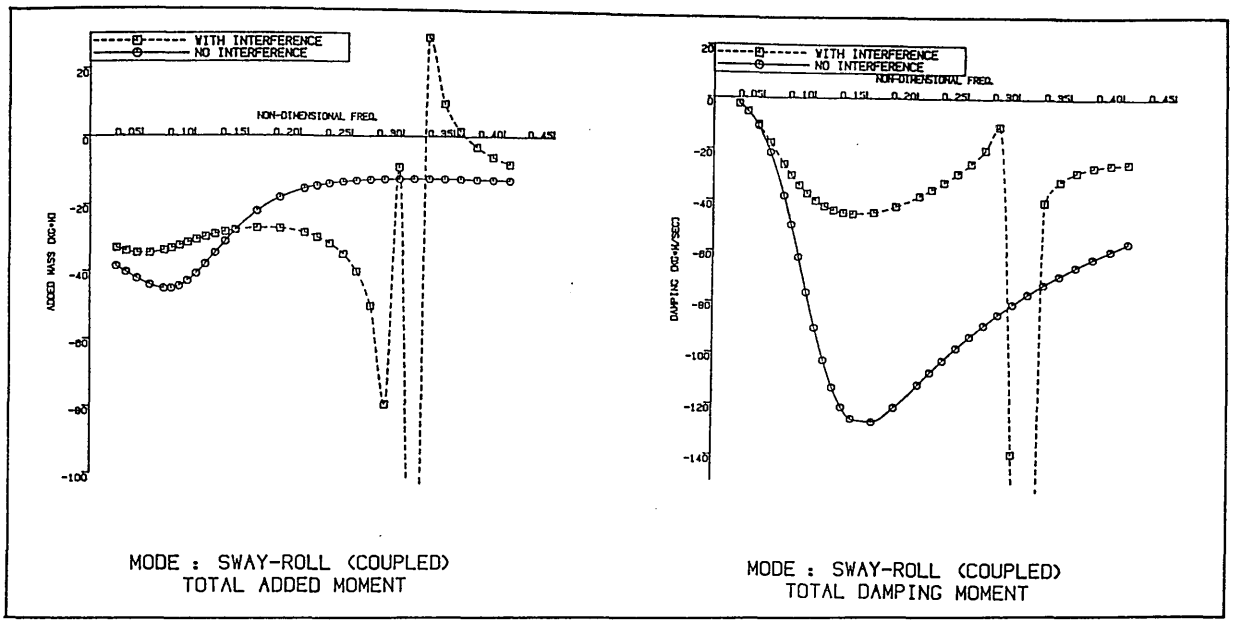

Fig. 108 - Comparison of the motion-induced coefficients of the model in the coupled sway-roll mode illustrating the hydrodynamic interaction effect between the hulls

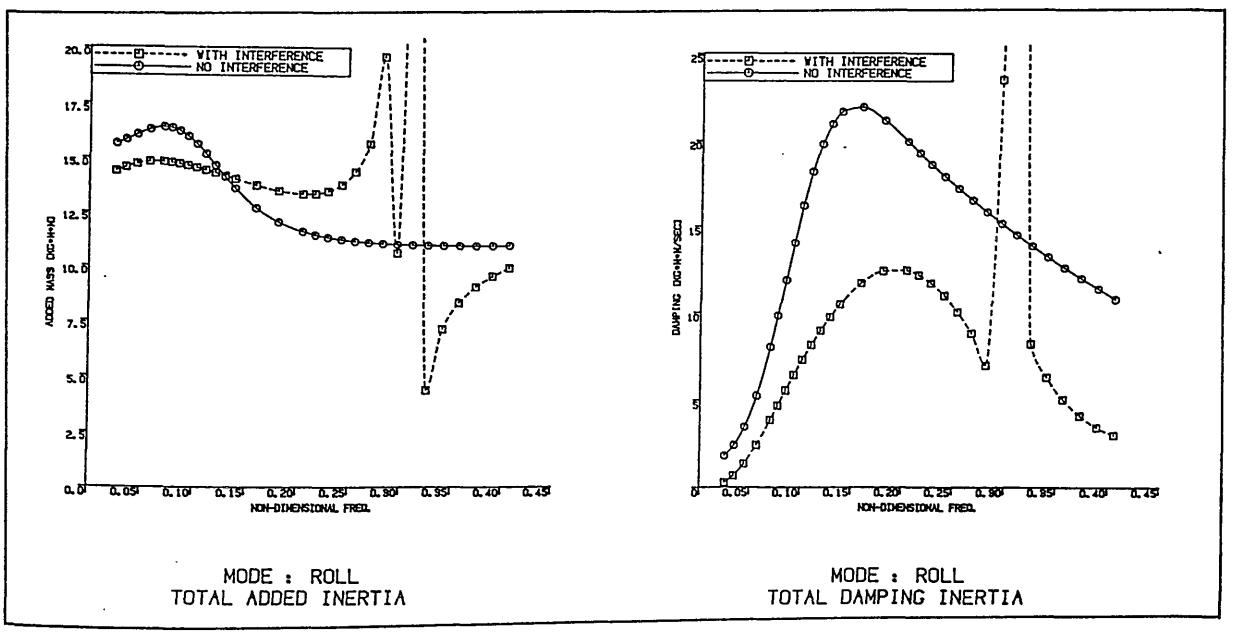

Fig. 109 - Comparison of the motion-induced coefficients of the model in the roll mode illustrating the hydrodynamic interaction effect between the hulls

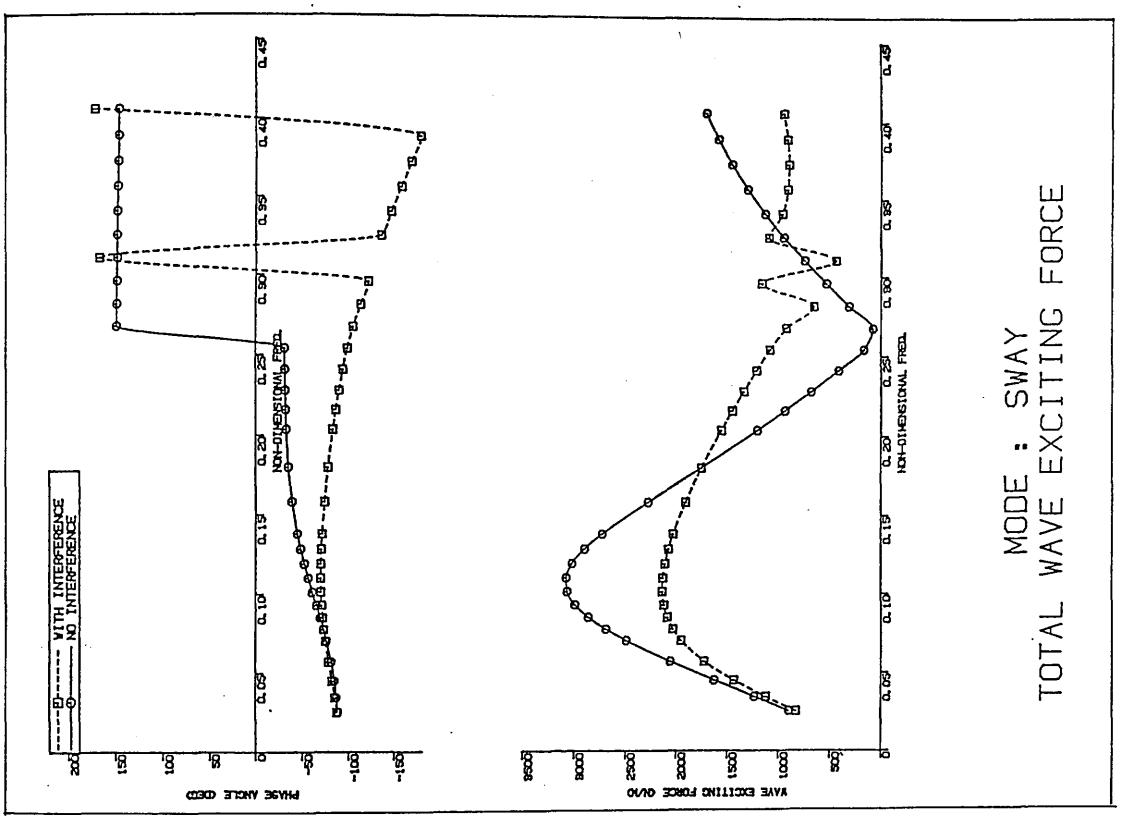

Fig. 111 - Comparison of the wave-induced forces of the model in the sway mode illustrating the hydrodynamic interaction between the hulls

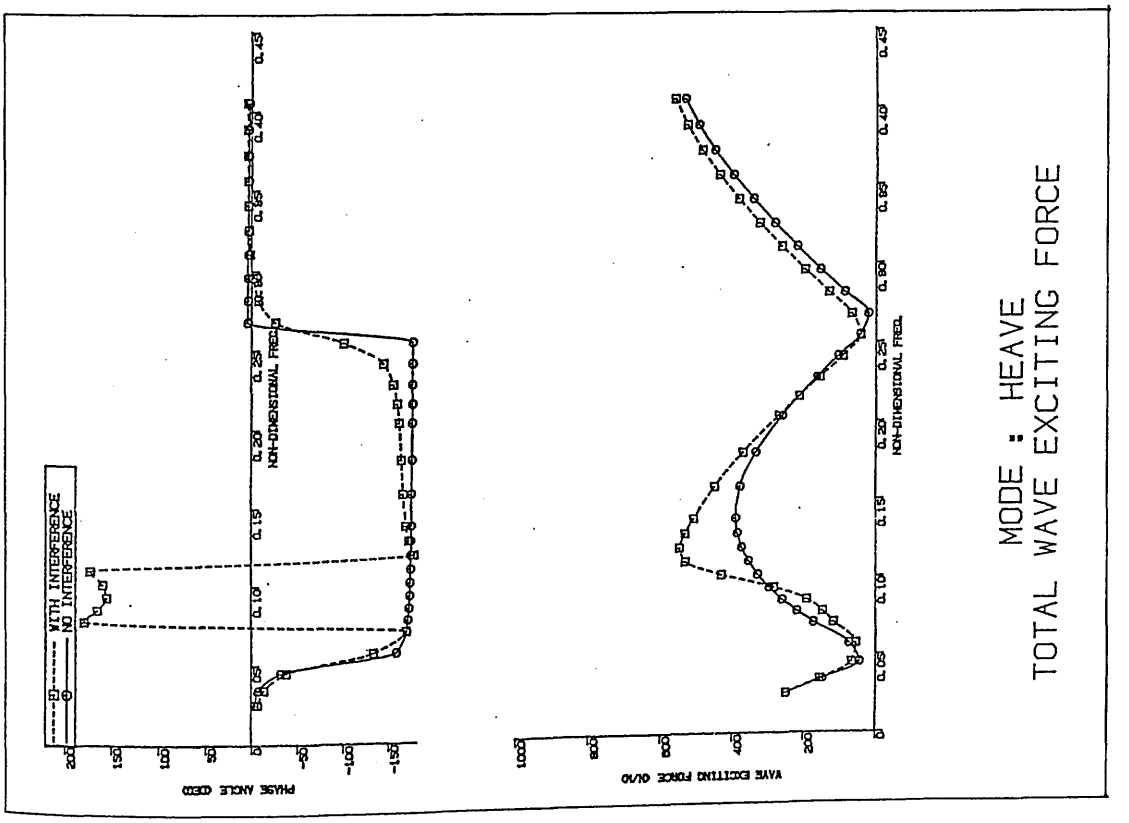

Fig. 110 - Comparison of the wave-induced forces on the model in the heave mode illustrating the hydrodynamic interaction effect between the hulls

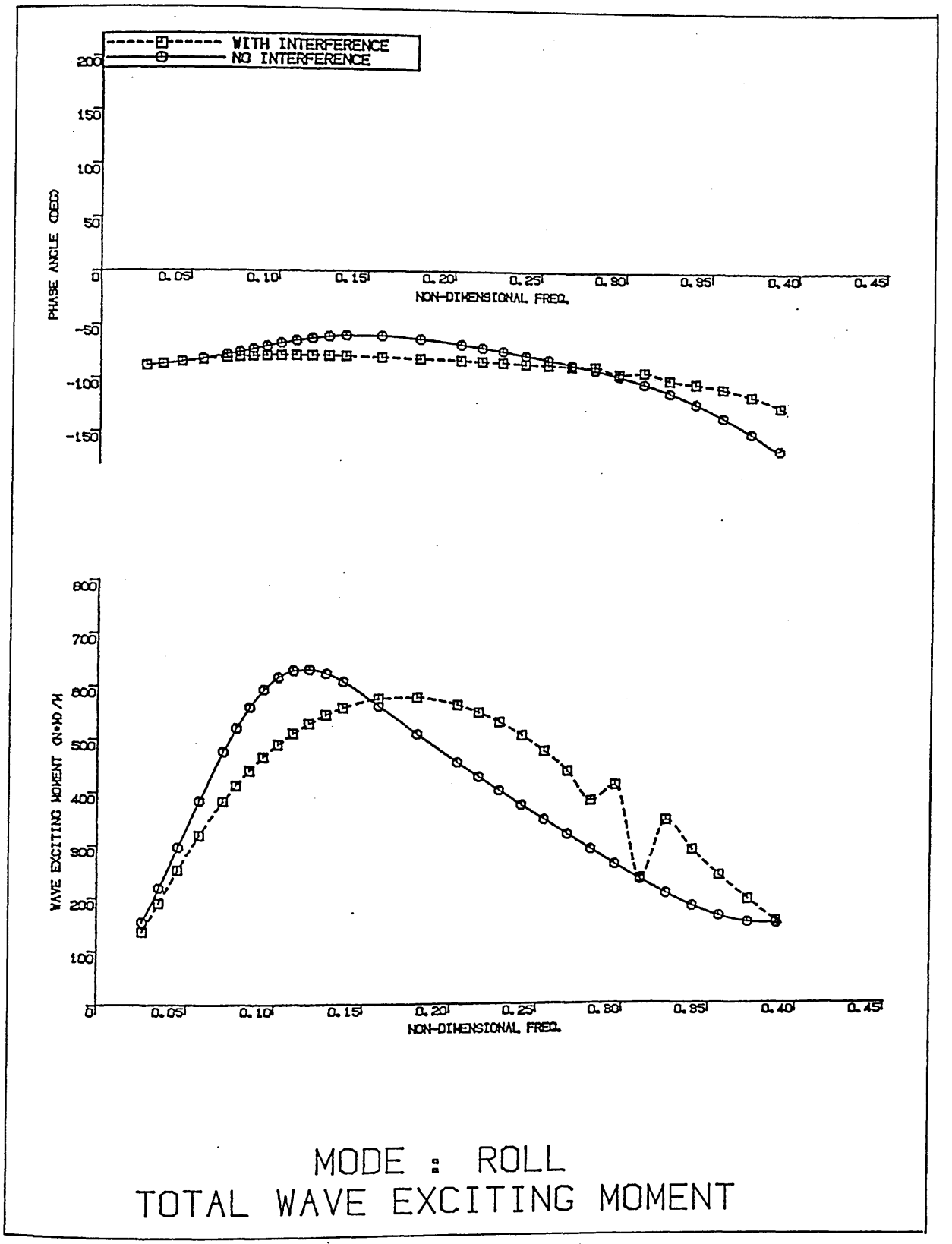

Fig. 112 - Comparison of the wave-induced moments of the model in the roll mode illustrating the hydrodynamic interaction effect between the hulls

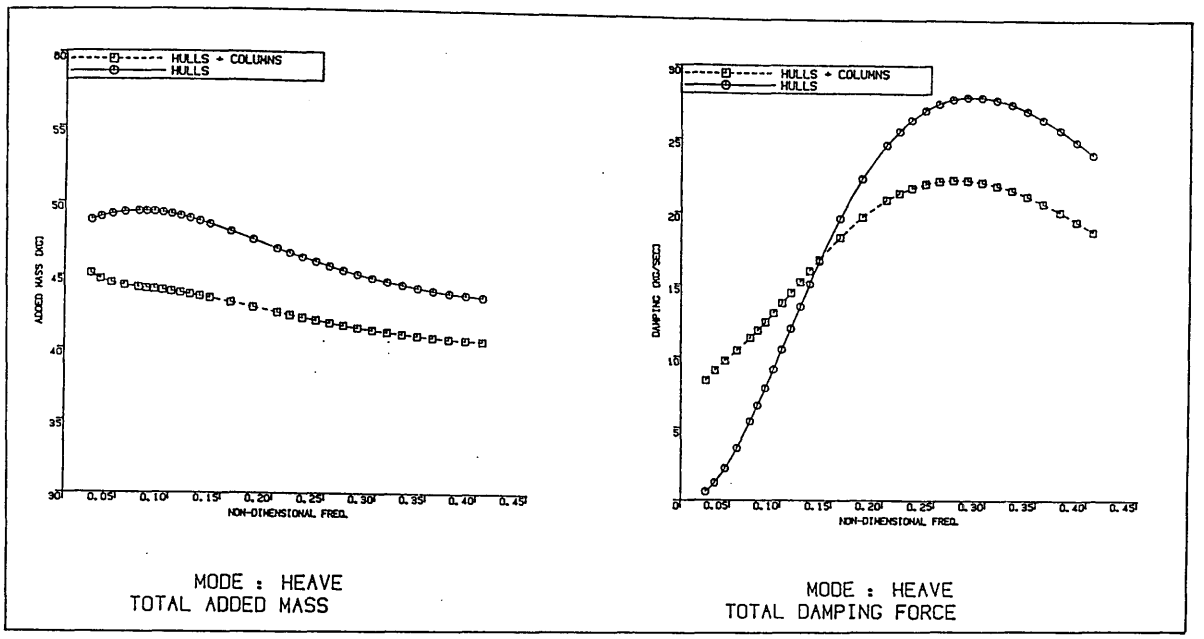

Fig. 113 - Effect of the surface-piercing columns on the motion-induced coefficients of the model in the heave mode

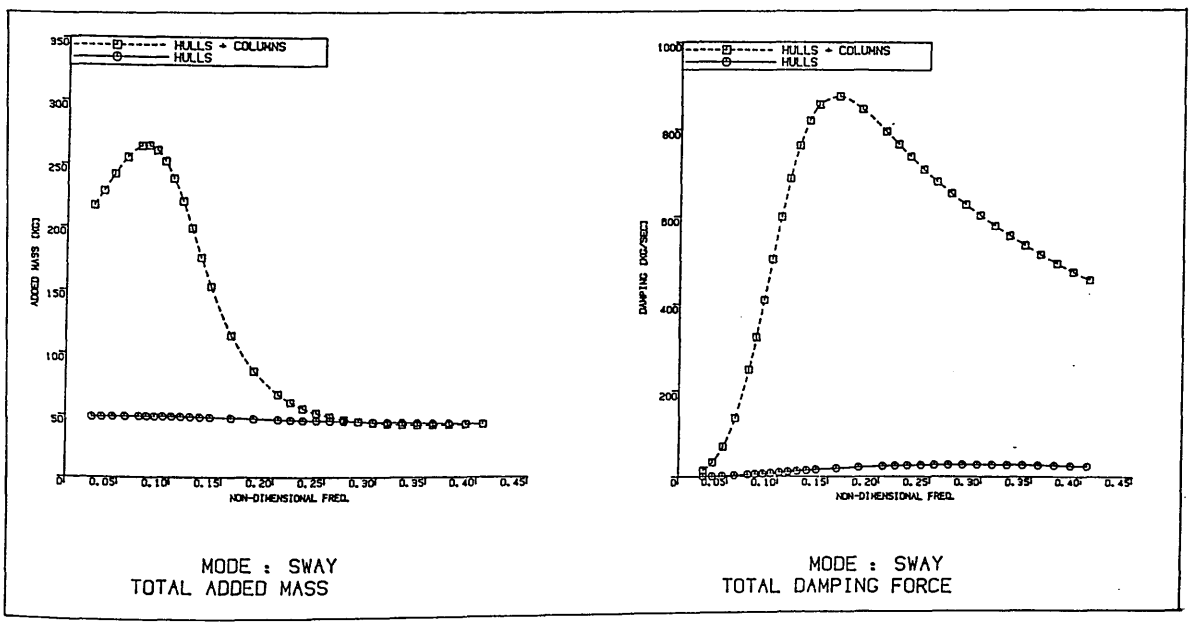

Fig. 114 - Effect of the surface-piercing columns on the motion-induced coefficients of the model in the sway mode

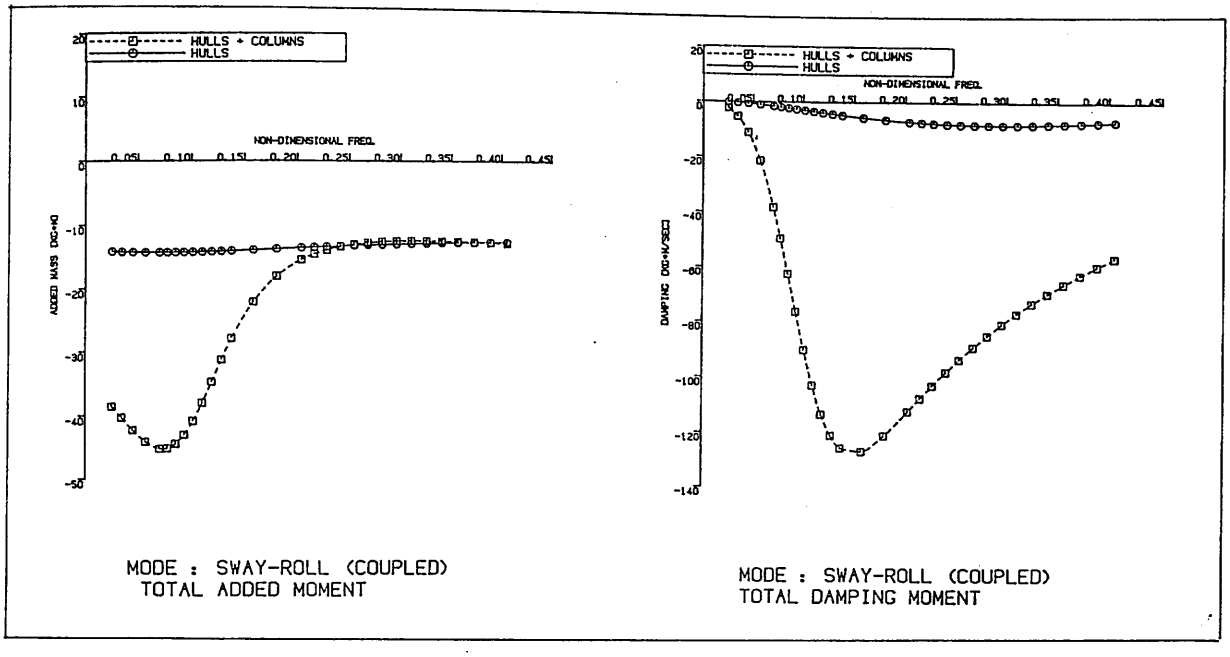

Fig. 115 - Effect of the surface-piercing columns on the motion-induced coefficients of the model for the coupled sway-roll mode

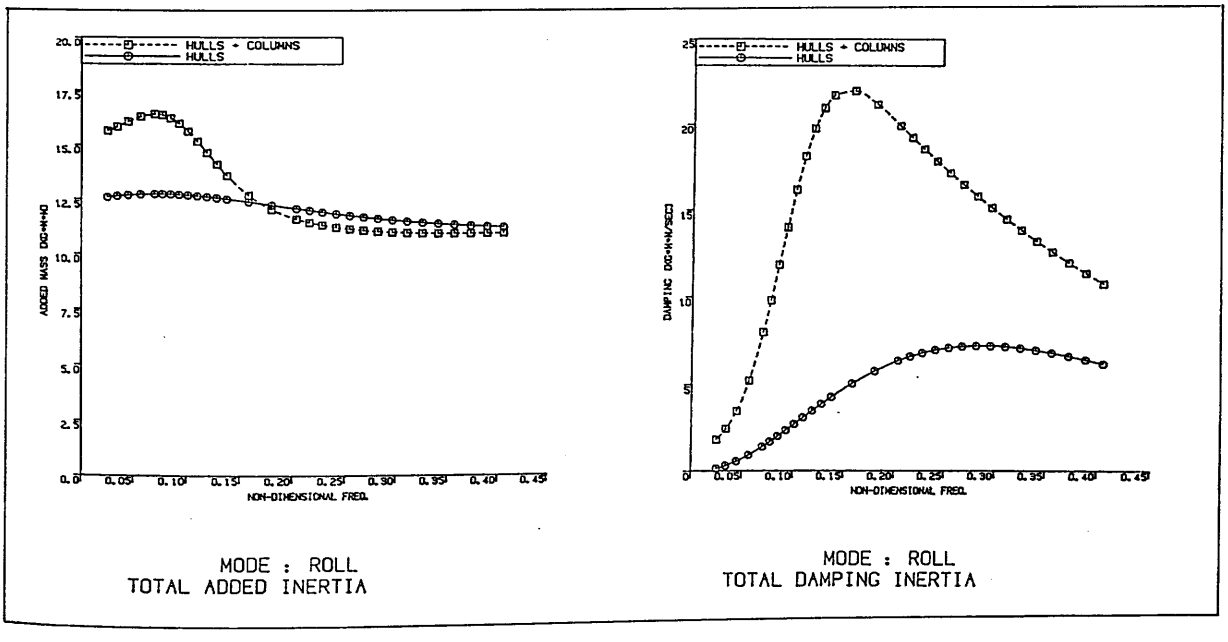

Fig. 116 - Effect of the surface-piercing columns on the motion-induced coefficients of the model in the roll mode

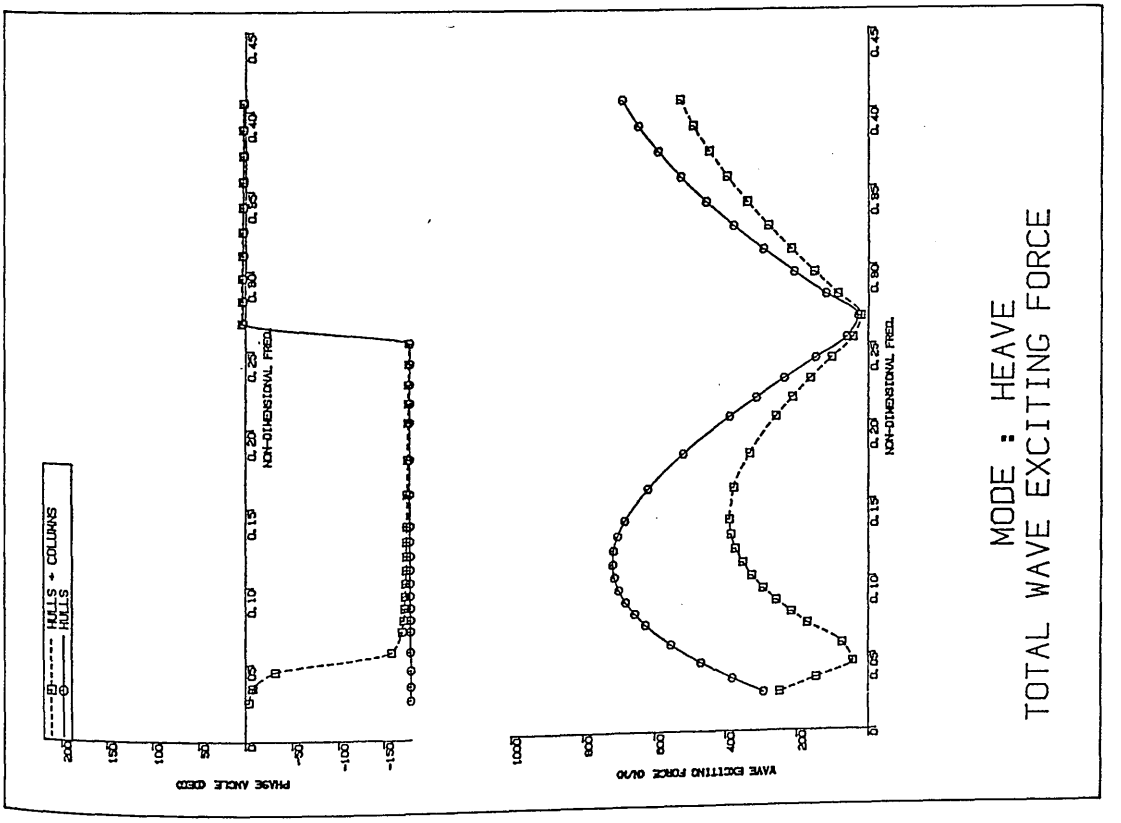

Fig. 117 - Effect of the surface-piercing columns on the wave-induced forces of the model in the heave mode

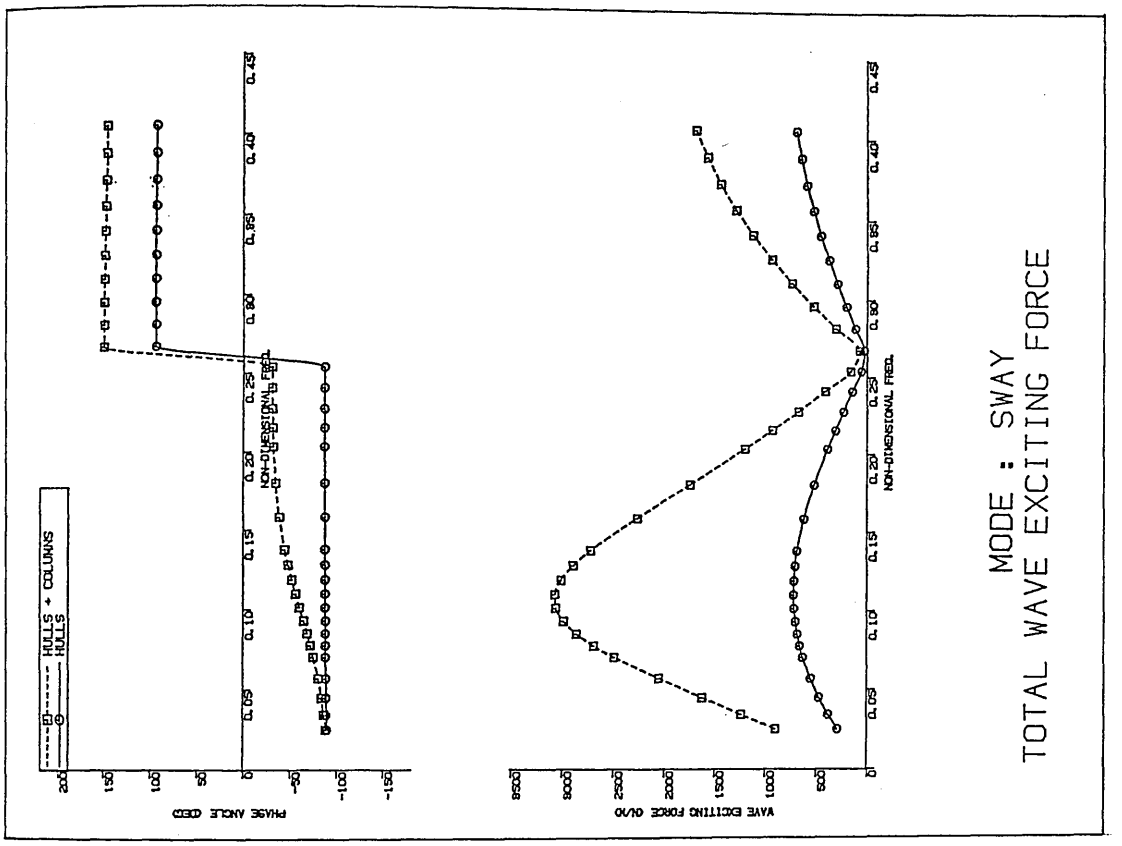

Fig. 118 - Effect of the surface-piercing columns on the wave-induced forces of the model in the sway mode

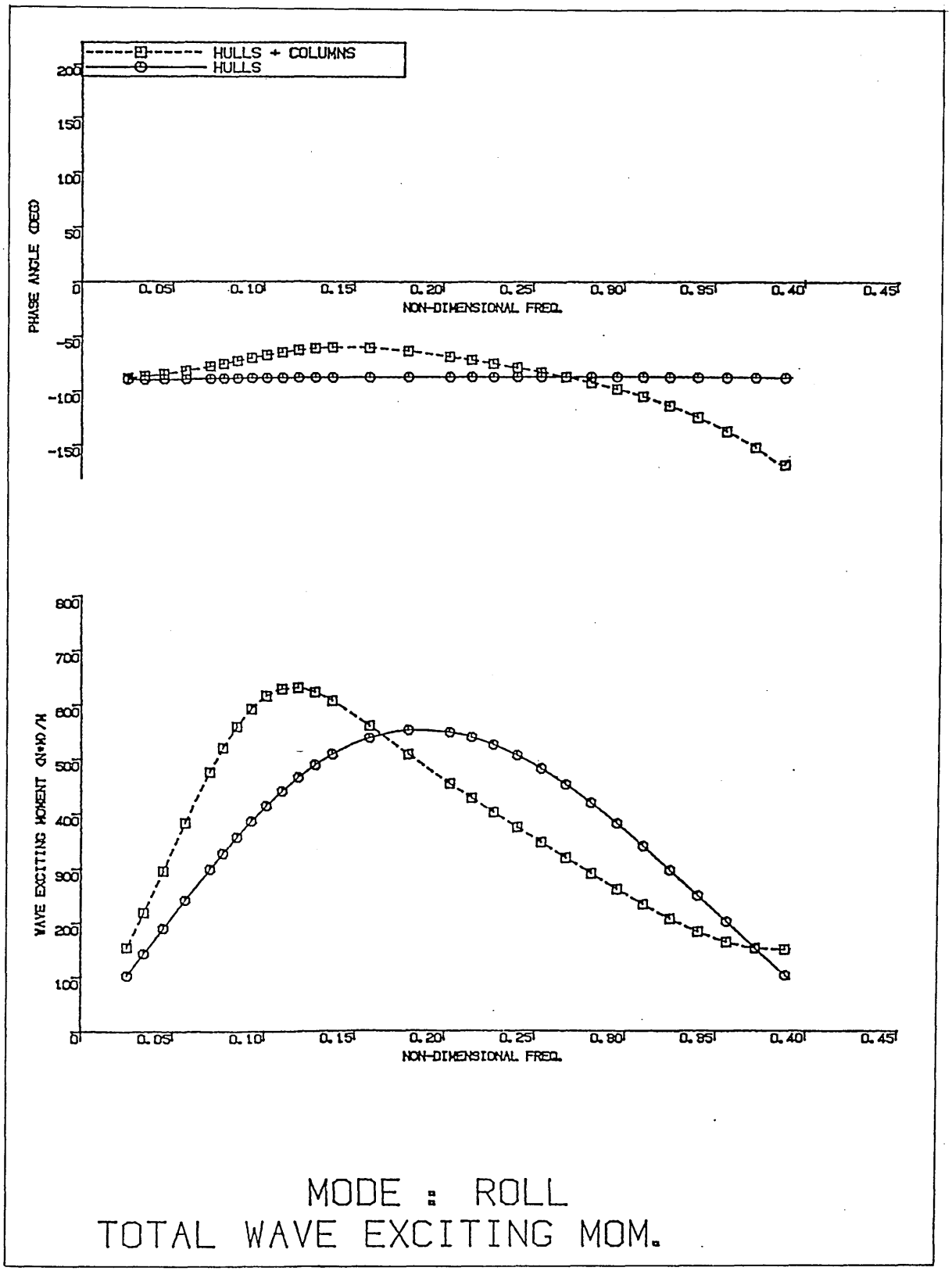

Fig. 119 - Effect of the surface-piercing columns on the wave-induced moment of the model in the roll mode

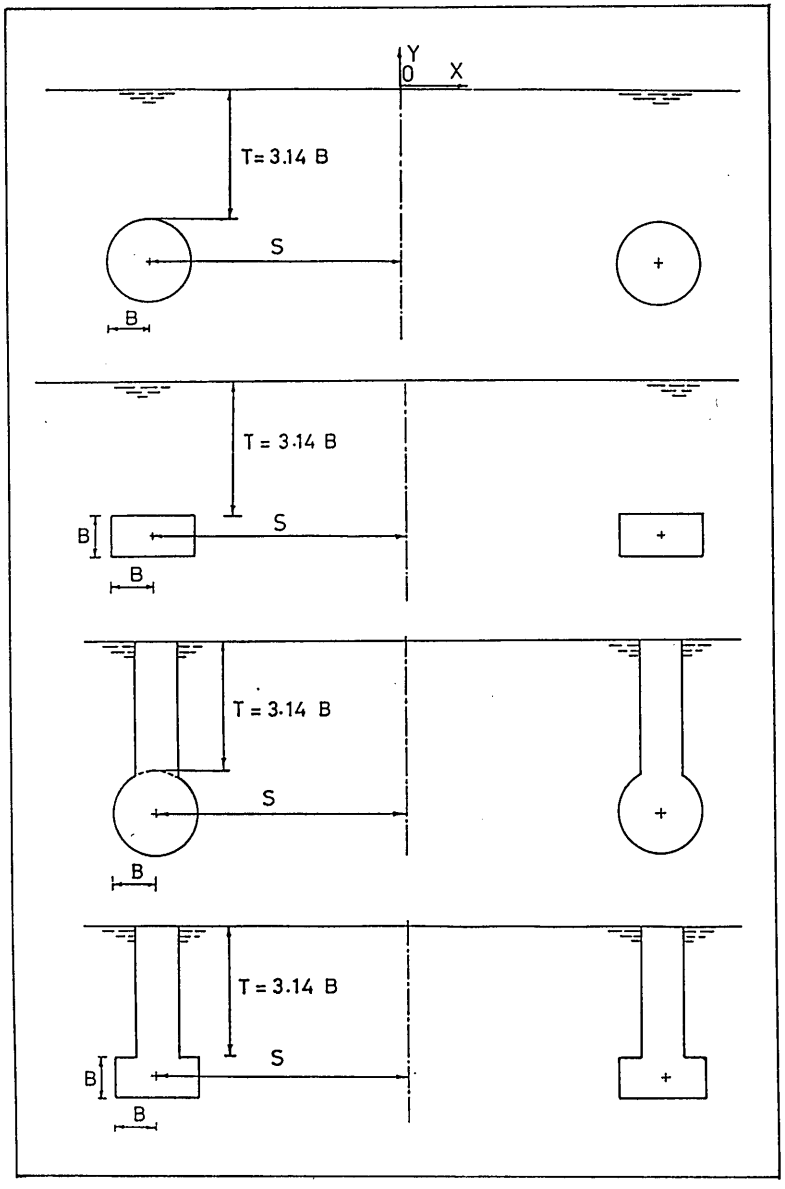

Fig. 120a - Definition of the cross-sections tested for the hydrodynamic interference investigation

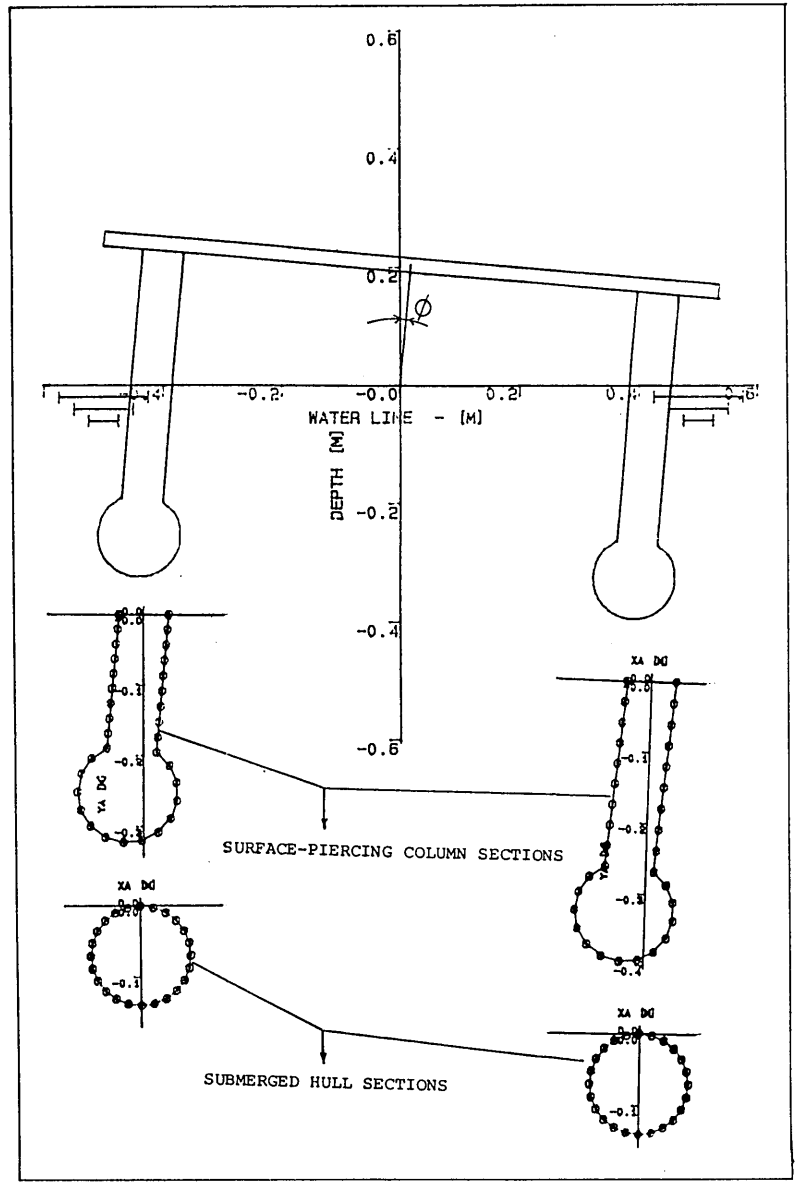

Fig. 120b - Typical segment distribution for the circular cross-sections in a tilted position

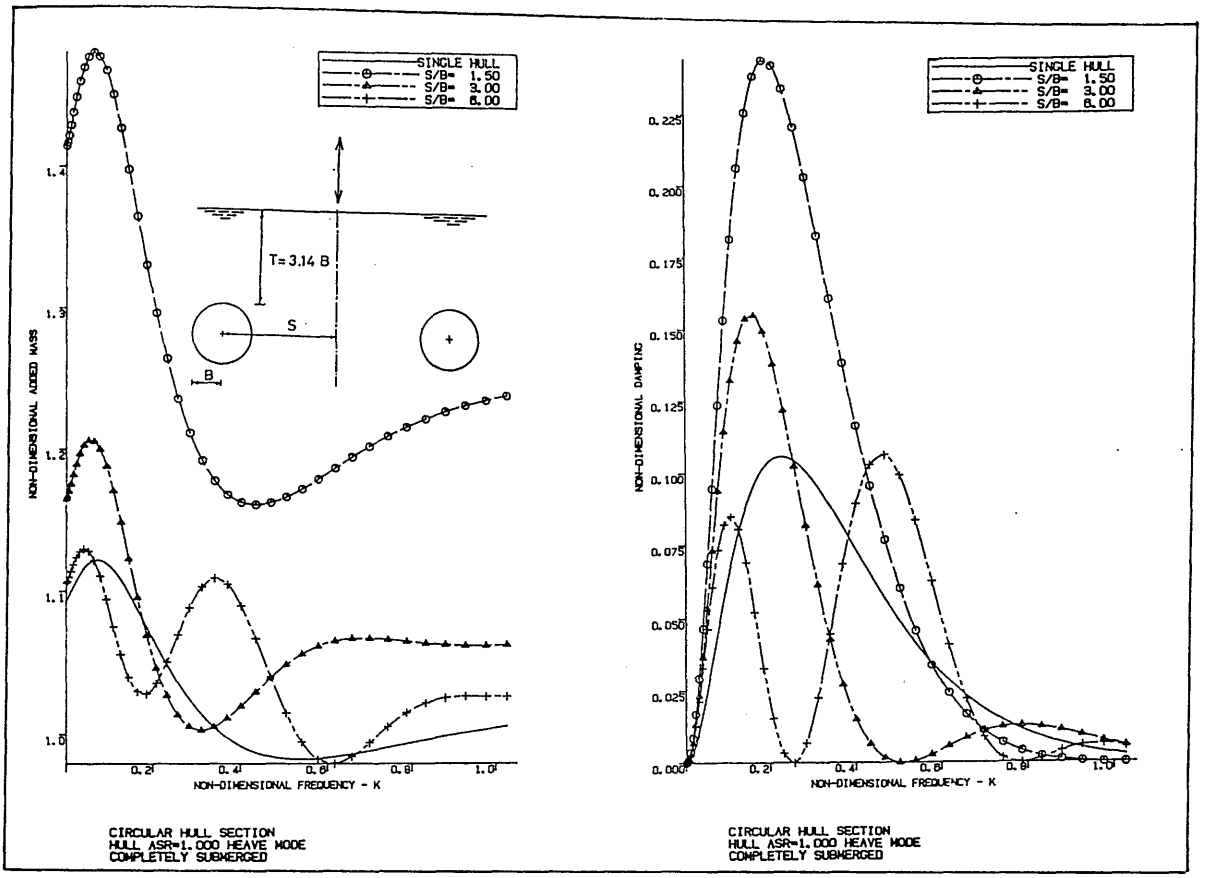

Fig. 121a - Effect of hull separation on the motion-induced coefficients of a submerged circular section in the heave mode

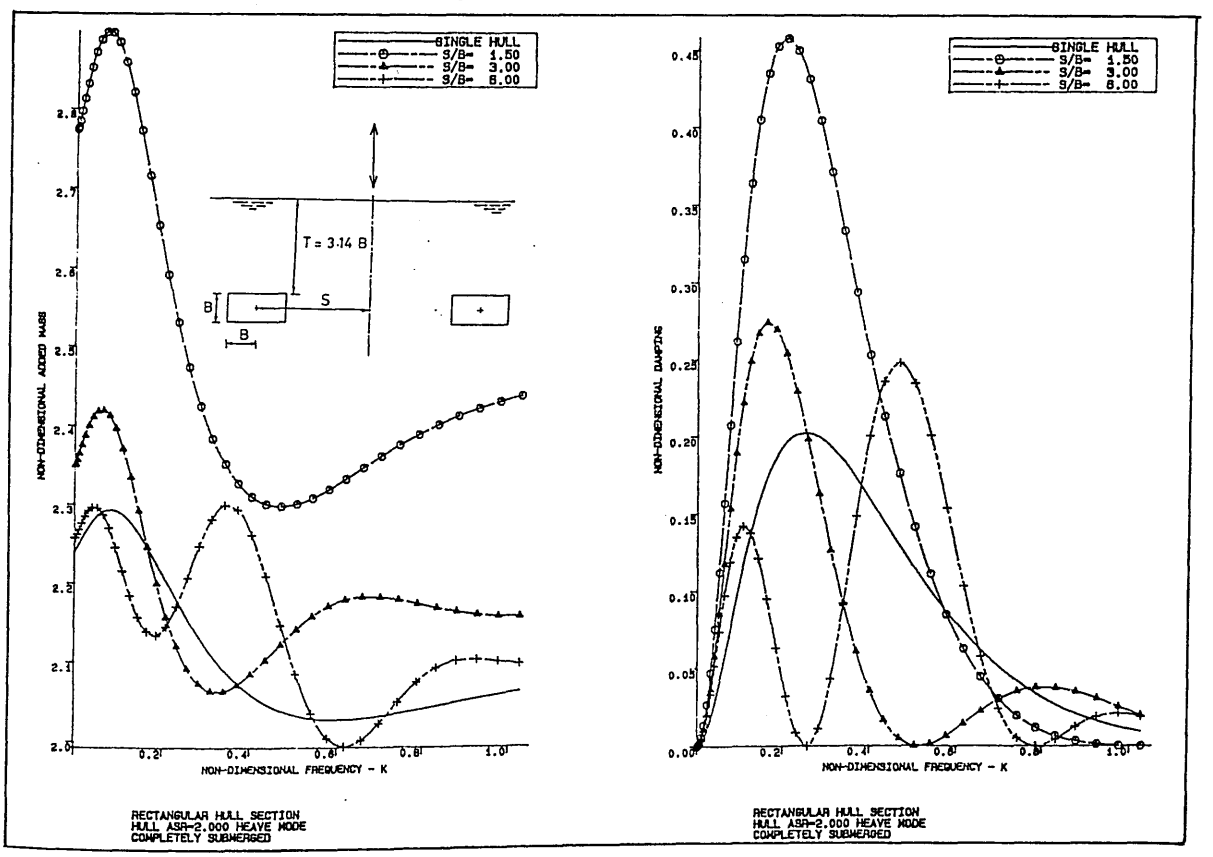

Fig. 121b - Effect of hull separation on the motion-induced coefficients of a submerged rectangular section in the heave mode

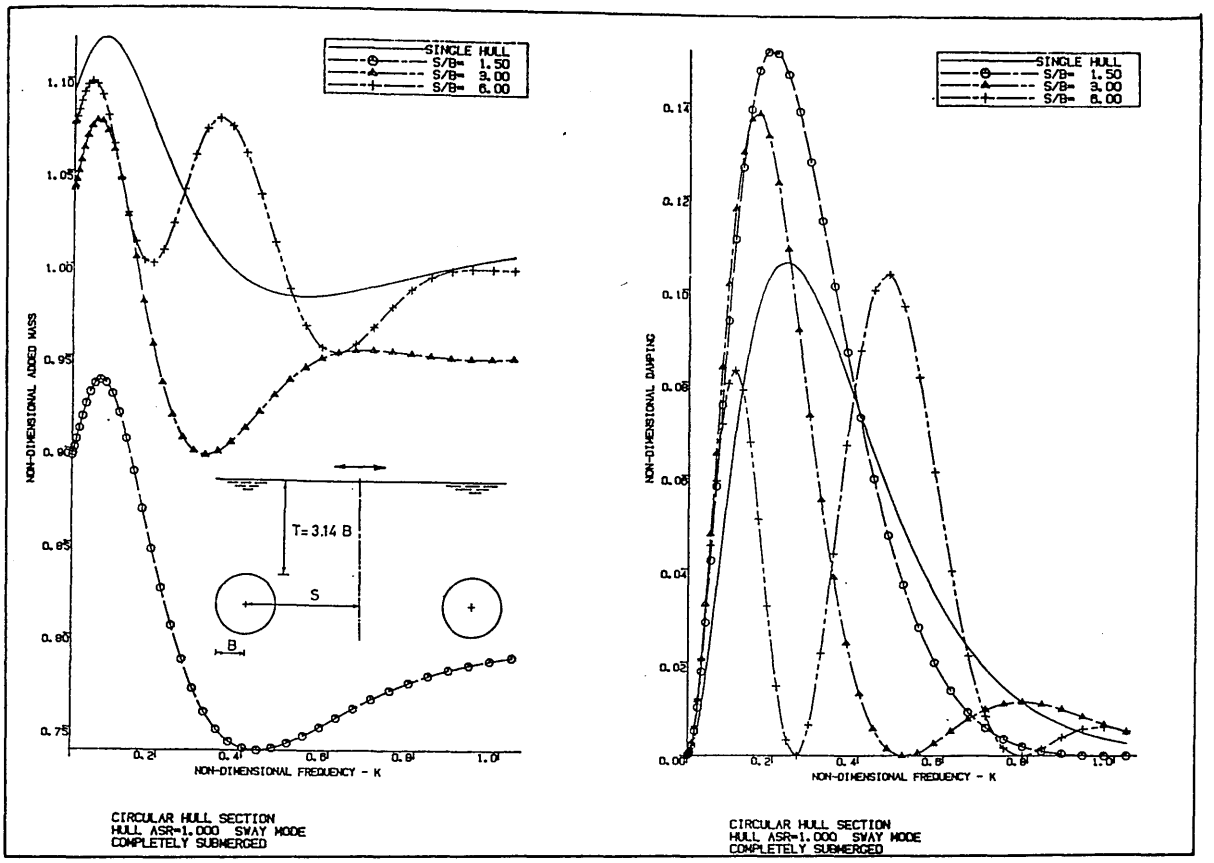

Fig. 122a - Effect of hull separation on the motion-induced coefficients of a submerged circular hull section in the sway mode

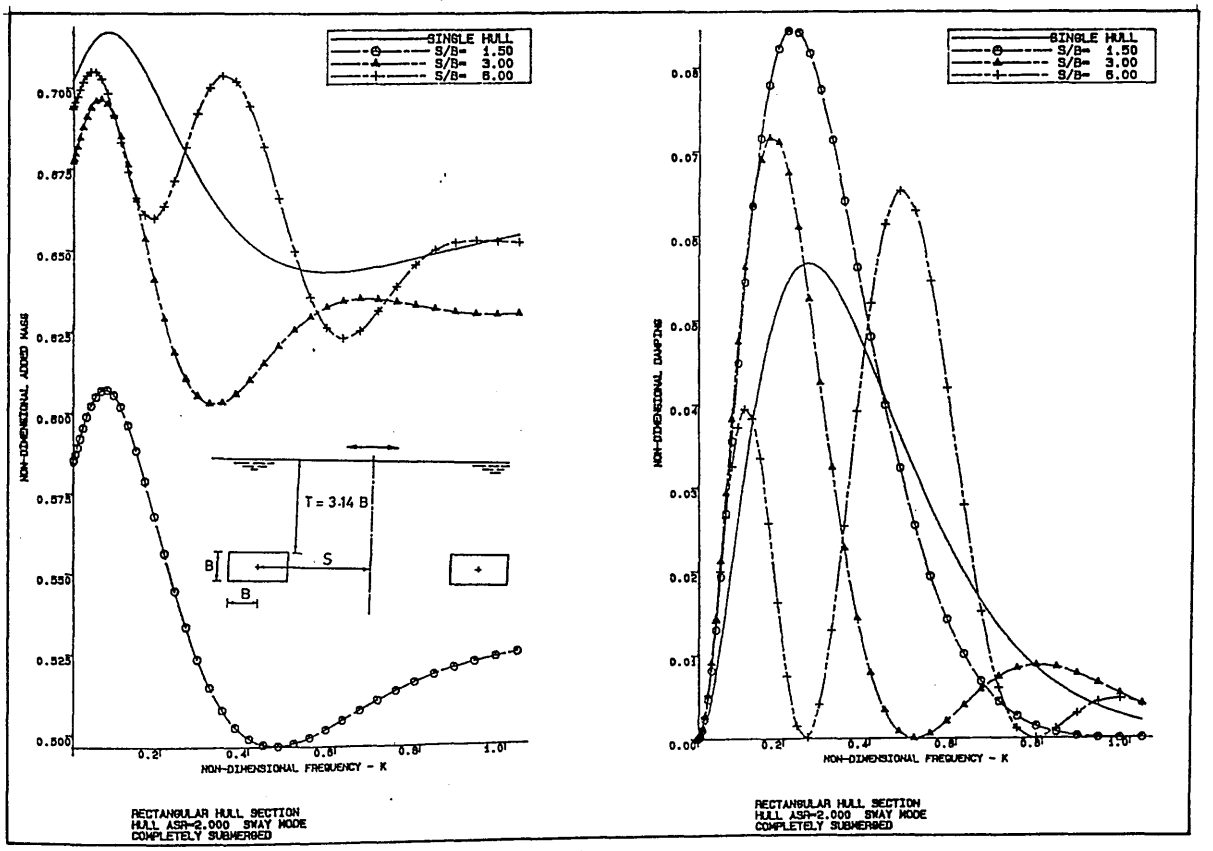

Fig. 122b - Effect of hull separation on the motion-induced coefficients of a submerged rectangular hull section in the sway mode

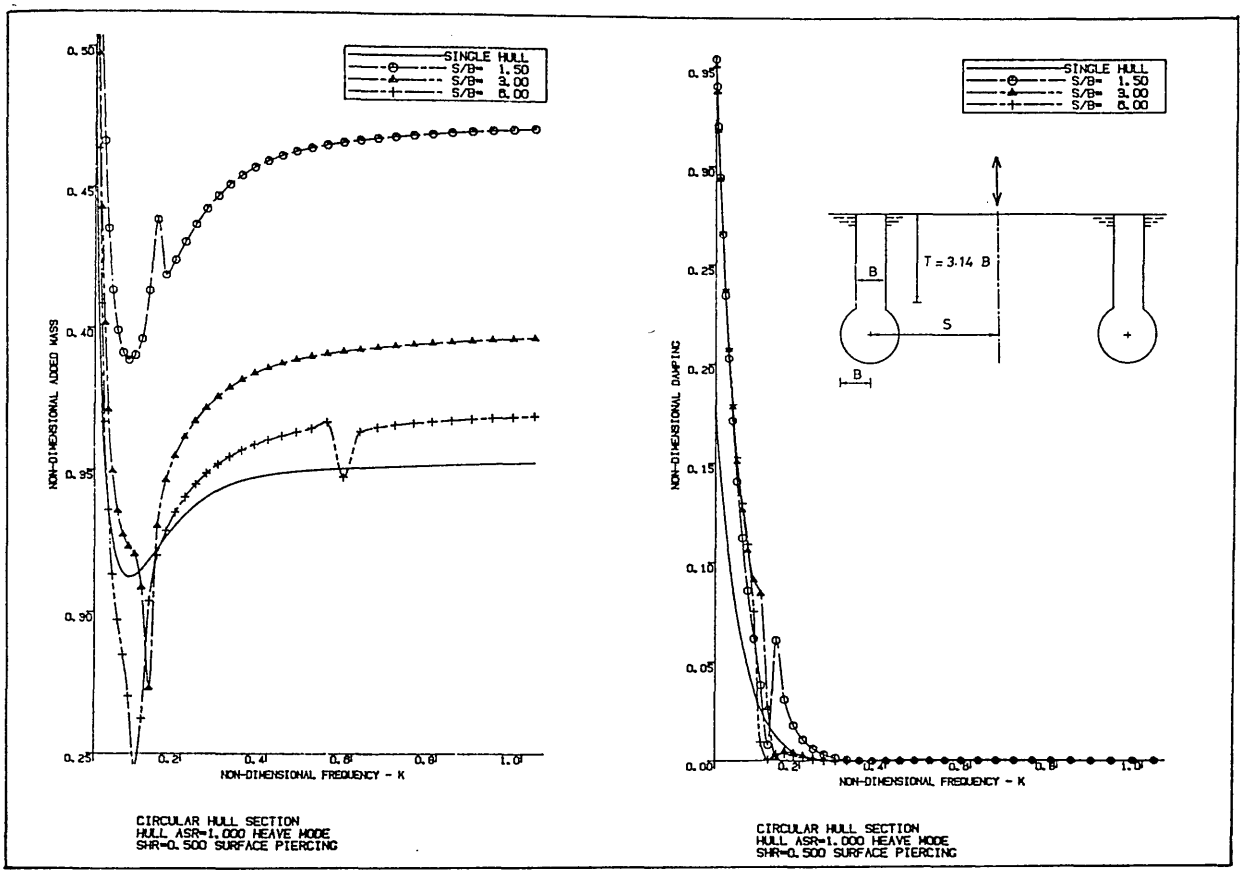

Fig. 123a - Effect of hull separation on the motion-induced coefficients of a surface-piercing circular column section in the heave mode

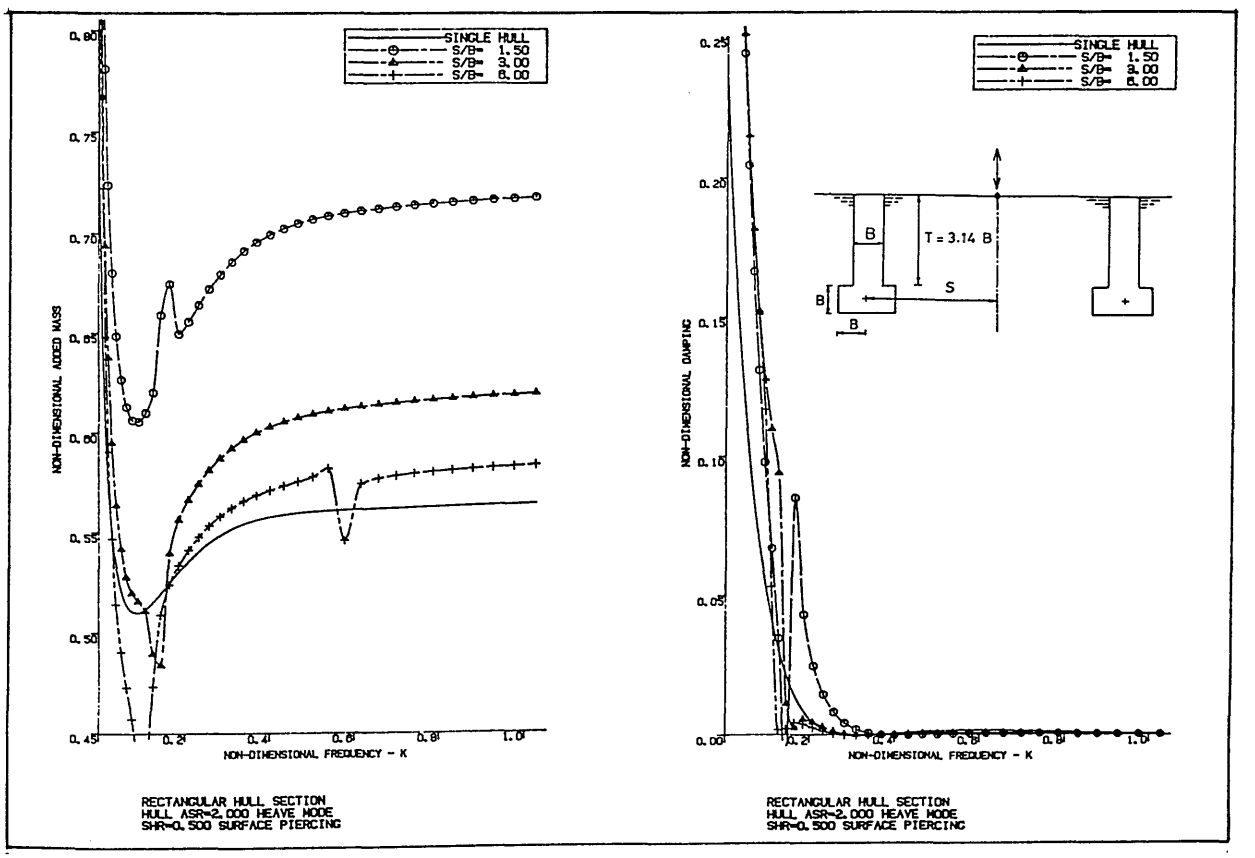

Fig. 123b - Effect of hull separation on the motion-induced coefficients of a surface-piercing rectangular column section in the heave mode

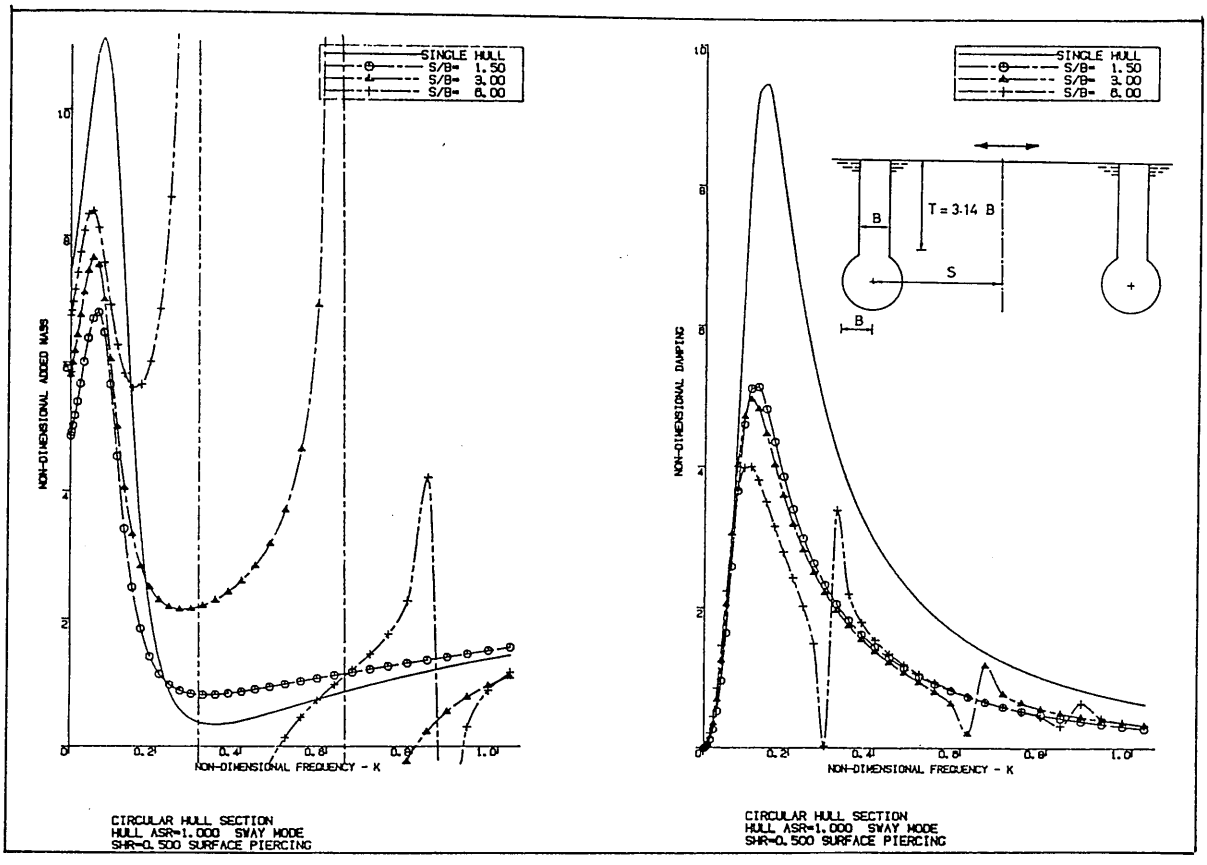

Fig. 124a - Effect of hull separation on the motion-induced coefficients of a surface-piercing circular column section in the sway mode

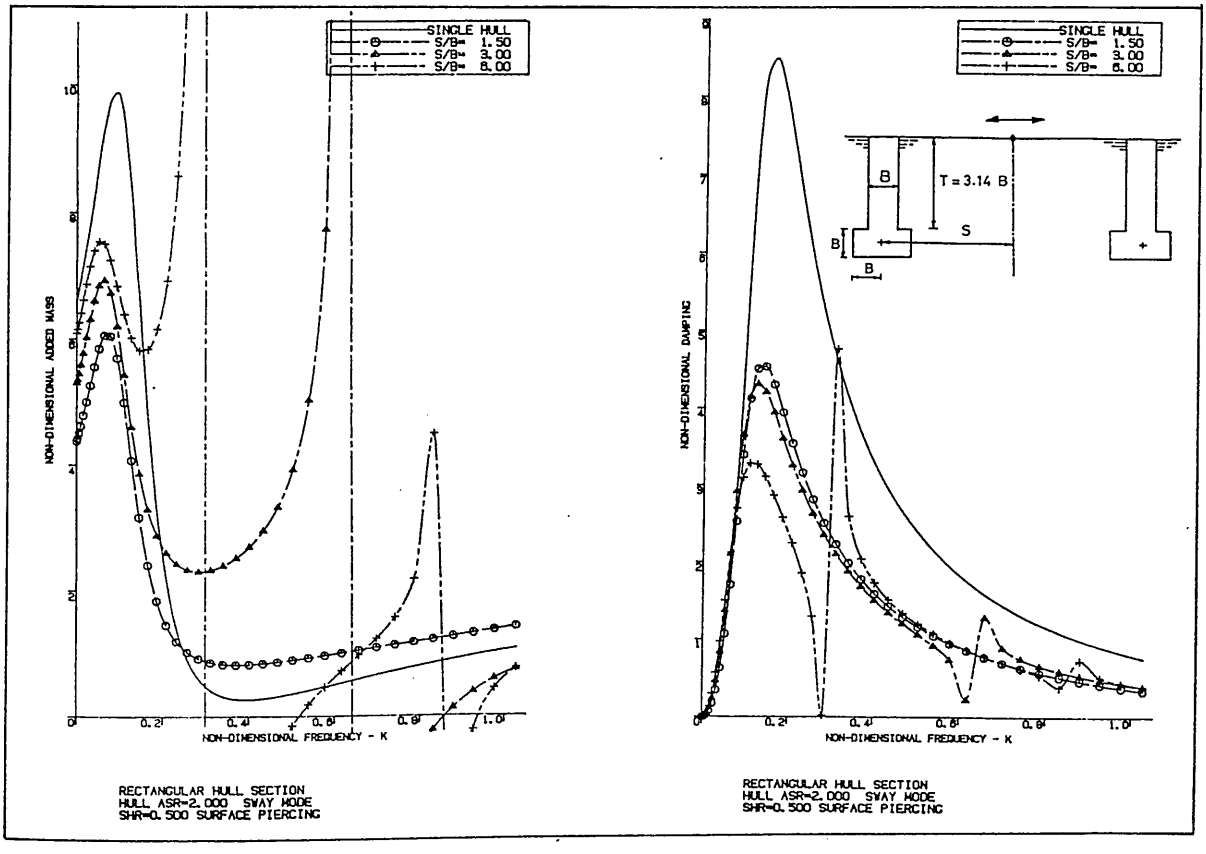

Fig. 124b - Effect of hull separation on the motion-induced coefficients of a surface-piercing rectangular column section in the sway mode

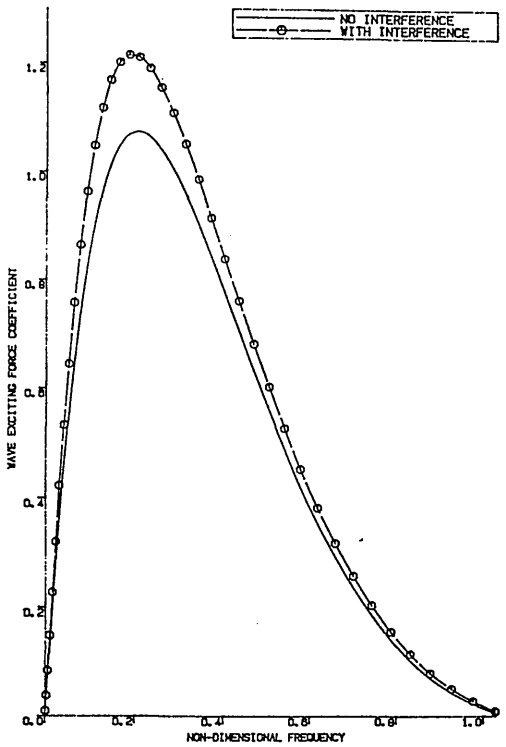

HEAVE - W. EXCITING FORCE
TWIN CS. [S/B = 1.5]

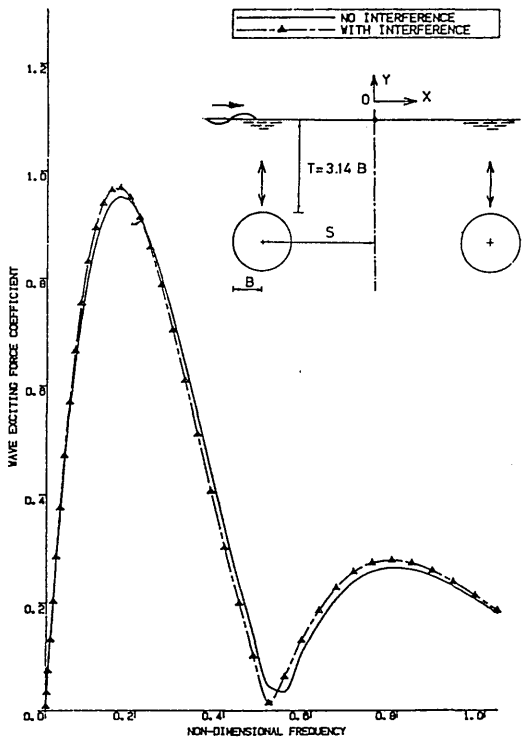

HEAVE - W. EXCITING FORCE
TWIN CS. [S/B = 3.0]

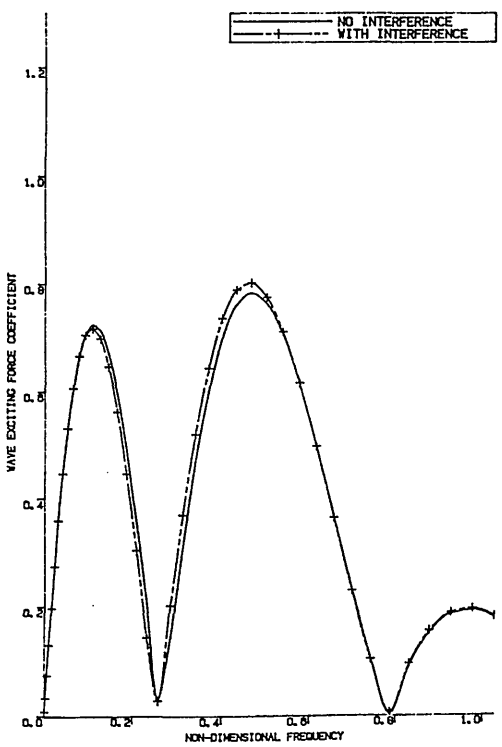

HEAVE - W. EXCITING FORCE
TWIN CS. [S/B = 6.0]

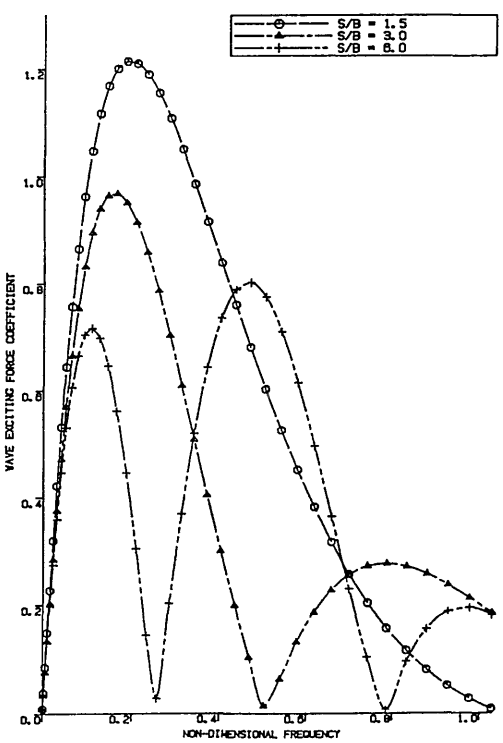

HEAVE - W. EXCITING FORCE
TWIN CIRCULAR SUBMERGED HULL

Fig. 125 - Effect of hull separation on the wave-induced coefficients of a submerged circular hull section in the heave mode

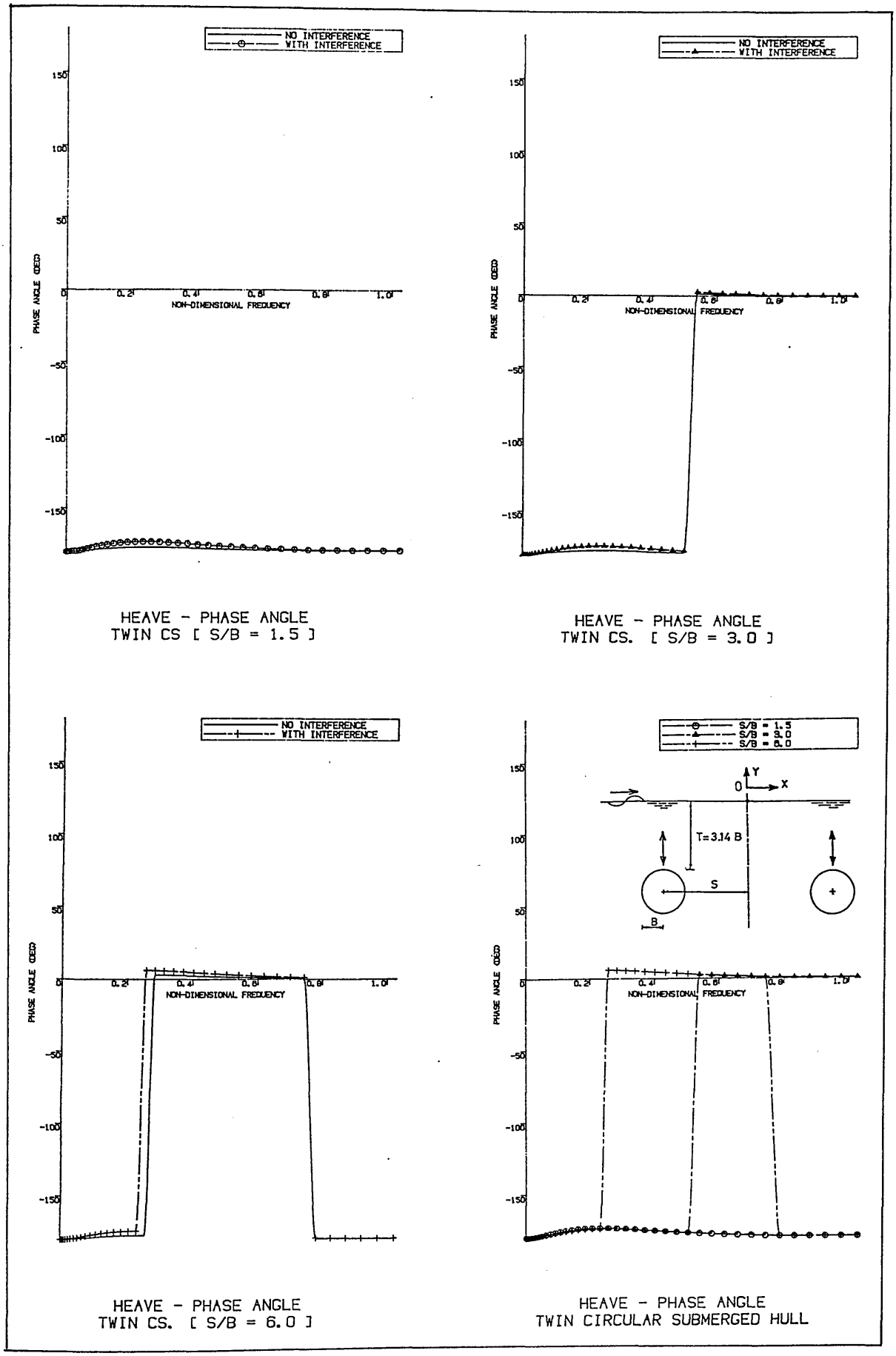

Fig. 126 - Effect of hull separation on the phase angles of the wave-induced force coefficients of a submerged circular hull section in the heave mode

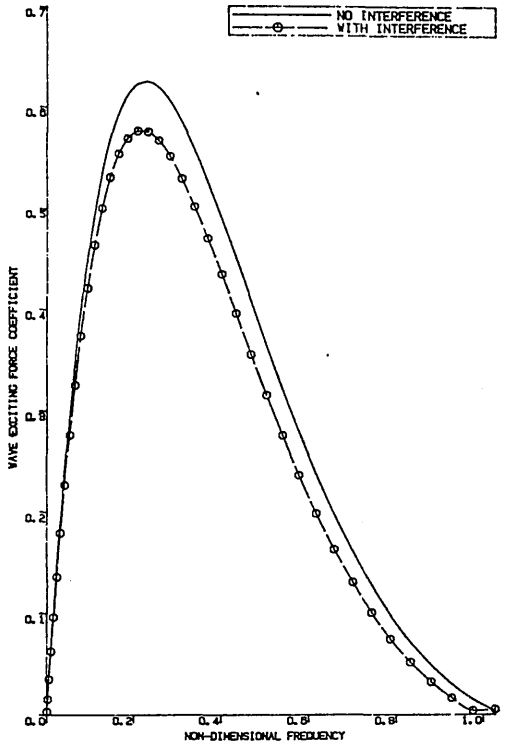

SWAY - W. EXCITING FORCE
TWIN RS. [S/B = 1.5]

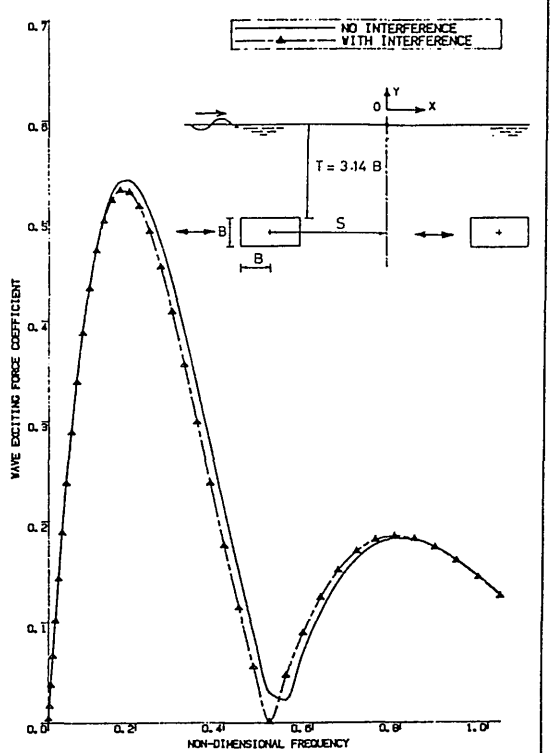

SWAY - W. EXCITING FORCE
TWIN RS. [S/B = 3.0]

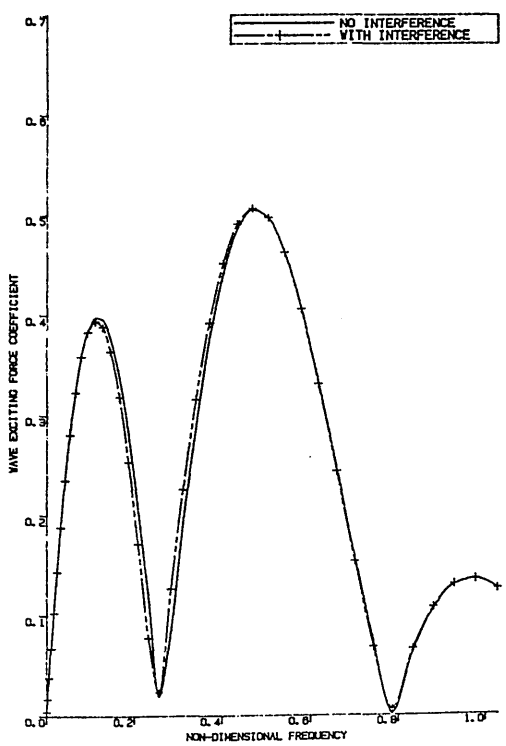

SWAY - W. EXCITING FORCE
TWIN RS. [S/B = 6.0]

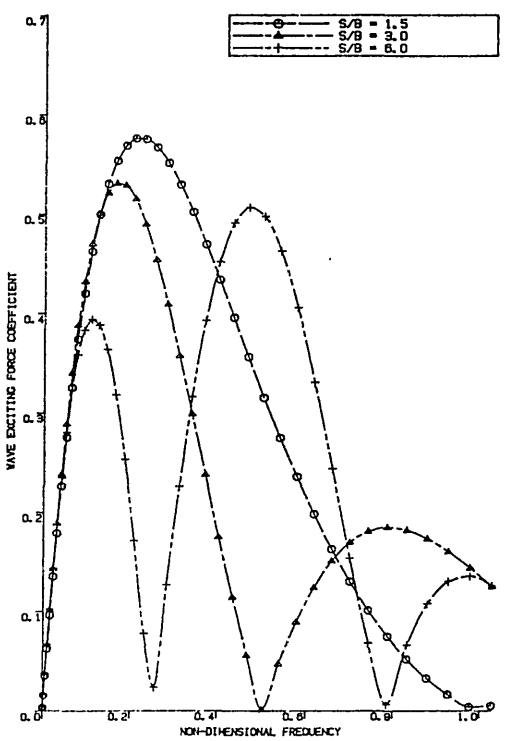

SWAY - W. EXCITING FORCE
TWIN RECTAN. SUBMERGED HULL

Fig. 127 - Effect of hull separation on the wave-induced force coefficient of a submerged rectangular hull section in the sway mode

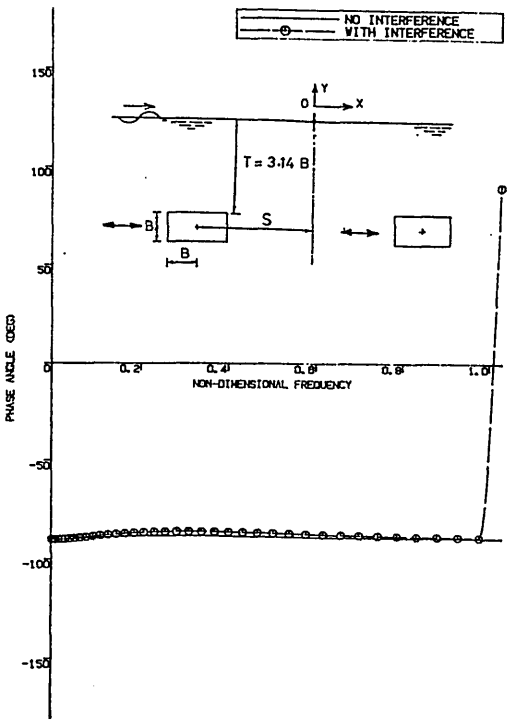

SWAY - PHASE ANGLE
TWIN RS. [S/B = 1.5]

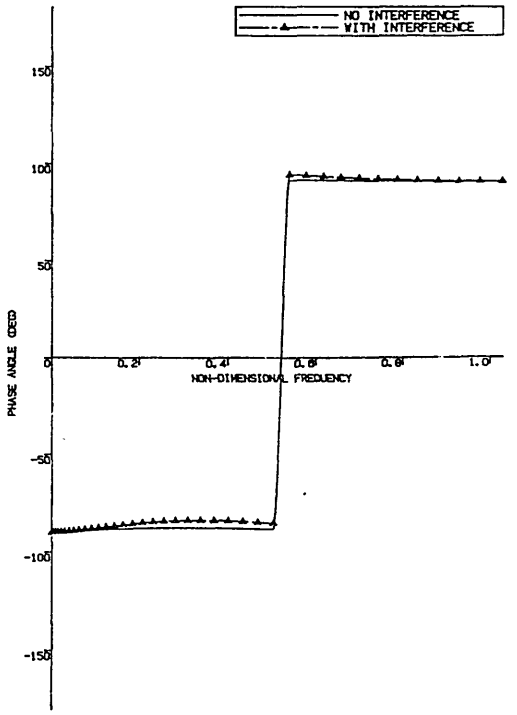

SWAY - PHASE ANGLE
TWIN RS. [S/B = 3.0]

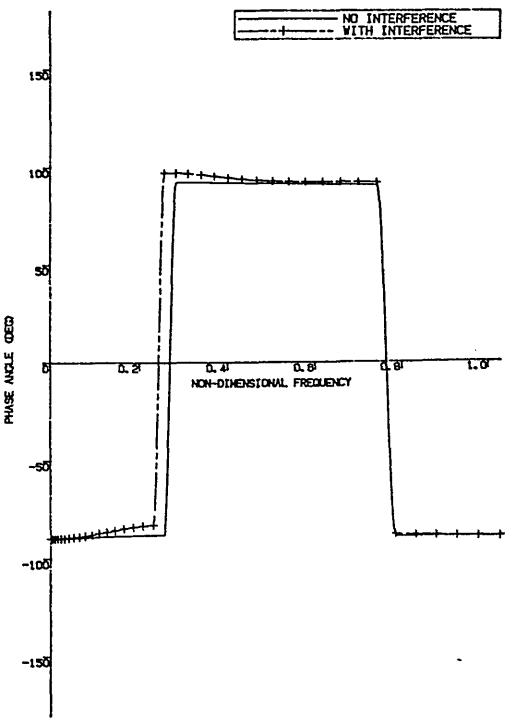

SWAY - PHASE ANGLE
TWIN RS. [S/B = 6.0]

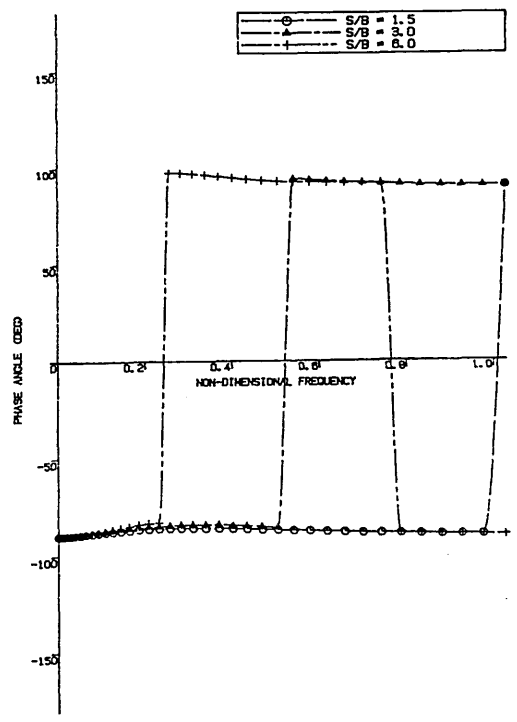

SWAY - PHASE ANGLE
TWIN RECTAN. SUBMERGED HULL

Fig. 128 - Effect of hull separation on the phase angle of the wave-induced force coefficients of a submerged circular hull section in the sway mode

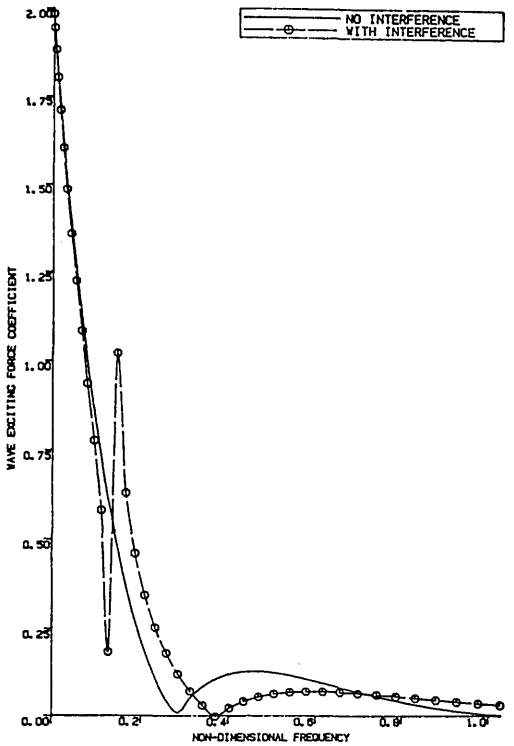

HEAVE - W. EXCITING FORCE
TWIN CF. [S/B = 1.5]

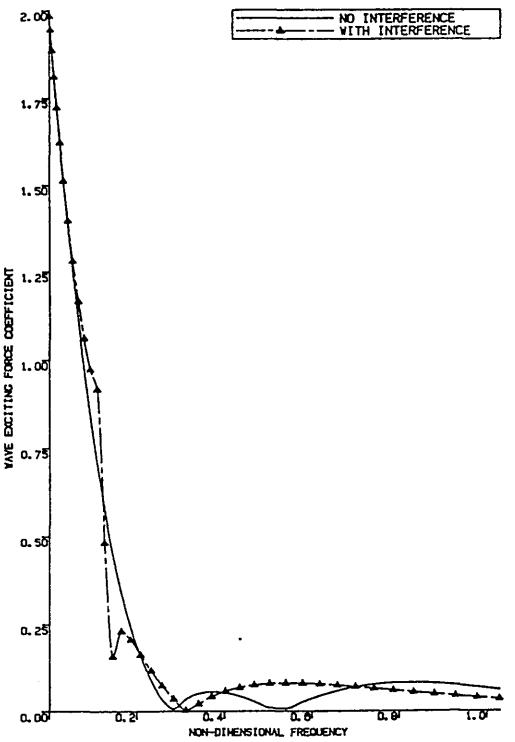

HEAVE - W. EXCITING FORCE
TWIN CF. [S/B = 3.0]

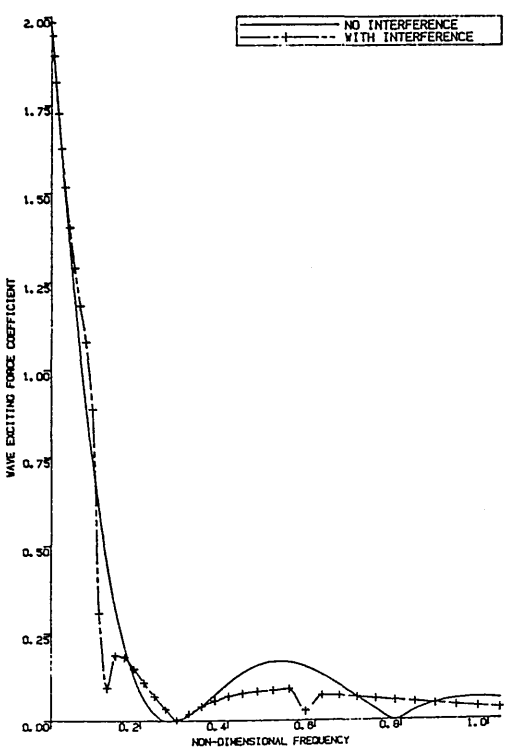

HEAVE - W. EXCITING FORCE
TWIN CF. [S/B = 6.0]

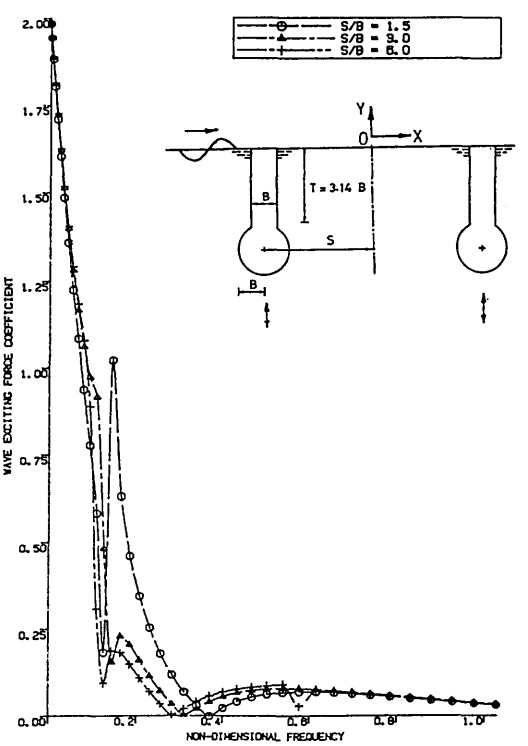

HEAVE - W. EXCITING FORCE
TWIN CIRCULAR FLOATING HULL

Fig. 129 - Effect of hull separation on the wave-induced force coefficients of a surface-piercing circular column-section in the heave mode

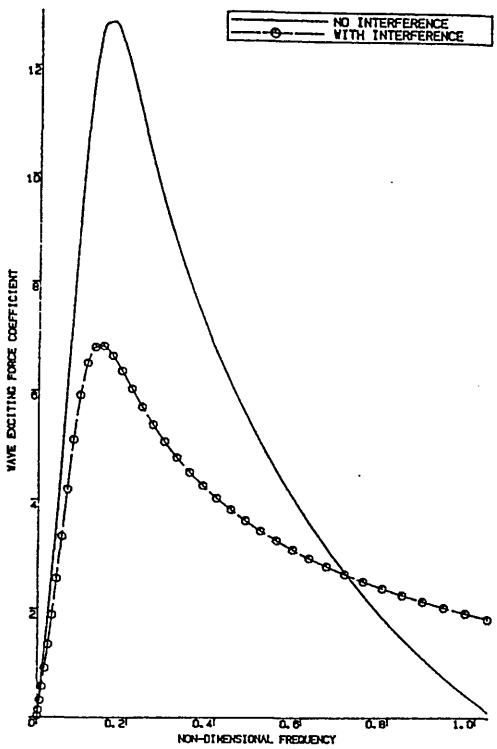

SWAY - W. EXCITING FORCE
TWIN RF. [S/B =1.5]

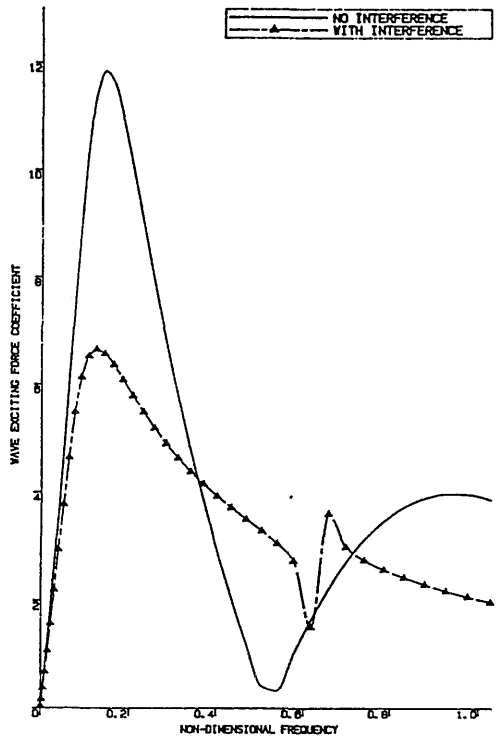

SWAY - W. EXCITING FORCE
TWIN RF. [S/B = 3.0]

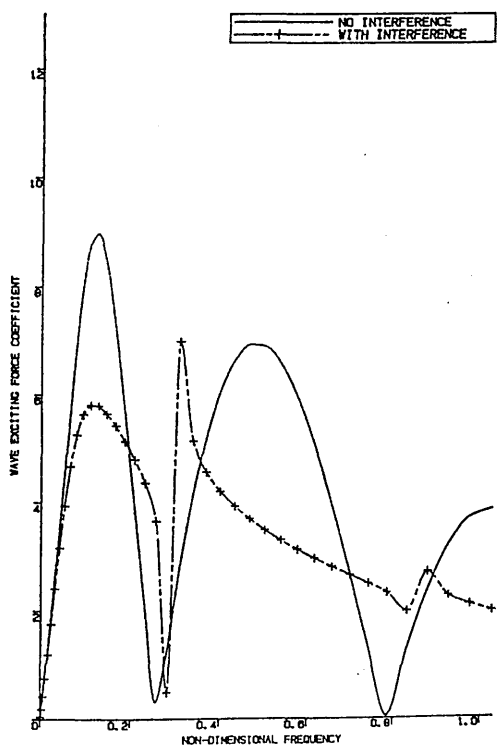

SWAY - W. EXCITING FORCE
TWIN RF. [S/B = 6.0]

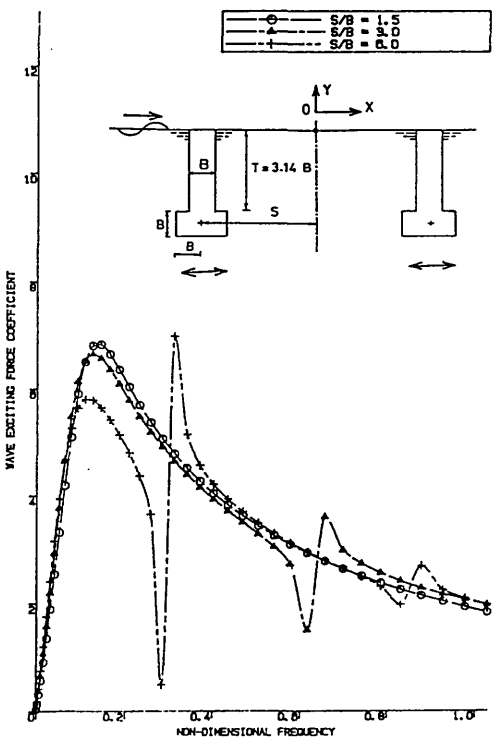

SWAY - W. EXCITING FORCE
TWIN RECTAN. FLOATING HULL

Fig. 130 - Effect of hull separation on the wave-induced force coefficients of a surface-piercing rectangular column section in the sway mode

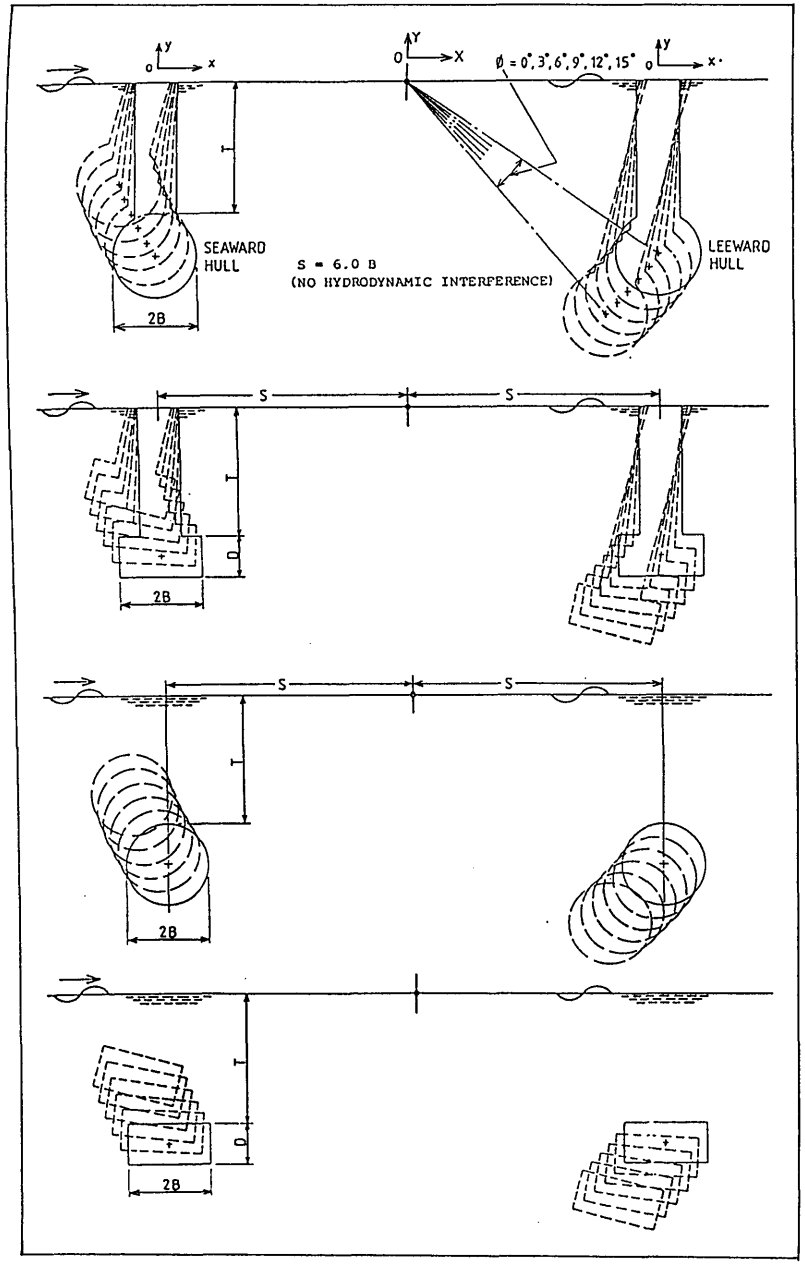

Fig. 131 - Range of the cross-sections and steady tilt angles examined

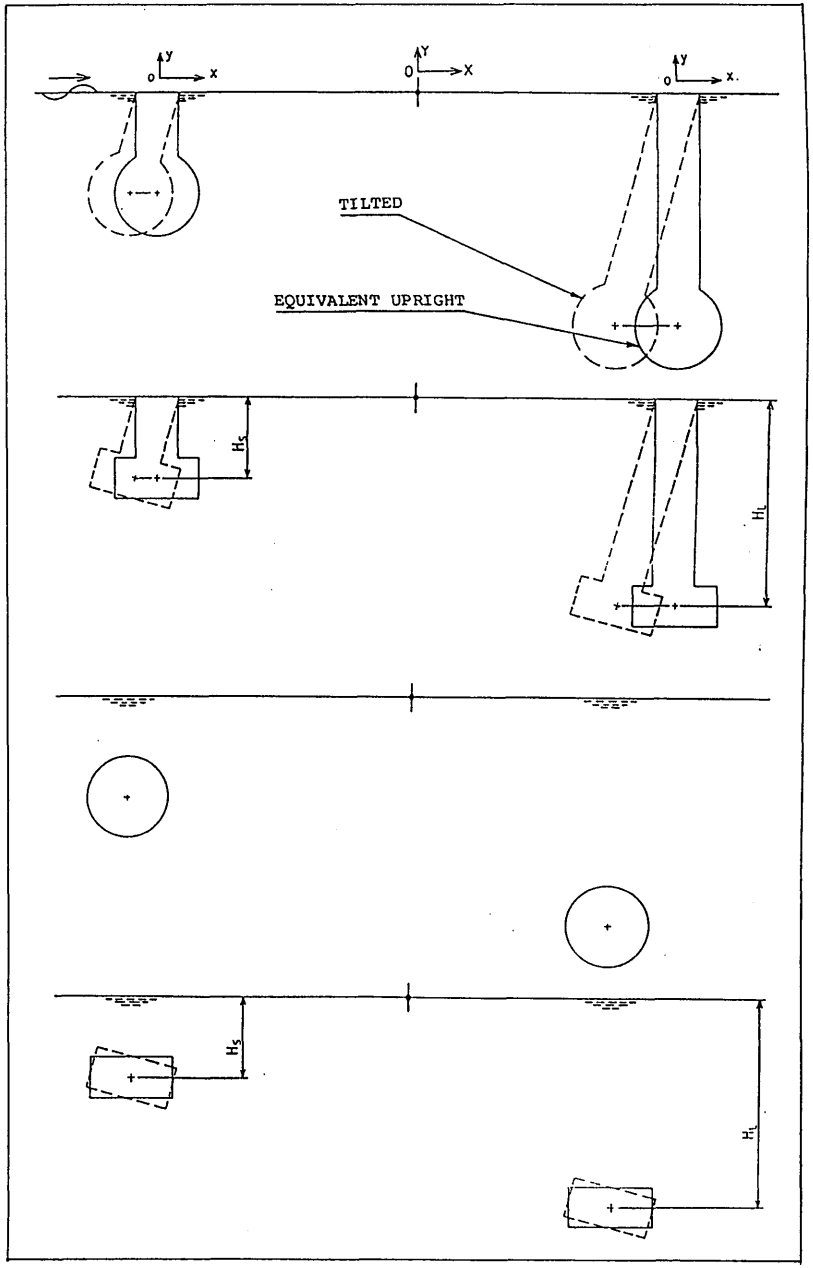

Fig. 132 - Presentation of the tilted seaward and leeward hull sections and their upright positions at equivalent depth of submergence (or draught) H_s, H_ℓ

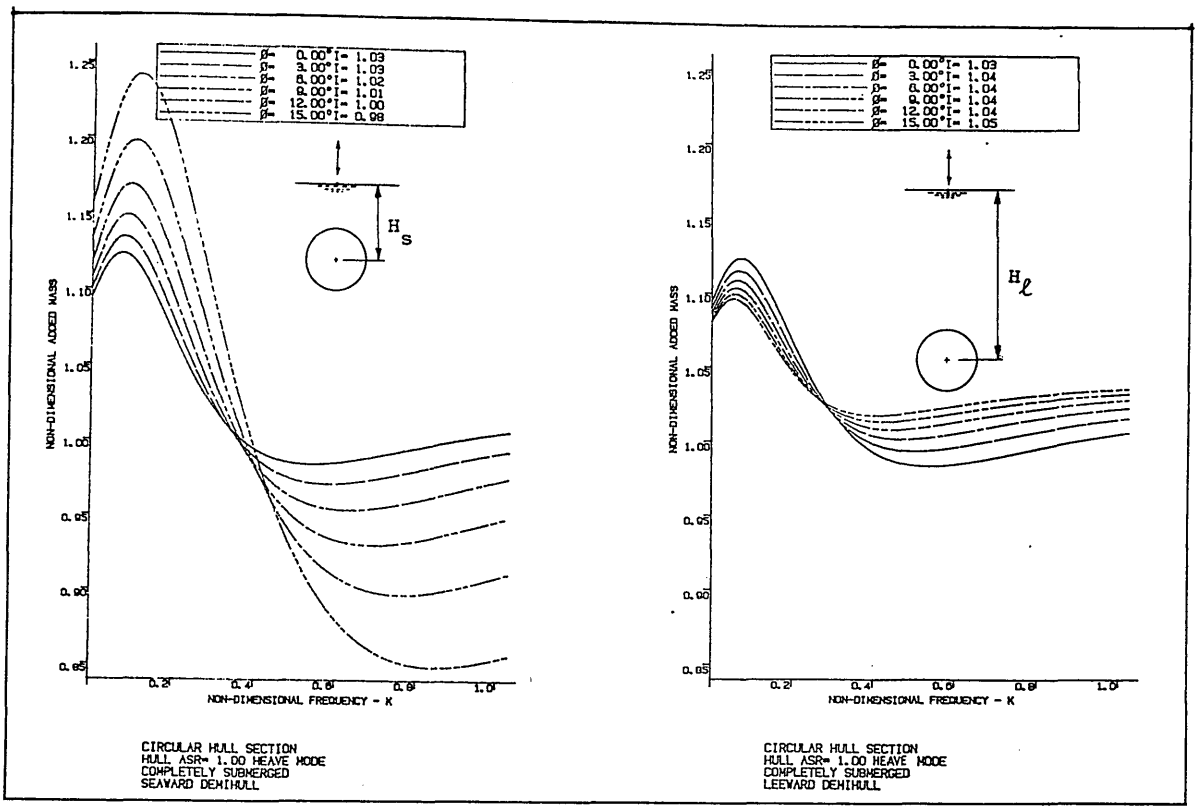

Fig. 133 - Effect of varying tilt angles on the heave added mass coefficient of circular hull section

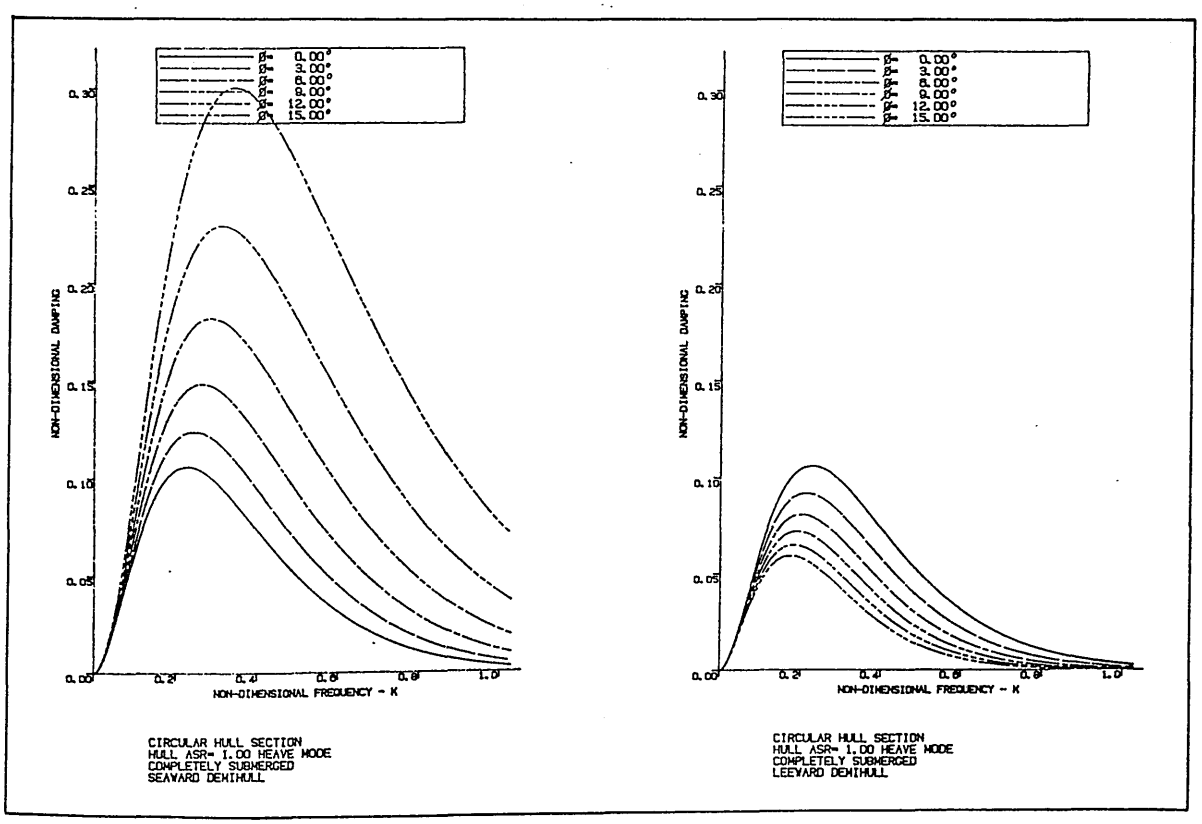

Fig. 134 - Effect of varying tilt angles on the heave damping coefficient of circular hull section

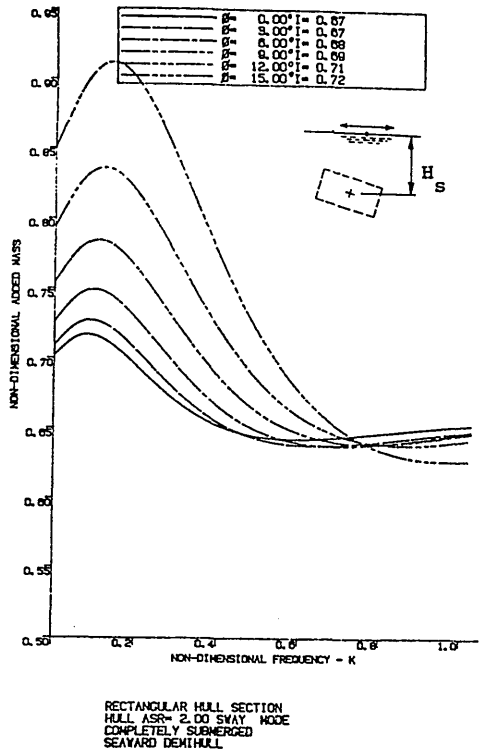

Fig. 135a - Seaward hull section in tilted position

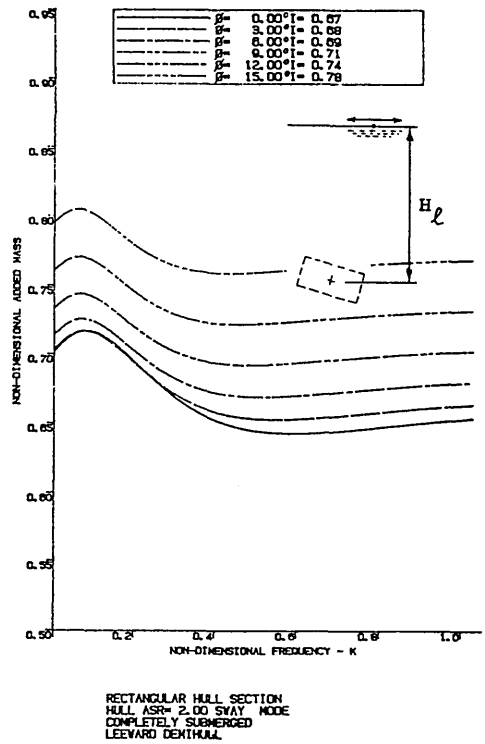

Fig. 135b - Leeward hull section in tilted position

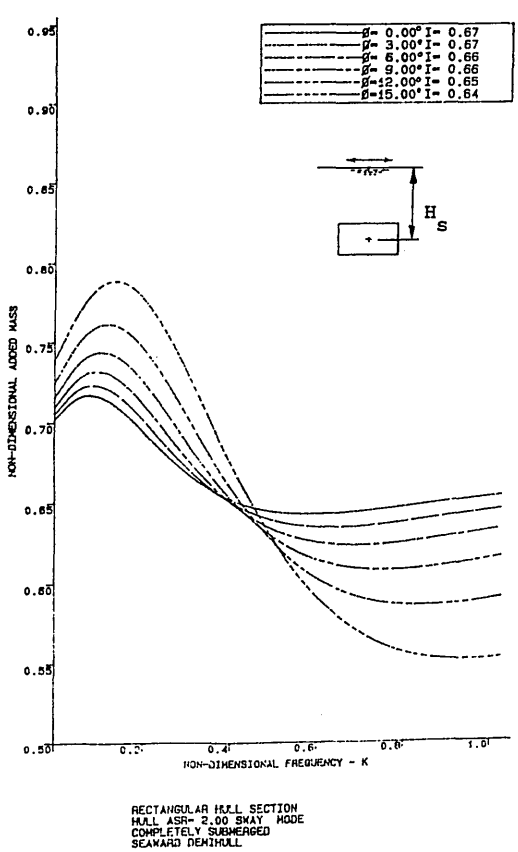

Fig. 135c - Seaward hull section in equivalent upright position

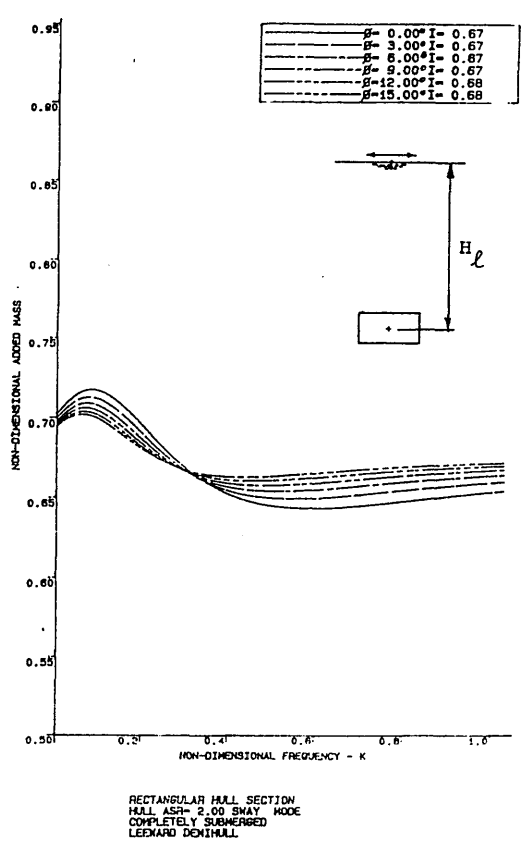

Fig. 135d - Leeward hull section in equivalent upright position

Fig. 135 - Effect of varying tilt angles on the sway added mass coefficients of rectangular hull section

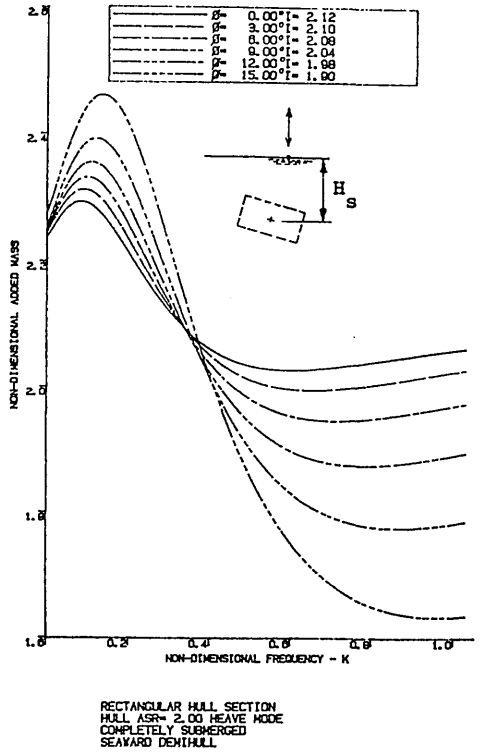

Fig. 136a - Seaward hull section in tilted position

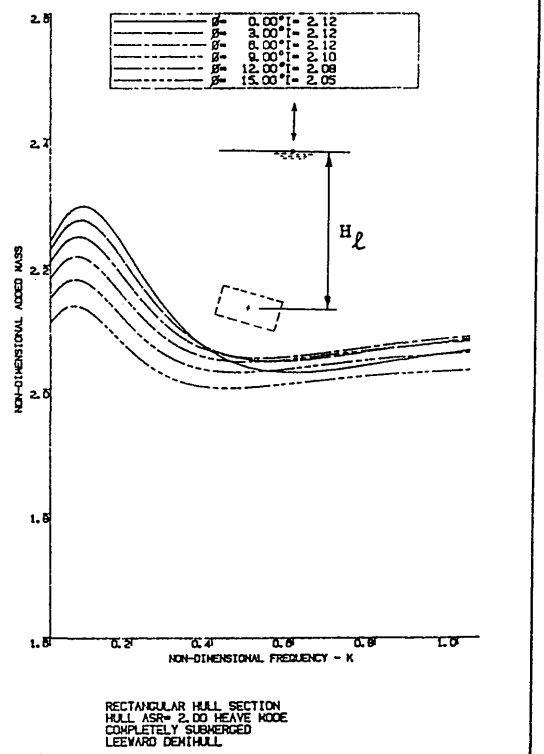

Fig. 136b - Leeward hull section in tilted position

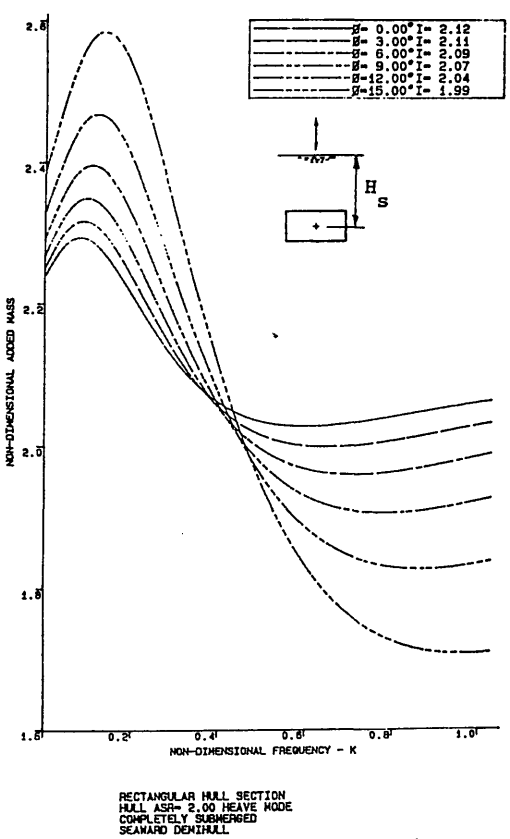

Fig. 136c - Seaward hull section in equivalent upright position

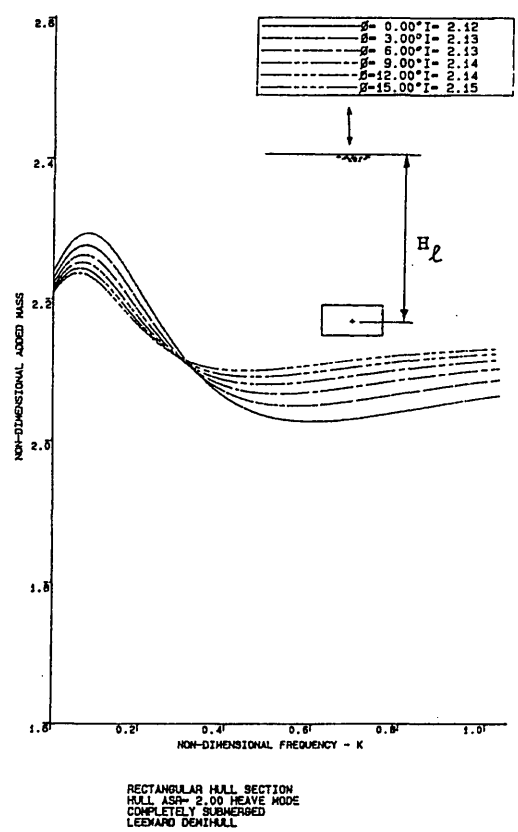

Fig. 136d - Leeward hull section in equivalent upright position

Fig. 136 - Effect of varying tilt angles on the heave added mass coefficient of rectangular hull section

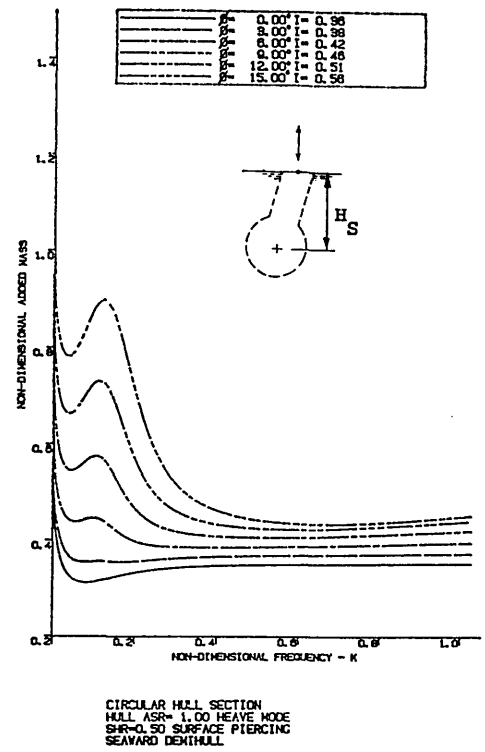

Fig. 137a - Seaward column section in tilted position

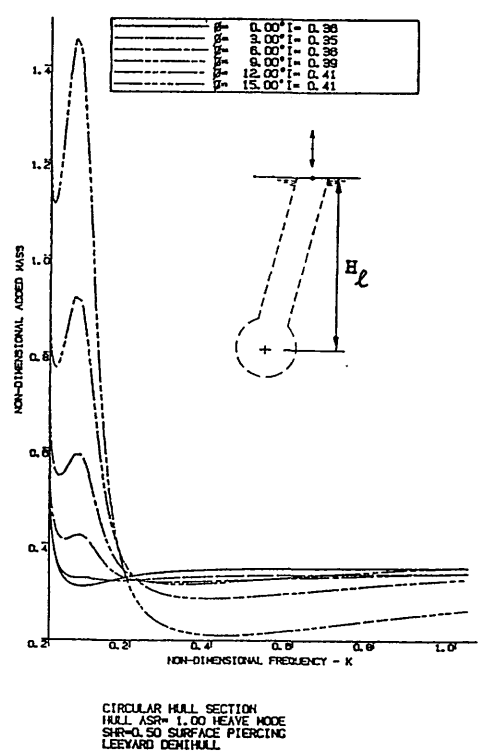

Fig. 137b - Leeward column section in tilted position

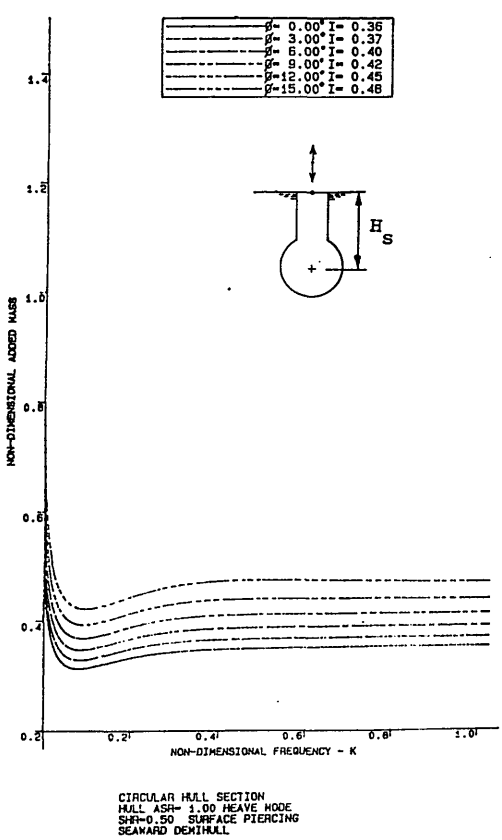

Fig. 137c - Seaward column section in equivalent upright position

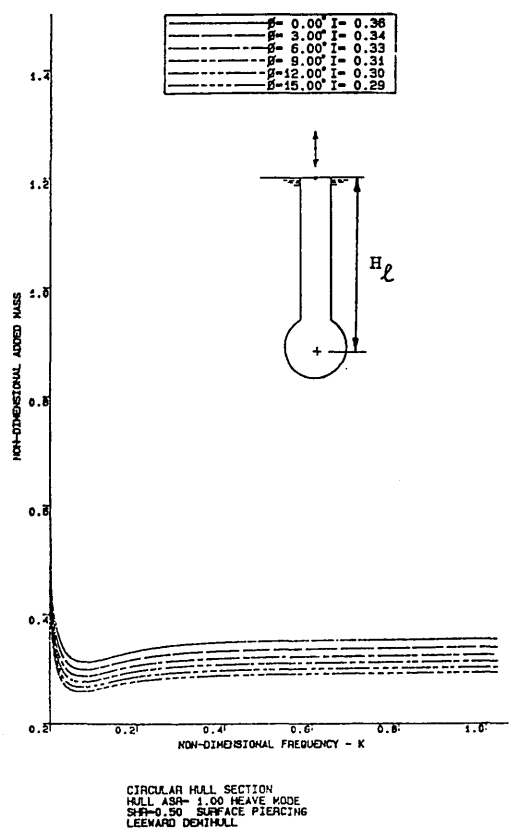

Fig. 137d - Leeward column section in equivalent upright position

Fig. 137 - Effect of varying tilt angles on the heave added mass coefficient of circular column section

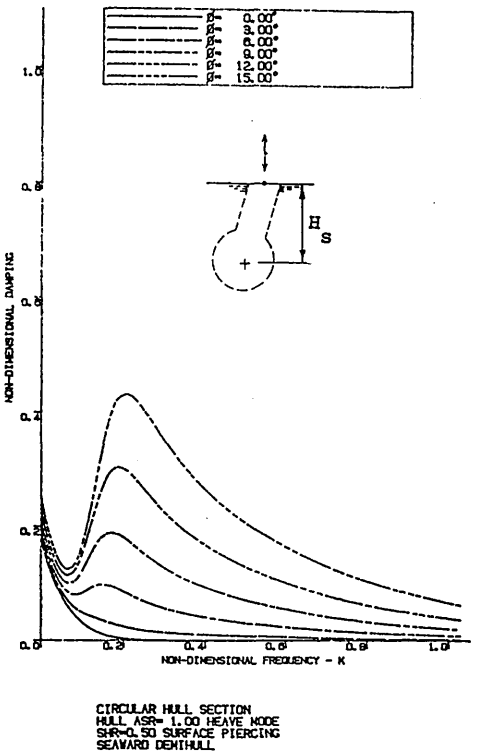

Fig. 138a - Seaward column section in tilted position

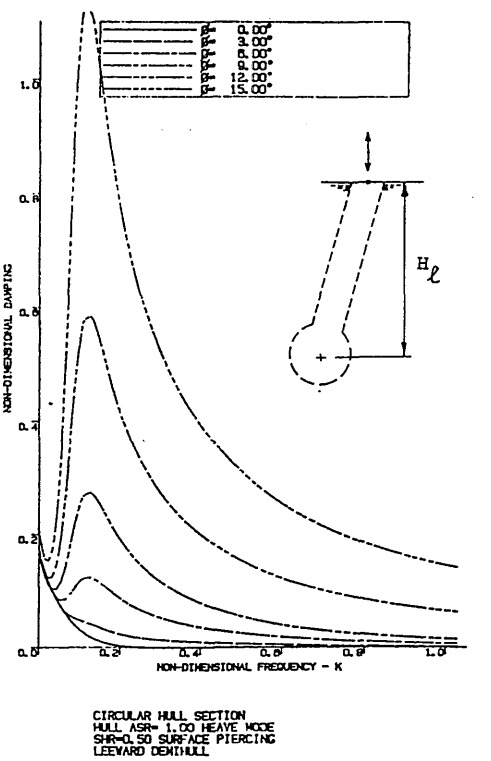

Fig. 138b - Leeward column section in tilted position

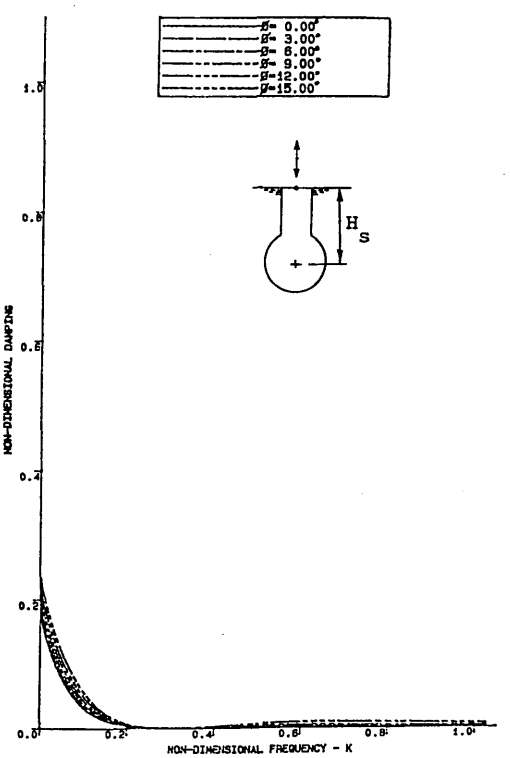

Fig. 138c - Seaward column section in equivalent upright position

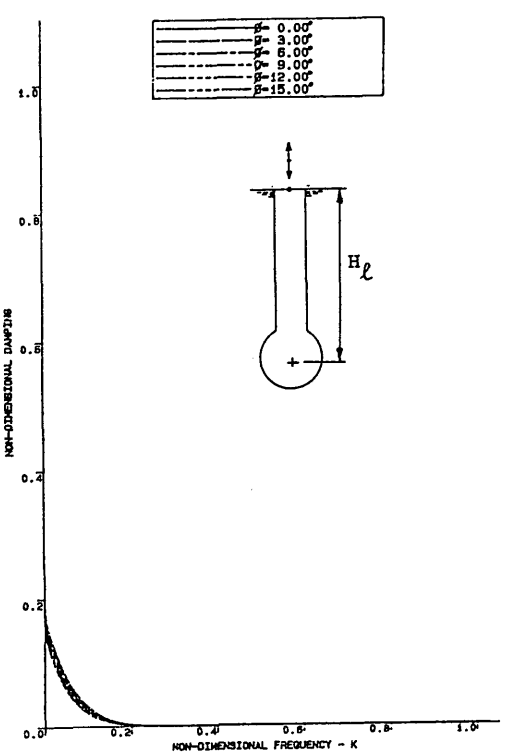

Fig. 138d - Leeward column section in equivalent upright position

Fig. 138 - Effect of varying tilt angles on the heave damping coefficient of circular column section

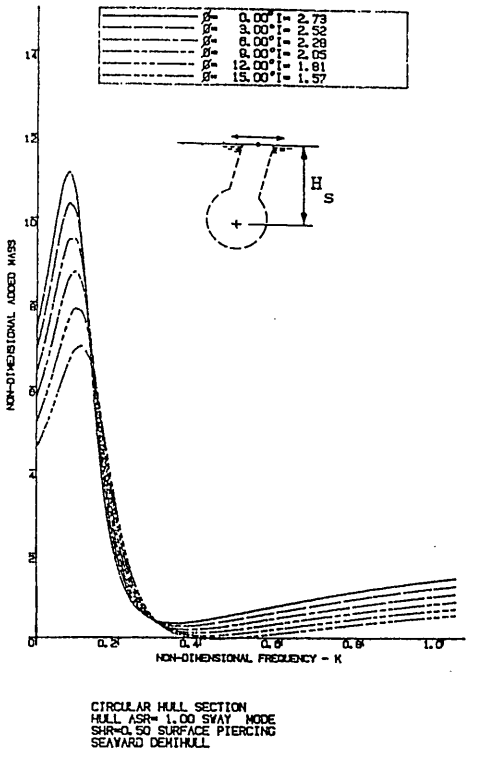

Fig. 139a - Seaward column section in tilted position

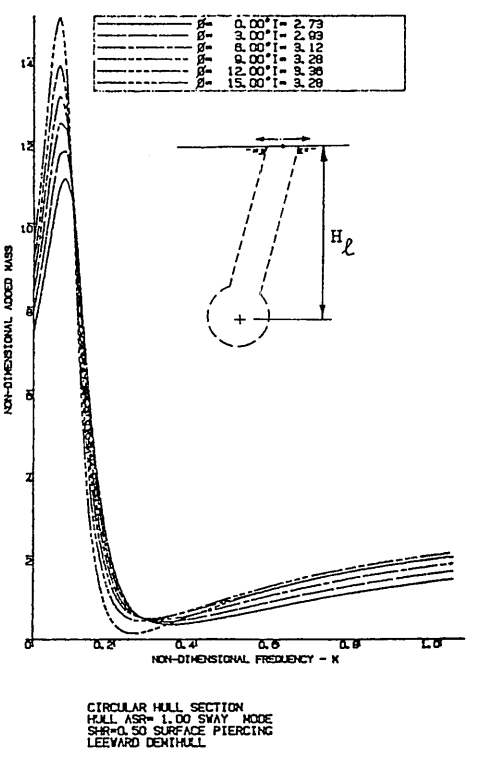

Fig. 139b - Leeward column section in tilted position

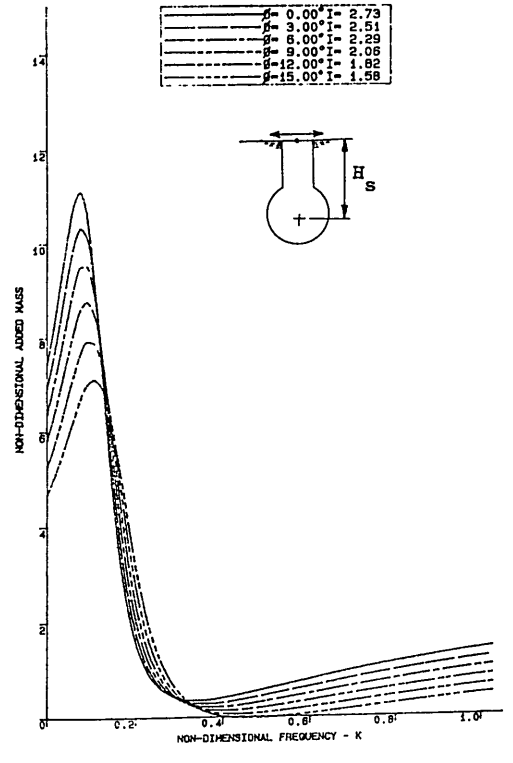

Fig. 139c - Seaward column section in equivalent upright position

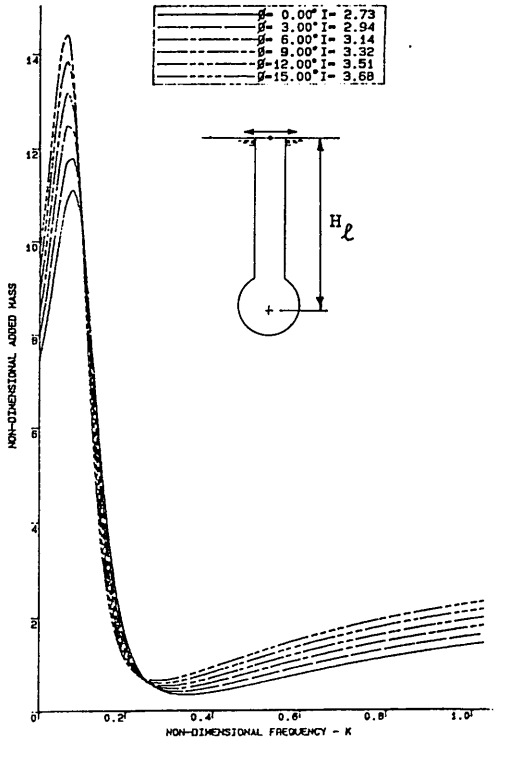

Fig. 139d - Leeward column section in equivalent upright position

Fig. 139 - Effect of varying tilt angles on the sway added mass coefficient of circular column section

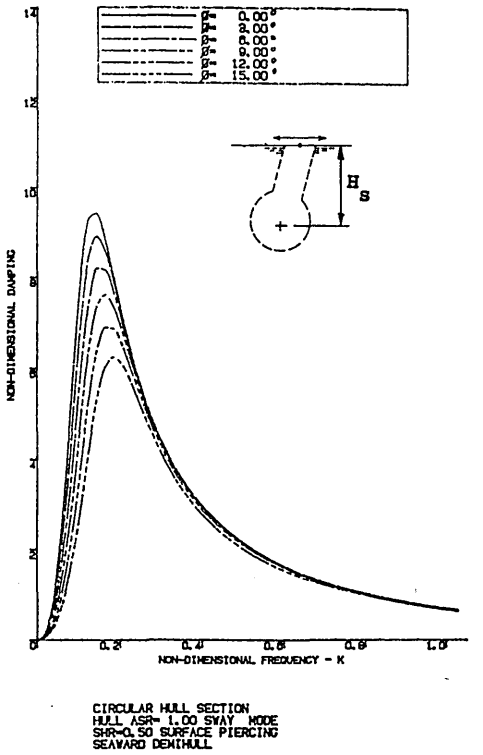

Fig. 140a - Seaward column section in tilted position

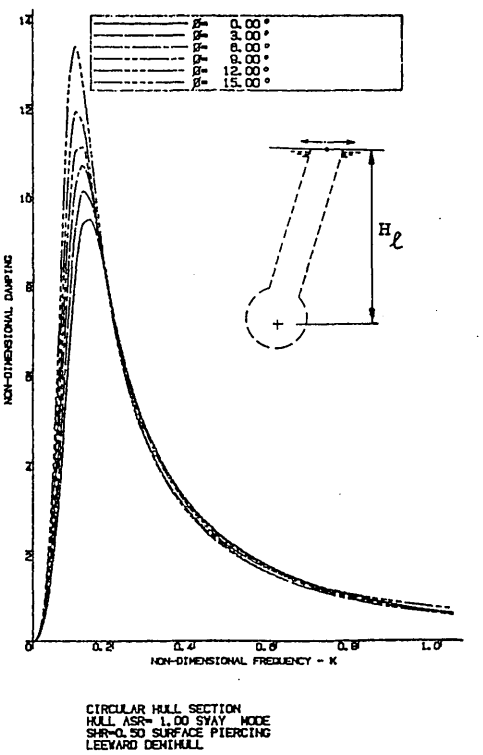

Fig. 140b - Leeward column section in tilted position

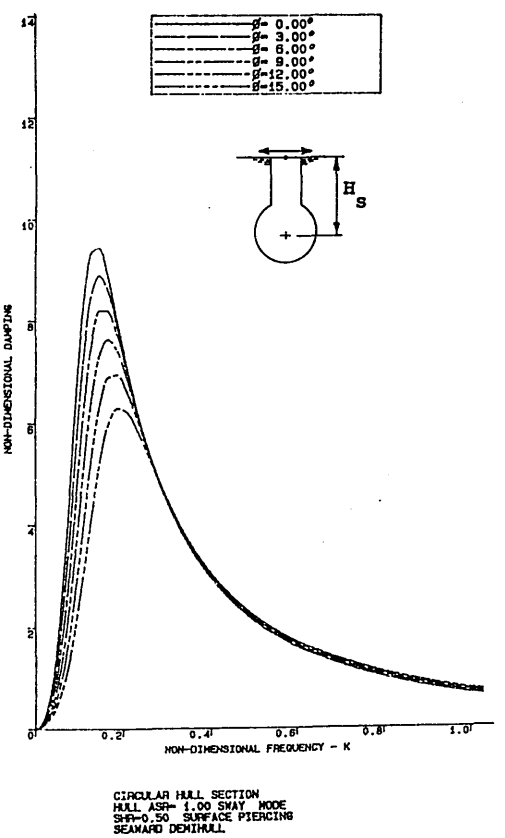

Fig. 140c - Seaward column section in equivalent upright position

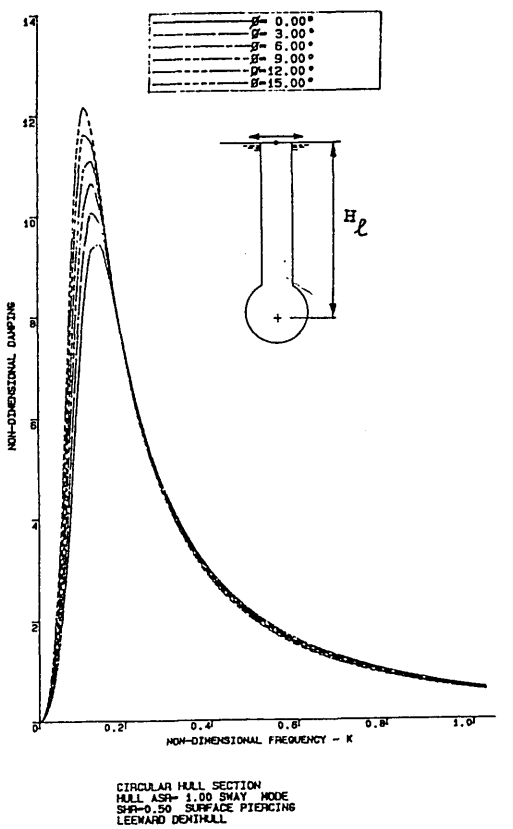

Fig. 140d - Leeward column section in equivalent upright position

Fig. 140 - Effect of varying tilt angles on the sway damping coefficient of circular column section

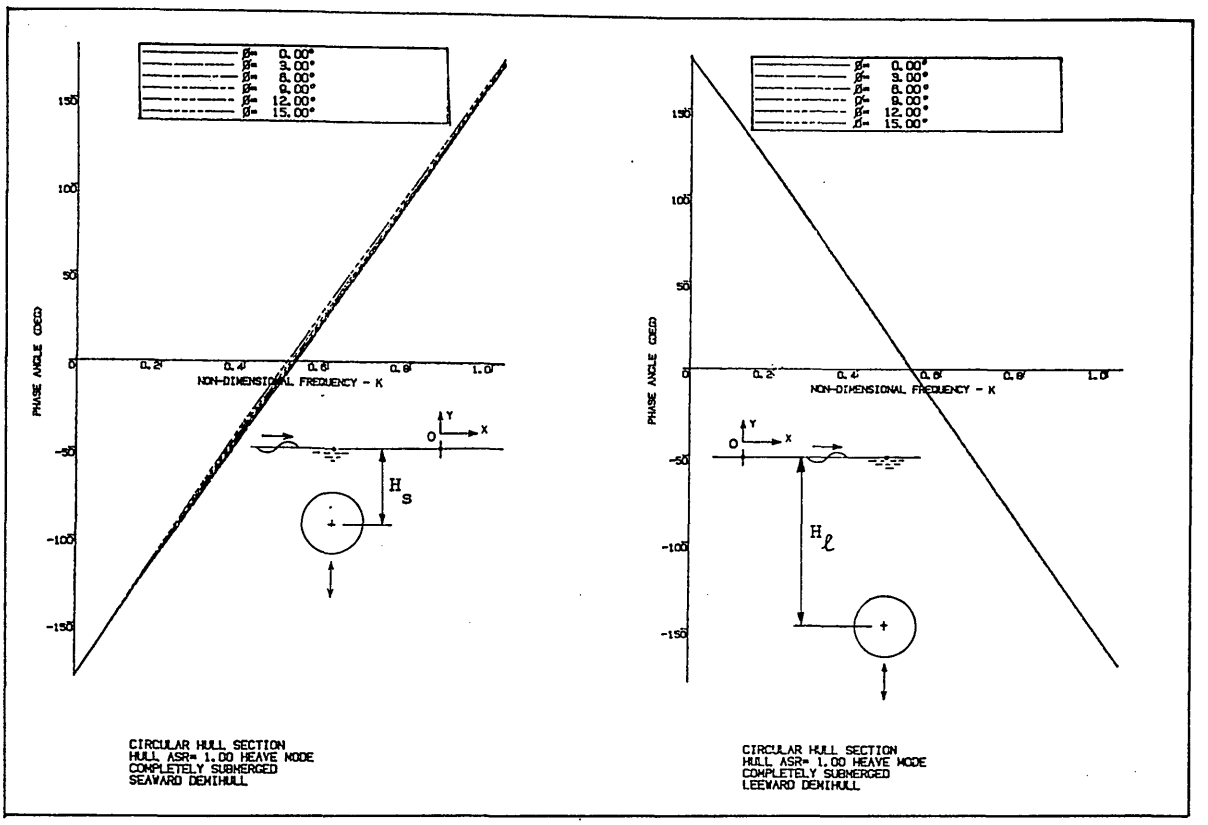

Fig. 141 - Effect of tilt angles on the phase angle of the heave exciting force for circular hull sections

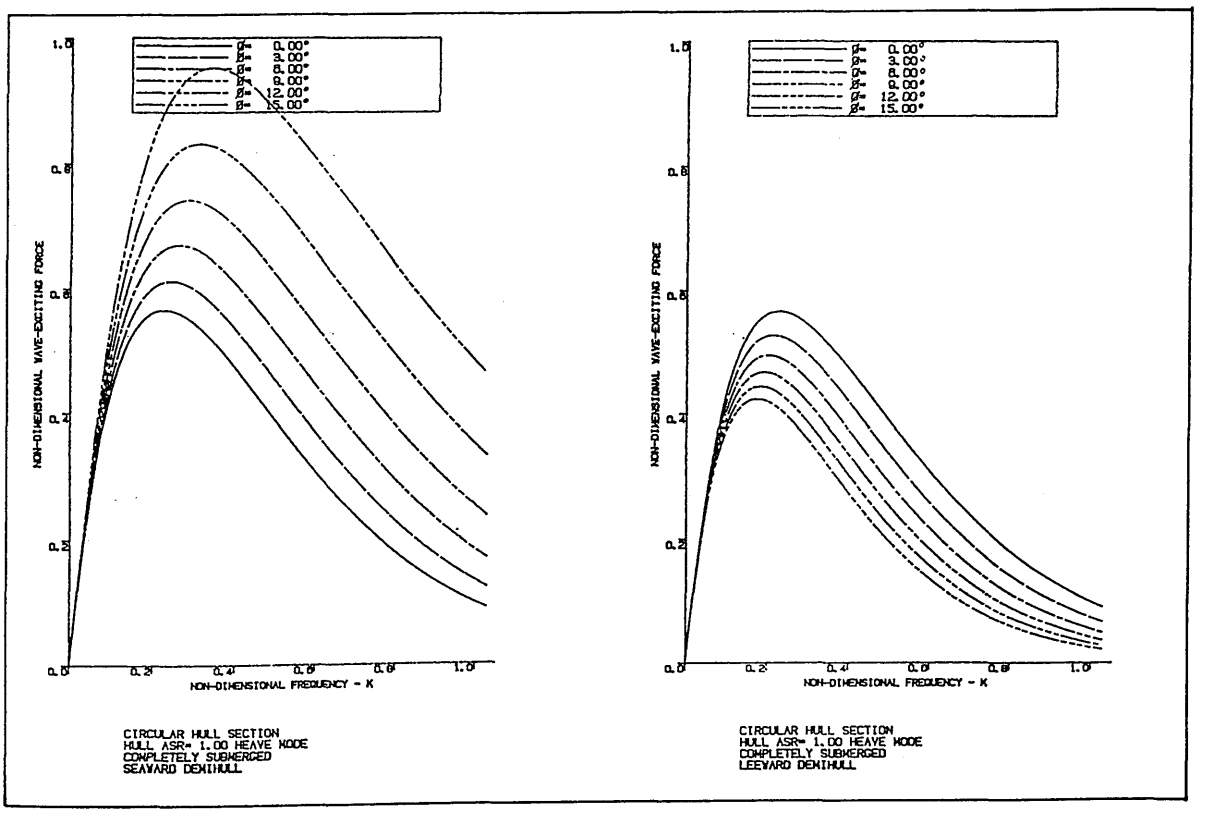

Fig. 142 - Effect of varying tilt angles on the heave exciting force of circular hull sections

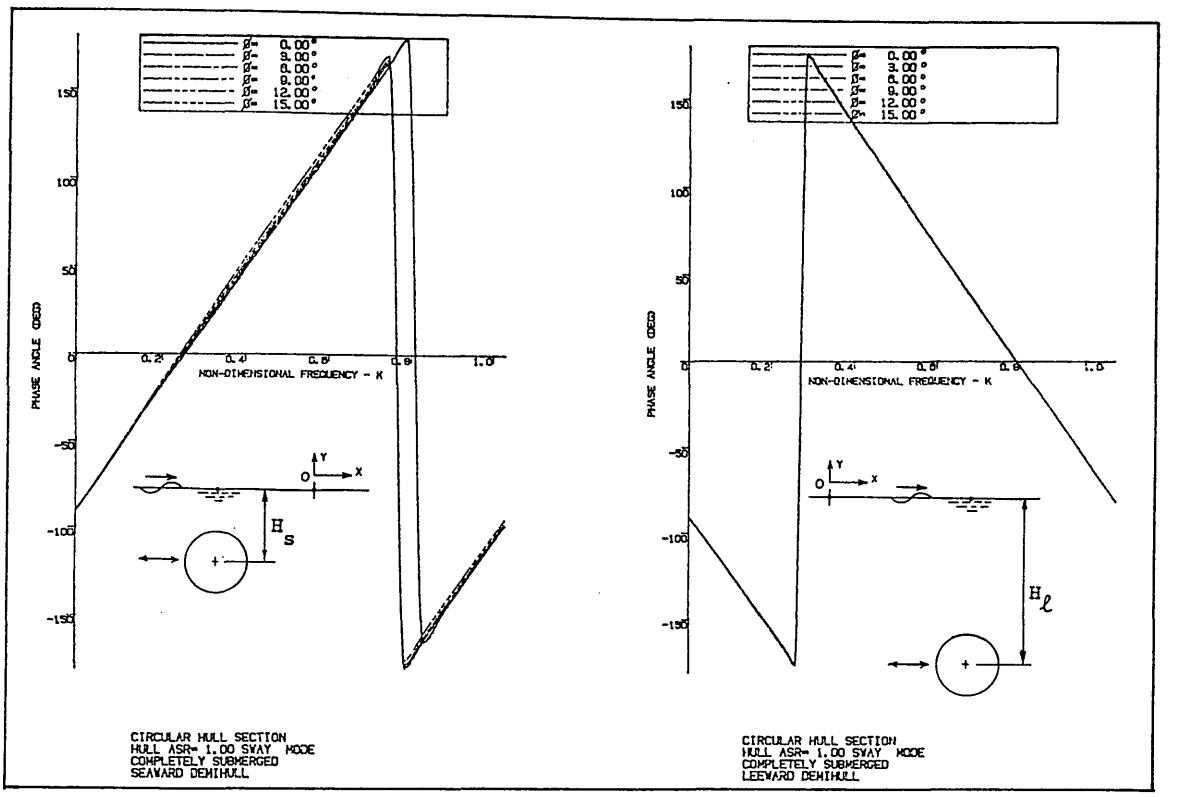

Fig. 143 - Effect of varying tilt angles on the phase angle of the sway exciting force for circular hull sections

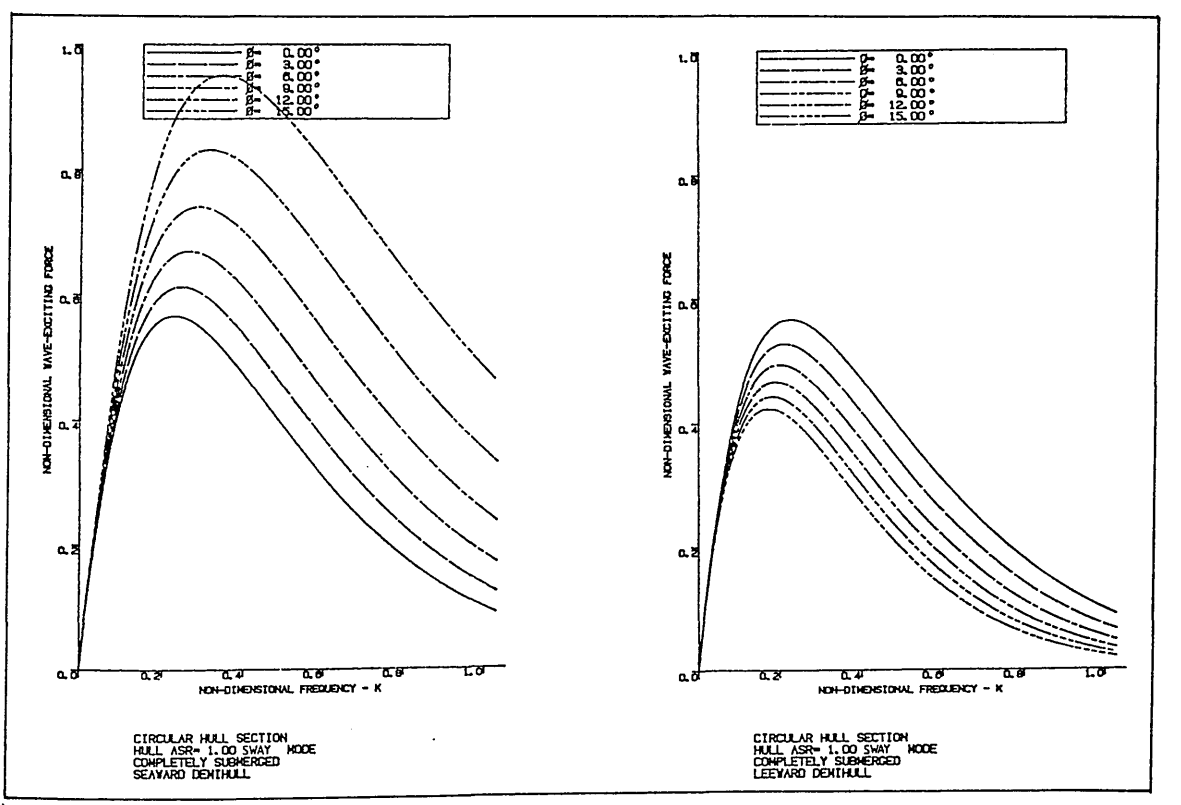

Fig. 144 - Effect of varying tilt angles on the sway exciting force of the circular hull sections

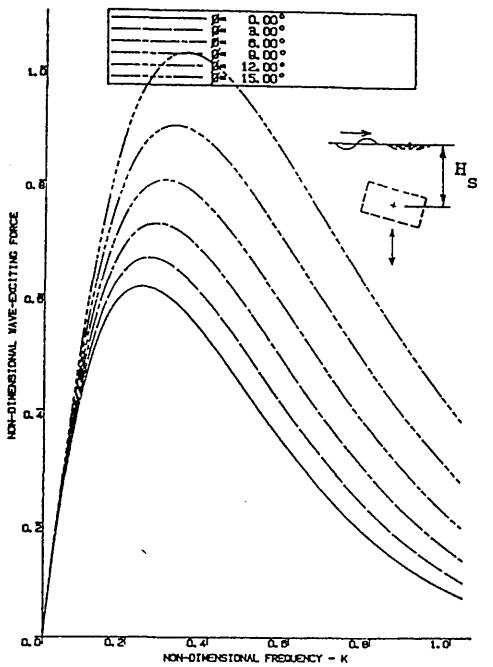

Fig. 145a - Seaward hull section in tilted position

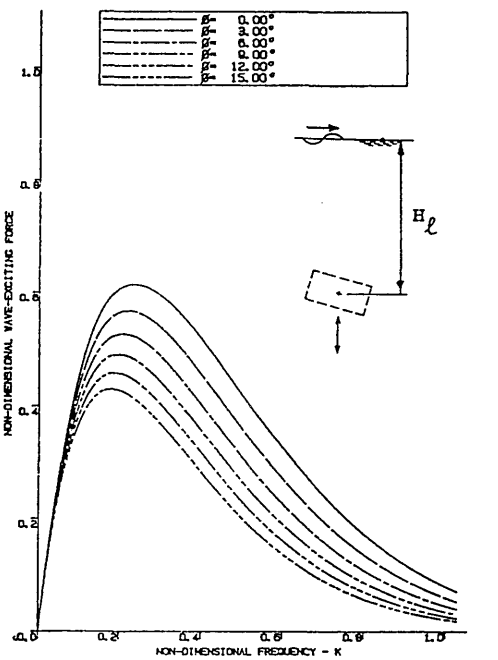

Fig. 145b - Leeward hull section in tilted position

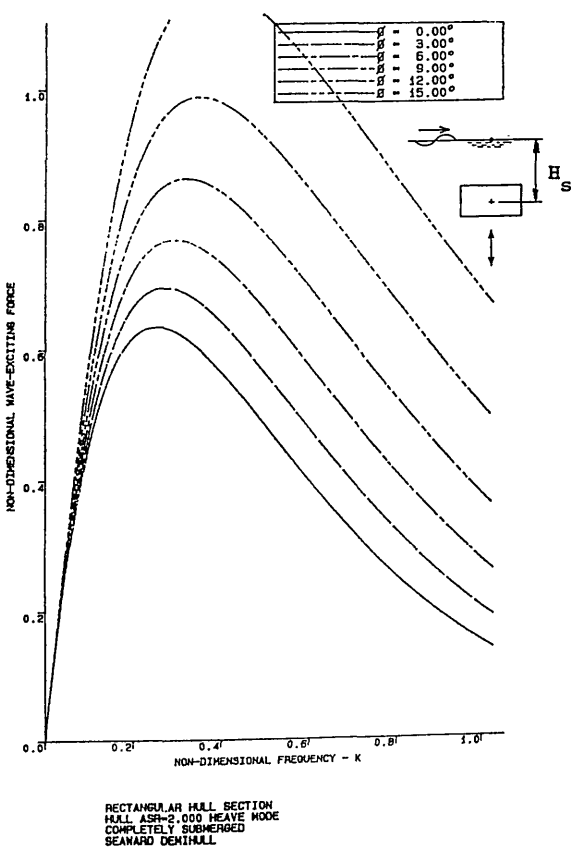

Fig. 145c - Seaward hull section in equivalent upright position

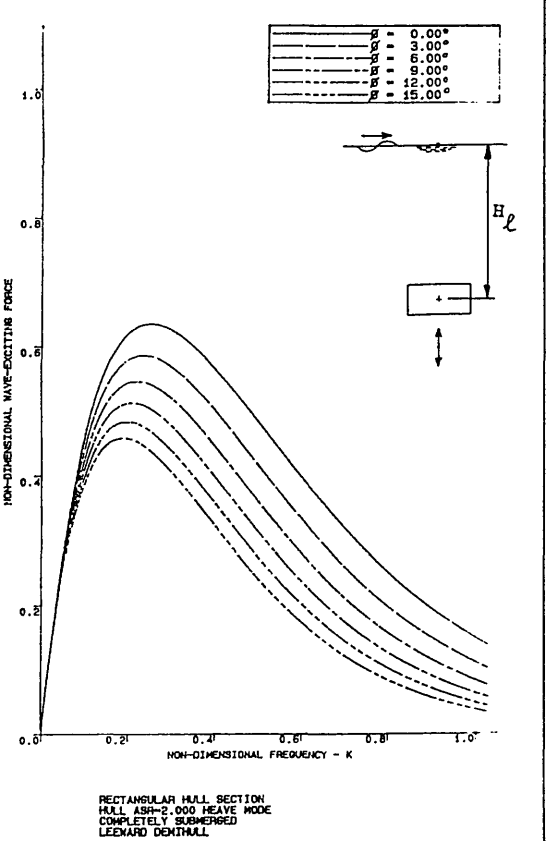

Fig. 145d - Leeward hull section in equivalent upright position

Fig. 145 - Effect of varying tilt angles on the heave-exciting force of the rectangular hull section

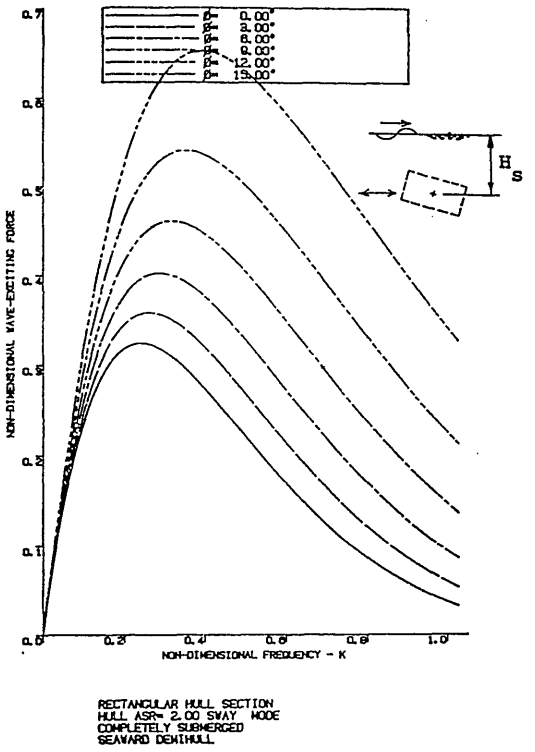

Fig. 146a - Seaward hull section in tilted position

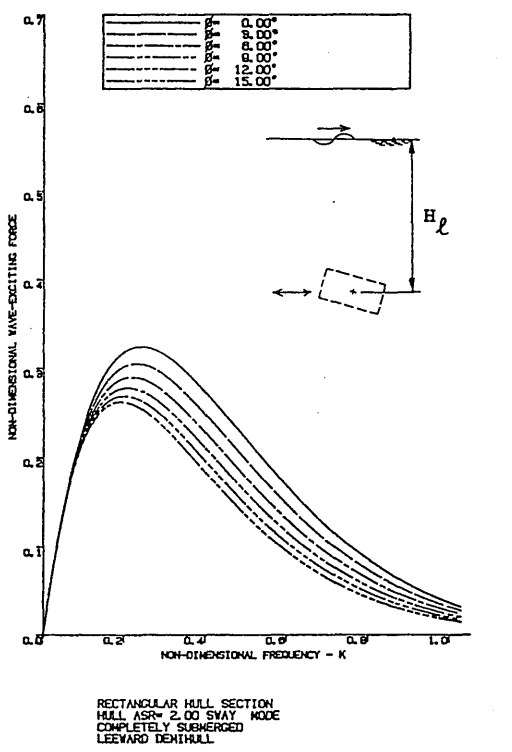

Fig. 146b - Leeward hull section in actual position

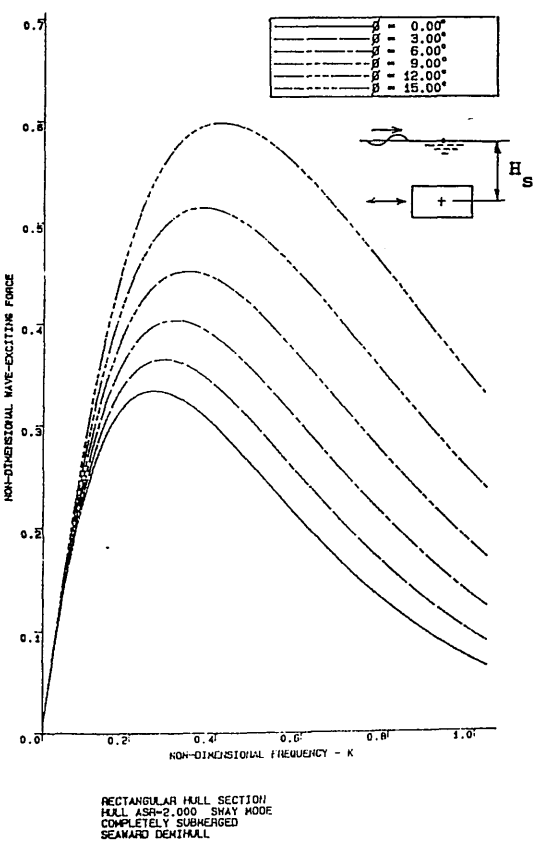

Fig. 146c - Seaward hull section in equivalent upright position

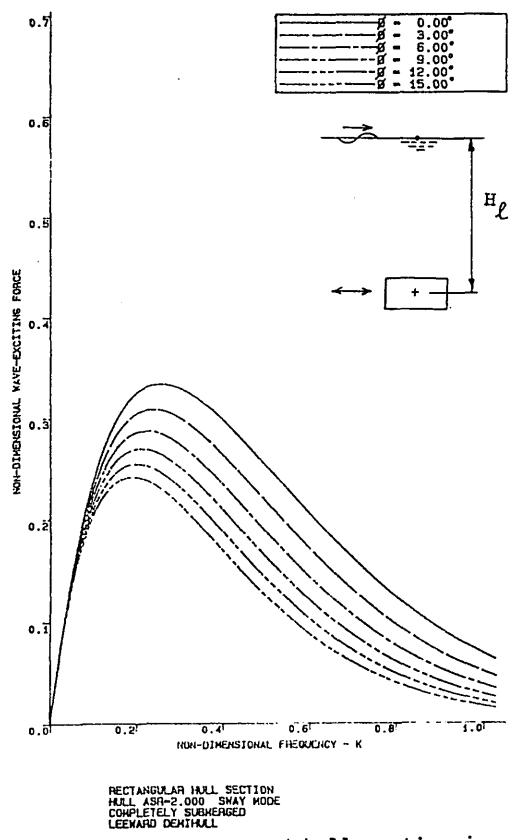

Fig. 146d - Leeward hull section in equivalent upright position

Fig. 146 - Effect of varying tilt angles on the sway exciting force on rectangular hull sections

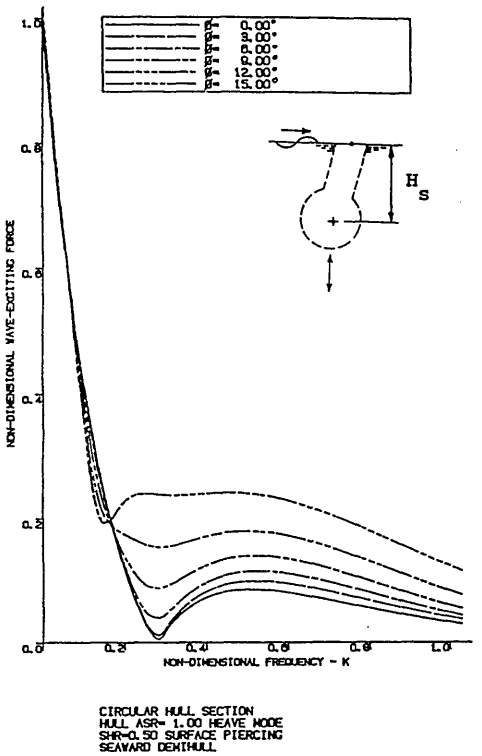

Fig. 147a - Seaward column section in tilted position

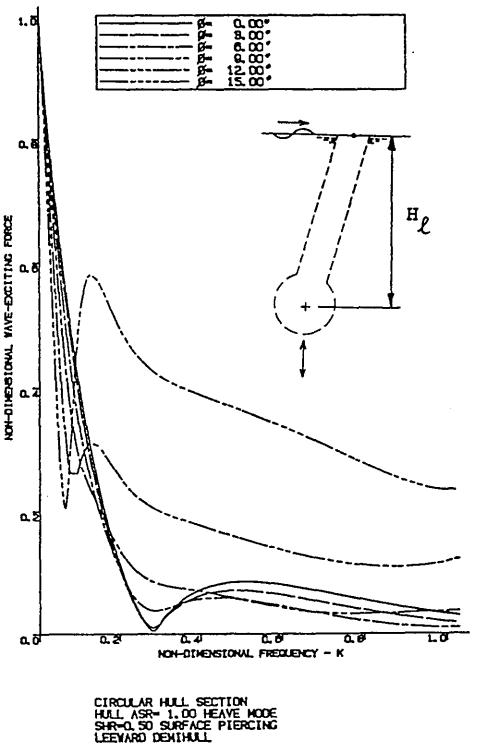

Fig. 147b - Leeward column section in tilted position

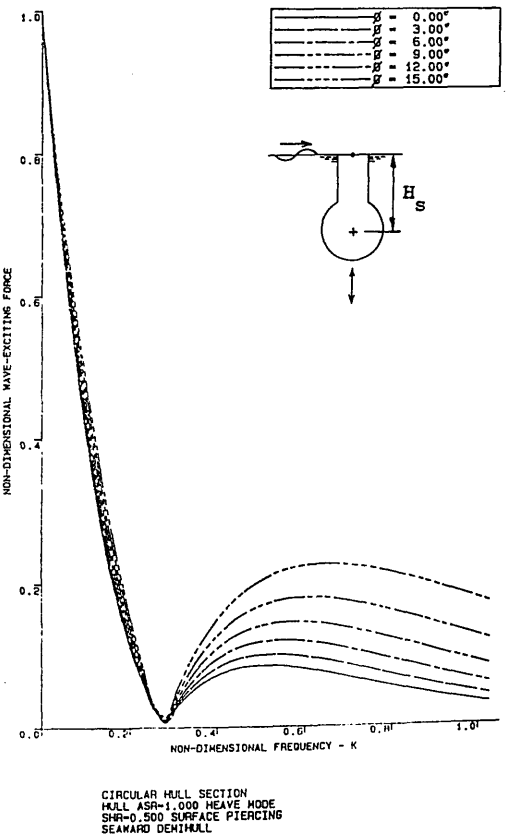

Fig. 147c - Seaward column section in equivalent upright position

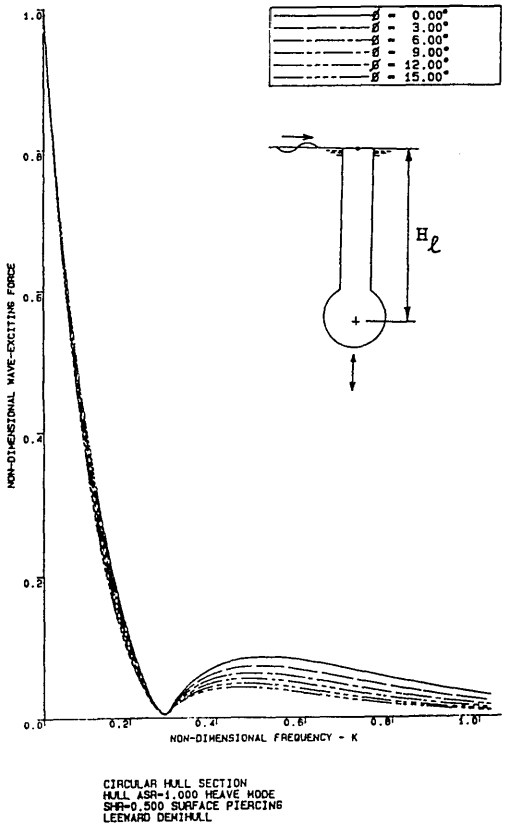

Fig. 147d - Leeward hull column section in equivalent upright positon

Fig. 147 - Effect of varying tilt angles on the heave exciting force of circular hull sections

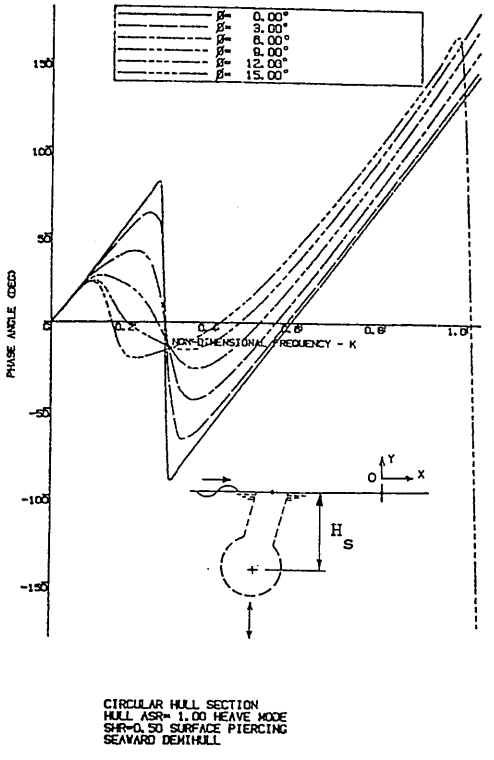

Fig. 148a - Seaward column section in tilted position

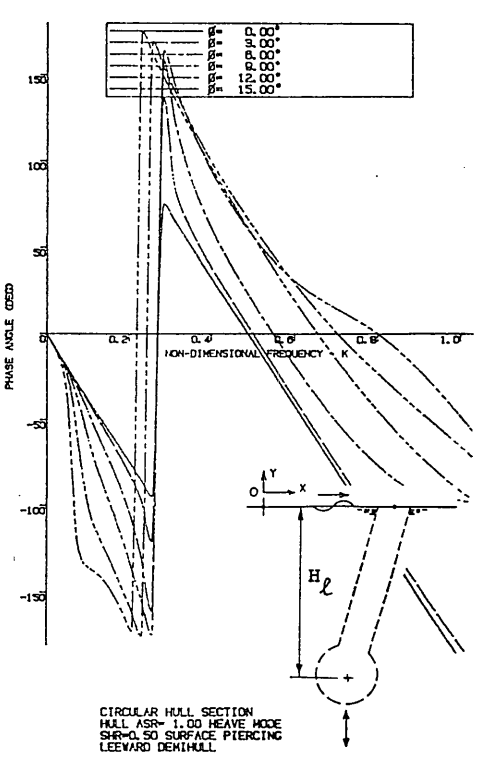

Fig. 148b - Leeward hull section in tilted position

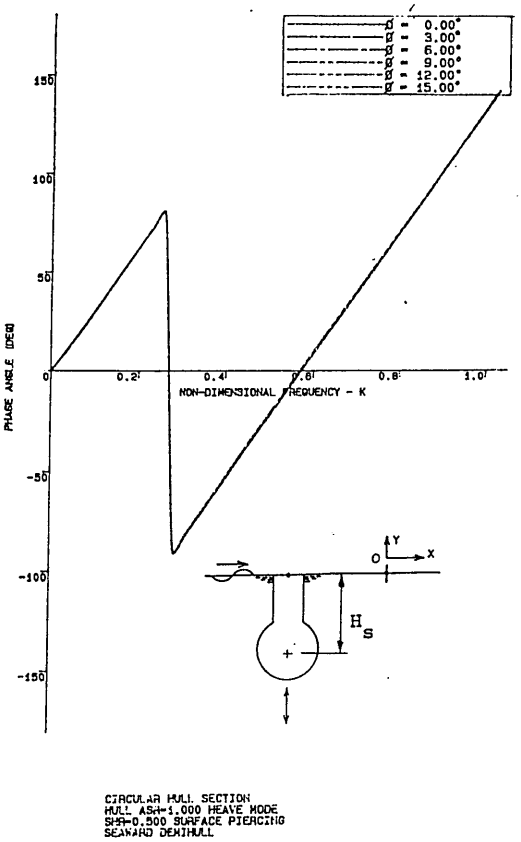

Fig. 148c - Seaward column section in equivalent upright position

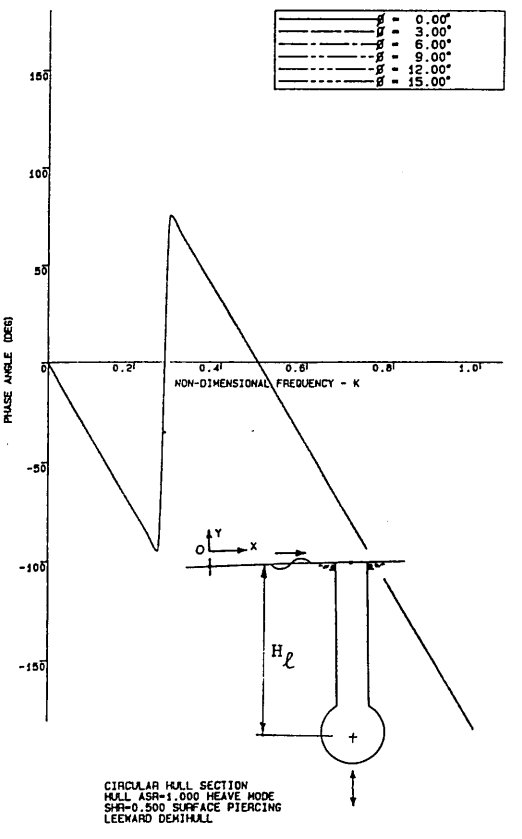

Fig. 148d - Leeward column section in equivalent upright position

Fig. 148 - Effect of varying tilt angles on the phase angle of the heave exciting force for circular column sections

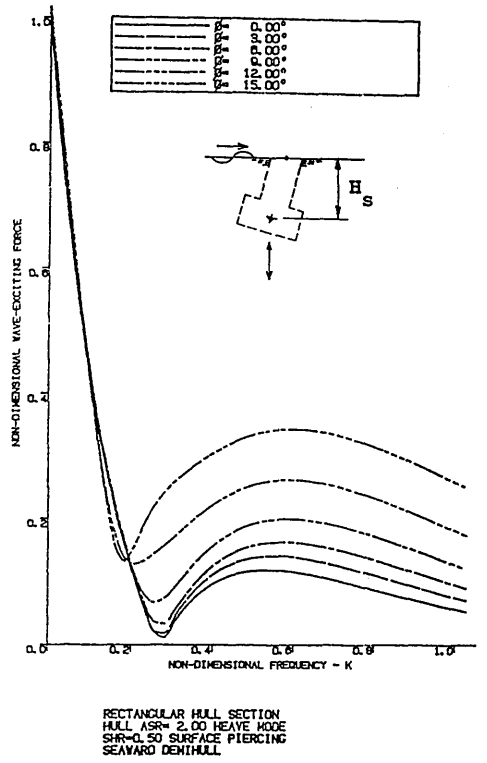

Fig. 149a - Seaward column section in tilted position

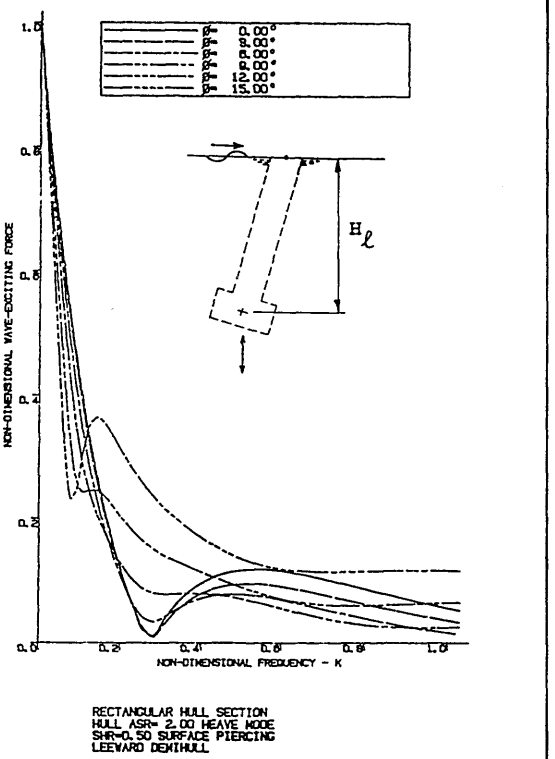

Fig. 149b - Leeward column section in tilted position

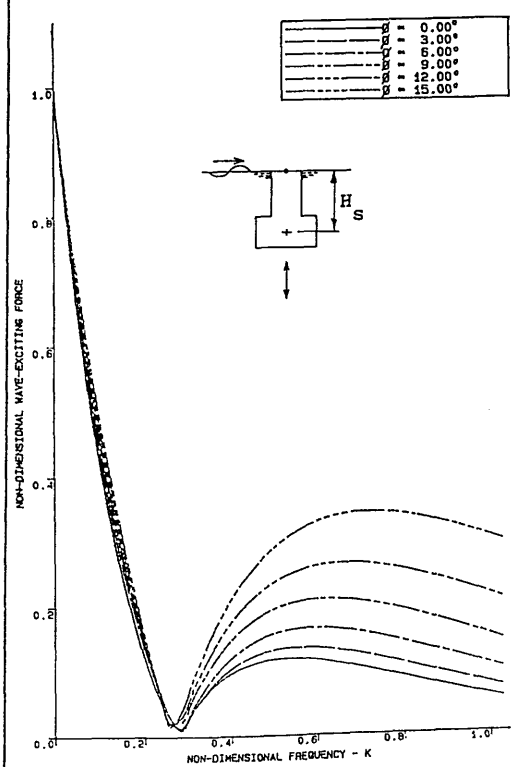

Fig. 149c - Seaward column section in equivalent upright position

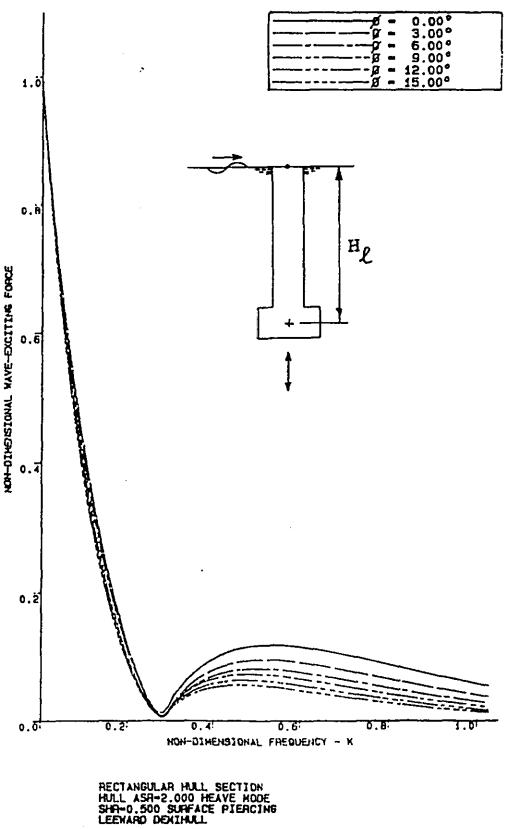

Fig. 149d - Leeward column section in equivalent upright position

Fig. 149 - Effect of varying tilt angles on the phase angle of the heave exciting force for rectangular column sections

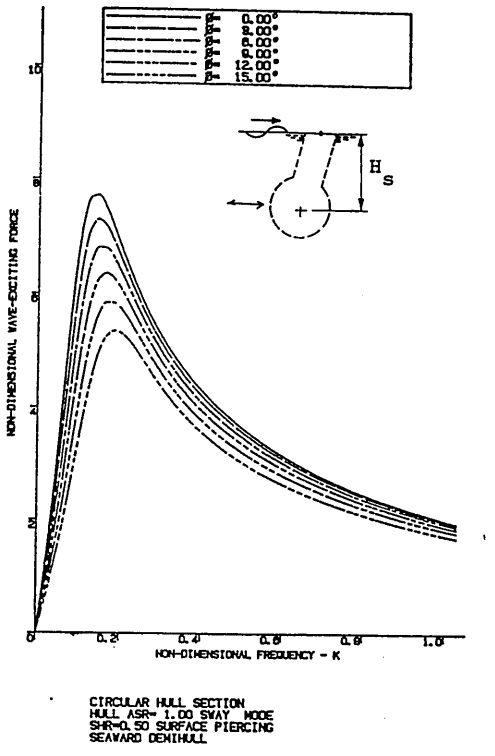

Fig. 150a - Seaward column section in tilted position

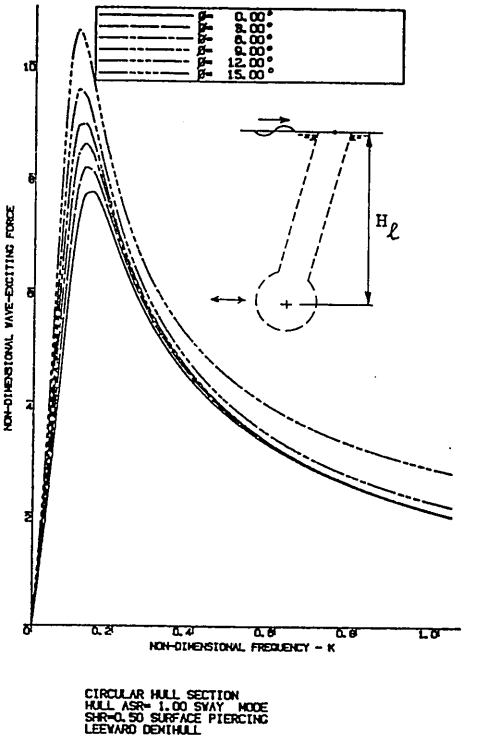

Fig. 150b - Leeward column section in tilted position

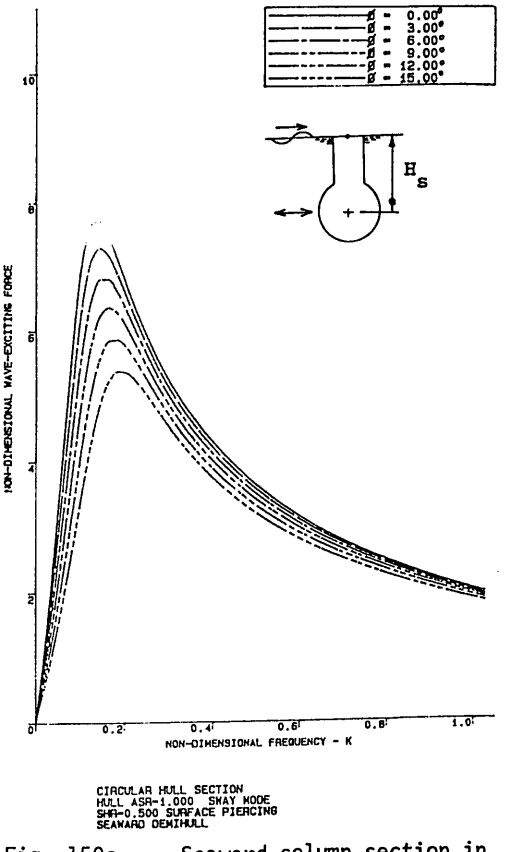

Fig. 150c - Seaward column section in equivalent upright position

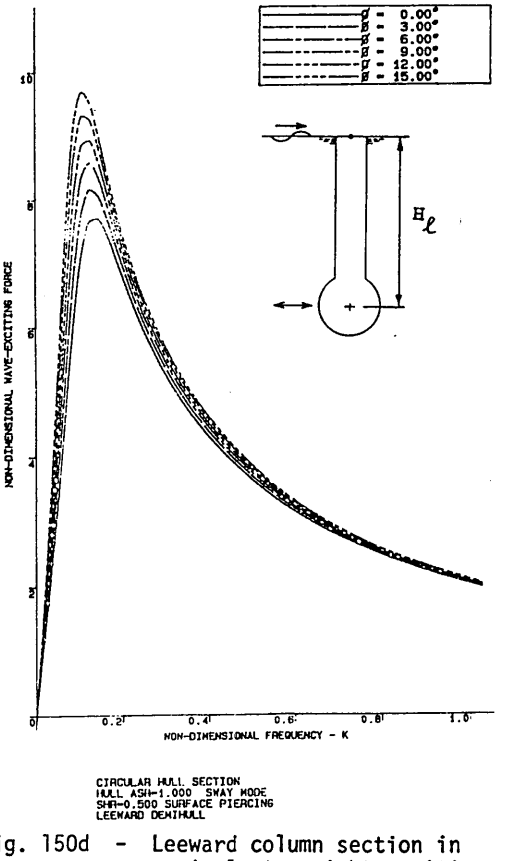

Fig. 150d - Leeward column section in equivalent upright position

Fig. 150 - Effect of varying tilt angles on the sway exciting force of circular column sections

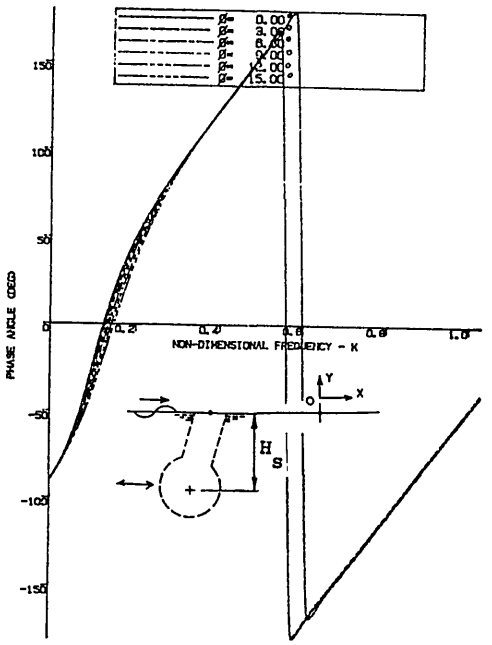

Fig. 151a - Seaward column section in tilted position

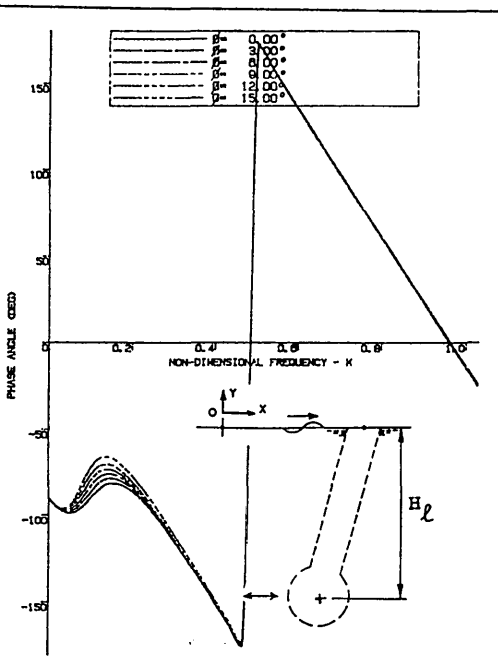

Fig. 151b - Leeward column section in tilted position

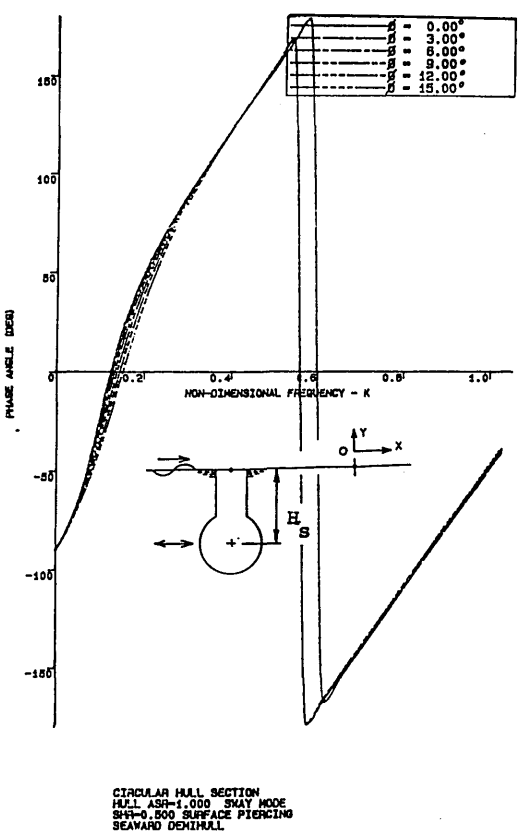

Fig. 151c - Seaward column section in equivalent upright position

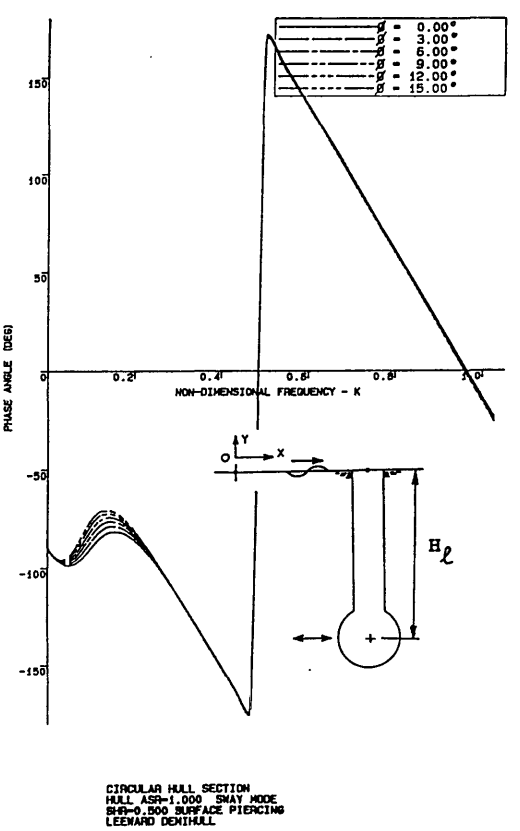

Fig. 151d - Leeward column section in equivalent upright position

Fig. 151 - Effect of varying tilt angles on the phase angle of the sway exciting force for circular column sections

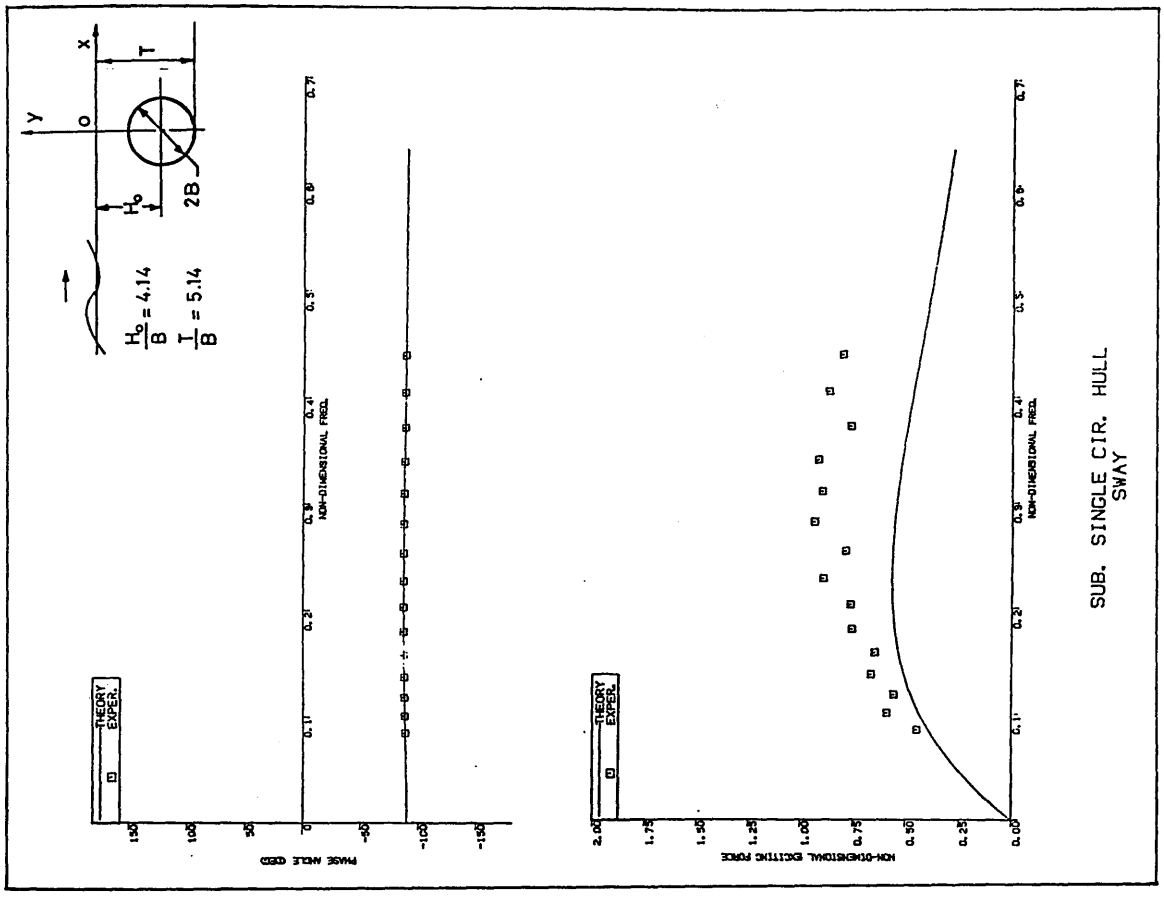

Fig. 153 - Comparison of the experiment and theory for the sway exciting force on the single submerged circular hull

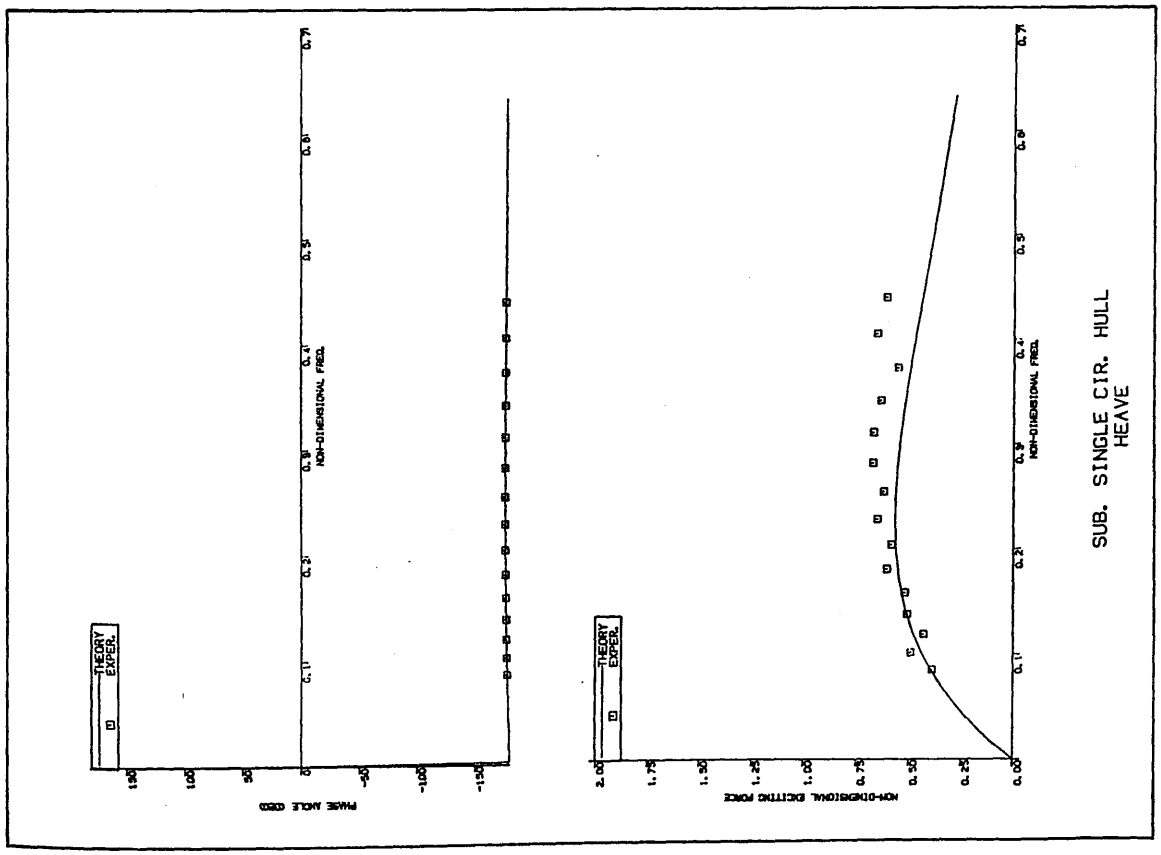

Fig. 152 - Comparison of the experiment and theory for the heave exciting force on the single submerged circular hull

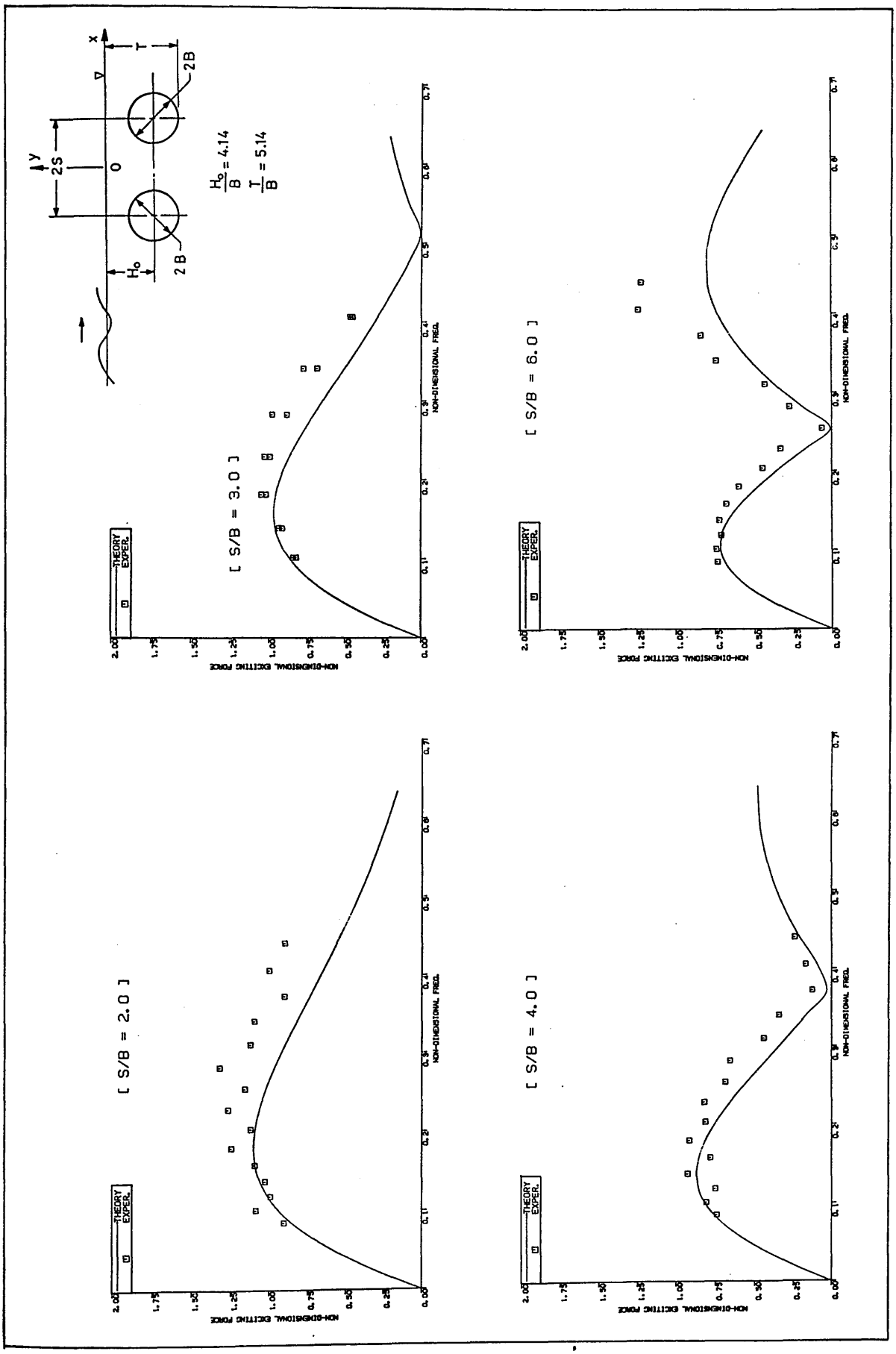

Fig. 154 - Comparison of the experiment and theory for the heave exciting force of twin circular hulls at various hull separations

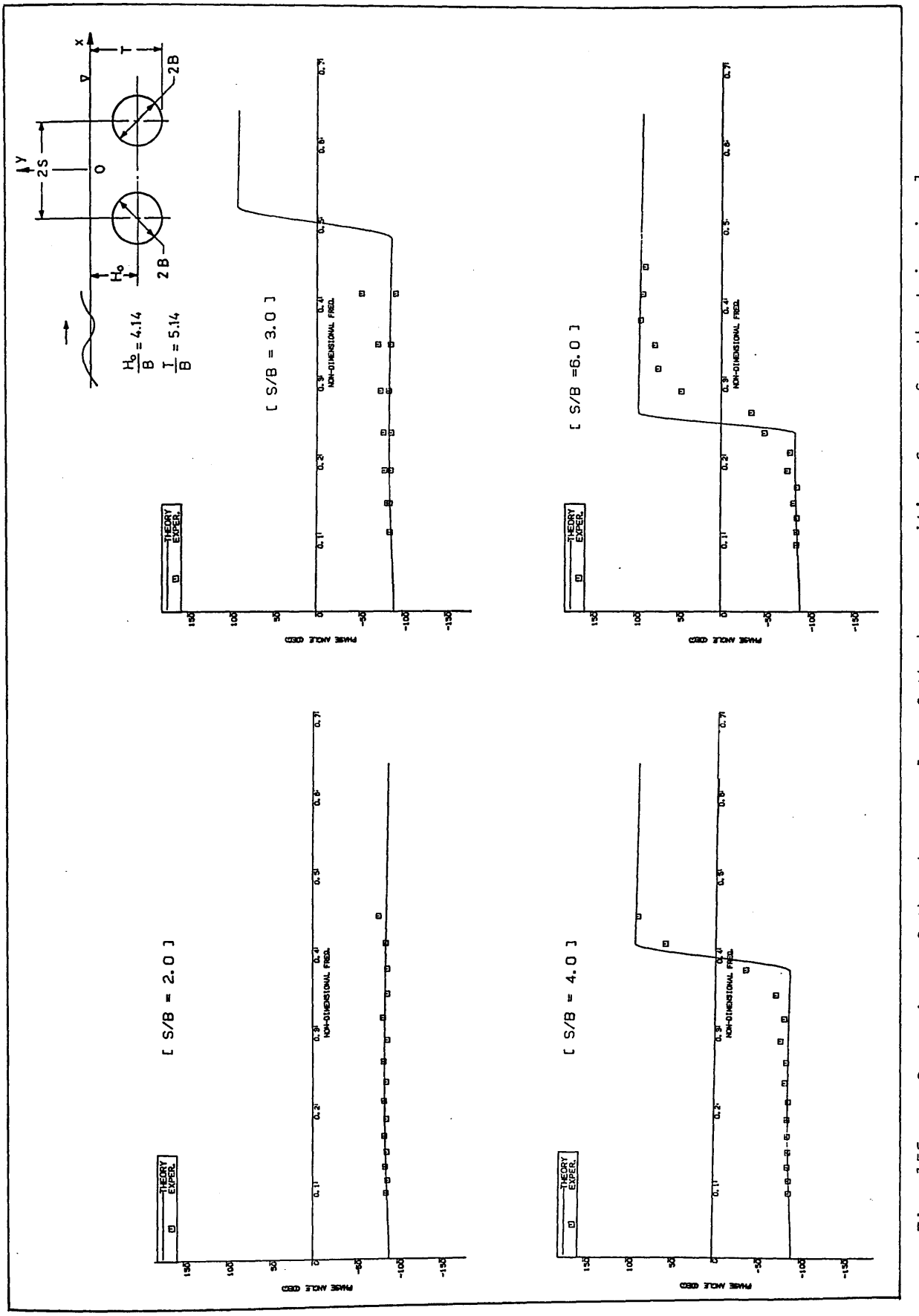

Fig. 155 - Comparison of the phase angles of the heave exciting force for the twin circular hulls at various hull separations

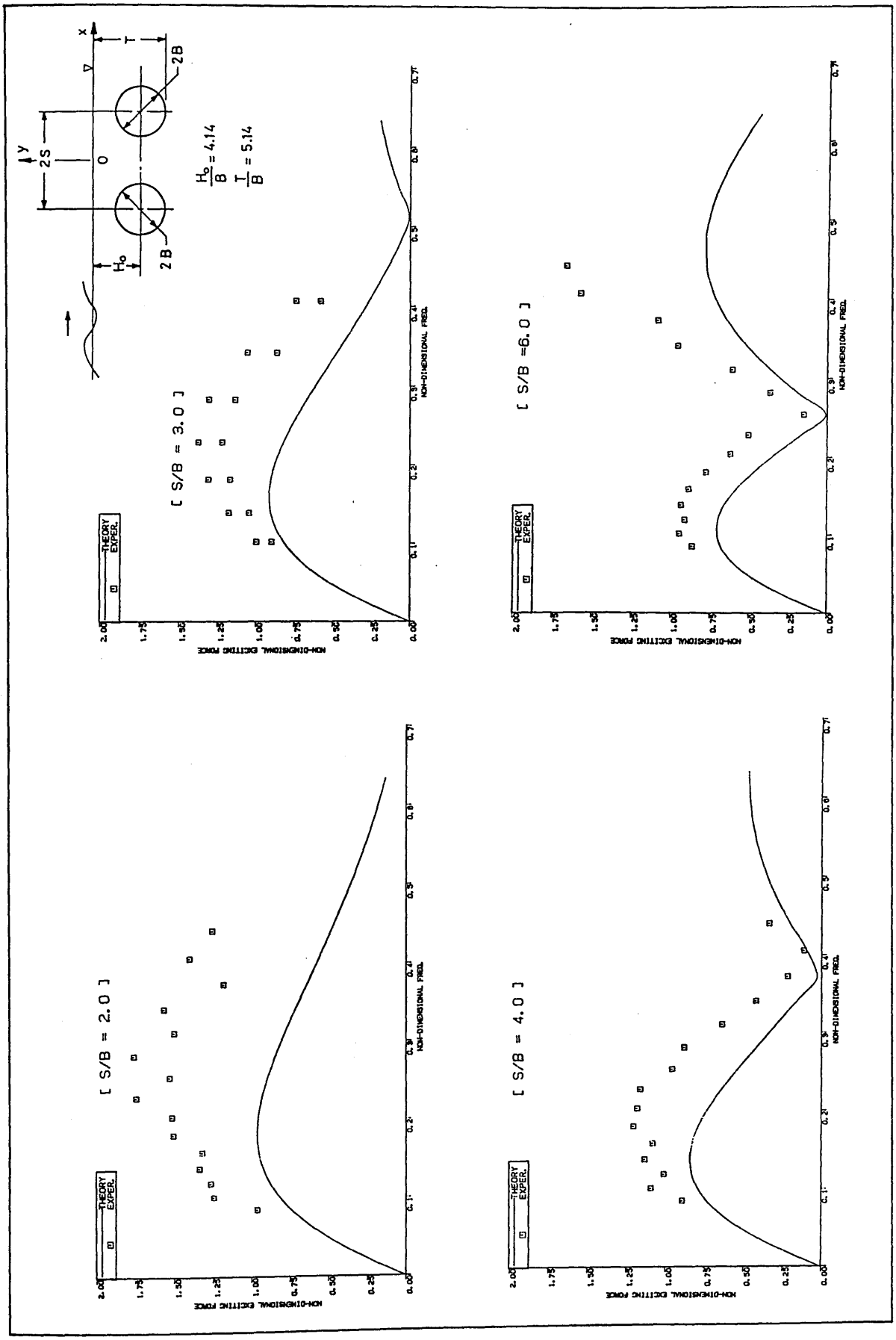

Fig. 156 - Comparison of the experiment and theory for the sway exciting force on the twin circular hulls at various hull separations

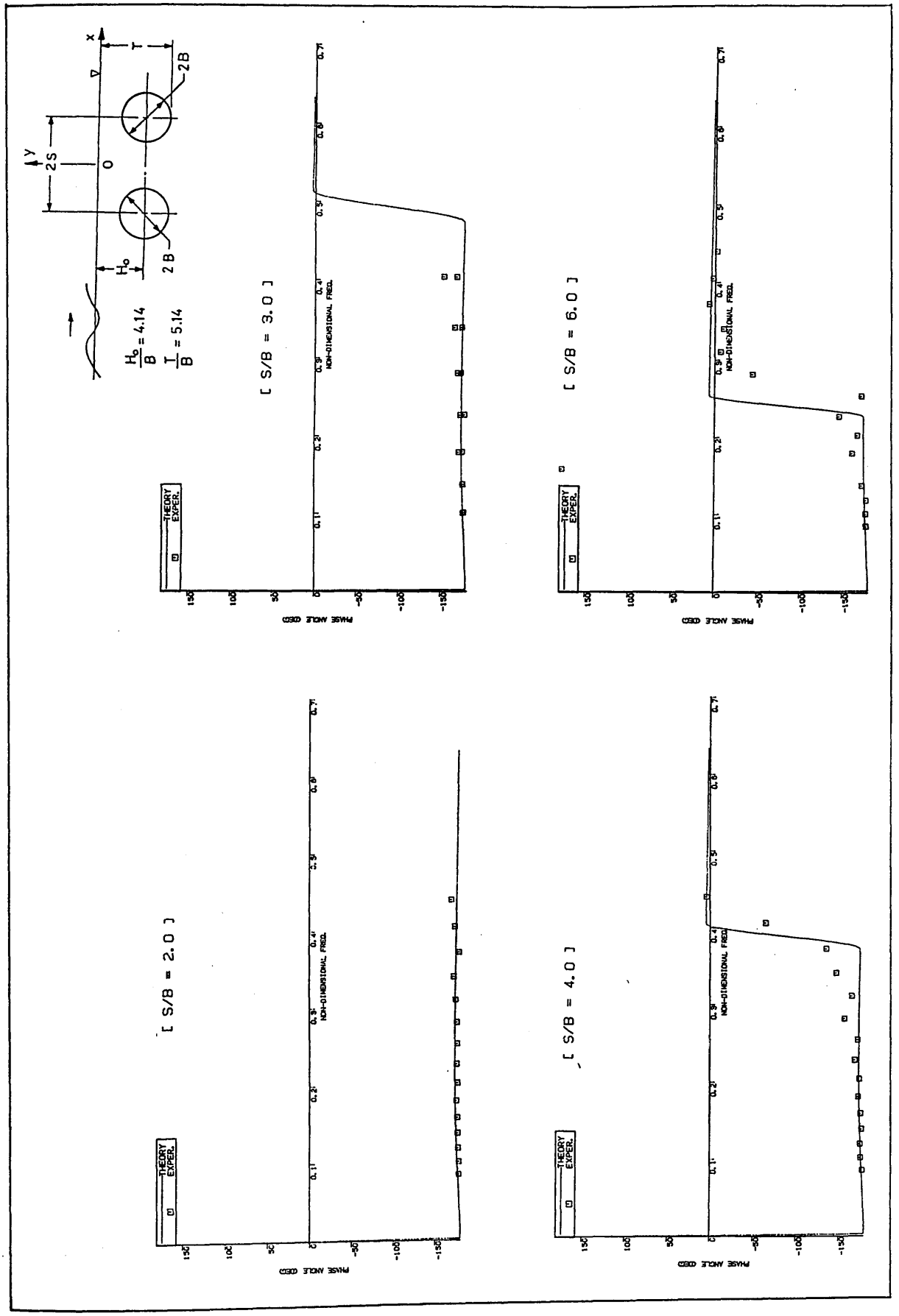

Fig. 157 - Comparison of the phase angles of the sway exciting force on twin circular hulls at various hull separations

4.3 FIRST-ORDER MOTION RESPONSE

In section 4.3 the first-order oscillatory hydrodynamic loads are formulated and computed in terms of the wave and motion-induced hydrodynamic coefficients. The wave-induced force/moment coefficients are assumed linearly proportional to the incident wave and presented as the wave-exciting force/moment per unit wave amplitude. The motion-induced coefficients, the added mass/inertia and damping, are assumed linearly proportional to the acceleration and velocity of the motion response and presented as the inertial force/moment, F_A, per unit acceleration and the potential damping force/moment, F_B, per unit velocity, Table 25.

In order to obtain these motion-induced force components (radiation forces) and their contribution to the steady wave-induced tilting moment, the vessel's oscillatory motion displacement should be known. From the motion displacements, the velocity, acceleration and thus the radiation force/moments are obtained by multiplying these terms with earlier computed added mass and damping coefficients. Moreover, the change in the direction of the distance vector, defined in section 4.2.1, induced by the roll motion can be calculated when the vessel's roll motion is known.

4.3.1 *Outline of Theoretical Approach for the First-Order Motions*

The prediction of the motions of a twin-hull semi-submersible are based on various methods (e.g. Morison's formula, strip theory, three-dimensional source distribution technique, etc.). In the following a method based on the strip theory[66,51] is used to predict the motion response of the model in regular beam seas and the computations are carried out for the upright position.

The solution of the first-order motion equation at a tilted position brings about a more complex motion problem compared to that in the upright position or alternatively the solution of this equation for the upright position has great simplifications compared to that in a more general tilted position in terms of the coefficients involved in the motion equation[89].

Therefore, although the formulation of the method is given in general form, numerical results are only presented for the semi-submersible model in the upright position. However, the effect of steady tilt on the motion equation is discussed wherever it is appropriate although the numerical calculations have not been carried out.

The effects of several parameters such as the hydrodynamic interference, the presence of surface-piercing columns, the hydrodynamic coupling and differing $\overline{GM}$s on the motion responses have been investigated.

4.3.2 *Formulation of the Theoretical Method*

It is assumed that when the semi-submersible oscillates about a mean position, which could be the upright or any tilted position, its response motions resulting from the first-order oscillatory loads are small in magnitude to justify the linear theory assumptions. The fluid is assumed ideal fluid and thus the effect of viscosity and the viscous fluid force, F_V, is neglected. Moreover, the semi-submersible has longitudinal and transverse symmetry in its upright condition and is positioned beam onto the regular wave trains. Thus, only the in-plane modes of motions (i.e. sway, heave and roll) take place.

According to Newton's second law, the previously defined hydrodynamic loads, F_R, F_W and the hydrostatic restoring load F_C, which is assumed linearly proportional to the motion displacement, will be

balanced by the inertial force, which is proportional to the acceleration of the motion. This results in the following 3 degrees of freedom motion equation:

$$\sum_{k=2}^{4} (M_{jk} + A_{jk})\ddot{s}_k + B_{jk}\dot{s}_k + C_{jk}s_k = F_j \qquad \ldots \quad (27)$$

where k = mode of motion and takes 2,3 and 4 for sway, heave and roll respectively

j = mode of excitation and takes the values similar to k for the corresponding modes

M_{jk} = mass matrix containing the mass, mass moment of inertia and products inertia of the body

A_{jk} = added mass and added moment of inertia matrix per unit acceleration

B_{jk} = damping force and moment of inertia matrix per unit velocity

C_{jk} = restoring force and moment matrix per unit displacement

F_j = complex wave-exciting force and moment matrix per unit wave amplitude

In eq. (27) since the right-hand side is complex

$$F_j = RE\ \{\bar{F}_j\ e^{-i\omega t}\} \qquad \ldots \quad (28)$$

the resulting motion displacements s_k are assumed to be complex as follows:

$$s_k = RE\ \{\bar{s}_k\ e^{-i\omega t}\} \qquad \ldots \quad (29)$$

where $\bar{F}_j = F_{jR} + i\ F_{jI}$ ... (30)

and $\bar{s}_k = s_{kR} + i\ s_{kI}$ ... (31)

From eq. 29, the velocity and acceleration of the motion are written as follows:

$$\dot{s}_k = -i\omega \bar{s}_k e^{-i\omega t}$$
$$\ddot{s}_k = -\omega^2 \bar{s}_k e^{-i\omega t} \quad \ldots \quad (33)$$

By substituting eqs 28 and 33 into 27 and omitting the time factor $e^{-i\omega t}$ in both sides of the equation:

$$\sum_{k=2}^{4} (M_{jk} + A_{jk})(-\omega^2 s_k) + B_{jk}(-i\omega \bar{s}_k) + C_{jk}(\bar{s}_k) = \bar{F}_j \quad \ldots \quad (34)$$

The elements of the matrices in eq. 34 are as follows.

Mass Matrix (M_{jk})

The elements of the generalised mass matrix take the following values in the upright position:

$$M_{22} = M_{33} = \rho\nabla,\ M_{44} = I_{44},\ M_{23} = M_{32} = M_{24} = M_{42} = M_{34} = M_{43} = 0$$

where ∇ is volume displacement,

I_{44} is the mass moment of inertia of the semi-submersible about the rolling axis.

In a tilted position the major change will be in the moment of inertia term since the instantaneous position of the members of the semi-submersible will be different relative to that in the upright position.

Added Mass (A_{jk}) *and Damping* (B_{jk}) *Matrix*

When the semi-submersible oscillates harmonically in the initially calm water, it induces symmetric or asymmetric flow-fields depending on the mode of oscillation. This can be observed as radiating surface waves in a form of cosine or sine wave as appropriate to the symmetric heave or asymmetric sway and roll motions respectively.

Consider in the general case a beamwise strip contour of the semi-submersible which is forced to oscillate in any of the k^{th} in-plane modes (e.g. heave, k=3) with the motion amplitude s_k (e.g. s_3 for heave).

The disturbance of the fluid caused by this mode of oscillation induces coupled forces on the strip contour in all the in-plane modes (e.g. if the section is forced to oscillate in the heave mode, it induces forces and moments in the sway and roll mode as well as the force in the heave mode). Thus, the induced forces and moments will have the acceleration component $\omega^2 a_{jk}$ and the velocity ωb_{jk} component in different directions depending on the flow-field generated (e.g. symmetric heave motion induces coupled sway forces ($\omega^2 a_{23}$, ωb_{23}), coupled roll moment ($\omega^2 a_{43}$, ωb_{43}) and pure heave forces ($\omega^2 a_{33}$, ωb_{33})).

As appropriate to the hulls of the semi-submersible, let subscript $\underline{s}$ and $\underline{\ell}$ denote the hydrodynamic quantities belonging to the seaward and leeward demi-hull separately. In Table 28, the sectional resultant added mass and damping for a twin-section by omitting the subscript ($\underline{s} + \underline{\ell}$) are presented by summation of the element loads for one demi-hull (e.g. seaward demi-hull $\underline{s}$ is chosen in Table 28). These relations are given in ref. [66] and based on the assumptions that the semi-submersible is symmetric with respect to the vertical centre plane and oscillates about the upright position with small motion amplitude.

Sectional Added Mass for Twin-Hull ($\underline{s}+\underline{\ell}$)	Sectional Damping for Twin-Hull ($\underline{s}+\underline{\ell}$)
$a_{22} = 2[a_{22}]_{\underline{s}}$	$b_{22} = 2[b_{22}]_{\underline{s}}$
$a_{23} = 0$	$b_{23} = 0$
$a_{24} = 2[a_{24}]_{\underline{s}}$	$b_{24} = 2[b_{24}]_{\underline{s}}$
$a_{32} = 0$	$b_{32} = 0$
$a_{33} = 2[a_{33}]_{\underline{s}}$	$b_{33} = 2[b_{33}]_{\underline{s}}$
$a_{34} = 0$	$b_{34} = 0$
$a_{42} = 2[a_{42}]_{\underline{s}}$	$b_{42} = 2[b_{42}]_{\underline{s}}$
$a_{43} = 0$	$b_{43} = 0$
$a_{44} = 2[a_{44}]_{\underline{s}}$	$b_{44} = 2[b_{44}]_{\underline{s}}$

Table 28 - The resultant sectional hydrodynamic forces and moments due to motion of the semi-submersible

In the above analysis the rotation centre has been taken at the origin (0) of the wave axis system which lies on the calm water surface. However, in practice the rotation centre is usually taken at the centre of the gravity. Therefore, in the following integral expression of the total hydrodynamic loads, the sectional element loads are transferred to the centre of the gravity in the vertical direction[66]. Eventually the elements of the added mass matrix A_{jk} and the damping matrix B_{jk} are obtained by integrating the sectional values along the z-axis as follows:

$$A_{22} = \int_{-L1}^{L2} a_{22}dz \qquad B_{22} = \int_{-L1}^{L2} b_{22}dz$$

$$A_{24} = A_{42} = \int_{-L1}^{L2} (a_{24} \pm \overline{OG}\, a_{22})dz \qquad B_{24} = B_{42} = \int_{-L1}^{L2} (b_{24} \pm \overline{OG}\, b_{22})dz$$

$$A_{33} = \int_{-L1}^{L2} a_{33}dz \qquad A_{33} = \int_{-L1}^{L2} b_{33}dz \qquad \ldots \quad (35)$$

$$A_{44} = \int_{-L1}^{L2} [a_{44} \pm \overline{OG}(2a_{24} \pm \overline{OG}\, a_{22})]dz \qquad B_{44} = \int_{-L1}^{L2} [b_{44} \pm \overline{OG}(2b_{24} \pm \overline{OG}\, b_{22})]dz$$

$$A_{23} = A_{32} = A_{34} = A_{43} = 0 \qquad B_{23} = B_{32} = B_{34} = B_{43} = 0$$

where $\int_{-L1}^{L2}$ = denotes integration of the sectional values along the semi-submersible length,

$\pm$ OG = distance between the origin (O) and the centre of gravity (G)

the (+) sign is taken for (G) above (O)

the (-) sign is taken for (G) below (O).

As stated above the relations given in Table 28 are based on the semi-submersible being in the upright condition. However, when the semi-submersible is in a tilted position, there will be a requirement to calculate the force coefficients of each demi-hull in its

tilted position. This will result in non-zero coupled coefficients (i.e. a_{32}, b_{32}, a_{23}, b_{23}, a_{34}, b_{34}, a_{43}, b_{43}) which are balanced out in the upright position due to symmetry.

Wave-Exciting Force Matrix (F_j)

Under the similar symmetry assumptions made for the radiation problem, when the strip contour, which is rigidly held in the upright position, encounters the incident wave the resultant forces exerted on the twin-hull are related to that on one hull in terms of the symmetric (even) and asymmetric (odd) component of the incident wave as follows[66]:

$$\begin{aligned} f_2 &= 2\left[f_2^{(o)}\right]_{\underline{s}} \\ f_3 &= 2\left[f_3^{(e)}\right]_{\underline{s}} \\ f_4 &= 2\left[f_4^{(o)}\right]_{\underline{s}} \end{aligned} \qquad \ldots \quad (36)$$

The integration of the sectional forces along the z-axis yields the total wave-exciting forces per unit amplitude of the incident wave as follows:

$$\begin{aligned} \frac{F_2}{a} &= \int_{-L1}^{L2} f_2 dz \\ \frac{F_3}{a} &= \int_{-L1}^{L2} f_3 dz \\ \frac{F_4}{a} &= \int_{-L1}^{L2} f_4 dz \end{aligned} \qquad \ldots \quad (37)$$

In a tilted position the relations given by eq. 36 will not be valid since the magnitude of the forces on each demi-hull will not be equal due to asymmetry. Therefore the forces on each demi-hull section should be calculated separately and the resultant force on the twin section should be the summation of these forces by taking into account the phase relation between them.

Restoring Force Matrix (C_{jk})

The elements of generalised restoring force matrix take the following values in the upright position:

$C_{22} = 0$ (or C_k if mooring or anchoring is considered),

$C_{33} = \rho g A_w$, $C_{44} = \rho g \nabla \overline{GM}$, $C_{23} = C_{32} = C_{24} = C_{42} = C_{43} = C_{34} = 0$

where C_k is stiffness of the mooring or anchoring,

A_w is the waterplane area, and

$\overline{GM}$ is the height of the transverse metacentre above the centre of gravity.

When the semi-submersible is in a tilted position the waterplane and the restoring moment arm will be different relative to that in the upright position. Moreover, the coupled elements in the heave and roll mode become non-zero[89]. However, since semi-submersibles usually have small waterplane areas and relatively small $\overline{GM}$s to develop large tilts, the changes, due to asymmetry, in the matrix coefficients may not be so important.

If eq. 34 is expanded for the three modes of motions by accounting for the simplifications in the upright position, resulting from the real and imaginary part of the equations, the following matrix form of the equation is obtained[51]:

$$\begin{bmatrix}
C_{22}-\omega^2(M_{22}+A_{22}) & 0 & -\omega^2 A_{24} & \omega B_{22} & 0 & \omega B_{24} \\
0 & C_{33}-\omega^2(M_{33}+A_{33}) & 0 & 0 & \omega B_{33} & 0 \\
-\omega^2 A_{42} & 0 & C_{44}-\omega^2(M_{44}+A_{44}) & \omega B_{24} & 0 & \omega B_{44} \\
-\omega B_{22} & 0 & -B_{24} & C_{22}-(M_{22}+A_{22}) & 0 & -\omega^2 A_{24} \\
0 & -\omega B_{33} & 0 & 0 & C_{33}-\omega^2(M_{33}+A_{33}) & 0 \\
-\omega B_{42} & 0 & -\omega B_{44} & -\omega^2 A_{42} & 0 & C_{44}-\omega^2(M_{44}+A_{44})
\end{bmatrix} \times \begin{bmatrix} S_{2R} \\ S_{3R} \\ S_{4R} \\ S_{2I} \\ S_{3I} \\ S_{4I} \end{bmatrix} = \begin{bmatrix} F_{2R} \\ F_{3R} \\ F_{4R} \\ F_{2I} \\ F_{3I} \\ F_{4I} \end{bmatrix}$$

By solving these six-linear equations for the real s_{kR} and imaginary s_{kI}, the resulting motion displacement s_k are obtained as follows:

from eq. 29, $$s_k = |s_k| \cos(\alpha_k - \omega t) \quad \ldots \quad (38)$$

with $$|s_k| = (s_{kR}^2 + s_{kI}^2)^{\frac{1}{2}} \quad \ldots \quad (39)$$

$$\alpha_k = \tan^{-1}(s_{kI}/s_{kR}) \quad \ldots \quad (40)$$

where $|s_k|$ = maximum of the motion displacement

α_k = phase shift of the maximum of the motion displacement from the maximum of the incident wave at the origin (0) of the wave-axis system.

4.3.3 *Computations for the First-Order Motion Response*

In this section the first-order oscillatory motions of the model used in the experiments are computed, based on the theoretical methods presented earlier. The three degrees of freedom motion equation is solved for sway, heave and roll response of the model in its upright position for regular beam seas. Theoretical results are compared with the experimental motion data for the largest $\overline{GM}$ value. The effect of hydrodynamic interference, presence of the columns, hydrodynamic coupling and differing $\overline{GM}$s on the motion response are investigated.

Presentation of Results

The motion response in each mode is represented by motion amplitude-to-wave amplitude ratio versus non-dimensional frequency. This provides the non-dimensional "Response Amplitude Operator" (RAO - m/m) in the heave and sway mode, whereas it has the units (degree/m) in the roll mode. The accompanying phase angle (α_k) are presented in degrees wherever it is appropriate. The experimental data is presented in the heave and roll mode since no experimental data was taken in the sway mode.

The data required for the computations of the elements in the hydrostatic and restoring matrix are obtained from the model characteristics at 0.36 m draught given in Chapter 3 and Appendix II.1.

In order to simulate the existence of moorings it is assumed that the model moves with a natural period of $T_m \simeq 18$ s which corresponds to a natural period of 150 s for the prototype. Thus the restoring force coefficient C_{22} (or C_k) can be obtained by the following relation:

$$C_{22} = 4\pi^2 \left(\frac{M_{22} + A_{22}}{T_m^2} \right) \simeq 28.52 \text{ N m}^{-1}$$

where $M_{22} = 58.3$ kg (at 0.36 m draught)

$A_{22} = 174.5$ kg (at a period of 18 sec)

In Figs 158 to 161 the results are presented for each mode of motion showing a comparison of the results when accounting for the hydrodynamic interference between the demi-hulls and for the demi-hulls in isolation. The figures for the heave and roll motion also include the experimental results at $\overline{GM} = 0.019$ m and 0.079 m.

In Figs 162 and 163 the effect of the hydrodynamic coupling between the sway and roll mode on the motion response are presented.

Figures 164 to 167 illustrate the effects of the columns on each mode of motion response without the hydrodynamic interference between the demi-hulls and the hydrodynamic coupling.

In Figs 168 and 169 the effect of metacentric height, $\overline{GM}$, on the sway and roll motion response curve is shown for two limiting $\overline{GM}$s tested ($\overline{GM}_{min} = 0.019$ m and $\overline{GM}_{max} = 0.079$ m).

Discussion of Results

The following theoretical results are based on the assumption that the model oscillates about its upright position. Therefore the experimental data with the highest $\overline{GM}$ tested, at which practically no tilt occurred, are essential for the comparison.

As shown in Figs 158 and 159 the agreement between the theory and experiment in the heave mode is good for the moderate and high frequencies while it is poor at low frequencies in particular at the resonance region.

In the roll mode as illustrated in Fig. 161, the agreement between the theory and experiment is worst at low frequencies and improves with increasing frequencies. The discrepancy in the low frequency region for both mode of motions can be attributed to several factors. Among these, the effect of viscosity, which is accentuated in this region with the large amplitude of resonant behaviour, three-dimensional effects due to the column parts and possible experimental errors.

(i) Effect of the Hydrodynamic Interference

As shown in Figs 158 to 161, the inclusion of the hydrodynamic interference into the computations brings about some fluctuations at the particular frequencies encountered during the analysis of the hydrodynamic forces.

The fluctuation in the heave mode at about the non-dimensional frequency of 0.10 is induced by the irregular frequency problem which does not represent any physical condition and thus it should be disregarded.

The fluctuation at about the non-dimensional frequency of 0.3 in the sway and to a lesser extent in the roll mode is induced by the resonant frequency phenomenon. As shown in Fig. 161, there is no scatter in the

experimental roll motion data about this frequency indicating the two-dimensional resonant behaviour.

However, if these fluctuations are disregarded the practical importance of the hydrodynamic interference is negligible, but slightly improves the motion prediction in the low frequency range for the heave and roll mode.

(ii) Effect of Hydrodynamic Coupling between the Sway and Roll

The inclusion of the hydrodynamic coupling between the sway and roll mode introduces the effect of $\overline{GM}$ on the sway motion response so that the sway motion increases with decreasing $\overline{GM}$ as shown in Fig. 162. The uncoupled motion equation automatically disregards the effect of $\overline{GM}$ on the sway motion.

As illustrated in Figs 162 and 163 the inclusion of the hydrodynamic coupling increases both sway and roll motion response. Despite the theoretical need to include this term, the inclusion of the coupling effect decreases the accuracy of the prediction in the roll mode, Fig. 163. This can be related to the increasing errors due to the three-dimensional effects, which are accentuated for the asymmetric modes, in (or by) the asymmetric coupling coefficient as well.

(iii) Effect of Columns

The above case is complicated due to the hydrodynamic interference and coupling effect, and therefore it is desirable to examine the situation when these effects are not present.

As shown in Figs 164 and 165, the inclusion of the columns within the theory presented demonstrates a much better prediction indicating that the beamwise strip method can be used to represent the column effect in the heave mode.

As illustrated in Fig. 166, the effect of columns increases the motion response of the model with two lower hulls throughout the frequencies tested.

In the roll mode, the inclusion of the columns decreases the response motion of the lower hulls displaying better accuracy in comparison with experiments, Fig. 167.

(iv) Effect of $\overline{GM}$

Since the coupling between the heave and roll is cancelled out in the upright position, the heave motion response will not be affected by any change in $\overline{GM}$. However, as shown in Figs 168 and 169, as the $\overline{GM}$ increases the sway and roll response decreases. This effect is strong in the low frequency region and diminishes with increasing frequency.

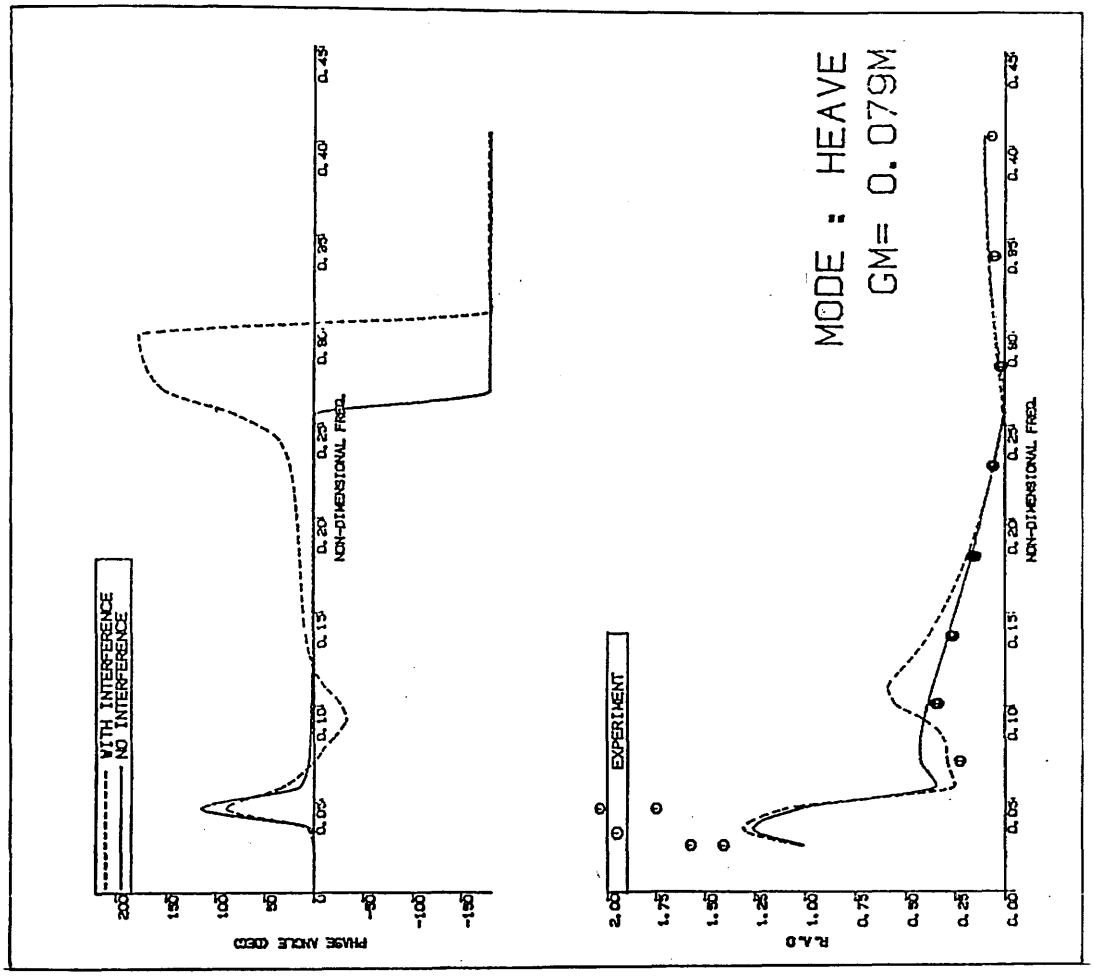

Fig. 159 - Heave motion response of the semi-submersible model displaying the effect of hydrodynamic interference for GM = 0.079 m

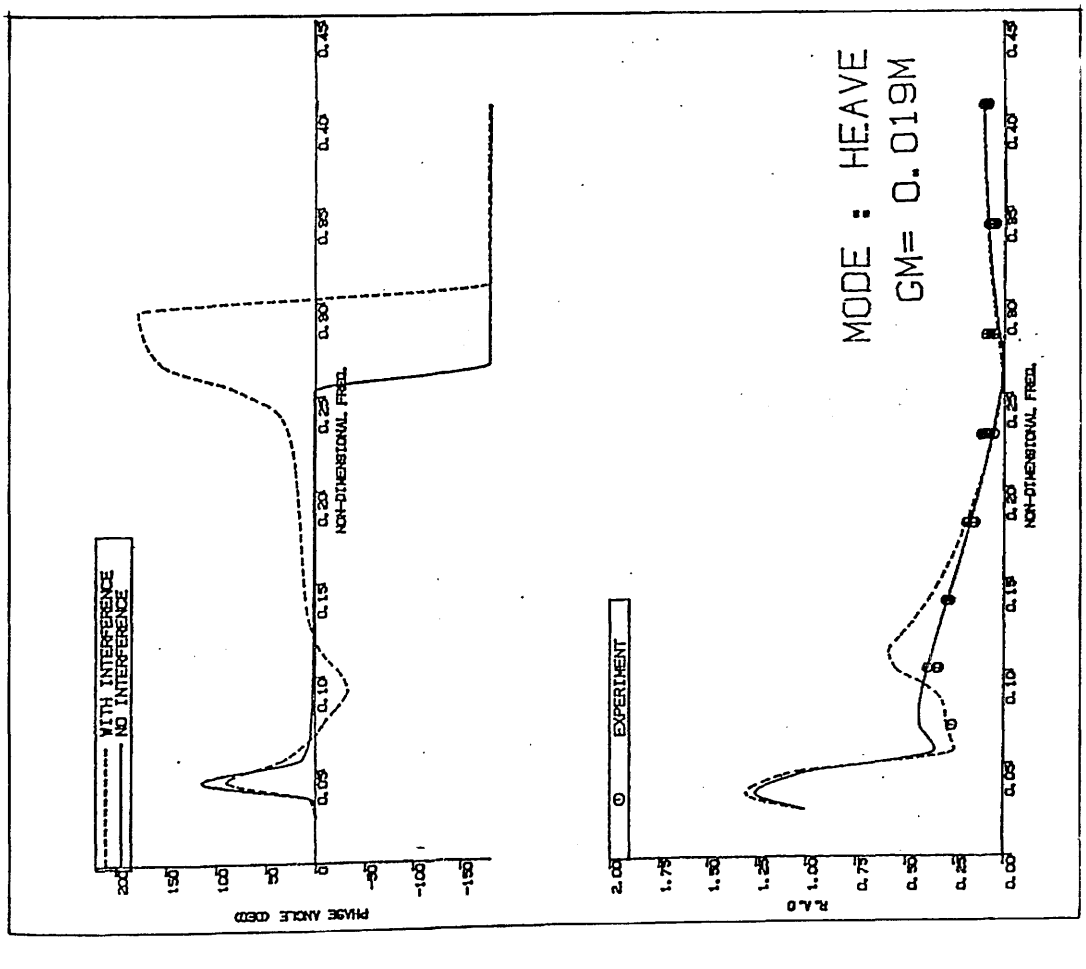

Fig. 158 - Heave motion response of the semi-submersible model displaying the effect of hydrodynamic interference effect for GM = 0.019 m

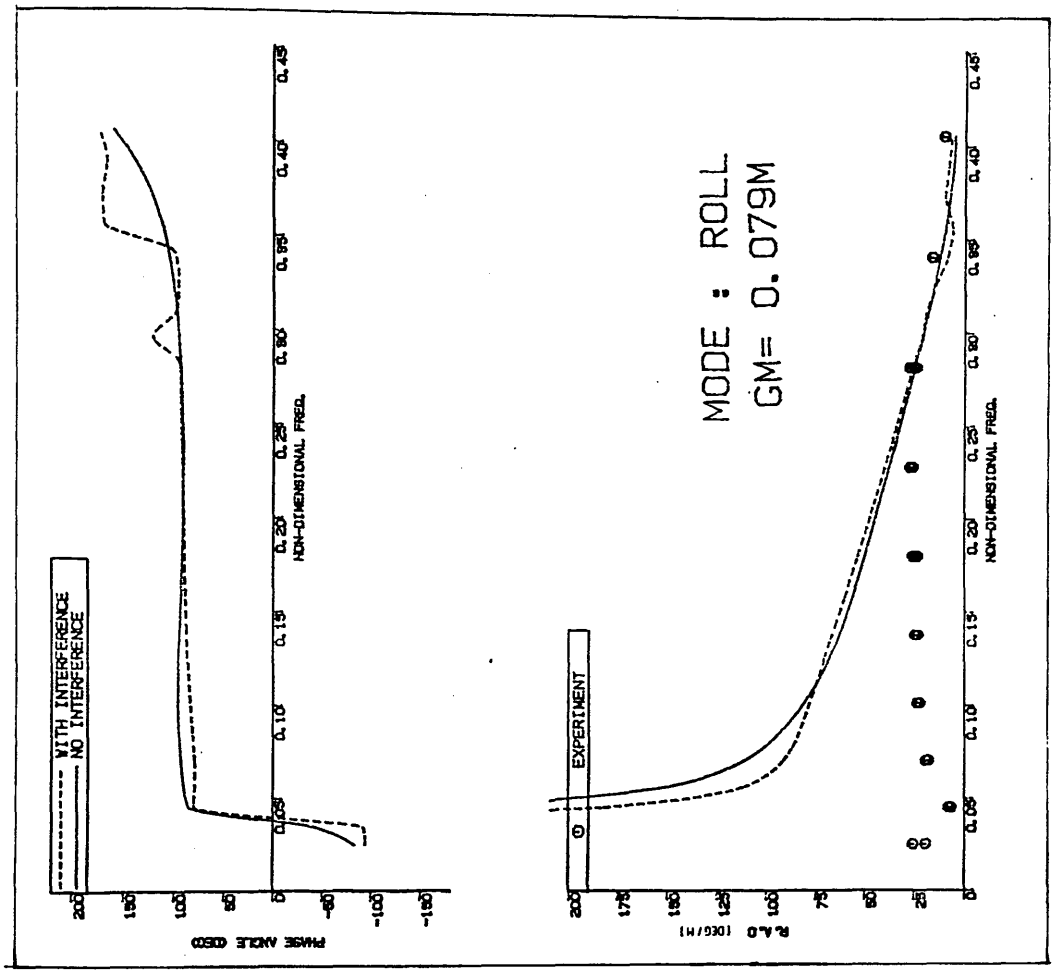

Fig. 161 - Roll motion response of the semi-submersible model displaying the effect of hydrodynamic interference for GM = 0.079 m

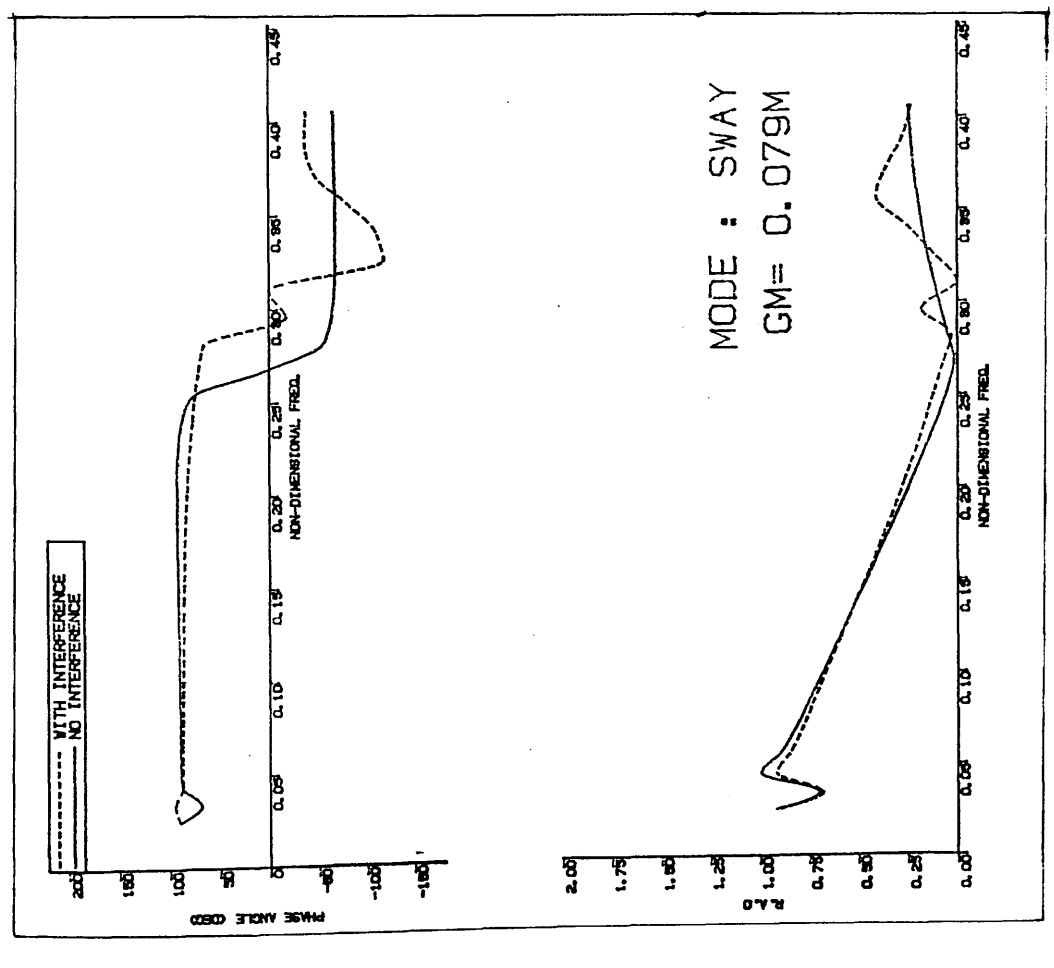

Fig. 160 - Sway motion response of the semi-submersible model displaying the effect of hydrodynamic interference for GM = 0.079 m

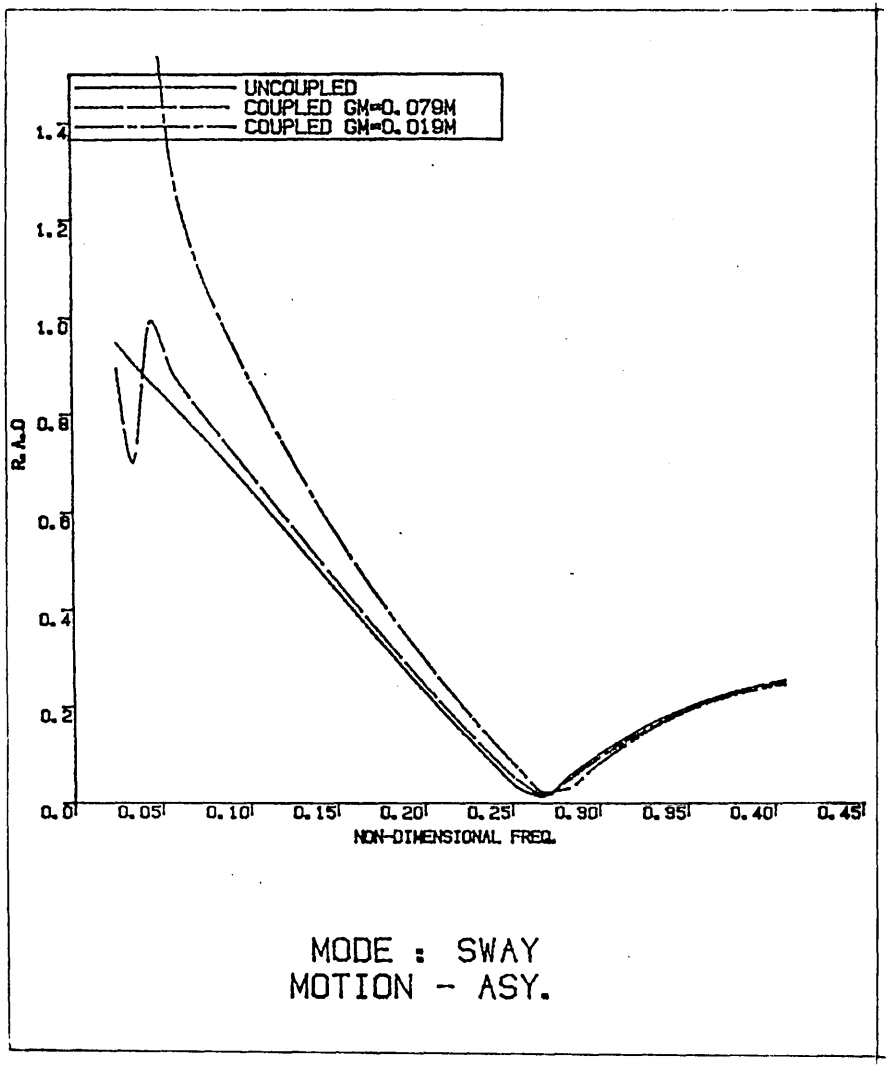

Fig. 162 - Illustration of the effect of hydrodynamic coupling between the sway and roll mode on the sway motion response of the model

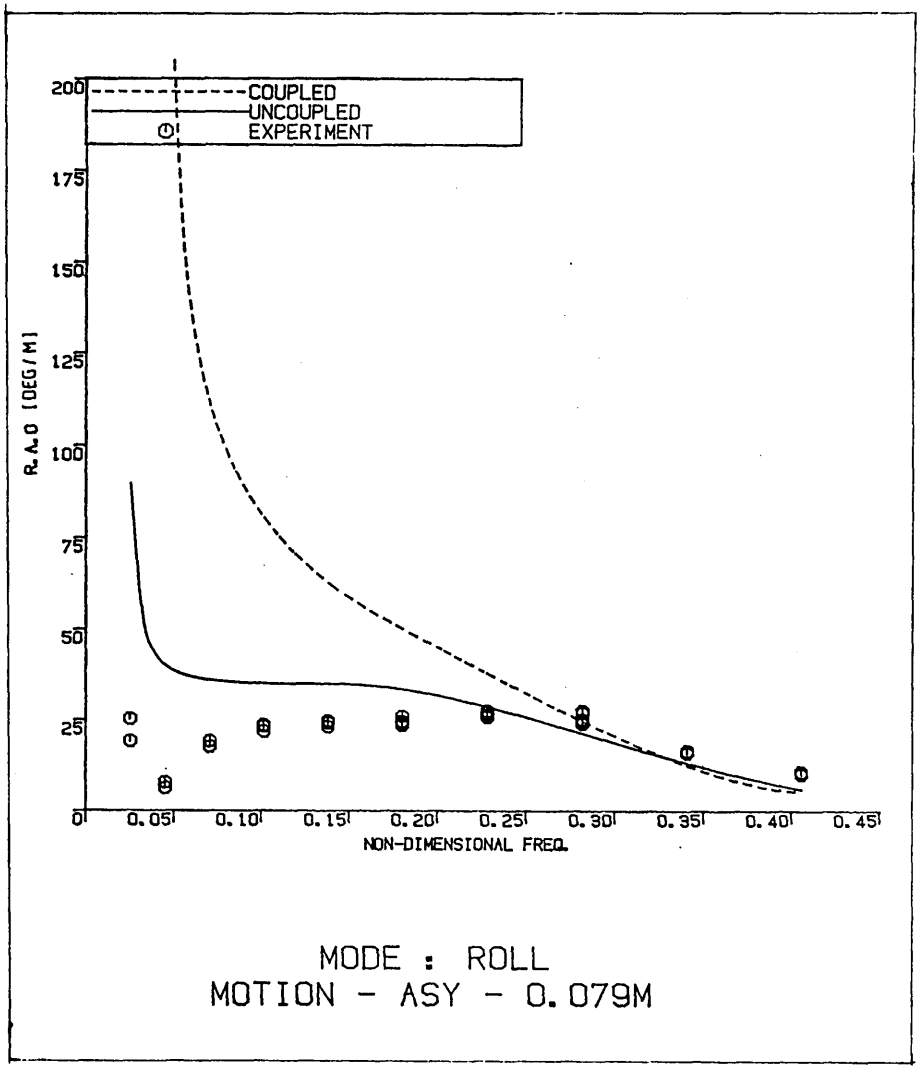

Fig. 163 - Illustration of the effect of hydrodynamic coupling between the sway and roll mode on the roll motion response of the model

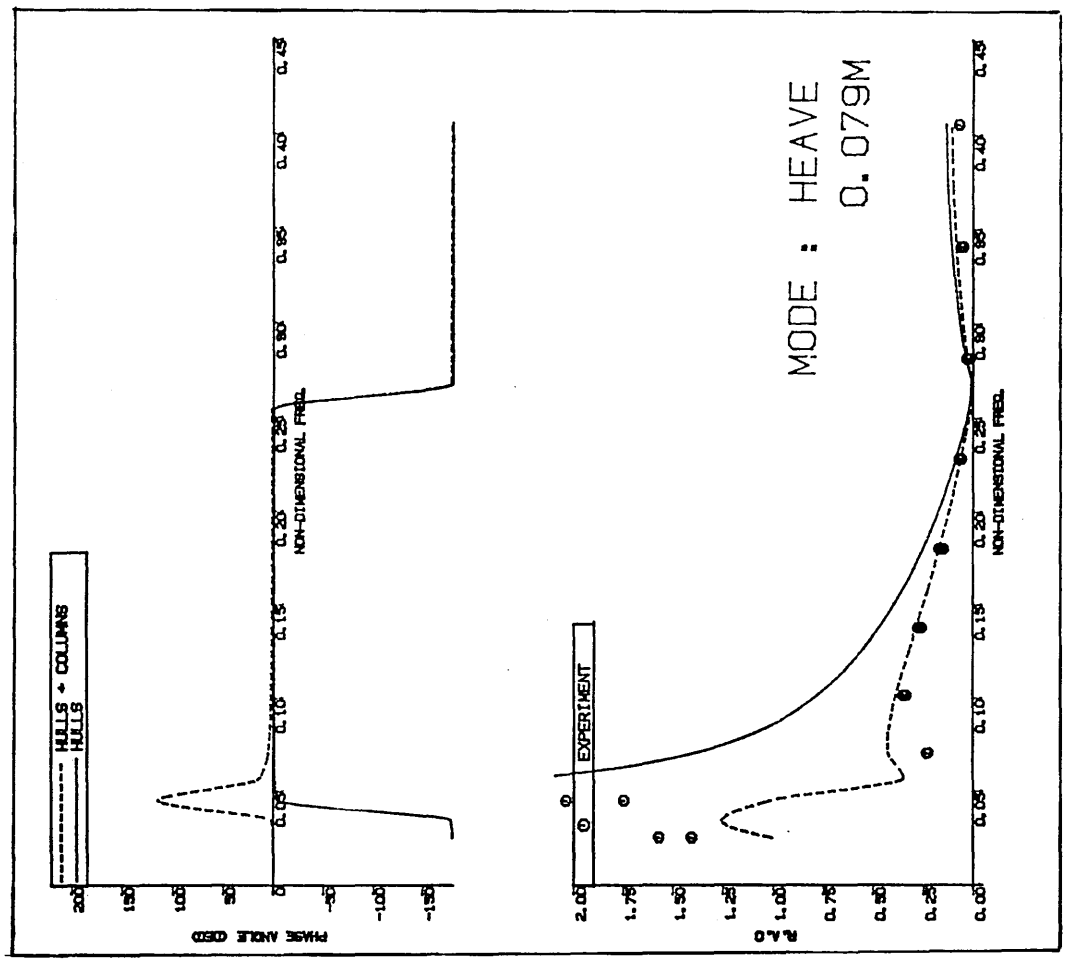

Fig. 165 - Effect of columns on the heave motion response of the model for $\overline{GM}$ = 0.079 m

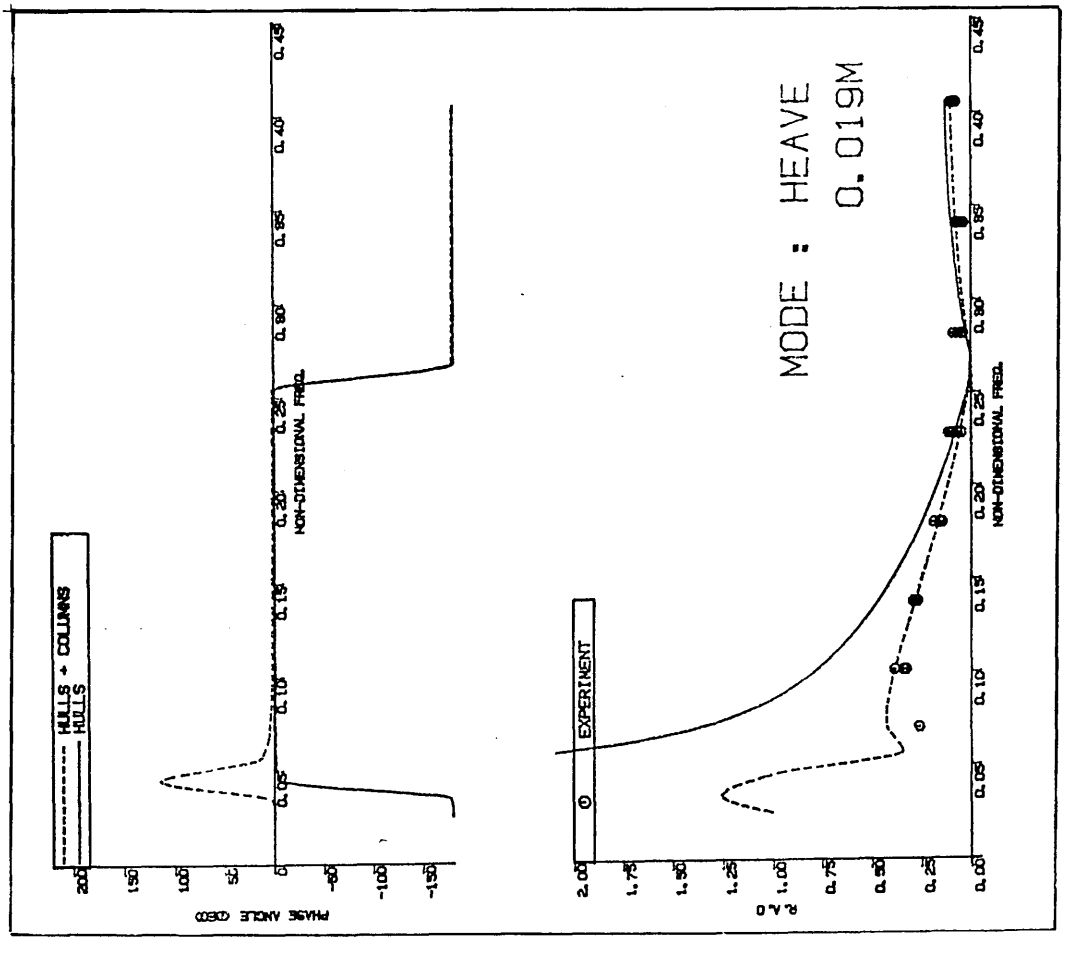

Fig. 164 - Effect of columns on the heave motion response of the model for $\overline{GM}$ = 0.019 m

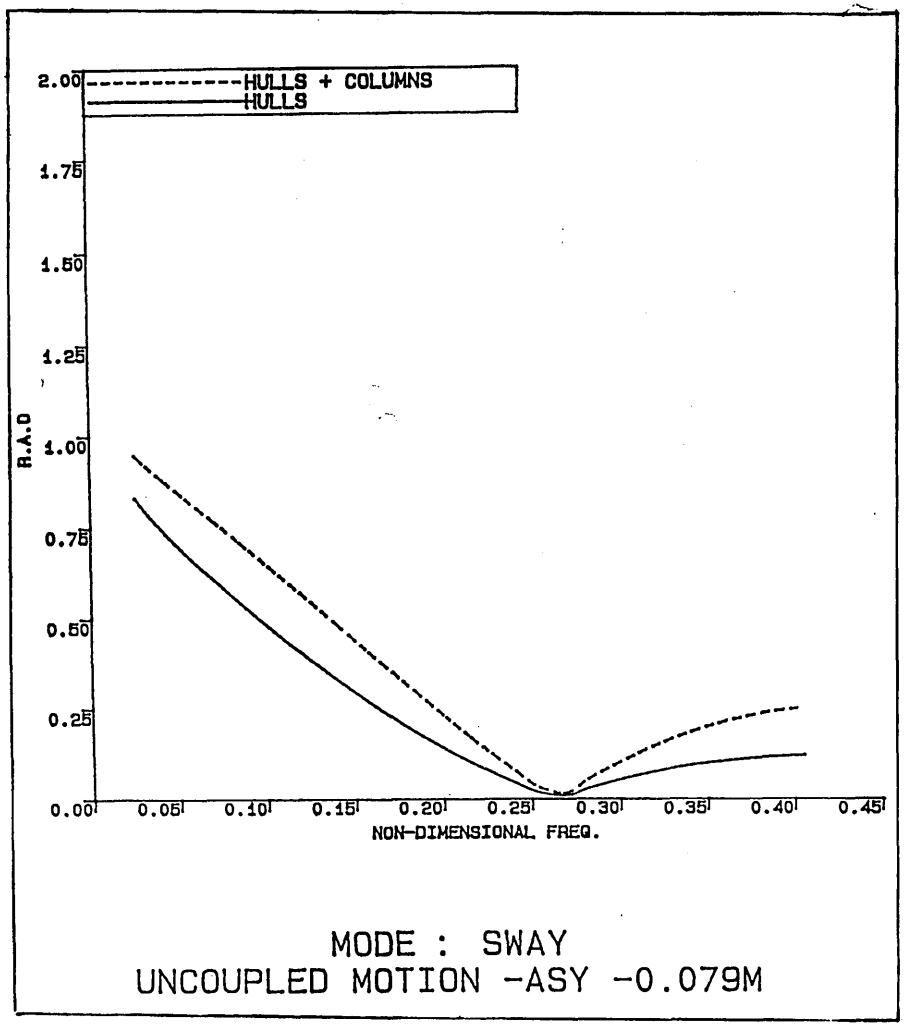

Fig. 166 - Effect of columns on the sway motion response of the model for $\overline{GM}$ = 0.079 m

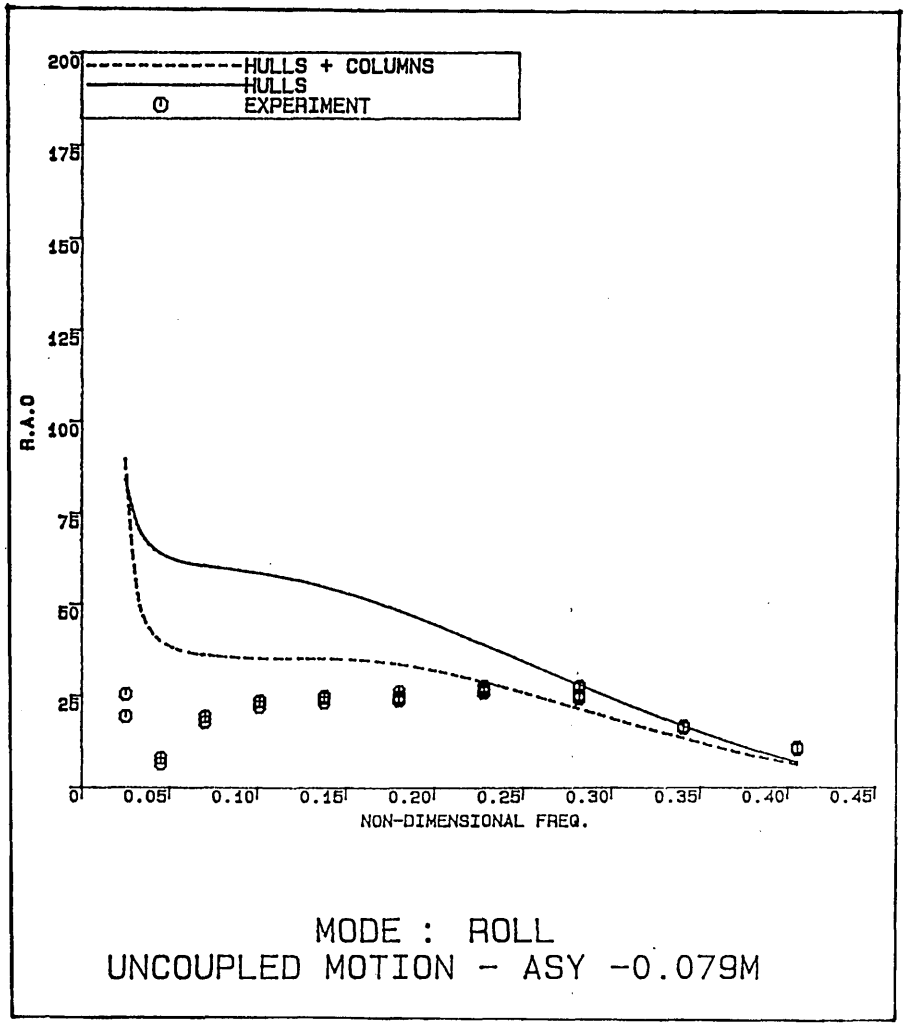

Fig. 167 - Effect of columns on the roll response motion of the model for $\overline{GM}$ = 0.079 m

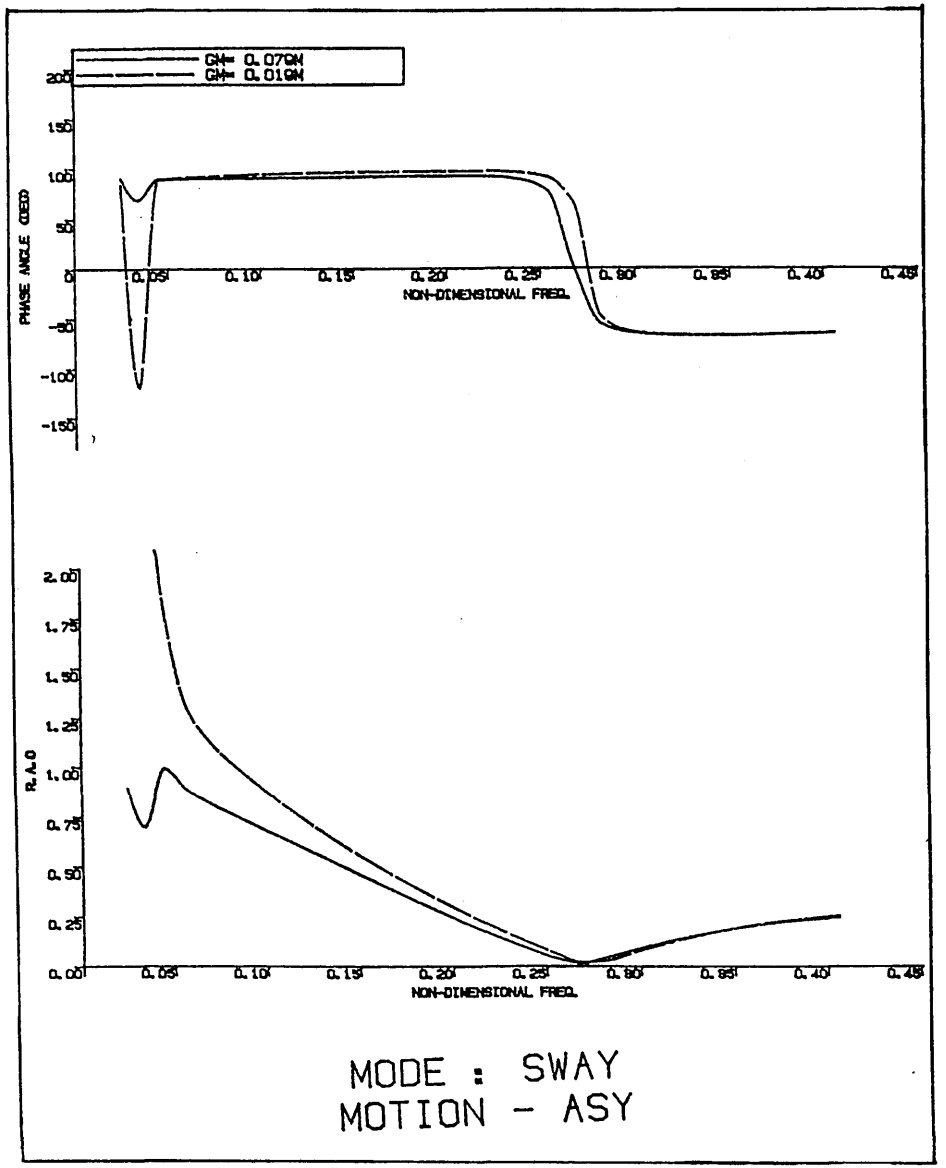

Fig. 168 - Effect of metacentric height ($\overline{GM}$) on the sway motion response of the model

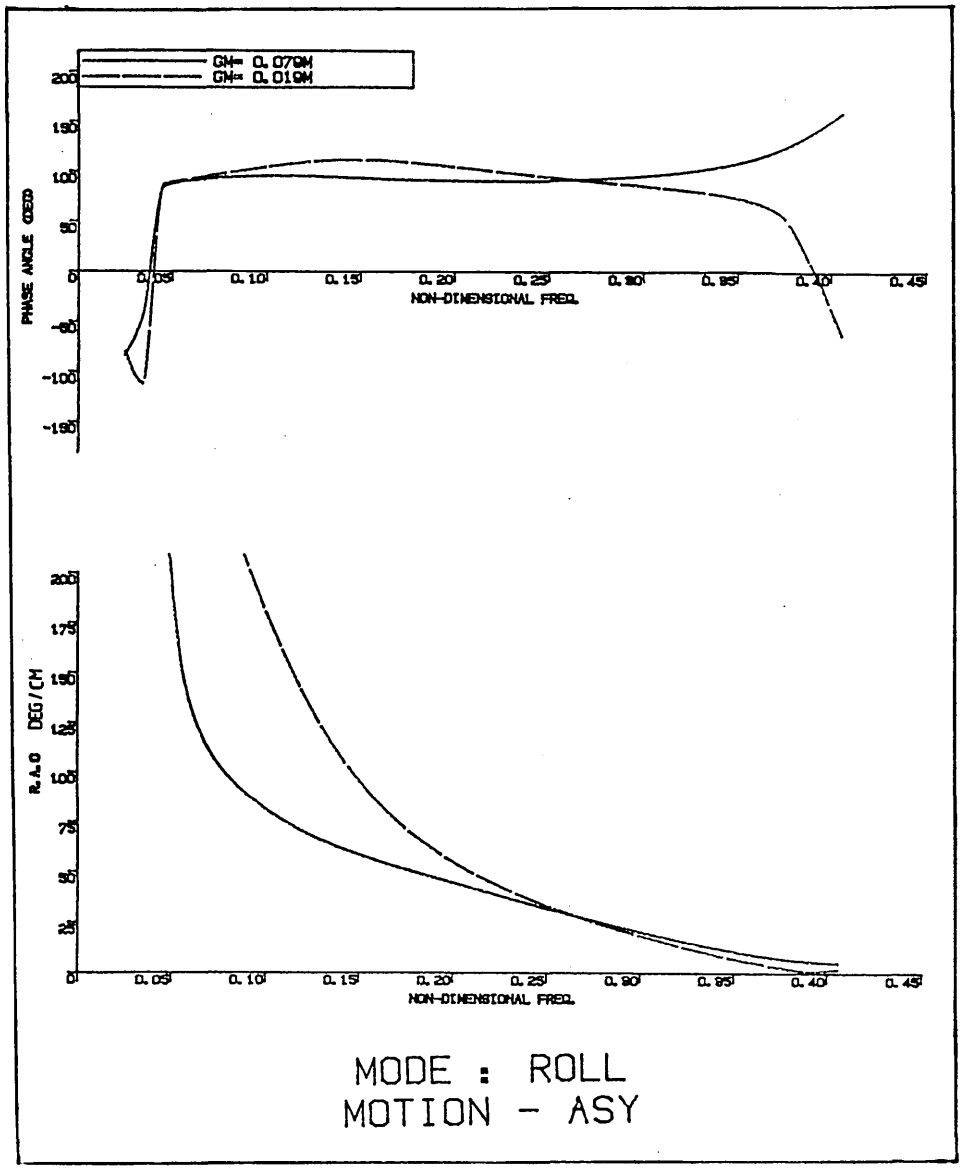

Fig. 169 - Effect of metacentric height ($\overline{GM}$) on the roll motion response of the model

4.4 SECOND-ORDER HYDRODYNAMIC FORCES

In spite of their small magnitudes, steady (mean) or slowly-varying (low-frequency) type of second-order forces and moments have important effects on semi-submersibles. Depending on the mode of excitation the response motion of the vessel can be magnified resulting in large excursions from the mean position when the vessel's restoring force or moment is such as to give a long natural period.

Semi-submersibles (and submarine vessels) experience relatively large second-order forces in the vertical direction as well as large drift forces in the horizontal direction because of their small (and non-existent) waterplane area and large submerged hulls. These forces are thought to be responsible for the long-period roll and heave motions of semi-submersibles[16,95] and for broaching problems of submarines near the free surface[30].

As reported in previous studies and observed in model tests referred to in Chapter 3, the steady tilt and heave motion of semi-submersible models with small $\overline{GM}$s has been also attributed to this steady vertical component.

Considering regular waves, the steady second-order forces can be defined as the time average of the hydrodynamic forces acting on a body. This steady component can be obtained by calculating the mean force over one period of a sinusoidal wave.

In section 4.1, it has been defined that the second-order forces are proportional to the square of wave height. However, in a general definition the term of second-order contains the product of two first-order terms which can be wave height, particle velocity, pressure, current velocity or vessel's motion response.

In the most general case the second-order forces can be grouped in two main categories based on the flow characteristics as follows:

(i) Potential Flow Forces (ii) Viscous Flow Forces

The research concerning second-order hydrodynamic forces was initially started for the prediction of the added resistance of ships[96,97,98]. Therefore attention was concentrated on the longitudinal component of potential steady forces in regular waves. In recent years with an increasing number of moored offshore structures, most of the research has been concentrated on these types of structures including random wave effects. Moreover there has been a need to calculate the steady viscous flow forces because of the range of dimensions of the members involved in these structures.

Major reviews of the theories developed and comparisons with some experimental work can be found in refs [14,58]. Briefly the existing theoretical methods can be grouped as follows:

(a) Using potential theory the steady forces are obtained by equating the change in the momentum of the surface waves in the far-field to the mean force exerted on the body. This method is called "The Far-field (Wave Momentum) Method" and the steady force depends on the first-order wave potential in the far-field (e.g. refs [99,100,101,102,103]).

(b) Using potential theory, the steady and the slowly-varying forces are obtained more straightforwardly from the direct integration of the fluid pressure on the instantaneous wetted surface. The method is termed "The Near-field (Direct Integration) Method" and the steady force depends on the first-order wave potential whereas the slowly-varying force depends on both the first- and second-order potential in the near-field (e.g. refs [31,104,14,58,105,106]).

(c) Using the empirical Morison Equation and the Relative Motion Concept the mean viscous drag component is obtained over one wave period (e.g. refs [12,92,93,94]).

(i) Steady Potential Flow Forces

From the point of view of the steady potential forces both methods, the near-field and the far-field, have some advantages relative to the other. Although the near-field method is more complicated and requires more computational effort it provides more insight into the mechanism by which waves and structures interact to produce these forces. Therefore it is used to illustrate the components of the steady potential forces in regular waves as follows.

The most comprehensive discussion of the second-order potential forces is given by Pinkster[14] who presented the contributions involved in these forces as follows:

I. Wave elevation II. Velocity head III. Body translation
IV. Body rotation V. Second-order wave

The first-order forces are induced by pressures acting over the mean wetted surface of the body. When the hydrostatic decay of this pressure, which includes diffraction effects, is considered from the mean waterline to the instantaneous free surface, this yields an additional steady force over one wave period. This is termed "wave-elevation (or relative wave height)" component.

The Bernoulli equation introduces a dynamic pressure in terms of the quadratic first-order wave particle velocities including diffraction effects. The integration of this dynamic pressure over the mean wetted surface yields a steady force component which is termed "Velocity head" component.

The first-order force represents pressures acting on the body as if it always occupies its mean position. In fact, because of the translational displacement of the body (heave, sway and surge) the pressure field slightly changes. Thus the integration of the product of this pressure gradient by the translational body displacement yields the steady "body translation" force component.

As the body rotates (in pitch, roll, yaw) the directions of the pressures, which act at right angles to the body's instantaneous surface, changes. For instance a roll angle will tilt the bottom of a rectangular pontoon so that the pressure in the vertical direction will give a horizontal force component which is the product of the heave pressure and the roll angle. Since the wave pressures integrated over the body surface can be expressed in terms of the body acceleration, the "body rotation" force component will be the product of the first-order rotational motion and body mass[91] and acceleration.

"The second-order wave" component is induced by the pressure gradient in the second-order waves.

(ii) Steady Viscous Flow Forces

Although Morison's equation does not perfectly represent the several aspects of the hydrodynamic loading it has the advantage of taking into account the viscous effect. In this formula the flow velocity in the viscous drag term, may have a constant part and a harmonic part. The constant part is induced by the mass transport of the waves ('Stokes' drift) and a possible current, whereas the harmonic part is induced by the wave particle motions[93].

The constant velocity components induce a steady "wave-current drag" force at a submerged location in terms of the form and friction factor[91,92]. The latter is a very small part of the form drag.

Since the wave particle velocity is harmonic, the drag force induced by this velocity at a submerged location has a zero-mean over one wave period. However, because of the changing surface elevation along the splash zone of a vertical cylinder, a mean "wave-drag" force in the horizontal direction is obtained due to the horizontal wave particle velocities[91,94].

Having explained the physics of the steady second-order forces, in the following section the vertical component of these steady forces is studied and used to compute the steady wave-induced tilting moment. In the formulation of this moment,potential steady forces in the horizontal direction are neglected assuming that they are balanced out by an artificially applied equivalent mooring force in the opposite direction.

Although the steady forces are neglected in the analysis, the author studied this component and presented a method to compute this force based on the two-dimensional beamwise strip method used earlier[53]. Briefly in this procedure, the sectional steady horizontal force in the beamwise direction is expressed by Maruo's formula derived from the far-field (wave momentum) method as follows[99]:

$$\bar{f}_x^t = \frac{1}{2}\rho g \quad |\bar{A}_{-\infty}|^2 \qquad \ldots \quad (41)$$

where $\bar{A}_{-\infty}$ is the complex form of the scattered wave amplitude at the far-field $(-\infty)$.

The reflected wave amplitude $\bar{A}_{-\infty}$ consists of the vector sum of the diffracted wave amplitude due to the presence of the fixed strip section and the radiated wave amplitude of the oscillating strip section for the in-plane modes. Both wave amplitudes are obtained from the asymptotic (far-field) expression of the velocity potentials which are represented by using the Frank Close-fit technique[103].

This method is based on a model of wave generation and reflection by the vessel. Since semi-submersibles are in general less obstructive to wave propagation, wave reflection is not a dominating factor in the steady horizontal force. Even the modelling of the columns, where the greater part of the reflection occurs, by two-dimensional methods may result in large three-dimensional errors. Therefore the author hesitates to use this method for this configuration.

Regarding the above review of the steady forces, for semi-submersibles with structural member dimensions at the waterline of the same order as the water particle motions, the wave drag force acting on the members may contribute significantly to the total steady force. Therefore it may be necessary to take into account this steady force component on the columns from the point of view of the wave-induced tilting moment calculation.

4.4.1 *Vertical Steady Second-Order Force on a Twin Hull Semi-Submersible*

Before semi-submersibles were introduced, the second-order vertical forces were investigated for control problems of submarines in the vertical direction near the free surface. Therefore the majority of the theoretical investigations were based on two-dimensional theories for completely submerged single slender bodies of simple cross-sections, in particular, circular sections.

Among these Ogilvie[31] gave a two-dimensional exact solution for the second-order horizontal and vertical force on a submerged circular cylinder under regular beam waves. The solution was given with no assumptions regarding the slenderness of the body or length scale of the problem.

Goodman[104] calculated the second-order vertical force on a slender body of revolution under regular and irregular head and beam seas. In this study it was assumed that the wave lengths were of the same order as the transverse dimensions of the body.

Lee and Newman[102] derived expressions for a submerged body of arbitrary cross-section under regular oblique waves retaining the assumption of slenderness with respect to the body length, wave length and depth of submergence.

The pioneering studies for the calculation of this force component relating to the steady tilt phenomenon were based on the above mentioned two-dimensional studies as reviewed in Chapter 2. Although more powerful three-dimensional methods were available to calculate this component perhaps because of the complexity of the tilt phenomenon in terms of other effects involved or because of the less practical importance of this phenomenon, they have not been utilised for the solution of tilt phenomenon. An additional reason might be that the forces acting on the submerged hulls are dominant compared to those on the vertical surface-piercing columns. Thus this type of approach for the twin-hull type semi-submersible could be justified.

In order to use these two-dimensional techniques, several approximations had to be made because of the complex geometry of semi-submersibles and restrictions due to the use of the theory. Among these, the effect of the vertical columns, lower hull cross-section, free surface, hydrodynamic interference between the hulls and heading angle can be accounted for.

In this section the second-order vertical force on a semi-submersible is calculated according to the methods given by Numata et al.[16], Martin and Kuo[20] and Morrall[29] in comparison with the

method suggested in the thesis based on Lee and Newman's solution[102]. Several hydrodynamic aspects such as the effects of cross-section, tilt, hydrodynamic interaction between the hulls, heading angle and surface-piercing columns are investigated. The calculated vertical steady force values by these methods are also compared with experimental measurements taken by Morrall.

4.4.1.1 *Outline of theoretical approach:*

1. Ogilvie[31] gives the exact solutions of the first- and second-order steady wave forces on a submerged circular cylinder under regular beam waves. The forces calculated are exact to second-order in non-viscous potential theory and are given for the following cases:

(i) The cylinder is fixed under the waves,

(ii) The cylinder is forced to oscillate sinusoidally in calm water, and

(iii) The cylinder is free to respond to the waves.

He also gives the approximate solutions for these forces. It is shown that over an appreciable range of radius and depth of submergence of the cylinder, the approximate solutions yield reasonable agreement in comparison with the exact solutions.

In both solutions, the exact one which was extended for twin cylinders by Martin and the approximate one which was used by Numata, the non-linear boundary value problem is solved by using the perturbation technique. The required velocity potential of the flow and other quantities derivable from this potential such as pressures, forces and motion of the cylinder are expanded in a convergent power series.

In the exact solution, the velocity potential is expressed in terms of the second- and first-order potential which is represented as a

combination of the incident wave and disturbance potential with unknown coefficients. The non-linear free surface and other boundary conditions are expanded in a Taylor series about the undisturbed positions of those boundaries. In this way higher-order non-linear conditions up to second-order are defined by lower linear ones. The application of the boundary condition required yields the unknown coefficients and thus the velocity potential. From this potential, pressures and forces are obtained by means of the Bernoulli and Blasius theorems[107].

Ogilvie assumes that if either the radius of the cylinder R is small or the depth of the submergence H (distance from the centre of the circle to the water level) is large, the free surface effects become unimportant and the disturbance potential can be represented in a simpler form by using the circle theorem[108] and thus the first sectional force expressions are given as follows:

(i) Cylinder is restrained

$$\bar{f}_y^t = 2\pi\rho g\, a^2 (\gamma R)^2\, e^{-2\gamma H}\, \frac{I_1[2\gamma R]}{\gamma R} \qquad \ldots \quad (42)$$

where $I_1[2\gamma R]$ is the modified Bessel Function of the first-kind[109].

(ii) Cylinder is free to respond to waves

$$\bar{f}_y^t = 2\pi\rho g\, a^2 (\gamma R)^2\, e^{-2\gamma H} \left\{ \frac{I_1[2\gamma R]}{\gamma R} - 1 \right\} \qquad \ldots \quad (43)$$

In eq. 43 it is assumed that the motion of the cylinder is similar to the motion of the water particles in the absence of the cylinder.

In both cases the steady force in the horizontal direction $\bar{f}_x^t$ is found to be zero. This is because a submerged circular cylinder, which is rigidly held in fixed position, or moving with the motion of equivalent water particles does not reflect any waves which could cause a net horizontal force but the incident waves suffer a phase shift in passing the cylinder[110,111].

In Figs 170 and 171 the comparison of the exact and approximate solutions are shown for the restrained and free cylinders[31].

On the other hand Goodman[104] gives the second-order vertical force expression for a slender body of revolution under regular beam seas by assuming that the wave length is of the same order of magnitude as the body radius.

The steady vertical force is given per unit length as follows (eq. 30 in ref. [104]):

$$\bar{f}_y^t = 2\rho g\, \gamma^2 a^2\, S_A\, e^{-2\gamma(H-\eta_o)}\, \frac{I_1[2\gamma R]}{\gamma R} + 2\rho g\, \gamma^2 a^2\, S_A\, e^{-\gamma(H-\eta_o)} \left\{ \frac{}{\eta' \sin(\omega t - \gamma\xi_o)}^t - \frac{}{\xi' \cos(\omega t - \gamma\xi_o)}^t \right\} \quad \ldots \quad (44)$$

where $S_A = \pi R^2$, is the body cross-sectional area.

In the formulation of this force problem Goodman assumes that the motions of the body consistsof a steady component ξ_o, η_o induced by the second-order force and an oscillatory component ξ', η' induced by the first-order forces in the horizontal and vertical direction.

When the body is restrained

$\eta_o = \xi_o = \eta' = \xi' = 0$ and eq. 44 becomes as follows:

$$\bar{f}_y^t = 2\rho g\, a^2\gamma^2\, S_A\, e^{-2\gamma H}\, \frac{I_1[2\gamma R]}{\gamma R} \quad \ldots \quad (45)$$

When the body is free to respond to regular waves, it is assumed that the oscillatory part of the motion ξ', η' is such that the body moves like a water particle, i.e.

$$\xi' = -\, a\, e^{-\gamma(H-\eta_o)} \sin(\omega t - \gamma\xi_o)$$

$$\eta' = \quad a\, e^{-\gamma(H-\eta_o)} \cos(\omega t - \gamma\xi_o) \quad \ldots \quad (46)$$

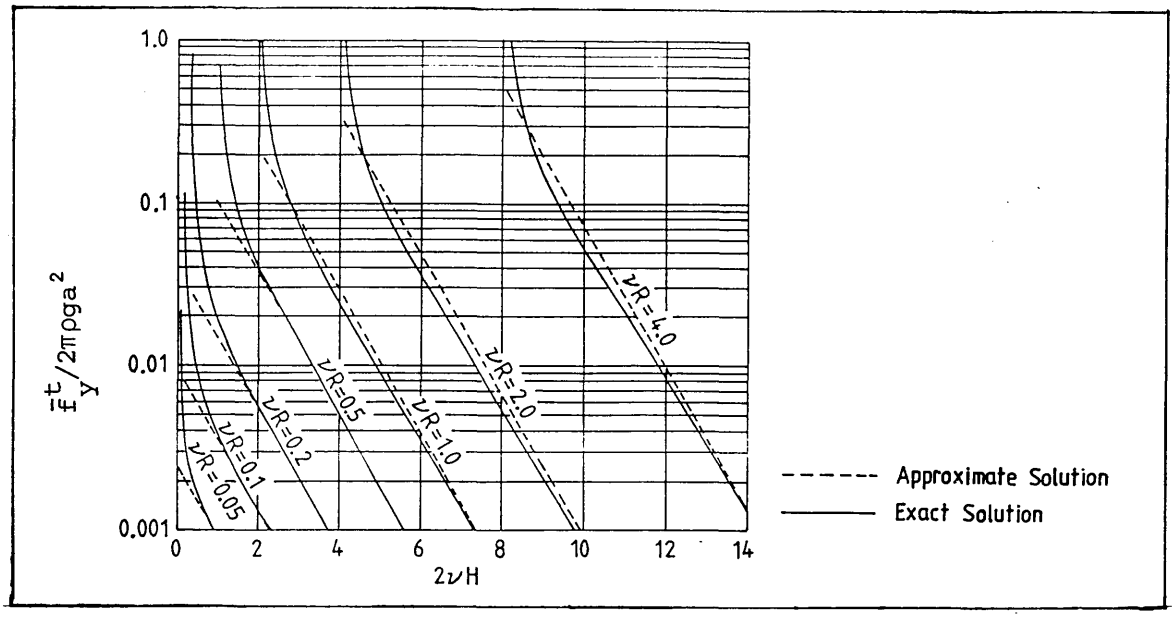

Fig. 170 - Steady vertical force on a restrained submerged circular cylinder[31]

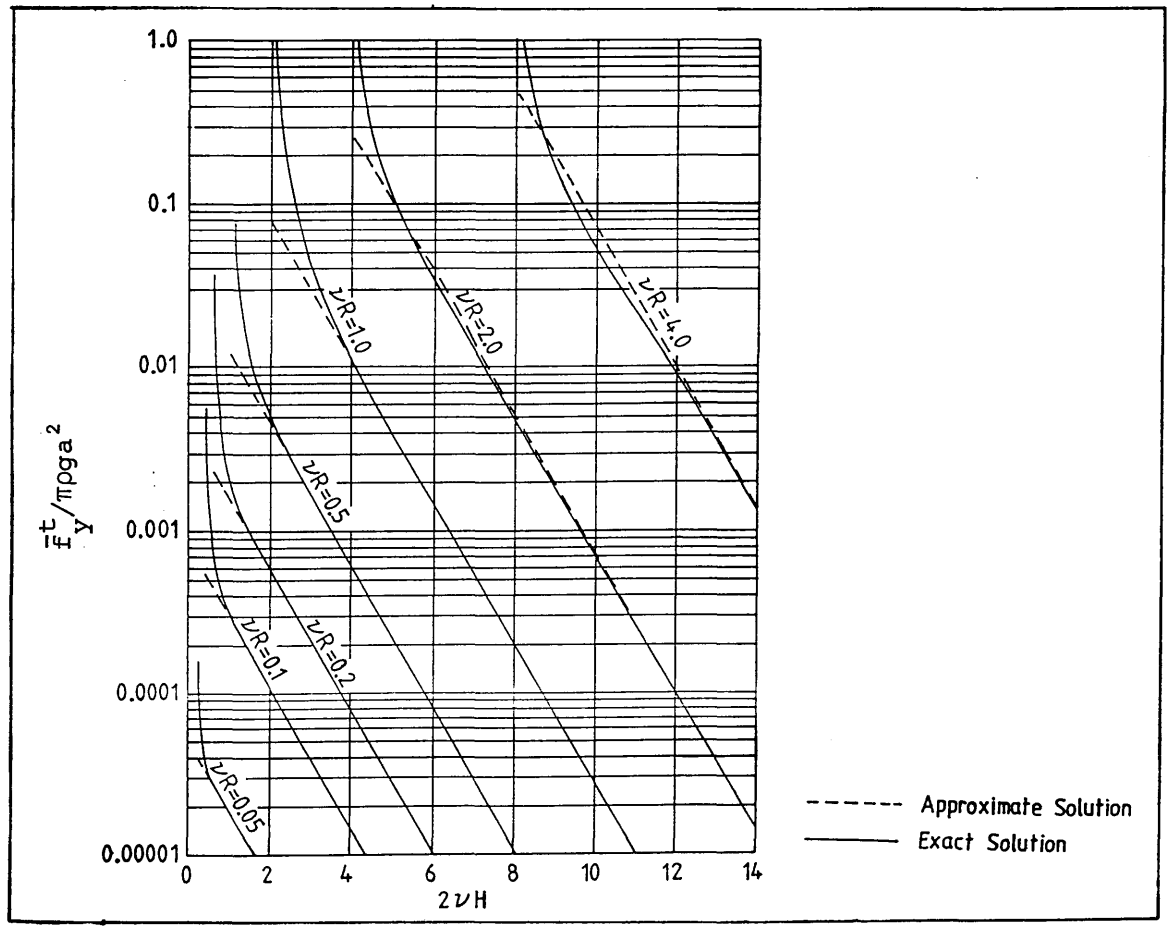

Fig. 171 - Steady vertical force on a freely floating submerged circular cylinder[31]

The substitution of eq. 46 into 44 yields the steady force expression as follows:

$$\bar{f}_y^t = 2\rho g\, a^2\gamma^2\, S_A\, e^{-2\gamma(H-\eta_o)} \left\{ \frac{I_1\, 2\gamma R}{\gamma_R} - 1 \right\} \qquad \ldots \quad (47)$$

In eqs 45 and 47 if $S_A = \pi R^2$, the results are similar to Ogilvie's approximate solutions except for η_o. Ogilvie assumes that the steady motion η_o induced by the steady upward force and ξ_o induced by the steady drift of the water are neglected since they are higher than second-order in order to formulate steady motion problem[31].

As stated in Chapter 2, Numata et al.[63] calculated the steady vertical force on the semi-submersible by using Ogilvie's approximate solution for the restraint case, eq. 42. The restrictions and approximations imposed by the use of this approximate solution have already been discussed in Chapter 2.

Martin and Kuo[20] calculate the steady vertical force by making use of Ogilvie's exact solution for twin circular cylinders. Therefore no assumption is made for the effect of free surface. Under linearised potential theory assumptions, the effect of the free surface, hydrodynamic interference between the cylinders and the oscillatory motions of the cylinders are taken into account.

Morral[29] gives the final expressions for the steady vertical force on a restraint submerged horizontal prism and circular footing as given by eqs (I.14) and (I.15) in Appendix I.

2. Lee and Newman[102] give an analytical solution for the steady vertical force on a submerged slender body with arbitrary cross-section under regular oblique waves. This theoretical study is based on the assumptions of slenderness with respect to the body length, wave length and depth of submergence. In non-viscous linear potential theory, the

disturbance potential of the fluid induced by an arbitrary shape of slender body is represented by "Kochin's Function" derived from Green's theorem, and by making use of momentum considerations the final steady vertical force is expressed in terms of the longitudinal distribution of cross-sectional area and added mass of the body. The assumption of slenderness with respect to the depth of submergence implies that the damping resulting from wave generation induced by the body oscillations can be neglected and that the added mass values can be approximated to the values for an unbounded fluid.

The formulation of this method is given in ref. [102]. In the following the final expression of the force is presented for use in the analysis of the steady-tilt problem.

Total steady vertical force $\bar{F}_y^t$ on a free slender body submerged under the regular oblique waves is given as follows:

$$\bar{F}_y^t = \frac{1}{2}\rho g(\gamma a)^2 e^{-2\gamma H}\left\{\cos^2\mu\left[I_1(0) - \frac{I_1^2(\gamma\cos\mu)}{I_1(0)}\right] + \sin^2\mu\left[I_2(0) - \frac{I_2^2(\gamma\cos\mu)}{I_2(0)} - \frac{I_4^2(\gamma\cos\mu)}{I_{b6}+I_{f6}}\right] + \left[I_3(0) + \frac{I_3^2(\gamma\cos\mu)}{I_3(0)} - \frac{I_5^2(\gamma\cos\mu)}{I_{b5}+I_{f5}}\right]\right\} \quad \ldots \quad (48)$$

where

$$\begin{bmatrix} I_1(\gamma\cos\mu) \\ I_2(\gamma\cos\mu) \\ I_3(\gamma\cos\mu) \end{bmatrix} = \int_L \cos(\gamma z\cos\mu)\begin{bmatrix} S_A \\ S_A + a_{22}/\rho \\ S_A + a_{33}/\rho \end{bmatrix} dz \quad \ldots \quad (49)$$

$$\begin{bmatrix} I_4(\gamma\cos\mu) \\ I_5(\gamma\cos\mu) \end{bmatrix} = \int_L z\sin(\gamma z\cos\mu)\begin{bmatrix} S_A + a_{22}/\rho \\ S_A + a_{33}/\rho \end{bmatrix} dz \quad \ldots \quad (50)$$

$$\begin{bmatrix} I_{f5} \\ I_{f6} \end{bmatrix} = \int_L \begin{bmatrix} a_{22}/\rho \\ a_{33}/\rho \end{bmatrix} z^2 dz \quad \ldots \quad (51)$$

a_{22} and a_{33} are the sectional added mass coefficients in the sway and heave mode,

I_{b5} and I_{b6} are the volume moment of inertia of the body with respect to the x- and z-axes of the body coordinate system whose origin is located at the centre of gravity with oy-axis towards the upward and oz-axis towards the bow,

μ is the angle of wave incidence relative to the positive z-axis.

In eq. 48 the first terms in the brackets $I_j(0)$, $(j=1,2,3)$, correspond to the force when the body is held in a fixed position, i.e.

$$\bar{F}_y^t = \frac{1}{2}\rho g(\gamma a)^2 e^{-2\gamma H} \int_L \left(2S_A + \sin^2\mu \frac{a_{22}}{\rho} + \frac{a_{33}}{\rho}\right) dz \quad \ldots \quad (52)$$

The terms containing the squares of I_j contribute to the forces induced by the body oscillations.

4.4.1.2 *Computations and discussion of results for the steady vertical force:* The precise determination of the wave-induced steady tilting moment is essential for the analysis of tilt behaviour. An equilibrium steady tilt occurs when this moment is balanced by the vessel's restoring moment.

As formulated in the following section and compared with the experimental measurements, this steady moment is assumed to be induced by the steady vertical force only. Therefore in this section by making use of the above stated theoretical solutions this force component is computed for a twin-hull semi-submersible. Its several aspects are discussed as follows.

Effect of cross-section

The solution given by Lee and Newman theoretically takes into account the effect of arbitrary shape exactly, whereas the others are for cylinders with circular cross-sections.

As shown in eqs 48 and 52 the effect of section shape in the force expression is represented by the longitudinal distribution of the cross-sectional area and the heave and sway added mass of the sections in an unbounded fluid. If one defines the following coefficients:

$$C_2 = \left(S_A + \frac{a_{22}}{\rho}\right) \Big/ 2S_A, \quad C_3 = \left(S_A + \frac{a_{33}}{\rho}\right) \Big/ 2S_A \qquad \ldots \quad (53)$$

These coefficients represent the relative difference between a lower-hull with arbitrary cross-section and an equivalent body of revolution having the same sectional area distribution. In Fig. 172 the variations of the hydrodynamic coefficients of two of the most common hull cross-sections, rectangular and rectangular with corner radius, for various aspect ratios are shown. Since the fluid is assumed unbounded the heave added mass of the section with an aspect ratio (x) is equivalent to the sway added mass of the section with the inverse of this ratio (1/x). By making use of these added mass coefficients and the sectional areas, coefficients C_2 and C_3 for the same cross-sections and aspect ratios are illustrated in Fig. 173. As shown in this figure, the replacement of a rectangular cross-section with the same sectional area of circular cross-section, which is suggested by Numata et al., is reasonable for aspect ratios about one. Deviations from the aspect ratio of one will result in increasing error.

If the hull is restrained, in eq. 52, the effect of cross-section is represented by the $\left(2S_A + \sin^2\mu \frac{a_{22}}{\rho} + \frac{a_{33}}{\rho}\right)$ term. This term is non-dimensionalised as follows:

$$C_o = \left(S_A + \sin^2\mu \frac{a_{22}}{\rho} + \frac{a_{33}}{\rho}\right) \Big/ 3S_A \qquad \ldots \quad (54)$$

The factor of 3 in eq. 54 is introduced to normalise the summation in the paranthesis for the sake of convenience.

In Fig. 174 the effect of aspect ratio on coefficient C_o is illustrated for beam seas. As shown in this figure as the aspect ratio deviates from unity (i.e. section gets elongated in either direction, vertical or horizontal), coefficient C_o and thus the steady force always increases in beam seas. The worst force is experienced at the peak values of aspect ratios considered while the least force is experienced on the circular cross-section. The rectangular cross-section with corner radius always demonstrates a lesser force compared to the rectangular with a maximum of 20% for an aspect ratio of one where the section converges to a circular section.

Effect of tilt

Except for the solution given by Martin and Kuo, in the other solutions presented the dynamic free surface effect is neglected because of the large depth of submergence assumption. However, its static effect is taken into account by the exponential term ($e^{-2\gamma H}$) in all. When the semi-submersible is in a tilted position, this effect will be taken into account via this term by the different depth of submergence of each hull. At the same time if the hull cross-section is non-circular, this may result in an additional change induced by the effect of instantaneous section shape at the tilted positions.

Since Lee and Newman's solution is applicable to non-circular cross-section bodies, this effect was investigated by using the solution for rectangular and rectangular with corner radius sections restrained under regular beam waves. The aspect ratios of both sections are 2 and the latter has a corner radius which equals half of the section depth. Figure 175 illustrates this effect on the non-dimensional added mass and coefficient C_o of these two typical sections. This figure shows that although the heave and sway added mass coefficient varies

with varying tilt angles, C_o does not change because of the counter acting behaviour of the added mass coefficients for these particular sections.

Effect of hydrodynamic interference

The use of Lee and Newman's solution in the twin-hull configuration excludes the hydrodynamic interaction between the hulls since it is given for a single body. As shown in eq. 52, the effect of hydrodynamic disturbance is introduced by the infinite added mass of the body. Therefore it is thought that the hydrodynamic interference can be taken into account by using twin-hull added mass coefficients which include the hydrodynamic interference between the hulls at first-order as studied earlier. Figure 176a illustrates the heave and sway added mass coefficients of deeply submerged twin circular hull sections at various hull separation and those of the same section in isolation by comparison. Practically for a hull separation to hull diameter ratio of less than 3, the heave added mass of the section deviates considerably from the isolated value compared to the sway added mass. This results in a slight increase in coefficient C_o and thus in the total steady vertical force on twin cylinders in the upright position, Fig. 176b.

Effect of heading angle

So far no experimental and theoretical work has been done for the effect of the heading angle on the steady tilt behaviour. Although this parameter has not been explored by experiments in the thesis, by making use of the force expression in eq. 52, in which this parameter is introduced by a term $\sin^2\mu$, one may deduce its importance. Figure 177 illustrates the effect of a heading angle on coefficient C_o for three typical cross-sections for the restrained case. As shown in

this figure while the worst force is induced in beam sea condition for the rectangular section, the least force is experienced in head or following sea conditions for the circular section. The variation of the heading angle from beam sea to head or following sea results in a maximum of 60% force increase for circular, 50% for rectangular with corner radius and 40% for rectangular cross-section.

Effect of vertical surface-piercing columns

The use of the above method neglects the presence of the surface-piercing columns because of the two-dimensional treatment. However, including the existing three-dimensional studies, there has been no study which demonstrates the contribution of the steady vertical force on surface-piercing columns of a semi-submersible compared to the total steady force on the vessel. Therefore the importance of this effect is discussed rigorously as follows.

Figure 178a shows the steady second-order vertical force on a floating hemisphere given by Pinkster in terms of its components, explained in section 4.3. As illustrated in this figure component II (velocity head force) and component III (body translation force) are the effective components. Since the body lines run vertically at the free surface, component I (wave elevation force) is zero. Component IV (body rotation force) does not contribute to the total force because no roll motion occurs. Thus the total force can change its direction from downward to upward under the two effective components.

Although the flow-field around a vertical column is different from than that around the sphere, both geometries are surface-piercing and have a similar shape of waterplane. Therefore there may be a similarity in trends of the curves of the forces on these two geometries so that, at least, the steady force may be either upward or downward depending on

the body motions. However, if the surface-piercing body is restrained, component III will be zero and thus the total steady vertical force will be dominated by the downward velocity head component II. This conclusion is supported by Taylor and Hung's results[106]. By using the same method they demonstrated a steady downward vertical force on fixed vertical surface-piercing column arrays (see table 3 of ref. [106]).

On the other hand the steady vertical force on a submerged circular cylinder is shown in Fig. 178b in the manner given by Pinkster. Since the body is fully submerged no contribution arises from component I. Because no roll motion occurs component IV is also zero. Thus the total force is dominated by components II and III as in the surface-piercing hemisphere case. However, contrary to this case, component II is always positive indicating an upward force, while component III is downward. Because of the dominant component II, the resultant force is always in the upward direction. As noticed in both Figs 178a and b, the inclusion of motion response decreases the total force considerably.

The above discussion may lead to a rough conclusion for the effect of the columns on the total steady force on the semi-submersible. The inclusion of the vertical columns, which induce a steady vertical force in the downward direction, reduces the total steady vertical force on a submerged circular hull which is positive in the upward direction. This trend is very strong when the assumption of a restrained body is made. The inclusion of the first-order motion may have a varying effect on this trend (see Fig. 178).

Comparison of the existing theoretical methods

In this section, the steady vertical force on each hull of a restrained semi-submersible model, which is similar in dimensions to the model tested, are computed under the steady tilt effect. The results

are obtained from the solutions given in the foregoing by Numata et al. (eq. 41), Martin and Kuo*, Morral (eqs I.14 and I.15 in Appendix I). Lee and Newman (eq. 52). The methods are also compared with the experimental measurements taken by Morral (see Chapter 2) on a submerged circular cylinder.

Figure 179 illustrates the comparison of the results obtained from these solutions for the model presented in this figure. The depth of submergence and the hull separation distance of the model is similar to the model tested. The effect of the vertical columns and the model's oscillatory motions are not taken into account. As shown in this figure, although the forces on the leeward hull are similar in magnitude, the differences in the solutions for the seaward hull increase with growing tilt angles. Since the method presented by Martin and Kuo theoretically takes into account the dynamic free surface effect, it demonstrates large forces in magnitude in the low and moderate frequency region compared to the others. Lee and Newman's solution, which is denoted as PRESENT in the key box of the figure, gives relatively less force over the range of frequencies compared to the other solutions.

In Fig. 180, the comparison of these solutions excluding Martin and Kuo's, which is only valid for circular sections, is illustrated for the same model but with a rectangular cross-section of pontoon with aspect ratio of 1.27. In Numata's solution equivalent radius is defined from the equivalent cross-sectional area of rectangular and circular section. As shown in this figure, the present method which theoretically accounts for the effect of cross-section exactly manifests greater force compared to the other two methods over most of the frequency range.

---

*The results are obtained from the computer program developed by Martin and Kuo in ref. [20].

In Fig. 181, these solutions are also compared with Morral's test results on a single submerged hull of circular cross-section including the theoretical result obtained from the three-dimensional near-field method (NMI-wave program). As reviewed in Chapter 2, in these tests, the steady vertical force was measured on the hull with the presence of the vertical columns at four different depths of submergence. As shown in Fig. 181 for the largest depth of submergence (H/R = 3.38) all the solutions are in reasonably good agreement with the experimental data. As the depth of submergence decreases Martin and Kuo's solution is still in good agreement with the test results indicating the importance of dynamic free surface effect while the others underestimate the test data. At the shallowest draught (H/R = 1.5) all the solutions present entirely different magnitudes and trend of forces compared to the test data in which the steady force changes its direction upwards to downwards.

Although this thesis concentrates on the twin-hull semi-submersible as a supplementary information, in Fig. 182, two solutions given by Numata and Morral for a footing type semi-submersible are compared. As stated in Appendix I, Numata's approach based on the equivalent volume of the footing and corresponding circular is shown at the top of Fig. 182. The figure indicates that Numata's approximate solution presents greater force compared to Morral's. The difference in magnitude of the forces from each method increases with increasing frequency. At large depths of submergence both solutions present similar results.

Effect of oscillations

The above results have been drawn under the assumption that the hulls or footings are restrained. In fact when the oscillation of the semi-submersible is taken into account the magnitude of the steady vertical force is reduced. Figure 183 demonstrates this effect for

twin circular hullsin beam seas obtained from eqs 42 and 43 for the hulls restrained and free to respond to waves. In the free case it is assumed that each hull moves similarly to the orbital motion of the wave with zero phase lag. As shown in this figure under this assumption the magnitude of the force on each pontoon is about a maximum of 8% of that on each pontoon in the fixed position.

Lee and Newman's solution, eq. 48, yields a vanishing steady vertical force when the body is free under regular beam seas because of the rigorous slender body approximations.

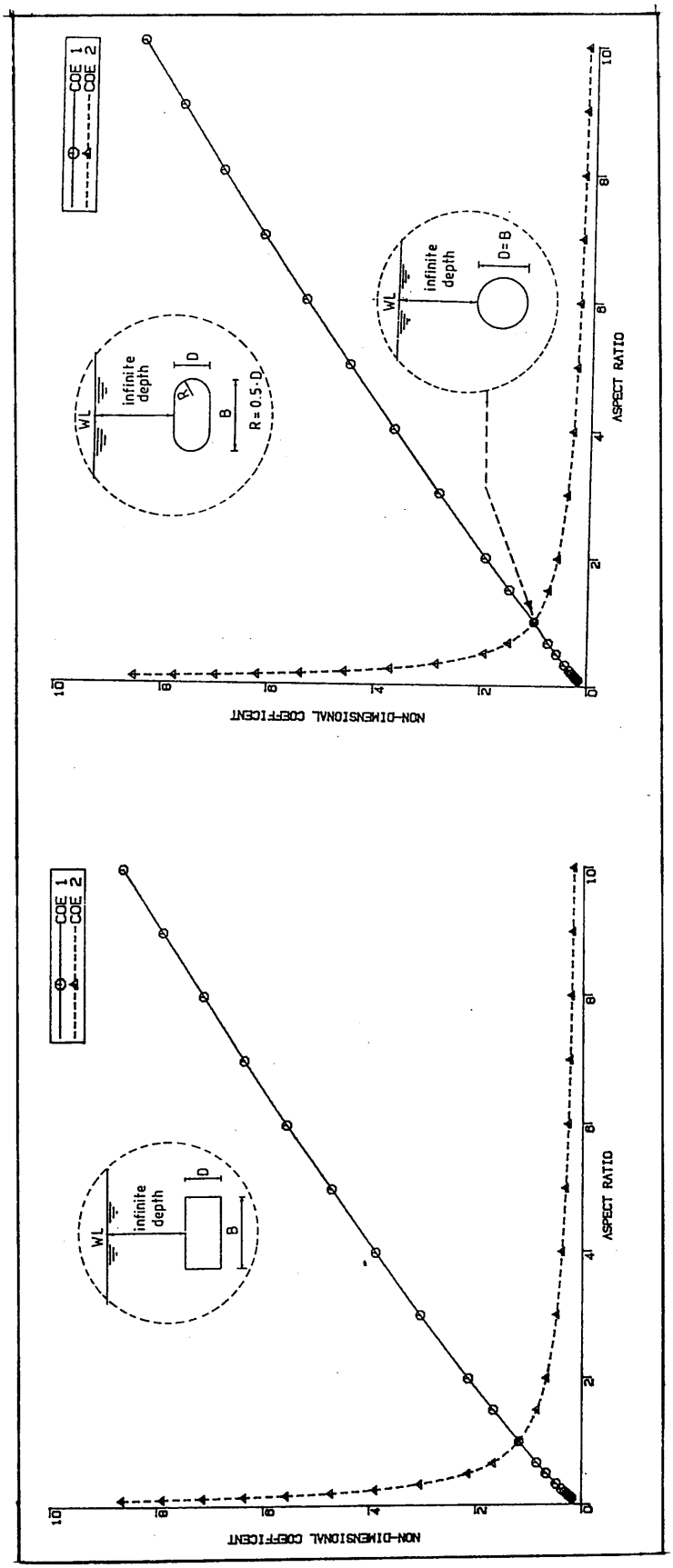

$$COE1 = \frac{a_{33}}{\rho S_A} \qquad a_{33} = \text{sectional heave added mass}$$

$$a_{22} = \text{sectional sway added mass}$$

$$S_A = \text{sectional area}$$

$$\rho = \text{density}$$

$$COE2 = \frac{a_{22}}{\rho S_A} \qquad \text{Aspect ratio} = B/D$$

Fig. 172 - Effect of aspect ratio on the added mass coefficients of various cross-sections

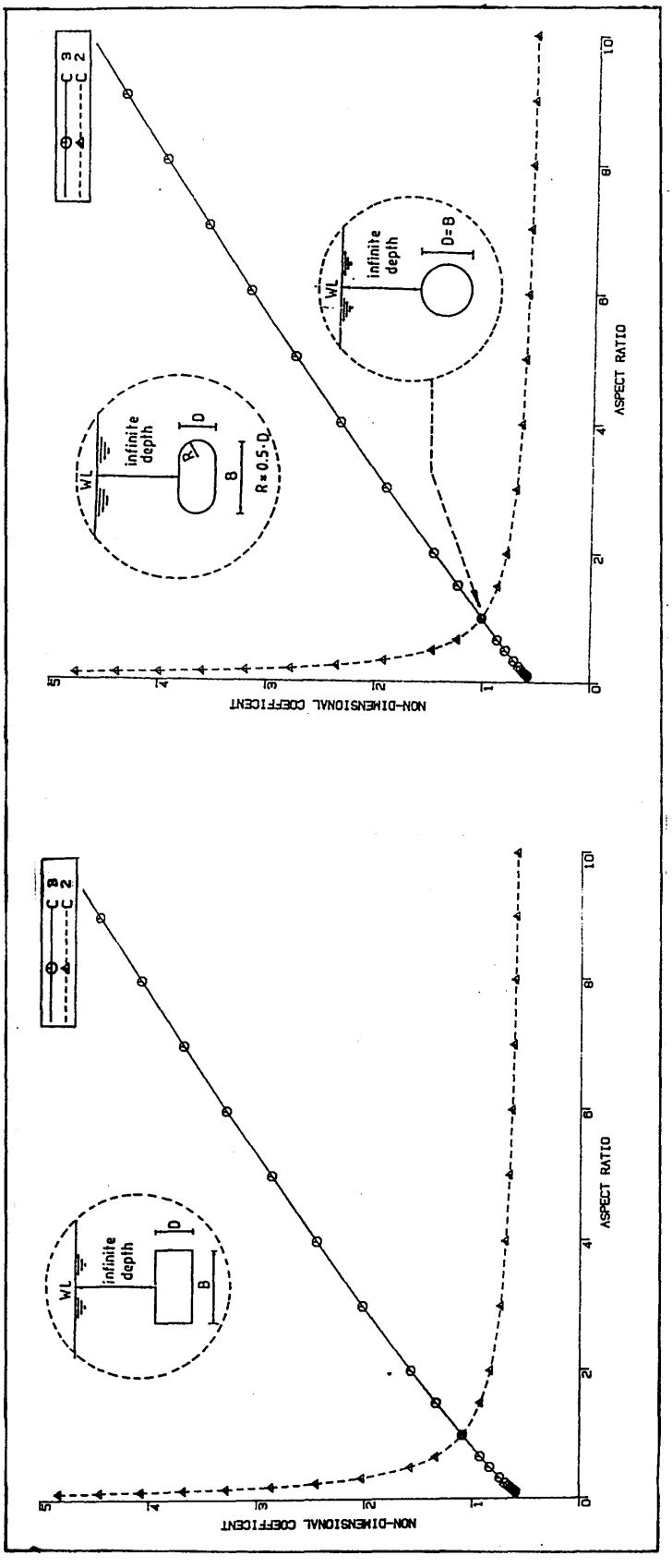

$$C_2 = \frac{S_A + \frac{a_{22}}{\rho}}{2S_A}$$

$$C_3 = \frac{S_A + \frac{a_{33}}{\rho}}{2S_A}$$

a_{22} = sectional sway added mass
a_{33} = sectional heave added mass
S_A = sectional area
ρ = density
Aspect ratio = B/D

Fig. 173 - Effect of aspect ratio on the hydrodynamic coefficient C_2 and C_3

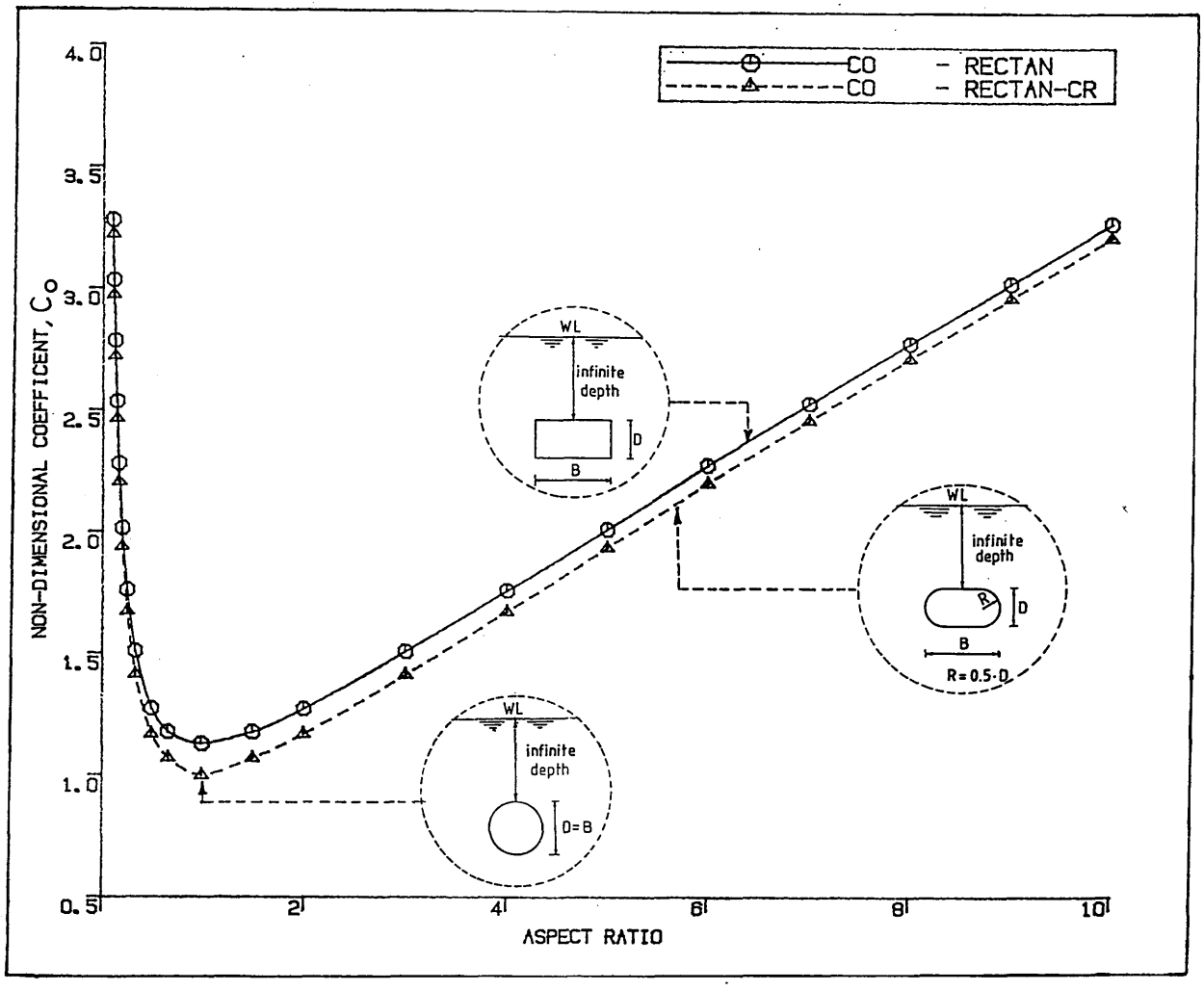

$$C_o = \frac{S_A + \frac{a_{22}}{\rho} + \frac{a_{33}}{\rho}}{3S_A}$$

Aspect ratio = B/D
a_{22} = sectional heave added mass
a_{33} = sectional sway added mass
S_A = sectional area
ρ = density

Fig. 174 - Effect of aspect ratio on the vertical second-order force coefficient C_o

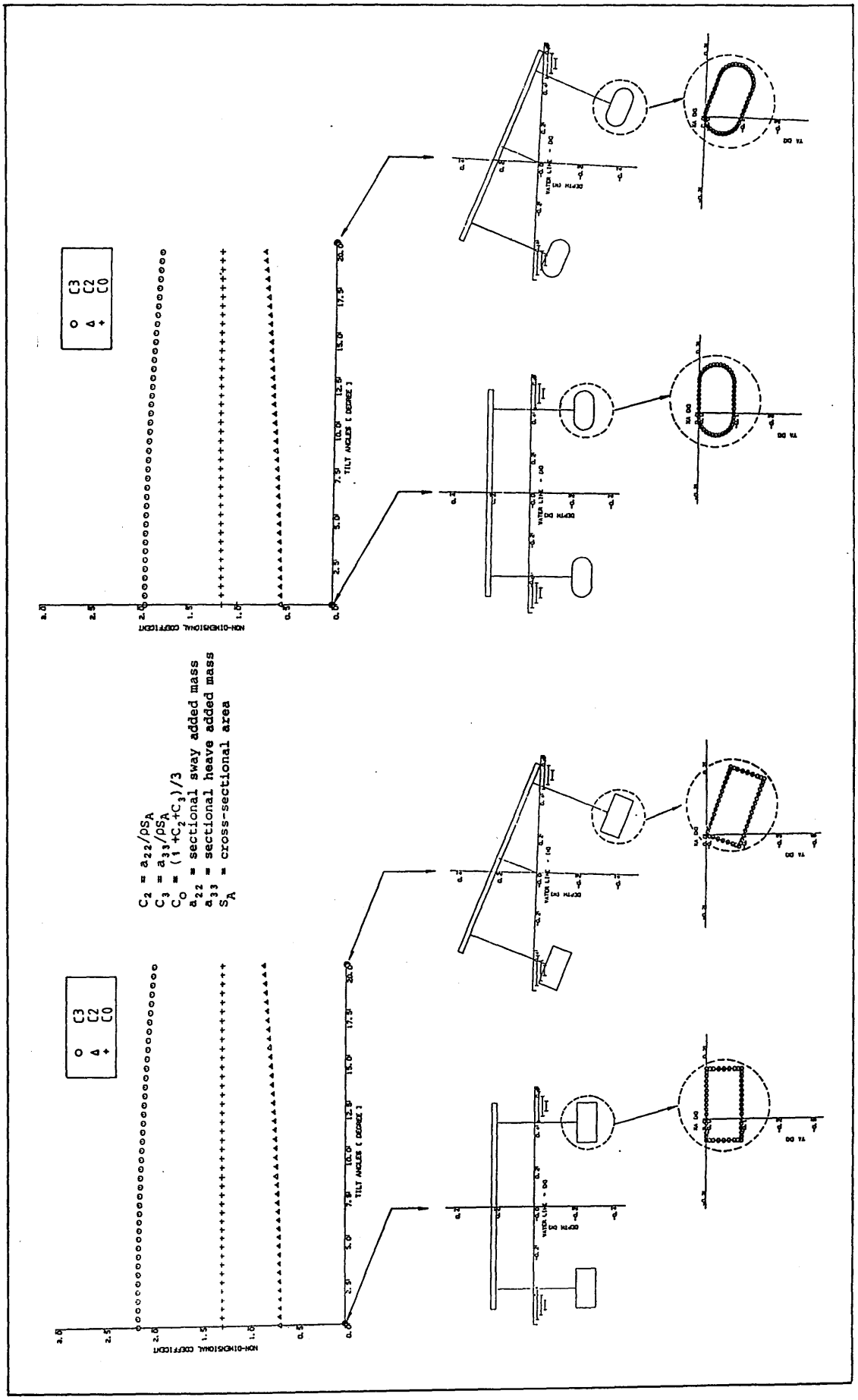

Fig. 175 - Effect of tilt on the hydrodynamic coefficients of submerged hull sections

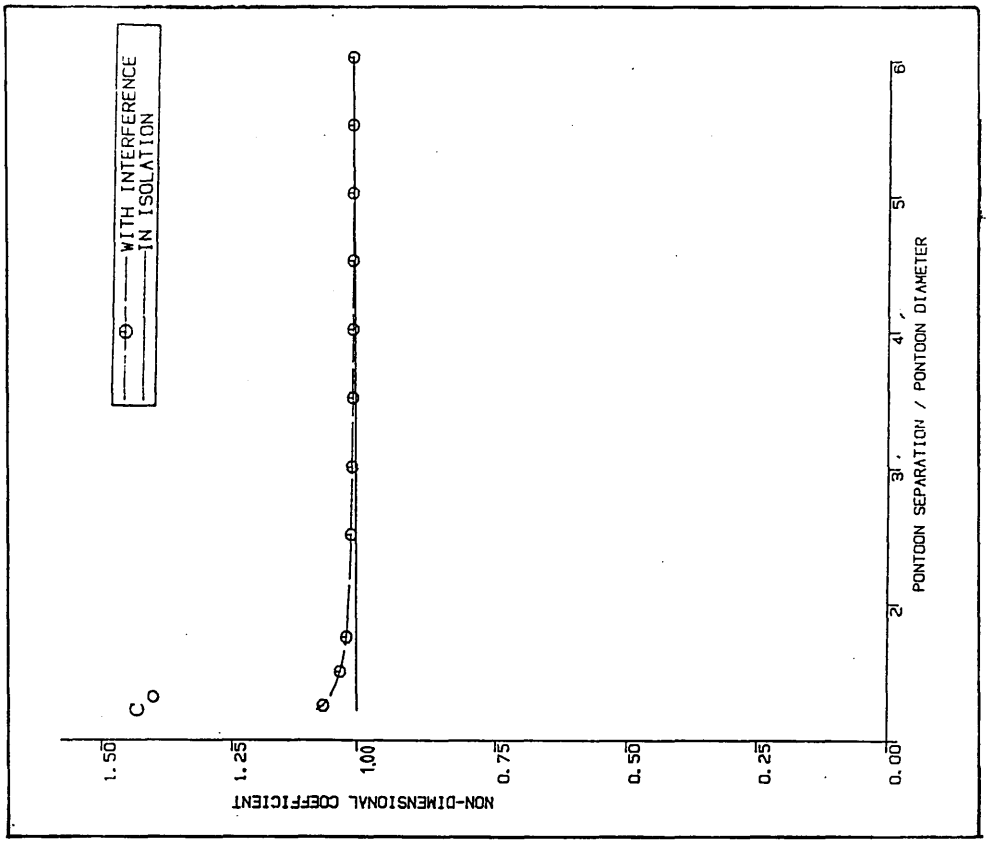

Fig. 176b - Effect of hydrodynamic interference on the steady vertical force coefficient C_o of twin circular hull sections

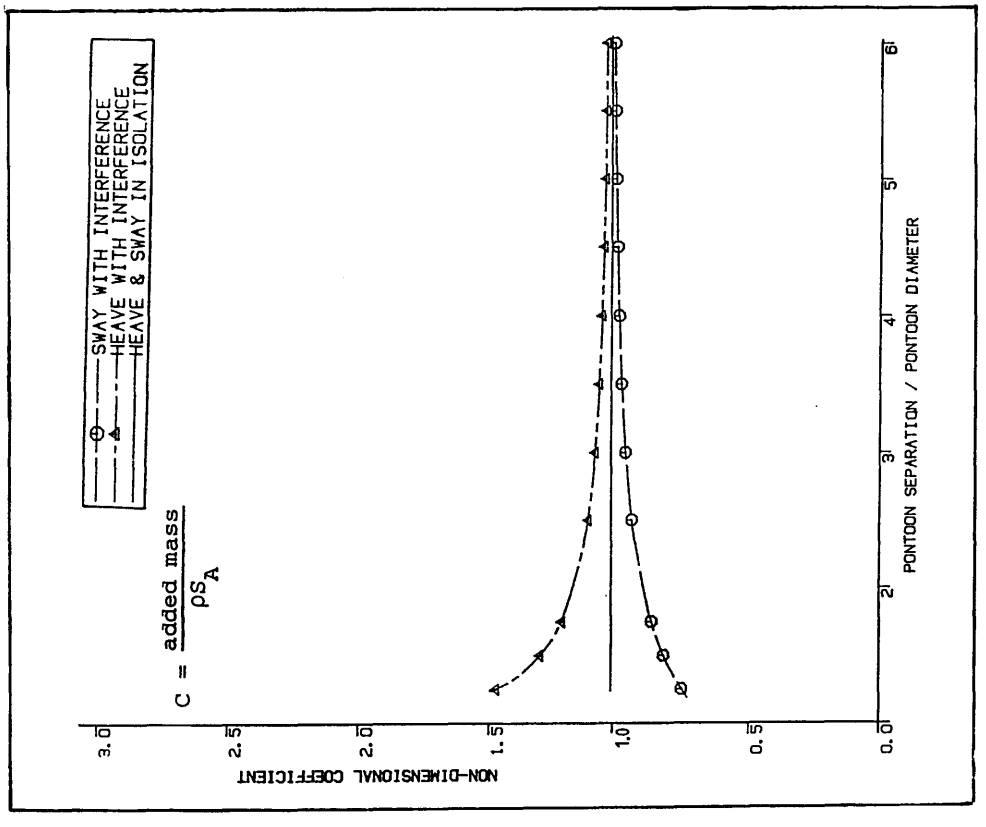

Fig. 176a - Effect of hydrodynamic interference on the added mass coefficients of deeply submerged twin circular hull sections

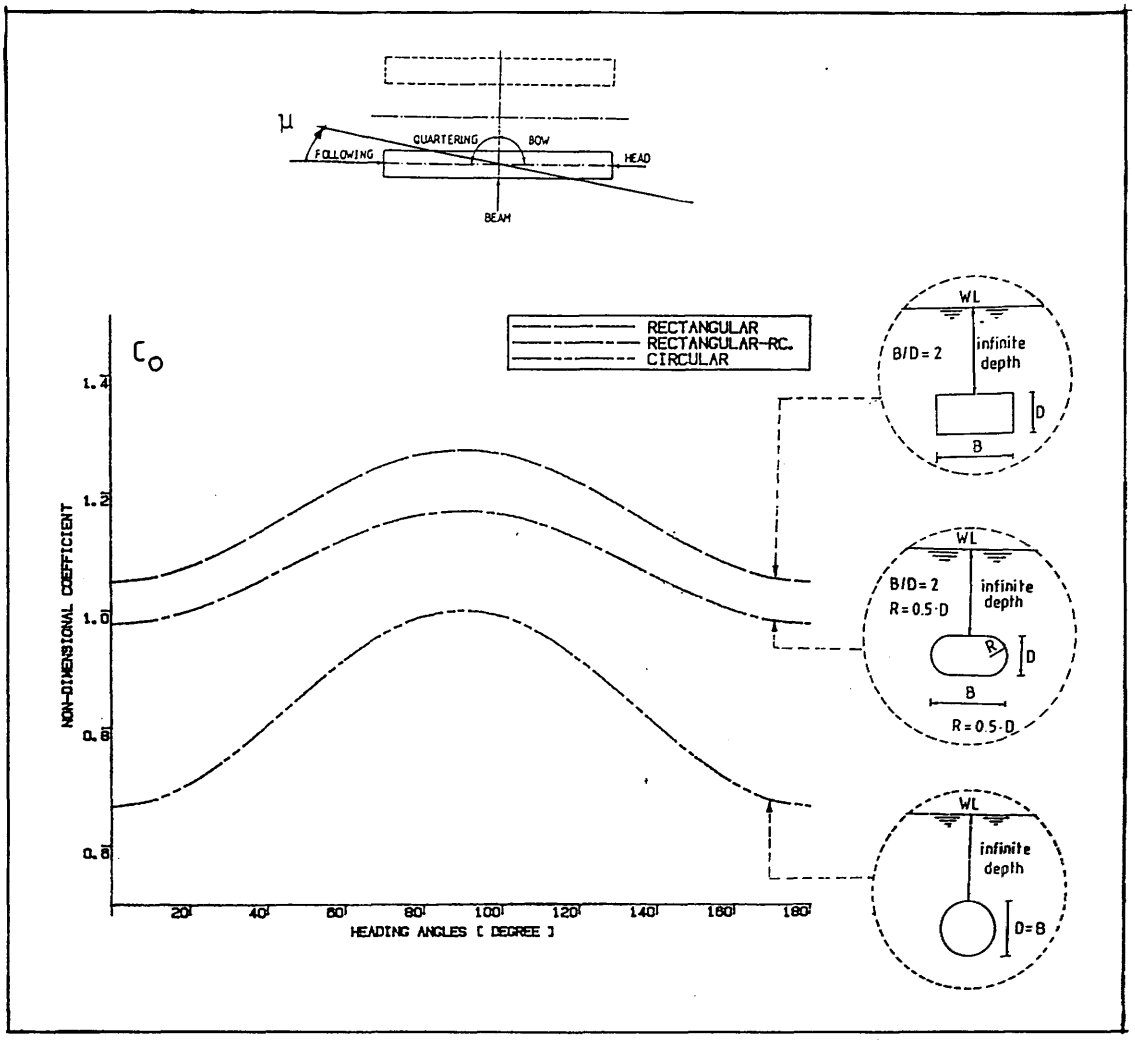

$$C_o = \frac{S_A + \frac{a_{22}}{\rho} + \frac{a_{33}}{\rho}}{3S_A} \sin^2\mu$$

a_{22} = sectional sway added mass
a_{33} = sectional heave added mass
S_A = sectional area
μ = heading angle

Fig. 177 - Effect of heading angle on vertical second-order force coefficient (C_o)

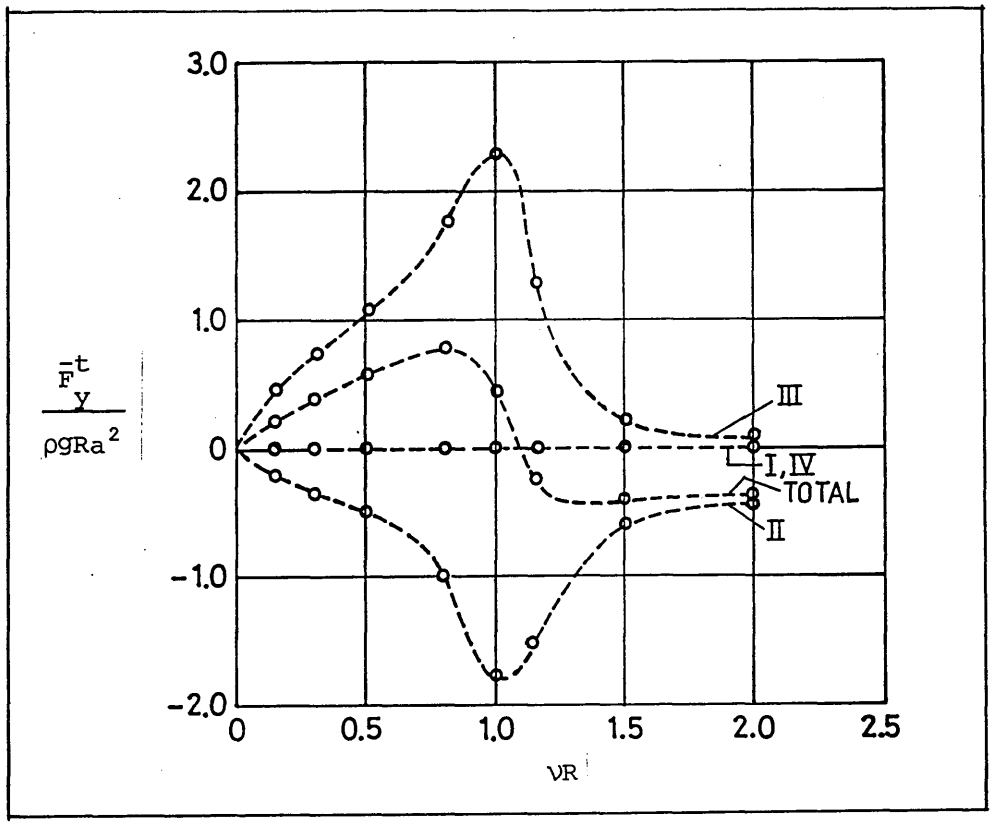

Fig. 178a - Breakdown of steady vertical force of a floating hemisphere into its components[14] (where R is radius of hemisphere)

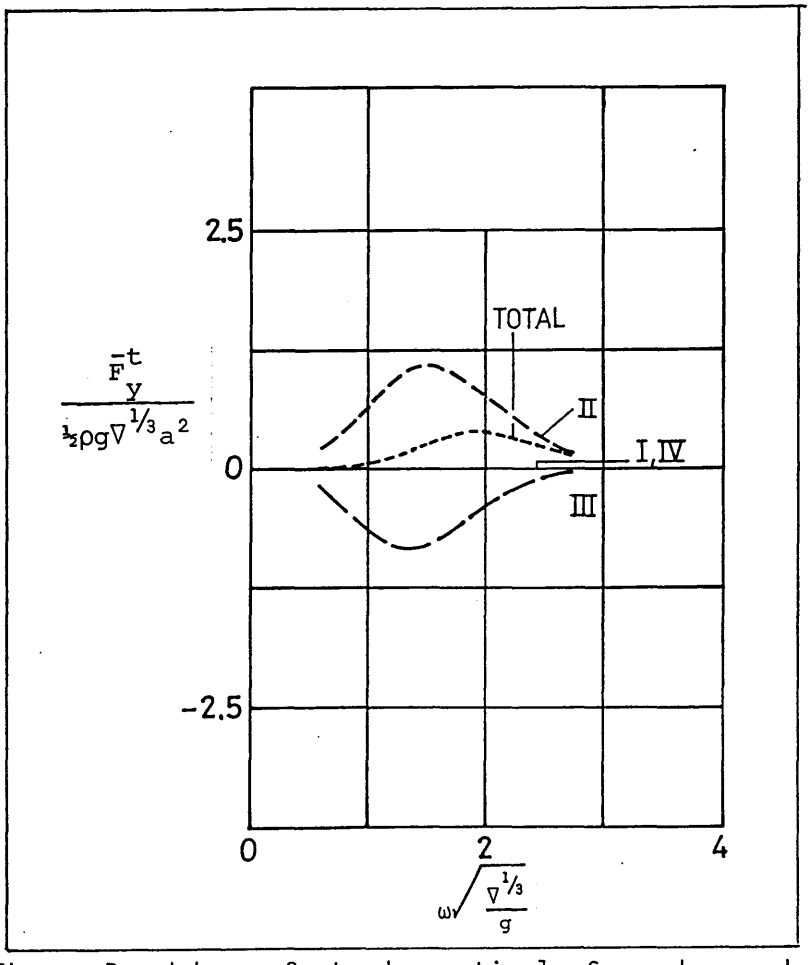

Fig. 178b - Breakdown of steady vertical of a submerged circular cylinder into its components[14] (where ∇ is the displacement volume of the cylinder)

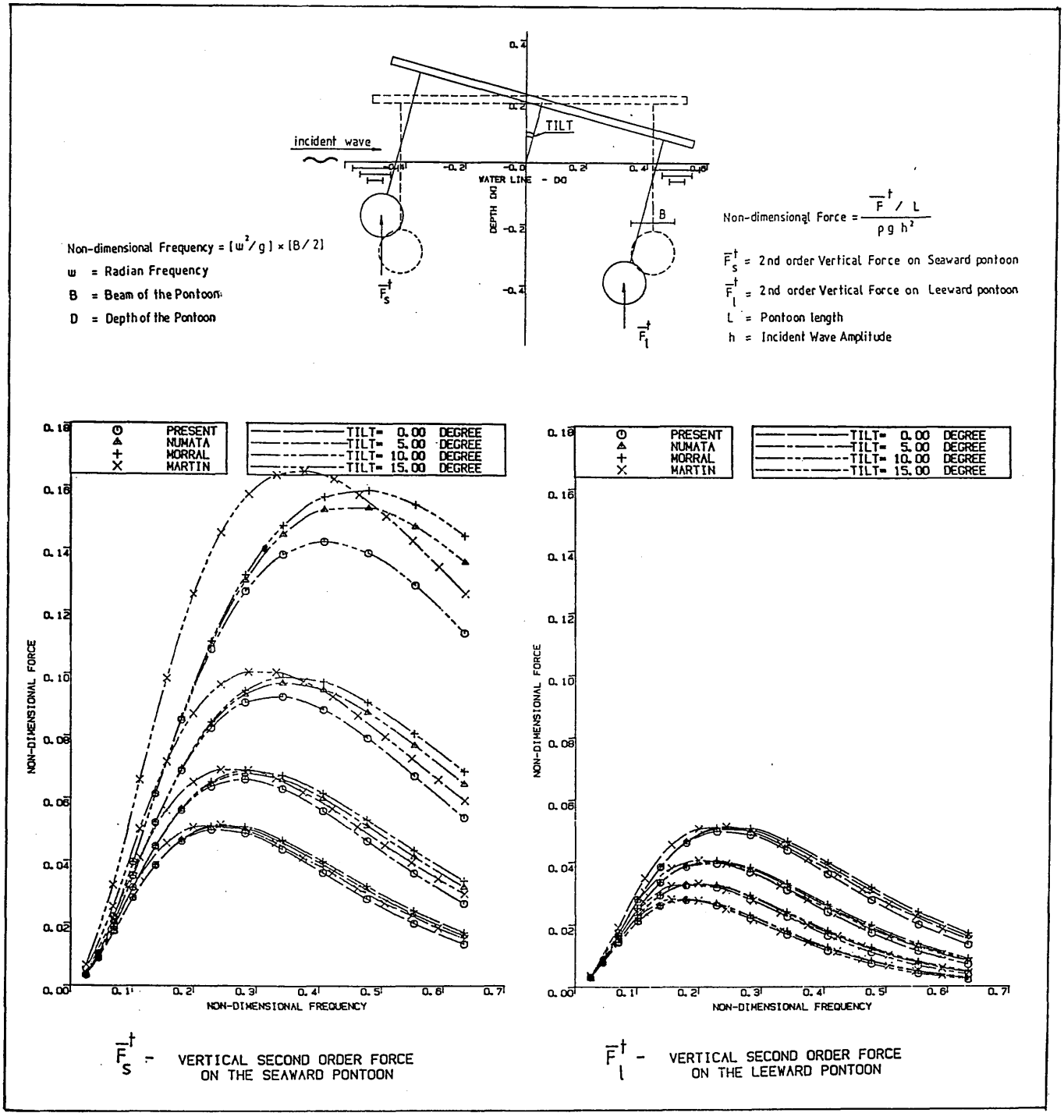

Fig. 179 - Comparison of various theoretical methods for the steady vertical force on the positions of twin circular hull semi-submersibles

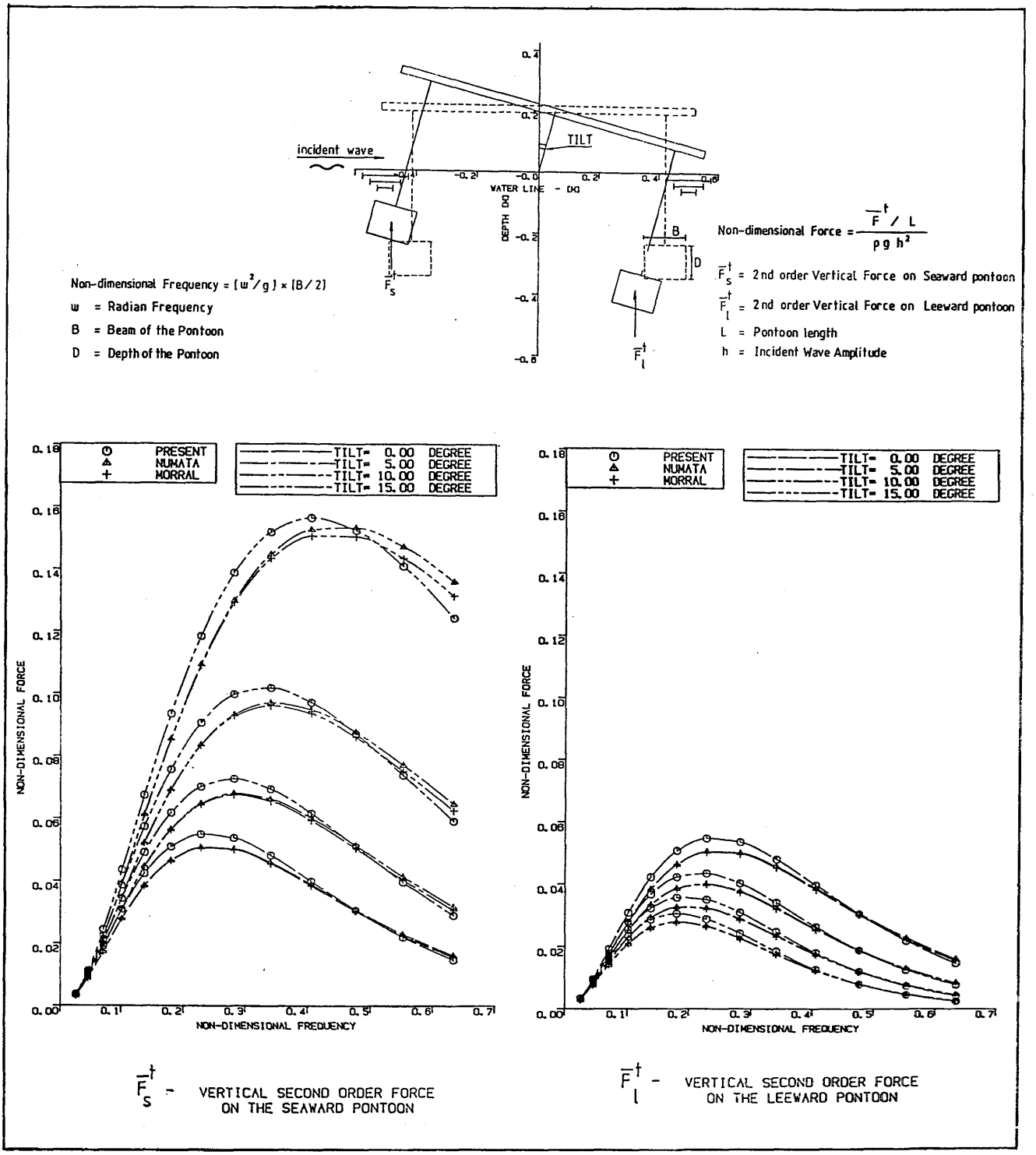

Fig. 180 - Comparison of the steady vertical forces on the basis of the different theoretical methods for the rectangular pontoons of a twin hull semi-submersible (B/D = 1.27)

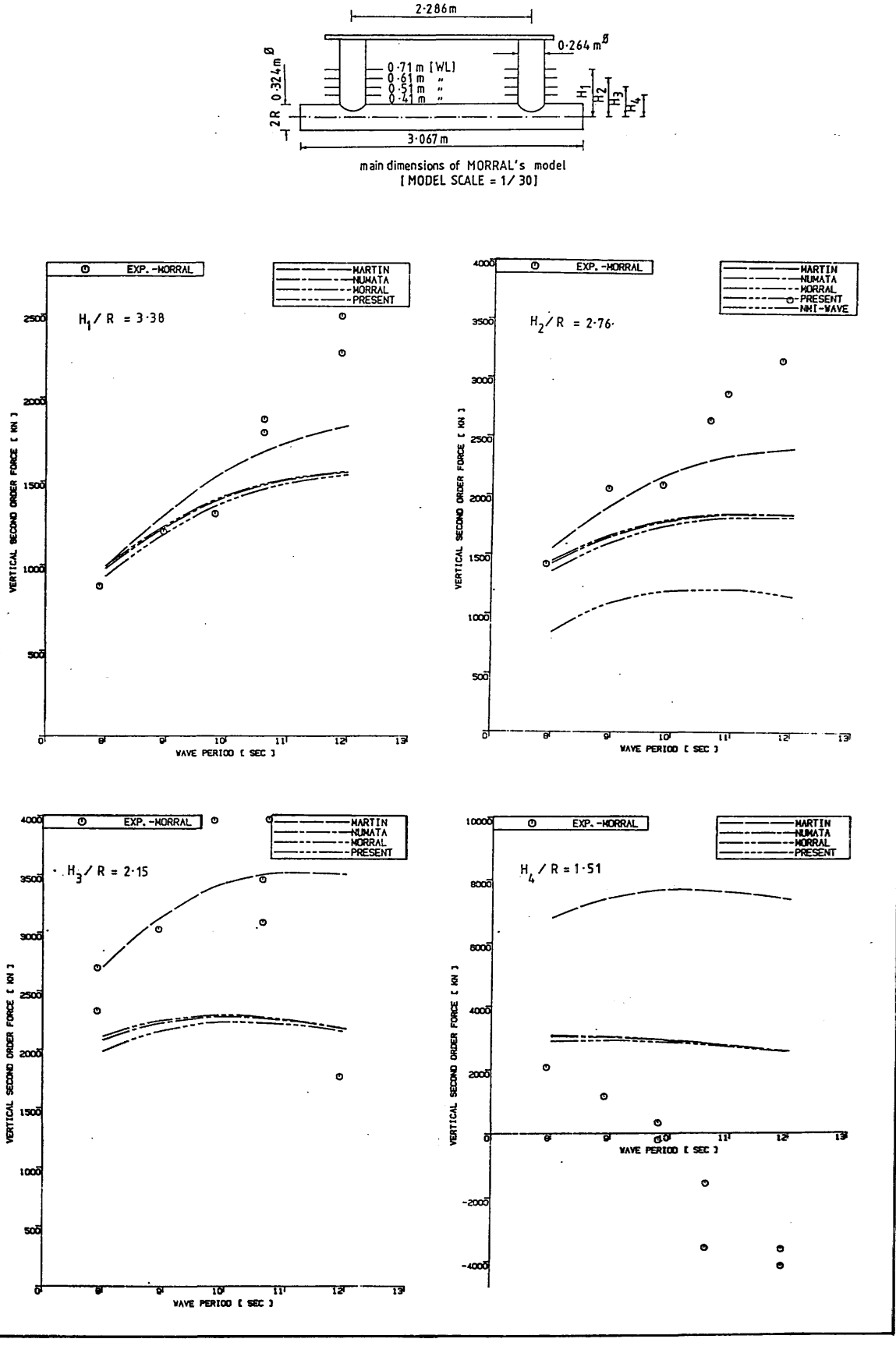

Fig. 181 - Comparison of experiment[29] and theory on the basis of the different methods for the steady vertical force on a circular pontoon

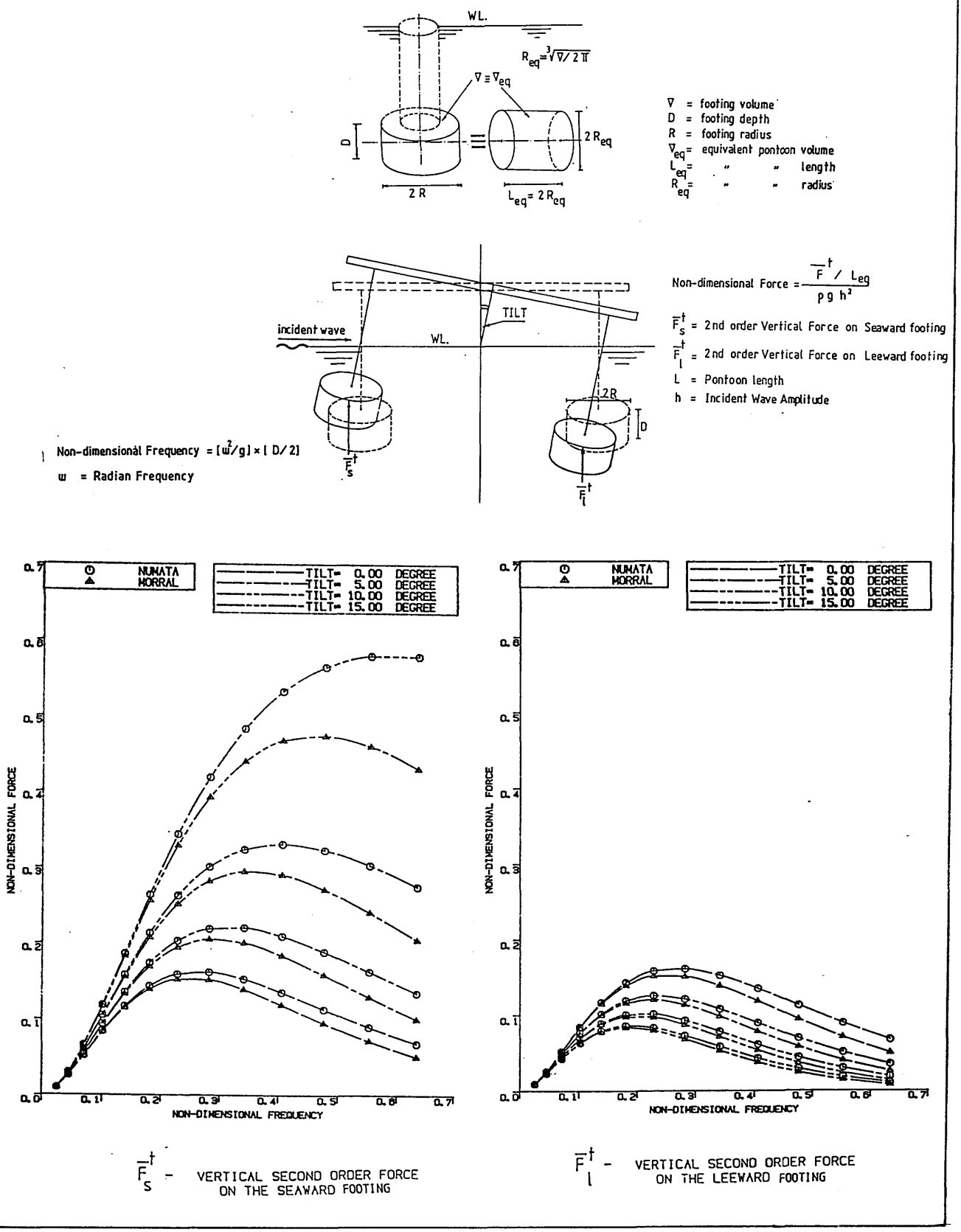

Fig. 182 - Comparison of the steady vertical force on the basis of the two different theoretical[16,29] methods for the seaward and leeward footing of a semi-submersible

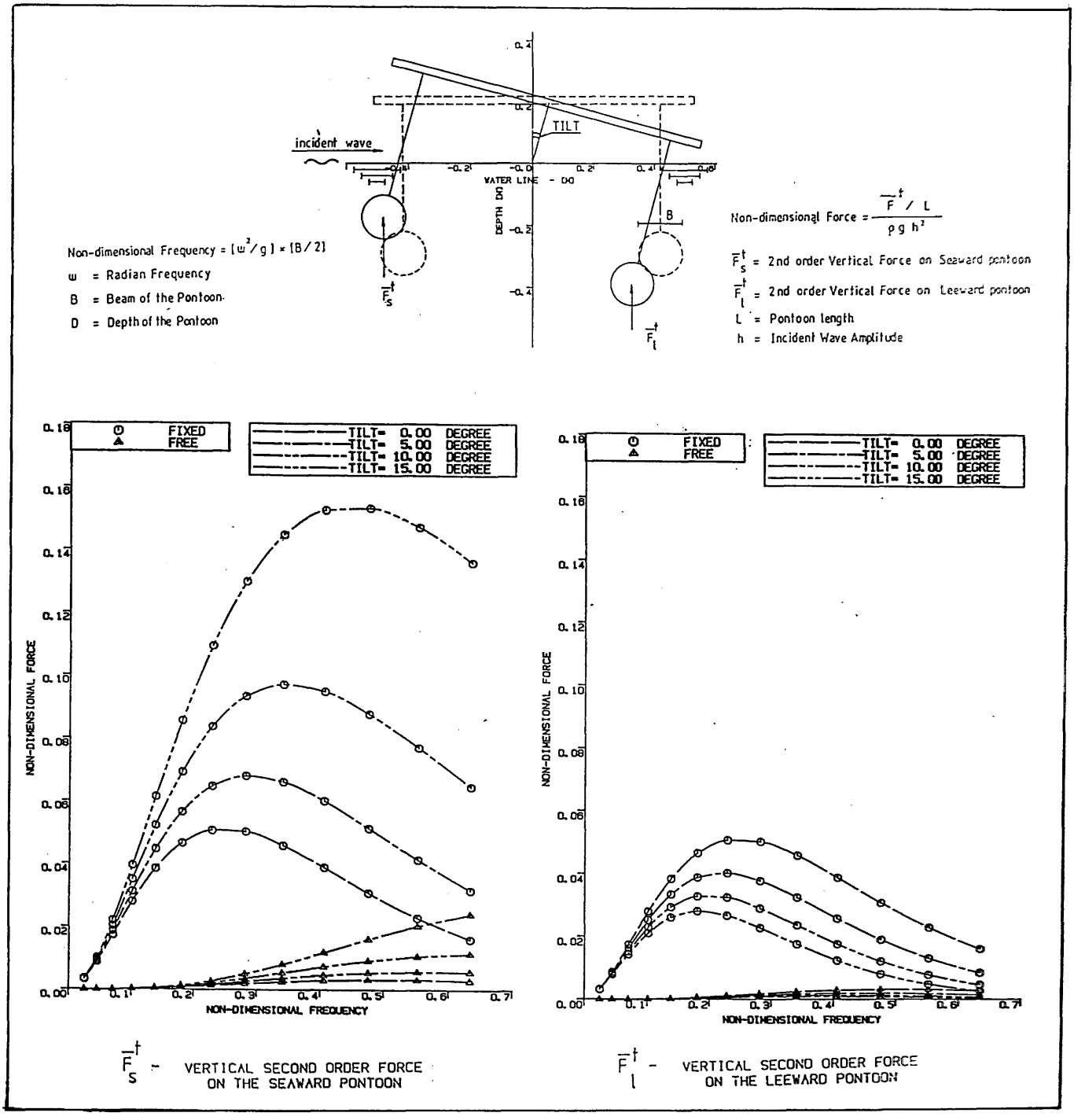

Fig. 183 - Effect of oscillations on the steady vertical force of the pontoons of a twin hull semi-submersible

4.4.2.1 *Steady tilting moment induced by the vertical second-order force:*

As reviewed in Chapter 2, Numata et al. predicted the steady tilt angles at the intersection points of the steady tilting moment induced by the vertical steady force and the static righting moment over a range of tilt angles expected. He demonstrated qualitative agreement between theoretically predicted and experimentally observed tilt angles.

In order to validate this approach by using the systematic test data generated in the thesis, the steady tilting moment expression is derived in this section. The similar rigorous assumptions and simplifications, which were made by Numata et al., are made but without the restriction for the shape of the lower hull. The vertical steady force in the moment expression is calculated using Lee and Newman's solution which theoretically accounts for the effect of slender hull shape exactly.

4.4.2.1.1 *Formulation of problem:*

It is assumed that the semi-submersible consists of two lower hulls which are slender with arbitrary cross-sections distributed along the hull length. The effect of surface-piercing columns is not taken into account. The hydrodynamic interference between the demi-hulls, which are assumed deeply submerged and sufficiently apart, is neglected.

The semi-submersible is assumed completely restrained under regular beam waves, with small amplitude in order to justify linear potential theory assumptions.

The use of the complete restraint assumption results in a larger value of steady tilting moment and thus a conservative result. Moreover there will be no oscillatory motion-induced forces with their steady moment. The oscillatory wave-exciting forces on the restrained body will induce the only oscillatory effects.

The steady horizontal force is assumed balanced out by an artificially applied mooring force at the application point of this force. Thus the steady tilting moment is induced only by the steady vertical forces which are assumed acting at the centroid of each hull.

Under the above stated assumptions, let the semi-submersible be tilted in the leeward direction. This induces a steady tilting moment $\bar{M}_T^t$ by the steady vertical force $\bar{F}_s^t$ and $\bar{F}_\ell^t$ on the seaward and leeward hull in different magnitudes due to the different depth of submergence H_s and H_ℓ, Fig. 184.

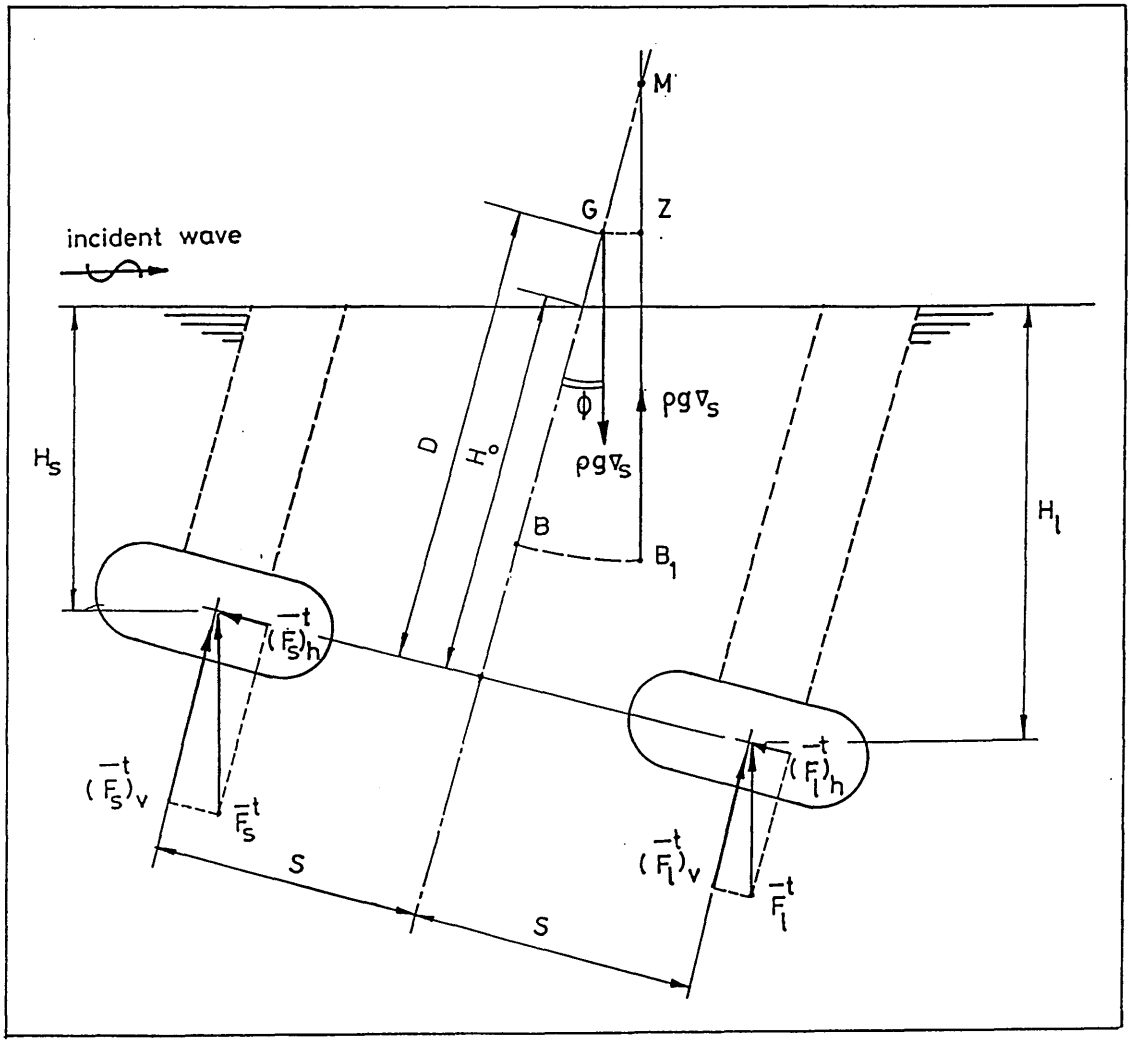

Fig. 184 - Quasi-static analysis of steady tilt induced by the steady vertical forces (potential)

Quasi-static analysis of the steady tilting moment $\bar{M}_T^t$ about the centre of gravity reduces to the following expression from Fig. 184:

$$\bar{M}_T^t = (\bar{F}_s^t)_v S + (\bar{F}_s^t)_h D - (\bar{F}_\ell^t)_v S + (\bar{F}_\ell^t)_h D \qquad \ldots \quad (55)$$

where suffices s, ℓ, h, v and T denote the quantities associated with the seaward hull, leeward hull, horizontal direction, vertical direction and tilting and the overbar $(-t)$ indicates the time average steady value.

By using eq. 52, the steady vertical forces on the hulls are as follows:

$$\bar{F}_s^t = \rho g \, (\gamma a)^2 \, e^{-2\gamma H_s} \nabla\left[1 + 0.5 \, (K_{22} + K_{33})\right]$$
$$\bar{F}_\ell^t = \rho g \, (\gamma a)^2 \, e^{-2\gamma H_\ell} \nabla\left[1 + 0.5 \, (K_{22} + K_{33})\right] \qquad \ldots \quad (56)$$

with
$$H_s = (H_o - S \tan\phi) \cos\phi$$
$$H_\ell = (H_o + S \tan\phi) \cos\phi \quad \text{(from Fig. 184)} \qquad \ldots \quad (57)$$

and $K_{22}(K_{33}) = \dfrac{\int_L a_{22}(a_{33})dz}{\rho\nabla}$ are the sway and heave added mass coefficients of one lower hull

$\nabla = \int_L S_A(z)dz$ is the volume displacement of one lower hull

The substitution of eq. 56 into eq. 55 yields the wave-induced steady tilting moment as follows:

$$\bar{M}_T^t = \rho g (\gamma a)^2 \nabla\left[1 + 0.5(K_{22} + K_{33})\right] \left\{ S \cos\phi \left(e^{-2\gamma H_s} - e^{-2\gamma H_\ell}\right) + D \sin\phi \left(e^{-2\gamma H_s} + e^{-2\gamma H_\ell}\right) \right\}$$
$$\ldots \quad (58)$$

4.4.2.2 *Steady tilting moment induced by the drag force*

A semi-submersible can be exposed to appreciable steady drag forces. This force component can make a significant contribution to the steady tilting moment as indicated by De Souza and Miller. In the following theoretical approach, the calculation of the steady moment on a twin-hull semi-submersible is based on Morison's Equation.

4.4.2.2.1 *Outline of theoretical approach:* The hydrodynamic forces on cylindrical members of a semi-submersible can be represented by Morison's equation including the viscous drag component. The use of this equation implies certain restrictions because of its empirical nature[60,112,113,114]. Amongst others, the restriction, which requires the wave length to be greater than five times the cylinder diameter, is essential. This enables one to use particle velocities and accelerations calculated at the centre of the members instead of integrating the corresponding pressure around the surface of the cylinder.

In terms of Morison's equation, the force on a unit length of the submerged portion of a fixed cylindrical member is expressed as the sum of an inertial force (f_I) and a drag force (f_D), i.e.

$$f = f_I + f_D = \rho C_M S_A \dot{V} + \frac{1}{2}\rho C_D D V|V| \quad \ldots \quad (59)$$

where C_M and C_D are the inertia and drag coefficients, S_A is the cross-sectional area, D is the cylinder diameter and V and $\dot{V}$ are the velocity and acceleration of the water particles in the incoming wave at the centre of the element.

In eq. 59 by substituting $V = V_o \cos\omega t$, where V_o is the maximum particle velocity it follows:

$$f(t) = -\rho C_M S_A \omega V_o \sin\omega t + \frac{1}{2}\rho C_D D V_o^2 \cos\omega t|\cos\omega t| \quad \ldots \quad (60)$$

The above force expression is harmonic in nature. The procedure to find its mean value is as follows:

$$\bar{f}^{t} = \frac{1}{T}\int_{t}^{T+t} f(t)\, dt \qquad \ldots \quad (61)$$

where T is one period of time.

Equation 61 yields a zero-mean value for f(t) given in eq. 60 at any submerged location.

However, in order to find the total force on a member, the force expression per unit length given by eq. 60 is integrated along the member. During this process, the integration is taken up to the wave surface for the horizontal forces on a surface-piercing member. Although Morison's equation is based on small amplitude linear wave theory and valid up to still water level, in practice it is stretched up to the wave crest. It is believed that the accuracy is improved by doing this[91-94]. Then the total horizontal force on a surface-piercing column becomes:

$$F_x(t) = \int_{o}^{H+\eta} \left(-\rho C_M S_A \omega V_o \sin\omega t + \frac{1}{2}\rho C_D D V_o^2 \cos\omega t|\cos\omega t|\right)dy \qquad \ldots \quad (62)$$

where D is column diameter, H is the column depth and η is the crest elevation.

Equation 62 can produce a non-zero mean if the crest elevation is not zero and is in phase with either of the inertia or the drag component. In such a case only the drag term, which is in phase with the crest elevation, yields a non-zero mean[91,92,115].

Based on the above approach, the steady horizontal drag forces on the columns of a semi-submersible will induce most of the tilting moment. In the following formulation this moment component

is given for a twin-hull semi-submersible in beam seas based on Morison's equation. The effect of vertical drag forces on the columns is ignored. Although the drag forces on the submerged lower hulls do not contribute to the steady moment they are included in the formulation for completeness and illustration.

4.4.2.2.2 *Formulation of problem:* Consider a twin circular hull semi-submersible fixed in beam on regular waves. The axis defining the wave system (o-xyz) lies on the free surface with the origin (o) at the middle of the two hulls as shown in Fig. 185.

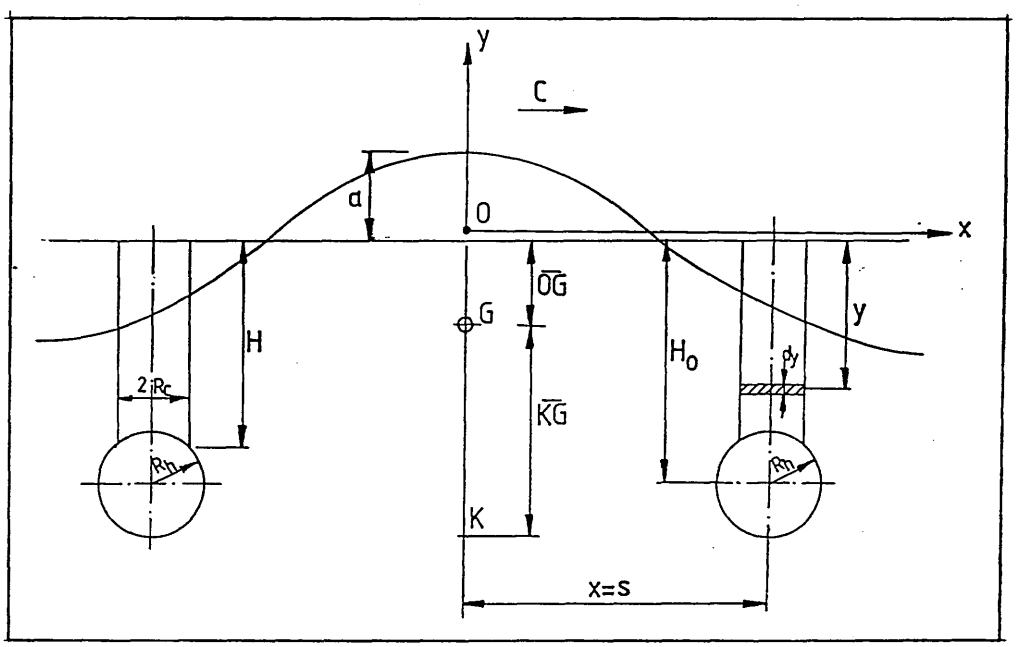

Fig. 185 - Twin circular hull semi-submersible in regular beam seas

Surface-Piercing Vertical Column

(a) Moment induced by the horizontal drag force

By using Fig. 185, the roll-exciting moment about the COG induced by the sway force on element dy of the column is:

$$= \frac{1}{2} \rho C_{D_c} A_{P_c} u|u| (\overline{OG} - y) \quad \ldots \quad (63)$$

where c indicates quantities associated with columns,

$$A_{P_c} = 2R_c \, dy \quad \ldots \quad (64)$$

and the horizontal wave particle velocity at a depth of y is:

$$u = - a\omega e^{\gamma y} \cos(\gamma x - \omega t) \quad \ldots \quad (65)$$

As a result of the small diameter member assumption the variation of the velocity across the diameter of the element dy is neglected. Moreover the variation of C_{D_c} along the depth of column and the hydrodynamic interference between members are also ignored. Then by substituting eqs 64 and 65 into eq. 63 and integrating from the bottom of the column up to the wave crest, the moment induced on one column is:

$$M_{x_c} = \frac{1}{2} \rho C_{D_c} (2R_c)(\gamma g \, a^2) \int_{-H}^{a\cos(\gamma x - \omega t)} \left[\overline{OG} \, e^{2\gamma y} - y \, e^{2\gamma y}\right] dy \; \cos(\gamma x - \omega t) \, |\cos(\gamma x - \omega t)|$$

$$= \frac{1}{2} C_{D_c} (2R_c)(\gamma g \, a^2)(INT) \cos(\gamma x - \omega t) \, |\cos(\gamma x - \omega t)| \quad \ldots \quad (66)$$

where $INT = \int_{-H}^{a\cos(\gamma x - \omega t)} \left[\overline{OG} \, e^{2\gamma y} - y \, e^{2\gamma y}\right] dy$

$$= \frac{1}{2\gamma} \left\{ \overline{OG} \left(e^{2\gamma a \cos(\gamma x - \omega t)} - e^{-2\gamma H} \right) - \left[\left(a\cos(\gamma x - \omega t) \; e^{2a\gamma \cos(\gamma x - \omega t)} + H \, e^{-2\gamma H} \right) \right.\right.$$

$$\left.\left. - \frac{1}{2\gamma} \left(e^{2\gamma a \cos(\gamma x - \omega t)} - e^{-2\gamma H} \right) \right] \right\} \quad \ldots \quad (67)$$

Submerged Lower Hulls

(a) Moment induced by the horizontal drag force

By using Fig. 185 the roll exciting moment about the COG induced by the sway force on a transverse hull element dz is:

$$= \frac{1}{2} \rho C_{D_h} A_{P_h} u|u| (KG - R_h) \quad \ldots \quad (68)$$

where index h indicates quantities associated with lower hulls,

$$A_{P_h} = 2R_h \, dz \quad \ldots \quad (69)$$

and it is the horizontal mean velocity at the lower hull axis H_o given by:

$$u = - a \omega e^{-\gamma H_o} \cos(\gamma x - \omega t) \quad \ldots \quad (70)$$

After substituting eqs 69 and 70 into eq. 68, integrating it along the hull length the moment induced on one lower hull is:

$$M_{x_h} = \frac{1}{2} \rho C_{D_h} (2R_h L) e^{-2\gamma H_o} \cos(\gamma x - \omega t) |\cos(\gamma x - \omega t)| (KG - R_h)(\gamma g a^2) \quad \ldots \quad (71)$$

(the variation of C_{D_h} along the length of the lower hull is neglected).

(b) Moment induced by the vertical drag force

By using Fig. 185, the roll-exciting moment about the COG induced by the heave force on a vertically taken hull element dz is:

$$= \frac{1}{2} \rho C_{D_h} A_{P_h} v|v|x \quad \ldots \quad (72)$$

where $A_{P_h} = 2R_h \, dz \quad \ldots \quad (73)$

and v is the mean vertical velocity at the lower hull axis H_o given by:

$$v = a \omega e^{-\gamma H_o} \sin(\gamma x - \omega t) \quad \ldots \quad (74)$$

By substituting eqs 73 and 74 into eq. 72 and integrating along the hull length the moment induced by one lower hull is:

$$M_{y_h} = \frac{1}{2} \rho C_{D_h} (2R_h L)(\gamma g a^2) e^{-2\gamma H_o} \sin(\gamma x - \omega t) |\sin(\gamma x - \omega t)| x \quad \ldots \quad (75)$$

The total roll-exciting moment induced by the drag force on the semi-submersible is obtained by summing eqs 66, 71 and 75 by considering the number of members on the leeward and seaward side of the vessel:

$$M_{T_D}(t) = \sum_{i=1}^{N_c} \left\{ \left[M_{x_c} \right]_{x=S} + \left[M_{x_c} \right]_{x=-S} \right\} + \left[M_{x_h} \right]_{x=S} + \left[M_{k_h} \right]_{x=-S} + \left[M_{y_h} \right]_{x=S} + \left[M_{y_h} \right]_{x=-S} \quad \ldots \quad (76)$$

where N_c is the number of columns on each hull, S is the half hull separation.

The above moment expression is formulated when the vessel is in the upright position. If the vessel has a tilt of ϕ, the effect on the column is to change the lower limit of the integral H to:

$$\begin{aligned} &(H - S \tan\phi) \cos\phi \quad \text{for the leeward column} \\ &(H + S \tan\phi) \cos\phi \quad \text{for the seaward column} \end{aligned} \quad \ldots \quad (77)$$

Similarly the upright depth of the lower hulls H_o is to change to:

$$\begin{aligned} &(H_o - S \tan\phi) \cos\phi \quad \text{for the leeward lower hull} \\ &(H_o + S \tan\phi) \cos\phi \quad \text{for the seaward lower hull} \end{aligned} \quad \ldots \quad (78)$$

The change in the transverse dimensions and force due to the small tilt is neglected since it is expected to have a very small effect.

The steady (mean) tilting moment induced by the total drag force on the semi-submersible is found by:

$$\bar{M}_{T_D}^{t} = \frac{1}{T} \int_{t}^{t+T} M_{T_D}(t)\, dt \quad \ldots \quad (80)$$

4.4.2.3 *Comparison of experiment and theory for the wave-induced tilting moment and discussion of results:*

Following the discussion on the components of the steady tilting moment the comparison and discussion is carried out in two groups: (i) the moment induced by the steady vertical force and (ii) the sum of the moment induced by the steady vertical force and the steady drag force.

(i) As reviewed in Chapter 2, Numata, et al. predicted the actual tilt angles observed in model tests by using the wave-induced tilting moment and the righting moment expression given by eqs I.5 and I.6 of Appendix I. In their procedure both moments were presented on the same axis over a range of possible tilt angles ($\phi \leq 16°$). The angles corresponding to the intersection points of the two moment curves indicated the predicted tilt angles. Over a series of six tests qualitative agreement was demonstrated between the predicted and actual tilt angles as shown in Fig. 5. The figure indicated that although the tilting moment curves are nearly linear, the restoring moment curve had a non-linear form. This non-linearity was due to the presence of the cross-members and bracings (see Figs I.1 and I.2 of Appendix I) causing an intersection of the two moment curves. The predicted tilt angles corresponding to the intersection points were in reasonable agreement with the actual tilt angles observed in their tests.

It was thought that the limited number of predictions published by Numata, et al. may not be satisfactory to justify their theory. Therefore it was decided to compare the extensive motion data produced in the thesis, Tables 10 to 14, with predictions obtained from the above procedure.

For the tilting moment computation eq. 58 was used. This was different from the Numata, et al. expression in terms of the steady vertical force expression involved. It was applicable to any cross-section lower hull. However, the use of the Numata, et al. expression or the expression suggested in eq. 58 would not yield any major difference for a circular section lower hull as discussed in section 4.3. The righting moment was expressed by $\Delta\overline{GM}\sin\phi$ where Δ was the total displacement of the model.

When the two moment curves for the model were plotted over a range of possible tilt angles, it was noted that both the curves were nearly linear with different slopes at the origin. Since the model did not have any bracing or cross-member, its righting moment for each $\overline{GM}$ was linear as shown in Fig. 186. This figure presents the righting moments for the first three $\overline{GM}$s at the actual tilt angles obtained from the static inclination tests. As shown in two typical examples at the smallest $\overline{GM}$ (0.019 m), Fig. 187a, and at the largest $\overline{GM}$ (0.079 m), Fig. 187b, the righting moment was always larger than the wave-induced tilting moment. The difference between the slopes increased rapidly demonstrating considerably larger slopes for the righting moment as the $\overline{GM}$ increased.

The above investigation demonstrated that there was no need to have a non-linearity in the righting moment curve to experience a steady tilt. Moreover the gap between the two lines of the actual equilibrium tilt angles suggested it was necessary to investigate further the difference between the two moment mechanisms. Therefore an alternative way of presenting the comparisons was carried out as follows:

The steady wave-induced moment for the model for each test run was predicted from eq. 58 at the actual tilt and wave data, which were

tabulated in Tables 10 to 14. The righting moments were also calculated at the corresponding tilt angles. Since the actual tilt angles theoretically indicates an equilibrium condition, the two moments computed at these angles should be equal or close in magnitude.

The results of such a comparison for typical frequencies, where the steady tilt occurred in the model tests, are presented in Figs 188 to 189. In these figures the wave-induced tilting moment is represented by a small circle corresponding to each test run. Since the righting moment is linearly dependent on the tilt angles, it is represented by the solid line passing through the values computed at the actual tilt angles. As shown in Figs 188a and 188b there is relatively close agreement between the magnitudes at the smallest $\overline{GM}$. However, as the $\overline{GM}$ increases the magnitude of the righting moment increases rapidly compared to that of the wave-induced tilting moment resulting in an increasing difference between them, Fig. 189.

The above investigation indicated that based on the Numata, et al. theory, the equilibrium between the magnitudes of the two moments at the actual tilt angles is highly dependent on $\overline{GM}$.

As discussed in Chapter 3, it was not possible to test the model with a smaller $\overline{GM}$ than 0.019 m because of practical difficulties. If it were possible and the resulting tilt angles could be measured accurately, the author has a strong feeling that the tilting moment could become larger than the righting moment at the actual tilt angles due to the strong influence of the $\overline{GM}$.

The above findings brought about the conflicting fact that whatever the model's $\overline{GM}$ was, if it had a steady tilt, at the equilibrium angle theoretically the tilting moment and the righting moment should be equal in magnitude; whereas the computations based

on the Numata, et al. theory demonstrated that this depended on the model's $\overline{GM}$.

The $\overline{GM}$ dependent gap between the two moments could be attributed to the inexact representation of the wave-induced moment mechanism. From the point of view of the righting moment mechanism, the variation of the moment arm under certain combinations of waves (trough or crest) relative to the position of the model may not be important because of the small waterplane area of the columns. Therefore the existing righting moment formula, which is valid for the static water level, can be justified. Whereas the inexact representation of the tilting moment due to the absence of the steady horizontal forces is important as explained below.

The steady horizontal forces acting on the columns form the major part of the total steady horizontal force on a semi-submersible. Figure 190 illustrates the components of the potential steady surge force on a three columns per hull twin rectangular hull semi-submersible referring to section 4.4[14,116]. As shown in this figure the wave-elevation component (component I) is the dominant component while the remaining only reduces somewhat the effect of contribution I. In addition to this potential component, steady effects of the horizontal drag forces on the surface-piercing columns will be important depending on the column diameter and wave height[91-94]. It is important that both force mechanisms originate due to wave motion about the free surface depending on wave height and diffraction of waves (for the potential component) from the columns.

On the other hand if the geometric characteristics of the model used in these tests are considered, its draught is 0.36 m and its KG varies between 0.28 m to 0.22 m corresponding to $\overline{GM}$s of

0.019 m and 0.076 m respectively. When the model has the smallest $\overline{GM}$, the COG about which the steady tilting moment is taken, is close to the free surface. Therefore the contribution of the horizontal forces to the tilting moment will be less due to a small moment arm. However, as the $\overline{GM}$ increases, the COG shifts downward while the horizontal forces still act about the free surface. This will introduce an increasing moment. Referring to Figs 188a and 188b it was noted that the tilting moments were in relatively close order of magnitude with the righting moment at the smallest $\overline{GM}$. In this case because of the small moment arm the absence of the horizontal forces on the column had less effect on the tilting moment. Whereas as the $\overline{GM}$ increased this effect becomes appreciable due to the increased moment arm resulting in an underestimated tilting moment.

(ii) The steady horizontal force due to the potential wave elevation component (component I) has been explained in section 4.4. It can be presented on a column by the time average value of the following expression[94]:

$$F_X = \frac{1}{2} \int_{-H}^{\eta} \int_{o}^{2\pi} p(\theta,y) R \cos\theta \, d\theta dy \qquad \ldots \quad (81)$$

its moment about the COG is the time average value of:

$$M_X = \frac{1}{2} \int_{-H}^{\eta} \int_{o}^{2\pi} p(\theta,y) R \, (\overline{OG}-y) \cos\theta \, d\theta dy \qquad \ldots \quad (82)$$

where H is column height, η is crest elevation, R is column diameter, p is the total pressure and θ is the polar angle.

In the above equations the pressure p includes the diffraction effect of the waves. This requires a three-dimensional representation because of the column configurations. Since the use of two-dimensional

beamwise strip theory demonstrated large three-dimensional errors in the column part, this contribution could not be taken into account by the close-fit method presented in the thesis. Therefore the absence of this component will cause an underestimation in the tilting moment results to be presented.

However, the effect induced by the drag component on the semi-submersible model is taken into account based on the theory given in section 4.4.3:

Figures 191 and 192 (a,b,c) present the roll exciting moment exerted on the model by the drag force for two extreme $\overline{GM}$s. For these illustrations the moments about the COG are broken down into the contributions from the vertical and horizontal directions in the upright position. The wave amplitudes at which the moments are computed are obtained from the modified ABS wave height formula as shown in Fig. 193. In the computations the drag coefficient for the column and hull was taken as 1.2.

As illustrated in Figs 191b and 192b the contribution due to the vertical drag force on the lower hulls is completely symmetric indicating a zero mean over one period. Whereas the contribution due to the horizontal drag force, Figs 191c and 192c, is asymmetric resulting in an asymmetric rolling moment as shown in Figs 191a and 192a. This asymmetry yields a mean moment over one period which is always in the leeward direction over the range of frequencies tested. (In Figs 191 and 192 negative y-axis indicates the moment in the leeward direction.)

Having computed the mean value of the oscillatory roll-exciting moment, these mean moments are presented in Fig. 194 for differing $\overline{GM}$s in the upright position. As shown in this figure as

the $\overline{GM}$ increases the tilting moment is increased. It should be noted that since the mean moment is always in the leeward direction the negative sign of this moment is disregarded.

According to the Numata, et al. theory, in order to develop a steady tilt there is a requirement for an initial starting mechanism. Depending on the direction of this mechanism a steady tilt could occur in either direction, leeward or seaward, since the theory provides a bi-stable tilting moment. The inclusion of the drag component automatically brings about a mechanism which provides an initial tilt always in the leeward direction. This finding confirms the model test results in terms of the preferred direction of tilt. However, in addition to this component the effect of the other components, which are not taken into account in the thesis, (e.g. the leeward column and hull is exposed to a wave diffracted by the presence of the seaward column and hull, the vessel's oscillatory motion about a tilted position) can cause a preferred direction of tilt.

In Figs 195 to 198 the sum of the moment induced by the steady vertical force and the drag force are compared to the righting moment at the actual tilt angles. As shown in these figures the inclusion of the drag component closes the gap between the two moments considerably particularly at the largest $\overline{GM}$, Fig. 197. However, there is still a difference between the two moments, Fig. 198, which indicates that tilting moment is still underestimated. However, it is noted that for large tilt angles the tilting moment becomes larger than the righting moment ($\phi \geq 12°$), Figs 195 and 196. This can be attributed to the combination of several factors which are induced by the non-linear behaviour of the forces in large waves, restrictions imposed by the measuring mechanism (LVDT strings) and moorings at

extreme tilts and sometimes green water at the deck due to wave splashing.

One important point is that during the tilting moment computations, it is assumed that the model is fixed. Therefore the computed moment theoretically should be overestimated. Whereas if the vessel's oscillation is taken into account the tilting moment will be reduced considerably as demonstrated by Martin and Kuo. In such a case to close the gap between the two moments will be impossible. Therefore the restraint body assumption may well be justified due to the existence of the moorings. Otherwise there is a need to take into account the effect of moorings into the moment computations.

Having predicted the tilting moment on the basis of the two force components (vertical potential force and horizontal drag force), the comparison with the righting moment at the actual tilts demonstrated an underestimation of tilting moment. Therefore the moment prediction still needs to be improved in terms of the other components involved. This underestimated tilting moment results in an underestimate of the tilt angles as shown in Figs 199 and 200. As illustrated in these figures, the initial tilting mechanism due to the drag component results in an intersection of the two moment curves although this was not possible by the Numata, et al. approach as demonstrated earlier (Figs 186a and 187b). However, Fig. 199 presents a predicted tilt of 2° for a $\overline{GM}$ = 0.019 m while the actual tilt is 6.92°. In Fig. 200 a predicted tilt of 0.7° is obtained for a $\overline{GM}$ = 0.079 m while the actual tilt is 1.36°.

From the above investigation it can be concluded that at the actual tilt angles a precise balance between the two moments is essential. An inexact representation of the moments, particularly the

tilting moment, will lead to large errors in the steady tilt predictions. Therefore unless a precise balance can be achieved between the two moments, a prediction of steady tilt will not be possible.

4.4.3 *Minimum $\bar{GM}$ to Limit Steady Tilt in Regular Beam Waves*

From the point of view of the present stability criteria, the most important parameter to be determined is the $\bar{GM}$ required to limit the steady tilt behaviour. If the regular sea state is known for a given range of frequency and wave height, a limiting $\bar{GM}$, which allows some minimum amount of tilt, can be established from the equilibrium condition of the wave-induced tilting moment and the righting moment. As given in eq. I.5 of Appendix I, Numata, et al. suggested the minimum $\bar{GM}$ criteria to avoid wave-induced tilt in regular beam seas. However, this criteria needs to be improved in terms of its interpretation and the representation of the tilting moment involved as explained below.

4.4.3.1 *Outline of theoretical approach and formulation of problem:* When the vessel has a steady tilt at an angle of ϕ, the vessel's righting moment $M_R(\phi)$ should be balanced by the total wave-induced tilting moment given by:

$$\Sigma \bar{M}_T^t(\phi) = \bar{M}_T^t(\phi) + \bar{M}_{T_D}^t(\phi) + \text{Others} \qquad \ldots \quad (83)$$

where $\bar{M}_T^t(\phi)$ is the moment induced by the steady vertical force given by eq. 58,

$\bar{M}_{T_D}^t(\phi)$ is the moment induced by the steady drag force given by eq. 80,

Others is the remaining moments which have been left out in the thesis but should be included for the exact representation of the tilting moment.

Then, at a tilted position:

$$\Sigma \bar{M}_T^t(\phi) = M_R(\phi) \qquad \ldots \quad (84)$$

with

$$M_R(\phi) = \rho g \nabla_s \bar{GM} \sin\phi \qquad \ldots \quad (85)$$

for relatively small angles. Where ∇_s indicates the vessel's total displacement volume.

The substitution of eqs 83 and 85 into eq. 84 results in a $\bar{GM}$ value given by:

$$\bar{GM}_{min} = \Sigma \bar{M}_T^t(\phi) \Big/ \rho g \nabla_s \sin\phi \qquad \ldots \quad (86)$$

where $\bar{GM}_{min}$ is the $\bar{GM}$ to limit the steady tilt to the angle ϕ.

For any $\bar{GM} > \bar{GM}_{min}$ the vessel will have a smaller angle than ϕ

for $\bar{GM} < \bar{GM}_{min}$ the vessel continues to develop tilt with growing magnitude until the leeward deck touches the water which could lead to a capsizing condition.

In order to demonstrate the consequence of the Numata, et al. approach in the following the minimum $\bar{GM}$ obtained on the basis of the steady vertical force is given:

If the tilting moment is induced by the steady vertical force only, eq. 83 becomes:

$$\Sigma \bar{M}_T^t = \bar{M}_T^t \qquad \ldots \quad (87)$$

where $\bar{M}_T^t$ is given by eq. 58. By substituting eq. 57 into 58 under the small angle approximations given by:

$\cos\phi \simeq 1$, $\sin\phi \simeq \tan\phi \simeq \phi$, it follows

$$\Sigma \bar{M}_T^t = \bar{M}_T^t = \rho g (\gamma a)^2 \nabla \left[1 + 0.5\ (K_{22} + K_{33})\right] \left\{ S(e^{2\gamma S\phi} - e^{-2\gamma S\phi}) + D\phi\ (e^{2\gamma S\phi} + e^{-2\gamma S\phi}) \right\} \qquad \ldots \quad (88)$$

The substitution of:

$$e^{2\gamma S\phi} + e^{-2\gamma S\phi} = 2 \cosh 2\gamma S\phi$$

$$e^{2\gamma S\phi} - e^{-2\gamma S\phi} = 2 \sinh 2\gamma S\phi \qquad \ldots \quad (89)$$

$$\underline{\cosh 2\gamma S\phi} \simeq 1$$

$$\underline{\sinh 2\gamma S\phi} \simeq 2\gamma S\phi$$

into eq. 88 yields:

$$\Sigma \bar{M}_T^t \simeq \rho g (\gamma a)^2 e^{-2\gamma H_o} \nabla \left[1 + 0.5 \left(K_{22} + K_{33}\right)\right] \left\{4\gamma S^2 + 2D\right\} \phi \qquad \ldots \quad (90)$$

By substituting eqs 90 and 85 into eq. 84 and assuming $\sin\phi \simeq \phi$, it follows:

$$\bar{GM}_{min} = (\gamma a)^2 e^{-2\gamma H_o} \frac{\nabla}{\nabla_s} \left[1 + 0.5 \left(K_{22} + K_{33}\right)\right] (4\gamma S^2 + 2D) \qquad \ldots \quad (91)$$

Equation 91 is similar to the min $\bar{GM}$ expression given by Numata, et al. and applicable to the lower hull with arbitrary cross-section. As noted in eq. 91, $\bar{GM}_{min}$ is independent of ϕ although it is derived from the equilibrium of the two moments at the tilted position ϕ. Numata, et al. defined $\bar{GM}_{min}$ in eq. 91 as the minimum $\bar{GM}$ to avoid steady wave-induced tilt in regular waves.

4.4.3.2 *Computations for minimum $\bar{GM}$ and discussion of results:*
The minimum $\bar{GM}$ criteria proposed by Numata, et al., eq. 91 (or eq. I.5 in Appendix I) needs to be improved on the following grounds.

Having the minimum $\bar{GM}$ expression independent of a tilt angle on the basis of the steady vertical force does not define it as the minimum $\bar{GM}$ to avoid steady tilt. However, according to eq. 86 theoretically to avoid steady tilt either the tilting moment should be zero or the $\bar{GM}$ should be infinitely large and for any normal level of $\bar{GM}$, some tilt will always occur. Since the minimum $\bar{GM}$ is highly dependent on the steady tilting moment it is essential to

account for all the forces which contribute to tilting moment or an erroneous minimum $\overline{GM}$ will be obtained.

In order to show the consequence of Numata, et al's criteria; the minimum $\overline{GM}$ of the model was computed at a range of wave frequencies and heights obtained from the ABS wave height formula. The results are presented in Fig. 201. As shown in this figure, a minimum $\overline{GM}$ curve is obtained corresponding to each of the original model test $\overline{GM}$s. Amongst the five minimum $\overline{GM}$ curves the largest minimum $\overline{GM}$ corresponds to the smallest test $\overline{GM}$ (1.33 m in full scale) and has a peak value at 0.0135 m (0.945 m on the full scale). According to Numata, et al's interpretation when the model has a $\overline{GM}$ just above this minimum value it will avoid steady tilt over the range of frequencies. However, the experimental findings do not confirm this criteria. As shown in Fig. 202, the model with original $\overline{GM}$s varying between 0.019 m and 0.079 m, which are well above the largest minimum $\overline{GM}$ (0.0135 m), still demonstrates steady tilt angles varying between 12° and 1° respectively.

The above investigation indicates that although the idea of a minimum $\overline{GM}$ criteria proposed by Numata, et al. is plausible, it needs to be improved in terms of the above stated points. Therefore it is believed that the following procedure will improve the criteria one step further:

The minimum $\overline{GM}$ should be obtained from eq. 86 in which the steady tilting moment should be represented as precisely as possible. This equation theoretically requires an acceptable amount of steady tilt to be specified. Therefore a proposed tilt (say $\phi < 3°$) is imposed. Then for a given sea state (e.g. ABS wave height formula can be used) by limiting the tilt motion to this specified value, the minimum $\overline{GM}$ required is calculated for each frequency. The largest of these must be used as the design criteria for the proposed steady tilt.

Using the above procedure the minimum $\overline{GM}$s to limit the model's tilt to 0.5°, 1°, 2° and 3° are presented in Fig. 203(a,b,c,d). For comparison, the minimum $\overline{GM}$s obtained from the Numata, et al. approach is also shown in Fig. 203 . As illustrated in this figure in order to limit the steady tilt to a very small amount of tilt (ϕ = 0.5°) the largest minimum $\overline{GM}$ varies between 0.065 m to 0.10 m (4.55 m to 7.0 m on the full scale). Such a large minimum $\overline{GM}$ is due to the very small magnitude of tilt proposed. If this limit angle is increased by a small amount, the $\overline{GM}$ reduces dramatically. As shown in Fig. 203d for 3° of proposed tilt, the largest minimum $\overline{GM}$ is 0.025 m (1.75 m on the full scale). This is nearly twice the minimum $\overline{GM}$ proposed by Numata, et al. to avoid steady tilt in the same wave range.

As noted in the above investigation, the minimum $\overline{GM}$ to limit steady tilt is highly dependent on the tilting moment and the specified limiting tilt angle. To impose a negligibly small tilt angle or to avoid steady tilt is practically impossible and would require a very large $\overline{GM}$.

In the presence of wind, its effect can be included into the tilting moment expression, eq. 83, and this will affect the minimum $\overline{GM}$ required. The inclusion of the wind effect brings problems of its accurate calculation (when combined with the wave-induced effects) which has been reviewed in Chapter 1. However, the above procedure on the basis of the equilibrium of the righting moment and the combined tilting moment at a specified tilt angle can still be used for the limiting $\overline{GM}$. For the validation and verification of the moment representation, model tests under the combined effect of wave and wind will be essential.

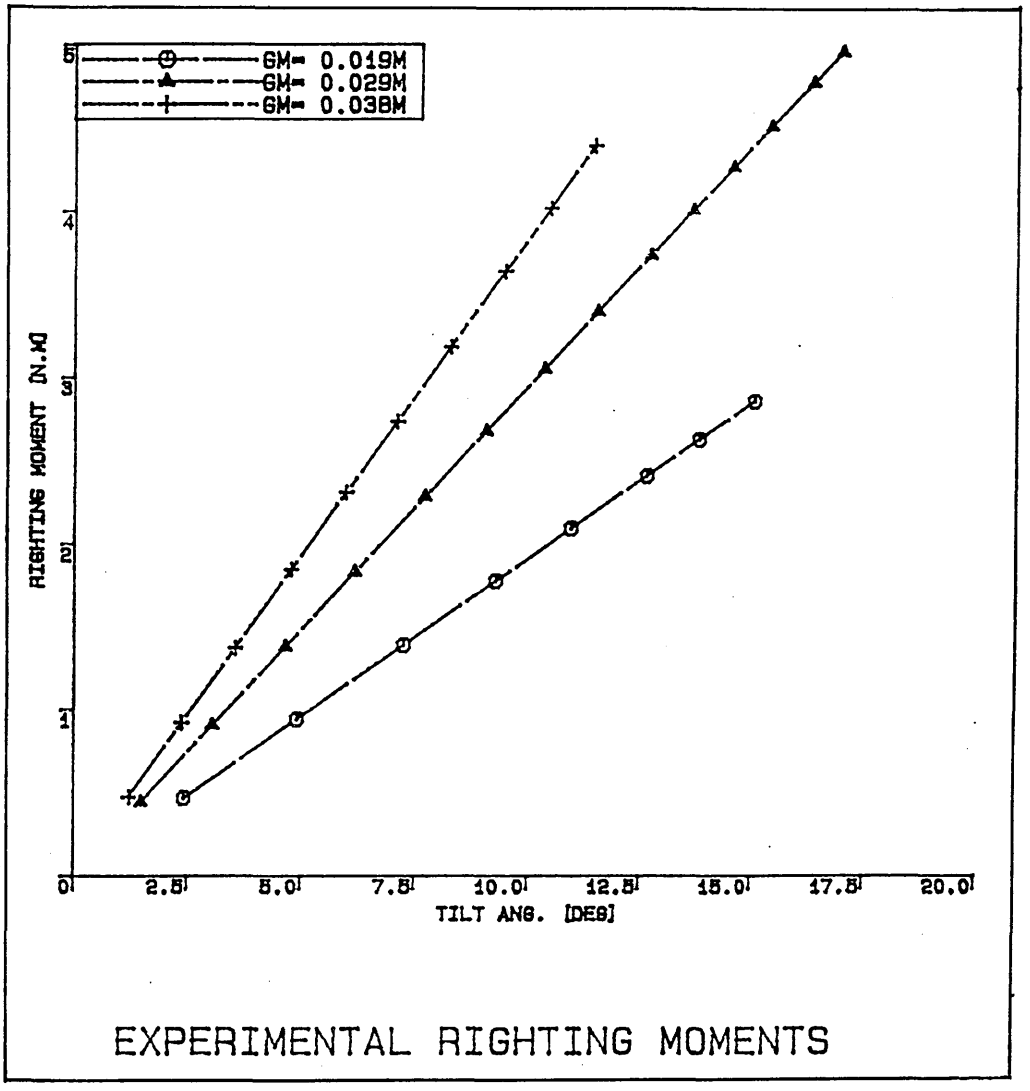

Fig. 186 - Righting moment of the semi-submersible model obtained from the model tests

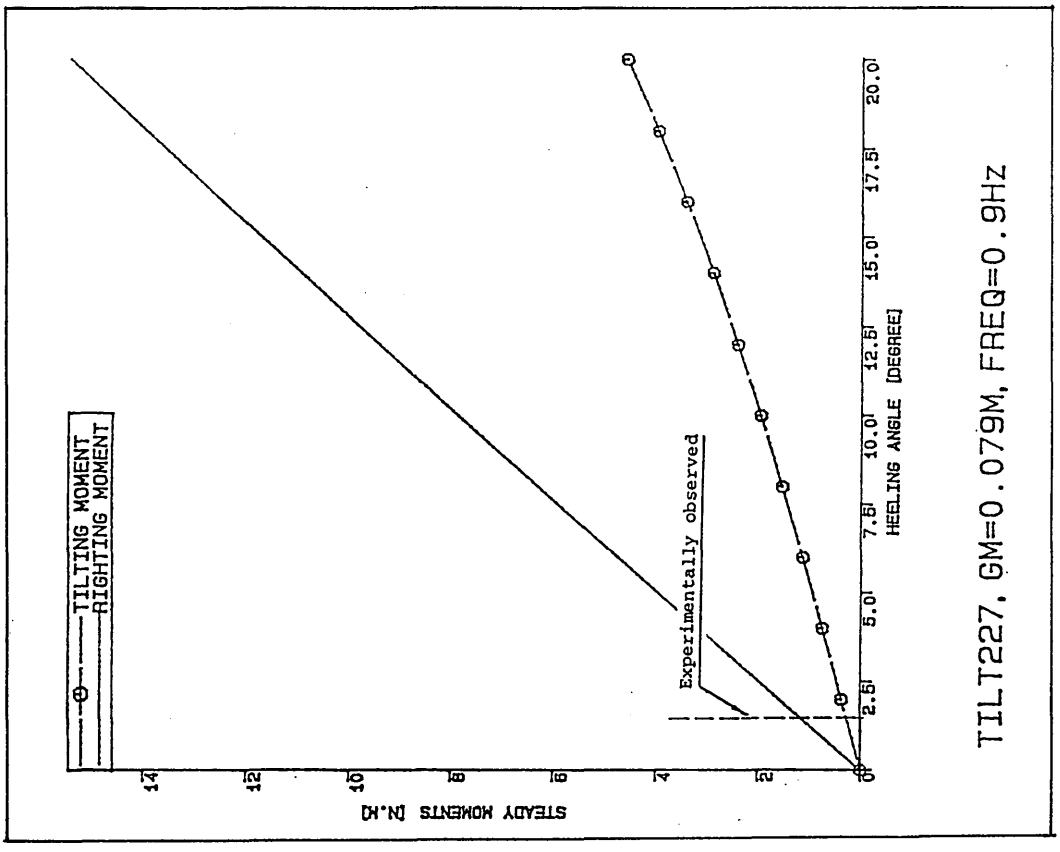

Fig. 187b - Comparison of righting moment against tilting moment predicted on the basis of steady vertical forces (potential) on hulls for GM = 0.079 m

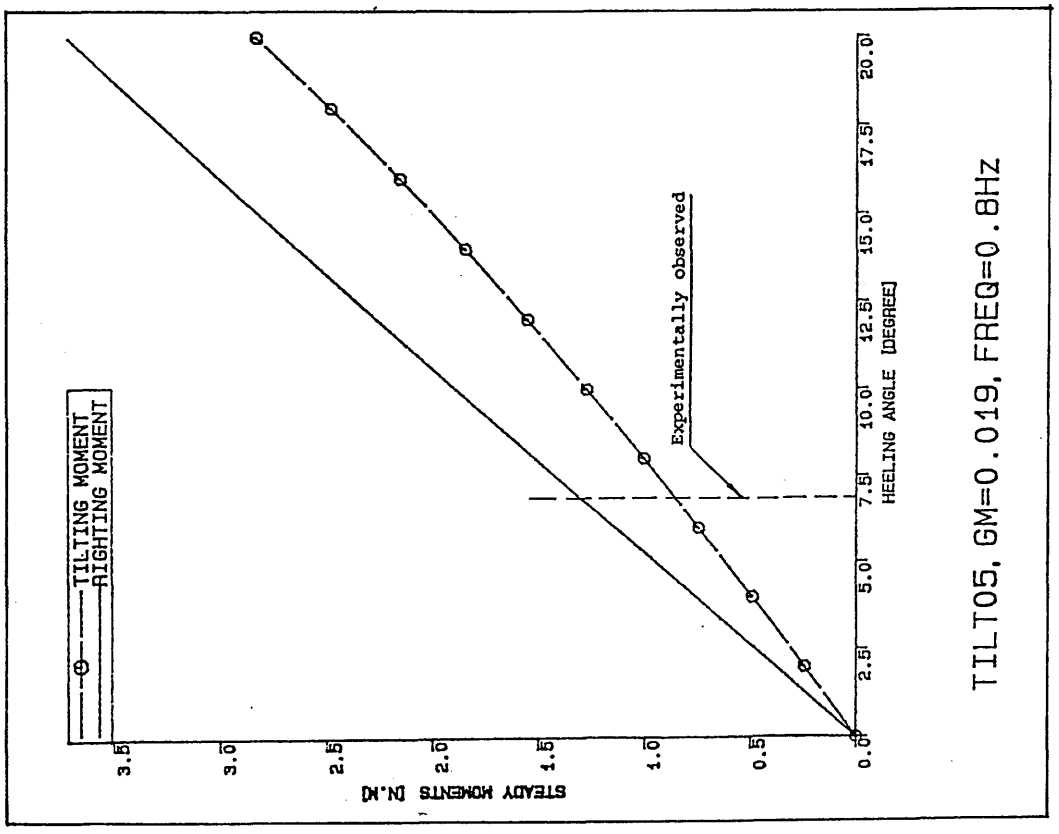

Fig. 187a - Comparison of righting moment against tilting moment predicted on the basis of steady vertical forces (potential) on hulls for GM = 0.019 m

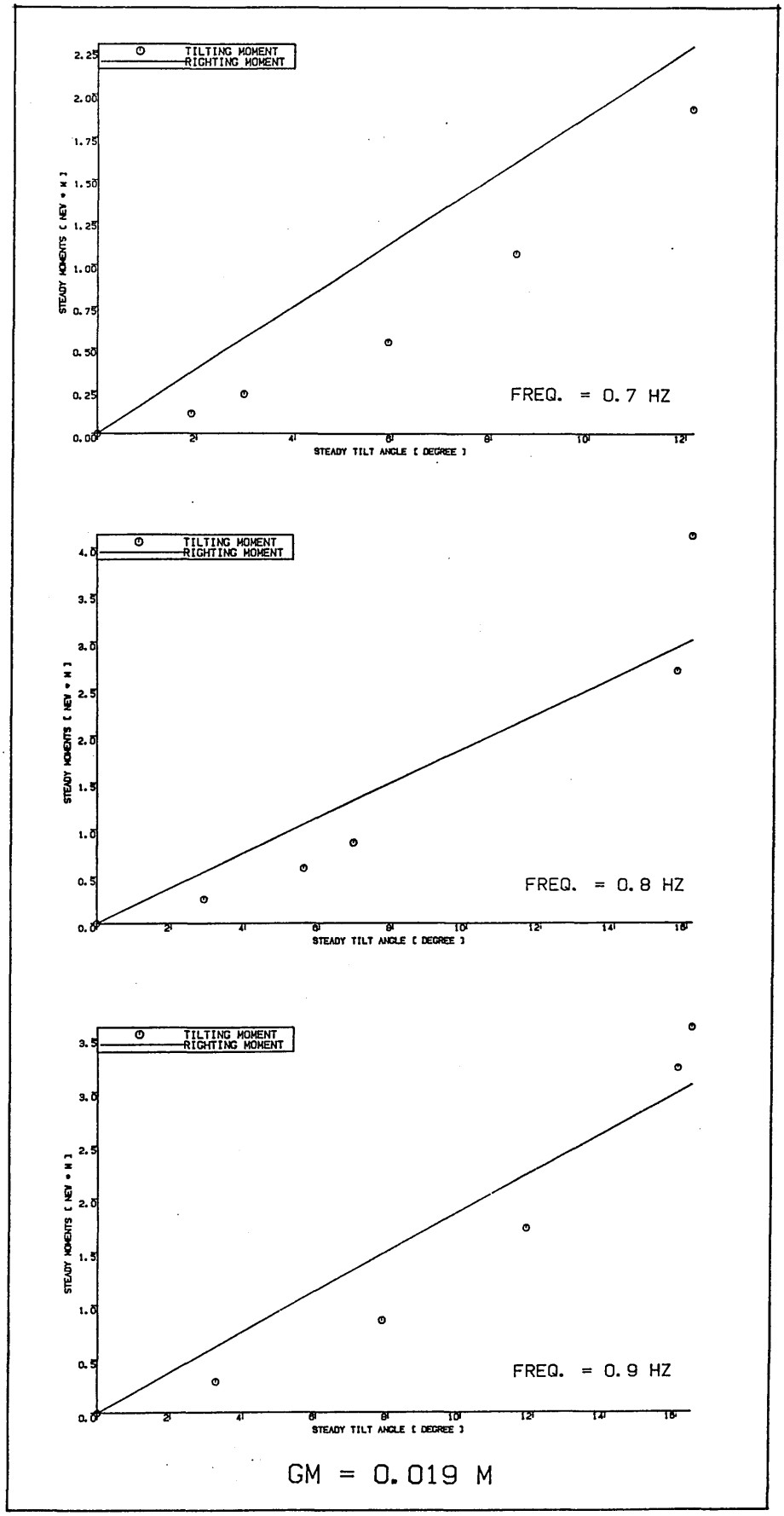

Fig. 188a - Comparison of righting moment against tilting moment predicted on the basis of steady vertical potential forces at actual tilt angles obtained from the tests for a frequency of 0.7 Hz to 0.9 Hz ($\bar{GM}$ = 0.019 m)

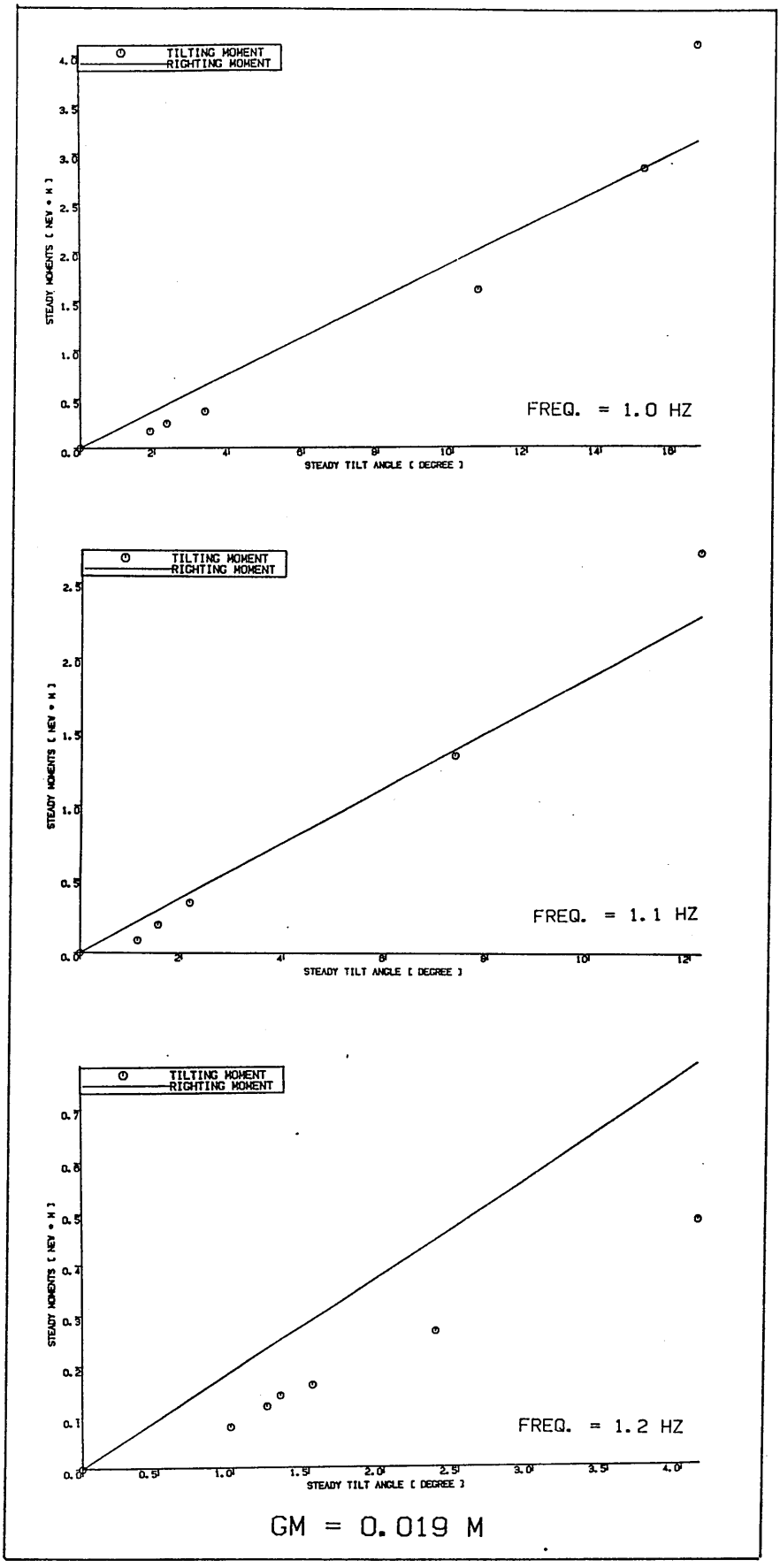

Fig. 188b - Comparison of righting moment against tilting moment predicted on the basis of steady vertical forces (potential) at actual tilts obtained from the tests for a frequency of 1.0 Hz to 1.2 Hz ($\overline{GM}$ = 0.019 m)

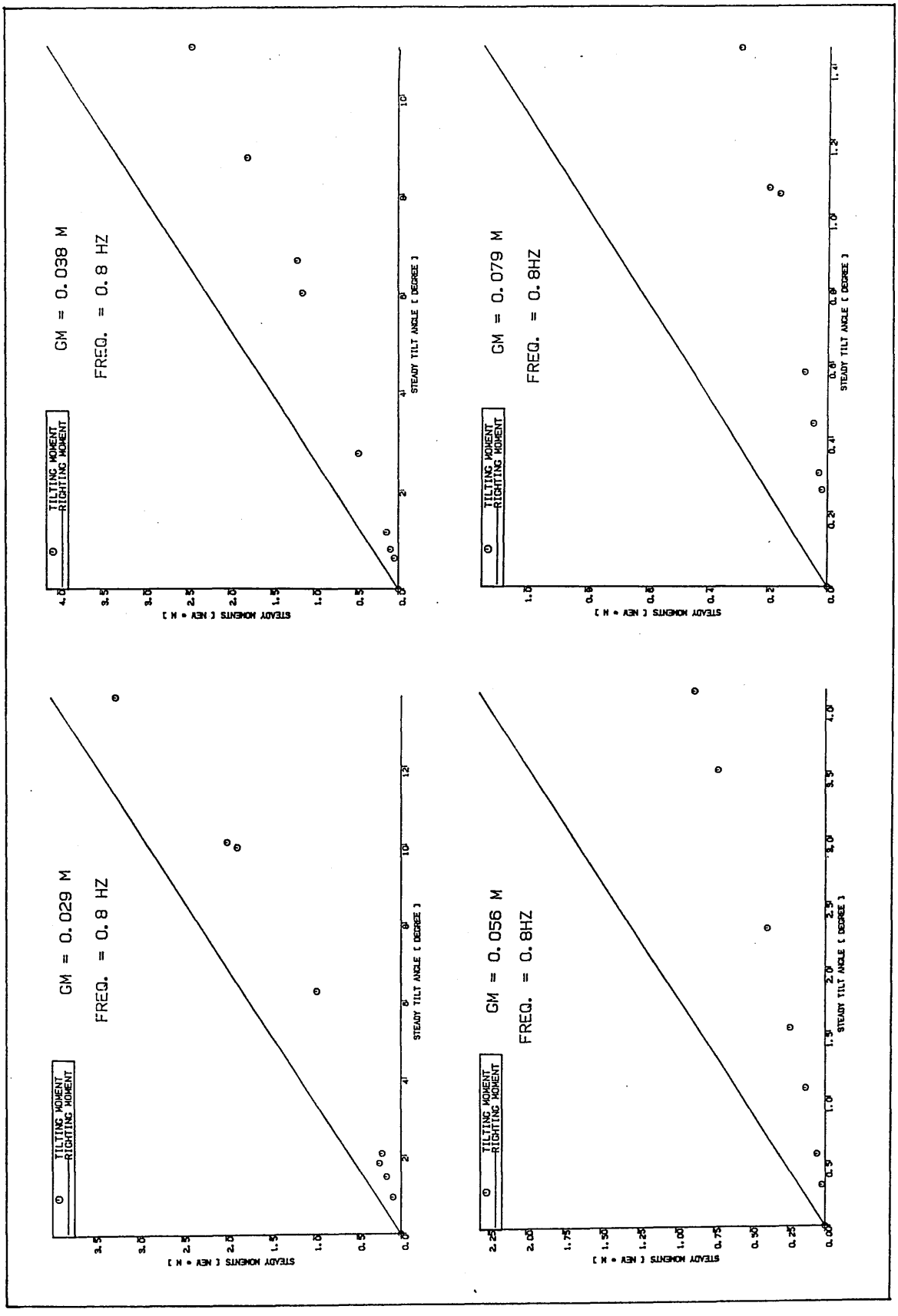

Fig. 189 - Comparison of righting moment against tilting moment predicted on the basis of steady vertical forces (potential) at actual tilt angles obtained from the tests for varying GM's at a frequency of 0.8 Hz

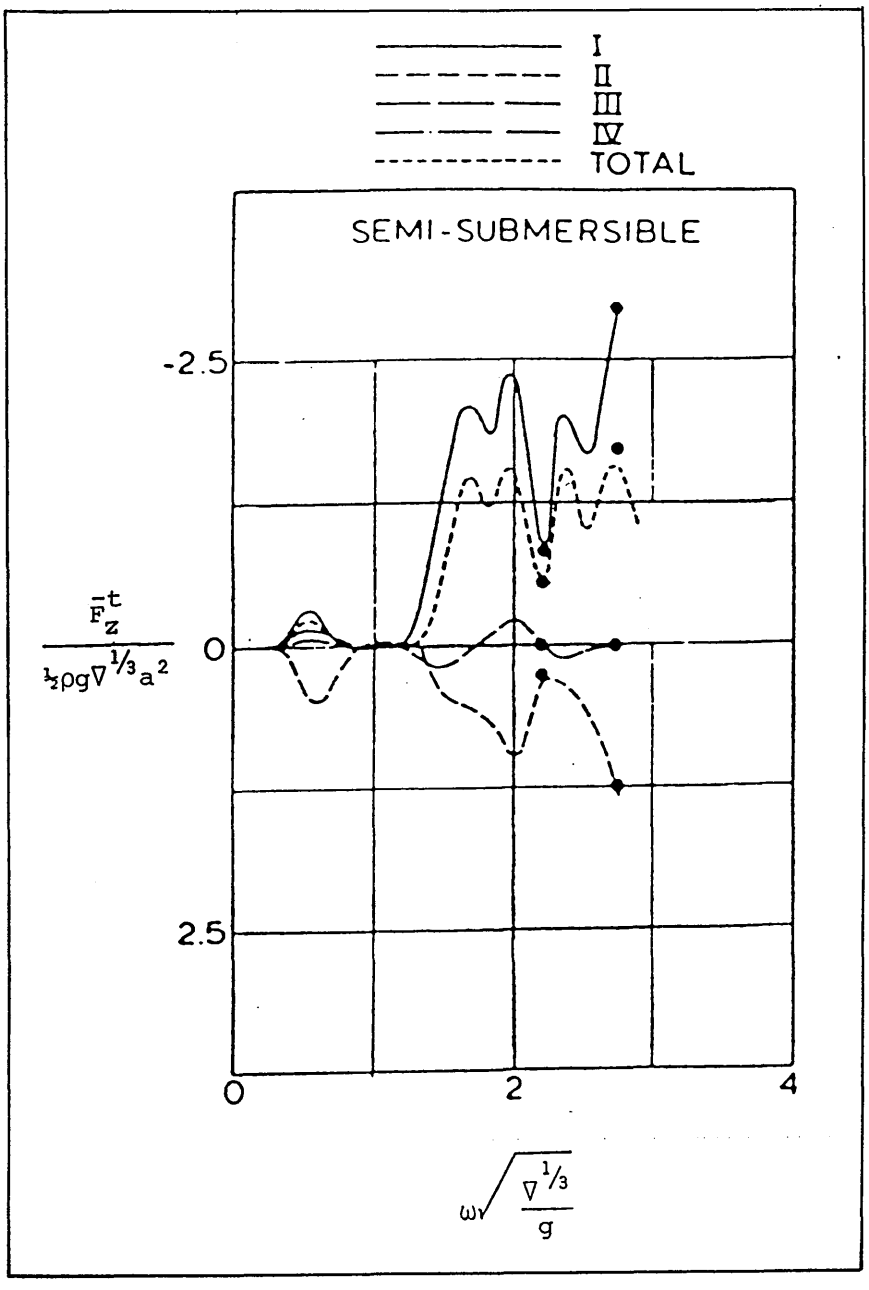

Fig. 190 - Potential surge force on a three column per hull twin rectangular semi-submersible[14,116]

(where ∇ is the displacement volume of the semi-submersible)

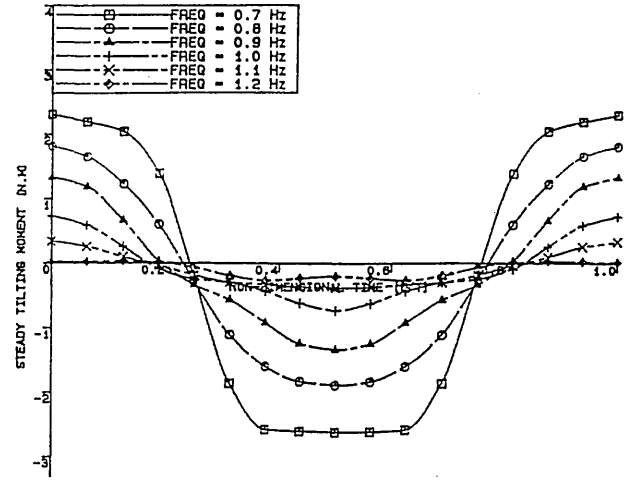

Fig. 191a

VIS. ROLL MT. - TOTAL
GM = 0.019 M.

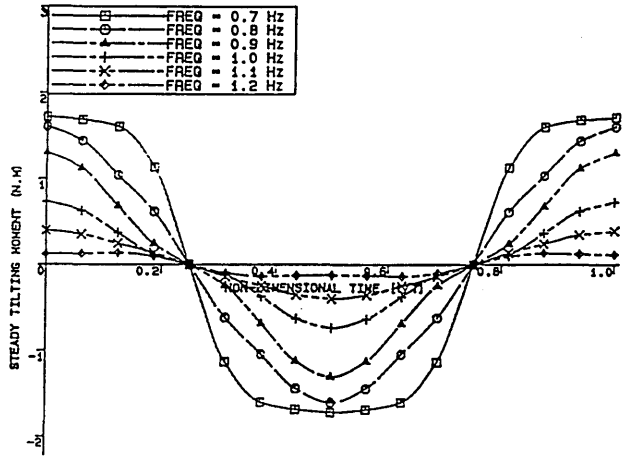

Fig. 191b

VIS. ROLL MT. - VERT. COMP.
GM = 0.019 M.

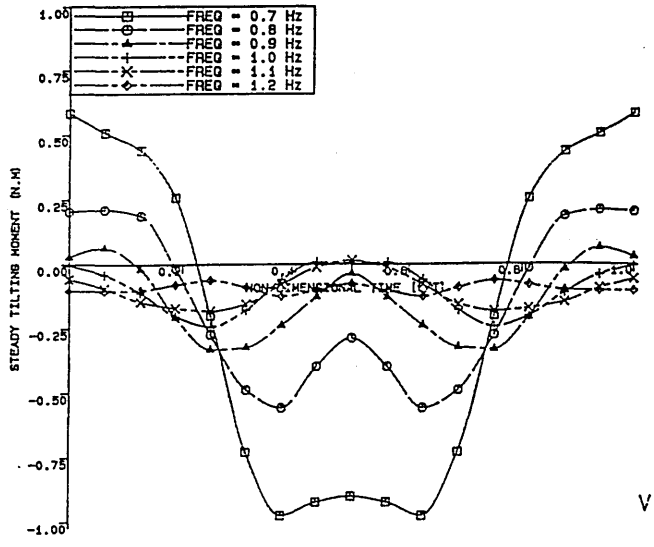

Fig. 191c

VIS. ROLL MT. - HORIZ. COMP.
GM = 0.019 M.

Fig. 191 - Breakdown of roll exciting moment due to the drag force into its vertical and horizontal components for $\overline{GM}$ = 0.019 m

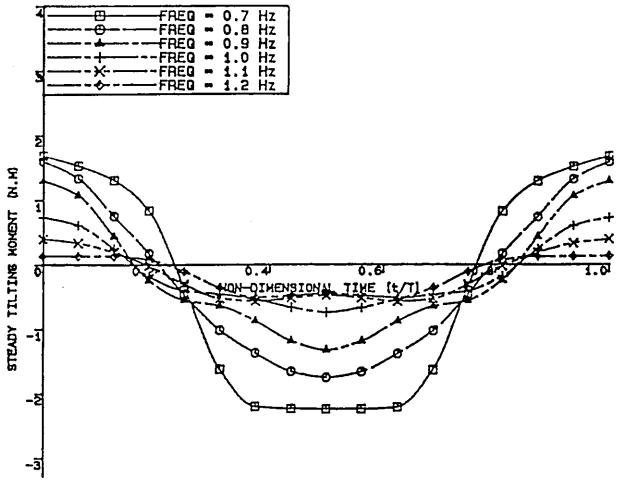

Fig. 192a

VIS. ROLL MT. - TOTAL
GM = 0.079 M.

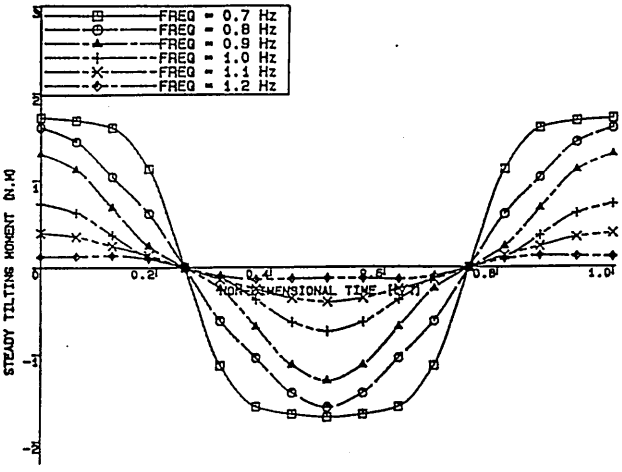

Fig. 192b

VIS. ROLL MT. - VERT. COMP.
GM = 0.079 M.

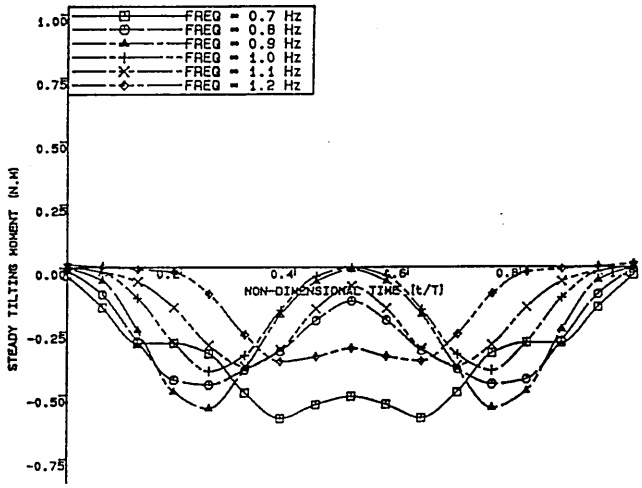

Fig. 192c

VIS. ROLL MT. - HORIZ. COMP.
GM = 0.079 M.

Fig. 192 - Breakdown of the roll exciting moment due to the drag force into its vertical and horizontal components for $\overline{GM}$ = 0.079 m

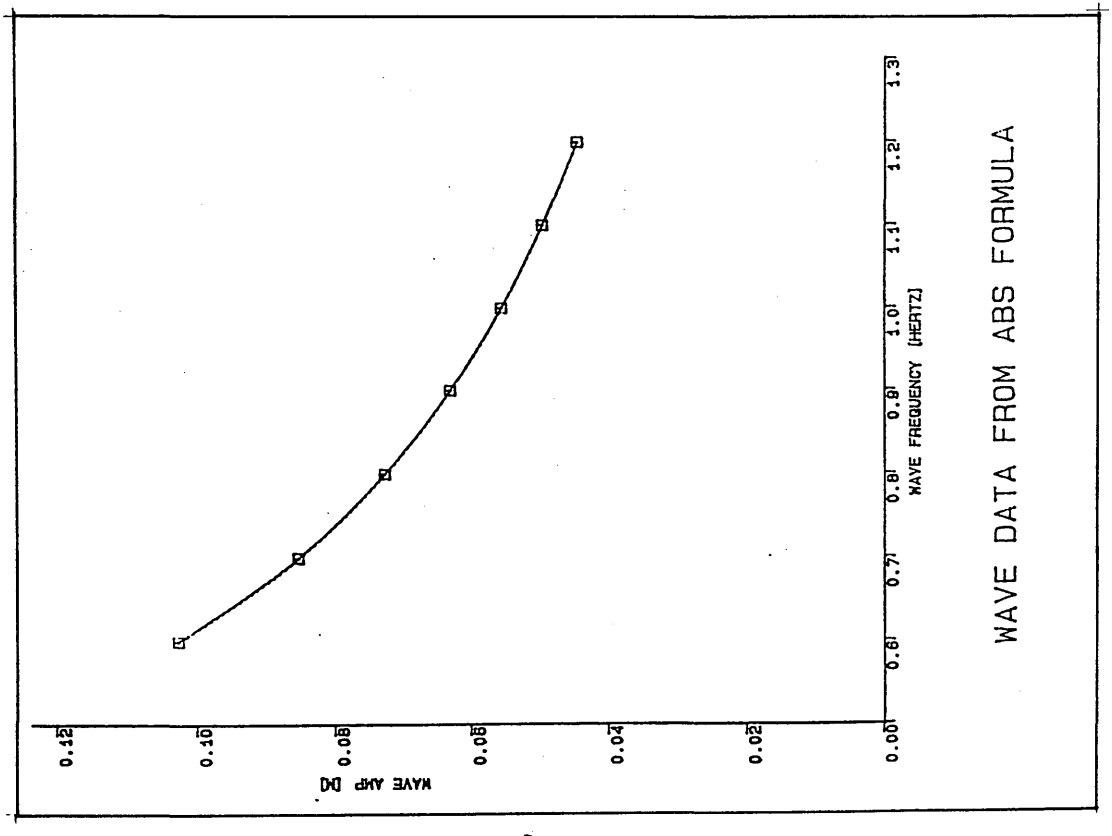

Fig. 193 - Variation of model scale wave amplitude with frequency on the basis of the ABS formula

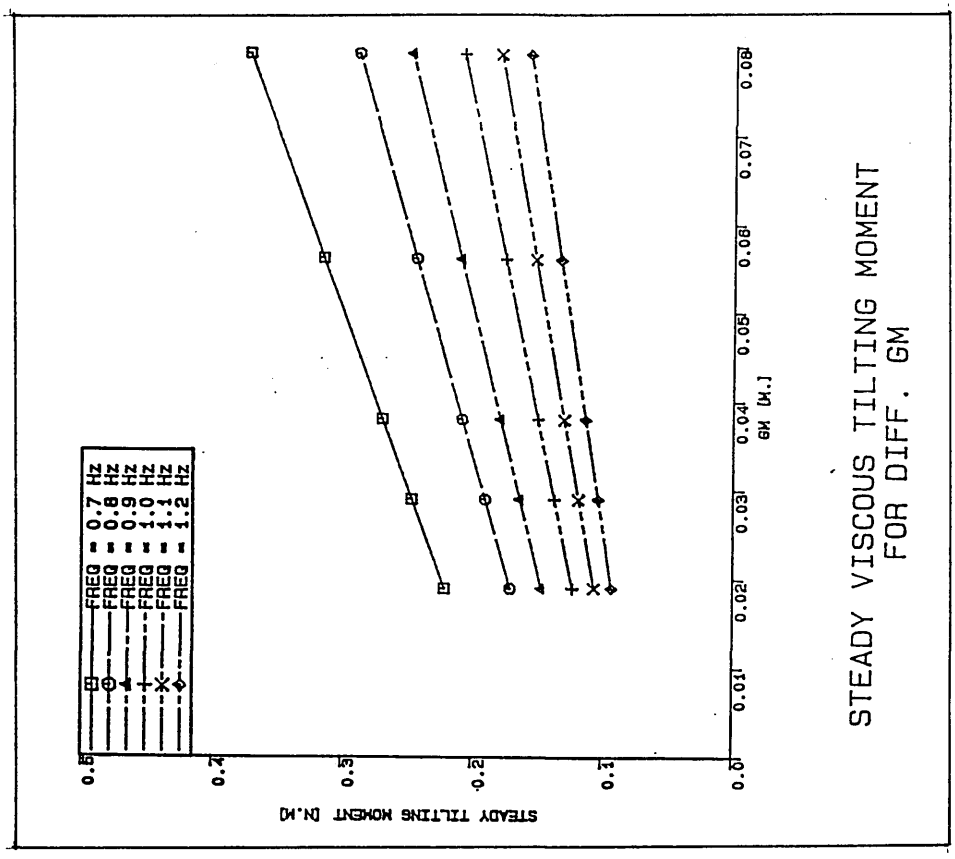

Fig. 194 - Variation of steady tilting moment induced by the drag force for varying $\overline{GM}$'s

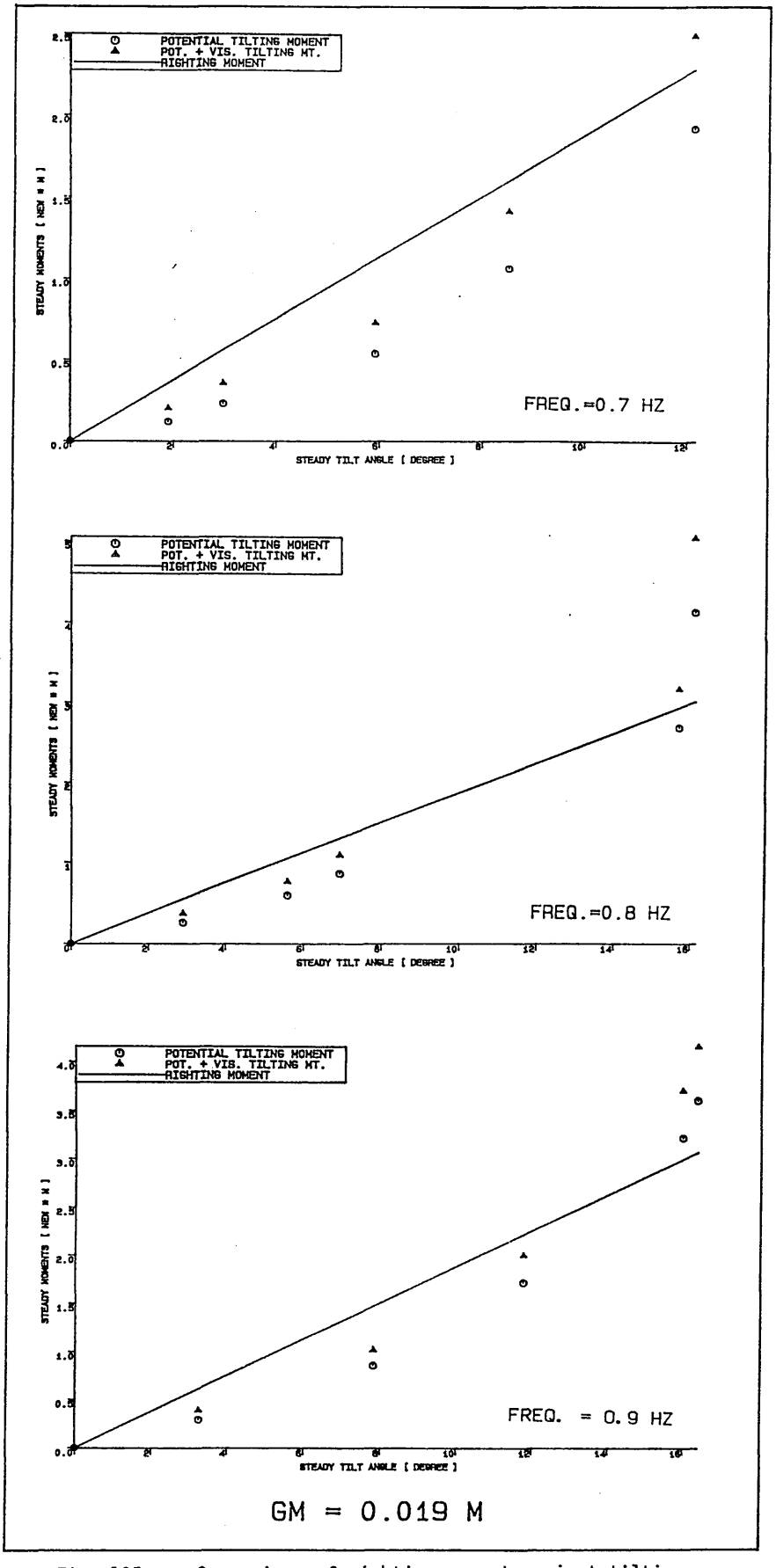

Fig. 195 - Comparison of righting moment against tilting moment on the basis of steady vertical forces (potential) and steady drag forces (viscous) at actual tilt angles obtained from the tests for a frequency of 0.7 Hz to 0.9 Hz ($\overline{GM}$ = 0.019 m)

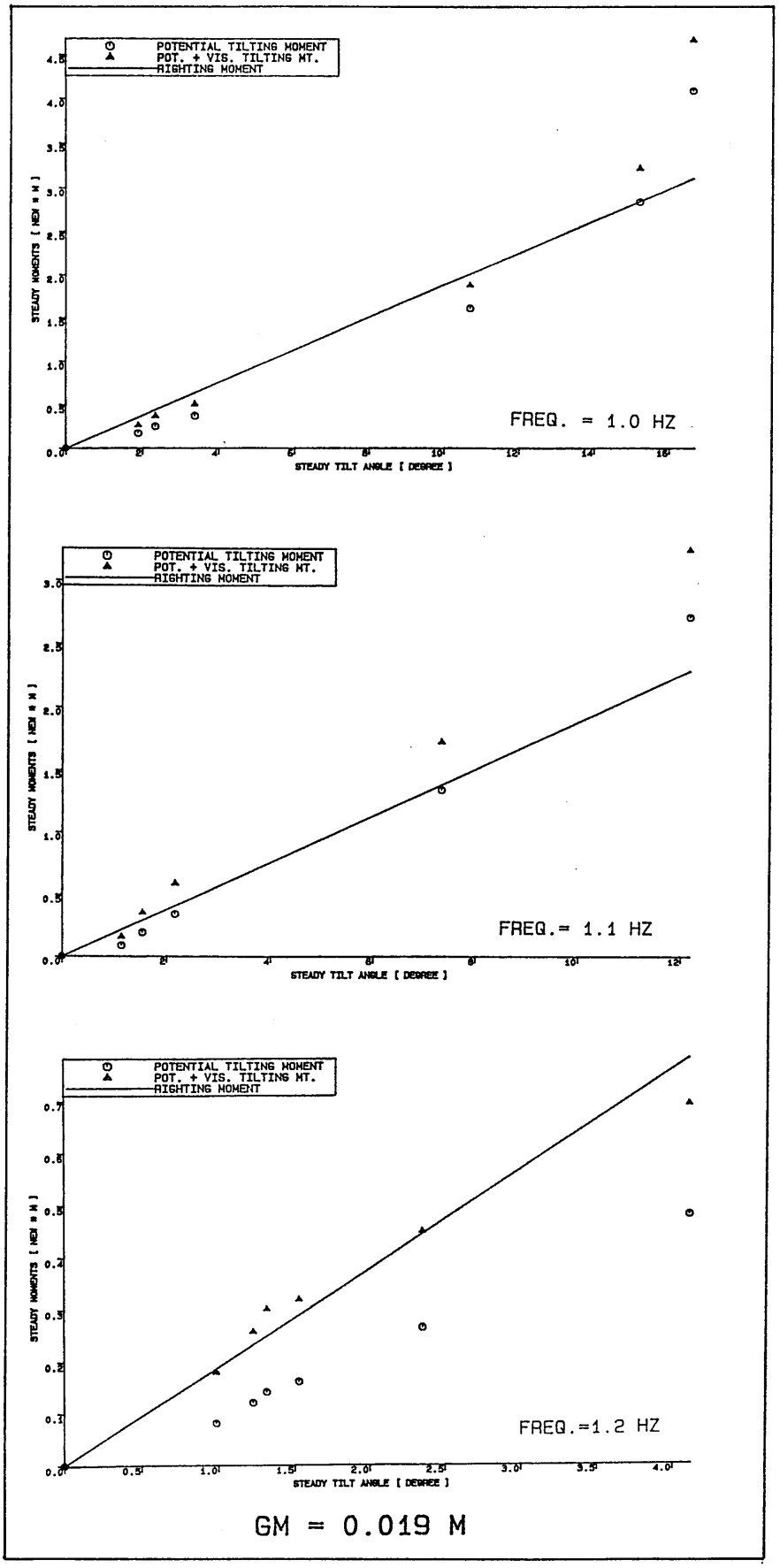

Fig. 196 - Comparison of righting moment against tilting moment on the basis of steady vertical force (potential) plus steady drag forces (viscous) at actual tilt angles obtained from the tests for a frequency of 1.0 Hz to 1.2 Hz ($\overline{GM}$ = 0.019 m)

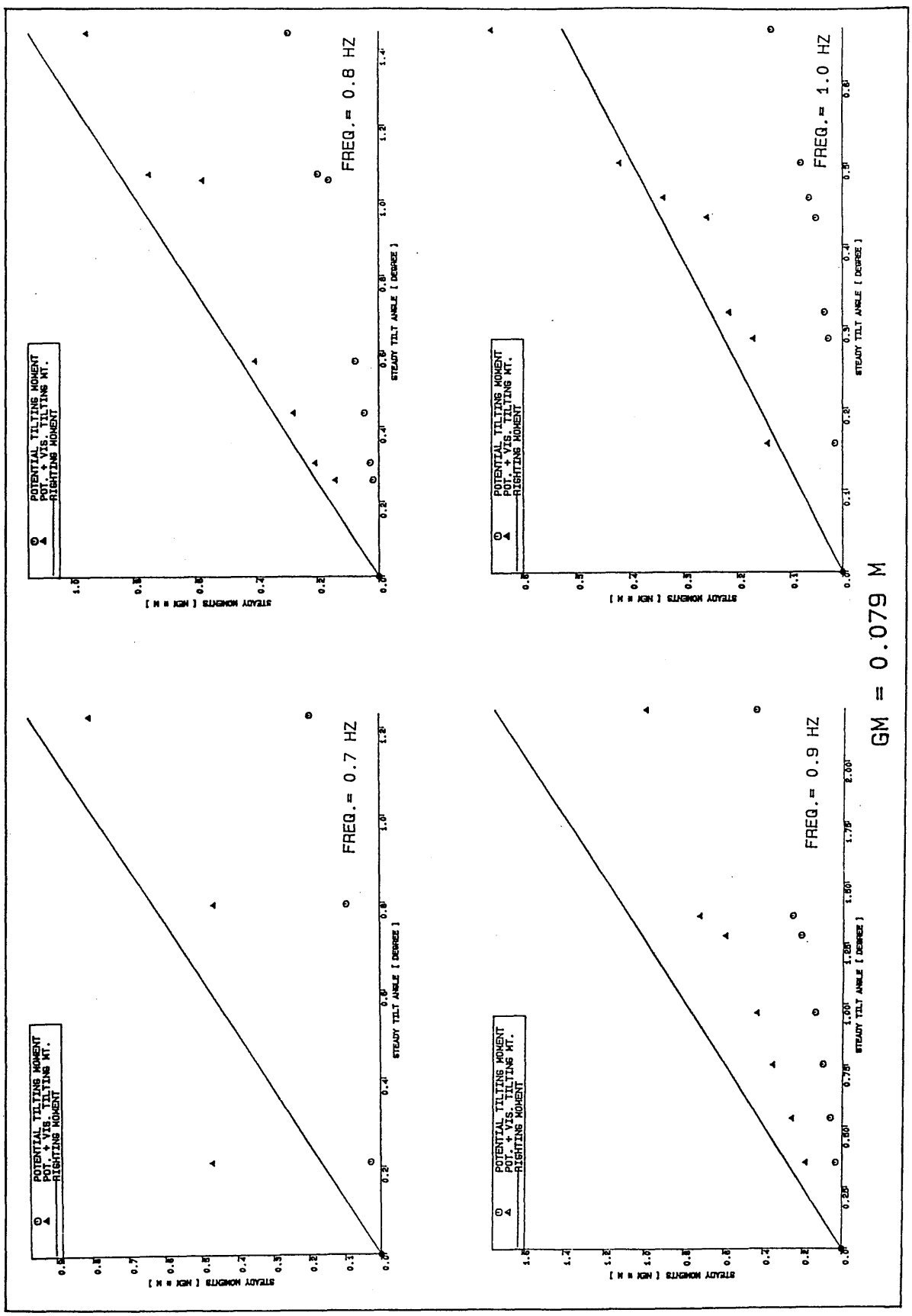

Fig. 197 - Comparison of righting moment against tilting moment on the basis of steady vertical forces (potential) plus steady drag forces (viscous) at actual tilt angles obtained from the tests for a frequency of 0.7 Hz to 1.0 Hz (GM = 0.079 m)

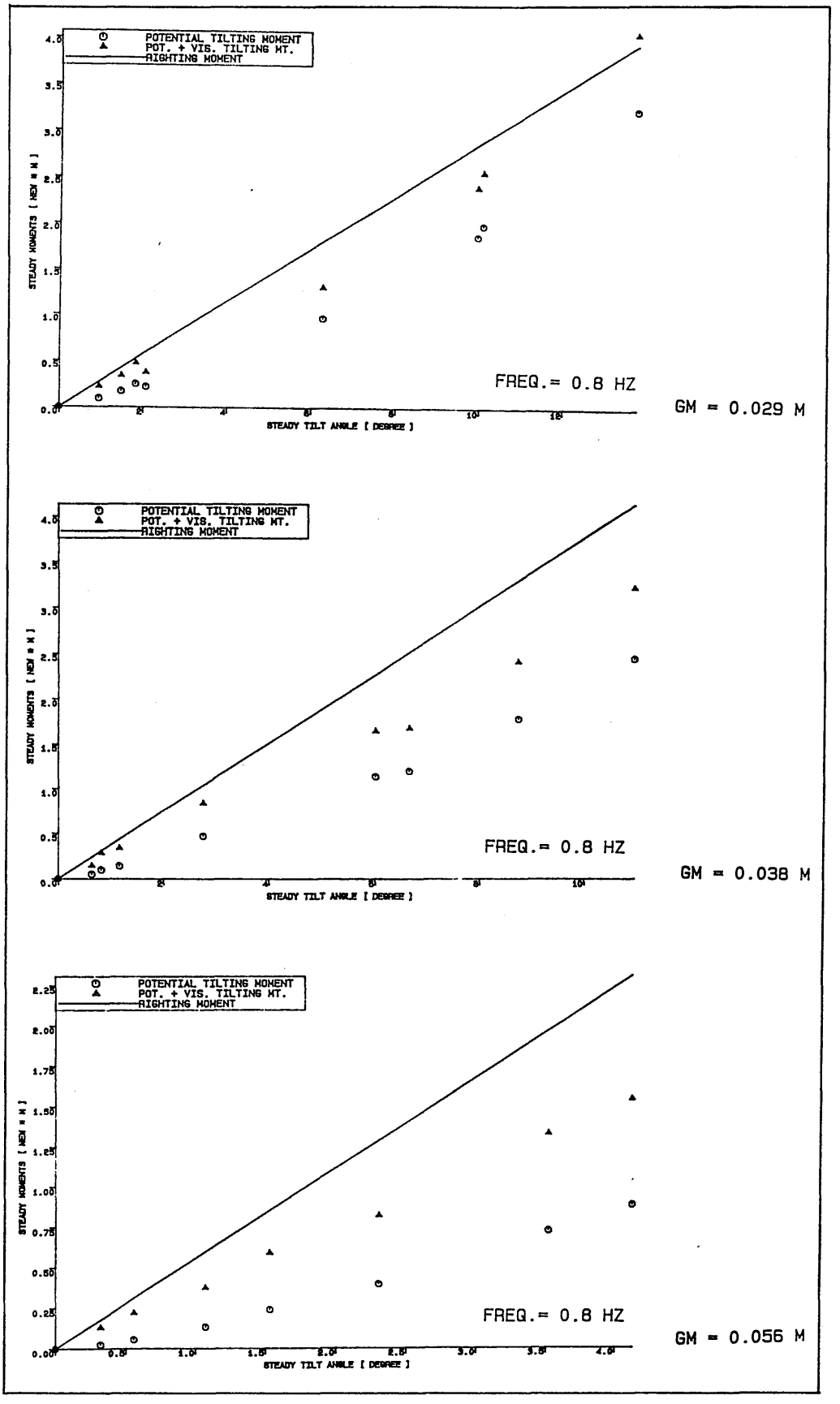

Fig. 198 - Comparison of righting moment against tilting moment on the basis of steady vertical force (potential) plus steady drag force (viscous) at actual tilt angles obtained from the tests for various $\overline{GM}$'s at a frequency of 0.8 Hz

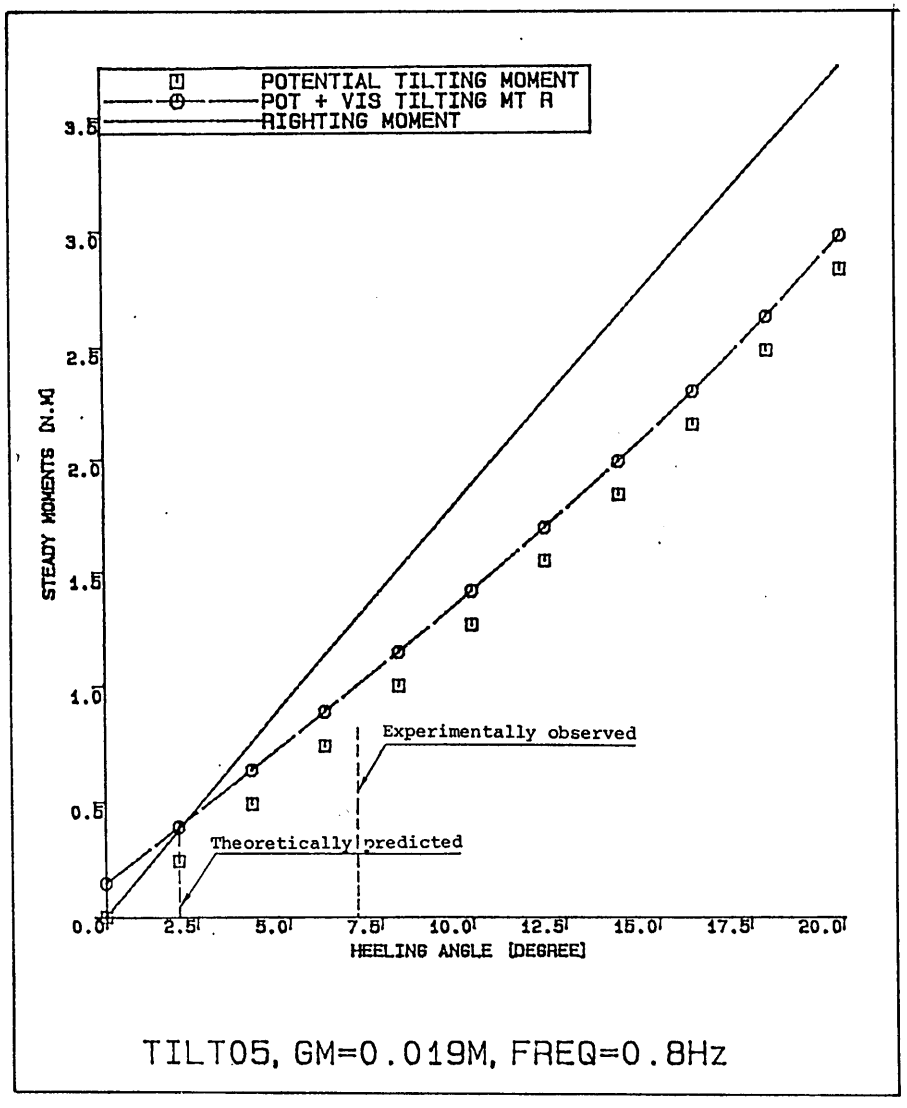

Fig. 199 - Comparison of righting moment against tilting moment on the basis of steady vertical forces (potential) plus steady drag force (viscous) at a frequency of 0.8 Hz for $\bar{GM}$ = 0.019 m

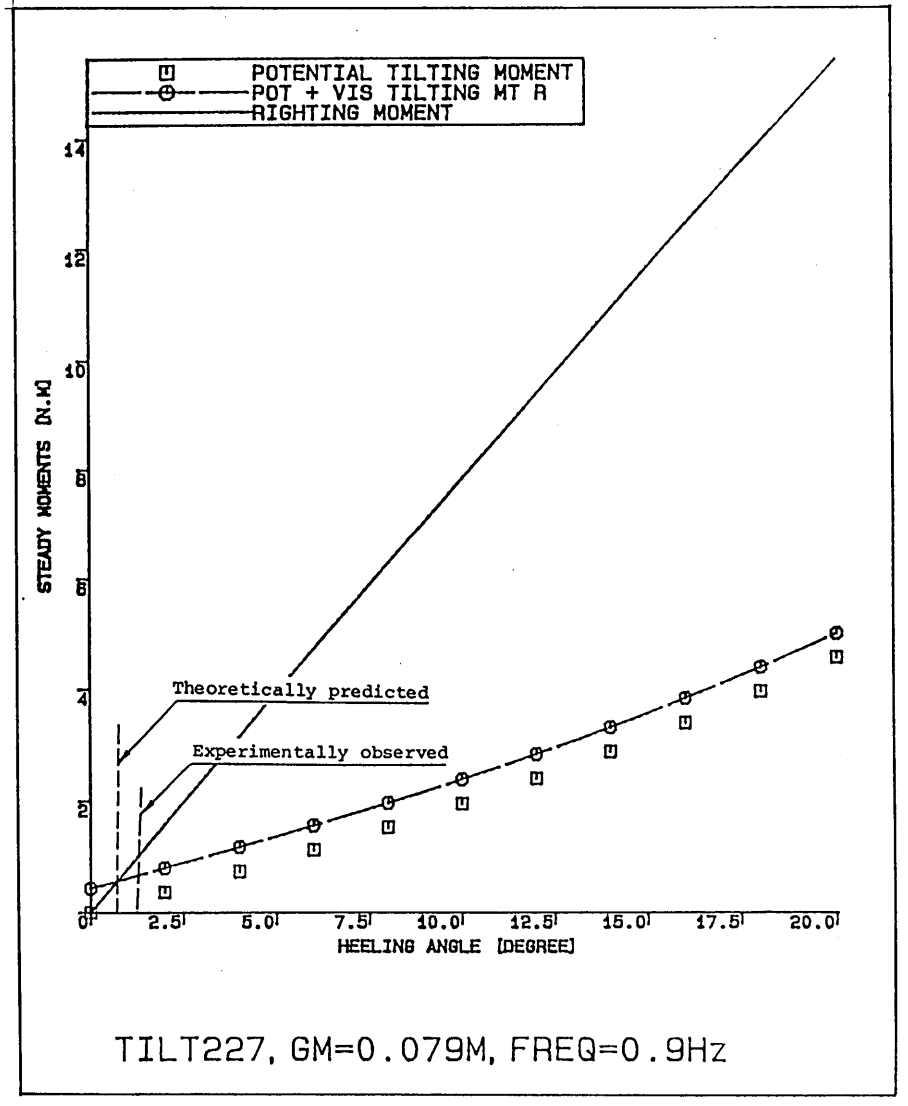

Fig. 200 - Comparison of righting moment against tilting moment on the basis of steady vertical forces (potential) plus steady drag forces (viscous) at a frequency of 0.9 Hz for $\bar{GM}$ = 0.079 m

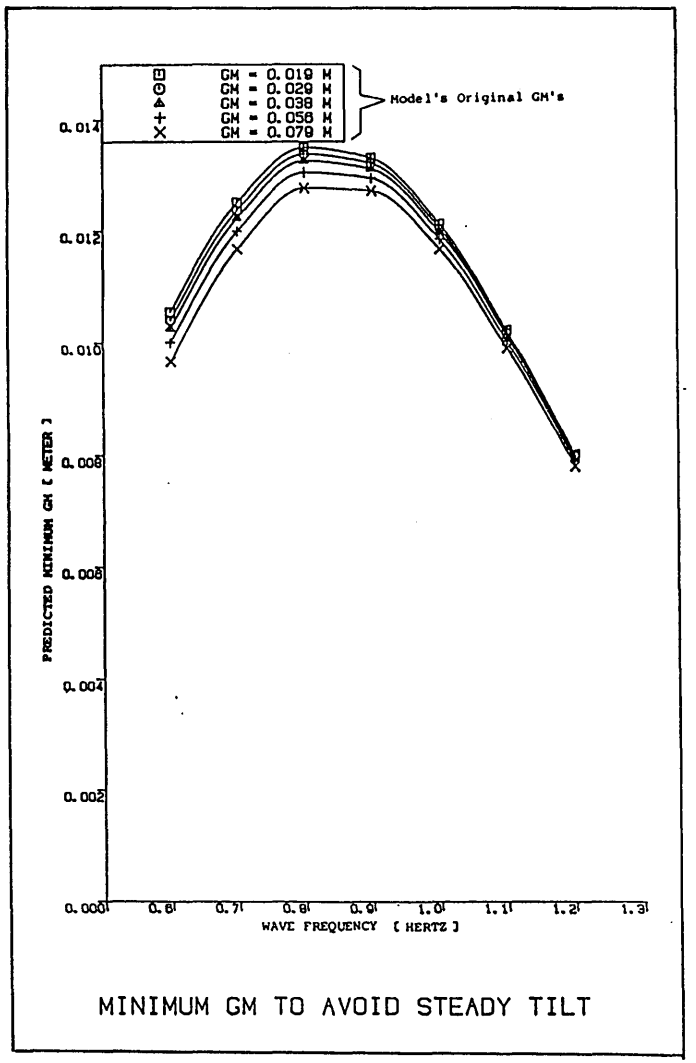

Fig. 201 - Minimum GM predicted to avoid the steady tilt on the basis of steady vertical forces (potential) for model's varying loading (GM) condition. [Wave heights are deduced from the ABS wave height formula.]

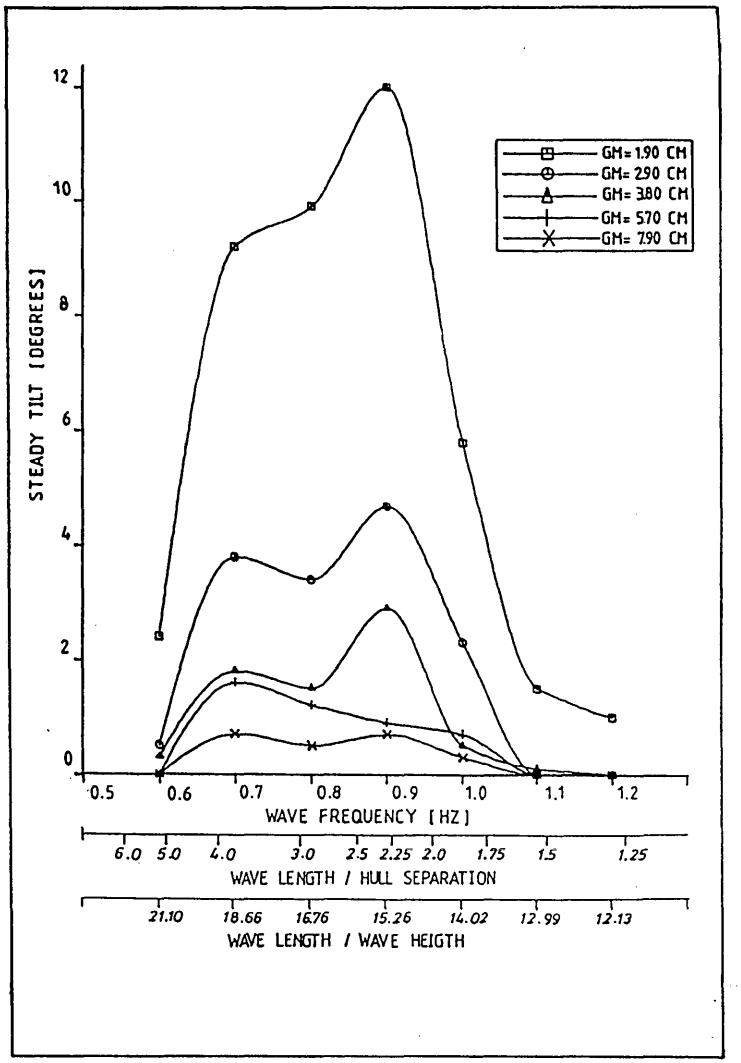

Fig. 202 - Steady tilt obtained from the tests for model's varying loading (GM) condition. [Wave heights are deduced from the ABS wave height formula.]

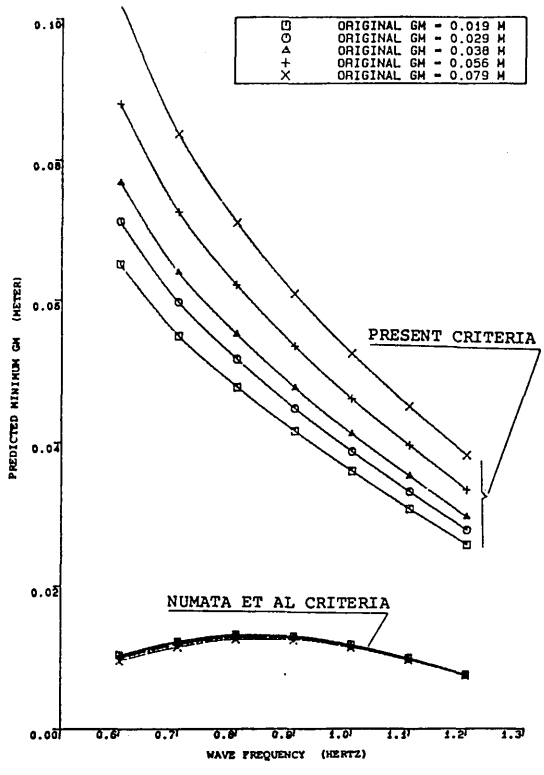

Fig. 203a - Max tilt allowed = 0.5°

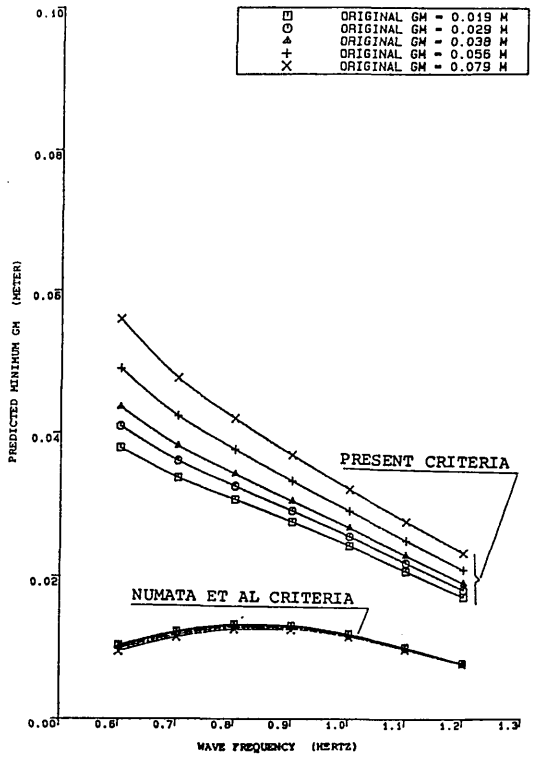

Fig. 203b - Max tilt allowed = 1.0°

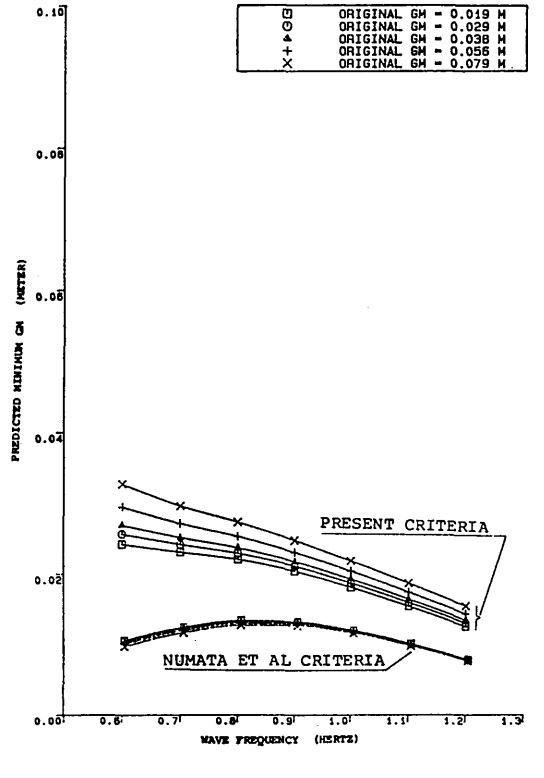

Fig. 203c - Max tilt allowed = 2.0°

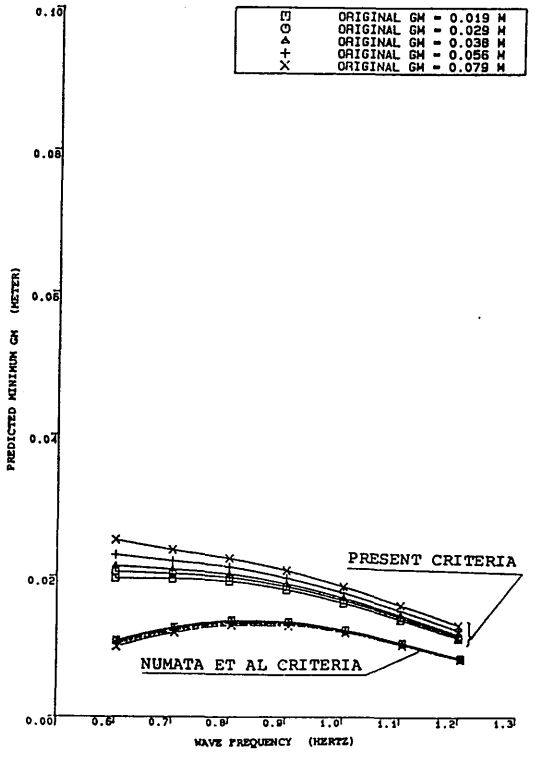

Fig. 203d - Max tilt allowed = 3.0°

Fig. 203 - Comparison of min $\overline{GM}$ criteria on the basis of steady vertical forces (Numata, et al. criteria) and steady vertical forces plus steady drag forces (present criteria) for model's various loading ($\overline{GM}$) conditions

4.5 CONCLUSIONS

The following conclusions are drawn from the theoretical work presented in this chapter and the comparisons with the experimental work given in Chapter 3.

1. A proper representation of the wave-induced steady tilting moment is an essential part of understanding the tilt phenomena. From the theoretical and experimental investigation of the components of this moment it is found that:

The main components are the steady potential vertical force on the lower hulls and steady horizontal forces on the columns induced by both the drag and potential effects.

The contribution of the horizontal forces is less when the COG is near the free surface. Then the total moment is dominated by the potential vertical force on the lower hulls. Increasing vertical shifts of the COG from the free surface give rise to an increasing contribution from the horizontal forces.

2. The comparison of the theoretical wave-induced tilting moment and the righting moment computed at the actual tilt angles (except at the extreme tilt angles $\phi \gtrsim 12°$) generally demonstrates an underestimation of the tilting moment. This is most likely due to the absence of the steady potential horizontal force and in particular the wave-elevation component on the columns. The computation of this force component on the columns requires a three-dimensional representation of the fluid potential including the diffraction effects of the waves.

3. The overestimated tilting moments computed at the extreme tilt angles are induced usually in large waves. Therefore non-linear effects particularly on the vertical components become dominant. Moreover, the restrictions due to the measuring system (LVDT strings) and the mooring system and the effects of the water splashing on the deck at large tilts will create equilibrium conditions which do not reflect the true full scale behaviour.

4. In the prediction of the wave-induced tilting moment it is assumed that the vessel is completely restrained. This produces an overestimated moment and thus more conservative results than the freely floating body assumption. However, if the vessel is assumed as freely floating the tilting moment predicted would be considerably underestimated in comparison to the experimental data. Therefore keeping in mind the restrictions due to the mooring system, the restrained body assumption may well be justified.

5. The moment induced by the vertical steady force has a bi-stable character. Depending on the direction of the initial disturbance it can induce tilt in either leeward or seaward direction. However, the moment induced by the horizontal drag force acts as a starting tilt mechanism and induces steady tilt always in the leeward direction, confirming the experimental observations. Although the effect of reflection due to columns is not considered in the thesis, this can contribute to the leeward tilt since the leeward column (and hull) is always exposed to a wave which has already lost some of its energy in passing the seaward columns.

6. A non-linearity in the righting moment curve due to the presence of the bracings and cross-members is not necessary to experience steady tilt.

7. Over a given range of regular beam waves a minimum $\overline{GM}$ to limit the vessel's steady tilt to a specified magnitude can be determined. This limiting $\overline{GM}$ is highly dependent on the precise determination of the tilting moment and the proposed limiting tilt. The absence of any component involved in the tilting moment could lead to a serious misjudgement in the determination of the minimum $\overline{GM}$. Practically, to avoid steady tilt or to have negligible tilt requires an undesirably large $\overline{GM}$.

8. The vertical steady force component is one of the main components contributing to the tilting moment. However, it has not been explored in the literature in terms of its several aspects. The further investigation on this component with emphasis on the tilt phenomena brings about the following conclusions:

(Unless it is stated the following conclusions apply to submerged lower hulls being held fixed under regular beam seas.)

(a) The steady force is mainly dominated by the depth dependent exponential term. The differences between the exact and the approximate methods for the calculation of this force are negligible at large depths of submergence. As the depth of submergence reduces the exact method produces a larger force and better agreement with the experimental data compared to the approximate theories. However, at very small depths of submergence both the exact and the approximate methods present different magnitudes and trend of forces compared to the test results which indicate the forces to be in a different direction.

(b) A rectangular shaped lower hull experiences a greater force compared to a circular one with the same sectional area. The modelling of a rectangular lower hull by a circular one having the same sectional area distribution leads to an underestimate of the force. This error increases with deviations of aspect ratio from unity.

(c) For a rectangular cross-section the deviation from unit aspect ratio increases the force (i.e. section gets elongated in either direction vertical or horizontal).

(d) A rectangular lower hull with rounded corners always experiences a smaller force than a purely rectangular hull with the same aspect ratio and the force decreases with increasing corner radius. When the hull cross-section converges to a circle whose diameter is equal to the beam of the rectangle, the maximum force on the circular hull is 20% less than the maximum force on a purely rectangular hull.

(e) For a rectangular hull and a rectangular hull with rounded corners in a tilted position there is no change in the magnitude of the force induced by the rotation compared to that in the upright position.

(f) The hydrodynamic interference between the lower hulls increased the force magnitude for a hull separation to lower hull diameter ratio of less than 3.

(g) The worst force is obtained in beam sea conditions and it decreases in magnitude with the deviation of heading angle from this condition.

(h) The inclusion of a surface-piercing column on a submerged lower hull reduces the force acting on the lower hull.

(i) The oscillatory motion of a lower hull in a similar manner to the orbital motion of the incident wave with zero phase lag results in a very small force compared to that of the lower hull being held fixed.

9. Although the steady contribution induced by the vessel's oscillatory motions is neglected because of the fixed body assumption, a two-dimensional method based on the beamwise strip theory for the forces and motions is presented. The following conclusions are drawn based on the results obtained from this method in regular beam seas:

(i) The computed sectional and total hydrodynamic loads on the semi-submersible model indicates the large contribution induced by the column mainly at lower and relatively moderate frequencies particularly in the asymmetric modes.

(ii) The method used presents satisfactory predictions for the heave mode and less satisfactory predictions for the roll mode particularly at lower and moderate frequencies compared to the experiments.

(iii) Theoretically, the motion response in regular beam seas requires hydrodynamic coupling between the sway and the roll mode. This introduces the effect of $\overline{GM}$ on the sway response. In spite of this fact the uncoupled motion response demonstrates a better correlation with the roll test data. This can be attributed to the increasing degree of three-dimensional effect due to the inclusion of the coupled motion induced force coefficient (sway into roll).

(iv) The findings (9)(i) to (9)(iii) indicate that the method is suitable for vertical motion predictions while it is not recommended for asymmetric motion predictions. This is mainly because the use of the method in way of the column neglects the three-dimensional effects which are considerable on circular columns for the asymmetric modes.

(v) At spacings of normal semi-submersible hulls the hydrodynamic presence of the other hull alters the hydrodynamic force coefficients of the single hull. The effect is more significant for the motion-induced coefficient, in comparison with the wave-exciting coefficients, increasing their magnitude in the vertical but decreasing it significantly in the horizontal direction.

(vi) In terms of the main underwater elements, the hydrodynamic interference between the hulls is most serious for columns, especially those which extend over a considerable part of the hull. Even if they are many wavelengths apart resonant frequencies, which induce standing waves between the hulls, can occur resulting in dramatic changes (peaks and troughs) in the force curves. For the submerged sections at hull separation-to-hull width ratio greater than 3 the interference is negligible for all practical purposes.

(vii) From the point of view of the semi-submersible model tested which had a large hull separation (S/R = 6.0) and circular columns, where the three-dimensional effects are dominant, hydrodynamic interference effects are not important.

(viii) If the shallowly submerged lower hulls have a wall-sided shape, this may work as a physical boundary to build

up a resonant condition. In such a case having circular or elliptical lower hulls may have an advantage compared to rectangular and rectangular with rounded corner lower hulls from the hydrodynamic design point of view.

(ix) Despite some of its theoretical weaknesses, the method of including the hydrodynamic presence of the columns improves the prediction of motion with high accuracy in the heave and less accuracy in the roll mode in comparison to the motion test data. This effect is considerable in the low frequency range tested.

(x) The hydrodynamic presence of the columns results in a 'wave-excitationless frequency' caused by the body (hull + column) - wave interaction. The location of this frequency changes: (a) by changing the ratio of the column waterplane area to underwater volume (in sectional case the ratio of column width to hull diameter), (b) by changing the separation distance between the columns.

(xi) Based on the investigation of two typical cross-sections of lower hulls which are circular and rectangular shape (see Fig. 120a) it is found that: at a relatively deep depth of submergence of the lower hull the hydrodynamic force coefficients for the rectangular section of aspect ratio larger than 1 are greater than that for the circular section in the vertical mode. The opposite is true in the horizontal mode and is also valid for the surface-piercing column sections.

(xii) The solution of the oscillatory motion equation under the tilt effect demands a proper representation of the hydro-

dynamic force coefficients at the tilted position. The theoretical investigation of these coefficients in the vertical and horizontal mode indicates that the influence of a tilt angle on the coefficients manifests itself through the change in the section area projected normal to the direction of motion and the depth of submergence.

For submerged rectangular sections the effect of pure tilt is negligible for all practical purposes except for tilt angles exceeding 10° for which slight variations occur.

For the surface-piercing column section the principal effect is in the heave mode. Marked changes occur at relatively small tilt angles. The wave-excitationless frequency completely vanishes for a tilted column section. Changes in the sway force coefficients are limited to tilt angles greater than 10° and are relatively minor. This conclusion applies to both circular and rectangular hull sections.

Chapter 5

CONCLUSIONS

In this last chapter, a general review of the whole study reported in this thesis is presented with emphasis on the overall conclusions and some recommendations for future design practice and research.

Dissatisfaction with the rules for the assessment of the intact stability of semi-submersibles in dynamic conditions has existed since their adoption in 1968. There has been considerable pressure from designers and operators of semi-submersibles to reduce the stability criteria which in turn would allow a higher deck load through a reduction in $\overline{GM}$. This pressure was somewhat reduced following the loss of the "Alexander L. Keilland" and the "Ocean Ranger". Although neither of these accidents was caused by inadequate statical stability, it became clear how quickly a minor structural weakness could lead to a major disaster. The rules and regulations regarding stability have been strengthened but the problem of tilt is not dealt with explicitly in these regulations.

Part of the reason for this is the lack of full scale data on the occurrence of tilt. So far there has been no well documented reports of tilt being observed on full scale semi-submersibles. Some verbal statements have been made suggesting tilt has occurred in one or two instances but it was attributed to wind, current and mooring effects. In the Ocean Ranger enquiry reference was frequently made by helicopter pilots and others to the vessel having a tilt which

was attributed to wind and bad ballasting with a possible low $\overline{GM}$ [88]. It is easy to confuse tilt due to hydrodynamic causes with tilt due to wind and possible current effects on a moored vessel. The high wave conditions, which give rise to tilt, are normally associated with co-linear wind and thus the tilt in the vessel is generally attributed to the effects of wind alone. However, in the thesis it is shown that tilt can occur in waves alone and that there will always be a preferred direction of tilt.

Results Deduced from Earlier Work

The majority of research studies concerned with this topic were originally intended to shed some light on certain dynamic aspects of semi-submersibles and tilt was a by-product of this work. Thus the problem was not explored rigorously and conflicting statements were made regarding certain experimental features. The different theoretical approaches based on the available test data indicated that there was still a need for further research work to fully understand the phenomenon. Numata, et al. demonstrated a qualitative agreement between theory and experiment over a limited range of tilt data on the basis of the potential second-order vertical force on the lower hulls if they were assumed to be held fixed in position. In De Souza and Miller's approach, this vertical force component was not considered but it was demonstrated that the steady drag forces on the columns produced an appreciable part of the induced tilt angles. Martin and Kuo solved the problem for a columnless twin circular hull model by calculating the potential forces on the freely oscillating hulls, exact to second-order and they indicated that the previous two approaches were too crude. The comparison of their predictions with the columnless model which had only freedom in the roll direction demonstrated a fair agreement for very small tilt angles.

Unfortunately the experimental work associated with these various investigations and certain other tests did not provide sufficiently accurate data over a wide enough range of predominant parameters (wave frequency, height and $\overline{GM}$) to validate any of these theories. In certain respects the experimental results were in conflict with one another and this was undoubtedly a major cause of delay in obtaining a complete understanding of this phenomenon.

Thus the first objective of this research was to obtain some accurate experimental work devoted entirely to the tilt problem so that some conflicting reports in the early studies could be clarified and to assist the theoretical developments.

Experimental Work

The experiments were concentrated on one of the most popular designs, the twin circular hull multi-column semi-submersible model in regular beam seas.

Systematic measurements of tilt were made over a wide range of the predominant parameters (five different $\overline{GM}$s, as wide a range of wave steepnesses as the tank would permit and wide frequency range). The collection of this extensive wave and motion data and their analysis was carried out using a computer based system by a specifically written package of programs. Although the results were analysed and presented in the frequency domain, it is possible to reproduce the time history of each test run for time domain investigations at some future date as illustrated in this study.

From the model tests, the frequency range and lower limit to the wave height necessary to cause tilt can form a basis for design

purposes and further research studies for this particular type of semi-submersible. Keeping in mind the effect of scale for the prototype it was found that steady tilt developed in regular beam seas with *a range of wave frequencies* varying between 0.7 Hz and 1.2 Hz (a range of period of approximately 12 sec to 7 sec on the full scale) and *wave height in excess of 8 cms* (about 6 m on the full scale). The worst tilt observed was around 15° for the smallest $\overline{GM}$ tested 0.019 m (1.33 m on the full scale) at a frequency of around 0.9 Hz (a period of about 9 sec on the full scale) and wave height in excess of 14 cms (about 10 m on the full scale). In this extreme case the leeward deck edge was frequently immersed and large wave impacts occurred but *no tendency to capsize* was observed. The tilt had a local maximum at a frequency around 0.7 Hz. The range of wave frequencies and heights over which tilt occurred was highly dependent on $\overline{GM}$. As $\overline{GM}$ increased the tendency to tilt disappeared but persisted around the local maximum 0.7 Hz, i.e. the range of tilt frequencies decreased with the lower end of the range remaining substantially fixed.

The systematic investigation of the effect of wave height on steady tilt required more tests with varying wave heights at each frequency in some cases including waves near to maximum steepness. However, for the analysis of the results and for preliminary design purposes it is desirable to use a constant wave slope in order that consistent results be obtained. In the thesis use was made of an ABS formula which gives smaller wave slopes than some other classification societies indicate, but which would thus give a conservative prediction of tilt conditions. Also, the model results indicated clearly considerable non-linear effects at very steep waves and it was desired to use essentially linear theoretical results.

As $\overline{GM}$ decreased the steady tilt increased non-linearly and the effects of the wave parameters on the behaviour became more accentuated. Although model tests with very low $\overline{GM}$s is very desirable in order to study the build-up of tilt with these parameters in practice this is extremely difficult due to the sensitivity of the model and experimental set-up to small changes in conditions.

Based on the several exploratory tests carried out it was concluded that the following effects, i.e. the first impact of the waves, the location and style of the moorings and fairleads, changes in viscous effects between model and full scale could affect the tilt but none of them were solely responsible for the development of tilt. Systematic measurements of the wave-exciting forces on the lower hulls at various hull spacings and on a single hull in isolation were provided at moderate and high waves over a wide range of frequencies. From these investigations it was found that the hydrodynamic interference between the lower hulls did not show any noticeable load difference which could induce a steady tilt at moderate heights. However, in high waves the forces on the leeward hull slightly increased relative to those on the seaward due to possible non-linear effects.

The model tests demonstrated that for this particular design *the steady tilt always developed in the wave travel direction* (leeward tilt). There is a mechanism in the waves for this preferred direction of tilt which is independent of the first impact of the waves, the moorings and the fairlead locations as concluded from the exploratory tests.

In some previous studies it was demonstrated that the non-linearity in the roll restoring moment (righting moment) due to the

presence of the bracings and cross-members caused an intersection of the wave-induced tilting moment and righting moment resulting in a steady tilt angle. However, the inclining experiments with the present model indicated that there was no non-linearity in the righting moment curve until the deck edge was immersed but the model could still develop steady tilt. Thus this non-linearity was not necessary to experience a tilt.

From the analysis of the oscillatory motions it was concluded that the heave and roll motion response of the model were affected non-linearly by the tilt effect. As the $\overline{GM}$ decreased higher heave and roll motion was recorded in the frequency range where steady tilt developed.

Theoretical Work

The tilt angles measured from the experiments enable one to obtain the righting moment which must exist and be equal and opposite to the steady wave-induced tilting moment.

To determine this tilting moment it is necessary to consider all the steady forces and their resulting moments which are applied to the vessel.

All the existing tilt theories and mechanisms have been examined in detail and computer programs developed to determine the numerical values of the tilting moment for the present semi-submersible model.

From the comparison of the righting moment and tilting moment at the measured tilt angle it was concluded that two most important

sets of wave forces contributing to the upsetting moment were:

(i) Steady vertical forces on the lower hulls due to potential effects, and

(ii) Steady horizontal forces on the columns due to drag effects.

However, the predicted tilting moment and the resulting tilt response on the basis of these components still demonstrated an underestimation of the test results which was believed to mainly originate from the steady horizontal forces due to potential effects particularly on the columns.

The steady vertical force on the lower hulls was obtained by the computer program developed from a solution of the linear far-field method for a single submerged slender body with arbitrary cross-section. The effect of the cross-sectional area shape and the hydrodynamic interference between the two hulls on this force was investigated. The computer program developed using the Frank Close-fit method was utilised to compute the added mass of arbitrary cross-sections and the hydrodynamic interference between twin sections.

From the theoretical investigations it was concluded that the replacement of a rectangular hull with a circular one based on the same sectional area distribution would underestimate the steady vertical force. The error in this underestimation increased with deviations of the aspect ratio from unity.

The hydrodynamic interference between the lower hulls increased the steady vertical force for hull separation to hull diameter ratio less than 3.

Moreover, the worst vertical force occurred in beam sea conditions and it decreased in magnitude with the deviation of heading

angle from this position. When the surface-piercing columns were included the steady vertical force decreased.

The steady horizontal force on the model due to drag effects was obtained by the computer program developed based on the Morison formula. The contribution of this force component into the tilting moment was sensitive to the vertical position of the COG. It acts as a starting tilt mechanism and induces steady tilt always in the wave travel direction confirming the experimental observations.

The computation of the above two force components and resulting tilting moment was based on the fixed body assumption which demonstrated consistently better agreement with the righting moment over the test data. In the case of a freely floating body the computed moment would be reduced considerably.

Although the oscillatory effects were not incorporated into the moment computations, the theoretical investigation of these effects was carried out in the thesis to assist further considerations of the hydrodynamic aspects of tilt. Two main computer programs were developed based on the Frank Close-fit technique, in which the two-dimensional Green's Function Integral Equation Method was utilised. They compute the motion-induced force coefficients (added mass inertia and damping) and the wave-induced force coefficients for the in-plane modes in regular oblique seas.

The versatility of this technique enabled investigations to be carried out for the effect of arbitrary cross-section (particularly asymmetric underwater geometry due to tilt), the effect of free surface and the hydrodynamic interference between the under water elements of the semi-submersible on the frequency dependent hydrodynamic coefficients in two-dimensions.

The hydrodynamic coefficients obtained from these programs were implemented in a package of computer programs developed to solve the oscillatory motion equation in regular beam seas on the basis of the beamwise strip method. It was believed that the primary requirement for the solution of the motion under the tilt effect was a proper determination of the hydrodynamic coefficients. Thus, from the investigation of these coefficients for circular and rectangular sections it was concluded that the influence of a tilt angle manifests itself through the change in the section area projected normal to the direction of motion and depth of submergence (for submerged section) or draught (for surface-piercing section).

The effect of pure tilt (isolated from the free surface effect) on the hydrodynamic coefficients should be taken into account even for small tilt angles in the vertical mode for the surface-piercing column sections. However, in the horizontal mode this effect was limited to tilt angles greater than 10° and was relatively minor. For the submerged rectangular section slight variations occurred after 10° and the effect can be changed by the depth of submergence.

The effect of depth of submergence on the motion-induced coefficients practically vanishes for a depth of submergence (from the top of a section contour to the water level) exceeding two and a half times the section depth or diameter and at this depth the potential damping also vanishes.

The effect of increasing the corner radii for a given aspect ratio of rectangular section will decrease the hydrodynamic coefficients as the rectangular geometry approaches to an ellipse.

The application of the Frank Close-fit method for the wave-exciting force predictions on the single and twin circular lower hull was found satisfactory by the model tests particularly in the heave mode. However, the motion predictions on the basis of the hydrodynamic coefficients obtained from this method was found satisfactory for the vertical heave mode while it was less satisfactory for the asymmetric roll mode. This was mainly because the use of the Close-fit method in the beamwise direction for the circular columns neglects the appreciable three-dimensional effects which are accentuated at the columns in the asymmetric modes. Thus the use of this method should be restricted to the vertical force and motion predictions for this type of geometry and it should be combined with three-dimensional methods for the column in the asymmetric modes. However, the method is still one of the most suitable for slender lower hulls and for twin-hull semi-submersibles with long struts (SWATH) or elongated waterplane area of columns where the three-dimensional effects are relatively smaller.

It was concluded that the hydrodynamic interference was most serious for surface-piercing members, particularly the columns which extended over a considerable part of the lower hulls and for submerged hull at hull separation-to-hull width ratio less than 3. However, in terms of the semi-submersible design considered which had a large hull separation and circular columns, this effect was not important since it did not build up a resonant condition due to large three-dimensional effects.

It was demonstrated that the exclusion of the hydrodynamic effects of the columns produced overestimated heave and roll motion in the low and moderate frequency range. Therefore their absence in the motion prediction may be justified only in the high frequency range.

Recommendations

In general design practice for semi-submersibles with low $\overline{GM}$s, the steady tilt behaviour should be checked by model tests and it should not be confused with other steady effects (wind, current, moorings, etc.).

As suggested by Numata, et al. over a given range of regular beam waves a minimum $\overline{GM}$ to limit the vessel's steady tilt motion can be determined by the following procedure:

Select a range of regular waves whose period varies between about 7 sec to 12 sec and height in excess of about 6 m but smaller than about 12 m. The variation of the period with wave height physically should reflect that at sea as the waves get longer the maximum steepness decreases (for this purpose the modified ABS wave formula given by eq. 9 can be used). Specify an acceptable amount of steady tilt angle to limit the vessel's tilt motion. Then obtain the minimum $\overline{GM}$ from eq. 86 for each wave period and corresponding height. The largest value of the $\overline{GM}$s calculated is the minimum $\overline{GM}$ to limit the vessel's tilt motion to this specified angle.

It is important to note that the limiting $\overline{GM}$ is highly dependent on the precise determination of the tilting moment and should be validated by model tests. As concluded in the thesis an underestimation in this moment would lead to a serious misjudgement in the minimum $\overline{GM}$ determination.

Future model tests are recommended for rectangular cross-section lower hulls, elongated waterplane area columns and other types of designs (e.g. footing types) by the manner described in this thesis. Moreover, the effect of draught, heading angle and irregular

seas are other requirements to be considered in the future studies.

Further work is required to compare the tilting moment determined from model tests with that predicted by the theoretical method developed herein. In this respect it is recommended to use three-dimensional methods to account for the effect of steady and oscillatory forces on the columns particularly for the horizontal mode. In this mode the effects of the actual mooring system used on the semi-submersible should be investigated since it will affect the magnitude of the tilt.

In the future research it is recommended to extend the force tests carried out on the lower hulls for the hull plus column combination to investigate the hydrodynamic interference phenomenon. These tests should include the precise measurement of the wave heights around the leeward and seaward columns. This is because although it was not included in the moment computations it is believed that there could be an additional mechanism causing such a strong preference for the leeward tilt induced by the reflection of the incident wave due to the number of columns in this particular design.

From the hydrodynamic design point of view it is recommended that designers avoid elongated waterplane area columns particularly with fairings (sloping sides). This would reduce the hydrodynamic interference between the hulls as well as tilt since wave reflection will be less.

When the lower hulls are shallowly submerged, circular or elliptical hulls may have an advantage compared to the rectangular and rectangular with round corners due to the reduction in interference effects and steady tilt.

ACKNOWLEDGEMENTS

The author is very grateful and would like to thank all those people who have contributed to the research work reported in this thesis. The following are gratefully acknowledged:

Professor D. Faulkner, Head of the Department, for making this research possible and his great understanding throughout the research period;

Mr. N.S. Miller, the Supervisor of this research work for his continuous encouragement and stimulating discussions which have been of immeasurable value to the author;

Dr. J. Martin (Edinburgh University) for making his computer programs available and his useful discussions with the author;

Dr. A.Y. Odabaşi (British Maritime Technology) for his guidance on several matters arising during the course of the research;

Dr. R.C. McGregor, the Project Supervisor, for his encouragement and support;

Dr. A.M. Ferguson, Superintendent of the Hydrodynamics Laboratory, Mr. R.B. Christison and Mr. D. Sinclair, the chief and deputy technician, and all the Mechanical Workshop technicians for making the tank testing facilities available, constructing the models and their continuous help during the tedious testing;

Mrs. C. MacEachen, the Computer Manageress and Miss M. Shields, Computing Assistant, for their assistance in the very large amount of computing involved;

Mr. P.S.K. Lai, the final year student, for his assistance in part of the computational work and his discussions with the author;

Mrs. M.C. Frieze for her excellent typing, and Mr. M. Söylemez for his contribution towards the completion of the drawings;

and to his Stepmother for her patient encouragement.

Finally, the author is greatly indebted to the financial support from the Turkish Ministry of Education, and the Marine Technology Directorate of the Science and Engineering Research Council, U.K.

Appendix I

The following figure and table give the geometry and dimensions of the semi-submersible-A used by Numata et al. in refs [15,16].

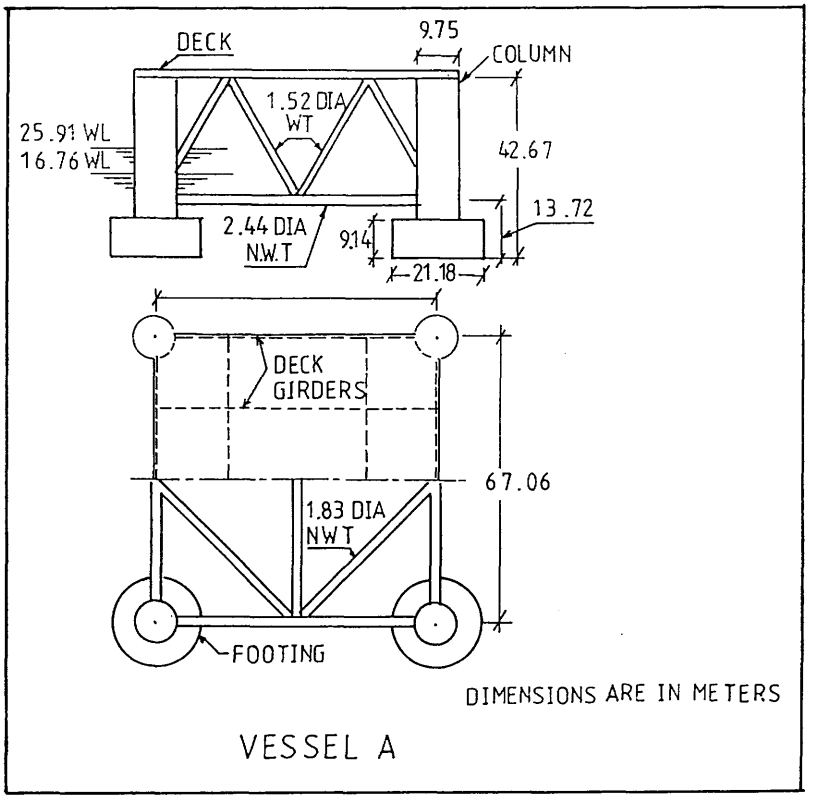

Fig. I.1 - 4-column footing type semi-submersible design[16]

Condition	Prototype		1/96 Model	
	Survival	Drilling	Survival	Drilling
Draught , m	19.81	25.91	0.206	0.27
Displacement, ton/kg	16562	18289	18.72	20.67
$\overline{GM}_1$	4.724	6.55	0.05	0.068
$\overline{GM}_2$ } m	2.286	3.05	0.024	0.032
$\overline{GM}_3$		0.945		0.0098
Natural heave period, sec	21.5		2.19	
Natural roll period , sec for $\overline{GM}_2$		55.5		5.66

Table I.1 - Main particulars of vessel A[16]

The following figure and table give the geometry and dimensions of the semi-submersible-B used by Numata et al. in refs [15,16].

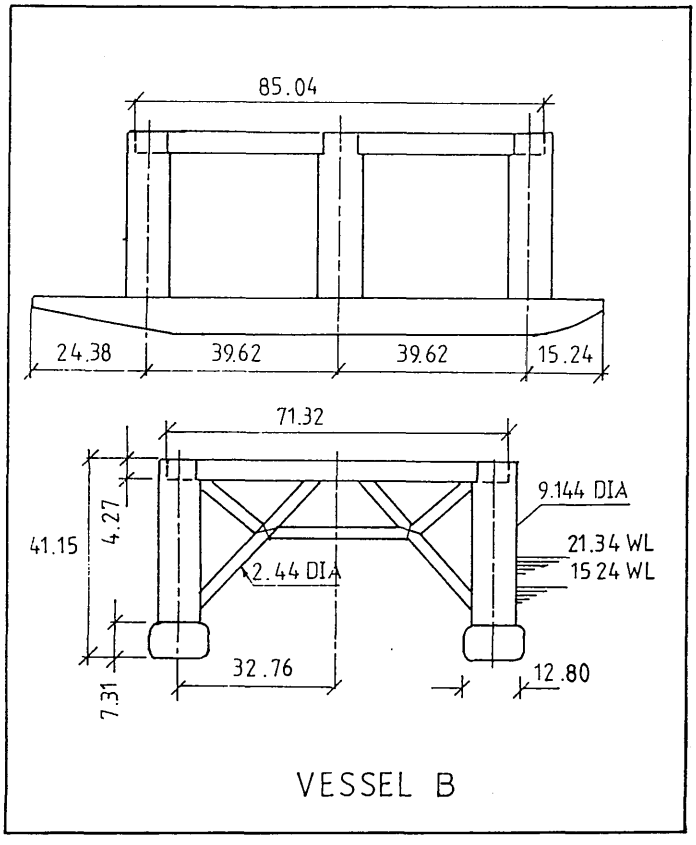

Fig. I.2 - 6-column twin rectangular hull type semi-submersible design[16]

Condition	Prototype		1/96 Model	
	Survival	Drilling	Survival	Drilling
Draught , m	15.24	21.34	0.158	0.222
Displacement, ton/kg	21947	24669	24.806	27.884
$\overline{GM}_1$	2.743	3.78	0.0286	0.0394
$\overline{GM}_2$		3.2		0.033
$\overline{GM}_3$ m		1.524		0.0158
$\overline{GM}_4$		0.8233		0.0086
$\overline{GM}_5$		0.396		0.0041
Natural heave period, sec	22.5		2.23	
Natural roll period , sec (for $\overline{GM}$ = 3.2 m)		55		5.613

Table I.2 - Main particulars of vessel B[16]

The Min $\overline{GM}$ Value for Semi-Submersibles to Avoid the Steady Tilt [16]

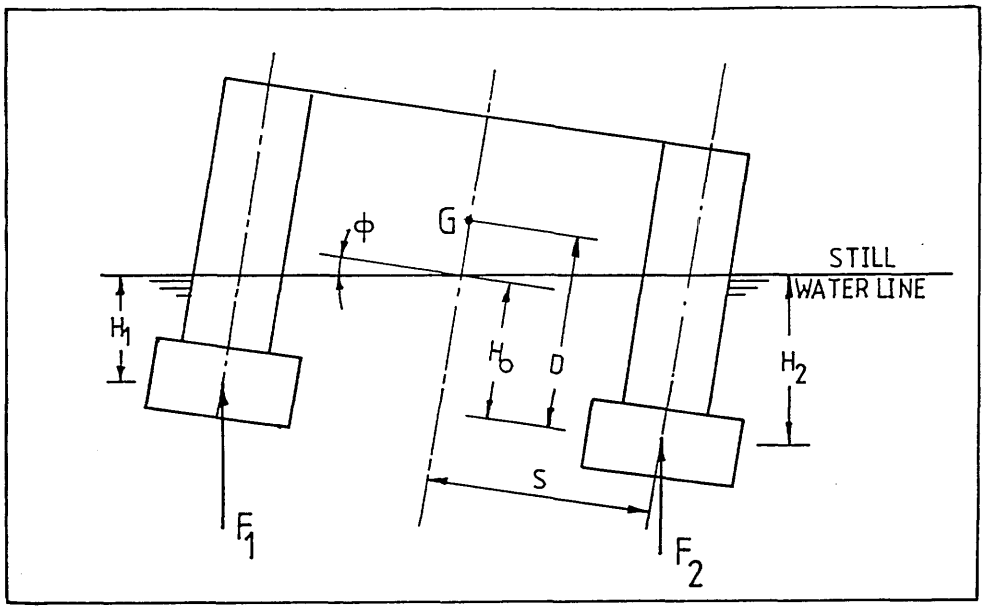

Fig. I.3 - The quasi-static analysis of the steady tilt [16]

The second-order vertical force on a circular cylinder restrained under the regular beam waves is given in the following form by using Ogilvie's solution [31]:

$$\bar{f}_y^t = 2\rho g(a^2\gamma^2)\, e^{-2\gamma H} S_A \frac{I_1[2\gamma R]}{\gamma R} \qquad \ldots \quad (I.1)$$

where $\bar{f}_y^t$ = steady second-order vertical force per unit length

a = incident wave amplitude

γ = wave number

I_1 = modified Bessel function of the first kind

H = depth of submergence of the cylinder axis

$S_A = \pi R^2$ = Cross-sectional area of cylinder $\qquad \ldots \quad (I.2)$

R = radius of cylinder

Although the solution given by eq. I.1 is valid for circular cylinders, Numata used this solution for vessel B, which had non-circular cross-

section of lower hull and vessel A, which had footing type lower hull by defining radius R as follows:

(i) For a pontoon with non-circular cross-section:

$$R = (S_A/\pi)^{\frac{1}{2}} \qquad \ldots \quad (I.3)$$

where S_A is non-circular cross-section area of pontoon.

(ii) For a footing:

$$R = (\nabla/2\pi)^{1/3} \qquad \ldots \quad (I.4)$$

where ∇ is the footing volume.

When the level position of the semi-submersible is disturbed, the steady vertical forces acting on each pontoon (or footing), $\bar{F}_1^t$ and $\bar{F}_2^t$, will create a steady tilting moment $\bar{M}_T^t$ due to the different depths of submergence H_1 and H_2. It is assumed that the forces applied at the pontoon (or footing) centre and the steady horizontal force is balanced out by the mooring force to restrain drift. By using Fig. I.3 the steady tilting moment $\bar{M}_T^t$, for relatively small angle of tilt ϕ, at about the CG reduces to:

$$\bar{M}_T^t = 2\rho g\, a^2\gamma^2\, e^{-2\gamma H_o}\, \nabla \left[\frac{I_1(2\gamma R)}{\gamma R}\right] (4\gamma S^2 + 2D)\phi \qquad \ldots \quad (I.5)$$

The righting moment M_R for small angle of tilt ϕ is given by:

$$M_R = \rho g \nabla_s\, \bar{GM}\phi \qquad \ldots \quad (I.6)$$

At the equilibrium position $\bar{M}_T^t$ will be balanced by M_R. Thus by equating eqs (I.5) to (I.6) the min $\bar{GM}$ value to avoid the steady tilt in regular beam seas is obtained as follows:

$$\bar{GM}_{min} = 2(\gamma a)^2\, e^{-2\gamma H_o}\, \frac{\nabla}{\nabla_s} \left[\frac{I_1(2\gamma R)}{\gamma R}\right] (4\gamma S^2 + 2D) \qquad \ldots \quad (I.7)$$

where ∇ = the volume of one lower hull for vessel B or the volume of two footings for vessel A

∇_s = the total volume displacement of the vessel

H_o, S and D are shown in Fig. I.3.

The following figure and table give the geometry and dimensions of the semi-submersible used by De Souza and Miller in refs [24, 27,17].

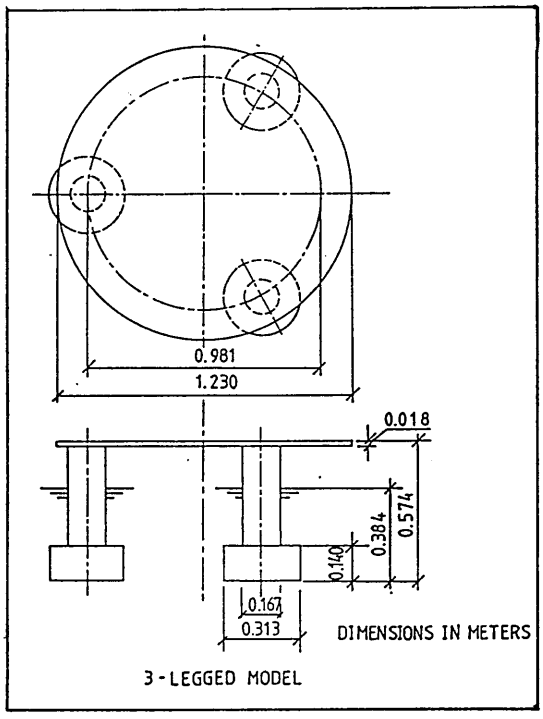

Fig. I.4 - 3-column footing type semi-submersible model [17]

Condition	Prototype	1/100 Model
Draught m	38.4	0.384
Displacement, m^3	48800	0.0488
$\overline{GM}_1$, m	6.9	0.069
$\overline{GM}_2$ / $\overline{KG}_2$	4.3 / 24.5	0.043 / 0.245
$\overline{GM}_3$ / $\overline{KG}_3$	2.7 / 26.8	0.027 / 0.268
Natural heave period, sec	22.5	2.25
Natural roll period , sec for $\overline{GM}_2$	47.2	4.72
for $\overline{GM}_3$	64.1	6.41

Table I.3 - Main particulars of 3-column footing type model [24,27]

The following figure and tables give the geometry and dimensions of the semi-submersible used by De Souza and Miller in refs [24,27,17]

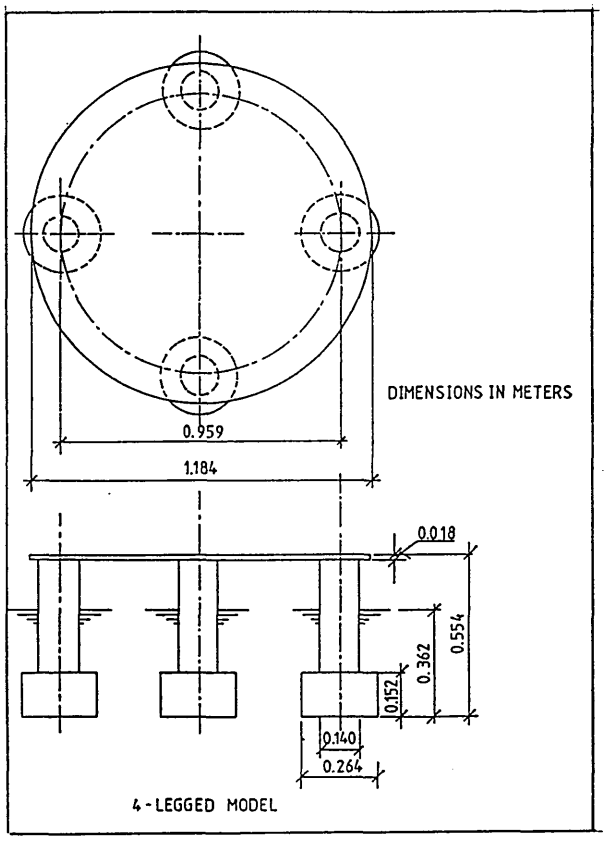

Fig. I.5 - 4-column footing type semi-submersible model[17]

Condition	Prototype	1/100 Model
Draught	36.2	0.362
Displacement, m^3	46600	0.0466
$\overline{GM}_1$, m	7.5	0.075
$\overline{GM}_2$ / $\overline{KG}_2$	4.7 / 23	0.047 / 0.23
$\overline{GM}_3$ / $\overline{KG}_3$	4.1 / 26	0.041 / 0.26
Natural heave period, sec	22.5	2.25
Natural roll period , sec for $\overline{GM}_2$	46.88	4.688
for $\overline{GM}_3$	76.6	7.66

Table I.4 - Main particulars of 4-column footing type semi-submersible model[24,27]

4 column footing type model	Wave period (sec)	Wave amplitude (m)	Steady tilt angle (degree)
Initial wind heel	0.889	0.041	6.306
$\phi_1 = 4.3°$	0.962	0.032	5.857
$\overline{GM}_1$ 0.075 m	1.05	0.047	5.181
$\phi_2 = 7.2°$	0.865	0.050	10.362
$\overline{GM}_2 = 0.047$ m	0.934	0.049	10.622
	1.017	0.060	9.939

Table I.5 - Test data for 4-column model under the wave plus wind effect [25]

The Wave-Exciting Forces Acting on the Footing Type Semi-Submersible [24]

Heave Mode:

$$\text{Pressure force} = \sum_{i=0}^{n-1} \pi\rho g\, aR_1^2\, e^{-\gamma H_1}\left[(R_2/R_1)^2\,(1-e^{-\gamma H_2}) - 1\right] \times \cos\gamma\,\left[R_c\cos(2\pi i/n+\mu) - ct\right] \quad \ldots \quad (I.8)$$

$$\text{Acceleration force} = \sum_{i=0}^{n-1} -\frac{2}{3}\pi\rho\gamma g\, Ja\, e^{-\gamma H_1}\left[(C_{v1}R_2^3 - C_{v2}R_1^3)(1+e^{-\gamma H_2}) + R_1^3\, e^{-\gamma H_2}\, C_{v3}\right] \times \cos\gamma\,\left[R_c\cos(2\pi i/n+\mu) - ct\right] \quad \ldots \quad (I.9)$$

$$\text{Velocity force} = \sum_{i=0}^{n-1} \frac{1}{2}\rho\pi R_2^2\, C_D\gamma g\, a^2 e^{-2\gamma(H_1+H_2)} \times \sin\gamma\left[R_c\cos(2\pi i/n+\mu) - ct\right] \times \left|\sin\gamma\left[R_c\cos(2\pi i/n+\mu) - ct\right]\right| \quad \ldots \quad (I.10)$$

Sway Mode:

$$\text{Pressure force} = \sum_{i=0}^{n-1} \pi\rho g\, aR_1^2 \left\{e^{2\gamma a\cos\sigma} - e^{-\gamma H_1}\left[1 - (R_2/R_1)^2\,(1-e^{-\gamma H_2})\right]\right\} \times \sin\gamma\,\left[R_c\cos(2\pi i/n+\mu) - ct\right] \quad \ldots \quad (I.11)$$

where $\cos\sigma = \cos\gamma\,\left[R_c\cos(2\pi i/n+\mu) - ct\right]$

Acceleration force = pressure force given by eq.(I.11) with $C_M = 2$ ... (I.1

$$\text{Velocity force} = \sum_{i=0}^{n-1} \frac{1}{2} \rho g a^2 \cos\sigma|\cos\sigma| \left[C_{D_{R_1}} R_1 \left(e^{2\gamma a\cos\sigma} - e^{-2\gamma H_1}\right) + C_{D_{R_2}} R_2 \left(e^{-2\gamma H_1} - e^{-2\gamma(H_1+H_2)}\right)\right] \quad \ldots \text{(I.1}$$

where $\cos\sigma = \cos\gamma[R_c \cos(2\pi i/n + \mu) - ct]$

n = number of columns

ρ = water density

g = gravitational acceleration

a = wave amplitude

γ = wave number

R_1 = radius of column

R_2 = radius of caisson

R_c = radius of circumscribing circle passing through the centre of the column

H_1 = depth of submergence of column of radius R_1 from the still water level

H_2 = depth of footing of radius R_2

μ = heading angle with respect to the wave travel

c = wave celerity

t = time

C_{v1} = added virtual mass coefficient in heave mode for a rectangle with aspect ratio $\pi R_2/2H_2$

C_{v2} = added virtual mass coefficient in heave mode for a rectangle with aspect ratio $\pi R_1/2H_2$

C_{v3} = added virtual mass coefficient in heave mode for a rectangle with aspect ratio $\pi R_1/2(H_1+H_2)$

J = 0.6366

C_D = drag coefficient for the whole column plus footing in heave

$C_{D_{R_1}}$ = drag coefficient for column of radius R_1 in sway

$C_{D_{R_2}}$ = drag coefficient for footing of radius R_2 in sway

The above equations from (I.8) to (I.13) are valid for:

R_1, R_2 ≤ wave length 1/10.

The following figure gives the geometry and dimensions of the idealised semi-submersible test configuration by Martin and Kuo in refs [20,21].

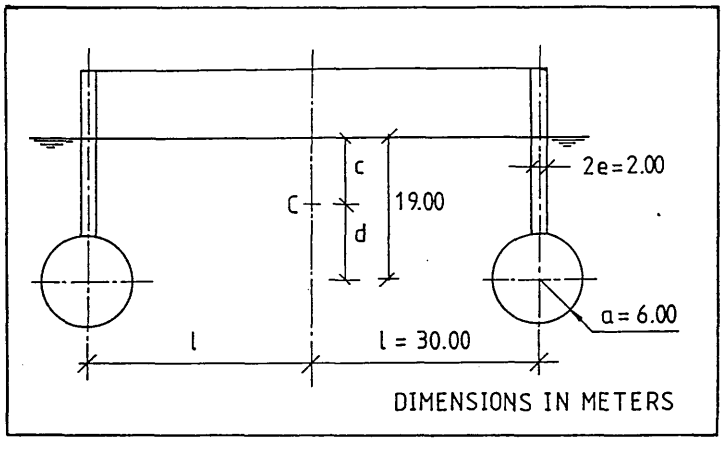

Fig. I.6 - Idealised semi-submersible test configuration (the centre of gravity is taken at C)[20]

Figure I.7 shows the simplified model used by Martin and Kuo in ref. [21]. It consisted of two parallel, circular cylinders rigidly connected to each other and could rotate about a fixed rolling axis through the CG and parallel to the cylinders in the middle of them.

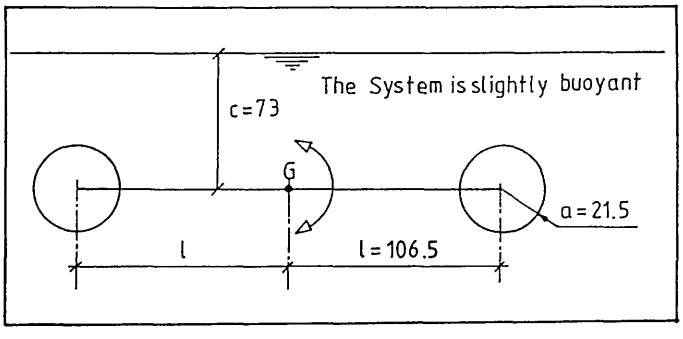

Fig. I.7 - Geometry of the simplified model[21]

The following figures give the geometry and dimensions of the models used by Morrall in ref. [29].

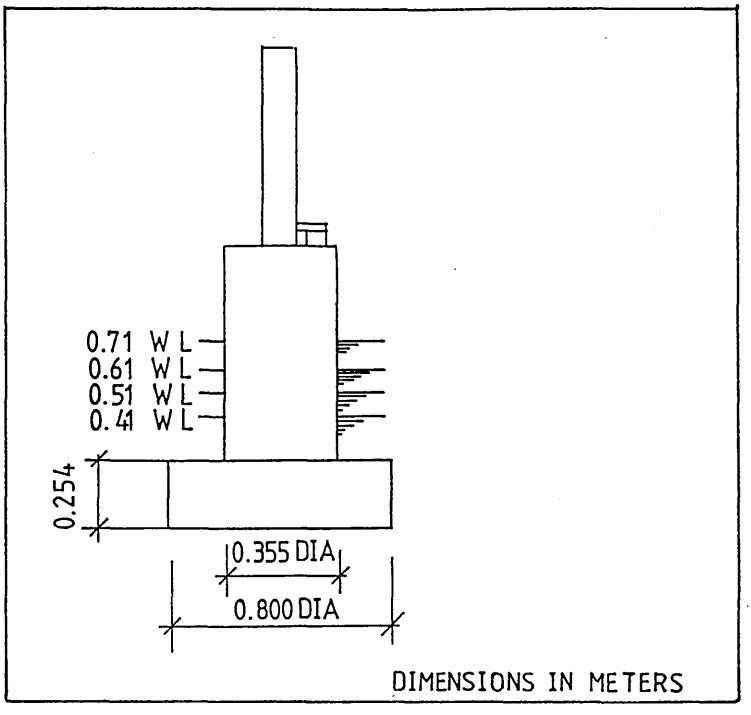

Fig. I.8 - Footing type semi-submersible model [29]

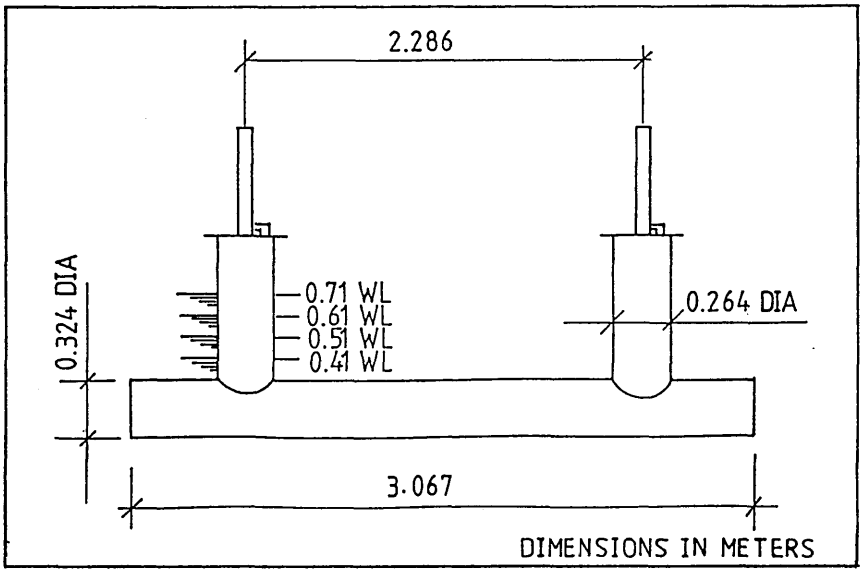

Fig. I.9 - Pontoon type semi-submersible model [29]

Steady Vertical Force on a Vertical Footing and Horizontal Lower Hull under the Regular Beam Waves[29]

The following steady vertical force expressions given by Morrall[29] were derived from simple linear wave theory by taking differences in fluid pressure due to the velocity of the particles moving over the top and bottom surface of a restrained vertical cylinder and horizontal prism.

For the vertical cylinder which represents the submerged footing:

$$\bar{F}^t_y = \rho g (\gamma a)^2 \, e^{-2\gamma H} \, (\pi R^2 D) \, \frac{\sinh \gamma D}{\gamma D} \qquad \ldots \quad (I.14)$$

For the horizontal prism which represents the submerged lower hull:

$$\bar{F}^t_y = \rho g (\gamma a)^2 \, e^{-2\gamma H} \, (B D L) \, \frac{\sinh \gamma D}{\gamma D} \qquad \ldots \quad (I.15)$$

where R = radius of the submerged footing

D = depth of the submerged footing or horizontal lower hull

H = depth of submergence of the centroid of the footing or lower hull

B = beam of the lower hull

L = length of the lower hull

The following figure shows the geometry and dimensions of the semi-submersible used by Hineno et al. in ref. [18].

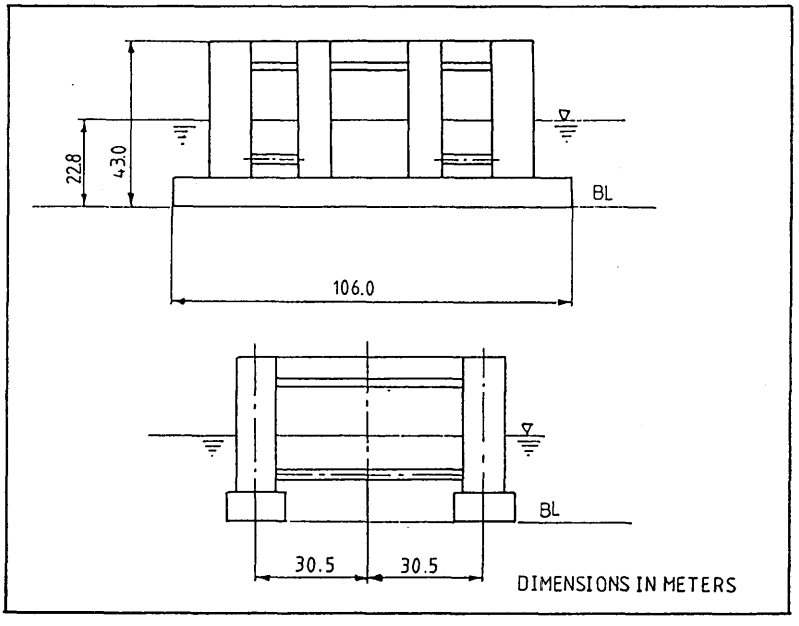

Fig. I.10 - 8-column twin rectangular hull type semi-submersible[18]

Table I.6 gives the testing conditions for the semi-submersible used by Hineno et al. in ref. [18].

Condition	Prototype	1/90 Model
Draught , m	22.8	0.2533
Displacement, ton/kg	36500	50.070
$\overline{GM}_1$ / $\overline{KG}_1$, m	0.4 / 22.6	0.00444/ 0.251
$\overline{GM}_2$ / $\overline{KG}_2$, m	2.1 / 21.0	0.0233 / 0.2333
Radius of gyration in roll direction, m	30.5 / 31.1	0.339 / 0.3455
Natural heave period, sec	23	2.424
Natural roll period , sec for $\overline{GM}_1$	152	16.022
for $\overline{GM}_2$	66	6.957

Table I.6 - Main particulars of 8-column twin rectangular hull type semi-submersible [18]

The following figure shows the geometry and dimensions of the tested model by Takarada et al. in ref. [8].

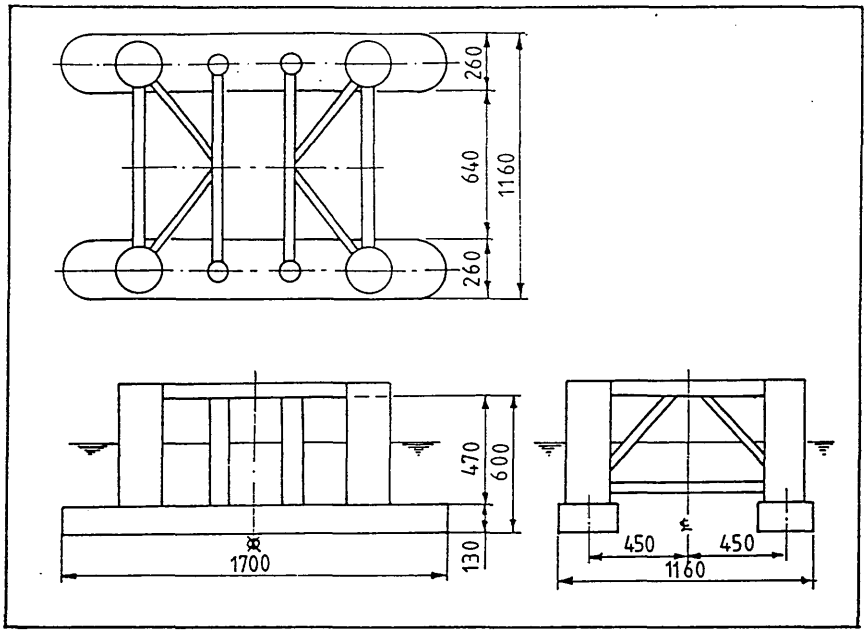

Fig. I.11 - 8-column twin rectangular hull type semi-submersible[8]

Condition		Prototype	1/60 Model
Draught	, m	24.00	0.40
Displacement	, ton/kg	35700 36200	161.40 [163.5]
$\overline{GM}_1$ / KG_1	, m	[0.48 / 19.2]	[0.008 / 0.32]
$\overline{GM}_2$ / KG_2	, m	1.62 / [1.68 / 18.0]	0.027 / [0.028 / 0.30]
$\overline{GM}_3$ / KG_3	, m	2.88 /	0.048 /
$\overline{GM}_1$ (longitudinal)	, m	[1.44]	[0.024]
$\overline{GM}_2$ (longitudinal)	, m	2.46 [2.64]	0.041 [0.044]
$\overline{GM}_3$ (longitudinal)	, m	[3.84]	[0.064]

[ ] indicates the moored condition.

Table I.7 - Main particulars of 8-column twin rectangular hull type semi-submersible[8]

The following figures show the mooring arrangement and fairlead positions of the model used by Takarada et al. in ref. [8].

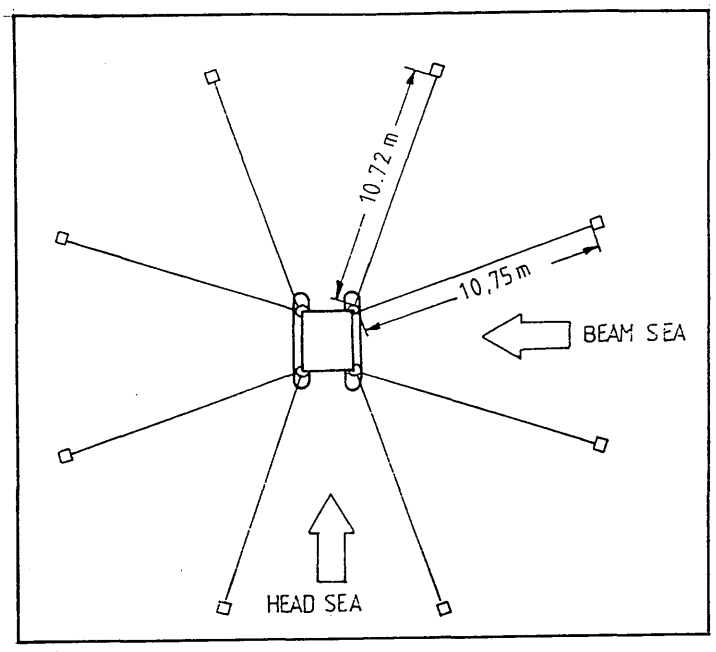

Fig. I.12 - Arrangement of mooring lines [8]

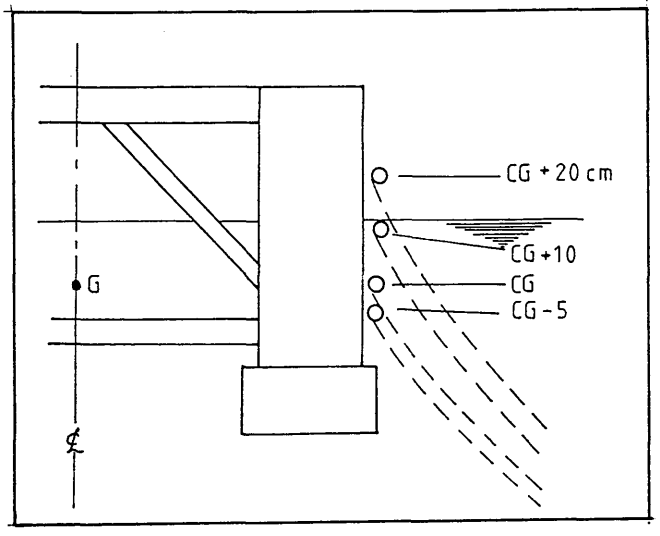

Fig. I.13 - Positions of fairleads [8]

The Quasi-Static Analysis of the Steady Tilt in the Moored Condition[8]

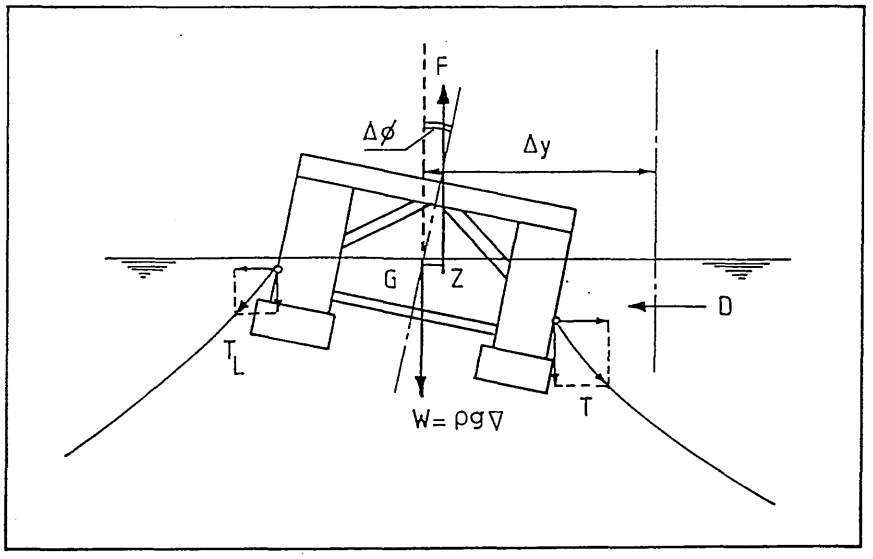

Fig. I.14 - The quasi-static analysis of the steady tilt in the moored condition[8]

$$\rho g \nabla + (T_s)_v + (T_\ell)_v = F \qquad \ldots \quad (I.16)$$

$$(T_s)_h - (T_\ell)_h = D \qquad \ldots \quad (I.17)$$

$$M_D + M_T = F \ \overline{GZ} \qquad \ldots \quad (I.18)$$

where Δy = horizontal drift,

$\Delta\phi$ = steady tilt,

∇ = displacement,

F = buoyancy,

T = line tension,

suffix s = seaward side,

ℓ = leeward side,

h = horizontal direction,

v = vertical direction,

D = steady drift force,

M_D = overturning moment due to the drift force,

M_T = overturning moment due to the mooring line tension.

Appendix II.1

CALCULATION OF MASS MOMENT OF INERTIA ABOUT ROLLING CENTRE AT THE C.O.G.

In the following the model is decomposed into the simple components with their known weights. The mass moment of inertia of each component is approximated to the known moment of inertia of various simple bodies [47] about their own axis. Then by transporting the moment of inertia of each component to the centre of rolling (assumed at the C.O.G.) of the semi-submersible the summed moment of inertia for the semi-submersible is found.

1. *Lower Hulls (2 off)*

r_a = 0.070 m
r_b = 0.066 m
y = 0.4175 m
i = 1 to 5
m = 6.55 kg

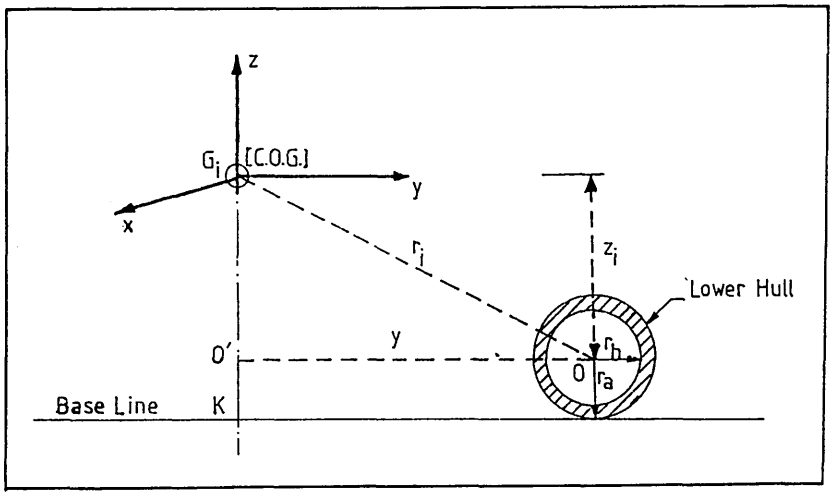

Fig. II.1 - Main particulars of the lower hull of the model

It is assumed that the hull is a hollow circular cylinder of outer radius r_a, inner radius r_b and the effects of inertia of the end caps are neglected but their weights are included. Then the moment of inertia for one hull about its rolling axis through 0 is:

$$I_o = \frac{1}{2} m (r_a^2 + r_b^2) = 0.030313 \text{ kg m}^2$$

where m = mass of the hull.

The calculation of the mass moment of inertia of one hull (I_{xx_i}) about 5 different C.O.G's for rolling is given in Table II.1.

$\overline{KG}_i$ (m)	$z_i = \overline{KG}_i - r_a$ (m)	$r_i^2 = y^2 + z_i^2$ (m^2)	$I_{xx_i} = I_o + mr_i^2$ (kg m^2)
0.28	0.21	0.2184	1.4608
0.27	0.20	0.2143	1.4340
0.26	0.19	0.2104	1.4084
0.243	0.173	0.2032	1.3613
0.22	0.15	0.1968	1.3193

Table II.1 - Rolling mass moment of inertia of a lower hull

2. *Vertical Columns (4 off)*

r_a = 0.057 m
r_b = 0.053 m
h = 0.525 m
y = 0.4175 m
h_1 = 0.041 m
m = 0.95 kg

(for one column)

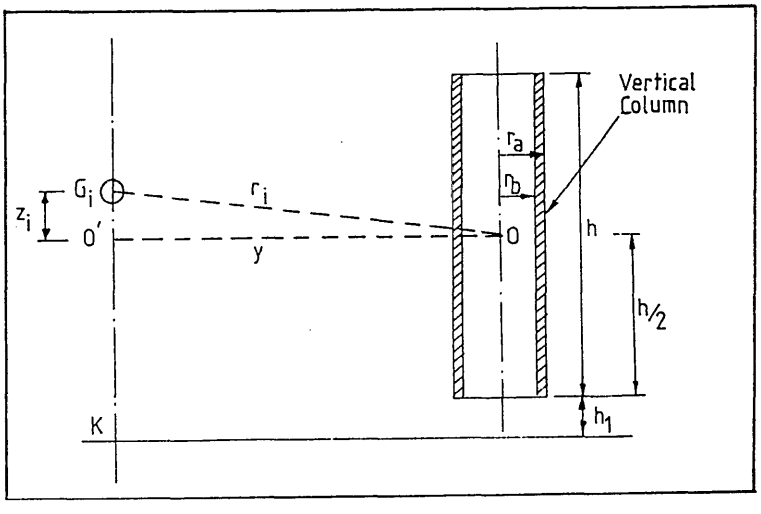

Fig. II.2 - Main particulars of the outer column of the model

If the column is considered to be a hollow circular cylinder of outer radius r_a, inner radius r_b, height h, its mass moment of inertia about its rolling axis through centre of mass (0) and perpendicular to cylindrical axis is:

$$I_o = \frac{1}{12} (3\, r_a^2 + 3\, r_b^2 + h^2) = 0.02326 \text{ kg m}^2$$

then

$\overline{KG}_i$ (m)	$z_i = \overline{KG}_i - (h/2+h_1)$ (m)	r_i^2 (m^2)	I_{xx_i} (kg m^2)
0.28	-0.0235	0.1745	0.1894
0.27	-0.0335	0.1754	0.1899
0.26	-0.0435	0.1762	0.1906
0.243	-0.0609	0.1780	0.1924
0.22	-0.0835	0.1813	0.1955

Table II.2 - Rolling mass moment of inertia of a corner column

3. *Inner Vertical Columns (4 off)*

$r_a = 0.0415$ m

$r_b = 0.039$ m

$h = 0.544$ m

$h_1 = 0.022$ m

$m = 1.050$ kg

$y = 0.4175$ m

$$I_o = \frac{1}{12} m\, (3\, r_a^2 + 3\, r_b^2 + h^2) = 0.026746 \text{ kg m}^2$$

$\overline{KG}_i$ (m)	$z_i = \overline{KG}_i - (h/2+h_1)$ (m)	r_i^2 (m^2)	I_{xx_i} (kg m^2)
0.28	-0.014	0.1745	0.2100
0.27	-0.024	0.1749	0.2104
0.26	-0.034	0.1755	0.2110
0.243	-0.051	0.17691	0.2125
0.22	-0.074	0.17978	0.2098

Table II.3 - Rolling mass moment of inertia of an inner column

4. *Ballast Containers (4 off)*

r_a = 0.044 m
r_b = 0.039 m
h = 0.31 m
y = 0.4175 m
m = 0.632
(for one container)

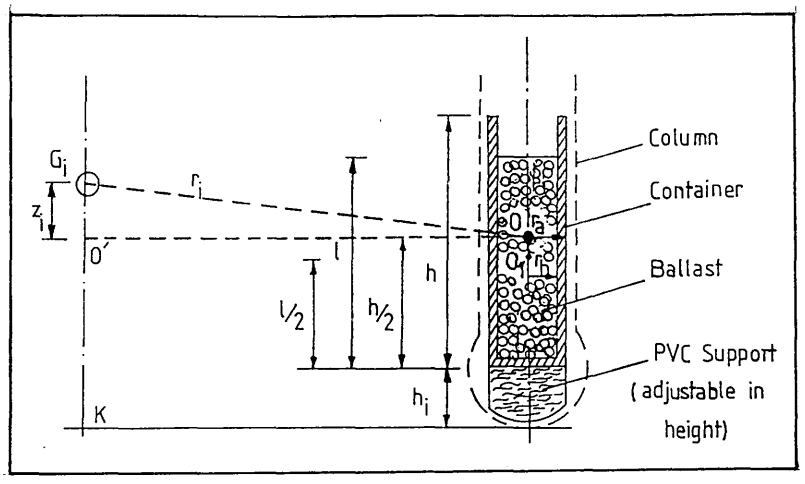

Fig. II.3 - Main particulars of a ballast container of the model

$$I_o = \frac{1}{12} m[3 r_a^2 + 3 r_b^2 + h^2] = 0.005607 \text{ kg m}^2$$

KG_i (m)	h_i (m)	$z_i = KG_i - (h/2+h_i)$ (m)	r_i^2 (m^2)	I_{xx_i} (kg m^2)
0.28	0.185	-0.06	0.1779	0.1180
0.27	0.165	-0.05	0.1768	0.1173
0.26	0.140	-0.035	0.1755	0.1165
0.243	0.10	-0.012	0.1744	0.1158
0.22	0.022	-0.043	0.1761	0.1169

Table II.4 - Rolling mass moment of inertia of a ballast container

5. *Ballast (4 off)*

r_b = 0.039 m

ℓ = 0.17 m

m = 5.712 kg (for one ballast)

It is assumed that the ballast is in a form of a right circular cylinder of radius r_b and height ℓ as shown in Fig. II.3. Its mass moment of inertia about the axis through O_1 and perpendicular to the

cylindrical axis is:

$$I_o = \frac{1}{12} m[3 r_b^2 + \ell^2] = 0.01593 \text{ kg m}^2$$

$\overline{KG}_i$ (m)	$z_i = KG_i - (h/2+h_i)$ (m)	r_i^2 (m^2)	I_{xx_i} (kg m^2)
0.28	-0.01	0.1744	1.0121
0.27	-0.02	0.1747	1.0138
0.26	-0.035	0.1755	1.0185
0.243	-0.058	0.1777	1.0307
0.22	-0.133	0.1871	1.0845

Table II.5 - Rolling mass moment of inertia of ballast

6. Aluminium Deck + Screws (2 off)

$t = 0.03$ m
$b = 0.203$ m
$b_1 = 0.10$ m
$b_m \simeq \frac{b+b_1}{2} = 0.15$ m
$h = 0.565$ m
$y = 0.4175$ m
$m = 1.5$ kg (one deck and screws)

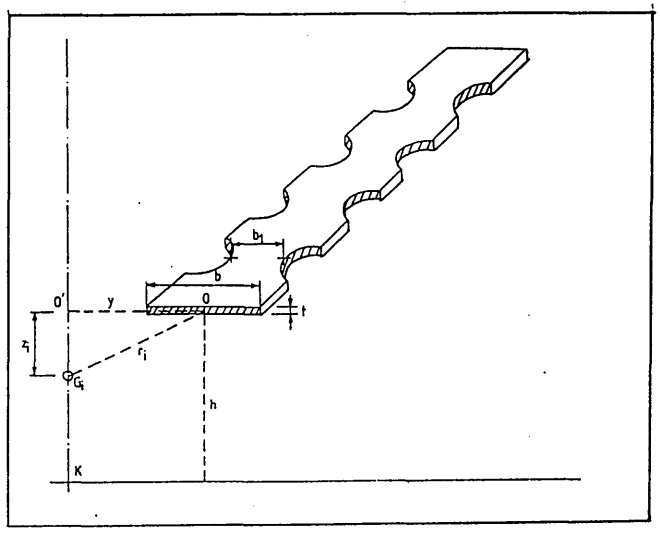

Fig. II.4 - Main particulars of the aluminium deck of the model

It is assumed that the deck is thin rectangular plate with mean beam b_m and thickness t. Its mass moment of inertia of rolling about [0] is:

$$I_o = \frac{1}{12} m[b_m^2 + t^2] = 0.002814 \text{ kg m}^2$$

$\overline{KG}_i$ (m)	$z_i = \overline{KG}_i - h$ (m)	r_i^2 (m^2)	I_{xx_i} (kg m^2)
0.28	-0.285	0.2555	0.3861
0.27	-0.295	0.2613	0.3948
0.26	-0.305	0.2673	0.4038
0.243	-0.322	0.2779	0.4196
0.22	-0.345	0.2933	0.4428

Table II.6 - Rolling mass moment of inertia of aluminium deck plus screws

7. Aluminium Lids at the Deck (4 off)

t = 0.003 m
b = 0.203 m
h = 0.567 m
y = 0.4175 m
m_1 = 0.268 kg
(shorter lid)
m_2 = 0.354 kg
(longer lid)

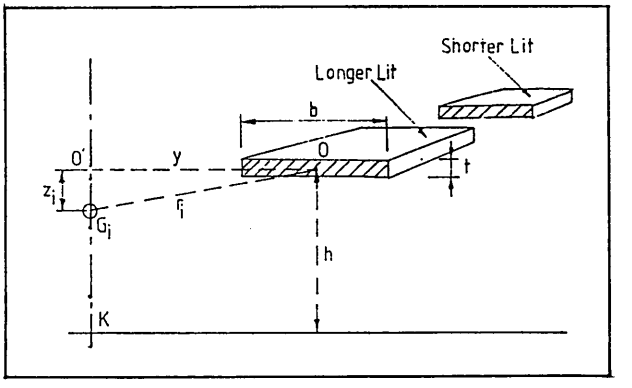

Fig. II.5 - Main particulars of the aluminium lids at the deck of the model

$$I_o = \frac{1}{2}(m_1 + m_2)[b^2 + t^2] = 0.02136 \text{ kgm}^2$$

$\overline{KG}_i$ (m)	$z_i = \overline{KG}_i - h$ (m)	r_i^2 (m^2)	I_{xx_i} (kg m^2)
0.28	-0.287	0.2566	0.1617
0.27	-0.297	0.2625	0.1654
0.26	-0.307	0.2685	0.1691
0.243	-0.324	0.2793	0.1758
0.22	-0.347	0.2941	0.1851

Table II.7 - Rolling mass moment of inertia of aluminium lids at the deck

8. PVC Deck (4 off)

t = 0.012 m
b = 0.204 m
y = 0.4175 m
h = 0.56 m
m_1 = 0.43 m
(shorter lid)
m_2 = 0.525 m
(longer lid)

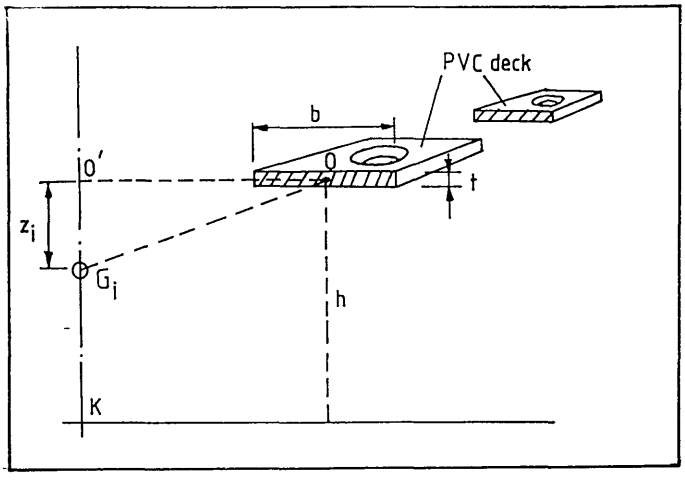

Fig. II.6 - Main particulars of the PVC deck of the model

By neglecting the effect of inertia of the holes:

$$I_o = \frac{1}{12}(m_1 + m_2)(b^2 + t^2) = 0.003323 \text{ kg.m}^2$$

$\overline{KG}_i$ (m)	$z_i = \overline{KG}_i - h$ (m)	r_i^2	I_{xx_i} (kg m^2)
0.28	- 0.28	0.2527	0.2446
0.27	- 0.29	0.2584	0.2501
0.26	- 0.30	0.2643	0.2557
0.243	- 0.317	0.2748	0.2657
0.22	- 0.34	0.2899	0.2802

Table II.8 - Rolling mass moment of inertia of the PVC deck

9. *Aluminium Beam at the Deck (4 off)*

t = 0.025 m
b = 0.4175 m
y = 0.2087 m
h = 0.58 m
m = 0.403 kg

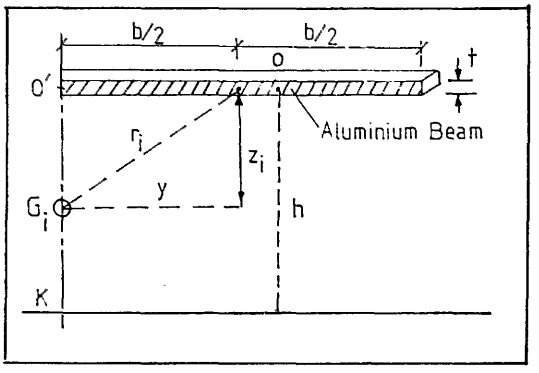

Fig. II.7 - Main particulars of the aluminium beam at the deck of the model

$$I_o = \frac{1}{12} m[b^2 + t^2] = 0.005875 \text{ kg.m}^2$$

$\overline{KG}_i$ (m)	$z_i = \overline{KG}_i - h$ (m)	r_i^2 (m^2)	I_{xx_i} (kg m^2)
0.28	-0.29	0.1277	0.0573
0.27	-0.31	0.1397	0.0622
0.26	-0.32	0.1459	0.0647
0.243	-0.337	0.1571	0.0691
0.22	-0.36	0.1732	0.0757

Table II.9 - Rolling mass moment of inertia of the aluminium beam

The total mass moment of inertia of the model is found by summing the above calculating individual moment values as follows:

$$\begin{aligned}
\Sigma I_{xx_i} &= 2 \times I_{xx_i} \quad \text{(lower hulls)} \\
&+ 4 \times I_{xx_i} \quad \text{(vertical column)} \\
&+ 4 \times I_{xx_i} \quad \text{(inner vertical column)} \\
&+ 4 \times I_{xx_i} \quad \text{(ballast container)} \\
&+ 4 \times I_{xx_i} \quad \text{(ballast)} \\
&+ 2 \times I_{xx_i} \quad \text{(aluminium deck + screws)} \\
&+ 4 \times I_{xx_i} \quad \text{(aluminium lids)} \\
&+ 4 \times I_{xx_i} \quad \text{(PVC deck)} \\
&+ 4 \times I_{xx_i} \quad \text{(aluminium beam)}
\end{aligned}$$

From the foregoing tables I_{xx_i} values are substituted into the above formula, thus the mass moment of inertia ΣI_{xx_i} and the radius of gyration $\bar{k}_{xx_i}$ of roll for the model is found as follows:

$\overline{GM}_i$ (m)	$\overline{KG}_i$ (m)	ΣI_{xx_i} (kg m^2)	$\bar{k}_{xx_i} = \sqrt{\frac{\Sigma I_{xx_i}}{\Delta}}$ (m)
0.019	0.28	11.666	0.4473
0.029	0.27	11.687	0.4477
0.038	0.26	11.729	0.4485
0.056	0.243	11.810	0.4500
0.079	0.22	12.115	0.4558

Table II.10 - Rolling mass moment of inertia and the radius of gyration of the semi-submersible model

Appendix II.2

EXPERIMENTAL DETERMINATION OF ADDED MASS AND DAMPING ABOUT NATURAL HEAVE AND ROLL FREQUENCY

The equation of motion for a linear single degree of freedom system subjected to a harmonic exciting wave force (and moment) is:

$$(M+A)\ddot{s} + B\dot{s} + C s = F_o \cos\omega t \qquad \ldots \quad II.1$$

where M = mass (or mass moment of inertia)

A = added virtual mass (or moment of inertia)

B = damping force (or moment) coefficient

C = restoring force (or moment) coefficient

ω = radian wave frequency

s = motion

$(\dot{\ })$ = time derivative

The solution of eq. II.1 is given[30]:

$$s = e^{-\nu t}(C_1 \cos\omega_d t + C_2 \sin\omega_d t) + S\cos(\omega t - \varepsilon) \qquad \ldots \quad II.2$$

where S = the maximum of the forced motion under the F_o wave exciting force

ε = the phase angle between the forced motion and the wave exciting force

If it is noticed eq.II.2 the resultant motion consists of two types of oscillations; the first term represents a 'free-damped oscillation' (i.e. the system oscillates freely under the effect of an initially applied force). The second term an oscillation with the same frequency as that of the wave exciting force. If both oscillations

remain effective the resultant motion will be a 'transient motion'. However, the free damped oscillation decays after a certain time depending on the magnitude of the decaying constant ν.

For the steady condition:

$$S = S_{st}\,\mu \qquad \ldots \quad II.3$$

where S_{st} = static motion amplitude $= \frac{F_o}{C}$ ... II.4

$$\mu = \text{magnification factor} = \frac{1}{[(1-\Lambda^2)^2 + 4K^2\Lambda^2]^{\frac{1}{2}}} \qquad \ldots \quad II.5$$

$$\Lambda = \text{tuning factor} = \frac{\textit{wave frequency}}{\textit{natural frequency}} = \frac{\omega}{\omega_n} \qquad \ldots \quad II.6$$

$$K = \text{non-dimensional damping factor} = \frac{\nu}{\omega_n} \qquad \ldots \quad II.7$$

$$\nu = \text{decaying constant} = \frac{B}{2(M+A)} \qquad \ldots \quad II.8$$

$$\omega_n = \text{natural frequency} = \left[\frac{C}{M+A}\right]^{\frac{1}{2}} \qquad \ldots \quad II.9$$

ω_d = radian frequency of the free damped oscillation $= [\omega_n^2 - \nu^2]^{\frac{1}{2}}$ ... II.10

$$\varepsilon = \text{phase angle} = \tan^{-1}\frac{2K\Lambda}{1-\Lambda^2}$$

C_1, C_2 = constants to be determined from the initial conditions.

The natural frequency ω_n is determined from eq. II.1 when there is no damping B=0 and exciting force F_o=0, i.e.

$$(M+A)\ddot{s} + Cs = 0 \qquad \ldots \quad II.12$$

This is a 'free, undamped oscillation' and the solution for this differential equation is:

$$s = C_{1n}\sin\omega_n t + C_{2n}\cos\omega_n t \qquad \ldots \quad II.13$$

where C_{1n} and C_{2n} are constants that can be determined from the initial conditions. The natural frequency ω_n is given by eq. II.9 and

considered to be a constant which does not depend on the amplitude of motion for small and moderate motions.

However ω_d, the radian frequency of the free damped oscillation whose solution is given by the first term of eq. II.2 is always smaller than the natural frequency because of the damping as given in eq. II.10 and shown in Fig. II.8.

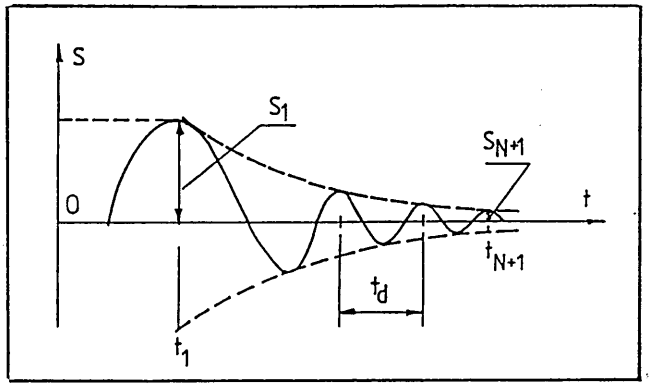

Fig. II.8 - Free damped oscillation

If S_1 is the amplitude of oscillation at t_1 and S_{N+1} the amplitude at t_{N+1} the ratio between these amplitudes is given by:

$$\frac{S_1}{S_{N+1}} = e^{-\nu N T_d} \qquad \ldots \quad II.14$$

where T_d = the period of damped oscillation = $\frac{2\pi}{\omega_d}$ ... II.15

N = number of cycles considered

By making use of eqs II.7, II.10, II.14 and II.15:

$$\frac{S_1}{S_{N+1}} = e^{-2\pi N \frac{K}{[1-K^2]^{\frac{1}{2}}}} \qquad \ldots \quad II.16$$

Since the non-dimensional damping factor K is usually small K^2 can be neglected giving:

$$K = -\frac{1}{2\pi N} \ell n \left[\frac{S_1}{S_{N+1}}\right] \qquad \ldots \quad II.17$$

As seen in eq. II.17 if the free damped motion amplitudes are known from the tests the non-dimensional damping factor can be determined for the small and moderate amplitudes.

Furthermore if the natural motion frequency ω_n is known from the tests, the added mass A can be calculated by eq. II.9. Then by using eqs II.7 and II.8 the decaying constant ν, and actual damping B can be determined about the natural frequency.

In the following these values are calculated for the semi-submersible model by using the natural frequency values determined from the free model tests. However, one should bear in mind that these tests are the free damped motion tests. Therefore the measured frequency is the free damped frequency rather than the undamped frequency (= natural frequency). Practically to perform an undamped free motion in the water is impossible. But for the practical purposes the natural frequency of the motion is assumed to be equal to the frequency of the free damped oscillation since the square of decaying constant ν will be negligible in formula II.10.

Heaving Motion

ρ = 1000 kg m^{-3}

g = 9.81 m sec^{-2}

A_w = waterplane area = 0.06244 m^2 (see Table 2, Chapter 3)

M = total displacement = 58.300 kg

C = restoring force coef = $\rho g A_w$ = 612.536 n/m

ℓ (mm)	S_N/S_{N+1}	ω_n (r s^{-1})	-K
24.5	32/28	2.564	0.0212
24.5	28/25	2.564	0.0180
25.0	25/22	2.513	0.02034
24.5	22/19	2.564	0.02333
24.0	19/16.5	2.618	0.0224
24.5	16.5/14.5	2.564	0.0206
24.5	14.5/12.5	2.564	0.0236

(Mean): $\omega_n = 2.564$ r s^{-1} K = 0.02135

Table II.11 - Experimental natural heave frequency and non-dimensional damping factor

where ℓ = the distance measured between each cycle considered

S_N/S_{N+1} = the ratio of the maximum of the motion measured for each successive cycle considered

ω_n = natural frequency = $\frac{2\pi}{T_n} = \frac{2\pi V}{\ell}$

T_n = natural period

V = chart speed = 10 mm s^{-1}

K = non-dimensional damping factor calculated from eq. II.17

By substituting ω_n, C, M into eq. II.9, the added mass about the natural frequency:

A = 34.874 kg (~ 40% of the total displacement of the model)

By using ω_n and K in eq. II.7, the decaying constant is found as:

$\nu = 0.0547$ r s^{-1}

and by substituting M, A and ν into eq. II.8 the actual damping is:

B = 10.20 n m^{-1} s

Rolling Motion

In the roll case the terms in eq. II.1 will be:

M = mass moment of inertia

A = added virtual moment of inertia

B = damping moment of inertia

C = restoring moment coefficient = $\rho g \nabla \overline{GM}$ ... II.18

∇ = underwater displacement of the model

Since 5 $\overline{GM}$ values are tested in the following 5 tables are presented.

GM = 0.0190 m

ℓ (mm)	S_N/S_{N+1}	ω_n (r s^{-1})	-K
89	60/34	0.706	0.0904
90	34/18	0.698	0.1012
90	71/39	0.698	0.0953
89	39/19	0.706	0.1144

Mean $\omega_n \simeq 0.702$ r s^{-1} K = 0.1003

Table II.12 - Experimental natural roll frequency and non-dimensional damping factor for $\overline{GM}$ 0.019 m

By using eq. II.18 with $\rho\nabla$ = 58.3 kg and $\overline{GM}$ = 0.019 m:

C = 10.866 n m

From Table 10 in Appendix II.1 mass moment of inertia for GM = 0.019 m is:

M = 11.666 kg m^2

By substituting ω_n into eq. II.9 added moment of inertia for this $\overline{GM}$ is:

A = 10.383 kg m^2

and decaying constant from eq. II.7 is:

ν = 0.0704 r s^{-1}

by using eq. II.8 the actual damping:

$$B = 3.104 \text{ n m s}$$

$\bar{GM} = 0.0290$ m

ℓ (mm)	S_N/S_{N+1}	ω_n (r s^{-1})	-K
70	54/38	0.897	0.060
71	38/25	0.885	0.066
70	54/35.5	0.897	0.067
71	35.5/22	0.885	0.076

Mean $\omega_n = 0.891$ r s^{-1} K = 0.0673

C = 16.585 n m
M = 11.687 kg m^2
A = 9.204 kg m^2
$\nu = 0.06$ r s^{-1}
B = 2.507 n m s

Table II.13 - Experimental natural roll frequency and non-dimensional damping factor for $\bar{GM} = 0.029$ m

$\bar{GM} = 0.0380$ m

ℓ (mm)	S_N/S_{N+1}	ω_n	-K
62	64/46.5	1.034	0.0508
62	46.5/34.5	1.034	0.0475
63	34.5/26	0.997	0.0450
63	26/18.5	0.997	0.0541
62	62.5/45.5	1.034	0.0505
63	45.5/34	0.997	0.0464
63	34/25.5	0.997	0.0457
63	25.5/18.5	0.997	0.0512
63	18.5/12.5	0.997	0.0624

Mean $\omega_n = 1.009$ r s^{-1} K = 0.0504

C = 21.733 n m
M = 11.729 kg m^2
A = 9.618 kg m^2
$\nu = 0.0508$ r s^{-1}
B = 1.99 n m s

Table II.14 - Experimental natural roll frequency and non-dimensional damping factor for $\bar{GM} = 0.038$ m

$\overline{GM}$ = 0.0560 m

ℓ (mm)	S_N/S_{N+1}	ω_n (r s^{-1})	-K
51.5	60/42	1.220	0.0568
50.0	42/32	1.257	0.0433
51.0	32/24	1.232	0.0458
50.5	24/18	1.232	0.0458
51.0	36.5/29	1.232	0.0366
51.5	29/22	1.220	0.0439
51.0	22/16	1.232	0.0506

Mean ω_n = 1.232 r s^{-1} K = 0.0461

C = 32.03 n m
M = 11.810 kg m^2
A = 9.291 kg m^2
ν = 0.0568 r s^{-1}
B = 2.397 n m s

Table II.15 - Experimental natural roll frequency and non-dimensional damping factor for $\overline{GM}$ = 0.056 m

$\overline{GM}$ = 0.0790 m

ℓ (mm)	S_N/S_{N+1}	ω_n	-K
39.5	52/41	1.591	0.0378
"	41/34	"	0.0298
"	34/27.5	"	0.0338
"	27.5/22	"	0.0355
"	22/18	"	0.0319
"	18/14	"	0.0399
"	41/34	"	0.0298
"	34/28	"	0.0309
"	28/22	"	0.0384
"	22/17.5	"	0.0364
"	17.5/14	"	0.0355
"	14/11	"	0.0384

Mean ω_n = 1.591 r s^{-1} K = 0.0348

C = 45.18 n m
M = 12.115 kg m^2
A = 5.733 kg m^2
ν = 0.0554 r s^{-1}
B = 1.9776 n m s

Table II.16 - Experimental natural roll frequency and non-dimensional damping factor for $\overline{GM}$ = 0.079 m

REFERENCES

1. Rules for Building and Classing Offshore Mobile Drilling Units, AMERICAN BUREAU OF SHIPPING, pp21-23, New York, 1973.

2. SARCHIN, T.H. and GOLDBERG, L.L. "Stability and Buoyancy Criteria for U.S. Naval Surface Ships", Trans SNAME, Vol. 70, pp418-458, 1962.

3. Rules for the Construction and Classification of Mobile Offshore Units, DET NORSKE VERITAS, pp35-37, Oslo, 1975.

4. Rules and Regulations for the Classification of Mobile Offshore Units, LLOYD'S REGISTER OF SHIPPING, Part 4, pp1-2, London, 1984.

5. PAULLING, J.R. "A Comparison of Stability Characteristics of Ships and Offshore Structures", Preproc. Second Int. Conf. on Stability of Ships and Ocean Vehicles, pp41-47, Tokyo, 1982.

6. OAKLEY, O.H., PAULLING, J.R. and WOOD, P.D. "Ship Motions and Capsizing in Astern Seas", Proc. Tenth Symp. on Naval Hydrodynamics, ACR-204, Office of Naval Research, pp297-350, 1974.

7. NUMATA, E. and MICHEL, W.H. "Experimental Study of Stability Limits for Semi-submersible Drilling Platforms", OTC paper 2032, Houston, 1974.

8. TAKARADA, N., OBAKATA, J., INOUE, R., NAKAJIMA, T. and KOBAYASHI, K. "The Stability on Semi-Submersible Platform in Waves (On the Capsizing of Moored Semi-Submersible Platform)", Preproc. Second Int. Conf. on Stability of Ships and Ocean Vehicles, pp49-61, Japan, 1982.

9. AGUIRRE, J.E. and BOYCE, T.R. "Estimation of Wind Forces on Offshore Drilling Platforms", Trans RINA, Vol. 116, pp93-111, 1974.

10. DAVENPORT, A.G. "The Spectrum of Horizontal Gustiness Near the Ground in High Winds", Quarterly Jour. Royal Met. Soc., 87, pp194-211, 1961.

11. MILLER, N.S. "Note on Wind Heeling Moments on Semi-Submersibles", Glasgow University NA & OE Dept. Report NAOE-HL-76-04, 1976.

12. HSU, F.H. and BLENKARN, K.A. "Analysis of Peak Mooring Force Caused by Slow Vessel Drift Oscillation in Random Seas", OTC paper 1159, Houston, 1970.

13. REMERY, G.F.M. and HERMANS, A.J. "The Slow Drift Oscillations of a Moored Object in Random Seas", OTC paper 1500, Houston, 1971.

14. PINKSTER, J.A. "Low Frequency Second Order Wave-Exciting Forces on Floating Structures", PhD Thesis, NSMB Publication No. 650, Wageningen, 1980.

15. NUMATA, E. and McCLURE, A.C. "Experimental Study of Stability Limits for Semi-Submersible Drilling Platforms", OTC paper 2285, Houston, 1975.

16. NUMATA, E., MICHEL, W.H. and McCLURE, A.C. "Assessment of Stability Requirements for Semi-submersible Units", Trans SNAME, Vol. 84, pp56-74, 1976.

17. MILLER, N.S. "Stability Tests on Two Designs of Semi-submersibles in Regular Waves", University of Glasgow NA & OE Dept. Report NAOE-HL-77-01, 1977.

18. HINENO, M., TAKEGAWA, H., ODA, T. and ABE, M. "The Effect of Low Frequency Roll Motion on Under-Deck Clearance of a Semi-submersible Platform", Preproc. Second Int. Conf. on Stability of Ships and Ocean Vehicles, pp29-35, Tokyo, 1982.

19. ATLAR, M. and MILLER, N.S. "The Tilt Problem in Semi-Submersibles", An Int. Conf. on Marine Safety, Dept. of NA & OE, University of Glasgow, 1983.

20. MARTIN, J. and KUO, C. "Calculations for the Steady Tilt of Semi-submersibles in Regular Waves", Trans RINA, Vol. 121, pp87-101, 1978.

21. MARTIN, J. and KUO, C. "The Steady Tilt of Semi-submersibles in Regular Waves: Calculations and a Simple Experiment", Mechanics of Wave-Induced Forces on Cylinders, edited by T.L. Shaw, University of Bristol, Pitman Advanced Publishing Ltd, pp704-713, 1979.

22. RUSAAS, S. "The Capsizing of "Alexander L. Keilland", Preproc. Second Int. Conf. on Ships and Ocean Vehicles, pp1-14, Tokyo, 1982.

23. FAULKNER, D. (Discussion to Ref. [20]), Trans RINA, Vol. 121, p96, 1978.

24. DE SOUZA, P.M.F.M. "Dynamic Response of Semi-submersibles", Glasgow University NA & OE Dept. Report NAOE-HL-76-03, 1976.

25. DE SOUZA, P.M.F.M., MILLER, N.S. and FERGUSON, A.M. "The Behaviour of a 4 column Semi-submersible Unit under Wind and Wave Loading", Glasgow University NA & OE Dept. Report NAOE-HL-76-06, 1986.

26. DE SOUZA, P.M.F.M. and MILLER, N.S. "The Intact and Damaged Stability Tests on a Three Column Semi-submersible Unit under Wind and Wave Loading", Glasgow University NA & OE Dept. Report NAOE-HL-77-02, 1977.

27. DE SOUZA, P.M.F.M. and MILLER, N.S. "The Intact and Damaged Stability Behaviour of Two Semi-submersible Models under Wind and Wave Loading", OTC paper 3298, Houston, 1978.

28. KUO, C., LEE, A., WELYA, Y. and MARTIN, J. "Semi-submersible Intact Stability - Static and Dynamic Assessment and Steady Tilt in Waves", OTC paper 2976, 1977.

29. MORRAL, A. "The Influence of the Steady Vertical Component of Wave Force on the Stability of Semi-submersibles", NMI Report, NMI R46, OT-R-7833, 1978.

30. BHATTACHARYYA, R. "Dynamics of Marine Vehicles", A Wiley-Interscience Publication, pp418-425, 1978.

31. OGILVIE, T.F. "First and Second Order Forces on a Cylinder Submerged under a Free Surface", Journal of Fluid Mechanics, Vol. 16, part 3, pp451-472, 1963.

32. NUMATA, E. (Written Discussion to Ref. [20]), Trans RINA, Vol. 121, pp97-98, 1978.

33. DEAN, W.R. "On the Reflection of Surface Waves by a Submerged Cylinder", Proc. Camb. Phil. Soc. 44, pp483-491, 1948.

34. URSELL, F. "Surface Waves on Deep Water in the Presence of a Submerged Circular Cylinder", Proc. Camb. Phil. Soc. 46, pp141-152, 1960.

35. SALTER, S.H., JEFFREY, D.C. and TAYLOR, J.R.M. "The Architecture of Nodding Duck Wave Power Generators", The Naval Architect, pp21-24, January 1976.

36. LONGUET-HIGGINS, M.S. "The Mean Forces Exerted by Waves on Floating or Submerged Bodies with Applications to Sand Bars and Wave Power Machines", Proc. R. Soc. Lond. A.352, pp463-480, 1977.

37. ARAI, S., NEKADO, Y. and TAKAGI, M. "Study on the Motions of a Moored Vessel Among the Irregular Waves", Journal of the Society of Naval Architects of Japan, No. 140, pp142-151, 1976.

38. INCECIK, A. "Design Aspects of the Hydrodynamic and Structural Loading on Floating Offshore Platforms under Wave Excitations", PhD Thesis, Glasgow University NA & OE Dept., pp395-423, 1982.

39. RUNDAT and CALIBR. Data Sampling Programs, Glasgow University NA & OE Dept. Hydrodynamics Lab.

40. McDOWALL, E.J. "A Study on the Problems of Wave Generation in a Tank", Final Year Project, Glasgow University NA & OE Dept., p6, 1979/80.

41. Rules for Classification of Mobile Offshore Units, Det norske Veritas, Pt 3, Ch 1, Sec 4, pp12-14, 1984.

42. DALLY, J.W. and WILLIAM, F.R. "Experimental Stress Analysis", Second Edition McGraw-Hill Book Company, pp216-271, 1978.

43. DataSpan 2000, Operating Instructions for Strain Gauge Amplifier Type 2028, RDP ELECTRONICS Ltd., West Midlands, December 1978.

44. WINDOW, A.L. and HOLISTER, G.S. "Strain Gauge Technology", Applied Science Publishers Ltd., 1982.

45. How to Instal Strain Gauges with Certified Eastman 910 Cement, Techniques in Experimental Stress Analysis Strain Gauge Series, VISHAY INTERTECHNOLOGY INC., Educational Products, Report T-101, Michigan.

46. Showa Foil Gauges, SHOWA MEASURING INSTRUMENTS CO. LTD., Cat No. E2003 11. 1975, Tokyo.

47. McCLEAN and NELSON, "Theory and Problems in Engineering Mechanics, Static and Dynamics", Schaum's Outline Series, pp224-225, 1962.

48. ATLAR, M. "A Study of the Frank Close-fit Method; Theory, Application and Comparison with Other Methods", Glasgow University NA & OE Dept. Report NAOE-HL-81-09, 1982.

49. ATLAR, M. "Method for Predicting First Order Hydrodynamic Loads on Single and Twin Sections by the Frank Close-fit Method", Glasgow University NA & OE Dept. Report NAOE-85-41, 1985.

50. ATLAR, M. "A Study of Hydrodynamic Radiation Pressures Around Two-dimensional Single and Twin Sections Oscillating in or below the Free Surface", Glasgow University NA & OE Dept. Report NAOE-84-53, 1984.

51. ATLAR, M. and LAI, P.S.K. "A Two-dimensional Method for Estimating Hydrodynamic Loads and Motions of a Twin-hulled Semi-submersible Associated with Some Hydrodynamic Aspects in Regular Beam Seas", Glasgow University NA & OE Dept. Report NAOE-85-34, 1985.

52. ATLAR, M., SEREN, D.B. and VALIDAKIS, J. "Investigation of the Hydrodynamic Coefficients of Semi-submersibles (or SWATH)-type Sections with Emphasis on the Effect of Tilt and Interference", Glasgow University NA & OE Dept. Report NAOE-85-32, 1985.

53. ATLAR, M. "A Study of the Wave-drift Forces on Single and Twin Sections Based on Maruo's Formula", Glasgow University NA & OE Dept. Report NAOE-85-39, 1985.

54. LONGUET-HIGGINS, M.S. and STEWART, R.W. "Radiation Stress in Water Waves; a Physical Discussion with Applications", Deep-Sea Research, Vol. 11, pp529-562, Pergamon Press, 1964.

55. FALTINSEN, O.M. "Slow-drift Excitation of a Ship in Irregular Beam Sea Waves", Det norske Veritas Report 76-083, 1976.

56. SALVESEN, N., TUCK, E.O. and FALTINSEN, O. "Ship Motions and Sea Loads", Trans SNAME, Vol. 78, pp250-287, 1970.

57. KIM, C.H. and CHOU, F.S. and TIEN, O. "Motions and Hydrodynamic Loads of a Ship Advancing in Oblique Waves", Trans SNAME, Vol. 88, pp225-256, 1980.

58. STANDING, R.G., DACUNHA, N.M.C. and MATTEN, R.B. "Mean Wave Drift Forces: Theory and Experiments", National Maritime Institute Report, OT-R-8175 NMI R124, Feltham, 1981.

59. NEWMAN, J.N. "Marine Hydrodynamics", the MIT press, pp45-46, 1977.

60. MORISON, J.R., O'BRIEN, M.P. and SCHAAF, S.A. "The Force Exerted by Surface Waves on Piles", Petroleum Transactions, AIME, Vol. 189, pp149-154, 1950.

61. SMITH, S.N. and ATLAR, M. "On the Large Amplitude and Extreme Motions of Floating Vessels", Proc. Third Int. Conf. BOSS, Vol. 2, pp608-617, MIT, 1982.

62. HOGBEN, N. and STANDING, R.G. "Wave Loads on Large Bodies", Proc. Int. Symp. on the Dynamics of Marine Vehicles and Structures in Waves (IMECHE), pp258-277, London.

63. NEWMAN, J.N., SØRTLAND, B. and VINJE, T. "Added Mass and Damping of Rectangular Bodies Close to the Free Surface", Journal of Ship Research, Vol. 28, No. 4, pp219-225, 1984.

64. NORDENSTRØM, N., FALTINSEN, O. and PEDERSEN, B. "Prediction of Wave-induced Motions and Loads for Catamarans", OTC paper 1418, Houston, 1971.

65. KIM, C.H. and CHOU, F.S. "Motions of a Semi-submersible Drilling Platform in Head Seas", Marine Technology, pp112-123, April, 1973.

66. KIM, C.H. "The Hydrodynamic Interaction between Two Cylindrical Bodies Floating in Beam Seas", Stevens Institute of Technology Report SIT-OE-72-10, Hoboken, 1972.

67. PAULLING, J.R. and HONG, Y.S. "Analysis of Semi-submersible Catamaran Type Platforms", OTC paper 2975, Houston, 1977.

68. ATLAR, M., SEREN, D.B. and VALIDAKIS, J. "Effect of Tilt and Hydrodynamic Interference on the Hydrodynamic Coefficients of SWATH-type Sections", Preproc. Int. Conf. on SWATH Ships and Advanced Multi-Hulled Vessels, RINA, paper 12, London, 1985.

69. SEREN, D.B. and ATLAR, M. "The SWATH Wave-load Program - Progress Report No. 6; An Overview of the Concepts Employed to Predict the Hydrodynamic Forces Imposed on an Unappended SWATH Ship Proceeding in a Seaway", Glasgow University NA & OE Dept. Report NAOE-84-63, 1984.

70. PAULLING, J.R., HONG, Y.S., STIANSEN, S.G. and CHEN, H.H. "Structural Loads on Twin-hull Semi-submersible Platforms", OTC paper 3246, Houston, 1978.

71. LEE, C.M. and CURPHEY, R.M. "Prediction of Motion, Stability and Wave Load of Small-waterplane-area, Twin-hull Ships", Trans SNAME, Vol. 85, pp94-130, 1977.

72. OHKUSU, M. "On the Heaving Motion of Two Circular Cylinders on the Surface of a Fluid", Reports of Research Institute of Applied Mechanics, Kyushu University, Vol. 17, No. 58, Japan, 1969.

73. WANG, S. "On the Hydrodynamic Forces of Twin-hull Vessels", Proc. 12th Coastal Eng. Conf., Vol. III, pp1700-1721, Washington D.C., 1970.

74. WANG, S. and WAHAB, R. "Heaving Oscillations of Twin Cylinders in a Free Surface", Journal of Ship Research, Vol. 15, No. 1, pp33-48, 1971.

75. LEE, C.M. and BEDEL, J.W. "Added Mass and Damping Coefficients of Heaving Twin Cylinders in a Free Surface", DTNSRDC Report No. 3695, 1971.

76. MAEDA, H. "Hydrodynamical Forces on a Cross-section of a Stationary Structure", Proc. Int. Symp. on the Dynamics of Marine Vehicles and Structures in Waves (IMECHE), pp80-91, London, 1974.

77. PRICE, W.G., TEMAREL, P. and YOUSHENG, W. "Structural Response of a SWATH or Multi-hull Vessel Travelling in Waves", Preproc. Int. Conf. on SWATH Ships and Advanced Multi-hulled Vessels, RINA, paper 13, London, 1974.

78. ABKOWITZ, M.A. "Stability and Control of Ocean Vehicles", The MIT Press, ppI-1, I-14, Cambridge, Massachusetts and London, 1969.

79. FRANK, W. "On the Oscillations of Cylinders in or below the Free Surface of Deep Fluids", DTNSRDC Report 2375, 1967.

80. MEYERS, W.G., SHERIDAN, D.J. and SALVESEN, N. "Manual NSRDC Ship-motion and Sea-load Computer Program", DTNSRDC Report 3376, 1975.

81. McCREIGHT, K.K. and LEE, C.M. "Manual for Mono-hull or Twin-hull Ship Motion Prediction Computer Program", DTNSRDC Report SPD-686-02, 1976.

82. BEDEL, J.W. and LEE, C.M. "Numerical Calculation of the Added Mass and Damping Coefficients of Cylinders Oscillating in or below the Free Surface", DTNSRDC Report 3551, 1971.

83. KIM, C.H. "Wave-exciting Forces and Moments on an Ocean Platform Fixed in Oblique Seas", OTC paper 1180, Houston, 1970.

84. WEHAUSEN, J.V. and LAITONE, E.V. "Surface Waves", Handbuch der Physik, (Encyclopedia of Physics) edited by S. Fluegge, Vol. 9, Fluid Dynamics 3, Springer Verlag, pp443-773, Berlin, 1960.

85. KIM, C.H. "An Introduction to Water Wave Theory in Ocean Engineering", Stevens Institute of Technology Report SIT-OE-80-2, pp56-70, Hoboken, 1980.

86. NEWMAN, J.N. "The Exciting Forces on Fixed Bodies in Waves", Journal of Ship Research, Vol. 6, pp10-17, 1962.

87. FALTINSEN, O.M. "A Study of the Two-dimensional Added Mass and Damping Coefficients by the Frank Close-fit Method", Det norske Veritas Report 69-10-S, 1969.

88. Marine Accident Report, Capsizing and Sinking of the US Mobile Offshore Drilling Unit Ocean Ranger off the East Coast of Canada 166 Nautical Miles East of St. John's, Newfoundland, February 15, 1982, National Transportation Safety Board Report NTSB-Mar-83-2, Washington, D.C. 20594.

89. KOBAYASHI, M. "Hydrodynamic Forces and Moments Acting on Two-dimensional Asymmetrical Bodies", Preproc. First Int. Conf. on Stability of Ships and Ocean Vehicles, Strathclyde University, Glasgow, 1975.

90. MOTORA, S. and KOYAMA, T. "On Wave-excitationless Ship Forms", Preproc. 6th Int. Naval Hydrodynamic Symp., Vol. I, pp14.1-14.19, Washington D.C., 1966.

91. LUNDGREN, H., SAND, S.E. and KIRKEGAARD, J. "Drift Forces and Damping in Natural Sea States", Proc. Third Int. Conf. BOSS, Vol. 2, pp592-607, MIT, 1982.

92. FERRETTI, C. and BERTA, M. "Viscous Effect Contribution to the Drift Forces on Floating Structures", Proc. First Int. Symp. on Ocean Engineering Ship Handling, paper 9, SSPA, Gothenborg, 1980.

93. PIJFERS, J.G. and BRINK, A.W. "Calculated Drift Forces of Two Semi-submersible Platform Types in Regular and Irregular Waves", OTC paper 2977, Houston, 1977.

94. CHAKRABARTI, S.K. "Steady Drift Force on Vertical Cylinder - Viscous vs. Potential", Applied Ocean Research, Vol. 6, No. 2, pp73-82, 1983.

95. NAESS, A. and BØRRESEN, R. "On Experimental Prediction of Low Frequency Oscillations of Moored Structures", OTC paper 2879, Houston, 1977.

96. HAVELOCK, T.H. "The Drifting Force on a Ship Among Waves", Phil. Magazine Series 7, Vol. 33, pp467-475, 1942.

97. MARUO, H. "The Excess Resistance of a Ship in Rough Seas", Int. Ship Building Progress, Vol. 4, No. 35, pp337-345, July 1957.

98. LIN, W.C. and REED, A. "The Second Order Steady Force and Moment on a Ship Moving in an Oblique Seaway", 11th Symp. on Naval Hydrodynamics, University College, pp333-351, London, 1976.

99. MARUO, H. "The Drift Force of a Floating Body in Waves", Journal of Ship Research, Vol. 4, No. 3, pp1-10, 1960.

100. Newman, J.N. "The Drift Force and Moment on Ships in Waves", Journal of Ship Research, Vol. 11, No. 1, pp51-60, 1967.

101. FALTINSEN, O.M. "Drift Force on a Ship in Regular Waves", DnV Report 75-4-S, 1975.

102. LEE, C.M. and NEWMAN, J.N. "The Vertical Mean Force and Moment of Submerged Bodies under Waves", Journal of Ship Research, Vol. 15, No. 3, pp231-245, 1971.

103. KIM, C.H. and CHOU, F. "Prediction of Drifting Force and Moment on an Ocean Platform Floating in Oblique Waves", Int. Shipbuilding Progress, Vol. 20, No. 230, pp388-401, 1973.

104. GOODMAN, T.R. "Forces on a Hovering Slender Body of Revolution Submerged under a Free Surface", Developments in Mechanics, Pergamon Press, pp525-549, N.Y., 1965.

105. DALZELL, J.F. and KIM, C.H. "An Analysis of the Quadratic Frequency Response for Lateral Drifting Force and Moment", Journal of Ship Research, Vol. 25, No. 2, pp117-129, 1981.

106. TAYLOR, E. and HUNG, S.M. "Wave Drift Enhancement Effects in Multi Column Structures", Marine Technology Report, Dept of Mechanical Eng., University College London, November 1984.

107. LAMB, H. "Hydrodynamics", Dover Publication, 6th edition, p91, N.Y.

108. MILNE - THOMSON, L.M. "Theoretical Hydrodynamics, p50, 3rd edition.

109. MURRAY, R.S. "Mathematical Handbook of Formulae and Tables", Schaum's Outline Series in Mathematics, p138, McGraw-Hill Book Company, 1968.

110. DEAN, W.R. "On the Reflection of Surface Waves by a Submerged Cylinder", Proc. Camb. Phil. Soc. 44, pp483-491, 1948.

111. URSELL, F. "Surface Waves on Deep Water in the Presence of a Submerged Circular Cylinder", Proc. Camb. Phil. Soc. 46, pp141-152, 1950.

112. HOOFT, J.P. "A Mathematical Method of Determining Hydrodynamically Induced Forces on a Semi-submersible", Trans SNAME, Vol. 79, pp28-70, 1971.

113. MILLER, N.S. and DE SOUZA, P.M.F.M. "The Wave Excited Forces and Dynamics Response of Semi-submersibles" in "Semi-submersibles and Tethered Buoyant Platforms - Some Design Considerations", Lectures for a course given 26-30th September, 1977, in Dept. of Naval Architecture and Ocean Engineering, Glasgow University, Part 2, pp55-140, 1977.

114. MATHISEN, J. and CARLSEN, C.A. "A Comparison of Calculation Methods for Wave Loads on Twin Pontoon Semi-submersibles", Int. Symp. on Ocean Eng. and Ship Handling, pp7:1-7:23, Gothenburg, 1980.

115. KEULEGAN, G.H. and CARPENTER, L.H. "Forces on Cylinders and Plates in an Oscillating Fluid", Journal of Research of the National Bureau of Standards, Vol. 60, No. 5, pp423-440, 1958.

116. HOOFT, J.P. "Advanced Dynamics of Marine Structures", A Wiley-Interscience Publication, pp156-170, 1982.

NOMENCLATURE

Chapter 1

$\overline{GM}$	metacentric height
ABS	The American Bureau of Shipping
DnV	The Det norske Veritas
$\overline{GZ}$	righting arm
R_e	Reynold's number

Chapter 2

USCG	The United States Coast Guard
$I_1(2\gamma R)$	the modified Bessel Function of the first kind
$\gamma = \frac{\omega^2}{g}$	wave number
ω	wave radian frequency
g	gravitational acceleration
R	radius of cylinder (in the text radius of a lower hull)
a	incident wave amplitude
T	wave period
λ	wave length
t	time
$\bar{F}^t$	steady force
$\bar{F}_x^t$	steady horizontal force
$\bar{F}_y^t$	steady vertical force
ρ	density
b	dissipation of energy
a_{2T}	amplitude of the second harmonic transmitted wave
CG	the centre of gravity
C_G	non-dimensional tilting moment
S	half of the pontoon separation

ϕ	steady tilt
ε	wave steepness
Δ	displacement weight
H_w	wave height
$H_{1/3}$	significant wave height
$\overline{T}$	mean wave period
L	pontoon length
$\overline{KG}$	vertical distance between the COG and the keel line
T_1, T_2	different periods of two regular components of a regular wave groups (Figs 28 and 29)
$S'_\eta(f)$	experimental wave spectrum
$S'_\phi(f)$	experimental roll motion spectrum

Chapter 3

$\overline{GM}_T$	transverse metacentric height
$\bar{k}_{xx}$	the radius of gyration for rolling about the COG
$\overline{KB}$	vertical distance between the centre of buoyancy and the keel line
W_i	mass of the i^{th} item of the semi-submersible model
$\overline{KG}_i$	vertical centre of gravity of the i^{th} item of the semi-submersible model
Δ	total displacement weight of the model
$\overline{BM}_T$	transverse metacentric radius
$\overline{BM}_L$	longitudinal metacentric radius
LCB	longitudinal position of the centre of buoyancy
LVDT	linear variable differential transformer
K	calibration factor
subscript i	number of shifts for inclining tests
w_i	sum of test weights transferred each time for inclining tests
d_i	horizontal shift of the i^{th} test weight for inclining tests

y_i total deflection of the pen on the chart due to transfer of the i^{th} test weight

Y_i total heel on the model

ϕ_i total heel angle due to transfer of the i^{th} test weight

ℓ horizontal distance between the vertical axes of the transducers

m_i static moment of the i^{th} test weight

$\overline{GM}_i$ metacentric height, which includes the effect of test weights

N maximum number of the shifts

subscript c values associated with correction due to the effect of test weights in inclining tests

Δ_c corrected model displacement weight which excludes the effect of test weights

$\overline{KG}_i$ corrected vertical centre of gravity of the model which excludes the effect of test weights

$\overline{Kg}_i$ vertical centre of gravity of the i^{th} test weight for inclining test

$\overline{KB}_c$ corrected vertical centre of buoyancy of the model which excludes the effect of test weights

$\overline{BM}_c$ corrected transverse metacentric radius which excludes the effect of test weights

K_v scale factor of the vertical axes of experimental chart records

K_t scale factor of the horizontal axis of experimental chart records

K_w calibration factor of wave probe

WL wave length

WH wave height

RAO motion amplitude/wave amplitude = response amplitude operator

ζ_M wave amplitude obtained from the wave probe by the model

ζ_R wave amplitude obtained from the wave probe on the right side of the bridge of the model tank

ζ_L wave amplitude obtained from the wave probe on the left side of the bridge of the model tank

ζ_B mean value of the experimental wave amplitude on the bridge of the model tank

F.S. full scale

T wave period

ϕ_o reference tilt angle

WH_o reference wave height

GM_o reference metacentric height

S half of the hull separation

R radius of circular lower hull (pontoon)

D diameter of circular lower hull (pontoon)

S/G strain gauge

R_1, R_2, R_3, R_4 resistance of each arm of the wheatstone bridge

V_{in} input voltage

V_{out} output voltage

K_L calibration factor of load cell transducer

N number of test weights used in the calibration of load cell transducers

L lower hull (pontoon) length

T draught (Figs 80 to 90)

Chapter 4

F_W wave exciting force

F_R radiation force

F_I incident wave (Froude-Krylov) force

F_D diffraction force

F_{AD} diffraction force component in phase with the acceleration of wave motion

F_{BD} diffraction force component in phase with the velocity of wave motion

F_A radiation force component in phase with the acceleration of body motion (hydrodynamic inertial force)

F_B radiation force component in phase with the velocity of body motion (hydrodynamic velocity force)

F_{VBW} viscous wave force caused by the wave-induced viscous fluid motion

F_{VB} viscous damping force caused by the body motion induced viscous fluid motion

F_V viscous fluid force resulting from the relative velocity due to both the wave and body motion in combination

D cylindrical member diameter

H wave height

λ wave length

Φ_I incident wave potential (Froude-Krylov potential)

Φ_D diffraction potential of the fluid motion

Φ_R radiation potential of the fluid motion

Φ total velocity potential of the fluid motion

V_n normal velocity component of a point on the section contour

h incident wave elevation

a wave amplitude

ω wave radian frequency

γ wave number

g gravitational acceleration

subscript $\underline{s}$ wetted contour of the strip section

$G(x,y;\xi,\eta)$ pulsating source potential of unit strength located at a point $(x,y;\xi,\eta)$ in the lower half plane

$Q_R(\xi,\eta)$ unknown strength of a point source in radiation potential

superscript m mode of oscillation takes 2, 3 and 4 for sway, heave and roll respectively

$A^{(m)}$ amplitude of the motion of the strip in the m^{th} mode of oscillation

$\cos(n,m)$ direction cosine depending on the m^{th} mode of oscillation

n outward unit normal vector

$\nabla = \frac{\partial}{\partial x}\vec{i} + \frac{\partial}{\partial y}\vec{j}$; the vector differential operator

$Q_j^{(m)}$ unknown source strength in the m^{th} mode associated with real part

$Q_{N+J}^{(m)}$ unknown source strength in the m^{th} mode associated with imaginar part

subscript j index for the terminal points of a segment

subscript N number of segments

$I_{ij}^{(m)}$ influence coefficient (normal derivative of the source potential) associated with real part in the m^{th} mode

$J_{ij}^{(m)}$ influence coefficient (normal derivative of the source potential) associated with imaginar part in the m^{th} mode

subscript i index for the mid-points of segments

P_o mid-point of segment

$|s|$ segment length

$\Phi_I^{(o)}$ odd component of the incident wave potential associated with the asymmetric flow field about the y-axis

$\Phi_I^{(e)}$ even component of the incident wave potential associated with the symmetric flow field about the y-axis

α_i segment slope of the i^{th} segment

$f^{(m)}$ sectional wave-exciting force in the m^{th} mode of excitation

$f_R^{(m)}$ sectional wave-exciting force in the m^{th} mode of excitation associated with real part

$f_I^{(m)}$ sectional wave-exciting force in the m^{th} mode of excitation associated with imaginar part

$\varepsilon^{(m)}$ phase shift of the force maximum in the m^{th} mode from the incident wave maximum at the origin of the wave axis (0)

(0-XYZ) wave axis system

(o-xyz) body axis system

R radius of lower hull

S_A instantaneous cross-sectional area

S	half of the hull separation
ρ	density of water
I	infinite frequency (in Figs 133 to 139)
B	half of the lower hull beam
ASR	aspect ratio
H_s	vertical distance from the centroid of a seaward lower hull section to the free surface
H_ℓ	vertical distance from the centroid of a leeward lower hull section to the free surface
K_r	non-dimensional resonant frequency
x	half column width at WL (in eq. 26)
n	natural mode of standing waves (1,2,3, ... for symmetric waves, 0.5, 1.5, 2.5, ... for asymmetric waves) (in eq. 26)
K	non-dimensional frequency
T	vertical distance from the top contour of a lower hull to the free surface
ϕ	steady tilt angle
SHR	column thickness to lower hull width ratio
subscript k	mode of motion takes 2, 3 and 4 for sway, heave and roll (in section 4.3.2)
subscript j	mode of excitation takes 2, 3 and 4 for sway, heave and roll (in section 4.3.2)
M_{jk}	mass matrix
A_{jk}	added mass matrix
B_{jk}	damping coefficient matrix
C_{jk}	restoring force coefficient matrix
F_j	wave-exciting force matrix
s_k	motion displacement in the k^{th} mode
$\bar{s}_k$	amplitude of the complex motion displacement in the k^{th} mode
$\bar{F}_j$	amplitude of the complex wave-exciting force in the j^{th} mode
F_{jR}	wave-exciting force associated with the real part in the j^{th} mode

F_{jI} wave-exciting force associated with the imaginar part in the j^{th} mode

s_{kR} motion displacement associated with the real part in the k^{th} mode

s_{kI} motion displacement associated with the imaginar part in the k^{th} mode

I_{44} rolling mass moment of inertia of the semi-submersible

∇ volume displacement of the semi-submersible (in section 4.3.2)

a_{jk} sectional added mass in the j^{th} mode induced by the k^{th} mode of excitation

b_{jk} sectional damping mass in the j^{th} mode induced by the k^{th} mode of excitation

subscript $\underline{s}$ seaward hull wetted contour (in section 4.3.2)

subscript $\underline{\ell}$ leeward hull wetted contour (in section 4.3.2)

$\int_{-L1}^{L2}$ integration along the semi-submersible length

$\overline{OG}$ vertical distance between the origin (0) and the centre of gravity (G)

A_w total waterplane area

C_k stiffness of mooring or anchoring

α_k phase shift of the motion maximum in the k^{th} mode from the incident wave maximum at the origin of the wave axis (0)

RAO motion amplitude/incident wave amplitude = Response Amplitude Operator

T_m natural heave period of the model

$\bar{f}_x^t$ sectional steady horizontal force

$|\bar{A}|_{-\infty}$ complex form of the scattered wave amplitude at the farfield $(-\infty)$

$\bar{f}_y^t$ sectional steady vertical force

$I_1[2\gamma R]$ the modified Bessel function of the first kind

H vertical distance from the centre of submerged cylinder to the water level

η_o steady vertical drift induced by the steady vertical upward force

ξ_o steady horizontal drift induced by the steady horizontal force

overbar $-t$ time average

η' oscillatory heave motion

ξ' oscillatory sway motion

μ the angle of wave incidence relative to the positive longitudinal z-axis

$\int_L$ integration along the slender body length

a_{22} sectional added mass coefficient in the sway mode

a_{33} sectional added mass coefficient in the heave mode

I_{b5} volume moment of inertia of the body with respect to the transverse x-axis

I_{b6} volume moment of inertia of the body with respect to the vertical y-axis

C_o steady vertical force coefficient

$\bar{M}_T^t$ steady tilting moment induced by the steady vertical force

$\bar{F}_s^t$ steady vertical force on the seaward pontoon

$\bar{F}_\ell^t$ steady vertical force on the leeward pontoon

D vertical distance from the centroid of a lower hull to the COG

subscript h horizontal

subscript v vertical

K_{22} sway added mass coefficient of deeply submerged lower hull

K_{33} heave added mass coefficient of deeply submerged lower hull

∇ volume displacement of one lower hull

H_o vertical distance from the centroid of a lower hull to the water level (in section 4.4.2.1.1)

f force on a unit length of the submerged portion of a fixed cylindrical member (in section 4.4.2.2.1)

f_I inertial force on a unit length of cylindrical member

f_D drag force on a unit length of cylindrical member

C_M inertia coefficient

C_D drag coefficient

D	cylinder diameter (in section 4.4.2.2.1)
V	velocity of the water particles in the incoming wave at the centre of the element (in section 4.4.2.2.1)
V_o	maximum particle velocity
F_X	total horizontal wave-exciting force on a surface-piercing column
H	column depth (in section 4.4.2.2.1)
η	crest elevation (in section 4.4.2.2.1)
subscript c	quantities associated with column
subscript h	quantities associated with hull
A_p	projected area
u	horizontal wave particle velocity
v	vertical wave particle velocity
subscript x	quantities associated with the horizontal direction
subscript y	quantities associated with the vertical direction
R_c	radius of column
R_h	radius of hull
M_{T_D}	roll exciting moment (tilting moment) induced by the drag force
N_c	number of columns
$\bar{M}^t_{T_D}$	steady tilting moment induced by drag force
$\rho(\theta,y)$	hydrodynamic pressure on a column element in polar coordinate system
$\Sigma\bar{M}^t_T$	total steady tilting moment on a semi-submersible
M_R	righting moment
∇_s	total displacement volume of the semi-submersible
$\overline{GM}_{min}$	minimum $\overline{GM}$ to limit the steady tilt to a specified tilt angle

H_1 vertical distance from the centroid of the upper pontoon to the mean water level in a tilted position

H_2 vertical distance from the centroid of the lower pontoon to the mean water level in a tilted position

ϕ steady tilt angle

D vertical distance from the centroid of a pontoon to the COG

H_o vertical distance from the centroid of a pontoon to the water level in the upright position

$\bar{F}_1^t$ steady vertical force on the upper pontoon of semi-submersible in a tilted position

$\bar{F}_2^t$ steady vertical force on the lower pontoon of semi-submersible in a tilted position

S half of the hull separation

$\bar{f}_y^t$ steady vertical force per unit length

S_A cross-sectional area of pontoon

H vertical distance from the centroid of submerged cylinder to the mean water level

R radius of cylinder

γ wave number

a incident wave amplitude

$I_1[2\gamma R]$ modified Bessel Function of the first kind

$\bar{M}_T^t$ steady tilting moment

M_R righting moment

∇ volume of one lower hull for vessel B or volume of two footings for vessel A

$\overline{GM}$ metacentric height

∇_s total volum displacement of the vessel

$\overline{KG}$ vertical distance from the baseline to the COG

n number of columns

ρ water density

g	gravitational acceleration
R_1	radius of column
R_2	radius of caisson
R_c	radius of circumscribing circle passing through the centre of column
H_1	depth of submergence of column of radius R_1 from the still water level
H_2	depth of footing of radius R_2
μ	heading angle with respect to the wave travel
c	wave celerity
C_{v1}	added virtual mass coefficient in the heave mode for a rectangle with aspect ratio $\pi R_2/2H_2$
C_{v2}	added virtual mass coefficient in the heave mode for a rectangle with aspect ratio $\pi R_1/2H_2$
C_{v3}	added virtual mass coefficient in the heave mode for a rectangle with aspect ratio $\pi R_1/2(H_1 + H_2)$
J	three-dimensional factor = 0.6366
C_D	drag coefficient for the column plus footing in the heave mode
$C_{D_{R_1}}$	drag coefficient for column of radius R_1 in the sway mode
$C_{D_{R_2}}$	drag coefficient for column of radius R_2 in the sway mode
R	radius of the submerged footing (in eq. I.14)
D	depth of the submerged footing or horizontal lower hull
B	beam of the lower hull
L	length of the lower hull
Δy	horizontal drift
$\Delta\phi$	steady tilt
∇	displacement volume
W	displacement weight
F	buoyancy
T	line tension

subscript s seaward

ℓ leeward

h horizontal

v vertical

steady drift force (in eq. I.17 to I.18)

M_D overturning moment due to the steady drift force

M_T overturning moment due to the mooring line tension

Appendix II.1

r_a outer radius of the cylindrical hull elements

r_b inner radius of the cylindrical hull elements

I_o rolling mass moment of inertia about the own axis of a model element

I_{xx_i} rolling mass moment of inertia about the COG of a model element for i^{th} $\overline{GM}$ tested

subscript i number of $\overline{GM}$s tested

z_i vertical distance between the COG of the i^{th} element and the COG of the model

m mass of a semi-submersible element

b_m mean beam of the aluminium deck of the model

t thickness

ΣI_{xx_i} rolling mass moment of inertia of the model for the i^{th} $\overline{GM}$ tested

$\bar{k}_{xx_i}$ radius of gyration of roll for the i^{th} $\overline{GM}$ tested

Appendix II.2

M mass (or mass moment of inertia)

A added virtual mass (or moment of inertia)

B damping force (or moment) coefficient

C	restoring force (or moment) coefficient
F_o	maximum of wave-exciting force (or moment)
ω	radian wave frequency
s	motion displacement
S	amplitude of motion displacement
ε	phase angle between the forced motion and the wave-exciting force
ν	decaying constant
S_{st}	static motion amplitude
μ	magnification factor
Λ	tuning factor
K	non-dimensional damping factor
ω_n	natural frequency
ω_d	radian frequency of the free damped oscillation
C_1, C_2	constants to be determined from the initial conditions
N	number of cycles considered
T_d	period of damped oscillation
A_w	total waterplane area
ρ	density of water
g	gravitational acceleration
ℓ	distance measured between each successive cycle on the pen recorder chart
T_n	natural period
V	chart speed
$\overline{GM}$	metacentric height